Poster Abstract

Casey O'Laughlin, Brent A. Law, Vanessa S. Zions, Thomas L. King, Brian Robinson, Yongsheng Wu. *The size versus settling relations of oil-mineral aggregates derived from diluted bitumen.* International Oil Spill Conference, May 15-18 2017, Long Beach, California.

A series of experiments to elucidate size versus settling velocity relationships of chemically- and physically-dispersed OMAs (oil-mineral aggregates) derived from diluted bitumen have been performed. Experiments are completed in an enclosed wave tank facility, and are designed to characterize warm water (>10 °C), high-sediment concentration (~50 mg/L) conditions in the presence and absence of chemical dispersant (Corexit®EC-9500A). Previous wave tank experiments operated at a low sediment concentration (~10 mg/L), and with a short 2-hour settling period, failed to produce OMAs. In these more recent experiments with higher sediment concentration, the settling phase is extended to 24 hours. The resulting occurrence of OMAs in wave tank experiment water is confirmed via microscope. Machine-vision floc cameras were used to produce high-resolution images of settling particles covering a size range from 45 microns to 1 millimeter, at image capture rates of up to 11 frames per second. These images are used to determine the settling velocity of individual particles. Size-settling relationships derived from similar imagery collected during previous lab experiments using lab-created OMAs show a broad range of settling velocities of OMA particles (0.04-23.9 mm/s). Analysis of images from recent 24 hour wave tank experiments is ongoing, and it is expected that a similarly broad range of size versus settling relationships will result from 'naturally' formed OMAs in these experiments.

**To:** Conmy, Robyn[Conmy.Robyn@epa.gov]; fingasmerv@shaw.ca[fingasmerv@shaw.ca]; tchazen@utk.edu[tchazen@utk.edu]; robert.jones@noaa.gov[robert.jones@noaa.gov]; mandyjoye@gmail.com[mandyjoye@gmail.com]; mbleigh@alaska.edu[mbleigh@alaska.edu]; karl.linden@colorado.edu[karl.linden@colorado.edu]; kmmcfarlin@alaska.edu[kmmcfarlin@alaska.edu]; msmiles@lsu.edu[msmiles@lsu.edu]; thomas.s.coolbaugh@exxonmobil.com[thomas.s.coolbaugh@exxonmobil.com]; mathijs.smit@shell.com[mathijs.smit@shell.com]; Sprenger, Mark[Sprenger.Mark@epa.gov]
**Cc:** nancy.kinner@unh.edu[nancy.kinner@unh.edu]
**From:** Mandsager, Kathy
**Sent:** Mon 10/24/2016 5:04:41 PM
**Subject:** State-of-Science for dispersant use in Arctic Waters: degradation & fate panel
2016.10.21_Degradation and Fate.docx
2016.10.24_Forwarded to Degradation group from public comment to Transport group.docx

Dear Degradation & Fate panel members,

Our next meeting is scheduled for **11/28 beginning at 1:00 pm ET**. Attached is the latest version of our document.

Additionally, there are 2 items that the Transport group have forwarded to you (see paragraphs attached) for your discussion/incorporation.

I believe we will need a few more meeting slots on the calendar in order to accomplish our tasks by end of the year. Could you please take a brief moment to fill out the doodle poll (by WE 10/28) so we can accommodate this?

http://doodle.com/poll/ybgsat2ub4cfipvk

Thank you!

---

Kathy Mandsager

Coastal Response Research Center

Center for Spills and Environmental Hazards

220 Gregg Hall, 35 Colovos Rd

University of New Hampshire

Durham, NH 03824

603.862.1545

Forwarded to Degradation group from public comment to Transport group:

Public Input:

Statements need to be added about persistence and transport of surface slicks especially after they emulsify or get frozen into ice. While there are uncertainties in details, there is a clear and significant known difference in fate and persistence of dispersed oil vs. surface slicks which is one of the key considerations for dispersants use, but is not currently evident in the document (NAS 2003, MMS 2003, vs. Hazen 2010).

Public Input:

Hazen et al (2010) reported "faster-than-expected hydrocarbon biodegradation rates at 5°C" in their studies, and suggested an intrinsic biodegradation of oil components in the deep water column. Several more resent publications, including Baelum et at (2012) suggested that nearly 75% of Macondo oil was degraded in deep waters at 5C temperature, which suggested that the dissolved constituents are not persistent.

**To:** Kavlock, Robert[Kavlock.Robert@epa.gov]
**Cc:** Gwinn, Maureen[gwinn.maureen@epa.gov]; Osaka, Anna[Osaka.Anna@epa.gov]; Smith, Kelly[Smith.Kelly@epa.gov]; Gilliland, Alice[Gilliland.Alice@epa.gov]; Conmy, Robyn[Conmy.Robyn@epa.gov]; Richardson, Teri[Richardson.Teri@epa.gov]; Geller, Andrew[Geller.Andrew@epa.gov]; Waits, Abby[Waits.Abby@epa.gov]
**From:** Sonich-Mullin, Cynthia
**Sent:** Wed 9/14/2016 9:09:37 PM
**Subject:** Advanced Notification: Deepwater Horizon Research Report
BSEE Report_E12PG00037_fact sheet.docx
E12PG00037_Draft Final Report__for IO review_august 2016.docx

Bob,

We are submitting the following EPA report to you under the Advanced Notification Policy (ANP):

*Dispersant Effectiveness, In-Situ Droplet Size Distribution and Numerical Modeling to Assess Subsurface Dispersant Injection as a Deepwater Blowout Oil Spill Response Option and Evaluation of Oil Fluorescence Characteristics to Improve Forensic Response Tools.*

This report has been developed as an EPA Report under an InterAgency Agreement with DOI, BSEE. The lead author of the EPA report is Robyn N. Conmy. Gregory Wilson, (OEM, OLEM) has reviewed this report.

We are flagging this report as a high profile product under the ANP since it relates to the Deepwater Horizon Oil Spill.

**Potential Implications/Impact**: This report addresses Sustainable Healthy Communities research on technical support for policy, guidance, and targeted research for oil spill response (SHC 3.62.2). We find that the dispersion of oil, both natural and enhanced due to dispersants, is influenced by factors such as water temperature, dispersant type and concentration, and jet release pressure. Undersea jet oil plumes simulated within wave / flume tanks offer an opportunity to monitor the movement of dispersed oil droplets. The results further inform aquatic spill preparedness efforts by the EPA, especially for subsurface oil spills like the 2010 Deepwater Horizon (DWH) spill in the Gulf of Mexico.

**Partners Engaged:** This report is a summary of the work conducted under an Interagency Agreement with the Department of Interior-Bureau of Safety and Environmental Enforcement (IAA No. E12PG00037). The work included colleagues from the EPA, Department of Fisheries and Oceans Canada (Canadian federal agency), The New Jersey Institute of Technology, The University of South Florida and Dalhousie University.

Attached are the Draft Final Report and Fact Sheet. Please let us know if you have any questions or if additional communications materials are needed.

Thanks,

Cindy

Cynthia Sonich-Mullin

Director, National Risk Management Research Laboratory

Office of Research and Development

U.S. Environmental Protection Agency

26 W. Martin Luther King Jr. Dr.

Cincinnati, Ohio 45268

Phone: 513-569-7923

Mobile: 513-560-5043

**Fact Sheet**

# Dispersant Effectiveness, In-Situ Droplet Size Distribution and Numerical Modeling to Assess Subsurface Dispersant Injection as a Deepwater Blowout Oil Spill Response Option
*and*
# Evaluation of Oil Fluorescence Characteristics to Improve Forensic Response Tools

*Submitted to be an EPA Report from IAA No. E12PG00037*

Robyn N. Conmy[1], Thomas King[2], Brian Robinson[2], Scott Ryan[2], Youyu Lu[2], Mary Abercrombie[3], Michel Boufadel[4], Haibo Niu[5]

[1]U.S. Environmental Protection Agency ORD NRMRL
26 MLK Drive West, Cincinnati, OH

[2]Department of Fisheries and Oceans Canada, Bedford Institute of Oceanography
1 Challenger Drive, Dartmouth, Nova Scotia, Canada B2Y 4A2

[3]University of South Florida, College of Marine Science
140 7th Ave South, St. Petersburg, FL 33701

[4]New Jersey Institute of Technology, Civil and Environmental Engineering
University Heights, Newark, NJ 07102

[5]Dalhousie University, Department of Engineering
PO Box 550, Truro, N.S. Canada

Impact Statement: This report addresses Sustainable Healthy Communities research on technical support for policy, guidance, and targeted research for oil spill response (SHC 3.62.2). We find that the dispersion of oil, both natural and enhanced due to dispersants, is influenced by factors such as water temperature, dispersant type and concentration, and jet release pressure. Undersea jet oil plumes simulated within wave / flume tanks offer an opportunity to monitor the movement of dispersed oil droplets. The results further inform aquatic spill preparedness efforts by the EPA, especially for subsurface oil spills like the 2010 Deepwater Horizon (DWH) spill in the Gulf of Mexico.

Background: The 2010 DWH oil spill in the Gulf of Mexico has highlighted the pressing need for a better understanding of the interaction of chemical dispersants and crude oil at ocean depth. This study assessed the operational performance of subsurface injection dispersant use on high pressure releases of oil within a flume tank.

Study Description: Oil dispersion experiments were conducted in the flow-through flume tank at BIO. A custom subsurface oil injection system was used to generate dispersed oil plumes in the tank, simulating underwater jet releases of oil (80°C oil temperature). A parametric study using three oil types (South Louisiana Crude, Alaskan North Slope Crude and Intermediate Fuel Oil 120), two dispersants (Corexit 9500 and Finasol OSR 52), and four dispersant-to-oil ratios (DOR 0, 1:20, 1:100, 1:200) was conducted at warm and cold temperatures. In situ oil plume dispersion was monitored for particle concentration and Droplet Size Distribution (DSD) using the LISST-100X Laser *in-situ* Scattering and Transmissometry System (Sequoia Scientific Inc. Seattle, WA) and fluorescence intensity from submersible fluorometers - an indication of dispersion effectiveness. Bottle samples were collected for analysis of Total Petroleum Hydrocarbons (TPH) and Benzene-Toluene-Ethylbenzene-Xylene (BTEX) concentrations. Empirical data was subsequently used as input variables to refine numerical models of droplet size formation (VDROP-J, JETLAG and Modified Weber Number). This project also included a stand-alone study to generate a fluorescence library of 25 oil types to expand community knowledge base on the optical signatures as a function of oil type.

Results: Simulated oil plume dispersion experiments demonstrated that the addition of dispersant decreased the Volume Mean Diameter (VMD) of oil and shifted the DSD to smaller droplets. Dispersions created DOR =1:20 yielded VMD smaller than 70 µm and exhibited bimodal DSD, suggesting that produced droplets dispersant injection would likely remain dispersed in the presence of mixing energy. Particle size analyses near the injection release (LISST Release) exhibited larger VMD compared to those generated further downstream from release in the tank (LISST Downstream) indicating a shift from larger to smaller droplets within the plume, with and without the presence of dispersant during the 12 minute experiments. Water temperature did not appear to influence the DSD or VMD for lighter crude oils, but a temperature effect was observed on the Total Particle Concentration (TPC), where lower temperatures were coincident with fewer particles dispersed within the plume for a given volume of oil injected. For experiments conducted at water temperatures less than 5°C, The LISST particle size analyzed yielded unexpected DSD where even a unimodal distribution was not measured. Chemistry and in situ fluorescence data indicate that the oil was in fact dispersed adequately. This suggests operational problems with the LISST below 5°C, even though it is within the operating temperature of the LISST (manufacturer manual).

Conclusion: In general, the addition of dispersant decreased the Volume Mean Diameter (VMD) of oil and shifted the DSD to smaller droplets, where Corexit 9500 produced smaller droplets compared to Finasol OSR 52 during the simulated oil plume experiments. Comparing DSD in the plume right after release and further downstream in the tank proved useful for examining the separation of particles within the plume. This has critical implications for the fate and transport of oil plumes and informs the tuning of numerical models. In situ fluorescence was found to be a reliable proxy for oil concentration during the subsurface injection experiments suggesting that

these measurements should be included during spill response monitoring, particularly when bottle samples cannot be obtained.

Partners Engaged: This report is a summary of the work conducted under an Interagency Agreement with the Department of Interior-Bureau of Safety and Environmental Enforcement (IAA No. E12PG00037). The work included colleagues from the EPA, Department of Fisheries and Oceans Canada (Canadian federal agency), The New Jersey Institute of Technology, The University of South Florida and Dalhousie University.

Contact: Robyn N. Conmy, Ph.D., ORD NRMRL Land Remediation Pollution Control Division, Environmental Stressors Management Branch, Tel: 513-569-7090, Fax: 513-569-7620, Email: conmy.robyn@epa.gov.

United States
Environmental Protection
Agency

EPA/600/R-15/xxx | June 2016 | www.epa.gov/research

# Dispersant Effectiveness, In-Situ Droplet Size Distribution and Numerical Modeling to Assess Subsurface Dispersant Injection as a Deepwater Blowout Oil Spill Response Option

*and*

# Evaluation of Oil Fluorescence Characteristics to

**Office of Research and Development**
**National Risk Management Research Laboratory**
**Land Remediation and Pollution Control Division**

EPA/600/R-15/XXX
June 2016

**IAA No. E12PG00037**

**Draft Final Report**

# Dispersant Effectiveness, In-Situ Droplet Size Distribution and Numerical Modeling to Assess Subsurface Dispersant Injection as a Deepwater Blowout Oil Spill Response Option
*and*
# Evaluation of Oil Fluorescence Characteristics to Improve Forensic Response Tools

*Submitted to:*

Bureau of Safety and Environmental Enforcement

*Submitted by:*

Robyn N. Conmy, Ph.D.
U.S. Environmental Protection Agency, Office of Research and Development
26 W. Martin Luther King Drive, Cincinnati, OH 45268
*Tel: 513-569-7090, Fax: 513-569-7620, Email: conmy.robyn@epa.gov

Thomas King, M.Sc.; Brian Robinson, M.Sc; Scott Ryan, M.Sc; Youyu Lu, Ph.D.;
Department of Fisheries and Oceans Canada, Bedford Institute of Oceanography
1 Challenger Drive, Dartmouth, Nova Scotia, Canada B2Y 4A2
Tel: 902-426-4172, Tom.King@mar.dfo-mpo.gc.ca

Mary Abercrombie, M.Sc.
University of South Florida, College of Marine Science
140 7th Ave South, St. Petersburg, FL 33701
*Tel: 727-553-1140, Email: mabercrombie@marine.usf.edu

Michel Boufadel, Ph.D.
New Jersey Institute of Technology, Civil and Environmental Engineering
University Heights, Newark, NJ 07102
Tel: 973-596-5657, Email: michel.boufadel@njit.edu

Haibo Niu, Ph.D.
Dalhousie University, Department of Engineering
PO Box 550, Truro, N.S. Canada
Tel: 902-893-6714, Email: haibo.niu@dal.ca

June 30, 2016



ED_001324_00000913-00002

# Notice/Disclaimer

The U.S. Environmental Protection Agency, through its Office of Research and Development, funded and conducted the research described herein under an approved Quality Assurance Project Plan (Quality Assurance Identification Number XXXXXX-XX-X-X). It has been subjected to the Agency's peer and administrative review and has been approved for publication as an EPA document. Mention of trade names or commercial products does not constitute endorsement or recommendation for use.

This draft report contains scientific observations from a series of subsurface oil injection experiments and high resolution fluorescence analyses. Findings are subject to institutional review and are considered draft, thus the information provided here should not be parsed. Refrain from citing or posting until report is considered final. Upon review, approval does not signify that the contents reflect the views of the U.S. EPA, DFO Canada, or BSEE, nor does the mention of trade names or commercial products constitute endorsement or recommendation for use.



ED_001324_00000913-00003

# Forward

The U.S. Environmental Protection Agency (US EPA) is charged by Congress with protecting the Nation's land, air, and water resources. Under a mandate of national environmental laws, the Agency strives to formulate and implement actions leading to a compatible balance between human activities and the ability of natural systems to support and nurture life. To meet this mandate, US EPA's research program is providing data and technical support for solving environmental problems today and building a science knowledge base necessary to manage our ecological resources wisely, understand how pollutants affect our health, and prevent or reduce environmental risks in the future.

The National Risk Management Research Laboratory (NRMRL) within the Office of Research and Development (ORD) is the Agency's center for investigation of technological and management approaches for preventing and reducing risks from pollution that threaten human health and the environment. The focus of the Laboratory's research program is on methods and their cost-effectiveness for prevention and control of pollution to air, land, water, and subsurface resources; protection of water quality in public water systems; remediation of contaminated sites, sediments and ground water; prevention and control of indoor air pollution; and restoration of ecosystems. NRMRL collaborates with both public and private sector partners to foster technologies that reduce the cost of compliance and to anticipate emerging problems. NRMRL's research provides solutions to environmental problems by: developing and promoting technologies that protect and improve the environment; advancing scientific and engineering information to support regulatory and policy decisions; and providing the technical support and information transfer to ensure implementation of environmental regulations and strategies at the national, state, and community levels.

Cynthia Sonich-Mullin, Director
National Risk Management Research Laboratory



ED_001324_00000913-00004

# Abstract

The 2010 Deepwater Horizon oil spill highlighted the need for better understanding the interaction of dispersants and crude oil during high-pressure releases. This report summarizes a study to assess the operational performance of subsurface injection dispersant use on high-pressure releases within a flume tank. Dispersion experiments were conducted using South Louisiana Crude, Alaskan North Slope Crude and Intermediate Fuel Oil 120 oils, with Corexit 9500 and Finasol OSR 52 dispersants and four dispersant-to-oil ratios (DOR 0, 1:20, 1:100, 1:200) at warm and cold temperatures. *In situ* plume dispersion was monitored for particle concentration and Droplet Size Distribution (DSD; LISST-100X), and fluorescence intensity. Samples were collected for Total Petroleum Hydrocarbons and Benzene-Toluene-Ethylbenzene-Xylene concentrations. Empirical data was subsequently used as input variables to refine numerical models of droplet size formation (VDROP-J, JETLAG and Modified Weber Number). This project also generated a fluorescence library of 25 oil types to expand community knowledge base on optical signatures as a function of oil type. In general, the addition of dispersant decreased the oil Volume Mean Diameter (VMD), creating smaller droplets. Dispersions at DOR =1:20 yielded VMD <70 µm and exhibited bimodal DSD, suggesting that produced droplets would likely remain dispersed in the presence of mixing energy. Water temperature did not appear to influence the droplets for lighter crude oils. DSD results suggest a separation of particles within the plume. *In situ* fluorescence was found to be a reliable proxy for oil concentration. These findings have implications for the fate and transport of oil plumes-both for spill response monitoring and numerical modeling.



ED_001324_00000913-00005

# Acknowledgements

The research presented in this report was funded by the Bureau of Safety and Environmental Enforcement (BSEE) through Interagency Agreement E12PG00037. Efforts were partially supported by the U.S. Environmental Protection Agency - Office of Research and Development (EPA ORD) and the Department of Fisheries Oceans Canada – Bedford Institute of Oceanography (DFO-BIO). This work was a highly collaborative effort and the authors would like to thank all of the contributors. The numerical modeling components are contributions by collaborators Dr. Michel Boufadel and Feng Gao (New Jersey Institute of Technology) and Dr. Haibo Niu and Linlu Weng (Dalhousie University). The high-resolution fluorescence component is a contribution of Mary Abercrombie (University of South Florida). A special thanks to all of the DFO and BDR Contracting staff who made the tank experiments possible: Patrick Toole, Claire McIntyre, Cody Sherren, Jennifer Mason, Peter Thamer, Gary Wohlgeschaffen, Susan Cobanli, and Rod Doane.



ED_001324_00000913-00006

# Table of Contents

Notice/Disclaimer ..... iii

Forward ..... iv

Abstract ..... v

Acknowledgements ..... vi

List of Figures ..... ix

List of Tables ..... x

Acronyms and Abbreviations ..... xi

Executive Summary ..... xii

Task A.1 Introduction & Relevance ..... 1

Task A.2 Experimental Methods ..... 5

A.2.1 Flume Tank Description, Flow Calibration, and Operation ..... 5

A.2.2 Waste Water Treatment ..... 8

A.2.3 Subsurface Oil Injection System ..... 8

A.2.4 Submersible Sensor Deployment ..... 12

A.2.5 VOC Air Monitoring ..... 14

A.2.6 Discrete Water Sample Collection ..... 14

A.2.7 Oil and Dispersant Samples ..... 14

A.2.8 Experimental Design – Core and Complimentary Experiments ..... 16

A.2.9 Submersible Sensor Calibration Experiments ..... 17

A.2.10 Submersible Fluorometer and LISST Data Processing ..... 18

A.2.11 Analytical Chemistry Analysis ..... 20

A.2.12 Numerical Modeling Methods ..... 21

TASK A.3 RESULTS ..... 22

A.3.1 ANS Dispersion Effectiveness ..... 22

A.3.2 IFO 120 Dispersion Effectiveness ..... 36

A.3.3 SLC Dispersion Effectiveness ..... 46

A.3.4 Gas Condensate Dispersion Effectiveness ..... 51

A.3.5 Tank Dilution Series Fluorescence Measurements ..... 53

A.3.6 VOC Air Monitoring ..... 58

A.3.7 VDROP-J and JETLAG Numerical Plume Modeling ..... 68



ED_001324_00000913-00007

A.3.8 Weber Number Scaling Numerical Plume Modeling ..... 70
Task B.1 Introduction & Relevance ..... 72
Task B.2 Experimental Methods ..... 81
B.2.1 Sample Preparation ..... 81
B.2.2 Artificial Seawater Protocol ..... 81
B.2.3 Dispersed Oil in Seawater Protocol ..... 81
B.2.4 Spectrophotometric Analysis ..... 82
Task B.3 Results & Discussion ..... 86
B.3.1 Oil Fluorescence Properties ..... 86
B.3.2 Fluorescence as a Function of Chemistry ..... 99
B.3.3 Flume Tank and Baffled Flask EEM Comparison ..... 110
B.3.4 PARAFAC Modeling ..... 112
DOR 0 ..... 114
DOR 1:100 ..... 119
DOR 1:20 ..... 123
PARAFAC Summary ..... 126
References ..... 128
Appendices (Separate Document) ..... 132
APPENDIX A – Experiment Logs ..... 132
APPENDIX B – Analytical Chemistry Results ..... 132
APPENDIX C – Jet Release LISST Oil Droplet Size Distribution Histograms ..... 132
APPENDIX D – Jet Release LISST Oil Droplet Size Distribution Time Series Contours ..... 132
APPENDIX E – Submersible Fluorescence Time Series ..... 132
APPENDIX F – Excitation Emission Matrix Contours ..... 132
APPENDIX G – VDROP-J and JETLAG Numerical Plume Modeling Report ..... 132
APPENDIX H – Weber Number Scaling Numerical Plume Modeling Report ..... 132



ED_001324_00000913-00008

# List of Figures

Figure 1. Photos of subsurface oil injection at the BIO flume tank showing the formation of the subsurface oil plume. Note that the background grid size is 1.5 cm x 1.5 cm.

Figure 2. Photo of the DFO BIO flume tank (top) and cross-section of the tank showing the high-flow manifolds used to generate horizontal water currents (not to scale).

Figure 3. Schematic diagram showing the location of the subsurface injector and *in situ* instrumentation submerged within the tank.

Figure 4A. Photo of the pressurized oil vessel used to hold the oil for the subsurface release.

Figure 4B. Schematic diagram of the pressurized oil vessel for subsurface oil release system in the flume tank.

Figure 5. LISST DSD and VMD (left panels) and time series of concentration and particle size (right panels) for ANS and Corexit 9500 warm water treatments. From top to bottom, DOR = 0, 1:200, 1:100, 1:20.

Figure 6. LISST DSD and VMD (left panels) and time series of concentration and particle size (right panels) for ANS and Corexit 9500 cold water treatments. From top to bottom, DOR = 0, 1:200, 1:100, 1:20.

Figure 7. *In situ* submersible fluorescence time series of sub-injection plume of ANS and Corexit 9500 warm water (left panels) and cold water (right panels) treatments. From top to bottom, DOR = 0, 1:200, 1:100, 1:20.

Figure 8. Downstream LISST DSD and VMD (left panels) and time series of concentration and particle size (right panels) for ANS and Corexit 9500 warm water treatments. From top to bottom, DOR = 0, 1:200, 1:100, 1:20.

Figure 9. Downstream LISST DSD and VMD (left panels) and time series of concentration and particle size (right panels) for ANS and Corexit 9500 cold water treatments. From top to bottom, DOR = 0, 1:200, 1:100, 1:20.

Figure 10. LISST DSD and VMD (left panels) and time series of concentration and particle size (right panels) for ANS and Finasol OSR 52 warm water treatments. From top to bottom, DOR = 1:200, 1:100, 1:20. Refer back to Figure 5 for ANS DOR = 0.

Figure 11. *In situ* submersible fluorescence time series of sub-injection plume of ANS and Finasol OSR 52 warm water treatments. From top to bottom, DOR = 1:200, 1:100, 1:20.

Figure 12. Downstream LISST DSD and VMD (left panels) and time series of concentration and particle size (right panels) for ANS and Finasol OSR 52 warm water treatments. From top to bottom, DOR = 1:200, 1:100, 1:20. Refer back to Figure 6 for ANS DOR = 0.



ED_001324_00000913-00009

Figure 13. LISST DSD with TPC for ANS with Corexit 9500 and Finasol OSR 52 warm water treatments. DOR = 0 (top panel); DOR = 1:20 experiments are middle and bottom panels.

Figure 14. LISST DSD with TPC (Total Particle Concentration) for DOR = 1:20 experiments of ANS and Corexit 9500 treatments. Water temperatures increase from top to bottom panels.

Figure 15. LISST TPC (Total Particle Concentration) for DOR = 1:20 experiments of ANS and Corexit 9500 treatments as a function of water temperature.

Figure 16. LISST DSD and VMD (left panels) and time series of concentration and particle size (right panels) for IFO 120 and Corexit 9500 warm water treatments. From top to bottom, DOR = 0, 1:200, 1:100, 1:20.

Figure 17. LISST DSD and VMD (left panels) and time series of concentration and particle size (right panels) for IFO 120 and Finasol OSR 52 warm water treatments. From top to bottom, DOR = 1:200, 1:100, 1:20. Refer to Figure 16 for IFO 120 DOR = 0.

Figure 18. Downstream LISST DSD and VMD (left panels) and time series of concentration and particle size (right panels) for IFO 120 and Corexit 9500 warm water treatments. From top to bottom, DOR = 0, 1:200, 1:100, 1:20.

Figure 19. Downstream LISST DSD and VMD (left panels) and time series of concentration and particle size (right panels) for IFO 120 and Finasol OSR 52 warm water treatments. From top to bottom, DOR = 0, 1:200, 1:100, 1:20. Refer to Figure 18 for ANS DOR = 0.

Figure 20. LISST DSD with TPC for IFO 120 with Corexit 9500 and Finasol OSR 52 treatments at warm temperatures. DOR = 0 (top panel); DOR = 1:20 experiments are middle and bottom panels.

Figure 21. LISST DSD and VMD (left panels) and time series of concentration and particle size (right panels) for IFO 120 and Corexit 9500 cold water treatments. From top to bottom, DOR = 0, 1:200, 1:100, 1:20.

Figure 22. Downstream LISST DSD and VMD (left panels) and time series of concentration and particle size (right panels) for IFO 120 and Corexit 9500 cold water treatments. From top to bottom, DOR = 0, 1:200, 1:100, 1:20.

Figure 23. LISST DSD and VMD for IFO 120 (top; DOR = 1:100) and ANS (bottom; DOR = 1:200) with Corexit 9500 during cold water treatments.

Figure 24. LISST DSD and VMD (left panels) and time series of concentration and particle size (right panels) for SLC and Corexit 9500 warm water treatments. From top to bottom, DOR = 0, 1:200, 1:100, 1:20.

Figure 25. Downstream LISST DSD and VMD (left panels) and time series of concentration and particle size (right panels) for SLC and Corexit 9500 warm water treatments. From top to bottom, DOR = 0, 1:200, 1:100, 1:20.

Figure 26. LISST DSD with TPC for SLC with Corexit 9500 treatments at warm temperatures. DOR = 0 (top panel); DOR = 1:20 experiments are bottom panels.

Figure 27. *In situ* submersible fluorescence time series of sub-injection plume of SLC and Corexit 9500 warm water treatments. From top to bottom, DOR = 0, 1:200, 1:100, 1:20.

Figure 28. LISST DSD and VMD (top panels),time series of concentration and particle size (middle panels), and fluorescence time series (bottom panels) for Gas Condensate and Corexit 9500 warm water treatments. Left panels are DOR = 0 and right panels are DOR = 1:20.

Figure 29. Calibration lines for fluorometer response vs TPH concentrations.

Figure 30. Calibration lines for fluorometer response vs BTEX concentrations.

Figure 31. Total Particle Concentration and fluorescence time series for ANS crude oil with Corexit 9500 dispersant.

Figure 32. VOC results for subsurface injection experiments (cold water season) using Alaska North Slope crude oil and four treatment conditions (no dispersant, DOR 1:200, DOR 1:100, DOR 1:20). Replicate treatments represented by light blue, dark blue and green colored lines.

Figure 33. VOC results for subsurface injection experiments (warm water season) using Alaska North Slope crude oil and four treatment conditions (no dispersant, DOR 1:200, DOR 1:100, DOR 1:20). Corexit 9500 was used as the treating agent. Replicate treatments represented by light blue, dark blue and green colored lines.

Figure 34. VOC results for subsurface injection experiments (warm water season) using Alaska North Slope crude oil and four treatment conditions (no dispersant, DOR 1:200, DOR 1:100, DOR 1:20). Finasol OSR 52 was used as the treating agent. Replicate treatments represented by light blue, dark blue and green colored lines.

Figure 35. VOC results for subsurface injection experiments (cold water season) using IFO 120 and four treatment conditions (no dispersant, DOR 1:200, DOR 1:100, DOR 1:20). Corexit 9500 was used as the treating agent. Replicate treatments represented by light blue, dark blue and green colored lines.

Figure 36. VOC results for subsurface injection experiments (warm water season) using IFO 120 and four treatment conditions (no dispersant, DOR 1:200, DOR 1:100, DOR 1:20). Corexit 9500 was used as the treating agent. Replicate treatments represented by light blue, dark blue and green colored lines.

Figure 37. VOC results for subsurface injection experiments (warm water season) using IFO 120 and three treatment conditions (DOR 1:200, DOR 1:100, DOR 1:20). Finasol OSR 52 was used as the treating agent (note – these treatments were not tested in triplicate).

Figure 38. VOC results for subsurface injection experiments using gas condensate and two treatment conditions (no dispersant, DOR 1:20). Corexit 9500 was used as the treating agent.

Figure 39. VOC results for subsurface injection experiments using Sweet Louisiana Crude oil and four



ED_001324_00000913-00011

treatment conditions (no dispersant, DOR 1:200, DOR 1:100, DOR 1:20). Corexit 9500 was used as the treating agent.

Figure 40. Fluorescence peaks of S. Louisiana sweet crude dispersed in ppb QSE (Quinine Sulfate Equivalents). Symbols represent Fluorescence Intensity Ratio (FIR) locations and the Center Wavelength (CWL) reported by sensor manufacturers. Bandwidths (BW) are not shown.

Figure 41. Twenty-five oil samples stored in glass bottles.

Figure 42. Trypsinizing baffled flasks containing dispersed oil in artificial seawater (top) and corresponding samples removed from each flask, ready for spectrofluorometric analysis.

Figure 43. Alaska North Slope dispersed oil in artificial seawater at DOR 1:20 with locations of $F_{max1}$, $F_{max2}$, $F_{max3}$ and $F_{max4}$ indicated. Note that maximum fluorescence intensity at $F_{max3}$ is mostly obscured by masking of second order Rayleigh scattering.

Figure 44. Photographs of pre-analysis samples and corresponding example EEMs of Type I (left) and II (right) oils; DOR = 1:20 for Arabian Light (light oil, API gravity > 31.1°), Mesa (medium oil, API gravity 22.3 – 31.1°) and heavy oils (IFO 40 and Santa Clara, API gravity < 22.3°).

Figure 45. $F_{max1}$ fluorescence for Light Oils (API gravity > 31°), in order of increasing density: 1. Scotian Shelf Condensate, 2. Federated, 3. Brent, 4. MC252—Discoverer Enterprise, 5. Hibernia, 6. MC252—generic, 7. Terra Nova, 8. Gullfaks, 9. Arabian Light. Note discrepancy in Scotian Shelf Condensate fluorescence pattern (circled) from that of all other Light Oils. It's particularly unusual that fluorescence intensity at highest DOR is lower than that at DORs 1:200 and 1:100.

Figure 46. $F_{max1}$ fluorescence for Heavy Oils (API gravity < 22.3°), in order of increasing density: 1. Santa Clara, 2. IFO 40, 3. Cold Lake Dilbit, 4. Access Western Blend Dilbit, 5. Hondo, 6. IFO 120, 7. IFO 180, 8. Belridge Heavy, 9. IFO 300. Note discrepancy in Intermediate Fuel Oils (circled) from that of all other Heavy Oils.

Figure 47. For all oil types at DOR 0, total concentration of 2-ring, 3-ring, and 4-ring PAHs (µg/L) against fluorescence intensity (RU) at $F_{max1}$ (top), and against $F_{max2}$ (bottom). Strong linear correlation exists between 2-ring PAHs and $F_{max1}$ fluorescence, but little to no correlation between 3-ring or 4-ring PAHs and $F_{max1}$ fluorescence intensity (top). Strong linear correlation also exists between 2-ring PAHs and $F_{max2}$, but no correlation between 3-ring PAHs or 4-ring PAHs and $F_{max2}$ (bottom).

Figure 48. For all oil types at DOR 0, total concentration of 2-ring, 3-ring, and 4-ring PAHs (µg/L) against fluorescence intensity (RU) at $F_{max3}$ (top), and against $F_{max4}$ (bottom). Strong linear correlation exists between 3-ring and 4-ring PAHs and both $F_{max3}$ and $F_{max4}$ fluorescence; however, only moderate correlation exists between 2-ring PAHs and $F_{max3}$ and $F_{max4}$ fluorescence intensity.

Figure 49. For all oil types at DOR 1:20, total concentration of 2-ring, 3-ring, and 4-ring PAHs (µg/L) against fluorescence intensity (RU) at $F_{max1}$ (top), and against $F_{max2}$ (bottom). A moderate logarithmic correlation is exhibited between 2-ring PAHs and fluorescence intensity (RU) at $F_{max1}$ and a weaker correlation between 2-ring PAHs and $F_{max2}$, but no correlation exists between 3-ring or 4-ring PAHs



ED_001324_00000913-00012

and fluorescence intensity at either $F_{max1}$ or $F_{max2}$.

Figure 50. For all oil types at DOR 1:20, total concentration of 2-ring, 3-ring, and 4-ring PAHs (µg/L) against fluorescence intensity (RU) at $F_{max3}$ (top), and against $F_{max4}$ (bottom). A strong logarithmic correlation is exhibited between 2-ring PAHs and fluorescence intensity at $F_{max3}$. Moderate correlations exist between 3-ring PAHs and $F_{max3}$ as well as between 2-ring PAHs and $F_{max4}$. However, only a weak logarithmic correlation exists between 4-ring PAHs and fluorescence intensity at $F_{max3}$, and there is no correlation between 3-ring or 4-ring PAHs and $F_{max4}$.

Figure 51. Chemical Dispersibility Ratio (CDR) vs. decreasing oil density (top) and Fluorescence Dispersibility Ratio (FDR) vs. decreasing oil density (bottom) show only a weak correlation between chemistry and oil density, and a moderate correlation between fluorescence and oil density. With the removal of the data point for Scotian Shelf Condensation, correlation between fluorescence and oil density improves to $R^2 = 0.71$.

Figure 52. Fluorescence Dispersibility Ratio (FDR) vs. Chemical Dispersibility Ratio (CDR) shows weak correlation between these two ratios.

Figure 53. South Louisiana Crude MC252 EEMS from BFT (left panels) and tank experiments (right Panels) for DOR = 0, 1:100 and 1:20.

Figure 54. Example of split half validation for the 6-component model of 25 oil types at DOR 0 showing individual fit of data splits (Set 1, left; and Set 2, right) compared to overall model for Mode 2 (top) and Mode 3 (bottom) loadings.

Figure 55. Mode 3 Loadings (Excitation) and Mode 2 Loadings (Emission) for all 25 oil types—DOR0 using 6-component model. Note difference in x-axis scales. Although components are tightly spaced, all appear as separate and distinct peaks.

Figure 56. Variation per Component shows Component 1 accounted for >20% to 40% (unique fit and fit) of the data, while Component 2-contributed 5-10% (unique fit and fit) and Components 3-6 accounted for 5% or less of the data, respectively. While Component 6 accounted for a very low percentage of the data, the 6-component model was still a better fit to the data than the 5-component model.

Figure 57. EEM views of the six components of PARAFAC model for 25 oil types at DOR 0. Component #1: $F_{max}$ = Ex 224nm/Em 335nm; Component #2: $F_{max}$ = Ex 230nm/Em 340nm; Component #3: Fmax = Ex 239nm/Em 363nm; Component #4: Fmax = Ex 218nm/Em 290 nm; Component #5: Fmax = Ex 221nm/Em 322nm; Component #6: Fmax = Ex 260nm/Em 474-511nm.

Figure 58. Mode 3 Loadings (Excitation) and Mode 2 Loadings (Emission) for all 25 oil types—DOR 1:100 using 5-component model. Note difference in x-axis scales. Although components are tightly spaced, all appear as separate and distinct peaks.



ED_001324_00000913-00013

Figure 59. Variation per Component shows Component 1 accounted for >35% to almost 50% (unique fit and fit) of the data, while Components 2-5 accounted for 5% or less of the data, respectively.

Figure 60. EEM views of the five components of PARAFAC model for 25 oil types at DOR 1:100. Component #1: $F_{max}$ = Ex 224nm/Em 335nm; Component #2: $F_{max}$ = Ex 254-266nm/Em 455-501nm; Component #3: $F_{max}$ = Ex 230nm/Em 344nm; Component #4: $F_{max}$ = Ex 242nm/Em 363 nm; Component #5: $F_{max}$ = Ex 218nm/Em 290nm.

Figure 61. Mode 3 Loadings (Excitation) and Mode 2 Loadings (Emission) for all 25 oil types—DOR 1:20 using 5-component model. Note difference in x-axis scales. Effect of full dispersion appears to broaden and shift emission peaks to longer wavelengths.

Figure 62. Variation per Component shows Component 1 accounted for 25 to 30% of the data (unique fit and fit) while Component 2 has increased to >10% to 25% (unique fit and fit) of the data. Contribution from Component 3 and 4 have increased, as well.

Figure 63. EEM views of the five components of PARAFAC model for 25 oil types at DOR 1:20. Component #1: $F_{max}$ = Ex 224nm/Em 335nm; Component #2: $F_{max}$ = Ex 233-266nm/Em 432-450nm; Component #3: $F_{max}$ = Ex 230-242nm/Em 501-520nm; Component #4: $F_{max}$ = Ex 233nm/Em 349nm; Component #5: $F_{max}$ = Ex 218nm/Em 290nm.



ED_001324_00000913-00014

# List of Tables

Table 1. List of hydrocarbon fluorometers used in this study. QSDE and PAH represent quinine sulfate dihydrate and petroleum aromatic hydrocarbons, respectively.

Table 2. Water sample collection strategy for the core and complimentary experiments. TPH and BTEX represent Total Petroleum Hydrocarbons and Benzene-Toluene-Ethylbenzene-Xylene, respectively.

Table 3. Physical and chemical property measurements of the oils used in this study.

Table 4. Step-wise sensor calibration experiment parameters.

Table 5. Calibration equations for the submersible fluorometers. Data in this report have fluorescence signal in the manufacturer recommended units.

Table 6. Summary of maximum VOC concentrations at the various treatment conditions tested in this study. Results are for only for warm water experiments.

Table 7. Sensor specifications as listed from manufacturers. Wavelengths listed as Center Wavelengths (CWL) with Full Width at Half Max (FWHM) and Bandpass (BP). Standards used are QS (Quinine Sulfate Dihydrate), NDD Salt (Napthalene Disulfonic Disodium) and PTSA Salt (Pyrenetetrasulfonic Acid Tetrasodium) (From Conmy et al., 2014b).

Table 8. List of oil samples used for EEM analyses. Oils separated by API (American Petroleum Institute) gravity.

Table 9. EEM fluorescence and chemical characteristics. Refer to Supplemental Table A for full table.

Table 10. Individual hydrocarbon compounds reported as Total Alkanes, Total 2-ring, 3-ring and 4-ring PAHs.



ED_001324_00000913-00015

# Acronyms and Abbreviations

| | |
|---|---|
| ADV | Acoustic Doppler Velocimetry |
| ANS | Alaskan North Slope |
| BIO DFO | Bedford Institute of Oceanography Dept. of Fisheries and Oceans Canada |
| BSEE | Bureau of Safety and Environmental Enforcement |
| BTEX | Benzene-Toluene-Ethylbenzene-Xylene |
| CRRC | Coastal Response Research Center |
| DCM | Dichloromethane |
| DE | Dispersion Effectiveness |
| DOR | Dispersant to Oil Ratio |
| DSD | Droplet Size Distribution |
| DWH | Deepwater Horizon Horizon |
| EEMS | Excitation Emission Matrix Spectroscopy |
| EPA | U.S. Environmental Protection Agency |
| GC-FID | Gas Chromatography-Flame Ionization Detector |
| GC-MS | Gas Chromatography Mass Spectrometry |
| GoM | Gulf of Mexico |
| IFO 120 | Intermediate Fuel Oil 120 |
| LISST | Laser In Situ Scattering Transmissometry |
| NEBA | Net Environmental Benefit Analyses |
| NJIT | New Jersey Institute of Technology |
| NRDA | Natural Resource Damage Assessments |
| NRT | National Response Team |
| OMA | Oil-Mineral Aggregate |
| PARAFAC | Parallel Factor Analysis |
| PSC | Particle Size Concentration |
| SLC | South Louisiana Crude |
| STP | Standard Temperatures and Pressures |
| TPC | Total Particle Concentration |
| TPH | Total Petroleum Hydrocarbons |
| UAC | Unified Area Command |
| VMD | Volume Mean Diameter |
| VOC | Volatile Organic Compounds |
| WG-50 | Wave Gauges |



ED_001324_00000913-00016

# Executive Summary

This report summarizes two projects covered under an Interagency Agreement between the Bureau of Safety and Environmental Enforcement (BSEE) and the U.S. Environmental Protection Agency (EPA) in collaboration with the Bedford Institute of Oceanography, Department of Fisheries and Oceans Canada (BIO DFO), New Jersey Institute of Technology (NJIT) and Dalhousie University. Both projects dovetail together in addressing the ability to differentiate physical from chemical dispersion effectiveness using dispersed oil simulations within a flume tank for improving forensic response monitoring tools. This report is split into separate Tasks based upon the two projects funded by BSEE:

1) Dispersant Effectiveness, In-Situ Droplet Size Distribution and Numerical Modeling to Assess Subsurface Dispersant Injection as a Deepwater Blowout Oil Spill Response Option.
2) Evaluation of Oil Fluorescence Characteristics to Improve Forensic Response Tools.

***TASK A: Dispersant Effectiveness, In-Situ Droplet Size Distribution and Numerical Modeling to Assess Subsurface Dispersant Injection as a Deepwater Blowout Oil Spill Response Option.***

The main objectives of work under Task A were to evaluate high velocity subsurface releases of physically and chemically dispersed oil using a flow-through wave (flume) tank. This project addressed three issues: (1) performance evaluation of dispersants for subsurface injection into sub-sea blowouts, (2) tracking, modeling, and predicting the movement and spread of the deepwater plume and oil surfacing from deepwater blowouts, and (3) evaluating the influence of dispersant applications in reducing the concentration of volatile organic compounds emanating from the water surface. Oil dispersion experiments were conducted in the flume tank at the Department of Fisheries and Oceans Canada, Bedford Institute of Oceanography (DFO BIO), which is equipped with an underwater oil release system to simulate a high-pressure release of oil (akin to a deepwater blowout). Subsea



ED_001324_00000913-00017

plume simulations were generated with a pressurized underwater oil release system adapted from existing technology developed by Masutani and Adams (2000). To mitigate wall effects and to generate oil droplets in the size range observed at depth during the Gulf of Mexico Deepwater Horizon (GoM DWH) oil spill, a high flow-rate of oil (3.8 L/min) was released through a small diameter nozzle (2.4 mm). Although it is impossible to simulate in the tank the extreme hydrostatic pressures that exist at 1500 m water depth, underwater high-pressure release of crude oil can be simulated with and without dispersant addition. The researchers also recognize that the shallow nature of the tank does not allow for investigating the rise velocity of the droplets that would be observed in a long (`1500m) water column. Rather, the tank allows for gathering data on the differences in droplet size and distribution during physical and chemical dispersion (akin to that observed during DWH) and for observing the vertical and horizontal movement of the droplets. Although results cannot be directly scaled or translated to a deepwater spill in the ocean, results are still useful for understanding the formation and movement of oil droplets under varying oil and dispersant type, dispersant amount and water temperature.

A total of 48 core and 24 complimentary flume tank experiments were conducted to evaluate the effectiveness of dispersant injection and attenuation of the plume as a function of oil type (US EPA reference oils: Alaskan North Slope (ANS) pipeline blend for a light-medium crude, IFO 120 for a heavy refined product and South Louisiana Crude (SLC) for a light crude, and also a gas condensate), chemical dispersant type (Corexit 9500 and Finasol OSR 52), dispersant-to-oil ratio (DOR of 0, 1:20, 1:100, and 1:200; corresponding to DOR concentrations of 0, 5, 1, and 0.5%) and water temperature (< 10 °C for low temperature and > 10 °C for higher temperature). Experiments were conducted at a fixed horizontal current flow rate of 1 cm/s (~ 1/8$^{th}$ of deep water flow rates in the GoM). Faster current was not permissible as it would have resulted insufficient time for collection of *in situ* measurements and discrete samples. Experiments were conducted using oil at 80 °C, although this is lower than the reservoir temperatures for the DWH Macondo wellhead (estimated at 130°C), this is as high as the experimental design would allow for safety reasons given the limits of the pressurized canister.



ED_001324_00000913-00018

Time series dispersion effectiveness was evaluated by measuring dispersed oil concentrations from samples collected in the flume tank, and via *in situ* droplet size distribution analysis and fluorescence measurements. Discrete samples were collected for oil chemical analysis of Total Petroleum Hydrocarbons (TPH) using gas chromatography coupled to a flame ionization detector (GC-FID) and the analysis of Benzene-Toluene-Ethylbenzene-Xylene (BTEX) via gas chromatography mass spectrometry (GC-MS), employed to quantify oil concentration and partitioning of hydrocarbon compounds in seawater.

The produced Droplet Size Distribution (DSD) was determined by using Laser *In-Situ* Scattering and Transmissometry instruments (LISST-100X, type C; Sequoia Scientific Inc. Seattle, WA) to track the full range diameters of chemically and physically dispersed oil droplets. Larger oil droplets, whether physically or chemically dispersed, may be capable of coalescing and rising to the surface under less energetic mixing conditions. The LISST measures particle size and outputs the concentration of particles in 32 logarithmically spaced size bins between 2.5 to 500 µm, thus facilitating a comparison between natural (physical) and chemical dispersion efficiency of crude oil. All submersible sensors were operated with real-time data acquisition throughout each experiment. *In situ* fluorescence was monitored real-time using two Chelsea Technologies Group AquaTrackas (crude and refined oil types), one Sea Bird – Wet Labs Inc. ECO (gelbstoff type), two Turner Designs Inc. Cyclops (crude and refined oil types) and one GmBH Trios (hydrocarbon type) fluorometers. Many of the fluorescence sensors used in this study are the same models employed to track the subsea plume during the DWH oil spill and confirm dispersion effectiveness. Sensors used in this work are also ones provided as examples in the National Response Team (NRT) *Subsea Dispersant Monitoring and Assessment Interim Guidance* Document, that states "the Risk Plan should use a properly calibrated oil-specific fluorometer (e.g., Chelsea UV AQUAtracka, Turner Designs Cyclops, Wet Labs ECO, or equivalent oil-specific instrument) to enable ongoing improvements in sampling".

Also monitored during experiments was the level of Volatile Organic Compounds (VOC) above the air-water interface of the tank using a handheld photo-ionization detector based



ED_001324_00000913-00019

meter to evaluate concentrations from the perspective of worker safety. Cautioned are the implications of these shallow water tank results, however as the short vertical water column did not allow for any stripping or dissolving of volatile compounds into the water column as would be expected during a deepwater oil release. Correlations between *in situ* fluorescence data, droplet size distribution, total particle concentration, and oil chemistry serve as inputs to the modeling activities of this project.

Oil droplet size distribution (DSD) data from this study is essential for the improvement of oil spill trajectory and ocean circulation modeling processes to predict the fate and transport of subsurface plumes and surface oil slick movement. This has implications for improving the scientific and response community's understanding on the impacts of dispersant application at depth, ultimate fate of subsurface dispersed oil plumes and potential natural resource damages. Recent advancements in the use of numerical modelling have allowed oil droplet size predictions resulting from a subsurface release. Several different mathematical approaches have been used to determine how oil would behave flowing out of an orifice at high pressure. This includes the modified Weber Number technique (Johansen et al., 2013) and the VDROP-J model (Zhou et al., 2014) to predict oil droplet breakup taking into account oil viscosity and interfacial tension. However, there is a limited amount of large scale real world data to help validate the output of these models. This study provided the opportunity to further test these techniques through the use of several different oil types and treatment conditions. Additional results from the numerical modelling using data obtained from tank experiments are presented in Appendix G, with Part 1 using the modified Weber Number and Part 2 using VDROP.

The premise for this research is that the evaluation and efficacy of chemical dispersants at depth will differ dramatically from conventional use of chemical dispersants for treating surface oil slicks. This is due to difference in mixing energy, where for surface slicks is provided mainly through naturally occurring surface waves and currents, particularly breaking waves. Monitoring of DSD is essential in differentiating between chemically and physically dispersed oil. Tank observations using underwater injection experiments provide



ED_001324_00000913-00020

evidence of stable dispersion that may be expected during subsea dispersant injection. Larger oil droplets, whether physically or chemically dispersed, may be capable of coalescing and rising to the surface under less energetic mixing conditions. The experimental results from this work demonstrate the chemical dispersion of oil into small droplets and help to predict the likelihood of coalescence and resurfacing of oil. Results of the project provide spill responders with critical information on the utility of subsurface dispersant application as an oil spill response option and the modeling capabilities that are available to predict oil trajectory during deep water blowouts. Both assist decision-making regarding countermeasures.

***TASK B: Evaluation of Oil Fluorescence Characteristics to Improve Forensic Response Tools.***

This project addresses the evaluation of oil fluorescence characteristics and sensor performance for improving response tools used to inform oil spill countermeasure decision-making. Fluorescence has long been used as 'one tool in the toolbox' for surface spills and used to supplement visual confirmation during response efforts. Recent oil and gas production in extremely remote locations brings an increased risk of spills in under-the-ice and/or deep-sea environments. For releases in these environs, responders will be evermore reliant on submersible sensors for plume tracking when the human eye cannot be employed. As such, the oil spill community has identified the need for better characterization of spilled oil by fluorometers.

Submersible fluorometers deployed during the 2010 DWH oil spill highlighted the challenges in ensuring selection of the optimum sensor configuration as fluorescence peaks occur over a wide nanometer range, vary in shape and wavelength position, are dependent on oil type due to chemical differences, and are affected by the addition of dispersants. This project addresses these concerns through the following objectives: (1) Characterization of oil optical properties as a function of oil type, DOR and concentration; (2) Generation of a comprehensive Excitation Emission Matrix Spectroscopy, or Matrices (EEMs) library that will



ED_001324_00000913-00021

be subjected to advanced statistical analyses for identification of wavelength regions best suited for oil detection; and (3) Evaluation of sensor performance through a series of experiments in a flume tank capable of static and flow-through operations, where sensor data will be validated with chemical and optical analyses.

A series of bench-scale dispersed oil-in-seawater experiments were conducted on 25 oils at 4 dispersant-to-oil ratios (DORs) using Corexit 9500 chemical dispersant. Analysis of the resulting 3D fluorescence EEMs show oil-specific results as well as differing effects of dispersant and DORs. Results will inform the identification of optimum oil detection wavelengths in the marine environment as well as confirmation of the chemical effectiveness of dispersant application. Samples were prepared using baffled flasks to physically disperse the oil within seawater. The effect of dispersant on oil-specific fluorescence is shown, where shifts in intensity and peak wavelengths were observed. Results were compared to chemistry results of oil components.

Results of the laboratory EEMs analysis were compared to EEMs collected under Task A of this project to compare the applicability of baffled flask fluorescence to large scale mixing experiments in the flume tank.

Given recent advances with *in situ* fluorometers, enabling detection at lower UV-wavelengths, these findings help to discern wavelength regions influenced by dispersed oil within seawater, improve the interpretation of fluorescence data, and inform decision-making by responders. Findings from this project will serve to improve confidence in field data, filling operational gaps and formulating operational guidelines.

***Findings: Tasks A and B***

Overall findings from both tasks of this project include:

1. Addition of either Corexit 9500 or Finasol OSR 52 chemical dispersants to Alaskan North Slope (ANS), IFO 120 and South Louisiana Crude (SLC) oils decreased the Volume Mean Diameter (VMD) and shifted the DSD to smaller droplets. In general, Corexit 9500 produced smaller droplets compared to Finasol OSR 52.



ED_001324_00000913-00022

2. Dispersions created without chemical dispersants or DOR = 1:200 yielded VMD larger than 70 µm and exhibited unimodal DSD. Dispersions created with DOR = 1:20 yielded VMD between 2.5 to 70 µm size range with a bimodal distribution. This suggests that produced droplets from a DOR = 1:20 dispersant injection with ANS would likely remain dispersed in the presence of mixing energy given the larger proportion of small droplet sizes observed.
3. Particle size analyses near the injection release (LISST Release) exhibited larger VMD compared to those generated further downstream from release in the tank (LISST Downstream) indicating a shift from larger to smaller droplets within the plume, with and without the presence of dispersant during the 12 minute experiments for ANS and SLC oils. This effect was not always observed with the heavier IFO 120 oil because small droplets were less predominant for this heavier oil.
4. For ANS, dispersion with < 70 um droplet VMD was observed for the DOR = 1:20 treatments at both cold and warm water temperatures. Water temperature did not appear to influence the DSD or VMD for this lighter crude oil. However, a temperature effect was observed on the Total Particle Concentration (TPC), where lower temperatures were coincident with fewer particles dispersed within the plume for a given volume of oil injected.
5. The addition of Corexit 9500 or Finasol OSR 52 to IFO 120 during warm temperature experiments resulted in a shift in DSD and a decrease in VMD; however bimodal distribution was not achieved and even DOR = 1:20 did not yield VMD less than 70 µm in most cases. At cold water temperatures, lower droplet sizes were not observed with the addition of dispersant, where DOR = 1:20 remained well above 200 µm. This suggests that dispersant addition to this oil at cold or warm temperatures would not yield droplet sizes that would likely remain in suspension.
6. For experiments conducted at water temperatures less than 5 °C, The LISST particle size analyzed yielded unexpected DSD where even a unimodal distribution was not measured. Chemistry and *in situ* fluorescence data indicate that the oil was in fact dispersed adequately. This suggests operational problems with the LISST below 5 °C,



ED_001324_00000913-00023

even though it is within the operating temperature of the LISST (manufacturer manual). Additional testing of the cold water temperature limits of the sensor is recommended.

7. SLC oil was more dispersible compared to ANS for treatments with and without chemical dispersant. Bimodal distribution was observed during DOR = 1:20 and some DOR = 1:100 experiments indicating that the jet release of this particular oil into warm water produced smaller droplets than the ANS.
8. *In situ* fluorescence serves as a good proxy for oil concentration during the subsurface injection experiments. Given the experimental design, fluorescence is better suited for correlation with particle size analysis and concentration. Heterogeneity of the produced plumes and the short time scale of experiments (~12 min) led to difficulties in correlations between the plume particle size analyses and chemistry results. This is in part due to discrete samples representing 15 second averages as opposed to instantaneous measures given by fluorometers and particle size analyzers.
9. VOC air monitoring was conducted above the tank at two horizontal locations during experiments. The gas condensate exhibited the highest surface VOC concentrations, followed by ANS and SLC which exhibited similar values. Lowest concentrations were observed for IFO 120 experiments. High VOC concentrations in the air were usually accompanied by lower BTEX concentrations in the water. For all oils tested, the addition of chemical dispersants (DOR = 1:20) resulted in a reduction in VOC concentrations within air compared to experiments without dispersant near the jet release location above the tank.
10. Computer programs for jet hydrodynamics, droplet size distribution, and movement of oil droplets within the jet/plume were employed where developed models were calibrated to experimental data obtained from the oil jet experiments in the flume tank. The models VDROP-J and JETLAG were used to predict the streamwise velocity and the holdup along the centerline of the plume, where both models were in agreement, implying that VDROP-J is capable of predicting the average droplet size



ED_001324_00000913-00024

distribution in the plume. In the absence of dispersant, the model VDROP-J predicted the oil DSD measured by the LISST. In the presence of dispersant, the VDROP-J model captured the overall trend of the DSD, but was challenged in capturing the peak in droplet concentration observed for 5 microns. The observed peak is could be due to tip-streaming (when high DORs oil droplets shed filaments from their edges resulting in smaller droplets), and VDROP-J does not yet have a module for this component.

11. The Modified Weber Number approach developed by SINTEF is a recent and promising approach for predicting DSD. Previously, the method has been validated solely by a light crude oil. For this project, median droplet diameters ($d_{50}$) and the relative droplet size ($d_{50}/D$) were calculated based on the measured droplet sizes obtained from the tank experiments, and the relations between $d_{50}/D$ and modified Weber number, Reynolds number, and oil concentration were quantified. Results demonstrate that chemical dispersants tested here reduced the droplet size of ANS in both cold and warm temperatures and that dispersants tested here are more effective in reducing droplet size with ANS compared to IFO 120. A two-step Rosin-Rammler approach was found to better predict the droplet size distribution in the empirical data as indicated by higher regression coefficients.
12. Fluorescence EEMs were generated for 25 oil types under varying DOR. Oils could be separated into two categories based on dispersiblity; where light, medium and heavy oils were found in each category. Fluorescence peaks are chemistry dependent and were well correlated with Total Petroleum Hydrocarbon (TPH) and Benzene-Toluene-Ethylbenzene-Xylene (BTEX) concentrations. EEMs generated from tank and Baffled Flask Test (BFT) experiments were in agreement with respect to fluorescence peak position and Fluorescence Intensity Ratio (FIR) values as an indication of dispersion effectiveness.



ED_001324_00000913-00025

## Task A.1 Introduction & Relevance

The 2010 Deepwater Horizon (DWH) oil spill in the Gulf of Mexico has highlighted the pressing need for a better understanding of the interaction of chemical dispersants and crude oil at ocean depth. Early in the blowout release, partial emulsification of oil was observed as it rose to the surface from 1500-m depth, and surface slicks were not continuous (JAG report, 2010). A decision was made to inject dispersants directly at the release point as a possible means to increase efficiency of dispersion and to potentially reduce the amount of dispersant needed if applied at the air-sea interface (CRRC Report, 2010). Large quantities of chemical dispersant were applied via subsurface injection and traditional spraying from aircraft onto the surface oil slick (Oil Budget Calculator, 2010). At a Coastal Response Research Center (CRRC) workshop to discuss the use of subsurface chemical dispersants as an oil spill response option, recommendations to the RRT (Regional Response Teams) by spill response and research expert attendees were made on potential advantages of subsurface dispersant injection given the rate of continuous oil release and preliminary evidence of the dispersant efficacy from the DWH spill (CRRC, 2010). Potential advantages of this application included the fact that the fresh (unweathered) oil was considered well suited for dispersion, operators were able to inject the dispersant directly into the oil stream thereby maximizing dispersant/oil contact, sufficient control of DOR (Dispersant-to-Oil Ratio) could be maintained, injection may minimize the need for surface dispersant application because of reduced oil surfacing and optimized subsurface application would likely promote formation of smaller, more stable droplets of oil, enhancing biodegradation (Lee et al., 2009).

As recommended by the interagency Unified Area Command (UAC) and on-site emergency spill response coordinators, a large-scale environmental monitoring program was implemented to detect and characterize dispersed oil based on field data and plume modeling outputs. This allowed for tracking the subsurface oil plume emanating from the blowout wellhead. Droplet Size Distribution (DSD) analysis using the LISST-100X Laser *in-situ*

Scattering and Transmissometry System (Sequoia Scientific Inc. Seattle, WA) and fluorescence intensity from submersible fluorometers were used as an indication of Dispersion Effectiveness onboard the research vessels, where particle concentrations were monitored to evaluate oil dispersion (presence of small droplets ≤ 70 µm) based on previous studies for surface dispersant applications (Li et al., 2009b). Data analysis of the monitoring samples provided sound evidence of the presence of oil-bearing small particles both in surface waters and in the subsurface plume (Lee et al., 2011). Furthermore, a negative correlation between subsurface dispersant injection and low molecular weight compounds in surface waters was observed. In contrast, a strong positive correlation was observed in the subsurface. These results suggest that subsurface dispersant use may have promoted the formation of small oil droplets in the deep sea. This would likely enhance the natural weathering and dissolution of oil in the water column, thus suppressing the presence of oil organic compounds in surface waters.

Although subsurface *in situ* dispersants were used to counter a deepwater spill blowout, much uncertainty still exists in terms of the DE (Dispersion Effectiveness) with this type of application. For example, assumptions of the optimal DOR are based on empirical data mostly obtained from bench-scale experimental protocols that have been designed for testing at standard temperatures and pressures (STP), whereas conditions at a wellhead on the ocean floor or anywhere along a riser beneath the ocean surface could be significantly different. Hence, DOR for direct injection needs to be better understood. Although theoretical analyses and experiments suggest that jet breakup of the oil is insensitive to the absolute value of system hydrostatic pressure for incompressible liquid-liquid systems (Masutani and Adams, 2000), the effects of several ambient environmental factors on subsurface dispersant effectiveness, including high release pressure, high oil temperature, low water temperature, and the presence of methane and suspended sediments in the oil plume and/or surrounding water column remain to be clarified. Improved understanding on the influence of these factors on DE and the interaction of crude oil and chemical dispersant under a range of turbulent regimes at depth is required for informed decision-making for future subsurface dispersant use.



ED_001324_00000913-00027

For evaluating chemical dispersion effectiveness, standard laboratory tests are inherently limited in simulating real field operational performance due to space constraints that are critical for transport and dilution efficiency (NRC, 2005). To address the need to evaluate chemical dispersion effectiveness under more realistic oceanographic and environmental conditions, a meso-scale wave tank capable of generating breaking and regular non-breaking wave conditions is currently in operation at the Bedford Institute of Oceanography (BIO), Dartmouth, Nova Scotia. This tank facility has been used previously to characterize the tank hydrodynamics and the efficacy of several oil dispersant formulations on dispersion of different oil types, including fresh and weathered crude oils and heavy fuel oils under breaking wave conditions (Figure 1) (Lee et al., 2009; Li et al., 2008; Wickley-Olsen et al., 2007). Mathematical modeling and experimental measurements have been used in the characterization of the fluid dynamics of the flume tank. In modeling, computer fluid dynamics software packages have been used to conduct numerical simulation of the fluid field and transport phenomena of the flume tank under both non-breaking and breaking wave conditions. Experimentally, wave gauges (WG-50) have been used to monitor wave profiling throughout the flume tank under various hydrodynamic conditions. Acoustic Doppler Velocimetry (ADV) has been employed to evaluate the *in situ* instantaneous three-dimensional velocity distribution, which is used to compute the velocity gradients and energy dissipation rates ($\varepsilon$) in the tank. Using this facility, previous experiments have assessed chemical dispersant effectiveness as a function of energy dissipation rate and particle size distribution (Li et al., 2009a) and demonstrated that the effectiveness of a dispersant is strongly dependent on wave conditions, dispersant type, and oil type (Lee et al., 2009). A strong correlation has been established between dispersion effectiveness and *in-situ* droplet size distribution within the hydrodynamic regime, particularly energy dissipation rate, under a variety of non-breaking wave and breaking wave conditions (Li et al., 2008; Li et al., 2009a). The flume tank has also been operated in flow-through mode to accommodate the effects of underwater currents on dispersion and dilution of oil (Li et al., 2009b; Li et al., 2010). Experiments have also shown the reliability of fluorescence measurements as a proxy for oil concentration within physically and chemically dispersed oil (Conmy et al., 2014).



ED_001324_00000913-00028

Experimental studies have also been conducted to better understand oil-mineral aggregate (OMA) formation and the influence of mineral fines on the physical and chemical dispersion of oil (Lee et al., 2009).

This report summarizes results from a project that addresses the operational performance of subsurface injection dispersant use on high pressure releases of oil within the flume tank. Developed methods were focused on monitoring subsurface oil transport by outfitting a new high-flow flume tank at the Department of Fisheries and Oceans Canada (DFO) Bedford Institute of Oceanography (BIO) facility with a new underwater high flow rate oil injection system. In this way, the efficiency of chemical dispersion during high pressure releases within the tank can be quantitatively evaluated and compared to experiments with physical dispersion (without dispersant addition). This work has implications for field response options. To this end, the **objectives** of this work were to:

1) Refine existing equipment, technologies, and methodologies for subsurface dispersant application evaluation and monitoring by measuring dispersed oil concentration, fluorescence, and *in situ* oil droplet size distribution,
2) Evaluate effects of water temperature and dispersant type on dispersion efficacy and dispersed oil droplet size distribution of oil at high temperatures,
3) Evaluate dispersion effectiveness (DE) as a function of oil type and dispersant-to-oil ratio (DOR) for subsurface dispersant injection,
4) Assess the effect of dispersant application on the VOC concentration in air above the air-sea interface of the flume tank,
5) Integrate droplet size distribution into deepwater blowout transport/behavior models to enable prediction of the dispersed oil droplets under high flow subsurface release velocities.

During the DWH spill, small droplet ($d \leq 70\mu m$) concentrations were monitored to aid in evaluating oil dispersion efficiency. The particle size and distribution data obtained from the field monitoring program during the DWH oil spill had a significant role in supporting



ED_001324_00000913-00029

emergency oil spill response operations, fate and transport modeling, and impact assessment. Findings from this study will have significant implications in further supporting emergency response operations, spill transport models and assessments for future deepwater spills.

# Task A.2 Experimental Methods

## A.2.1 Flume Tank Description, Flow Calibration, and Operation

Oil dispersion experiments were conducted in the flow-through flume tank at BIO. The BIO flume tank is rectangular shaped with dimensions of 32 m in length x 2 m in height x 0.6 m in width, with an operational water height of 1.65 m. It was fabricated with carbon steel (3/16") and the interior and exterior surfaces are coated with a marine epoxy paint finish to reduce corrosion while operating under marine conditions. Two sets of manifolds consisting of five inflow and outflow pipes (each constructed of 4" PVC pipe and equipped with a ball valve so that the flow rate can be controlled) are fixed (1.1 m from the outer edges) at both ends of the tank (Figure 2). Two high flow centrifugal pumps (Magnatex 3575 Series, 3" suction, 4" discharge, 600 gpm, Houston, TX), one connected to the inflow manifold and the second connected to the outflow manifold provide a flow-through system used to generate horizontal water currents in the tank. A fiberglass holding tank is used to supply seawater for the system to ensure that a constant flow rate is maintained.

Seawater was obtained from the Bedford Basin, which is directly adjacent to the tank. Two smaller pumps (5 HP Pacer S Series Centrifugal Pump, 110 gpm, Lancaster, PA) were used to pull seawater (~50 cm below the surface) through a 3" suction hose from the Basin. A foot valve was installed at the end of the hose to maintain prime water in the line between fillings. Prior to entering the tank, the seawater was filtered through high-flow polypropylene bag filters (5 µm and 25 µm, Atlantic Purification, Dartmouth, NS).

During normal operations, the flume tank (31,500 L) and holding tanks (25, 000 L) were filled



ED_001324_00000913-00030

with filtered seawater. A stainless steel baffle was mounted (~0.5 m) in front of the influent manifold to control current flow. Flow gauges on the influent and effluent lines were monitored and valve adjustments were made to obtain a balanced flow rate, and so that the operational volume was maintained throughout the experiment. Water current velocities were measured at various depths and locations in the tank using an ADV (Nortek Vectrino+, Boston, MA) and the flow rates adjusted until the horizontal water current velocities (3.5 cm/s) were consistent at all measured depths.

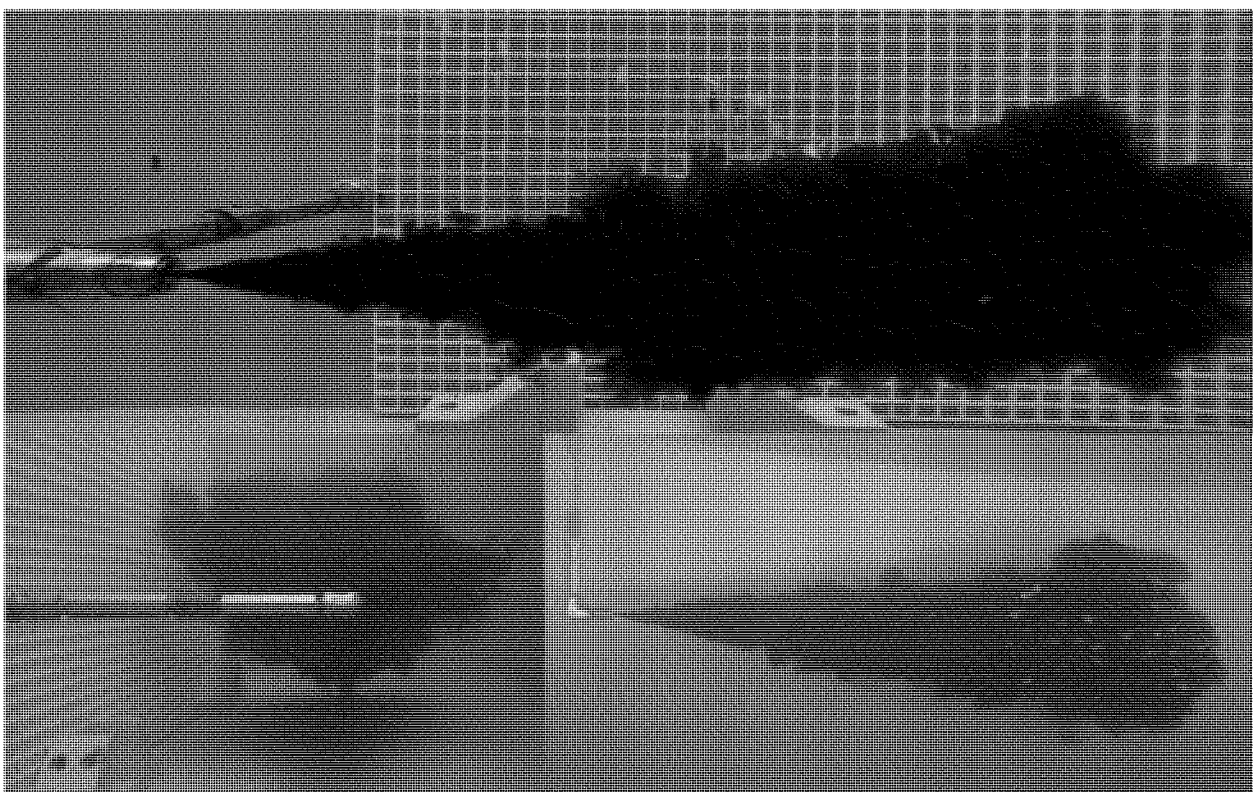

**Figure 1. Photos of subsurface oil injection at the BIO flume tank showing the formation of the subsurface oil plume. Note that the background grid size is 1.5 cm x 1.5 cm.**



ED_001324_00000913-00031

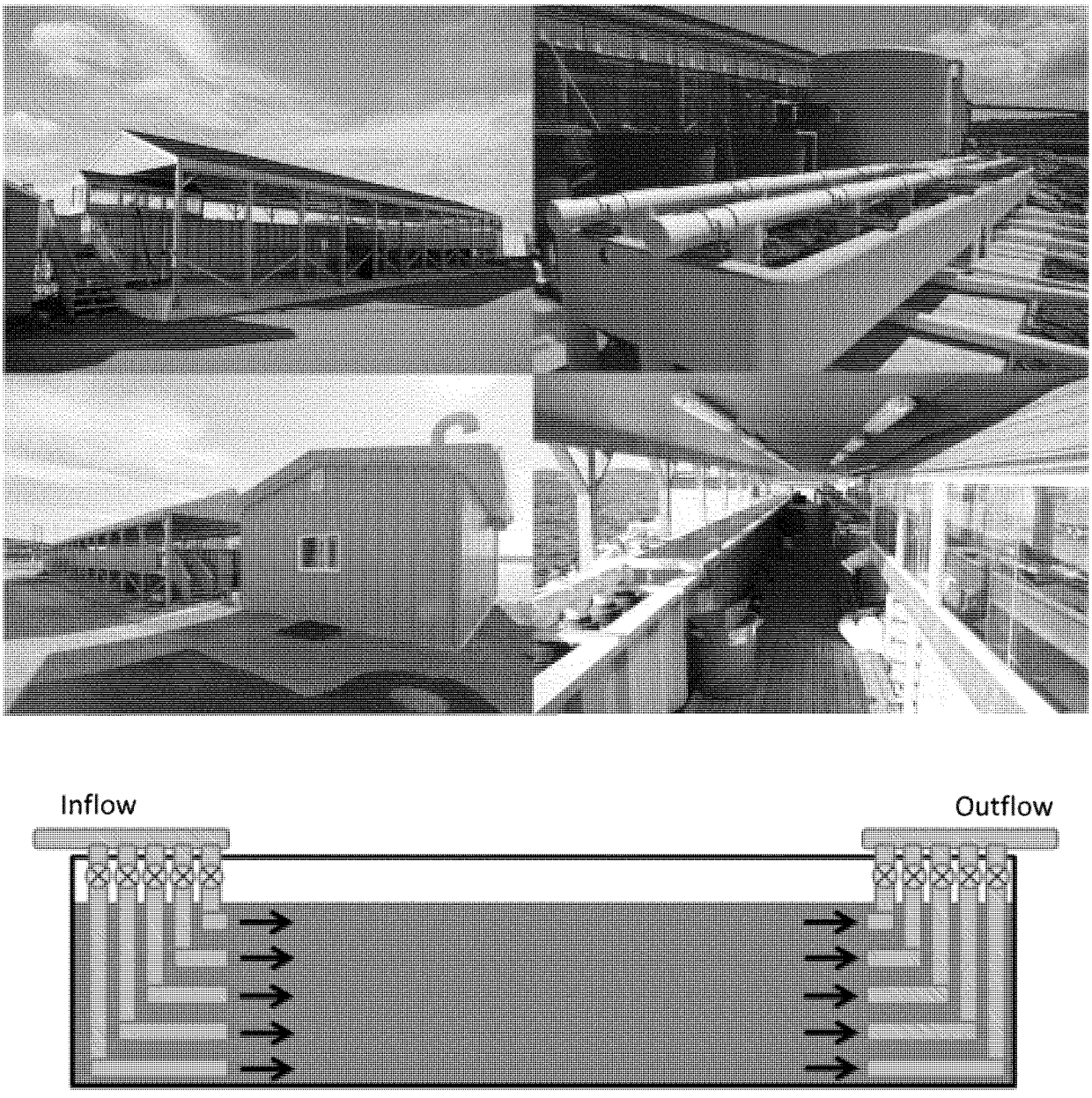


**Figure 2. Photo of the DFO BIO flume tank (top) and cross-section of the tank showing the high-flow manifolds used to generate horizontal water currents (not to scale).**



ED_001324_00000913-00032

### A.2.2 Waste Water Treatment

Oil absorbent pads (New Pig, Tipton, PA) are used to manually remove oil from the water surface. The remaining water in the tank is removed by pumping it through an effluent pipe that discharges the waste water over layers of polypropylene PomPom Oil-Mops (New Pig, Tipton, PA) that filter the waste water by removing any remaining insoluble oil prior to discharging it back into the Bedford Basin. Water samples are collected from the treated effluent and the PomPom's are changed if total petroleum hydrocarbon concentrations exceed the minimum guidelines (10 ppm) for wastewater discharge in Canada. Pads and Oil-Mops are discarded as oily waste disposal.

### A.2.3 Subsurface Oil Injection System

A custom (engineered in-house) subsurface oil injection system was used to generate dispersed oil plumes in the tank (Figure 3). Briefly, the system consists of a 2 L stainless steel pressure vessel that rests in a support rack. A series of valves and pressure gauges are connected to the pressure vessel. The assembled system is fastened to the outer wall of the tank by way of a quick connect bulkhead fitting. From the same location inside the tank, the fitting connects the outer assembly to a nozzle (2.4 mm inner diameter), which extends mid-width perpendicular to the tank wall (20 cm off the bottom and 9 m downstream from the inflow manifold) and is angled at the tip, so as to direct the discharge plume downstream. Given the shallow nature of the tank, this release setup enabled using the horizontal length of the tank to capture the plume movement.

For each experiment, oil or oil/dispersant premix is added to the pressure vessel (Figure 4A) in order to reduce the influence of any additional confounding factor of mixing effectiveness. Inside the pressure vessel is a copper coil that is connected to a water bath to permit the oil to be heated to 80°C, which takes 30 minutes. Although lower than the estimated oil temperature during the DWH release (~130°C), this is the highest temperature permissible in the pressure vessel to avoid risk of explosion. The vessel is then pressurized (40 psi for ANS, SLC and Condensate; 60 psi for IFO 120) with compressed Nitrogen. A ball valve connected to



ED_001324_00000913-00033

the pressure vessel is manually opened and oil is released through the subsurface nozzle into the flume tank (Figure 4B). The release time and total volume (determined by mass) of oil injected are recorded. After each experiment, the entire subsurface injector system was cleaned by flushing repeatedly with toluene, acetone and fresh water until no visible oil remained prior to next experiment.

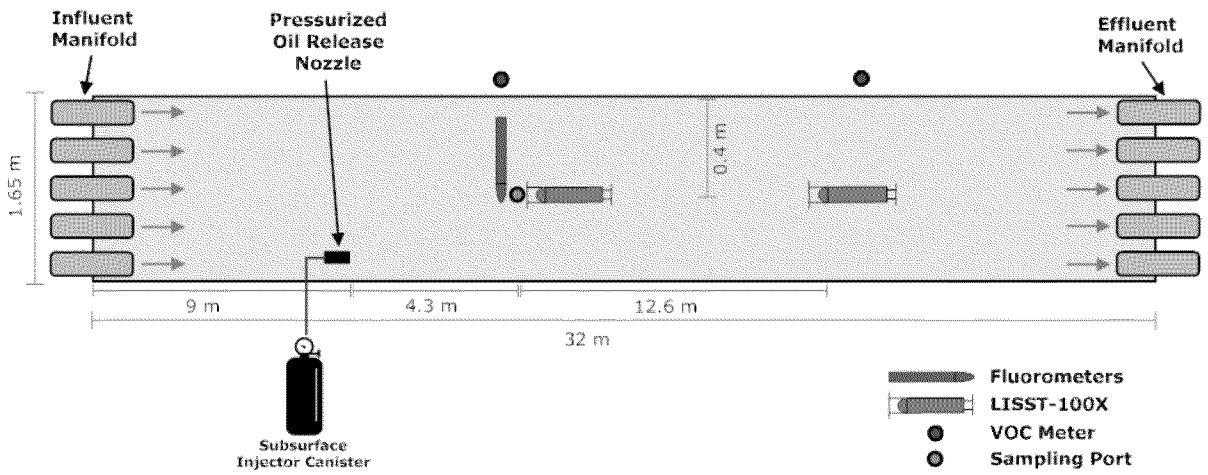


**Figure 3. Schematic diagram showing the location of the subsurface injector and *in situ* instrumentation submerged within the tank.**

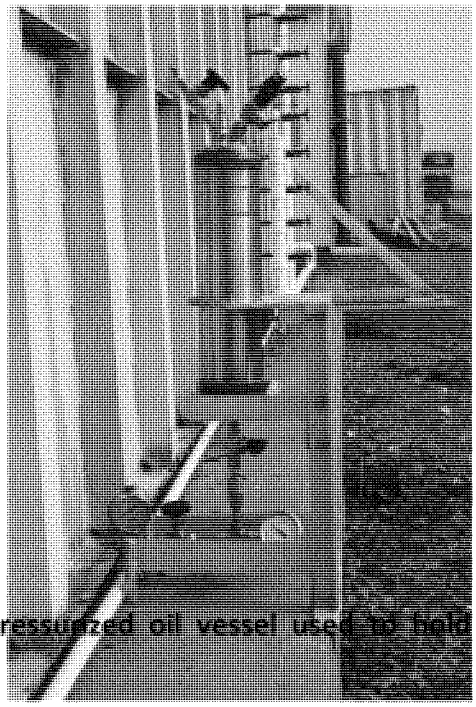

**Figure 4A. Photo of the pressurized oil vessel used to hold the oil for the subsurface release.**



ED_001324_00000913-00035

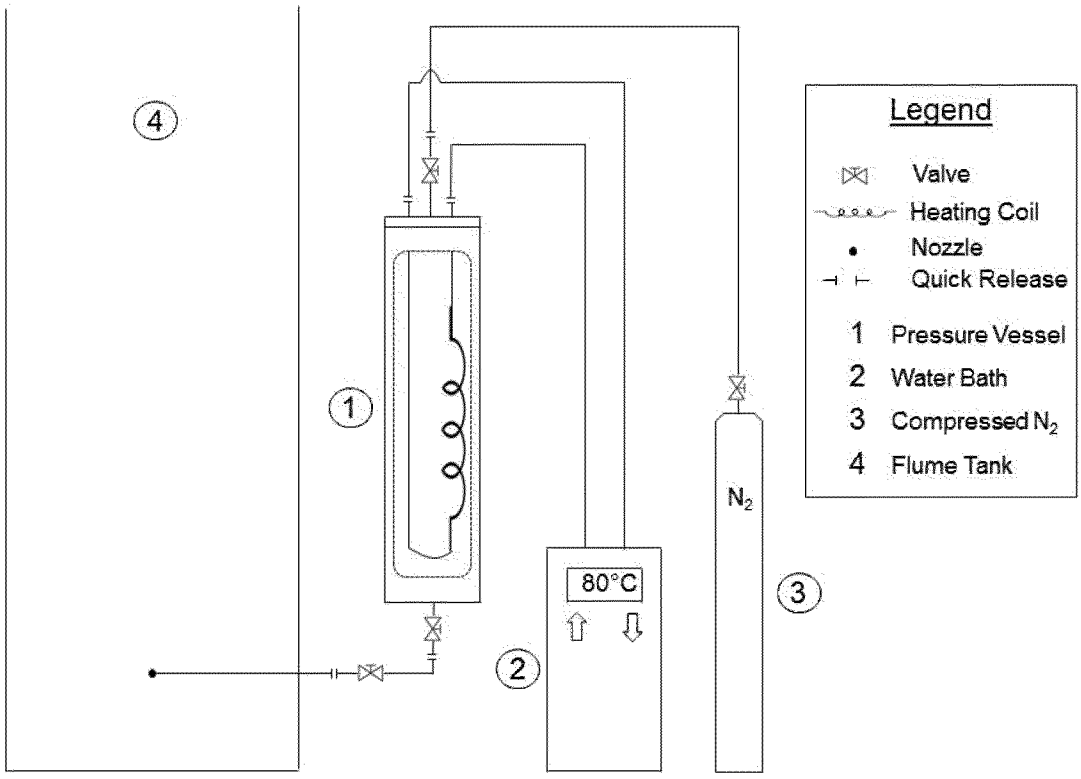


**Figure 4B. Schematic diagram of the pressurized oil vessel for subsurface oil release system in the flume tank.**



ED_001324_00000913-00036

### A.2.4 Submersible Sensor Deployment

*Fluorescence*- A total of six hydrocarbon fluorometers that are used worldwide during oil spill response were evaluated during this study (Table 1). The fluorometers were mounted on an aluminum frame located 4.3 m from the oil release point with their UV windows and at a depth of 0.4 m. The instruments were attached to a crosspiece support bar, so that they were all located the same distance downstream from the oil release point with the UV window pointed directly down at the bottom of the tank.

**Table 1. List of hydrocarbon fluorometers used in this study. QSDE and PAH represent quinine sulfate dihydrate and petroleum aromatic hydrocarbons, respectively.**

| Instrument | Excitation/Emission wavelengths and Units |
|---|---|
| Chelsea UV AQUAtracka (Refined) | 239/360nm, µg/L Perylene |
| Chelsea UV AQUAtracka (Crude) | 239/440nm, µg/L Carbazole |
| Turner Designs Cyclops (Fine Oil) | 254/350nm, Volts |
| Turner Designs Cyclops (Crude Oil) | 365/510nm, Volts |
| Sea Bird – WET Labs ECO-FLU | 370/460nm, µg/L QSDE |
| GmbH Trios | 254/360nm, µg/L PAH |

Several different data acquisition systems were used to control and collect data from the *in situ* fluorometers. The GmBH Trios was operated by the manufacturer's power supply and data acquisition system using the MSDA_DE software, which provided a real-time display of the signal intensity in calibrated units of µg/L PAH. The sampling rate was set at one reading every five seconds and raw data was saved as a comma delimited (.csv) file. The two Turner instruments were connected to a Databank Handheld Datalogger (Turner Designs, Sunnyvale, CA), which powered both instruments and recorded data at a sampling rate of 1 reading



ED_001324_00000913-00037

every 3 seconds. The datalogger auto-gain feature cycles through settings of 1x, 10x, and 100x depending on the signal intensity. Raw data was recorded as signal intensity in mV and was offloaded from the datalogger via USB connection to a laptop and saved as a text (.txt) file. The Sea Bird - WET Labs and Chelsea instruments were connected to a custom-built power supply and data acquisition system (Pace Scientific XR5-SE datalogger; Mooresville, NC), which collected data from the instruments at a sampling rate of one reading per second. The signal was recorded internally on the datalogger and then sent via wireless connection to a laptop in real-time display. Raw data was recorded as signal intensity in mV and offloaded as a .txt file.

*Particle Size Analysis* - Oil droplet size was measured *in situ* using two LISST-100X particle size analyzers (Sequoia Scientific, Seattle, WA). The instrument measures particle sizes in the range of 2.5 – 500 µm in 32 logarithmically spaced bins. The first LISST was located immediately after the aluminum frame supporting the fluorometer package at a distance of 5.1 m from the oil release point and the second LISST was located at 16.9 m from the oil release point and both at a depth of 0.4 m (Figure 3). Placement was informed by the numerical modeling team of this project to maximize oil droplet detection without saturating the instrument. Both instruments were connected via a 20 m cable to laptops running the LISST-SOP data acquisition software (version 5). Prior to the start of each experiment, a background scatter file of the seawater quality in the tank was generated and used later to subtract from the final experimental data file. The instruments were operated in real-time mode with a sample acquisition rate of one measurement every three seconds.

*Supplemental Measures* - Weather conditions (air temperature, wind speed, wind direction, humidity, rainfall) for all experiments were recorded using a Vantage VUE Weather station (Davis Instruments, Hayward, CA). Water temperature and salinity were measured using a YSI handheld probe. Underwater video of oil droplets and the transport of the plume were captured using a GoPro Hero4 digital camera, as well as a Sony RX100 III digital camera with underwater housing.



ED_001324_00000913-00038

### A.2.5 VOC Air Monitoring

Surface volatile organic compound (VOC) concentrations were monitored using handheld ToxiRAE Pro PID portable gas detectors (RAE Systems, San Jose, CA). Two detectors were used for each experiment, and they were positioned 0.4 m above the water surface at distances of 5.1 and 16.9 m from the oil release point (Figure 3). The detectors were calibrated using a certified 25 ppm benzene calibration gas (AirLiquide, Dartmouth, NS) according to the manufacturer's recommended procedure. Instrument drift was checked periodically against the calibration gas and recalibrated if necessary. During the experiments, the handheld meters were set to datalogging mode, which recorded VOC concentrations as ppm of benzene every three seconds. This data was offloaded and saved as a .txt file for processing.

### A.2.6 Discrete Water Sample Collection

Water samples for chemical analysis were collected at various time points throughout the experiments (Table 2). Three ¼" stainless steel tubes were attached to the aluminum fluorometer frame, so that the end of the tube was located at the same depth as the instrument UV windows (0.4 m). These were attached via peroxide cured silicon tubing (Cole Parmer, Vernon Hills, IL) to a Masterflex L/S multi-channel digital peristaltic pump (Cole Parmer, Vernon Hills, IL) which flowed to a three-way valve system. When the valve was set to bypass mode, the water in the lines was continuously primed and flowing, so it could instantaneously be switched to sample mode to allow for sample collection. The pump flow rate was set to approximately 120 mL/min, and all tubing was flushed with clean seawater for 5 minutes prior to the start of any experiment. Tubing was replaced on an as needed basis. Water samples from the effluent manifolds were also collected through a 1" sampling valve at the exit of effluent pipe prior to it entering the treatment system.

### A.2.7 Oil and Dispersant Samples

Four different hydrocarbon products were tested in this study to cover a range of viscosity



ED_001324_00000913-00039

and physico-chemical characteristics: Two crude oils, a fuel oil, and a gas condensate. Samples of Alaska North Slope crude oil (ANS) and Intermediate Fuel Oil 120 (IFO 120) were obtained from BSEE. Sweet Louisiana Crude was obtained from NOAA. Gas Condensate was obtained from Exxon Mobil and originated from the Sable Offshore Energy Project. Physical properties of the samples (Table 3) were measured using an Anton Paar SVM 3000 Stabinger Viscometer (Anton Paar, Saint Laurent, QC). Supplies of chemical dispersants (Corexit 9500 and Finasol OSR 52) were purchased from the manufacturers.

**Table 2. Water sample collection strategy for the core and complimentary experiments. TPH and BTEX represent Total Petroleum Hydrocarbons and Benzene-Toluene-Ethylbenzene-Xylene, respectively.**

| Time (min) | TPH (Tank) | TPH (Effluent) | BTEX (Tank) | BTEX (Effluent) | Fluorometry (Tank) | Fluorometry (Effluent) |
|---|---|---|---|---|---|---|
| Background | X | | X | | X | |
| T = 0 | X | X | X | | | |
| T = 0.5 | X | | | | | |
| T = 1.0 | X | | X | | X | |
| T = 1.5 | X | | | | | |
| T = 2.0 | X | X | X | | X | |
| T = 2.5 | X | | | | | |
| T = 3.0 | X | | X | | | |
| T = 3.5 | X | | | | | |
| T = 4.0 | X | X | X | X | | |
| T = 4.5 | X | | | | | |
| T = 5.0 | X | | X | X | | |
| T = 6.0 | X | X | X | X | | |
| T = 8.0 | X | X | X | X | | X |
| T = 10.0 | X | X | X | X | | |
| T = 12.0 | X | X | X | X | | |
| Total # Samples/Expt | 16 | 7 | 11 | 5 | 3 | 1 |
| Total # of Samples | TPH – 1725 | | | | | |



ED_001324_00000913-00040

| | |
|---|---|
| Analyzed | BTEX – 1200<br>Fluorometry – 300 |

**Table 3. Physical and chemical property measurements of the oils used in this study.**

| Oil Type | Measurement Temperature (°C) | Density (g/mL) | Kinematic Viscosity (centistokes) | BTEX Content (%) |
|---|---|---|---|---|
| Alaska North Slope (ANS) | 50 | 0.8529 | 6.4 | 2.3 |
| | 40 | 0.8600 | 8.3 | |
| | 25 | 0.8704 | 13.1 | |
| | 15 | 0.8777 | 18.9 | |
| Intermediate Fuel Oil (IFO 120) | 50 | 0.9345 | 134.0 | 0.2 |
| | 40 | 0.9411 | 240.3 | |
| | 25 | 0.9515 | 781.4 | |
| | 15 | 0.9587 | 2481.5 | |
| Gas Condensate (CND) | 50 | 0.7247 | 0.4 | 13.4 |
| | 15 | 0.7466 | 0.5 | |
| Sweet Louisiana Crude (SLC) | 50 | 0.8219 | 3.2 | 2.4 |
| | 40 | 0.8291 | 4.0 | |
| | 25 | 0.8733 | 5.8 | |
| | 15 | 0.8473 | 8.2 | |

### A.2.8 Experimental Design – Core and Complimentary Experiments

Both the flume tank and holding tanks were filled with filtered seawater as described above. Seawater temperature and salinity were recorded using a handheld probe (YSI Incorporated,



ED_001324_00000913-00041

Yellow Springs, OH). After the flume tank was filled, the *in situ* instrumentations including the fluorometers, LISSTs, and VOC meters were positioned in desired locations as indicated previously. The subsurface oil release system was filled with oil or oil/dispersant premix, which was heated to operating temperature. The water supply lines leading to the high flow pumps were primed and the inflow and outflow pumps were started. The system was run in recirculation mode for 10 minutes to allow current flow to stabilize in the flume tank. At a set time point prior to oil injection (5 minutes), data-logging on all instruments was started and background seawater samples were collected. After the oil was injected into the tank, the real-time readout of the fluorometer signal was monitored. Once the first spike in signal intensity was observed (usually after 2 minutes based on the fluorometer signal readout), a stopwatch was started and the first chemistry samples were collected. At this point the high flow system was switched from recirculation mode to flow through, which diverted the water flow into the effluent treatment system instead of returning it to the holding tank. The experiment ran for 12 minutes, at which point the high flow pumps were turned off and the instrument data acquisition was stopped. The tank was cleaned and drained as described above. Tank and instruments were cleaned using Big Orange Degreaser (Zep Superior Solutions, Atlanta, GA), to prevent any potential contamination between experiments. Instrument windows were cleaned using disposable alcohol wipes (Bausch and Lomb, Vaughan, ON). Water samples were returned to the lab and stored at 4°C.

### A.2.9 Submersible Sensor Calibration Experiments

The calibration experimental setup was similar to the core and complimentary experiments, except that the oil was added in a step-wise (tank dilution series measurements) fashion to the flume tank as shown in Table 4. Calibration experiments were conducted in such a way to create a series of known concentrations of dispersed oil in the flume tank. Predetermined amounts of oil and dispersant (Corexit 9500) premix were added to the tank (Alaska North Slope, ANS, crude was used at a DOR of 1:20) using the subsurface injector.

The flume tank was operated in recirculation mode and oil/dispersant premix injections



ED_001324_00000913-00042

occurred every 45 minutes, which provided a sufficient time for the dispersed oil concentrations to stabilize in the tank (previous testing of this system showed that hydrocarbon concentrations in the tank are homogenous after 45 minutes of recirculation). The recirculation of water in the tank provided sufficient mixing energy to allow small droplets generated by the subsurface injector to remain dispersed in the water column. *In situ* instrumentation was located at the same locations as all other experiments. Water samples were collected at 45 minute time intervals after each oil addition.

Upon reaching homogeneity in the tank (i.e. 45 minutes after each oil addition), the average fluorometric intensity signal collected over a 4 minute time period was calculated. Fluorometers were calibrated to manufacturer suggested units using factors provided. Triplicate water sample analysis results for Total Petroleum Hydrocarbons (TPH) and Benzene-Toluene-Ethylbenzene-Xylene (BTEX) were averaged that correspond with the same time points. Fluorescence and chemistry averages were regressed to generate calibration curves of TPH and BTEX vs signal intensity for oil additions ranging from 1 to 18 ppm. Higher variability at low concentrations resulted in the exclusion of some data points in the regression calculation.

### A.2.10 Submersible Fluorometer and LISST Data Processing

Raw LISST data files were processed using a statistically-based quality control script written using the R statistical package (www.r-project.org). In summary, this script identifies and removes "Over Range" samples (defined as 0 µL/L across all particle size bins) and outliers. Outliers are defined as any reading that is greater than the moving mean (5 data points before and after the targeted time point) of the dataset multiplied by four times the standard deviation (over the same interval as the moving mean). Due to the potential for one or more extreme outliers to skew both the moving mean and standard deviation calculations for points around them, this outlier detection routine is run iteratively, excluding previously flagged points, until no more outliers are detected. Once these QC steps have been performed, the script calculates a number of parameters from the data such as Total Particle Concentration (TPC), Volume Mean Diameter (VMD), and Particle Size Concentration (PSC). It



ED_001324_00000913-00043

then goes on to detect the plume curve (if present) and time-normalizes the data based on that location. Data are presented as Droplet Size Distribution (DSD). Plots presented include data 2 minutes before and 8 minutes after the start of the plume curve. Data from the Downstream LISST were normalized so that the plume began at t = 5 min in order to visually convey that the plume was detected in the tank roughly 3 min after detection by the LISST further upstream near point of injection release.

Similar to the LISST data, a script was used to detect outliers in data collected from the *in situ* fluorometers. Curve detection was then performed and the data was time-normalized to include 2 minutes of data before, and 8 minutes of data after the start of the plume curve. The baseline of the plume curve was then calculated using data points observed in the first minute preceding the start of the curve and this baseline was subtracted from the data. Finally, factory calibration factors were applied to the data values for each instrument before plotting.

**Table 4. Step-wise sensor calibration experiment parameters.**

| Oil Addition # | Mass of Oil Added for each Addition (g) | Cumulative Oil Concentration in Tank (mg/L) |
|---|---|---|
| 1 | 9.45 | 0.3 |
| 2 | 9.45 | 0.6 |
| 3 | 12.6 | 1 |
| 4 | 63 | 3 |
| 5 | 94.5 | 6 |
| 6 | 189 | 12 |
| 7 | 189 | 18 |



ED_001324_00000913-00044

### A.2.11 Analytical Chemistry Analysis

*Total Petroleum Hydrocarbon (TPH) Analysis* - The method used for extraction and processing of TPH samples was developed by DFO in-house (Cole et al., 2007; King et al., 2015). Water samples were collected in pre-weighed 125 mL amber glass bottles and filled to approximately 90 mL. Sample bottles were weighed and a mass difference was used to determine the total volume of the collected water sample. The samples were immediately stored at 4°C until ready for further processing. Within 24 hrs of collection, 10.0 mL of dichloromethane (DCM) was added to each sample. The samples were shaken by hand for 30 seconds, and then placed on a Wheaton R2P roller (Wheaton, Millville, NJ) set at 9 rpm. After 18 hours on the roller, a Pasteur pipette was used to transfer the DCM solvent layer into a pre-weighed 15 mL graduated centrifuge tube. The solvent was then evaporated under a gentle stream of nitrogen using an N-Evap (Organomation, Berlin, MA) and topped up with DCM to a final volume of 1.00 mL. The solvent extract was transferred into an auto-sampler vial and stored at -20°C for GC-FID analysis.

Sample extracts (1 µL) were injected using an Agilent 7683 auto-sampler into an Agilent 7890B GC, using splitless injection set to oven track mode (2°C higher than the oven temperature program). The column used for separations was a Supelco MDN-5s 30 m × 250 µm × 0.25 µm (length × i.d. × film thickness). Hydrogen was used as a carrier gas with a flow rate of 3.0 mL/min. The GC oven is programmed to an initial oven temperature of 35°C, held for 2 min, followed by an increase to 320°C at 20°C/min, and held at 320°C for 10 min, with a total run time of 26.25 min. The GC flame ionization detector (FID) was operated at 320°C with the hydrogen flow set at 30 mL/min and the air flow set at 400 mL/min. An eight point calibration was generated using standards prepared from the appropriate crude oil stock that



ED_001324_00000913-00045

was used to generate the TPH samples (e.g. ANS, IFO 120, SLC or Gas Condensate). Peak quantification was performed using relative response factors. Routinely the method of extraction was tested for efficiency by a spike and recovery study. Typically, a mean percent recovery of >90% was calculated from filtered seawater spiked with crude oil. Lab and field blanks were incorporated in the method.

*BTEX Analysis* - EPA Method 8240 (purge and trap) was modified by running a gas chromatograph/mass spectrometer in selected ion monitoring mode to include ethylbenzene (Cole et al., 2007). To summarize, water samples for BTEX (benzene, toluene, ethylbenzene and [m,p & o] xylene) analysis were collected in 40 mL purge and trap vials. The vials were spiked with 40 µL of 6N HCl to serve as a preservative, so that they can be stored at 4°C for up to 14 days.

The purge and trap system was a Teledyne Tekmar Stratum PTC purge and trap concentrator equipped with a Tenax/silica gel/charcoal trap. The auto-sampler was a Teledyne Tekmar Aquatek 70-vial unit. The auto-sampler transferred a 5 mL aliquot of sample into the purge and trap chamber, where it was purged with helium for 11 minutes. During this process, the volatiles were trapped on the Tenax trap and then desorbed at 225°C for 2 min. The desorbed gases enter a heated transfer line connected to the Agilent 6890 GC injector and subsequently proceed to the GC column (Supelco MDN-5s 30 m × 250 µm × 0.25 µm length × i.d. × film thickness).

The GC oven was programmed at an initial oven temperature of 50°C, held for 8 min, followed by an increase to 280°C at 40ºC/min, and held at 280°C for 2 min, for a total run time of 18 min. The gases exiting the GC column were detected by an Agilent 5973 mass selective detector (MS) used in selective ion mode (SIM) monitoring for six ions: 77, 78, 91, 92, 105 and 106 amu. BTEX standards were prepared in 40 mL purge and trap vials. Samples and standards were analyzed using this method, along with sample blanks and duplicate samples.



ED_001324_00000913-00046

### A.2.12 Numerical Modeling Methods

Refer to Appendices G and H for numerical modeling components.

# TASK A.3 RESULTS

The overarching objective for this project was to evaluate the operational performance of the subsurface injection of dispersants during deepwater blowouts. Presented here are the results from a series of flume tank subsurface injection experiments where dispersion effectiveness was evaluated via response monitoring tools (fluorescence and particle size analyzers), discrete water sample chemistry analysis and VOC air monitors. The logs for all experiments conducted can be found in Appendix A. Corresponding chemistry results for each experiment are tabulated in Appendix B.

## A.3.1 ANS Dispersion Effectiveness

Injection experiments were conducted using ANS crude oil, chemically dispersed with Corexit and Finasol. Regardless of warm ($\geq$ 11°C) or cold (5.4 – 10.7°C) water temperatures, the addition of the two tested dispersant lowers the VMD of ANS and shifts the DSD to smaller droplets within the plume. An example of this trend is shown in Figures 5 and 6. Note that LISST histogram plots have constrained Y-axes; thus lines that extend slightly above the top of the plot area represent values that were truncated. Histograms in these figures correspond to time points at the leading edge of the plume (~2-3 min from oil release). Contour plot X-axis represents experiment elapsed time. Plots for triplicate experiments for each treatment are shown in Appendices C and D. All plots represent data from the LISST positioned closest to the jet release (denoted as Jet Release LISST throughout the document) and in close proximity to the submersible fluorometers. Histograms represent the particle concentration for a given size class (Y axes). Contour plots represent the 10 minute time series of the plume, where colored contours represent



ED_001324_00000913-00047

the particle concentration (normalized to max value for comparison purposes), Y axes represent the droplet sizes in µm and X axes are time in minutes. Time is elapsed time since oil injection into the tank. These contours allow for ascertaining how the DSD shifts over the duration of the release. A second LISST positioned further downstream of release (denoted as Downstream LISST throughout the document) allows for comparing the evolution of the plume in space and time since release of the plume. For warm temperature experiments, there is a slight decrease in VMD for DOR = 1:200 and 1:100 (Corexit) compared to the no-dispersant treatment (DOR = 0), in this case ~130 µm down to ~80 µm (exact numbers are within text of the figures). A large shift in DSD is observed for the DOR 1:20 treatment, where VMD is ~ 10 µm. The cold water treatments exhibit this same trend, where VMD is ~ 10 µm for the DOR = 1:20 treatment (Figure 6). *In situ* submersible fluorescence from multiple fluorometers was recorded during experiments. Example time series for each dispersant and temperature treatment are shown in Figure 7 and illustrate the impact of dispersant at DOR = 1:20 in the plume. With DORs of 0, 1:200 and 1:100, the plumes tend to exhibit a spike in fluorescence shortly after release (within 2 min), and then a sharp decline in signal that is brought to extinction by 4 minutes. For DOR = 1:20, however, the signal remains elevated and with variability for up to 6 minutes. This indicates that more oil is remaining submerged in the plume for a longer time period. Time series fluorescence plots for triplicate experiments for each treatment are shown in Appendix E.

The Downstream LISST positioned further from the jet release and the fluorometers serves as an indication of plume evolution through the tank. Plots of the Downstream LISST DSD and VMD for all dispersant treatments for warm and cold water experiments are shown in Figures 8 and 9, respectively. Comparing these to the LISST results near the jet release illustrates the decrease in Total Particle Concentration (TPC; represents the maximum concentration for the entire plume) as the plume disperses through the tank (note the change of Y axis scale). Also evident is a shift to smaller particles for all DOR treatments as the plume moves through the tank. Where the decrease in TPC suggests plume dilution in



ED_001324_00000913-00048

the tank, the DSD shift to smaller particles suggests that within each experiment larger droplets were removed from the plume within 6 minutes of the oil release, most likely rising to the surface of the tank.

Warm water experiments conducted with ANS and Finasol OSR 52 dispersant also yield a shift in DSD towards smaller VMD for DOR = 1:20 (Figure 10). However the shift is smaller than that observed with Corexit 9500 (Figure 5), with lowest VMD on the order of ~50-60 µm. DOR = 1:200 and 1:100 treatments exhibited spikes in fluorescence signal that taper off within 3 minutes of oil release (Figure 11). Fluorescence for DOR = 1:20 Finasol OSR 52 treatments exhibited a decrease in intensity at ~4 minutes which is faster than that for treatments with Corexit 9500. The Downstream LISST exhibited a similar shift in DSD and TPC that was observed with Corexit 9500 treatments (Figures 12 and 13).

Water temperatures for experiments ranged between 5.4 – 20.8 °C. In general there was no clear trend on the influence of temperature on DSD, VMD fluorescence intensity, or oil concentrations for the time series for DOR = 0, 1:200 or 1:100 treatments. This suggests that water temperature has little effect on the dispersibility of ANS (80 °C oil temperature) when released as a jet with little or no exposure to chemical dispersant (in this case the pre-mixing process prior to release). In contrast, DOR = 1:20 experiments showed a decrease in total particle concentration (TPC) with decreasing temperature even though no effect was observed on DSD for the two temperatures. Figure 14 shows three examples of this effect, where TPC values for each DOR = 1:20 experiment increase as a function of temperature (Figure 15). It is important to note that for all treatments using ANS, the experiment at the lowest temperature (SubANS-10R; 5.4 °C) exhibited anomalous dispersion compared to the other DOR = 1:200 treatments (Appendices C and D). Because this occurred in only one experiment out of 33 experiments with ANS, it is difficult to ascribe a cause for this other than an improper jet release of oil.



ED_001324_00000913-00049

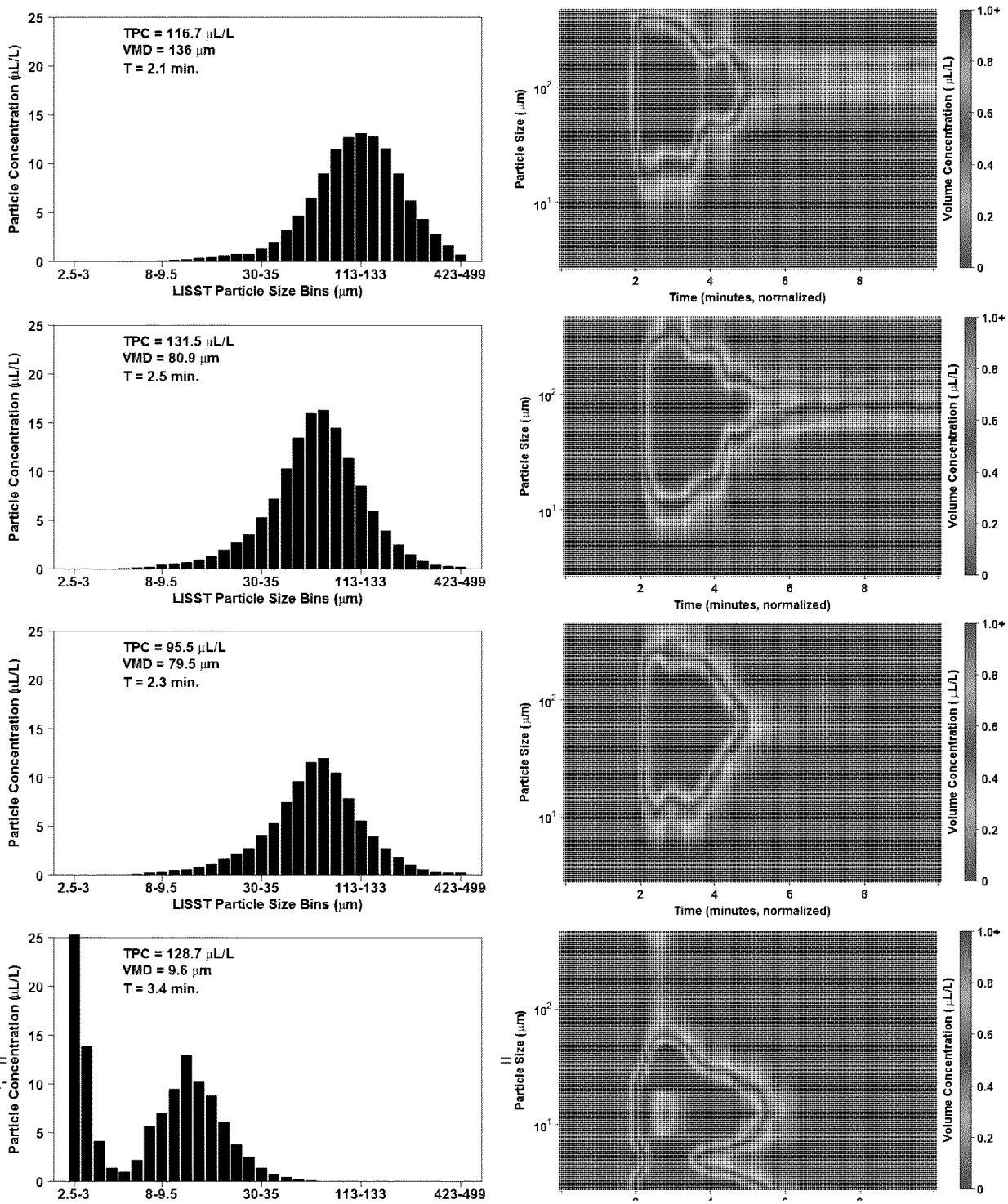
TPC = 116.7 µL/L
VMD = 136 µm
T = 2.1 min.
TPC = 131.5 µL/L
VMD = 80.9 µm
T = 2.5 min.
TPC = 95.5 µL/L
VMD = 79.5 µm
T = 2.3 min.
TPC = 128.7 µL/L
VMD = 9.6 µm
T = 3.4 min.
Particle Concentration (µL/L)
LISST Particle Size Bins (µm)
2.5-3
8-9.5
30-35
113-133
423-499
Particle Size (µm)
Time (minutes, normalized)
Volume Concentration (µL/L)

Fig
siz
bo
t

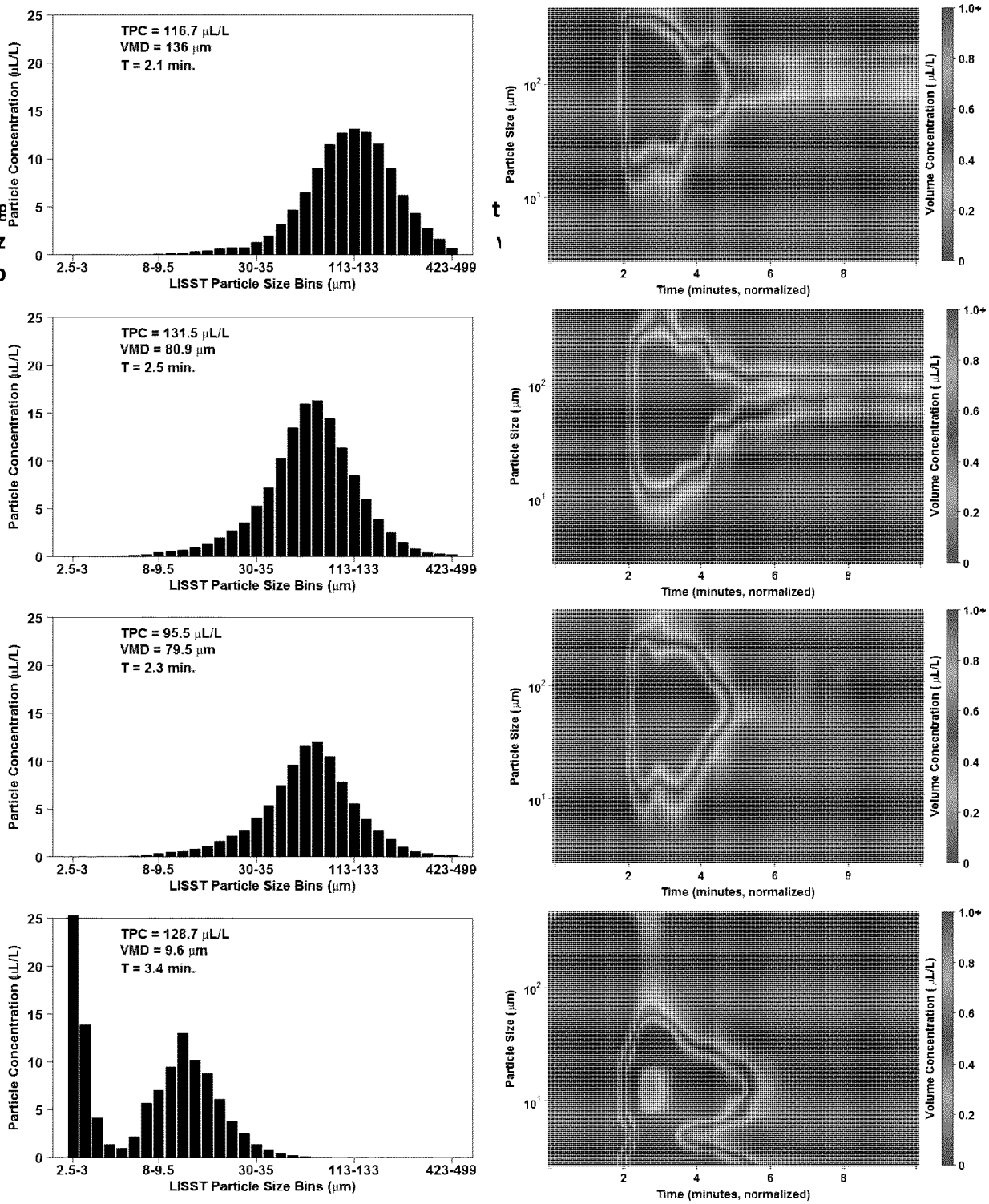
TPC = 116.7 µL/L
VMD = 136 µm
T = 2.1 min.
TPC = 131.5 µL/L
VMD = 80.9 µm
T = 2.5 min.
TPC = 95.5 µL/L
VMD = 79.5 µm
T = 2.3 min.
TPC = 128.7 µL/L
VMD = 9.6 µm
T = 3.4 min.
Particle Concentration (µL/L)
LISST Particle Size Bins (µm)
2.5-3
8-9.5
30-35
113-133
423-499
Particle Size (µm)
Time (minutes, normalized)
Volume Concentration ( µL/L)

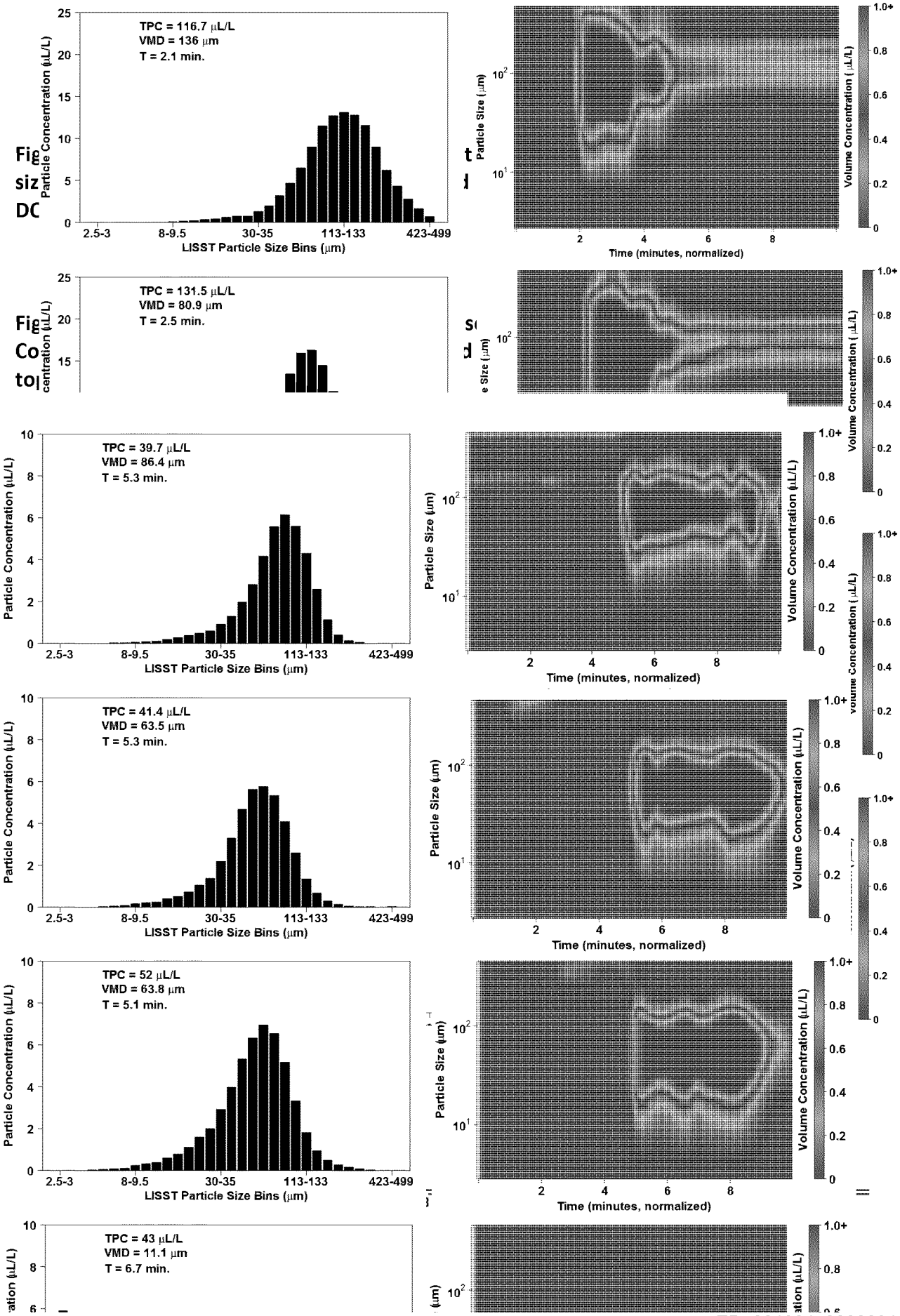
TPC = 116.7 µL/L
VMD = 136 µm
T = 2.1 min.
TPC = 131.5 µL/L
VMD = 80.9 µm
T = 2.5 min.
TPC = 39.7 µL/L
VMD = 86.4 µm
T = 5.3 min.
TPC = 41.4 µL/L
VMD = 63.5 µm
T = 5.3 min.
TPC = 52 µL/L
VMD = 63.8 µm
T = 5.1 min.
TPC = 43 µL/L
VMD = 11.1 µm
T = 6.7 min.
Particle Concentration (µL/L)
LISST Particle Size Bins (µm)
2.5-3
8-9.5
30-35
113-133
423-499
Particle Size (µm)
Time (minutes, normalized)
Volume Concentration (µL/L)

**Figure 8. Downstream LISST DSD and VMD (left panels) and time series of concentration and particle size (right panels) for ANS and Corexit 9500 warm water treatments. From top to bottom, DOR = 0, 1:200, 1:100, 1:20.**

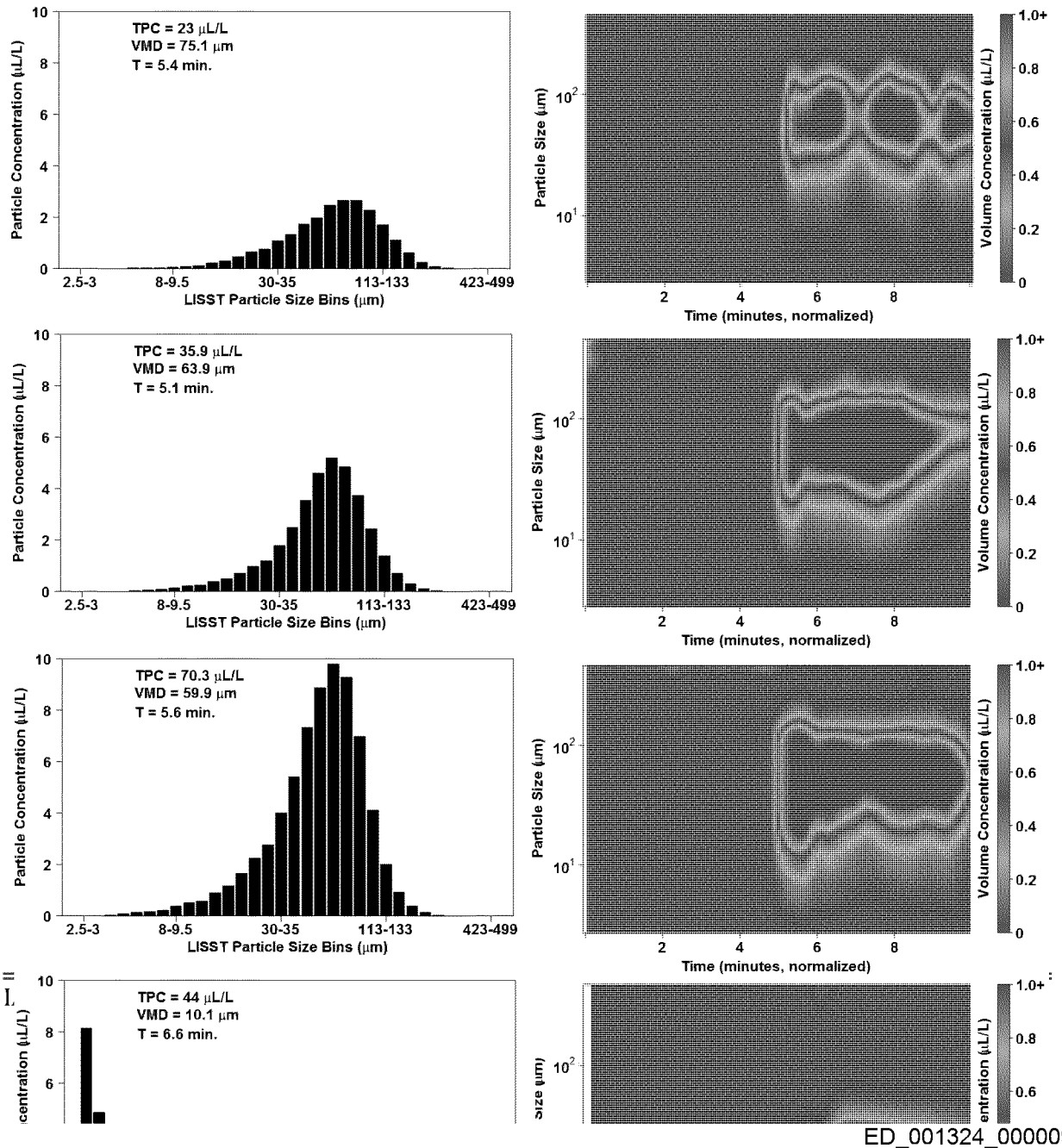

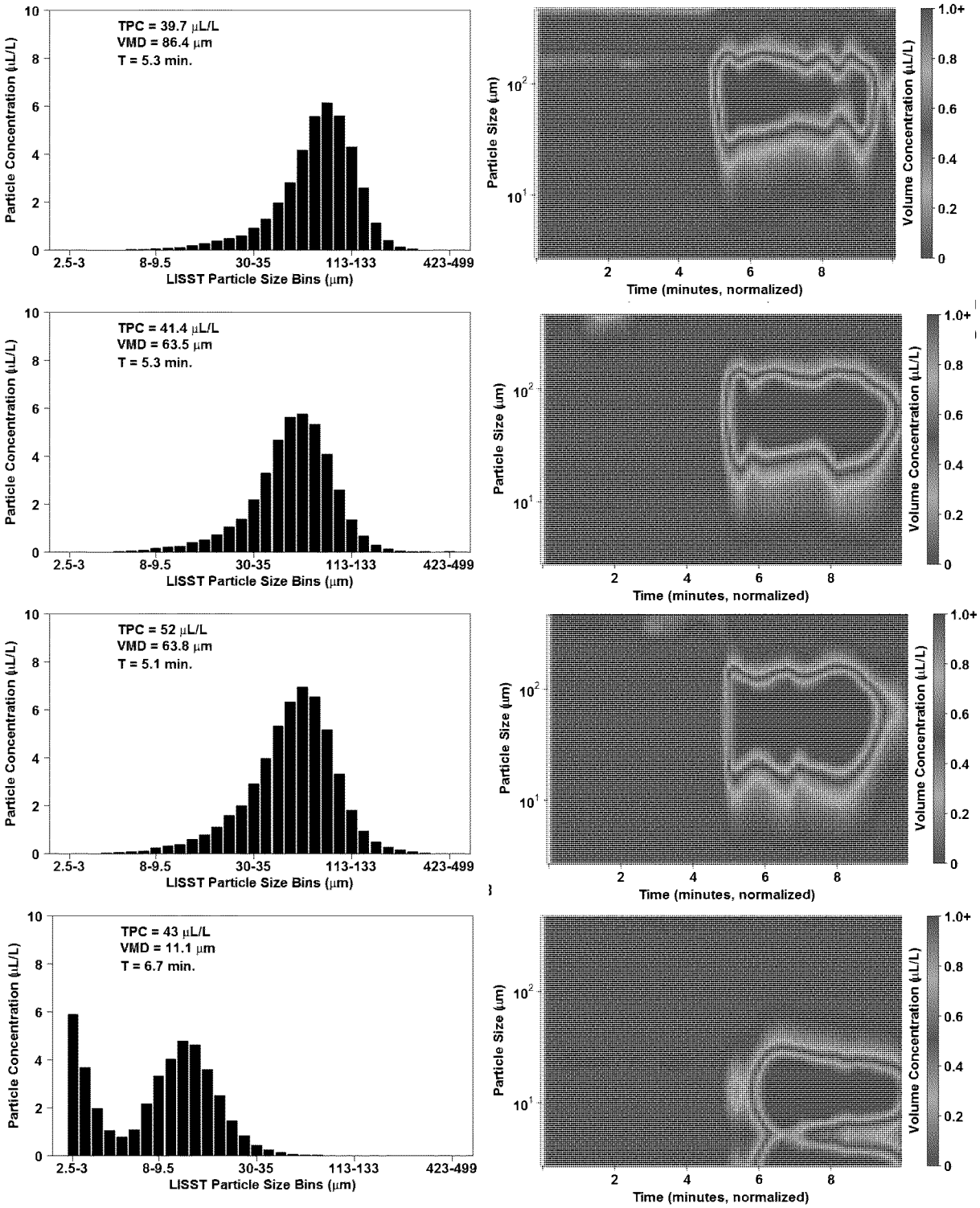
TPC = 39.7 µL/L
VMD = 86.4 µm
T = 5.3 min.
TPC = 41.4 µL/L
VMD = 63.5 µm
T = 5.3 min.
TPC = 52 µL/L
VMD = 63.8 µm
T = 5.1 min.
TPC = 43 µL/L
VMD = 11.1 µm
T = 6.7 min.
Particle Concentration (µL/L)
LISST Particle Size Bins (µm)
2.5-3
8-9.5
30-35
113-133
423-499
Particle Size (µm)
Time (minutes, normalized)
Volume Concentration (µL/L)

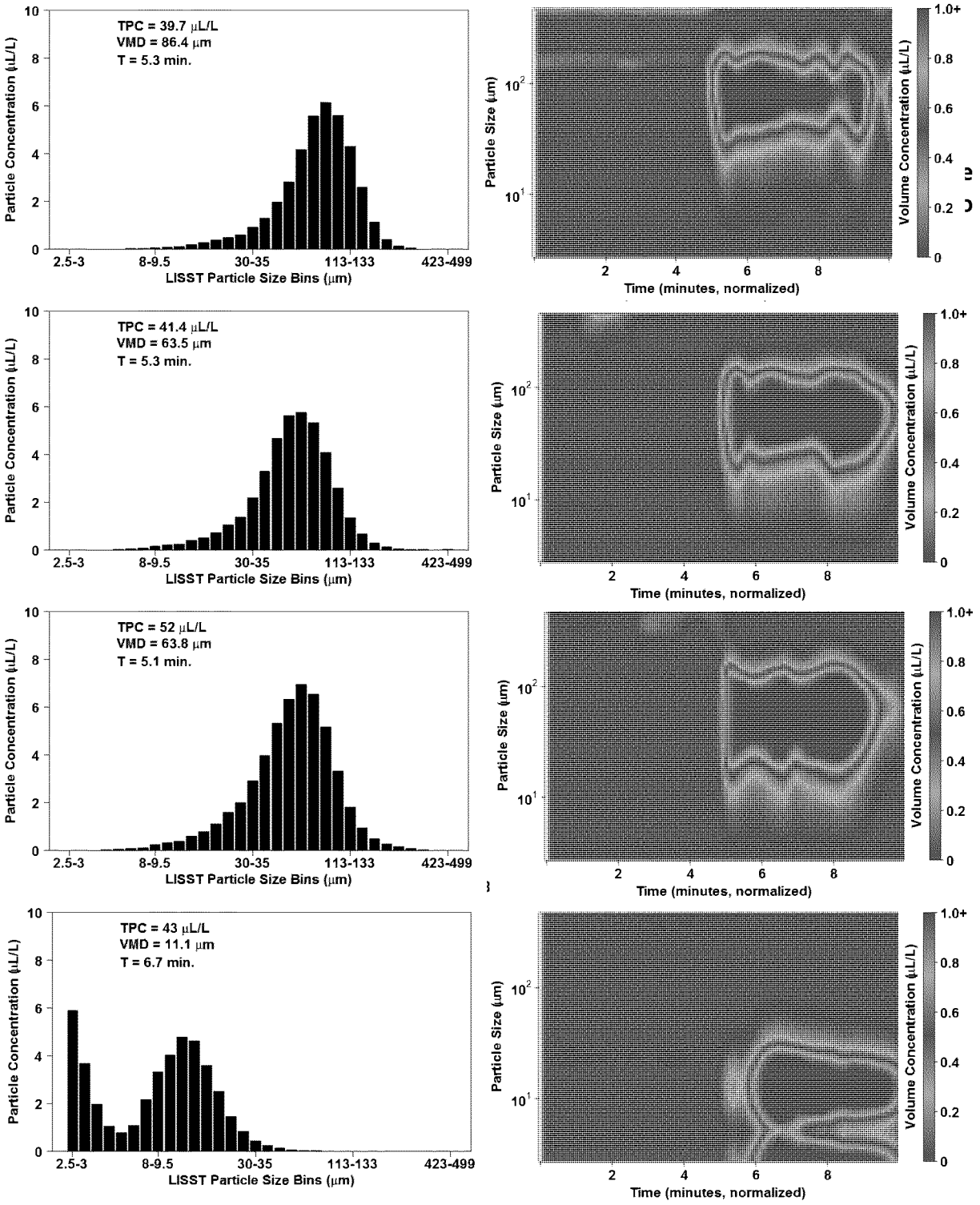
TPC = 39.7 µL/L
VMD = 86.4 µm
T = 5.3 min.
TPC = 41.4 µL/L
VMD = 63.5 µm
T = 5.3 min.
TPC = 52 µL/L
VMD = 63.8 µm
T = 5.1 min.
TPC = 43 µL/L
VMD = 11.1 µm
T = 6.7 min.
Particle Concentration (µL/L)
LISST Particle Size Bins (µm)
2.5-3
8-9.5
30-35
113-133
423-499
Particle Size (µm)
Time (minutes, normalized)
Volume Concentration (µL/L)

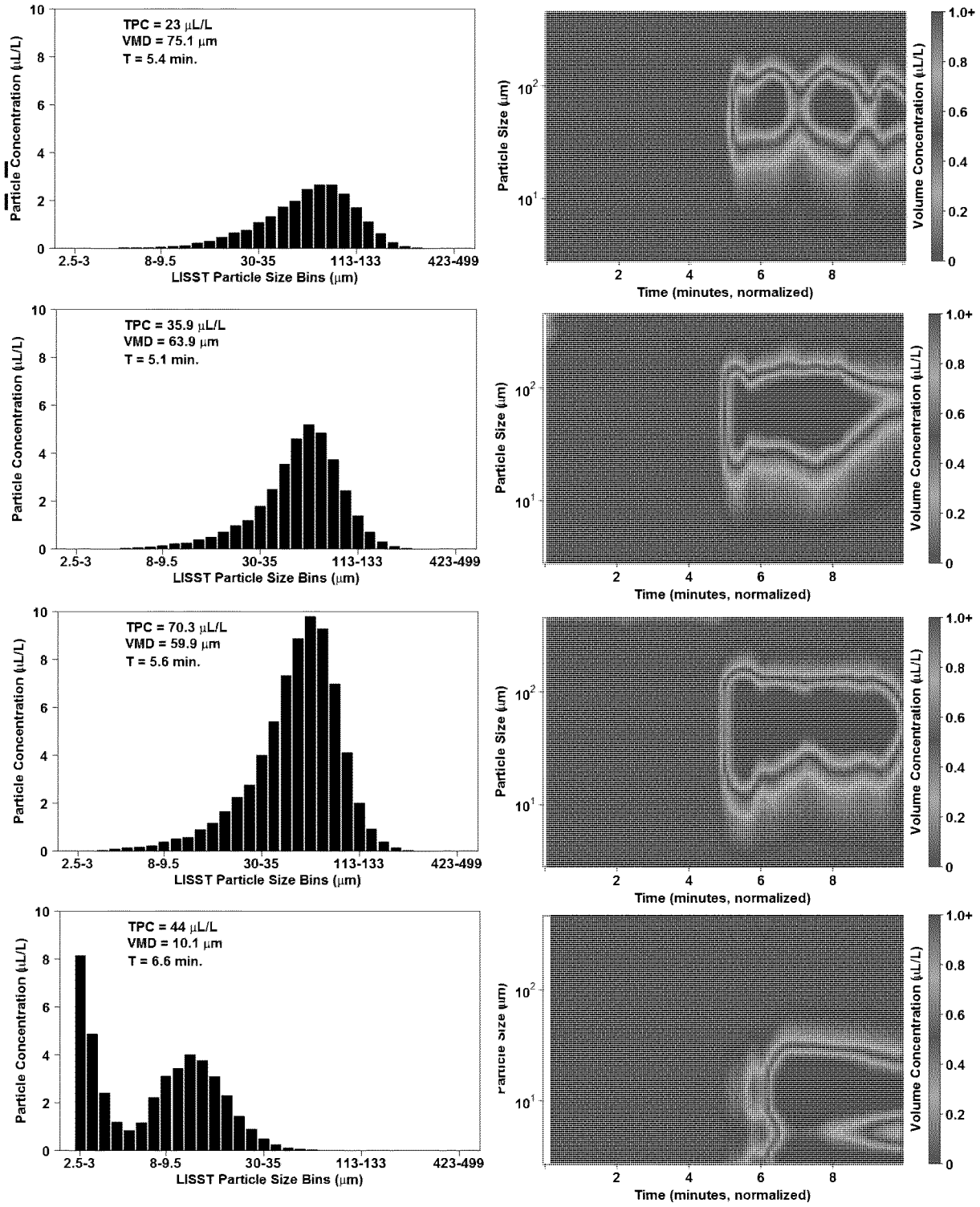
TPC = 23 µL/L
VMD = 75.1 µm
T = 5.4 min.
TPC = 35.9 µL/L
VMD = 63.9 µm
T = 5.1 min.
TPC = 70.3 µL/L
VMD = 59.9 µm
T = 5.6 min.
TPC = 44 µL/L
VMD = 10.1 µm
T = 6.6 min.
Particle Concentration (µL/L)
LISST Particle Size Bins (µm)
2.5-3
8-9.5
30-35
113-133
423-499
Particle Size (µm)
Time (minutes, normalized)
Volume Concentration (µL/L)

**Figure 12. Downstream LISST DSD and VMD (left panels) and time series of concentration and particle size (right panels) for ANS and Finasol OSR 52 warm water treatments. From top to bottom, DOR = 1:200, 1:100, 1:20. Refer back to Figure 6 for ANS DOR = 0.**



ED_001324_00000913-00057

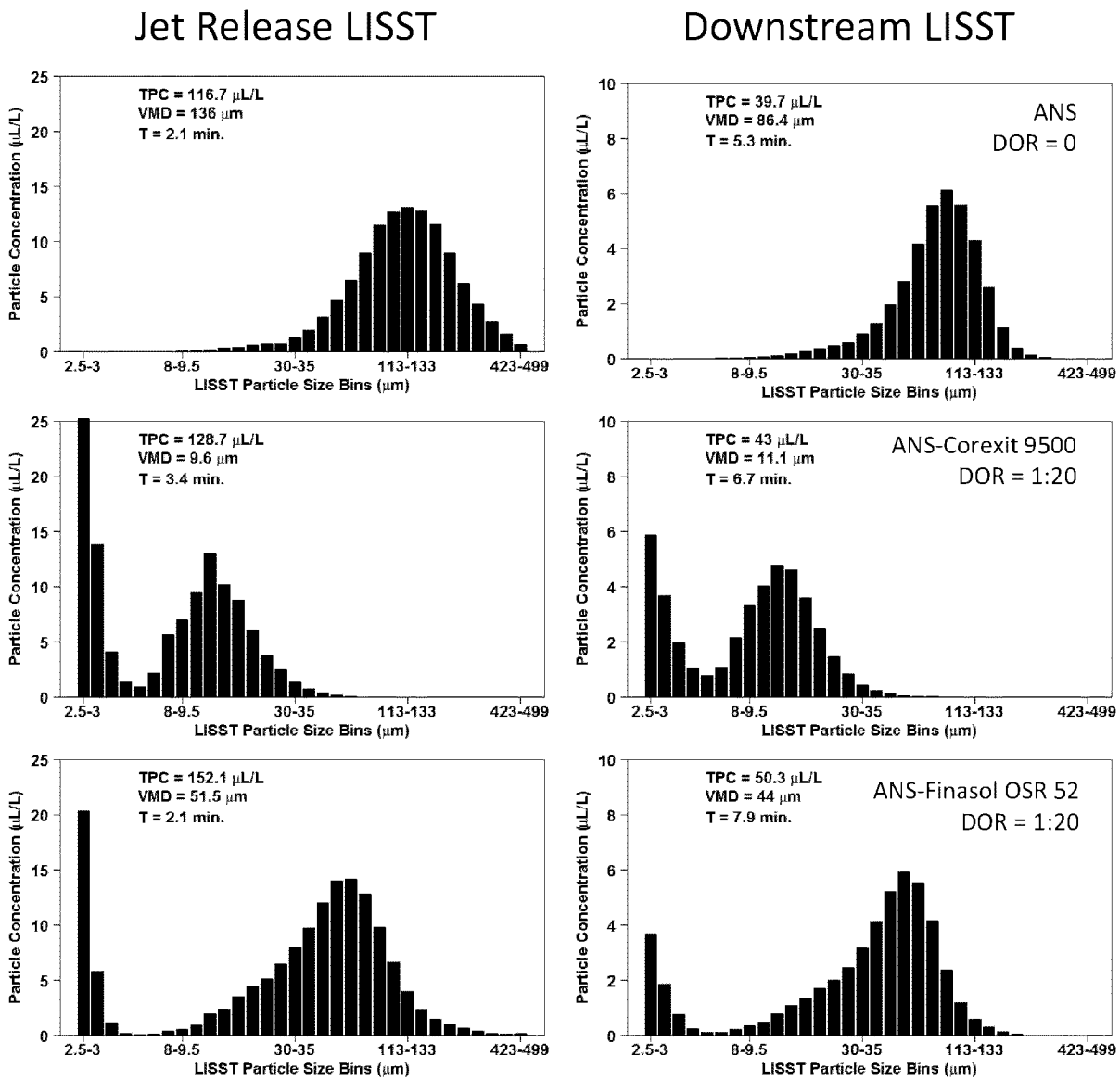


**Figure 13. LISST DSD with TPC for ANS with Corexit 9500 and Finasol OSR 52 warm water treatments. DOR = 0 (top panel); DOR = 1:20 experiments are middle and bottom panels.**



ED_001324_00000913-00058

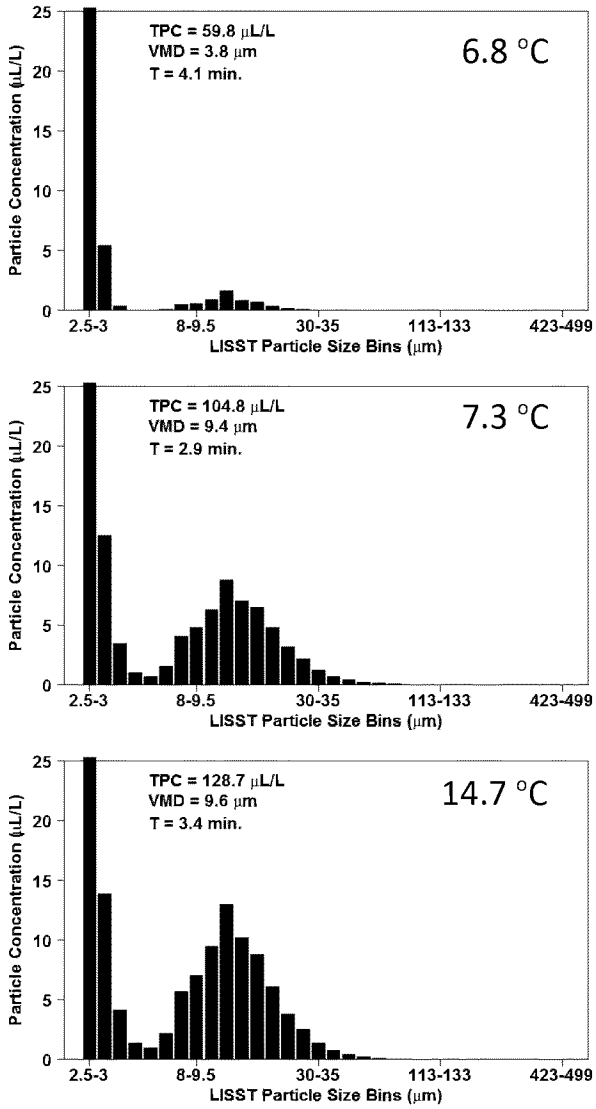


**Figure 14. LISST DSD with TPC (Total Particle Concentration) for DOR = 1:20 experiments of ANS and Corexit 9500 treatments. Water temperatures increase from top to bottom panels.**



ED_001324_00000913-00059

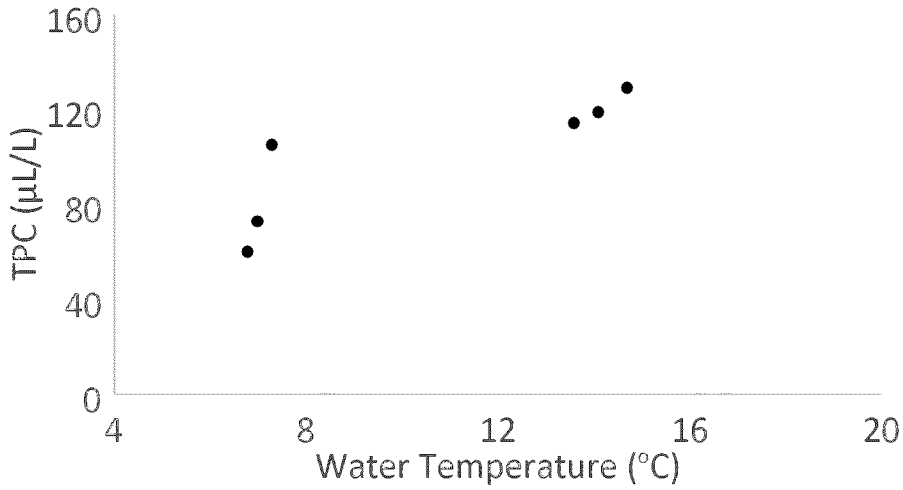


**Figure 15. LISST TPC (Total Particle Concentration) for DOR = 1:20 experiments of ANS and Corexit 9500 treatments as a function of water temperature.**



ED_001324_00000913-00060

### A.3.2 IFO 120 Dispersion Effectiveness

Injection experiments were conducted using Intermediate Fuel Oil (IFO 120), chemically dispersed with Corexit 9500 and Finasol OSR 52. For warm water experiments, temperatures ranged between 13.5 – 16 °C for treatments with Corexit 9500 and between 17.5 – 20.3 °C for treatments with Finasol OSR 52. In the DOR = 0, 1:200 and 1:100 treatments using Corexit 9500, VMD typically remained > 200 µm (Figure 16). VMD values were smaller for DOR = 1:20 treatments (~66-120 µm), indicating a shift in DSD, but to a lesser extent than the shift observed for ANS experiments. Fluorescence data exhibited scatter and noise in the signal for all but the DOR = 1:20 treatments (Appendix E). A similar trend in DSD, VMD and fluorescence signal was observed for IFO 120 exposed to Finasol OSR 52 at warm temperatures (Figure 17), where DOR = 1:200, 1:100 and 1:20 exhibited VMD values of 376.5, 209.5 and 125.8 µm, respectively. Unlike experiments with ANS, which is less viscous and dense, IFO 120 exposed to dispersant tended to result in larger oil droplets for a given amount of dispersant added. Comparing the results of IFO 120 with the two dispersants is challenging because no triplicate experiments were conducted for Finasol OSR 52 treatments, as the latter treatments were add-on experiments and not central to the project. In general, from the data collected, Finasol OSR 52 yielded higher VMD for a given DOR compared to Corexit 9500 at warm temperatures. As with ANS, the Downstream LISST measured a decrease in TPC and shift to smaller droplet sizes as the plume moved through the tank for all treatments, but to a lesser extent with DOR = 1:20 (Figures 18, 19 and 20).

For cold water experiments using IFO 120 exposed to Corexit 9500, temperatures ranged between (4.9 – 7.5 °C). At these colder temperatures a shift in DSD and VMD was not as apparent (Figure 21). For DOR = 0, 1:200 and 1:100 VMD typically remained > 223 µm but was as high as 344 µm. The DOR = 1:20 treatment exhibited VMD of 178-327 µm, suggesting that this oil was not well dispersed at cold temperatures. Fluorescence time series data were noisy for all experiments except the DOR = 1:20 (Appendix E). The Downstream LISST recorded extremely low particle concentrations, further suggesting poor dispersion (Figure 22). During the IFO 120 cold water treatments, one experiment resulted



ED_001324_00000913-00061

in an anomalous DSD histogram that was similar to an anomalous one observed during one of the ANS experiments (Figure 23). In both cases, the experiments were conducted at the coldest temperatures during the course of this study (4.9 and 5 °C). Suspected as a possible cause may be the LISST instrument itself. The manual reports that the lower operating temperature for the LISTT-100X is -10 °C. However, the data suggests that our particular unit may have experienced some complications at low temperatures. This is supported by the fact that the fluorescence signal and chemistry data for these experiments indicate no anomalies. Further testing would be needed to confirm the effect of low temperatures on particle size analysis results using our instrument to rule out any potential issues with operating at temperatures between 5 and -10 °C.

One aspect to note with the IFO 120 cold water experiments is that a few of the treatments were conducted at water temperatures of ~12 °C, which overlaps with the temperatures of the warm water group. This was the result of erratic weather patterns that at times were difficult to work around. Thus, when interpreting the temperature data, caution must be exercised for these particular experiments (refer to Appendix A for temperature log), and for the interpretation in this section, they were excluded as they do not represent cold conditions.



ED_001324_00000913-00062

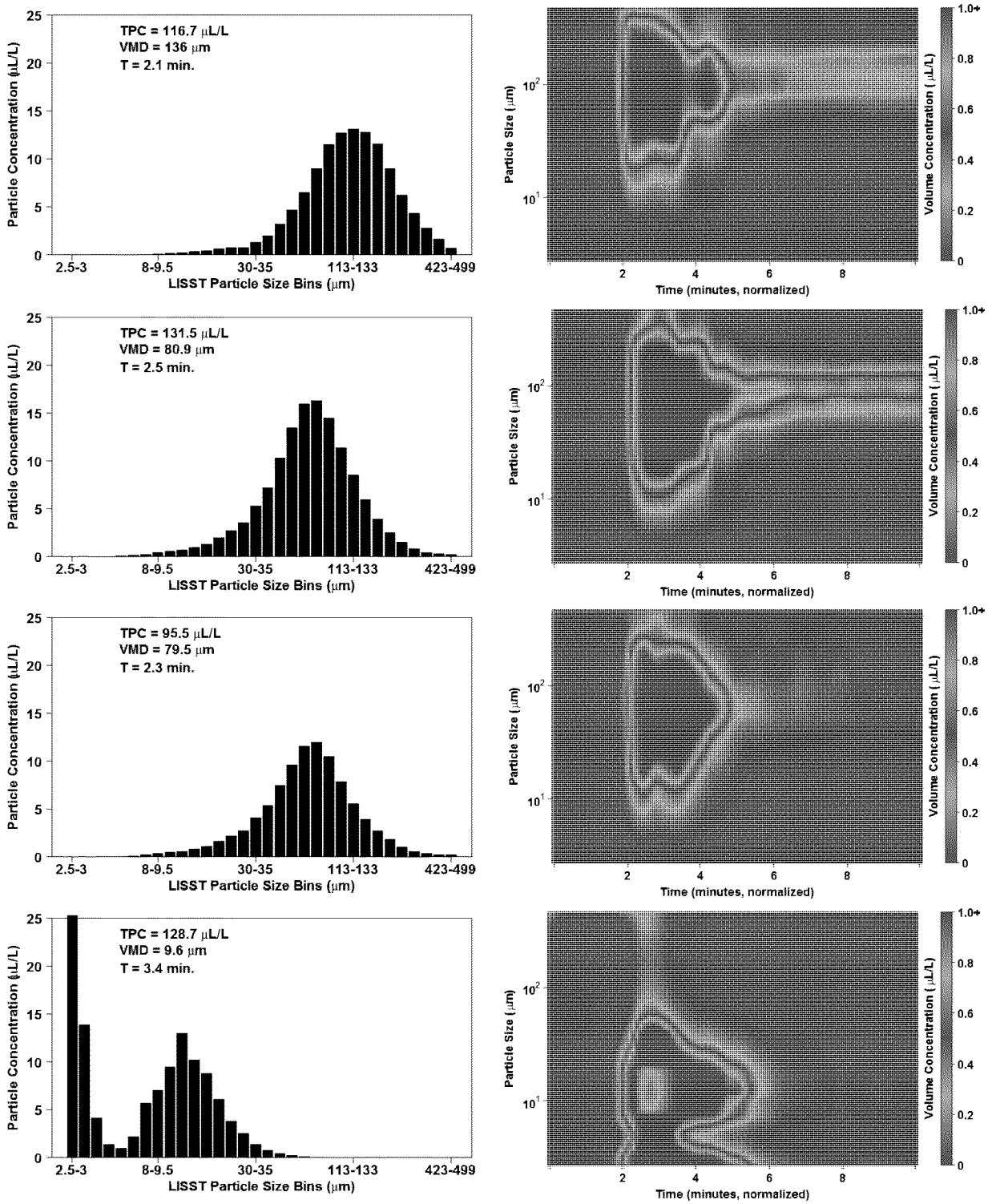


**Figure 16. LISST DSD and VMD (left panels) and time series of concentration and particle size (right panels) for IFO 120 and Corexit 9500 warm water treatments. From top to bottom, DOR = 0, 1:200, 1:100, 1:20.**

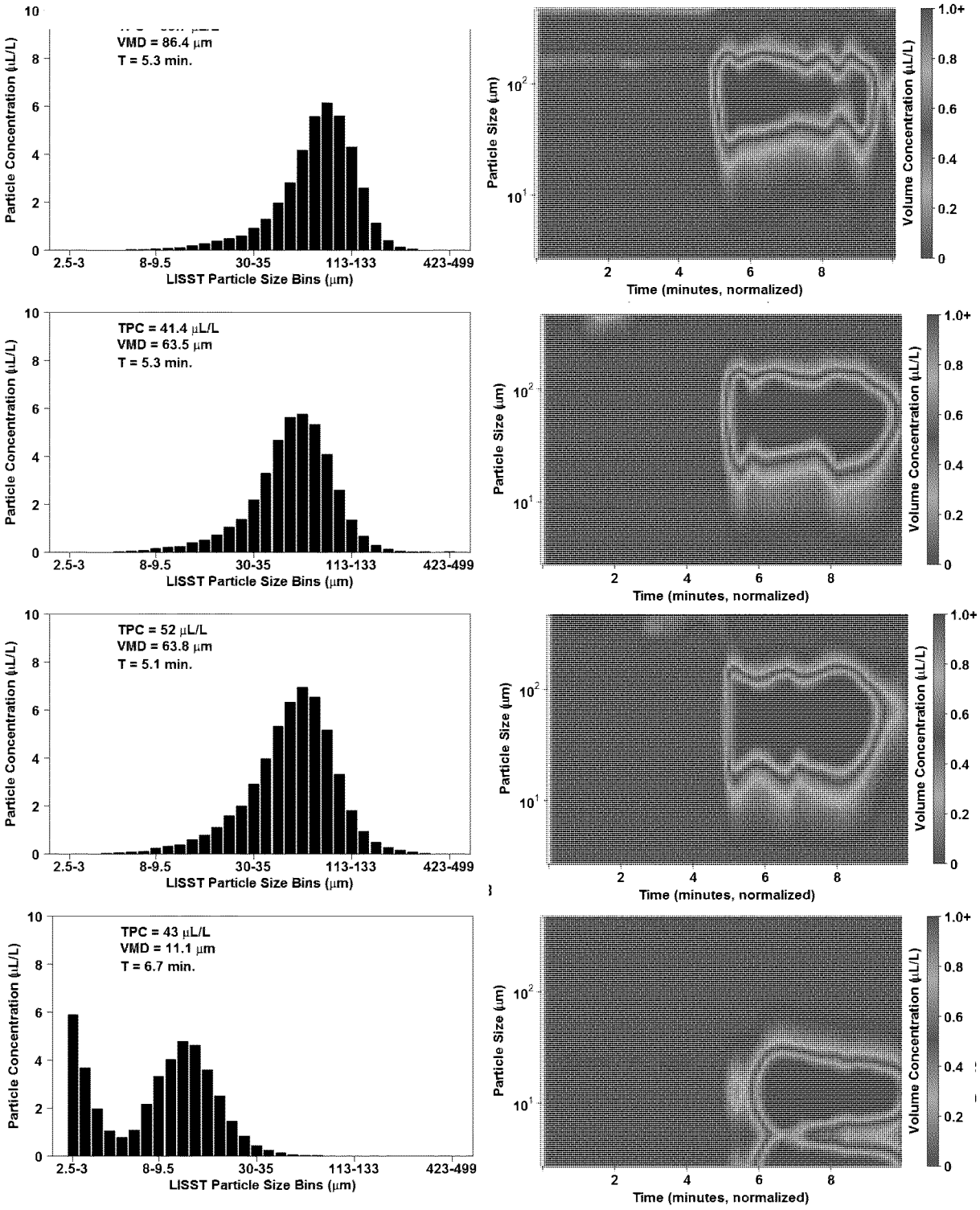
VMD = 86.4 µm
T = 5.3 min.
TPC = 41.4 µL/L
VMD = 63.5 µm
T = 5.3 min.
TPC = 52 µL/L
VMD = 63.8 µm
T = 5.1 min.
TPC = 43 µL/L
VMD = 11.1 µm
T = 6.7 min.
Particle Concentration (µL/L)
LISST Particle Size Bins (µm)
2.5-3
8-9.5
30-35
113-133
423-499
Particle Size (µm)
Time (minutes, normalized)
Volume Concentration (µL/L)

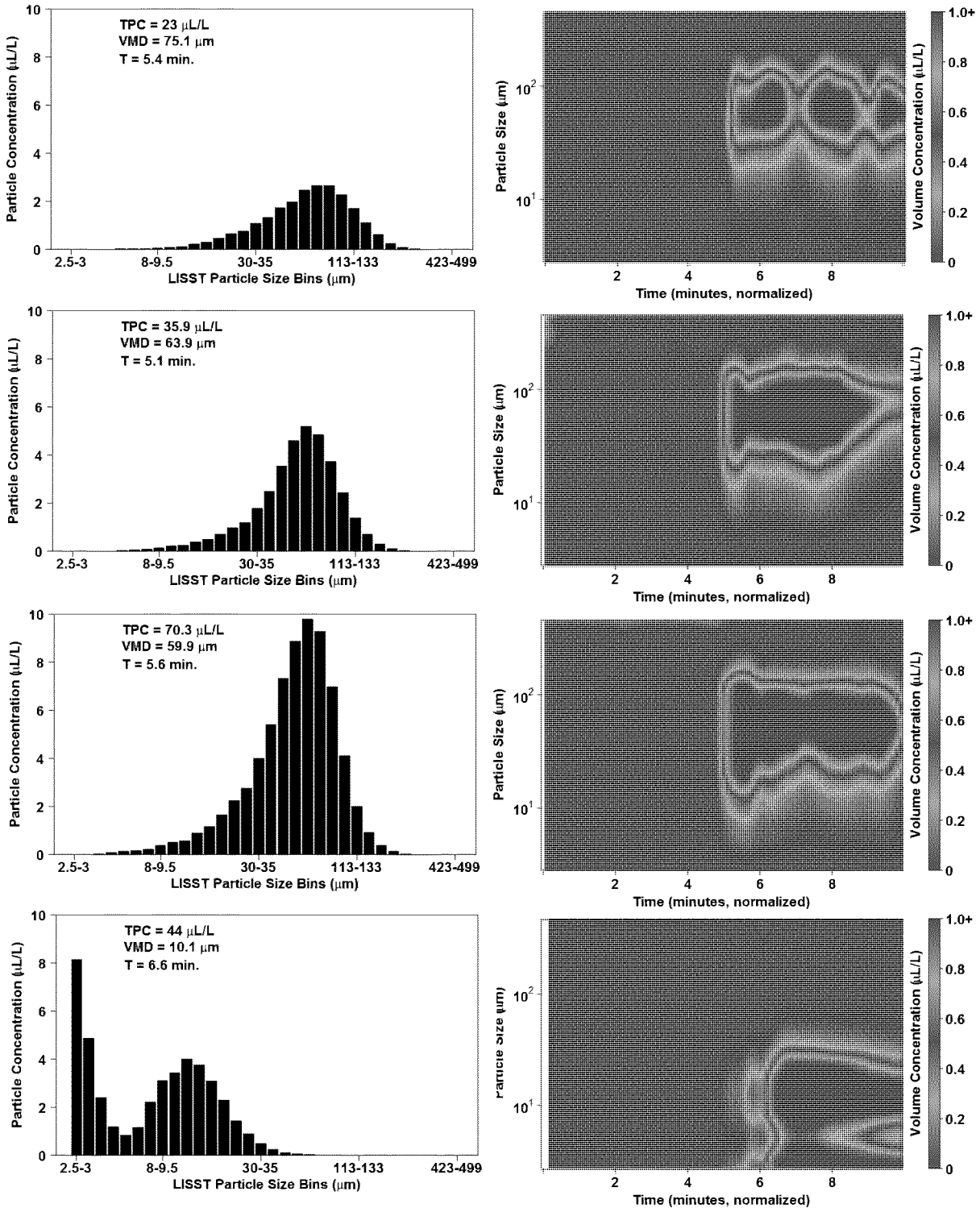


**Figure 18. Downstream LISST DSD and VMD (left panels) and time series of concentration**

**and particle size (right panels) for IFO 120 and Corexit 9500 warm water treatments. From top to bottom, DOR = 0, 1:200, 1:100, 1:20.**

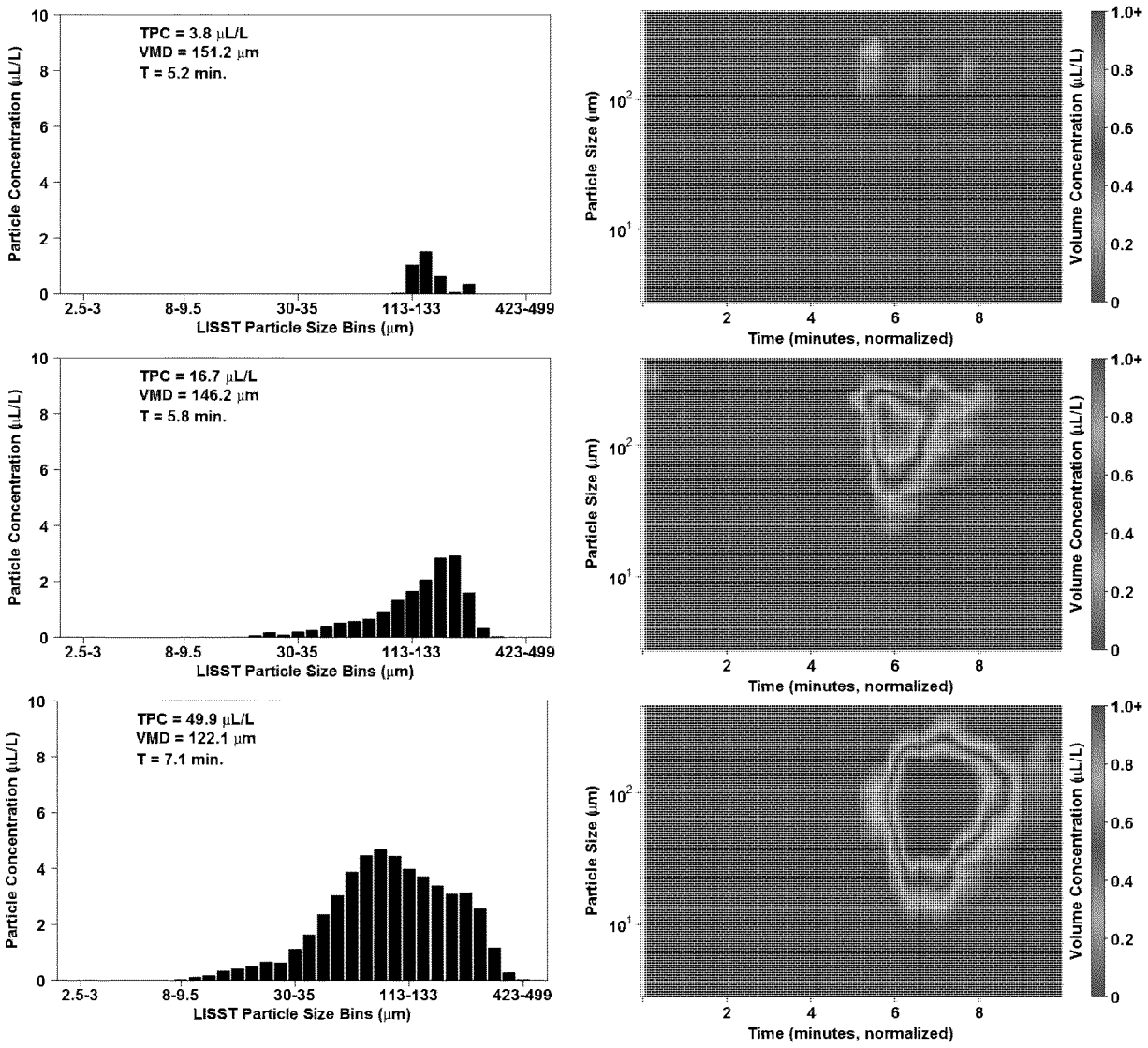


**Figure 19. Downstream LISST DSD and VMD (left panels) and time series of concentration and particle size (right panels) for IFO 120 and Finasol OSR 52 warm water treatments. From top to bottom, DOR = 0, 1:200, 1:100, 1:20. Refer to Figure 18 for ANS DOR = 0.**

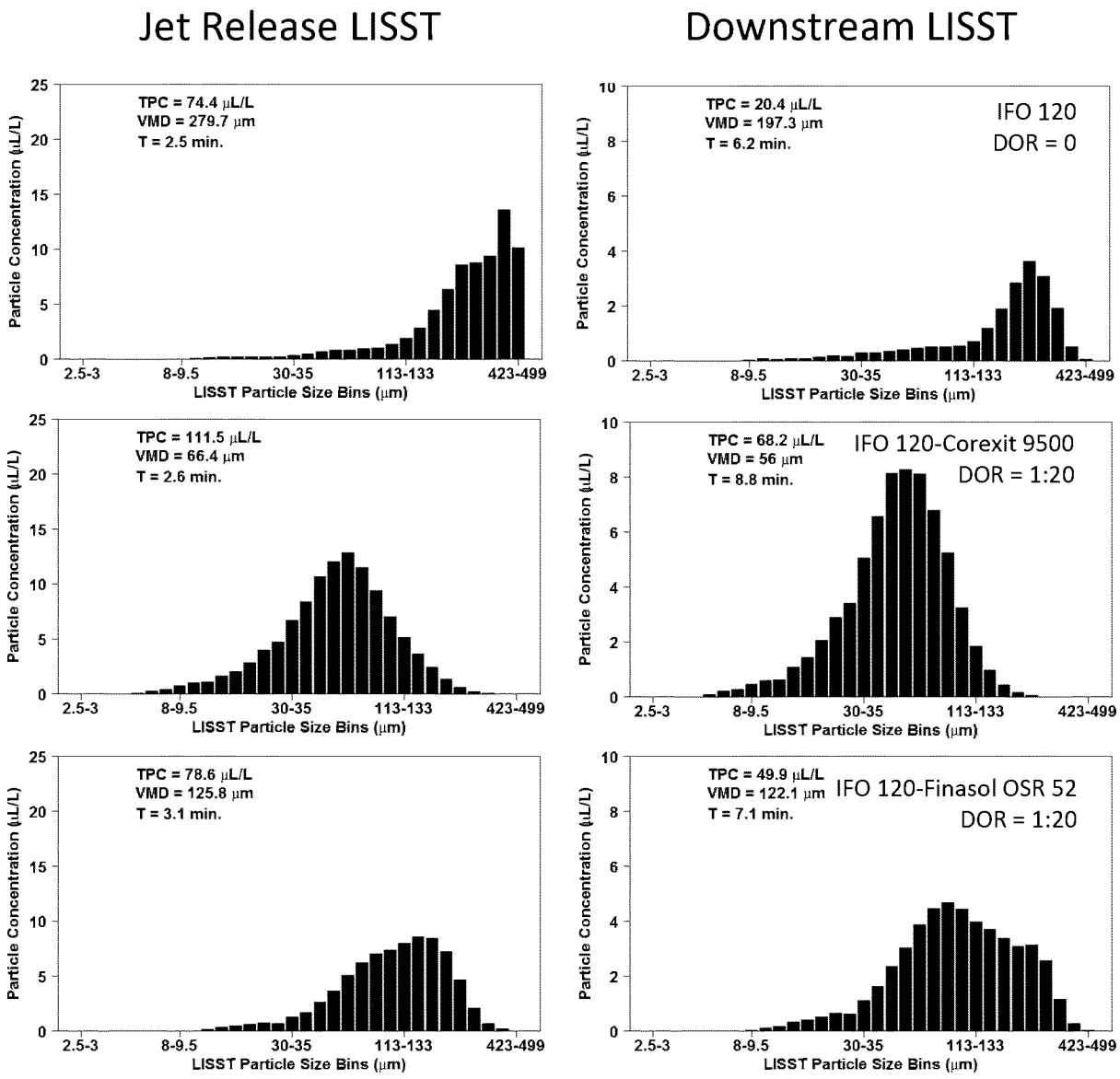


**Figure 20. LISST DSD with TPC for IFO 120 with Corexit 9500 and Finasol OSR 52 treatments at warm temperatures. DOR = 0 (top panel); DOR = 1:20 experiments are middle and bottom panels.**

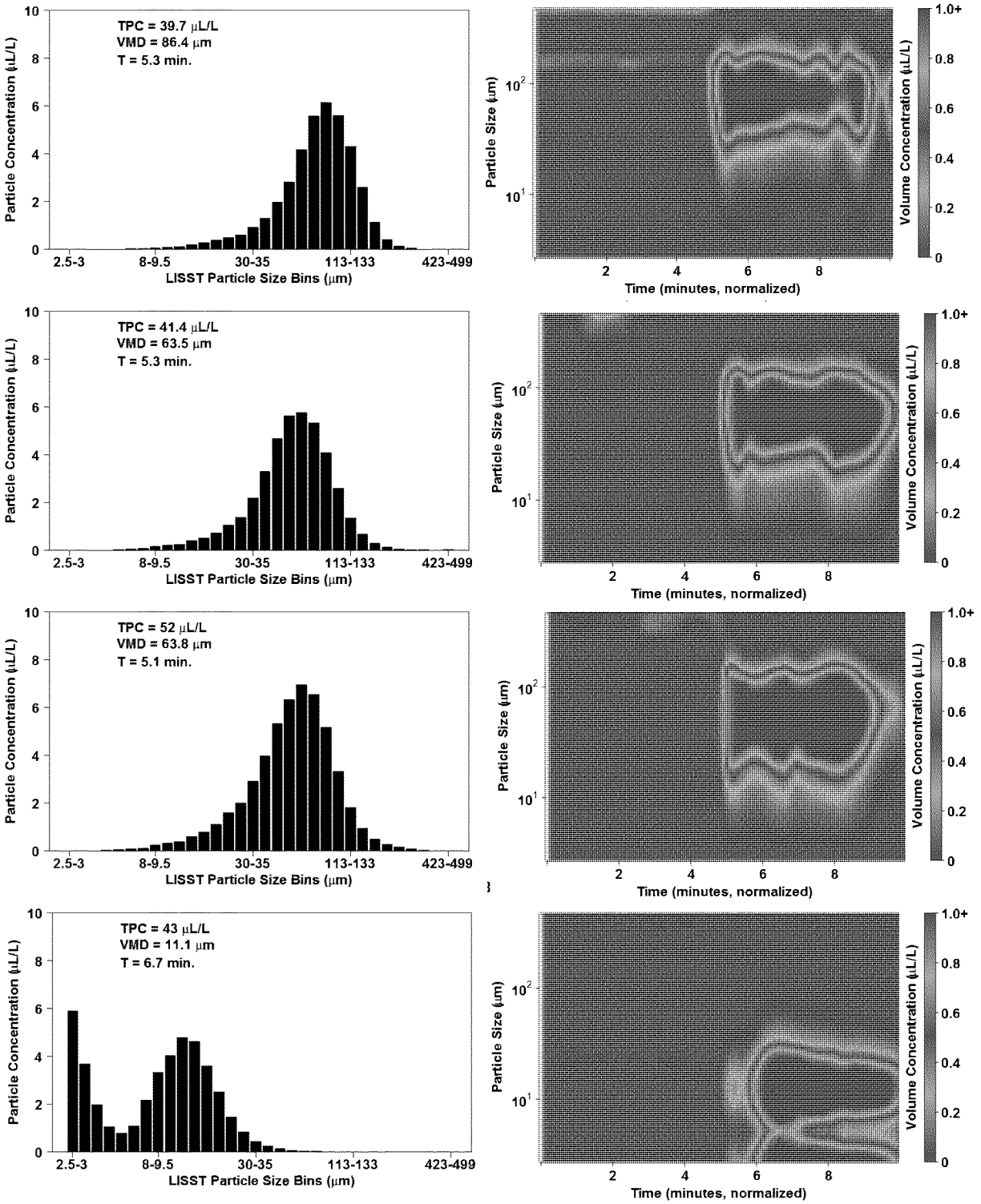
TPC = 39.7 µL/L
VMD = 86.4 µm
T = 5.3 min.
TPC = 41.4 µL/L
VMD = 63.5 µm
T = 5.3 min.
TPC = 52 µL/L
VMD = 63.8 µm
T = 5.1 min.
TPC = 43 µL/L
VMD = 11.1 µm
T = 6.7 min.
Particle Concentration (µL/L)
LISST Particle Size Bins (µm)
2.5-3
8-9.5
30-35
113-133
423-499
Particle Size (µm)
Time (minutes, normalized)
Volume Concentration (µL/L)

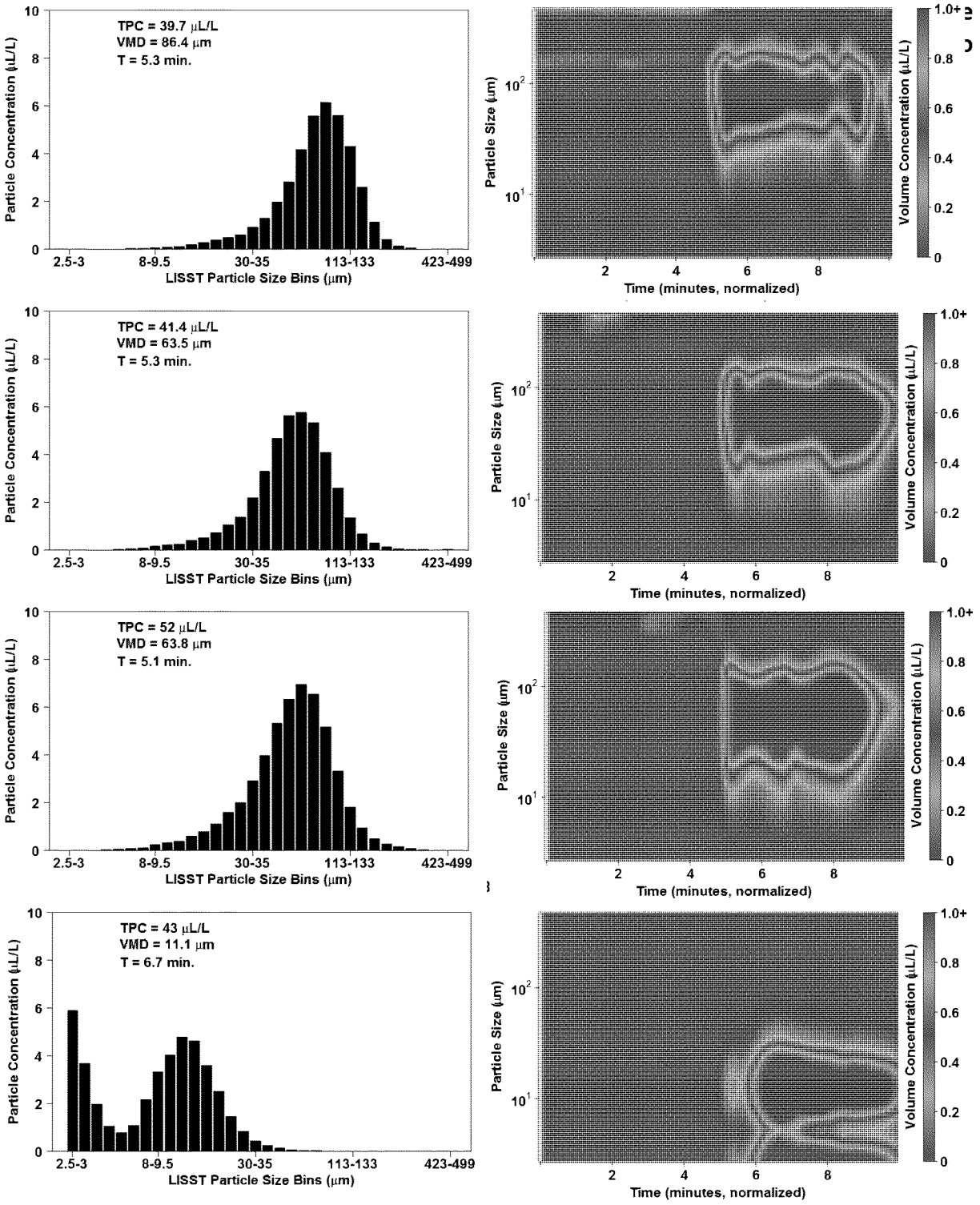
TPC = 39.7 µL/L
VMD = 86.4 µm
T = 5.3 min.
TPC = 41.4 µL/L
VMD = 63.5 µm
T = 5.3 min.
TPC = 52 µL/L
VMD = 63.8 µm
T = 5.1 min.
TPC = 43 µL/L
VMD = 11.1 µm
T = 6.7 min.
Particle Concentration (µL/L)
LISST Particle Size Bins (µm)
2.5-3
8-9.5
30-35
113-133
423-499
Particle Size (µm)
Time (minutes, normalized)
Volume Concentration (µL/L)

Fi
an
to

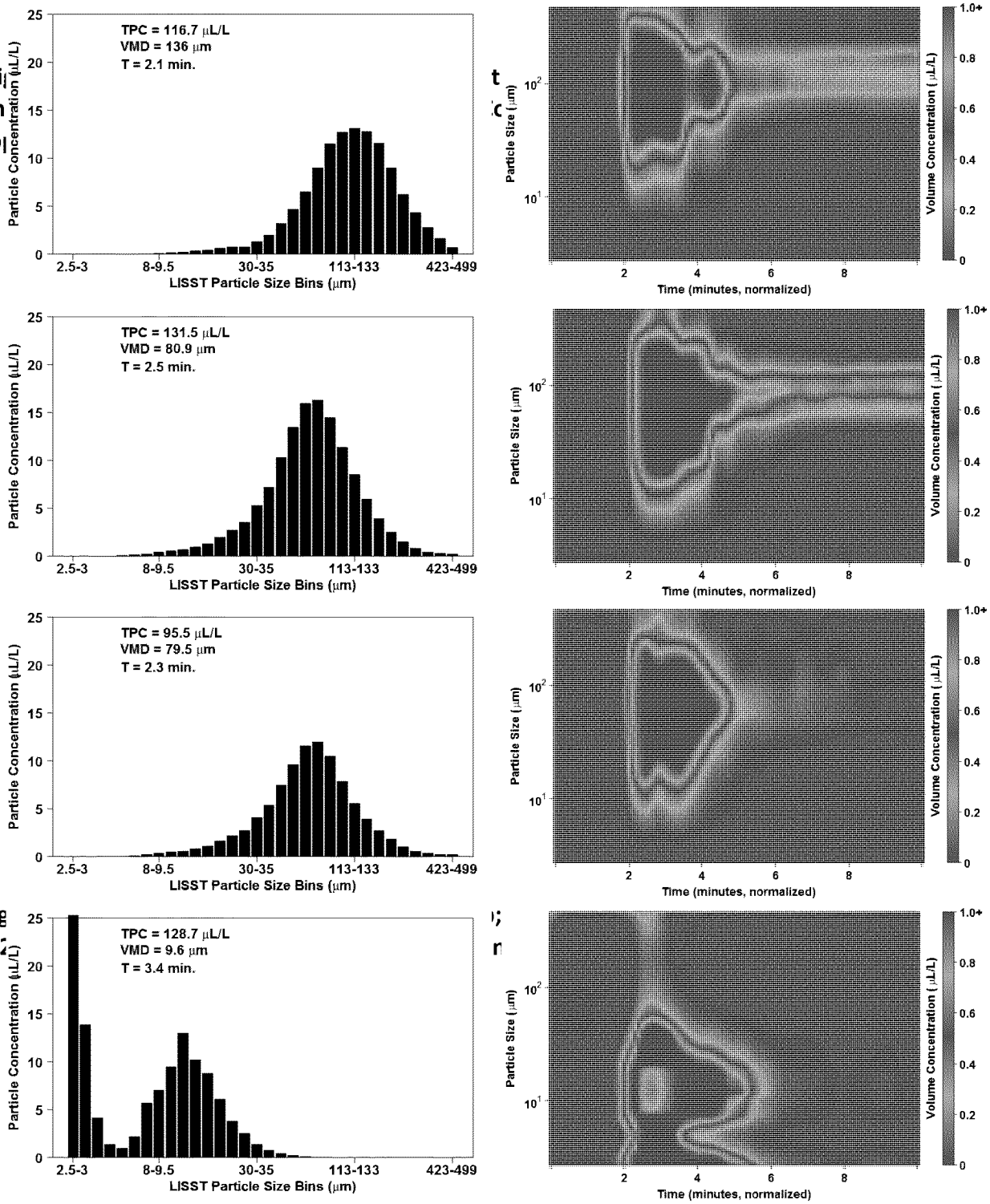
TPC = 116.7 µL/L
VMD = 136 µm
T = 2.1 min.
TPC = 131.5 µL/L
VMD = 80.9 µm
T = 2.5 min.
TPC = 95.5 µL/L
VMD = 79.5 µm
T = 2.3 min.
TPC = 128.7 µL/L
VMD = 9.6 µm
T = 3.4 min.
Particle Concentration (µL/L)
LISST Particle Size Bins (µm)
2.5-3
8-9.5
30-35
113-133
423-499
Particle Size (µm)
Time (minutes, normalized)
Volume Concentration (µL/L)

Fig
1:

### A.3.3 SLC Dispersion Effectiveness

Experiments involving South Louisiana Crude (SLC) oil treated with Corexit 9500 were conducted for warm water conditions (16.6 – 19.6 °C) to compare dispersion between ANS and SLC. Experiments with SLC yielded higher TPC values compared to ANS results, most likely the result of slightly larger amounts of oil added to the pressure canister (~25-50 g) due to the lower viscosity of SLC resulting in more oil injected by the injector, so comparisons shouldn't be made regarding TPC. The observed VMD of physically-dispersed SLC oil (neat; DOR = 0; ~123-148 µm) was found to be less than that of ANS (>200 µm). The addition of dispersant yielded a shift in DSD and VMD to smaller particles, where DOR = 1:200 and 1:100 exhibited diameters of ~91-108 µm, and DOR = 1:20 ranged between ~15 - 21 µm, as depicted in Figure 24. The Downstream LISST results indicate smaller droplet size as the plume moves through the tank (size fractionation) and a decrease in TPC (plume dilution), further demonstrating this trend for all oils (Figures 25 and 26). The fluorescence data indicates a strong signal with little scatter for up to 4 min in these treatments (Figure 27; Appendix E). Using these results, comparisons can be made to results of SLC with Corexit 9500 from surface plume simulations (oil released into tank via pour in from flask) from Conmy et al., 2014a (and unpublished data) from those experiments. No apparent differences between DSD and VMD for DOR = 0 treatments were found. For DOR = 1:20 VMD values are similar, however, the range of droplet diameters for surface simulations is larger with particles up to 200 µm. In subsurface injection jet experiments the range of diameters is narrower, where particles > 100 µm were not observed. This suggests that the combination of the chemical dispersant tested here, elevated turbulent mixing from the jet release and higher oil temperature of 80 °C yielded smaller droplets. To discern the dominant factor controlling the difference, additional testing would need to be conducted.



ED_001324_00000913-00071

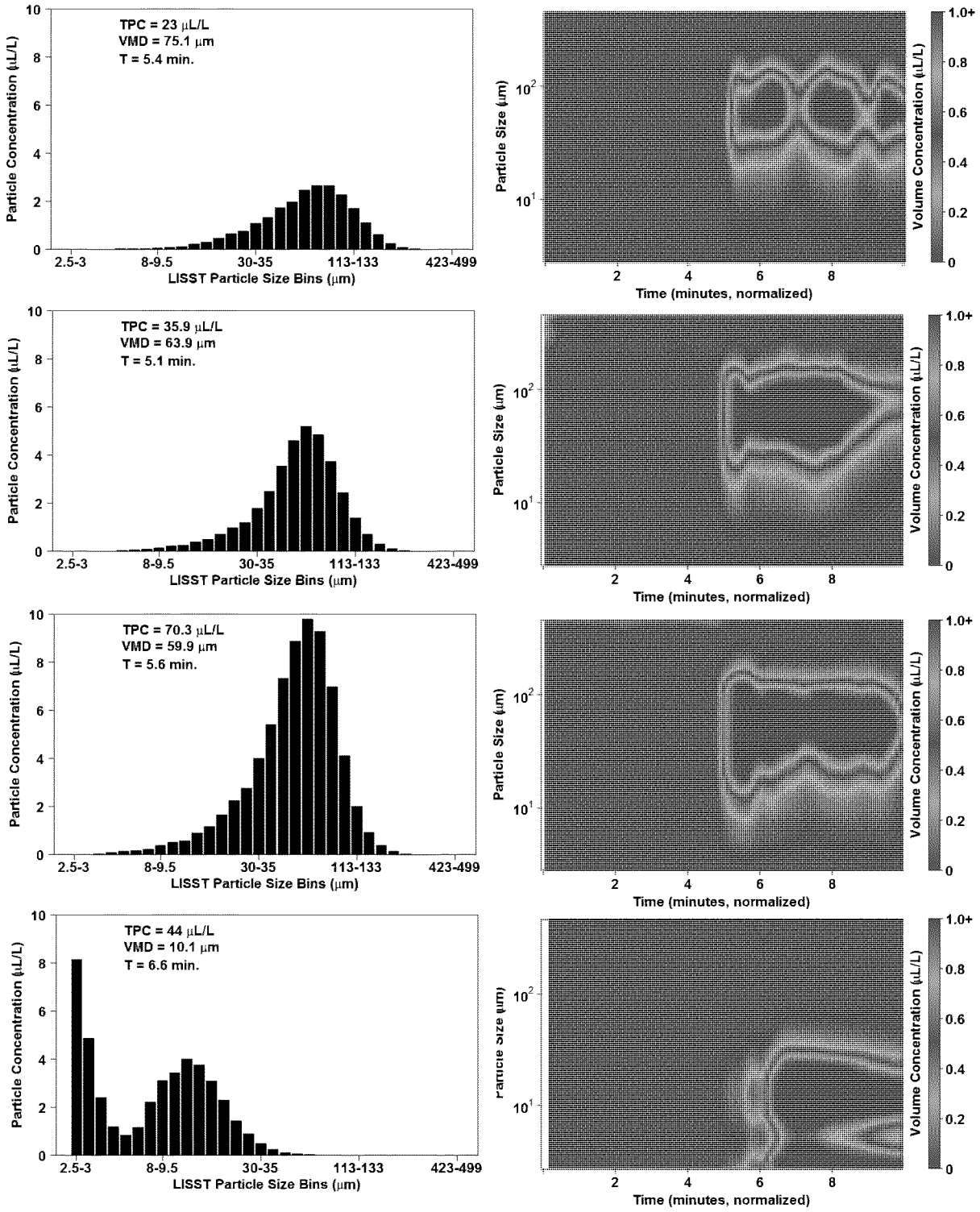
TPC = 23 µL/L
VMD = 75.1 µm
T = 5.4 min.
TPC = 35.9 µL/L
VMD = 63.9 µm
T = 5.1 min.
TPC = 70.3 µL/L
VMD = 59.9 µm
T = 5.6 min.
TPC = 44 µL/L
VMD = 10.1 µm
T = 6.6 min.
Particle Concentration (µL/L)
LISST Particle Size Bins (µm)
2.5-3
8-9.5
30-35
113-133
423-499
Particle Size (µm)
Time (minutes, normalized)
Volume Concentration (µL/L)

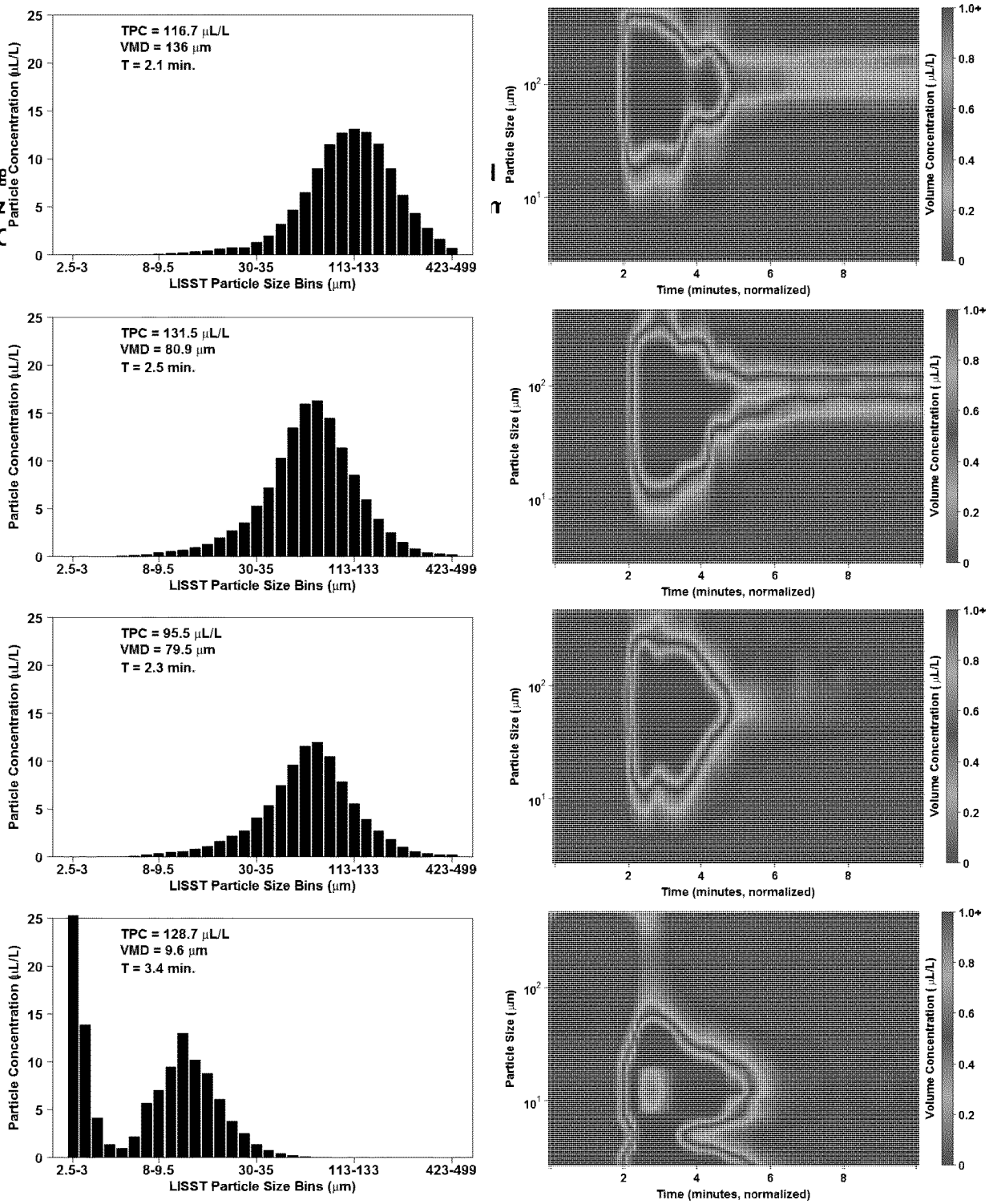
TPC = 116.7 µL/L
VMD = 136 µm
T = 2.1 min.
TPC = 131.5 µL/L
VMD = 80.9 µm
T = 2.5 min.
TPC = 95.5 µL/L
VMD = 79.5 µm
T = 2.3 min.
TPC = 128.7 µL/L
VMD = 9.6 µm
T = 3.4 min.
Particle Concentration (µL/L)
LISST Particle Size Bins (µm)
2.5-3
8-9.5
30-35
113-133
423-499
Particle Size (µm)
Time (minutes, normalized)
Volume Concentration ( µL/L)

**Figure 25. Downstream LISST DSD and VMD (left panels) and time series of concentration and particle size (right panels) for SLC and Corexit 9500 warm water treatments. From top to bottom, DOR = 0, 1:200, 1:100, 1:20.**

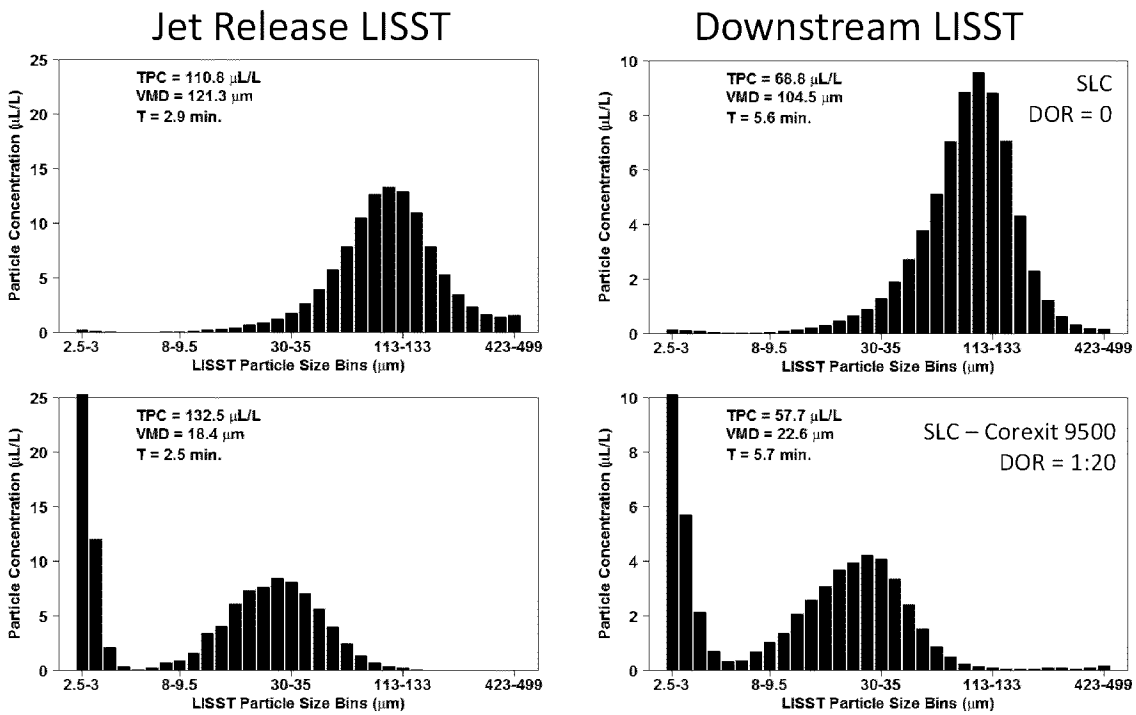


**Figure 26. LISST DSD with TPC for SLC with Corexit 9500 treatments at warm temperatures. DOR = 0 (top panel); DOR = 1:20 experiments are bottom panels.**



ED_001324_00000913-00074

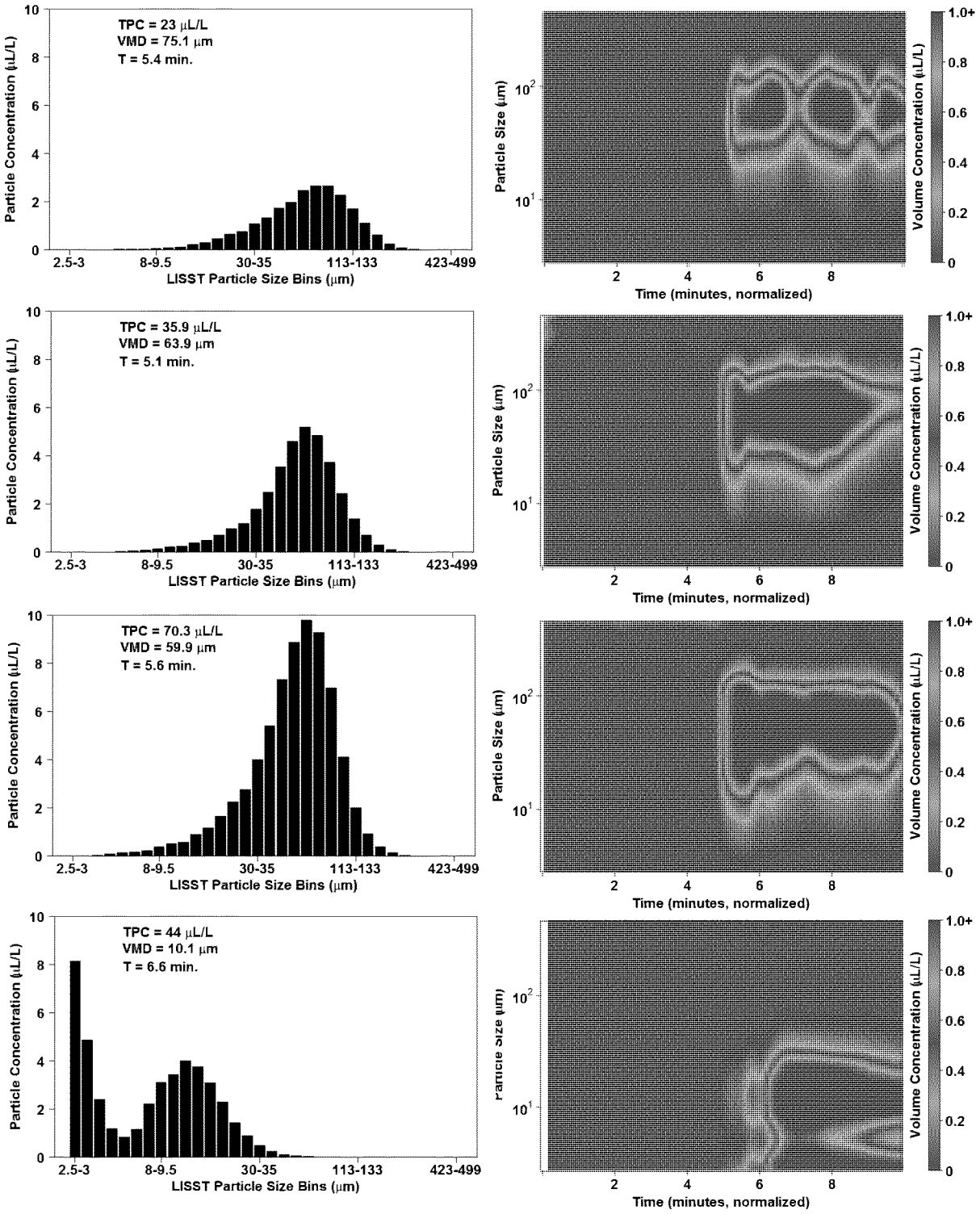
TPC = 23 µL/L
VMD = 75.1 µm
T = 5.4 min.
TPC = 35.9 µL/L
VMD = 63.9 µm
T = 5.1 min.
TPC = 70.3 µL/L
VMD = 59.9 µm
T = 5.6 min.
TPC = 44 µL/L
VMD = 10.1 µm
T = 6.6 min.
Particle Concentration (µL/L)
LISST Particle Size Bins (µm)
2.5-3
8-9.5
30-35
113-133
423-499
Particle Size (µm)
Time (minutes, normalized)
Volume Concentration (µL/L)

**Figure 27. *In situ* submersible fluorescence time series of sub-injection plume of SLC and Corexit 9500 warm water treatments. From top to bottom, DOR = 0, 1:200, 1:100, 1:20.**

### A.3.4 Gas Condensate Dispersion Effectiveness

Injection experiments were conducted with Gas Condensate and Corexit 9500 for warm water conditions (10 – 12 °C temperature range) and DOR = 0 and 1:20 only. The Gas Condensate consisted of mostly C15 alkanes and lower PAHs (napthalene and alkylated derivatives. The VMD for Gas Condensate with no dispersant added ranged between ~150 – 215 µm (Figure 28). With the addition of dispersant, VMD for the triplicates were 60.4, 68.2 and 170.4 µm suggesting that dispersant at DOR = 1:20 shifts the DSD to smaller particles for most experiments. Large variability in the triplicates was observed, however at this time there is no clear explanation as to the cause. The corresponding fluorescence data for these treatments indicate a strong signal with little scatter for up to 3 min in both treatments (Figure 28; Appendix E).



ED_001324_00000913-00076

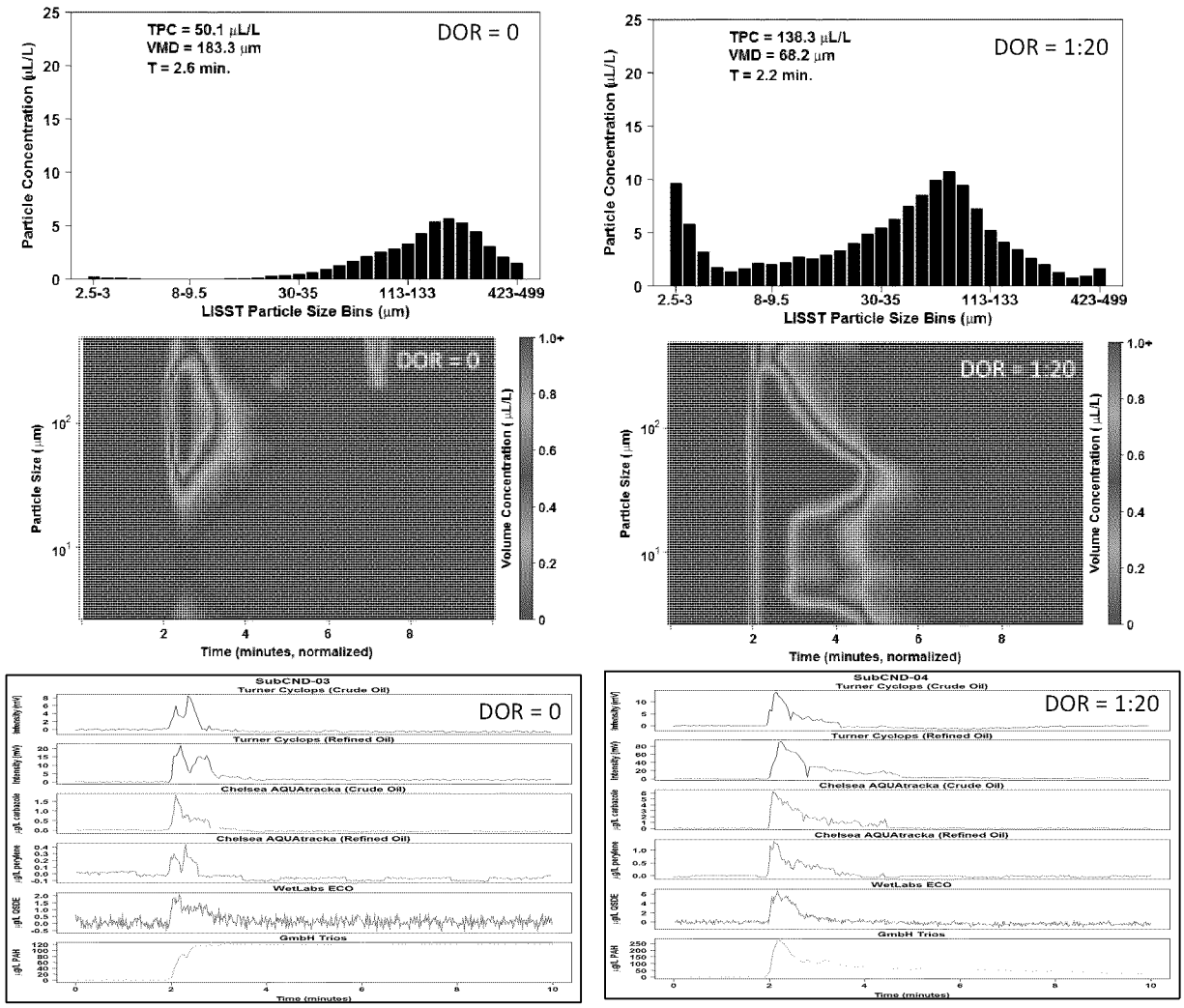


**Figure 28. LISST DSD and VMD (top panels),time series of concentration and particle size**

**(middle panels), and fluorescence time series (bottom panels) for Gas Condensate and Corexit 9500 warm water treatments. Left panels are DOR = 0 and right panels are DOR = 1:20.**

### A.3.5 Tank Dilution Series Fluorescence Measurements

Submersible fluorescence results are presented in units recommended by manufacturers and using calibration factors provided by the manufacturers. Efforts were made to correlate the fluorescence intensity with TPH and / or BTEX concentration but were not possible due to issues inherent with the discrete sample collection. In order to fill bottles for chemical analysis, a 30 second time period was needed. Due to the short time period of the experiments and the heterogeneity of the plume concentration through time (evident from the fluorescence time series), oil concentrations within the bottles represent an average over a 30 second time period that cannot be aligned with the time series data, which are generated on the time scale of seconds. Given this fact, a dilution series within the tank using ANS was conducted to provide a calibration curve for fluorometers to a known concentration of oil in a homogeneous tank akin to Conmy et al., 2014a. Calibration regression results for all submersible fluorometers can be found in Figures 29 and 30 for TPH and BTEX, respectively and regression equations are tabulated in Table 5. Strong correlations between oil concentration and fluorescence intensity were observed, suggesting that fluorescence signal may serve as a proxy for TPH or BTEX at specific time points within the tank. This is an advantage as fluorescence intensity and oil droplet concentrations time series can therefore be calibrated and employed to provide for chemistry estimates that can be correlated with particle / oil droplet concentrations at fine time scales within the tank during experiments. For example, comparing the TPC and fluorescence signature for ANS with and without dispersant illustrates the differences in the oil droplet concentration and dissolved oil during injection experiments and the utility of monitoring both to understanding



ED_001324_00000913-00078

plume dynamics (Figure 31).

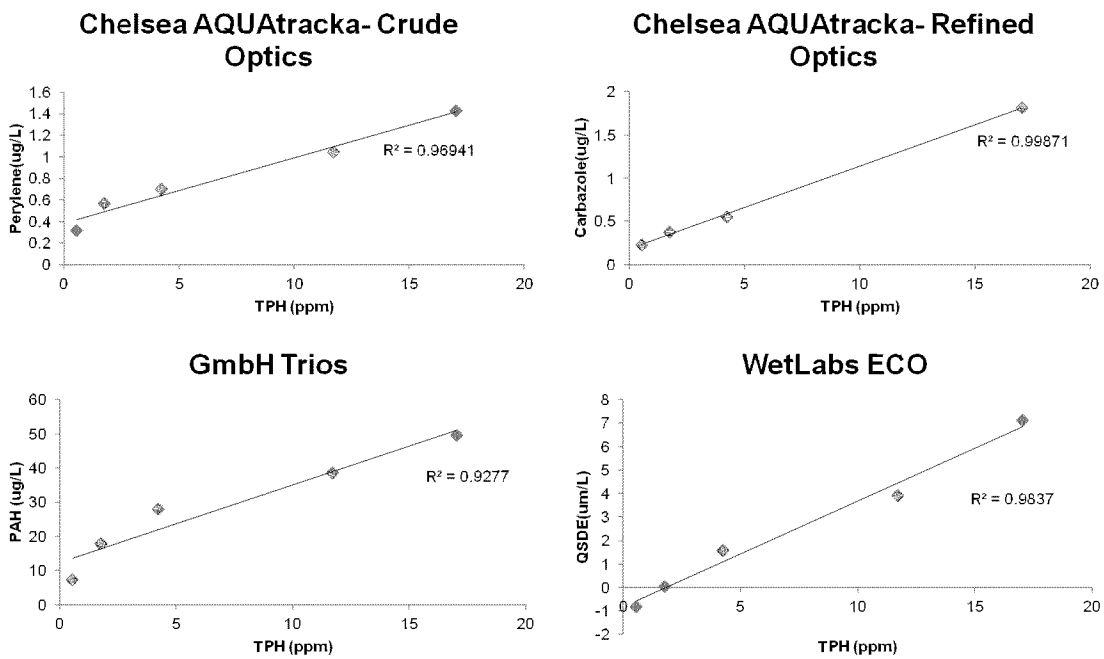

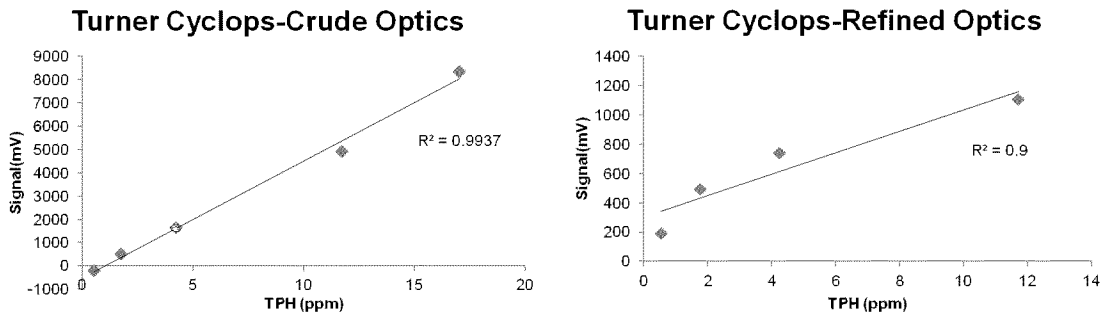


**Figure 29. Calibration lines for fluorometer response vs TPH concentrations.**

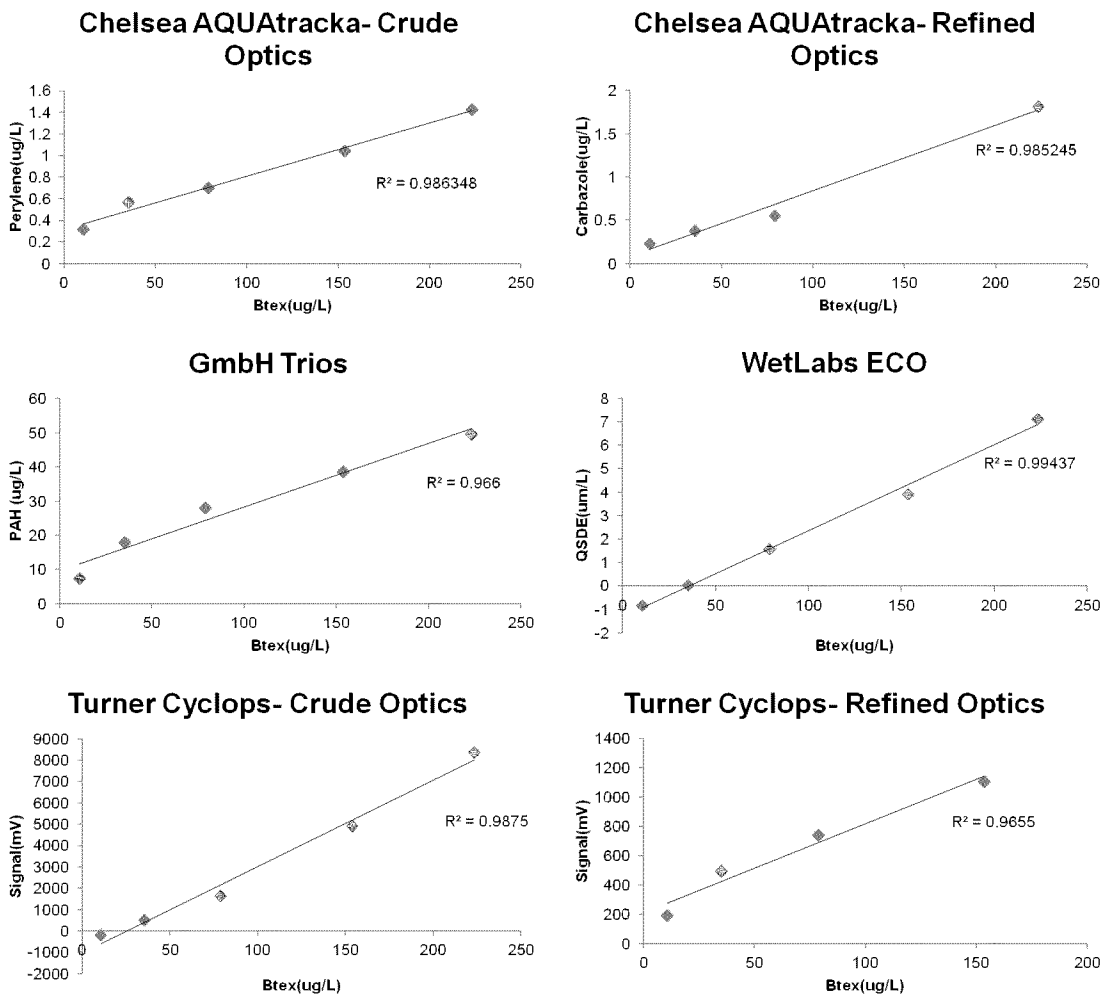


**Figure 30. Calibration lines for fluorometer response vs BTEX concentrations.**



ED_001324_00000913-00080

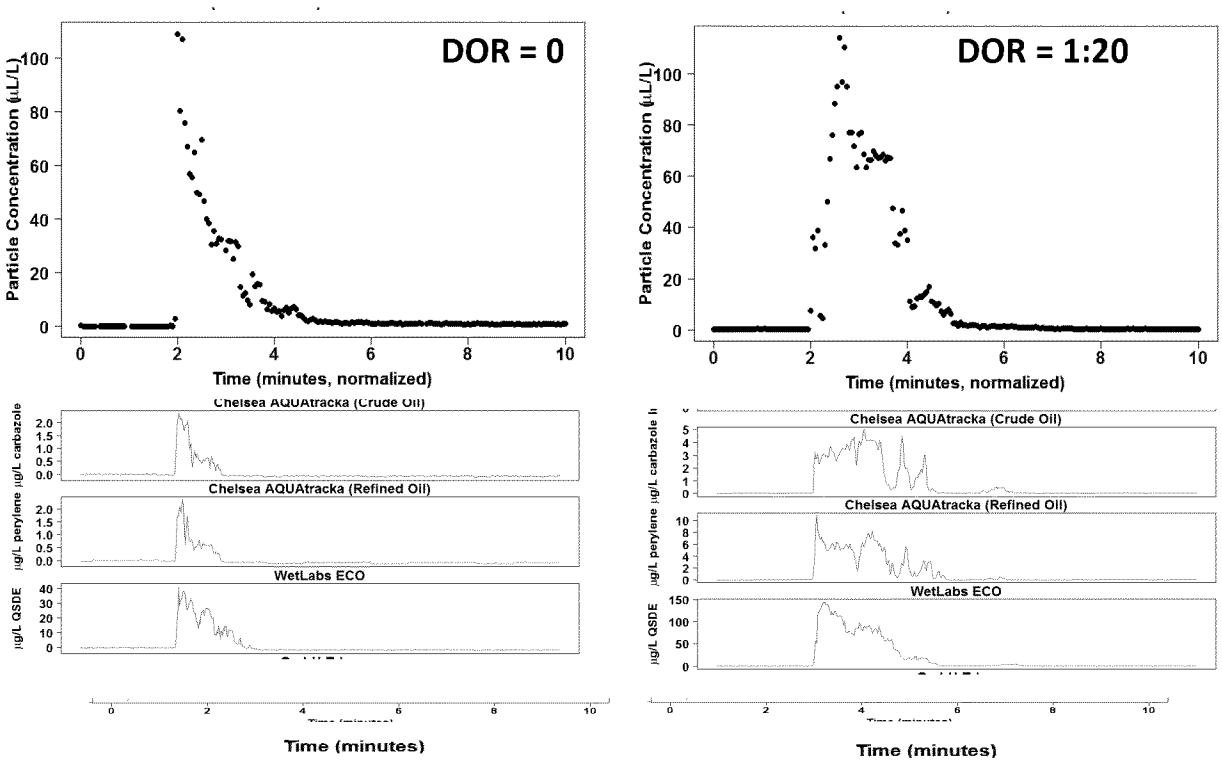
DOR = 0
Particle Concentration (µL/L)
Time (minutes, normalized)
Chelsea AQUAtracka (Crude Oil)
µg/L carbazole
Chelsea AQUAtracka (Refined Oil)
µg/L perylene
WetLabs ECO
µg/L QSDE
Time (minutes)
DOR = 1:20
Particle Concentration (µL/L)
Time (minutes, normalized)
Chelsea AQUAtracka (Crude Oil)
µg/L carbazole
Chelsea AQUAtracka (Refined Oil)
µg/L perylene
WetLabs ECO
µg/L QSDE
Time (minutes)

**Figure 31. Total Particle Concentration and fluorescence time series for ANS crude oil with Corexit 9500 dispersant.**

**Table 5. Calibration equations for the submersible fluorometers. Data in this report have fluorescence signal in the manufacturer recommended units.**



ED_001324_00000913-00082

| Instrument | Factory Calibration Standard (units) | TPH Calibration Equation | BTEX Calibration Equation |
|---|---|---|---|
| Chelsea Aquatracka (Crude Optics) | Perylene (ug/L) | [TPH] = ([Perylene]-0.3834)/0.06051 | [BTEX] = ([Perylene]-0.3165)/0.004922 |
| Chelsea Aquatracka (Refined Optics) | Carbazole (ug/L) | [TPH] = ([Carbazole]-0.1804)/0.09575 | [BTEX] = ([Carbazole]-0.08487)/0.007584 |
| GmbH Trios | PAH (ug/L) | [TPH] = ([PAH]-12.288)/2.2733 | [BTEX] = ([PAH]-9.559)/0.1871 |
| Turner Cyclops (Crude Optics) | Signal (mV) | [TPH] = (Signal+320.26)/503.94 | [BTEX] = (Signal+1152.2)/42.429 |
| Turner Cyclops (Refined Optics) | Signal (mV) | [TPH] = (Signal-299.29)/73.339 | [BTEX] = (Signal-212.05)/6.0593 |
| Wetlabs ECO | QSDE (uM/L) | [TPH] = (QSDE-0.2102)/0.4362 | [BTEX] = (QSDE+0.5403)/0.03697 |

### A.3.6 VOC Air Monitoring

For all experiments, the Volatile Organic Compounds (VOC) measurements exhibited higher variability compared to the in water sensor measurements. The installation of a wind curtain along the western side of the tank helped to reduce the prevailing winds coming directly off

the water, however the effects of wind were not completely eliminated. The observed variability is likely caused by differences in wind speed and direction both among the triplicate experiments (typically run on the same day), and among the different treatments (which were run over days/weeks). The VOC meters were installed with the air intakes pointing down and were 0.4 m above the water surface at the top edge of the tank. This positioning helped to reduce the effects of wind, given that the tank walls acted as an additional wind blocker.

Two VOC meters were deployed above the tank, but only results from the VOC meter closest to the oil release are presented here (Jet Release VOC meter; the VOC meter directly above the fluorometer rack). Results from the second VOC meter (Downstream VOC meter) installed 11.8 m farther downstream are more variable, both in concentrations between triplicate runs and in the time it takes for airborne VOC concentrations to reach the meter. In general, readings from the second meter showed a broader plume with a lower peak VOC concentration. Due to an instrument malfunction, approximately 17 experiments are missing data from the Downstream VOC meter. All results from the Jet Release VOC meter are presented in Figures 32-39. Note that the Y-axis scale differs depending on the oil type (20 ppm for IFO, 45 ppm for ANS & SLC, 250 ppm for Gas Condensate).

Of the four different hydrocarbon products tested, experiments using the gas condensate exhibited the highest surface VOC concentrations, followed by ANS and SLC which exhibited similar values. The lowest concentrations were observed for IFO 120 experiments. Higher concentrations of VOC in the air were usually accompanied by lower BTEX concentrations in the water for each oil type (analytical chemistry results in Appendix B). Chemistry results from the water column (effluent, listed in Appendix B tables) samples help to verify the findings from the VOC meters. In general, the measured concentrations of BTEX in the effluent water samples were higher for experiments using dispersant compared to the untreated experiments. The effluent port in the flume tank during normal operation produces a depth integrated water sample which does not draw off the water surface. Therefore, oil that rises to the surface is not drawn into the effluent, and so the tank effluent



ED_001324_00000913-00084

can be used as a measure of how much oil was dispersed into the water column. Regardless of the oil product tested, the use of chemical dispersants resulted in a reduction in VOC concentrations in the air above the water compared to corresponding experiments without dispersant. These results comparing the mean maximum VOC concentrations (30 second before/after peak readings) measured during each experiment are summarized in Table 6. A general trend was also observed where increasing the DOR resulted in lower surface VOC concentrations near the jet release location. Statistical analysis using ANOVA followed by confidence interval test (Tukey's test) to compare the means found that there were significant differences between VOC readings for ANS at a DOR of 1:20 versus no dispersant (both Corexit and Finasol), as well as significant differences for SLC at a DOR of 1:20 versus no dispersant and DOR 1:100 and 1:200. Caution should be used when extrapolating these results to other spill scenarios, given that this was a shallow water tank so the effects of dissolution of VOCs from oil droplets in a deepwater blowout would not be accounted for in these experiments. Due to wind effects mentioned previously, trends in VOC concentrations above the plume further down the tank could not be established. Further, wind conditions may have contributed to the observed variability in the measurements. The effects of wind on the dilution and transport of VOCs should also be considered during a real world spill scenario, and so the absolute values of VOC concentrations measured in this study should only be used to compare the relative differences between treatments, and should not be used as a guide for worker exposure. Caution must be exercised however in that these results merely represent VOCs that make it to the air-sea interface from a very shallow wave tank. They cannot simulate the dissolution of VOCs into water that would be expected in a deep water column.

**Table 6. Summary of maximum VOC concentrations at the various treatment conditions tested in this study. Results are for only for warm water experiments.**



ED_001324_00000913-00085

| | Avg. Peak VOC Concentration (ppm), n = 3 | | | | ANOVA |
|---|---|---|---|---|---|
| Oil Type | No Dispersant | DOR 1:200 | DOR 1:100 | DOR 1:20 | p-value, α = 0.05 |
| ANS (Corexit 9500) | 23.07 | 13.27 | 12.43 | 0.13 | 0.023 |
| ANS (Finasol OSR 52) | 23.07 | 16.56 | 7.17 | 2.9 | 0.024 |
| IFO 120 | 1.00 | 0.90 | 7.37 | 0.17 | 0.133 |
| Condensate | 121.23 | -- | -- | 19.73 | 0.152 |
| SLC | 28.53 | 27.5 | 16.75 | 1.53 | 0.001 |



ED_001324_00000913-00086

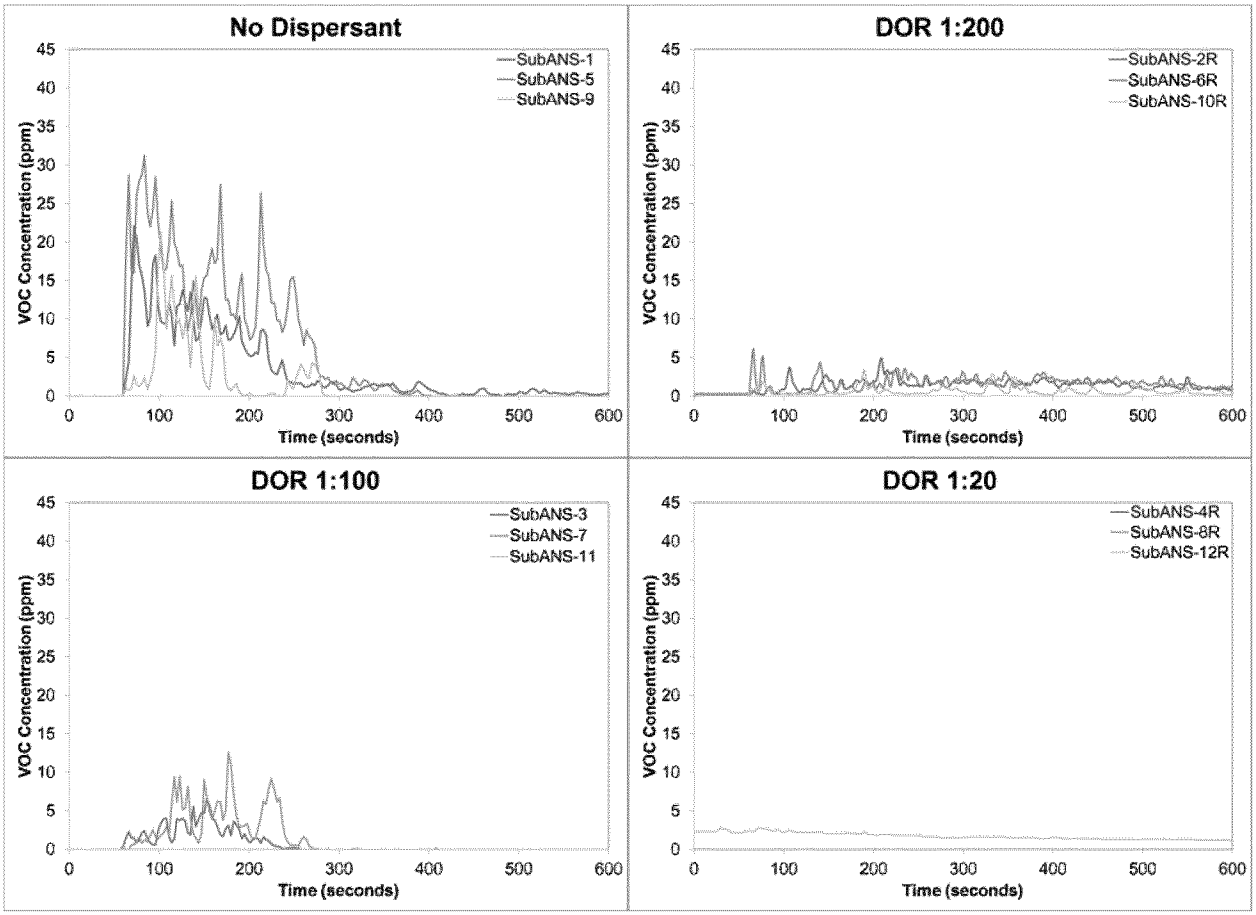


**Figure 32. VOC results for subsurface injection experiments (cold water season) using Alaska North Slope crude oil and four treatment conditions (no dispersant, DOR 1:200, DOR 1:100, DOR 1:20). Replicate treatments represented by light blue, dark blue and green colored lines.**



ED_001324_00000913-00087

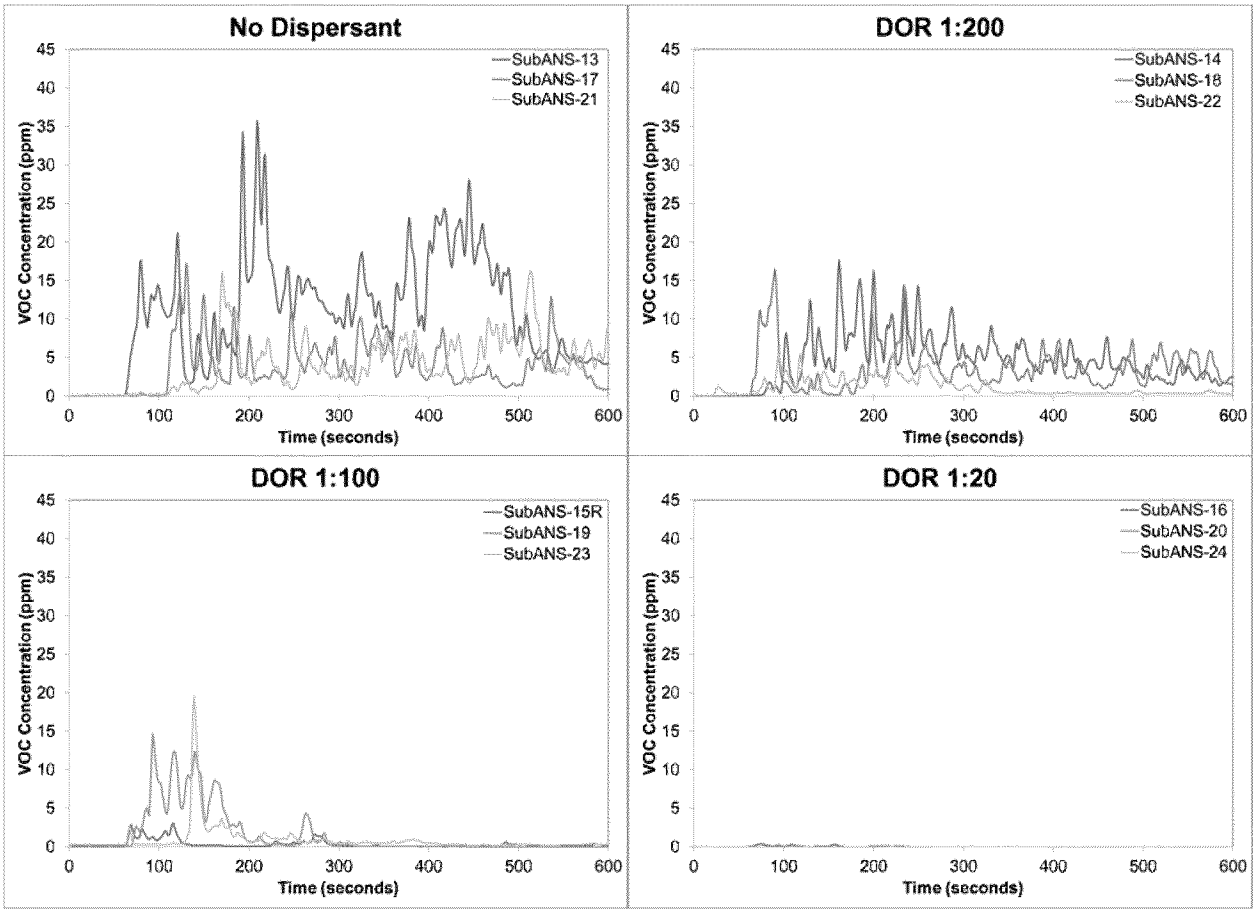


**Figure 33. VOC results for subsurface injection experiments (warm water season) using Alaska North Slope crude oil and four treatment conditions (no dispersant, DOR 1:200, DOR 1:100, DOR 1:20). Corexit 9500 was used as the treating agent. Replicate treatments represented by light blue, dark blue and green colored lines.**



ED_001324_00000913-00088

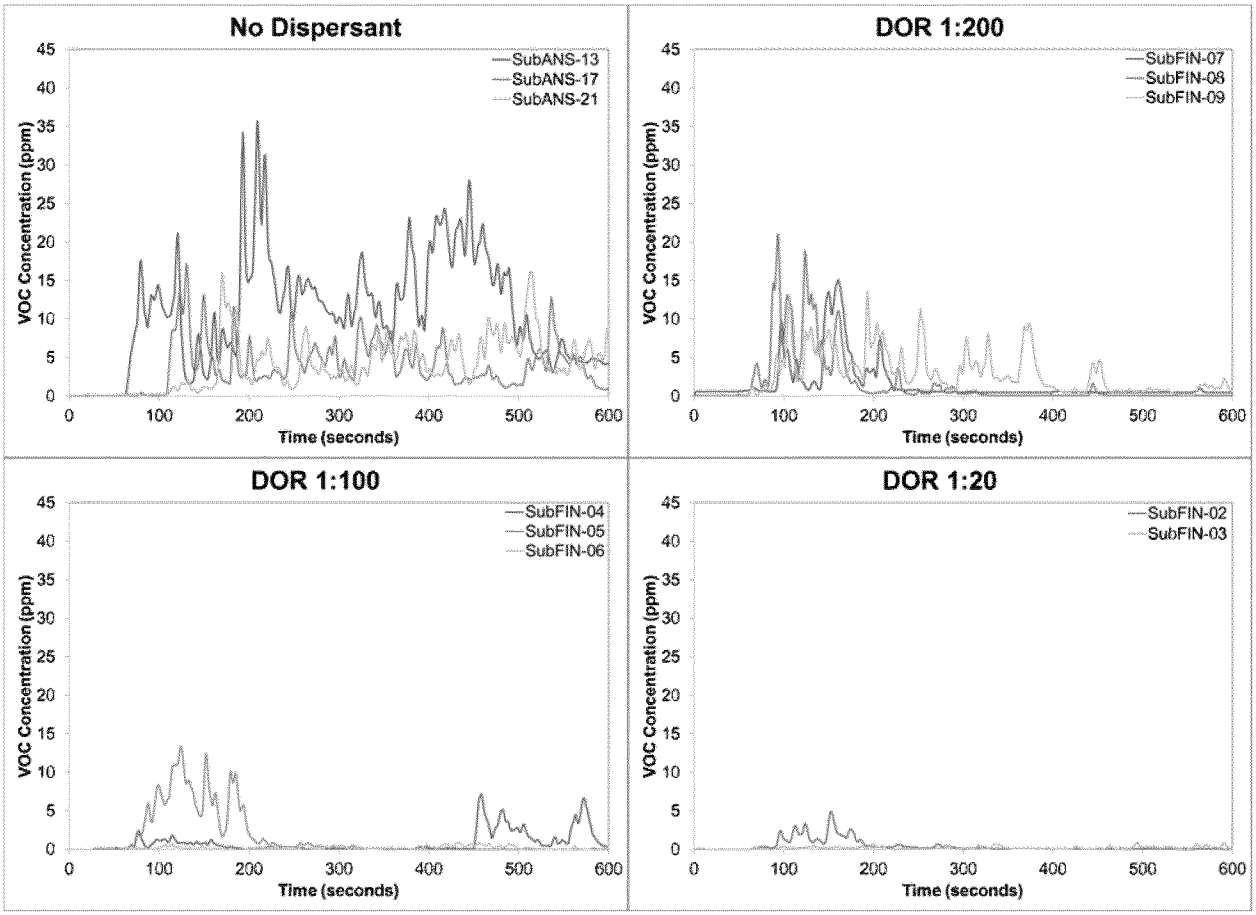


**Figure 34. VOC results for subsurface injection experiments (warm water season) using Alaska North Slope crude oil and four treatment conditions (no dispersant, DOR 1:200, DOR 1:100, DOR 1:20). Finasol OSR 52 was used as the treating agent. Replicate treatments represented by light blue, dark blue and green colored lines.**



ED_001324_00000913-00089

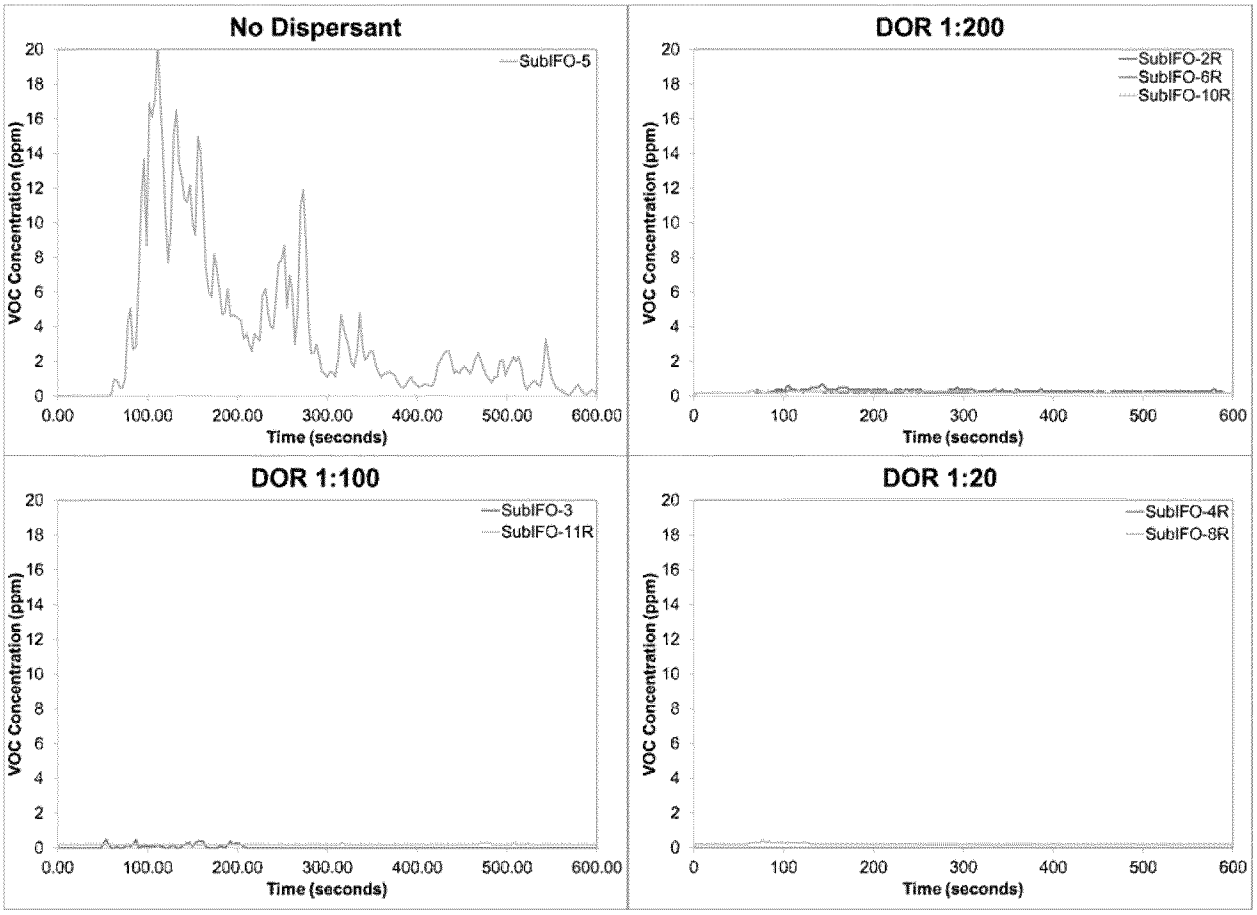


**Figure 35. VOC results for subsurface injection experiments (cold water season) using IFO 120 and four treatment conditions (no dispersant, DOR 1:200, DOR 1:100, DOR 1:20). Corexit 9500 was used as the treating agent. Replicate treatments represented by light blue, dark blue and green colored lines.**



ED_001324_00000913-00090

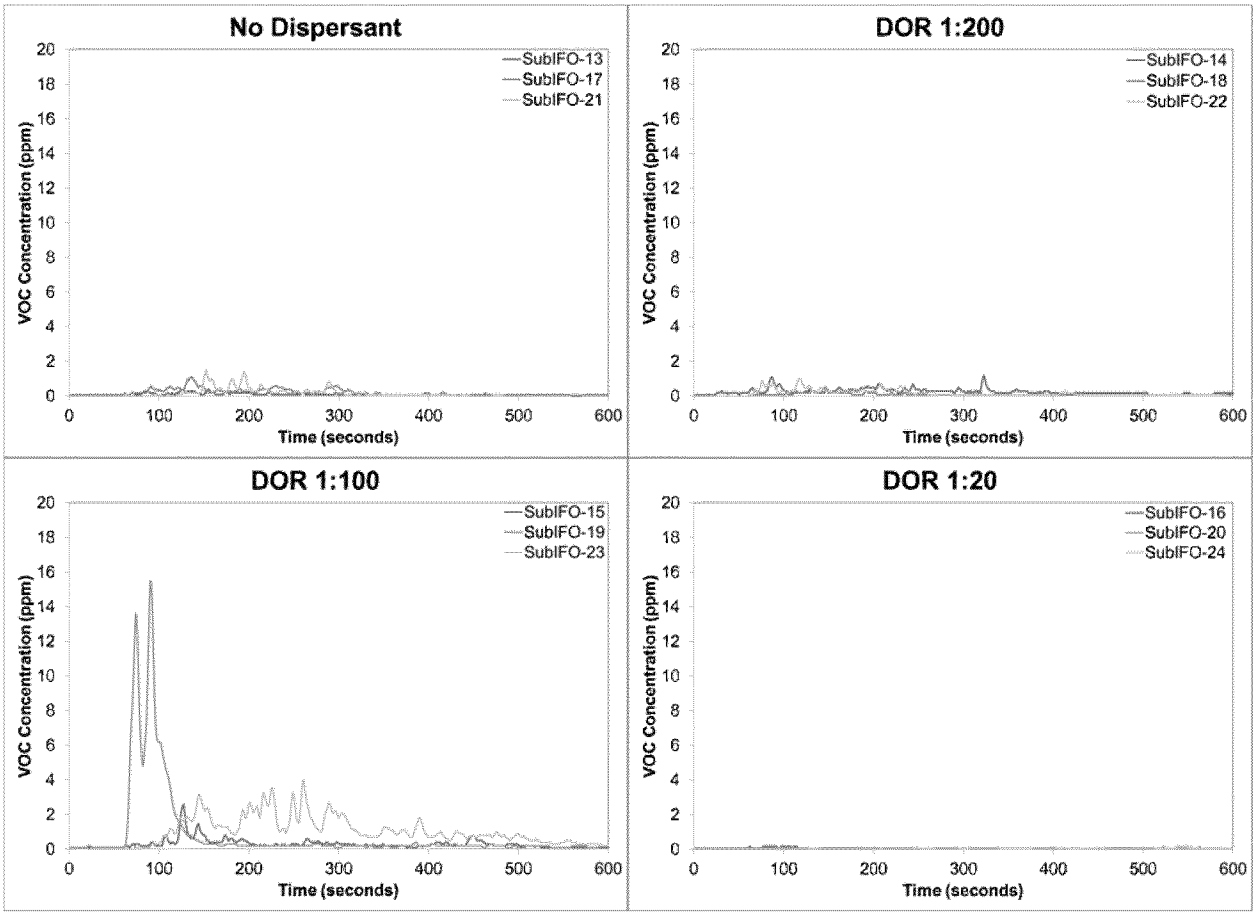


**Figure 36. VOC results for subsurface injection experiments (warm water season) using IFO 120 and four treatment conditions (no dispersant, DOR 1:200, DOR 1:100, DOR 1:20). Corexit 9500 was used as the treating agent. Replicate treatments represented by light blue, dark blue and green colored lines.**



ED_001324_00000913-00091

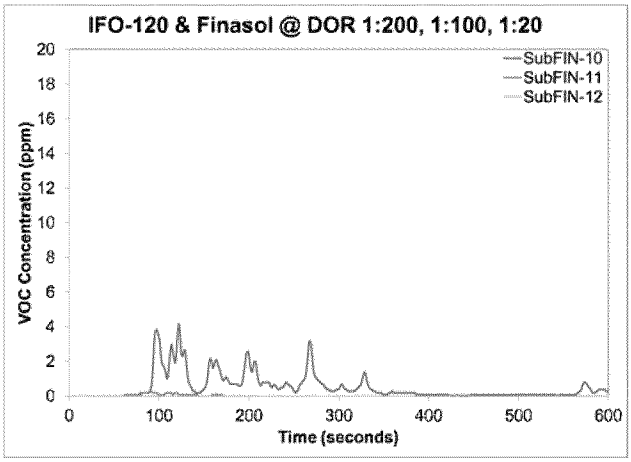


**Figure 37. VOC results for subsurface injection experiments (warm water season) using IFO 120 and three treatment conditions (DOR 1:200, DOR 1:100, DOR 1:20). Finasol OSR 52 was used as the treating agent (note – these treatments were not tested in triplicate).**

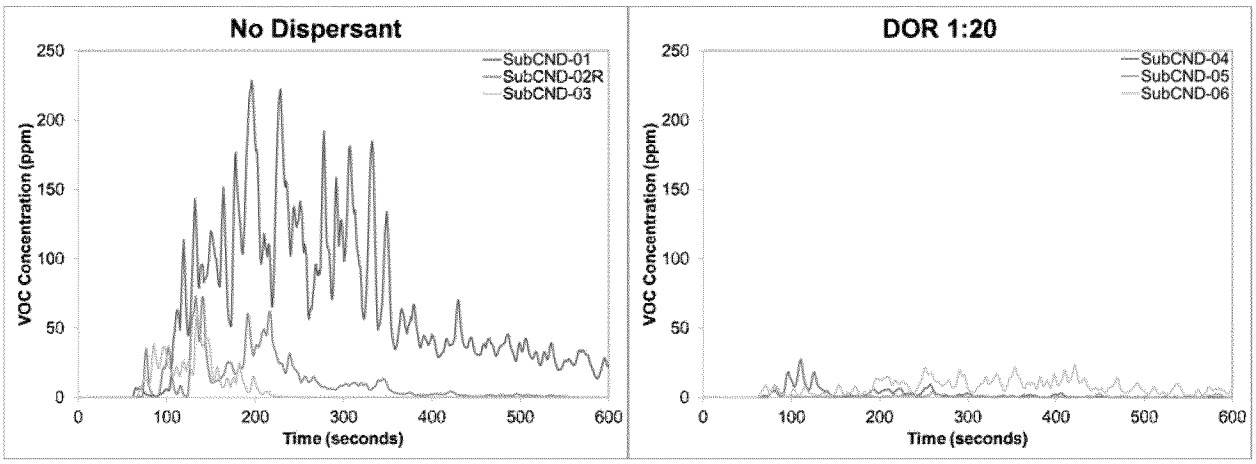


**Figure 38. VOC results for subsurface injection experiments using gas condensate and two treatment conditions (no dispersant, DOR 1:20). Corexit 9500 was used as the treating agent.**



ED_001324_00000913-00092

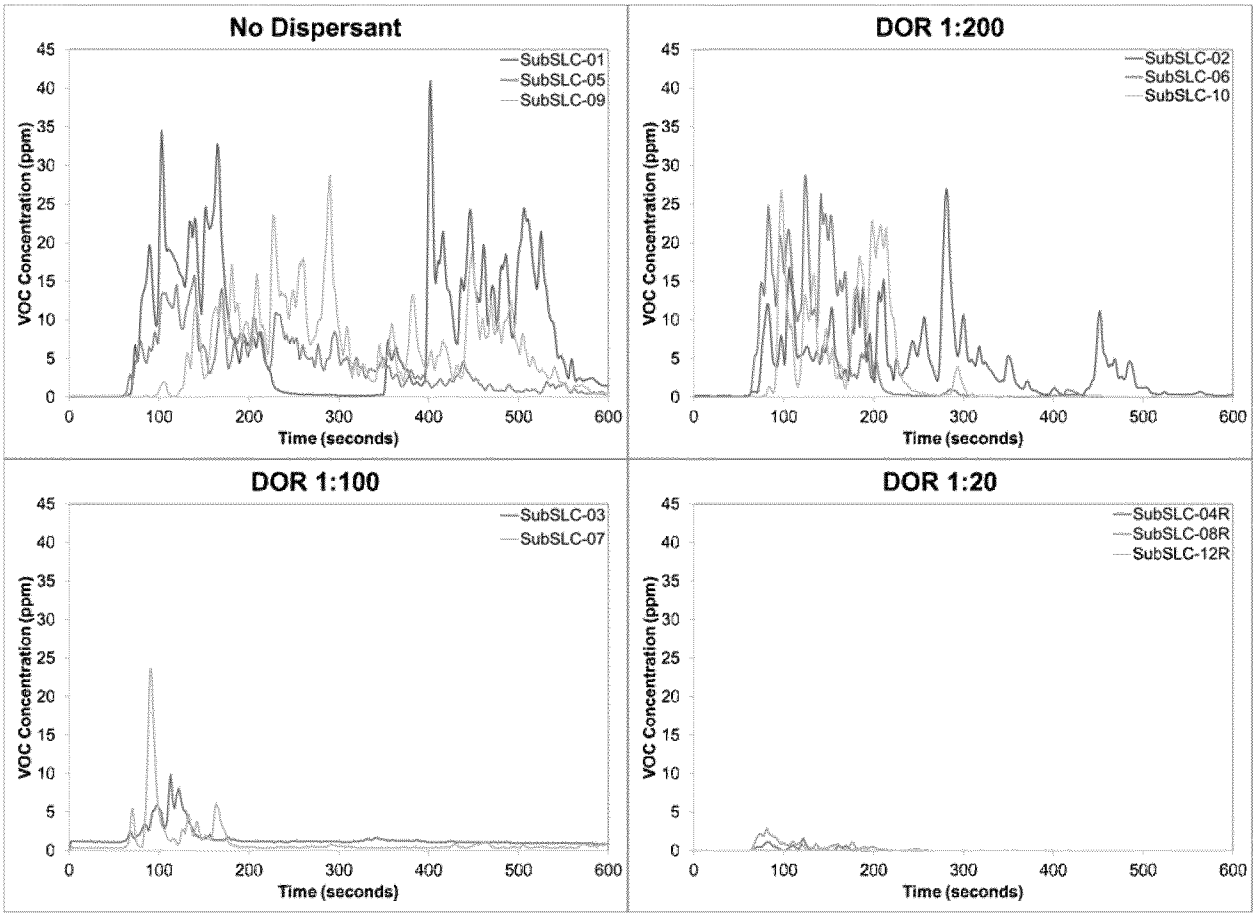


**Figure 39. VOC results for subsurface injection experiments using Sweet Louisiana Crude oil and four treatment conditions (no dispersant, DOR 1:200, DOR 1:100, DOR 1:20). Corexit 9500 was used as the treating agent.**

### A.3.7 VDROP-J and JETLAG Numerical Plume Modeling

Refer to Appendix G for detailed summary of the VROP-J and JETLAG numerical modeling component along with figures. Modeling the movement of oil released underwater is a challenging task due to limitations in measuring hydrodynamics in an oil-water system. Computational Fluid Dynamics (CFD) models are capable of reproducing the hydrodynamics provided they have sufficient resolution. However, current CFD models cannot predict the droplet size distribution. For this reason, we used a suite of programs to understand jet hydrodynamics, the droplet size distribution, and the movement of oil droplets within the jet/plume. The developed models were calibrated to experimental data of oil jet released underwater in the BIO tank. Based on the properties of the jet (mass flow rate 3.8 L/min through a 2.4 mm orifice), the regime of the jet is atomization, which indicates that the jet would break into small droplets. The models VDROP-J and JETLAG were used to predict the streamwise centerline velocity and the holdup (volume of oil divided by the total volume of fluids in a control volume) along the centerline of the plume, where both models were in agreement. This implies that VDROP-J is adequate to predict the average droplet size distribution in the plume. In the absence of dispersant, the model VDROP-J predicted oil DSD that is very close to that measured by the LISST instrument. However, In the presence of dispersant premixed with the oil, the VDROP-J model captured the overall trend of the DSD, but could not capture the peak in droplet concentration observed at 5 µm. The observed peak is most likely due to tip-streaming (when at high DORs, oil droplets shed filaments from their edges resulting in smaller droplets), and VDROP-J does not have such a module at this time but is considered for future development.

The computational fluid dynamics (CFD) program Fluent (www.ansys.com) was used to model the hydrodynamics of the horizontal jet experiments. The standard $k-\varepsilon$ model was used to model turbulence, and the Volume of Fluid (VOF) was used to model the two phases (oil and water). The profiles of the holdup (ratio of oil volume to total volume), velocity magnitude, eddy diffusivity and turbulent dissipation rate were presented. Findings indicate that the holdup drops sharply with distance from the source to a few percent within 0.50 m from the source, suggesting the occurrence of water entrainment into the plume. A



ED_001324_00000913-00094

significant reduction in the energy dissipation rate was also observed, by orders of magnitude along the centerline, starting from $10^4$ watt/kg to $10^{-4}$ watt/kg. Both holdup and energy dissipation values have important consequences on oil droplet breakup and coalescence. The plume exhibited a core of high velocity and high mixing, while the edge of the plume had more or less violent conditions, which is probably due to the entrained water squishing the edges of the plume. The velocity and eddy diffusivity are needed to predict the movement of individual oil droplets. The shape of the plume was circular near the orifice, but became oblate horizontally at a centerline distance of 2.0 m, which is due to both the buoyancy of the whole plume and its inertia. This suggests that the narrow width of the tank (0.60 m) did not affect the jet hydrodynamics (otherwise the jet would be elongated in the vertical). The width of the tank had an effect on the jet dynamics only near the surface as the plume became elongated along the tank near the surface.

The CFD approach has its limitations as it smooths out the edge of the oil jet/plume, and thus does not allow for the formation of large eddies around the plume. Here, large eddy simulations (LES) were used to capture the large eddies where the movement of individual oil droplets employed a lagrangian approach. Water velocity and the eddy diffusivity were used to transport oil droplets, and the effect of individual oil droplet buoyancy and inertia were accounted for. Accounting for the inertia of oil droplets has not been done previously in the oil spill literature. Neglecting the inertia of the droplets results in overestimates of their rise rate as the inertia from a horizontal jet tends to propel the droplet more horizontally, and thus their rise gets delayed also by turbulent mixing. Results suggest that oil droplets with a diameter less than 100 µm would mix uniformly in the plume, while those close to 500 µm would tend to be above the centerline of the plume. This indicates that, when measuring the droplet size distribution using the LISST, the placement of the LISST would not affect the reading of droplets that are less than 100 microns. But the LISST needs to be placed judicially to capture particles that are 300 to 500 µm, otherwise LISST placement below the centerline would underestimate the actual droplets in that range. In contrast, LISST placement above the centerline does not allow for determining that the concentration values represent the whole cross section of the plume.



ED_001324_00000913-00095

### A.3.8 Weber Number Scaling Numerical Plume Modeling

Refer to Appendix H for detailed summary of the Weber Number Scaling numerical modeling component. During the Deepwater Horizon oil spill, modeling activities for predicting oil droplet size distribution formed in subsea oil blowouts was critical given their direct influence on the fate and transport of oil in the marine environment. The scientific community's knowledge on droplet size distributions and our capability to predict the distributions are still limited. A recent and promising approach for predicting DSD is the Modified Weber Number approach developed by SINTEF. Thus far, this method has been based on experimental results, validated by a light crude oil (Oseberg Blend crude oil). Here, this approach is validated over a range of oil types (IFO 120 and ANS) using a series of experiments conducted with a subsurface release of oil within the DFO horizontal flow tank.

Based on the measured droplet sizes obtained from the tank experiments, corresponding median droplet diameters ($d_{50}$) and the relative droplet size ($d_{50}/D$) were calculated, where D is the nozzle diameter. Accordingly, the relations between $d_{50}/D$ and modified Weber number, Reynolds number, and oil concentration were quantified. With regression analyses, the empirical coefficients for the prediction of droplets size distribution based on the modified Weber number were determined for a certain type of oil (e.g., IFO 120 and ANS). The results indicated that chemical dispersants play an important role in reducing the droplet size of ANS in both cold and warm temperatures. The effectiveness of dispersant in reducing droplet size is higher for ANS compared to IFO 120. There may be thresholds for the dose of chemical dispersant to some oils (e.g., IFO 120) but further data analyses are needed to confirm this. There may also be over dose of dispersant to some oils (e.g., ANS) when the DOR is high, eventually affecting the droplet size distribution. Furthermore, the data indicate that the distributions of the data with $d/d_{50} <= 1$ and $d/d_{50} > 1$ are significantly varied. Therefore, a two-step Rosin-Rammler approach was introduced to more accurately predict the droplet size distribution. The regression coefficients for the two-step Rosin-Rammler are higher compared to the single step in most cases (Appendix H), indicating the advantage of the proposed two-step Rosin-Rammler approach. It should also be noted that the measured



ED_001324_00000913-00096

interfacial tension (IFT) for the IFO 120 and ANS with different DORs appear to be significantly different compared to the measured results from SINTEF for the modified Weber number approach, possibly due to the characteristics of different oils.



ED_001324_00000913-00097

# Task B.1 Introduction & Relevance

BSEE's *Remote Sensing & Surveillance of Oil Spills* broad agency announcement that funded this work states that "In remote sensing, a sensor other than human vision or conventional photography is used to detect or map oil spills." Thus, although certain remote sensing of oil spills is traditionally linked to detection of oil on the sea surface from above, the scope of the technology can be extended to include the detection of oil in the deep-sea and/or under-the-ice conditions using various sensors, as responders cannot use vision within the water column. As demonstrated during the 2010 Gulf of Mexico Deepwater Horizon (DWH) oil spill, oil detection by fluorescence can enable responders to discern trajectory of plumes and assess effectiveness of dispersant countermeasures (ACT, 2008; Joint Analysis Group Report, 2010). The information gained from such technologies was used to track oil in the water column and inform response strategies to protect natural resources potentially at risk; thus supporting both Net Environmental Benefit Analyses (NEBA) and Natural Resource Damage Assessments (NRDA). To advance the application of this methodology, this project evaluated fluorescence characteristics of various oils with and without dispersants to aid in the selection and refinement of *in situ* sensors for use in oil spill response operations.

The overall objective of this work was to translate oil fluorescence R&D into operational tools for oil spill response. Tabulating information on the optimum fluorescence wavelengths for oil detection as a function of oil type and DOR assists responders selecting sensors and establishing Best Practices for rapid decision making during spill response. The results of this project are timely and can be used in conjunction with the National Response Team (NRT) guidance document, Environmental Monitoring for Atypical Dispersant Operations: Including Guidance for Subsea Application and Prolonged Surface Application, for incident-specific decisions concerning monitoring subsea dispersant use (www.nrt.org). It specifically calls upon using oil-specific submersible fluorometers with laboratory and on-board ship analyses using fixed wavelength and scanning spectrofluorometers to enable improvements to monitoring sampling during dispersant application. Findings from this project provide additional scientific

information in support of implementing guidance recommendations.

*Fluorescence characteristics* - All fluorophores (molecules that fluoresce) have characteristic wavelengths for maximum absorption of light and characteristic wavelengths at which they emit light as fluorescence. Absorption and fluorescence can occur at either narrow or wide wavelength ranges depending on the chemistry and complexity of the fluorophores. A variety of naturally occurring fluorescent compounds occur in the ocean, from ones with narrow wavelength ranges with sharp fluorescence peak maxima (pigments, proteins) to complex compounds with wide diffuse peaks over long wavelength ranges, such as the ubiquitous Colored Dissolved Organic Matter (CDOM) or petroleum oils.

Fluorescence characteristics of complex mixtures can overlap if structurally similar compounds are shared. Such is the case with CDOM and the aromatic fraction of crude oils. Both are comprised of a variety of organic molecules and both exhibit complex, three-dimensional EEM spectra. In general, crude oils have a broad excitation peak centered in the ultraviolet spectrum (< 300 nm) and two emission peaks, one centered in the ultraviolet spectrum around 340 nm and a much larger and broader peak in the visible around 445 nm (Bugden et al., 2008). These peaks result from the single ring benzene derivatives and the "polynuclear aromatic" fraction that are particularly susceptible to UV excitation wavelengths. EEMs exhibit distinct fingerprints for different oils as illustrated by previous studies (Bugden et al., 2008; Kepkay et al., 2008).

*DWH in situ oil fluorescence* - Deployment of submersible fluorometers during the DWH oil spill response illustrated the utility of this forensic tool that enabled large-scale monitoring of oil concentrations to a depth of approximately 1600 m. Co-deployment of the fluorometers alongside other response sensors [Conductivity-Temperature-Depth (CTD), Dissolved Oxygen (DO), Laser *In-Situ* Scattering and Transmissometry (LISST)] from multiple platforms (e.g. profilers) with real-time capabilities improved our understanding of the processes influencing the fate and behavior of the oil in the presence and absence of chemical dispersants. Added to this, extensive water column sampling also involved discrete sample collection for oil particle concentration and size, Total Petroleum Hydrocarbons (TPH), Volatile Organic Carbon (VOC)



ED_001324_00000913-00099

and other physical, chemical, biological factors. To date, the in-depth reviews by the Joint Analysis Group (JAG) charged with data analysis have found that of all the variables measured, the most highly correlated in the subsea plume are *in situ* DO and oil fluorescence intensity (Joint Analysis Group Report, 2010). Such a correlation is not unexpected as laboratory tests show that enhanced oxygen utilization can result from microbial respiration in the presence of oil compounds (Venosa et al., 2002b). Beyond the underlying biochemical mechanisms however, likelihood of correlation is increased based on the fact that variables measured *in situ* at high sampling rates are better to capture plume heterogeneity. Hence, the utility of *in situ* fluorescence as a tool was ascertained early in the response due to such correlations, the high temporal and spatial resolution provided by the sensors, and also the advantages afforded by real-time capability compared to discrete analyses.

However, the multitude of submersible fluorometers used in the DWH response called to attention differences in the sensitivity and analytical capability of the instruments used due to differences in configuration of excitation and emission wavelengths, methods of calibration, sensitivity, and correlation to oil concentration (Figure 40, Table7). Many are not customized to capture oil fluorescence peak maxima, rather only a fraction of the signal (Fuller et al., 2003; Conmy et al., 2004 Conmy et al., 2014b). Furthermore, the ability of any fluorescence sensor (laboratory or field submersible) to detect oil is a function of (1) how well the sensor matches the excitation and emission wavelengths of the oil (including bandwidth of the wavelength filters or bandpasses from gratings, (2) the power of the light source, and (3) the sensitivity of the detector.

When tracking in the subsea became necessary early in the response, fluorometers used for detection of CDOM (i.e., WET Labs ECO series) were deployed on the vertical profilers as they were widely available, were capable of full ocean depth deployment and had been previously shown to detect oil in water (Wet Labs, Inc. website, www.wetlabs.com). These sensors typically have light sources that excite at wavelengths slightly longer than peak absorption by hydrocarbons and detect emission in the visible. They employ filters centered on excitation (Ex) and emission (Em) wavelengths at 370 and 460 nm ($ExEm_{370/460nm}$). Although the center



ED_001324_00000913-00100

wavelength of the filters does not capture the peak of the oil fluorescence signal, the wide bandwidth of the emission filters (120 nm Full Width at Half Max) and the broad nature of the fluorescence peaks means that CDOM sensors are capable of detecting a large portion of the visible fluorescence signal. CDOM fluorometers were used to detect oil during the response in part because of their accessibility, but also because these sensors capture some portion of the oil fluorescence peak that occurs at the longer UV wavelengths where CDOM peaks also exist.

To quell questions regarding the ability of the ECO CDOM fluorometer to detect oil in the subsea plume, calibration tests were conducted at Louisiana State University (LSU) using Mississippi Canyon 252 (MC252) source oil. They provided a means to convert raw fluorescence data to Quinine Sulfate Dihydrate Equivalents (QSDE, the standard typically used for CDOM) to ppm of oil (JAG report, 2010). The calibrations were conducted in flasks on orbital shakers at 90 revolutions per minute (rpm), where oil concentrations ranged between 1-50 ppm. Dispersant (Corexit 9500) was added at a DOR of 1:2.5 and 1:25. The response of the fluorometer was linear with respect to oil but varied as a function of DOR, with a quenching of fluorescence in the presence of more dispersant per unit oil. Results of this test indicated that the ECO sensor was a sufficient proxy for oil concentrations greater than 1 ppm (NOAA, 2010). However, as the response continued and after the well was capped, oil concentrations in the subsea plume decreased as well as the magnitude of the fluorescence anomaly due to dilution and degradation of the oil, particularly at further distances from the wellhead. Concern was raised that a fluorometer with higher sensitivity for oil (one with a hydrocarbon-specific configuration) was needed. At that time, Chelsea UV Aquatrackas ($ExEm_{239/360nm}$) were deployed to track the plume in the far field of the response geographic region with the expectation (and subsequent confirmation) that it would detect fluorescence signal at lower oil concentrations.



ED_001324_00000913-00101

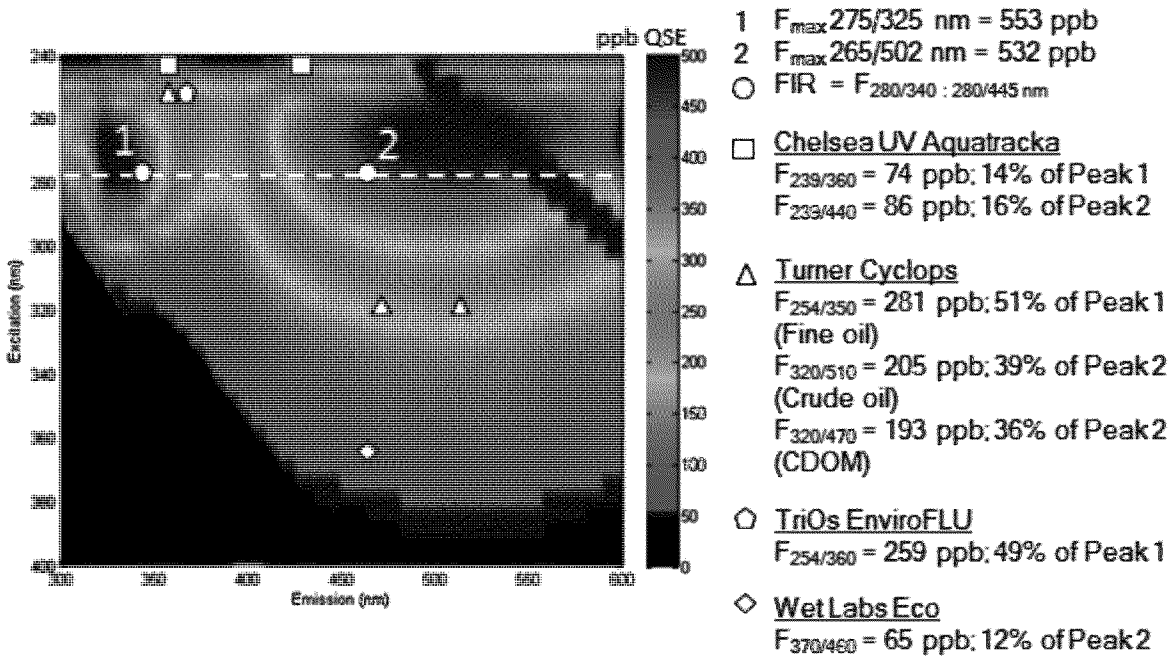


**Figure 40. Fluorescence peaks of S. Louisiana sweet crude dispersed in ppb QSE (Quinine Sulfate Equivalents). Symbols represent Fluorescence Intensity Ratio (FIR) locations and the Center Wavelength (CWL) reported by sensor manufacturers. Bandwidths (BW) are not shown.**



ED_001324_00000913-00102

**Table 7. Sensor specifications as listed from manufacturers. Wavelengths listed as Center Wavelengths (CWL) with Full Width at Half Max (FWHM) and Bandpass (BP). Standards used are QS (Quinine Sulfate Dihydrate), NDD Salt (Napthalene Disulfonic Disodium) and PTSA Salt (Pyrenetetrasulfonic Acid Tetrasodium) (From Conmy et al., 2014b).**

| Manufacturer | Instrument | Light source | Excitation λ (nm) | Emission λ (nm) | Detector | Dynamic Range |
|---|---|---|---|---|---|---|
| Chelsea Technologies Group | UV AQUAtracka | Xenon lamp | 239 CWL | 360 CWL | PMT | 0.001- 10 μg/L Carbazole |
| | UV AQUAtracka | Xenon lamp | 239 CWL | 440 CWL | PMT | 0.001 - 10 μg/L Perylene |
| Seapoint Sensors | SUVF | LED | 370, 12 FWHM | 440, 40 FWHM | Photodiode | 0.1 - 1500 μg/L QS |
| TriOS, GmbH | EnviroFLU-HC, DS | Xenon lamp | 254, 25 FWHM | 360, 50 FWHM | Photodiode | 0 - 5000 ppb Phenanthren |
| Turner Designs | Cyclops (Fine oil) | LED | 254, 40 nm BP | 350, 50 nm BP | Photodiode | 0 - 10,000 ppb NDD Salt |
| | Cyclops (Crude oil) | LED | 320, 130 nm BP | 510, 180 nm BP | Photodiode | 0 - 2700 ppb PTSA Salt |
| | Cyclops (CDOM) | LED | 320, 130 nm BP | 470, 60 nm BP | Photodiode | 0 - 2500 ppb QS |
| WetLabs | WetStar | LED | 370, 10 FWHM | 460, 120 FWHM | Photodiode | 0.100 - 1000 ppb QS |
| | ECO-FLU, triplet, puck | LED | 370, 10 FWHM | 460, 120 FWHM | Photodiode | 0.01 - 500 ppb QS |

*Post-DWH response sensor tank testing* -To address persisting uncertainties regarding sensor performance in the subsea, a team of scientists conducted experiments in May 2011 to study the dynamic range, sensitivity, and response *of in situ* fluorometers to changing excitation or emission properties of fresh and weathered MC252 oil (NOAA Science Box Award, PI: Michelle Wood; Co-PI's from EPA, NOAA, University of South Florida). The experiment was conducted within the flow-through flume tank at the BIO in Dartmouth, Nova Scotia, taking into consideration environmental factors such as wave energy and ocean currents. Experiments included the stepwise addition of oil and dispersant (DOR of 1:25; 0.3 - 12 ppm of MC252 SLC oil) to the flume tank while collecting *in situ* fluorescence and droplet-size distribution data, as well as coincident discrete samples for chemistry and EEM analyses. The flume tank was operated in static mode and each addition of oil and dispersant was allowed to homogenize prior to collecting discrete samples and coincident sensor measurements to calculate the least linear squares regressions. Results indicated that all sensors tested were responsive to changes in MC252 oil concentration regardless of wavelength configuration. Linear response of the WET



ED_001324_00000913-00103

Labs ECO, Turner Designs Cyclops and the Chelsea Technologies Group AQUAtrackas sensors as a function of oil concentration was observed, where lowest concentrations were not below the detection limit of any sensor tested (Conmy et al., 2014a). Results demonstrated that all sensors exhibited a wide dynamic range of detection for MC 252 oil and were capable of detecting oil at the lowest concentration (approximately 300 ppb oil), which is significantly lower than the LSU calibration study (1 ppm) and a common misconception during the response (Conmy et al., 2014a). Differences in the detection limit between the studies may be explained by differences in the design, scale and the amount of physical dispersion of the tests, where the tank can provide mixing energies similar to those found in the field.

The 2011 study findings answered critical questions about sensor performance to detecting MC252 oil. However, the experiment highlighted the need for future studies to evaluate sensor performance using a variety of DORs and for multiple oil types. Evident from the DWH spill and post-spill research was that further R&D is needed to transfer knowledge gained through laboratory 3-D Excitation Emission Matrix (EEM) Spectroscopy into practical information for fluorescence tools used during spill response. Fluorescent properties are oil specific and investigating variations in EEMs as function of oil type and dispersant-to-oil ratios better prepares the community in identifying sensors for response options. To that end, the objectives of this project were to:

I. Generate a comprehensive EEMs database, building upon existing data at the Department of Fisheries and Oceans Canada, to provide fluorescence peak information as a function of oil type, weathering state, concentration and Dispersant-to-Oil Ratios (DORs).
II. Critically examine the database using advanced statistical methods and models to identify wavelengths best suited for oil monitoring during dispersant application and degradation.
III. Conduct flume tank experiments to determine submersible sensors capable of providing data comparable to scanning and/or fixed wavelength laboratory fluorometers for rapid deployment during response efforts.

Through this project, a comprehensive EEMs library database was generated covering a wide variety of oils from light to heavy fuel and crude oils and diluted bitumen. Varying DORs (1:20, 1:100, 1:200, 0) and oil concentrations were evaluated as the presence of dispersant alters EEM fingerprints. EEMs were subjected to advanced statistical analyses and models to identify wavelengths best suited for oil monitoring during dispersant application and subsequent tracking. Fluorescence is a non-destructive characterization tool that is routinely used to examine complex organic mixtures (foods, wine, medical compounds, aquatic organic matter, oils). Unlike single compound solutions, they exhibit broad, diffuse peaks that result from overlapping smaller peaks with similar chemistry. Although EEMs can be a substantial source of information on chemical composition and variability amongst samples, the high-dimensionality (intensity by emission by excitation) and nonlinearity of the data equates to difficulties in data interpretation and extraction of practical information as a characterization tool (Bieroza et al., 2010). Therefore, it is difficult to determine which underlying chemical components are responsible for which portion of the fluorescence fingerprint. Combining standard techniques for EEM analysis such as assessment of particular fluorescence peak features including peak height and wavelength position via 'peak picking' with Parallel Factor Analysis (PARAFAC) modeling results in a more comprehensive understanding of the chemical constituents. The use of advanced multivariate analyses such as PARAFAC has gained popularity as an effective means to deconvolve complex, broad peaks into their underlying smaller components (Stedmon et al., 2003; Boehme et al., 2004; Christensen et al., 2005; Stedmon and Bro, 2008). Here, we processed EEMs data with scripts in the N-way toolbox for Matlab (Andersen and Bro, 2000) and SOLO software (Eigenvector, Inc) and used the algorithms to isolate wavelengths to best characterize an oil type. An excellent review of these chemometric techniques and applications is provided in Bieroza et al., 2010. This approach will allow for comparing oil in water mixtures for similarities and contrasting features.

Results were evaluated for the Fluorescence Intensity Ratio (FIR) technique (Bugden et al. 2008; Kepkay et al. 2008). The latter calculates the ratio at $ExEm_{280/340nm}$ to $ExEm_{280/445nm}$ as an



ED_001324_00000913-00105

indicator of oil dispersion. Previous studies at DFO COOGER have shown that dispersed oil fluoresces over two peaks centered on emission wavelengths of 340 nm and 445 nm, at excitation wavelength 280 nm, and that chemical dispersion enhances the emission intensity at 445 nm (Bugden et al. 2008; Kepkay et al. 2008). Postulated is that the fluorescence intensity at $ExEm_{280/340nm}$ represents the dispersion of lower molecular weight aromatic hydrocarbons, while intensity at $ExEm_{280/445nm}$ corresponds to higher molecular weight aromatic compounds.

Finally our work addresses the disconnect that exists between fluorescence research conducted in laboratories and the collection of fluorescence data from submersible sensors. By conducting laboratory-based and tank-based experiments on the same oil type and DOR, comparisons between EEMs can be made across scales. This helps to determine how well the *in situ* sensors are aligned in detecting dispersed oil.



ED_001324_00000913-00106

# Task B.2 Experimental Methods

B.2.1 Sample Preparation - Twenty-five oil samples from the DFO and EPA stockpiles (covering a wide range of viscosity and oil type) were used for spectrofluorometric testing, where oil characteristics were tabulated for the test oils based on an extensive literature search (Table 8; Supplemental Material A). All glassware used in this study was cleaned to ensure highest analytical integrity including solvent rinsing, deionized water rinsing and baking in a muffle furnace at 450˚C where appropriate. Samples were stored in 125mL amber glass bottles with PTFE-lined caps (Figure 41).

B.2.2 Artificial Seawater Protocol - Artificial seawater was used for DOR mixing to avoid interference of fluorophores found in natural seawater with oil fluorescence signal. Fresh artificial seawater was made to salinity of 28 ppt and was prepared in 1 L quantity at the beginning of each experiment by adding Tropic Marin® salts (Appendix A) to 1 L ultrapure water dispensed from a Millipore Milli-Q unit (≤ 4 ppb DOM) into a 1.5 L glass beaker, covering the beaker with aluminum foil, and stirring with a magnetic stir-bar on electric stir plate for 20 minutes at room temperature (~24°C).

B.2.3 Dispersed Oil in Seawater Protocol - A series of dispersed-oil-in-seawater experiments were performed using baffled trypsinizing flasks (baffled flasks) with artificial seawater, MC252 oil and Corexit 9500 chemical dispersant (Venosa et al., 2002a). Four petroleum oil / dispersant solutions were prepared for each oil type at the following DORs: 0, 1:20, 1:100, and 1:200. Oil was pipetted into an 8.6 ml amber vial, followed by addition of the appropriate amount of Corexit 9500 chemical dispersant into the vial. Teflon-lined capped vials were shaken by hand for 60 seconds and 10 µL of dispersant / oil mixture was pipetted (Eppendorf positive displacement micropipettes, 1-20 µL) into 100 mL artificial seawater contained in each of three replicate flasks. Flasks were covered with parafilm and placed on a New Brunswick Scientific Innova 2100 platform shaker (orbit = 1.9 cm) for 12 minutes at 200 rpm. Approximately 3.5mL of the resulting dispersed-oil-in-seawater was immediately dispensed through a spigot near the bottom of each flask into three 4.0-mL UV-grade quartz cuvettes, which were immediately



ED_001324_00000913-00107

covered with Teflon stoppers to prevent evasion of volatile components during fluorescence analyses (Figure 42). After removal of spectrophotometric samples, additional volumes of sample were removed from the baffled flasks for extraction of total petroleum hydrocarbons (TPH) by dimethylene chloride (DCM). TPH analysis follows the same Gas Chromatography-Mass Spectrometry (GC-MS) method as in Task A of this project.

B.2.4 Spectrophotometric Analysis - A Horiba Scientific AquaLog spectrofluorometer was used to analyze the 25 oil types with varying DOR. A series of analyses were initially performed while varying the instrument's settings (excitation and emission increments, gain setting, integration time) in order to determine optimal settings for the entire experimental protocol. Excitation-Emission Matrices (EEMs) were generated using the following instrument parameters: 200 – 800 nm excitation (3 nm increments), 249 – 828 nm emission range (CCD detector at 534 nm 8 pixel increments), medium gain setting and integration time of 0.1 sec. A quinine sulfate dihydrate dilution series was created consisting of: 0.5N $H_2SO_4$ solvent; 100 ppm 1° (primary stock) solution; 100 ppb 2° (secondary stock) solution; 1,3,5,10 and 20ppb quinine sulfate solutions. Dilutions were analyzed for fluorescence and used for cross-calibration with instrument software built-in quinine sulfate tool to convert results into Quinine Sulfate Equivalents (QSE) and demonstrate linearity of fluorescence in a dilution series. All data processing and spectral corrections follow the manufacturer's manual. Dilution series with oil concentrations between 1 – 500 ppb were also generated to determine lower detection limits for oils. EEMs are presented in Raman Units (RU).



ED_001324_00000913-00108

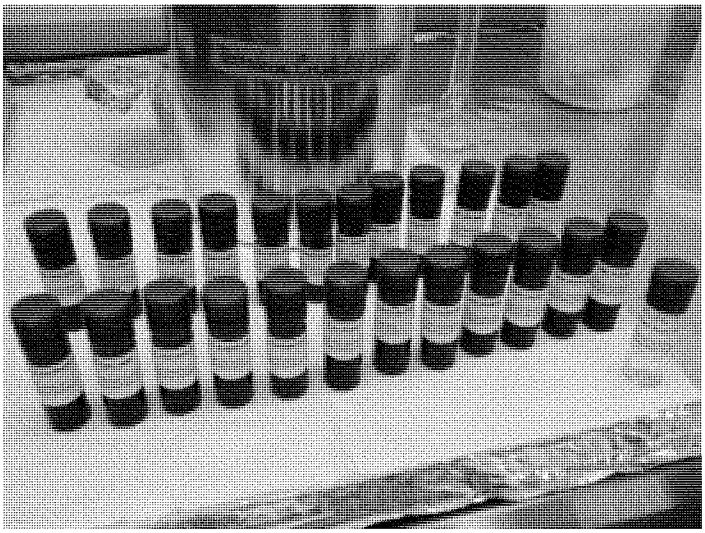

**Figure 41. Twenty-five oil samples stored in glass bottles.**



ED_001324_00000913-00109

Table 8. List of oil samples used for EEM analyses. Oils separated by API (American Petroleum Institute) gravity.

| Light (API >31.1°) | Medium (API 22.3 – 31.1°) | Heavy (API <22.3°) |
|---|---|---|
| Arabian Light (32.2°) | Alaska North Slope (29.7°) | Access Western Blend Dilbit (21.3°) |
| Brent (38.2°) | Alaskan North Slope (10% weathered) | Belridge Heavy (13.6°) |
| Federated (39.4°) | Heidrun (28.6°) | Cold Lake Dilbit (21.5°) |
| Gullfaks (32.7°) | Lago (25.0°) | Hondo (19.5°) |
| Hibernia (35.6°) | Mesa (30.3°) | IFO 40 (21.9°) |
| MC252—Discoverer Enterprise (37.2°) | Sea Rose (29.8°) | IFO 120 (18.4°) |
| MC252—generic (35.2°) | Vasconia (26.3°) | IFO 180 (14.1°) |
| Scotian Shelf Condensate (53.2°) | | IFO 300 |
| Terra Nova (33.8°) | | Santa Clara(22.1°) |



ED_001324_00000913-00110

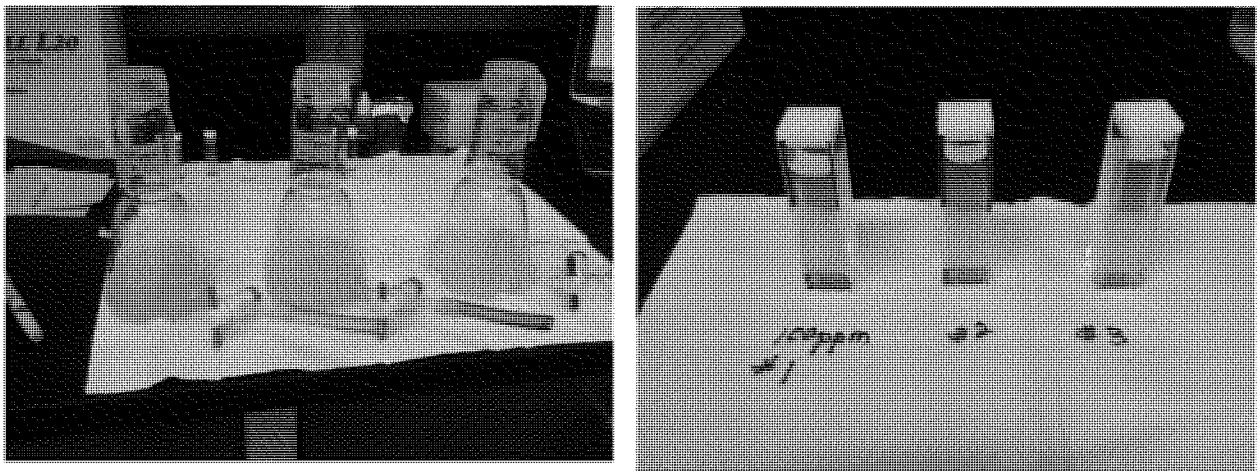

**Figure 42. Trypsinizing baffled flasks containing dispersed oil in artificial seawater (top) and corresponding samples removed from each flask, ready for spectrofluorometric analysis.**

# Task B.3 Results & Discussion

## B.3.1 Oil Fluorescence Properties

Four characteristic excitation/emission (Ex/Em) peak locations were identified: $F_{max1}$ – $F_{max4}$ (Figure 43) for all 25 oil types at four DORs (Figure 43). The highest intensity peak ($F_{max1}$) occurred, without exception, at Ex 221-239 nm/Em 335-344 nm and was paired with a blue-shifted, lower intensity peak ($F_{max2}$) at Ex 215-221 nm/Em 285-308 nm in all oil types. A third broad, low-intensity peak ($F_{max3}$) was observed at Ex 215-305 nm/Em 418-571 nm, to varying degrees across oil types, corresponding with oil categories determined by API gravity (Table 8). Light crude oils exhibited $F_{max3}$ fluorescence at all DORs with the exception of Scotian Shelf



ED_001324_00000913-00111

Condensate. Of note is that Scotian Shelf Condensate appeared physically unlike any of the other light oils: clear in color with apparent very low viscosity. Since viscosity is largely determined by the size and relative weight of component hydrocarbons (Fingas 2011), fewer complex fluorophores would likely be present in this oil type. Fluorescence in the $F_{max3}$ region was identified at all DORs in only one medium weight oil (Heidrun), and was not present at any DOR in one medium oil (Vasconia). Two medium-weight oils emitted measurable fluorescence in the $F_{max3}$ region only with full dispersion (Lago and Mesa), while Sea Rose showed fluorescence at DORs 1:100 and 1:20. One medium weight oil, Alaska North Slope (both fresh and 10% weathered), exhibited unusual $F_{max3}$ behavior, with measureable fluorescence at DOR 0, 1:100 and 1:20, but not at DOR 1:200. Finally, for the heavy weight oils, $F_{max3}$ was almost completely absent at all DORs, with the exception of fluorescence at DOR 1:20 for Cold Lake Dilbit (Diluted Bitumen) and IFO 40, and across all DORs for one anomalous member of this group—Access Western Blend Dilbit. Dilbit is a mixture of bitumen—essentially a heavy crude oil with API gravity < 10.0°—and a diluent—either a light condensate or naptha (Priaro 2016). The combination of characteristics from both oil types may account for the unusual $F_{max3}$ fluorescence observed in this oil type. Additionally, Intermediate Fuel Oils (IFOs) are not true crude oils, but marine fuels consisting of a mixture of post-refinery heavy residual oil and refined diesel fuel, which may also help to explain the appearance of $F_{max3}$ fluorescence in IFO 40. Clearly, the presence of fluorescence in the $F_{max3}$ region, especially at DOR 1:20, appears to be related to API gravity, and thus to density as well as kinematic viscosity since API gravity = (141.5/Specific Gravity) – 131.5 (Fingas, 2011). The absence of $F_{max3}$ region fluorescence in heavy weight oils may be due to retention of energy within the large, complex hydrocarbons which make up the highest density oils. Additionally, the appearance of fluorescence in the $F_{max3}$ region at highest DORs for the medium weight oils (Lago, Mesa, and Sea Rose) suggests that smaller droplet sizes were created via the dispersion which could lead to a decrease in reabsorption of fluorescence within the oil – water mixture. A fourth region of broad, low-intensity fluorescence ($F_{max4}$) was identified at Ex 269-291 nm/Em 326-353 nm for all oil types at all DORs. $F_{max1}$ and $F_{max4}$ oil-in-water fluorescence regions appear to be analogous to the characteristic colored dissolved organic matter (CDOM) fluorescence regions '$A_C$' at Ex 260/Em

400-460 and 'C' at Ex 320-365/Em 420-470 (Coble, 2014).

In addition to maximum intensity for each fluorescence peak (in RU), full width at half maximum (FWHM) was also recorded. Further, fluorescence intensity at Ex/Em 281/340 and 281/456 nm was recorded to enable calculation of the FIR for all samples. Optimum settings for signal collection on the HORIBA AquaLog necessitated excitation at 3 nm intervals, which accounts for the 1 nm discrepancy from the published FIR wavelengths (Bugden, et al. 2008). Fluorescence intensity at the specified Ex/Em wavelength settings of five off-the-shelf *in situ* fluorometers (Conmy et al., 2014a & b), which were all employed in the response to the DWH spill, was recorded. Those wavelengths were also adjusted slightly to compensate for signal collection intervals on the HORIBA AquaLog. Selected results are presented in Table 9 along with results of chemical analyses, and complete fluorescence results are included as a Supplemental Table A. EEM contour 'fingerprint' plots for all oils, which characterize each oil type and illustrate the effect of dispersant on the fluorescence properties, are presented in Appendix F. The ability to identify oil source can be useful in the prevention and abatement of oil spill pollution. To that end, efforts to determine characteristic fluorescence fingerprints have existed since the 1970s (Frank, 1978) and have received renewed attention with the advent of improved fluorescence detection systems (Bugden, 2008).

Intensity of $F_{max1}$ was consistently strong across oil types, with no ambiguity in peak location. The observed Ex/Em range of significant fluorescence intensity was fairly narrow with FWHM of only 37-50 nm, and little to no change in peak location with increasing DOR. However, Six of the nine light oil types, but just one of the seven medium oil types and one of the nine heavy oil types[1] displayed this slight increase (approximately 4.5 nm) in FWHM with maximum dispersion (DOR 1:20). One medium weight oil (Lago) and one heavy oil (Access Western Blend Dilbit) showed the same slight increase in FWHM at both DORs 1:100 and 1:20. The impact of applying the Inner Filter Effect correction tool (IFE) to fluorescence intensity was also calculated for $F_{max1}$. This correction utilizes the measured absorbance of the sample to correct for fluorescence emitted by fluorophores within the sample, but re-absorbed within the sample itself. Of note is

[1] Increase of approximately 4.5 nm in FWHM in $F_{max1}$ seen in light oils Arabian Light, Brent, Federated, Gullfaks, Hibernia, and Terra Nova; in medium oil Mesa; and in heavy oil IFO 120 at DOR 1:20.



ED_001324_00000913-00113

that application of the IFE resulted in only a small magnification of the fluorescence signal at DORs 0, 1:200 and 1:100 for all oil types; however, there was a clear delineation between two categories of oil types at DOR 1:20: Oil Type I, with IFE effect > 2.5 and Oil Type II, with IFE effect < 2.5 (Table 9). This appears to be due to the increase in optical density, and thus absorbance, possibly caused by interaction between Corexit 9500 and well dispersed Type I oils. Photographs of four representative pre-analysis samples, along with the resulting EEMs of oil type are shown in Figure 44 to illustrate the difference in fluorescence between the types regardless of being a light, medium or heavy crude oil.

Due to variation from laboratory to laboratory, and even differences in instrument to instrument performance from the same manufacturer, it is necessary to convert fluorescence intensity "raw counts" to a standardized unit for useful reporting purposes. Traditionally, the fluorescence community has utilized a dilution series of quinine sulfate dihydrate in weak acid to convert instrument output to Quinine Sulfate Equivalents (QSE) (Coble, 1996). However, in recent years the alternate method of reporting in Raman Units (RU) has gained favor (Murphy et al., 2010). Due to inherent properties of water molecules, the Raman scatter peak is a reliable feature which can be used through collecting a scan of ultra-pure water at the beginning of each day, and then using the ratio of raw counts to the area under the curve of the Raman peak (approximately 381-426 nm) to convert fluorescence to RU. As the Quinine Sulfate SRM is no longer available from NIST (National Institute of Standards and Technology), we have reported results in RU and offer a conversion factor to QSE using the highest quality quinine sulfate dihydrate readily available.

Overall, $F_{max1}$ intensity ranged from a minimum of 39.58 RU (Access Western Blend Dilbit DOR 0) to 3090.23 RU (IFO 120 DOR 1:100). Since all of the Intermediate Fuel Oils and the Scotian Shelf Condensates showed unusual fluorescence profiles which tended to skew the results for the aforementioned reasons (Figures 45 and 46), these will be eliminated from the remaining discussion. $F_{max1}$ intensity within Type I oils ranged from 357.62 RU (Arabian Light DOR 1:200) to 1998.60 RU (MC252 Discoverer Enterprise DOR 1:20), while the range in Type II Oils was the overall low of 39.58 previously mentioned to a high of 1098.90 (Heidrun DOR 1:20).



ED_001324_00000913-00114

While the excitation wavelength of maximum intensity for $F_{max2}$ remained relatively consistent, the emission wavelength varied within, as well as among, oil types. The occurrence of double and triple peaks, as well as minor sub-peaks, within the $F_{max2}$ region was fairly common. It was sometimes difficult to distinguish the $F_{max2}$ peak from the shoulder of a very strong $F_{max1}$ peak, especially at higher DORs. For this reason, determination of the true FWHM was sometimes problematic. For $F_{max2}$ intensity, Type I Oils ranged from 63.95 RU (Brent DOR 1:200) to 437.32 RU (MC252 Discoverer Enterprise DOR 1:20), and Type II Oils ranged from 25.07 RU (Belridge Heavy DOR 0) to 164.07 RU (Heidrun DOR 1:20).

For oil types exhibiting an $F_{max3}$ peak, it was most apparent at the highest DOR (1:20) and some oils exhibited a strong $F_{max3}$ peak across all DORs (e.g., Brent, Federated). However, for those oils the $F_{max3}$ peak at DOR 1:20 was significantly blue shifted (peak moved to lower wavelengths) from the $F_{max3}$ location observed at lower DORs. FWHM of the $F_{max3}$ peak was much greater than that of any other peak (145-283 nm), with the exception of the three lower DORs of Access Western Blend Dilbit (52-56 nm). Identification of highest $F_{max3}$ intensity proved somewhat problematic as it tended to lay within the second order Rayleigh region, a band of high intensity light resulting from scattering by water molecules. The edge of highest intensity could also lie in this region, so determination of the true FWHM was also problematic for many oil types. Traditionally, second order Rayleigh is eliminated by simply masking this region (10-12 nm). Although algorithms have been developed to model the character of fluorescence peaks lying within (Zepp, et al. 2004; Bahram, et al. 2006), assumptions about the linearity of fluorescence must be made, and the true signal behavior cannot be known. For this reason, as our goal was to identify signals which could also be detected by *in situ* instruments, the decision was made to identify the maximum fluorescence intensity lying outside of the second order Rayleigh region rather than to try to interpolate the data.

As previously mentioned, $F_{max3}$ intensity was not always present, and it was observed far more often in Type I Oils with a range of 2.64 RU (Arabian Light DOR 1:200) to 744.69 (MC252 Discoverer Enterprise DOR 1:20). Only four of the Type II Oils exhibited $F_{max3}$ peaks and these ranged from 2.45 RU (Access Western Blend Dilbit DOR 0) to 174.93 RU (Heidrun DOR 1:20).



ED_001324_00000913-00115

As with $F_{max2}$, the $F_{max4}$ region sometimes contained double peaks. Unique spectral shapes for this region were also observed, especially in higher-density oils such as Access Western Blend Dilbit, Belridge Heavy, and Cold Lake Dilbit. FWHM ranged from 27 nm to 73 nm, for all oil types but one. The exception was Access Western Blend Dilbit, with FWHM of 77-110. Intensity at $F_{max4}$ ranged from 33.53 RU (Arabian Light DOR 1:200) to 231.86 RU (MC252 Discoverer Enterprise DOR 1:20) in Type I Oils and from 4.93 RU (Access Western Blend Dilbit DOR 0) to 116.97 RU (Heidrun DOR 1:20) in Type II Oils.

Results of the concentration dilution series showed that the HORIBA AquaLog was consistently capable of detecting dispersed oil in artificial seawater in the three oil types tested (Alaska North Slope, IFO 120, and MC252 Discoverer Enterprise) at all four DORs down to at least 50 ppb. However, detecting dispersed oil below 100 ppb necessitated increasing the integration time to 10 sec. per scan in order to collect sufficient data, which resulted in a total analysis time of approximately 30 minutes for each sample. Since the HORIBA AquaLog scans from high to low wavelengths and much of the fluorescence signal from petroleum resides in the UV region, photobleaching of the sample as well as temperature effects certainly may have impacted these results.



ED_001324_00000913-00116

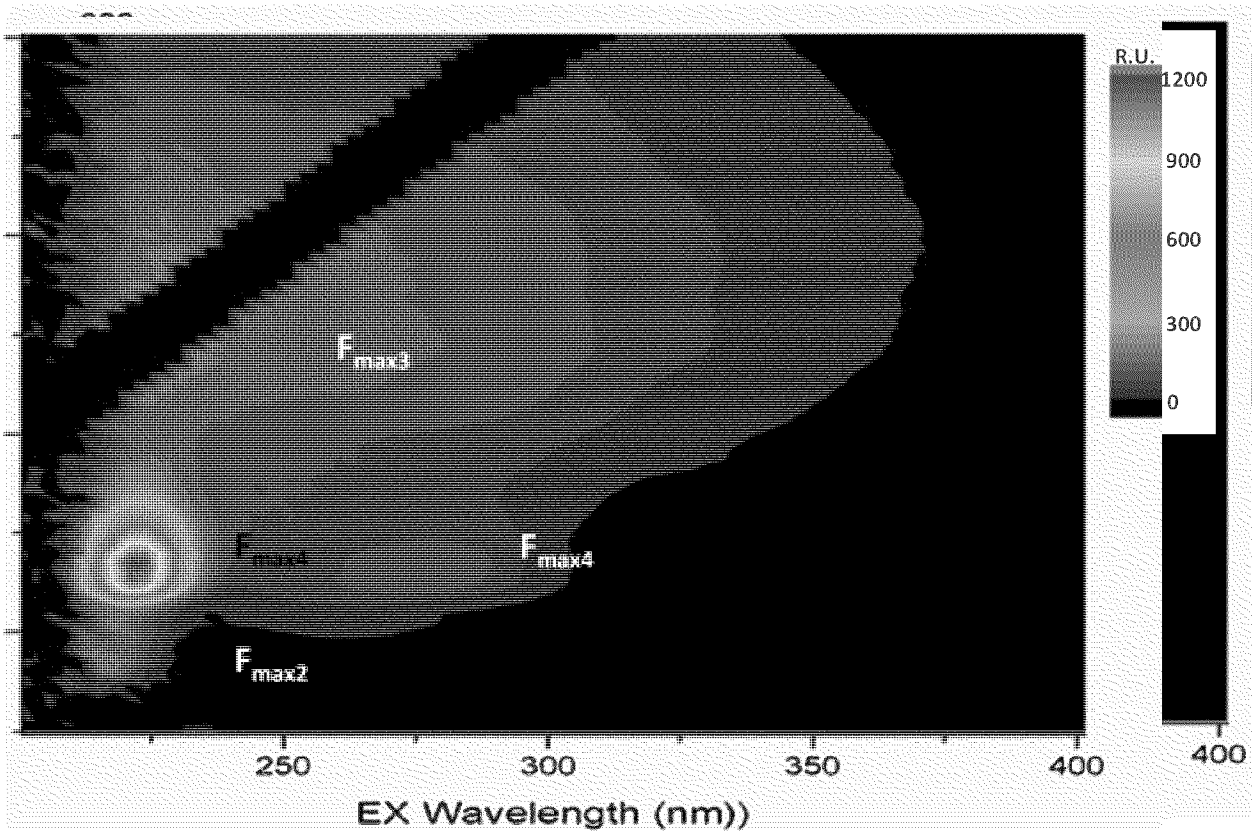


**Figure 43. Alaska North Slope dispersed oil in artificial seawater at DOR 1:20 with locations of $F_{max1}$, $F_{max2}$, $F_{max3}$ and $F_{max4}$ indicated. Note that maximum fluorescence intensity at $F_{max3}$ is mostly obscured by masking of second order Rayleigh scattering.**



ED_001324_00000913-00117

**Table 9. EEM fluorescence and chemical characteristics. Refer to Supplemental Table A for full table.**

| Type I Oils | DOR | $F_{max}$[1] (RU) | IFE | FIR | Alkanes (µg/L) | 2-ring PAHs (µg/L) | 3-ring PAHs (µg/L) | 4-ring PAHs (µg/L) |
|---|---|---|---|---|---|---|---|---|
| Alaska North Slope | 0 | 697.07 | 1.16 | 21.59 | 375 | 145 | 15 | 8 |
| | 1:200 | 715.01 | 1.15 | 35.41 | | | | |
| | 1:100 | 839.60 | 1.32 | 6.59 | | | | |
| | 1:20 | 1171.63 | 3.33 | 0.88 | 3019 | 477 | 89 | 65 |
| Alaska North Slope (10% weathered) | 0 | 812.97 | 1.19 | 21.70 | 545 | 182 | 19 | 14 |
| | 1:200 | 831.70 | 1.21 | 21.70 | | | | |
| | 1:100 | 828.06 | 1.28 | 9.08 | | | | |
| | 1:20 | 1109.51 | 3.01 | 0.91 | 3312 | 499 | 99 | 74 |
| Arabian Light | 0 | 400.42 | 1.18 | 7.29 | 733 | 113 | 11 | 12 |
| | 1:200 | 357.62 | 1.07 | 11.61 | | | | |
| | 1:100 | 426.82 | 1.26 | 2.70 | | | | |
| | 1:20 | 701.75 | 4.19 | 0.39 | 6004 | 571 | 71 | 103 |
| Brent | 0 | 646.18 | 1.15 | 7.59 | 1068 | 162 | 21 | 12 |
| | 1:200 | 660.37 | 1.16 | 6.65 | | | | |
| | 1:100 | 708.16 | 1.37 | 1.97 | | | | |
| | 1:20 | 1098.42 | 3.05 | 0.68 | 5954 | 456 | 97 | 58 |
| Federated | 0 | 574.35 | 1.14 | 3.70 | 1921 | 197 | 41 | 30 |
| | 1:200 | 607.97 | 1.21 | 2.01 | | | | |
| | 1:100 | 645.28 | 1.37 | 0.94 | | | | |
| | 1:20 | 1223.17 | 4.37 | 0.36 | 6501 | 488 | 129 | 87 |
| Gullfaks | 0 | 937.00 | 1.24 | 5.79 | 762 | 326 | 47 | 26 |
| | 1:200 | 934.42 | 1.27 | 5.57 | | | | |
| | 1:100 | 933.08 | 1.35 | 3.24 | | | | |

| | | | | | | | | |
|---|---|---|---|---|---|---|---|---|
| | 1:20 | 1524.21 | 3.73 | 0.71 | 1943 | 642 | 107 | 60 |
| Hibernia | 0 | 938.08 | 1.24 | 6.91 | 2289 | 296 | 39 | 24 |
| | 1:200 | 951.49 | 1.34 | 3.22 | | | | |
| | 1:100 | 978.62 | 1.47 | 1.69 | | | | |
| | 1:20 | 1812.41 | 4.02 | 0.49 | 6095 | 541 | 94 | 59 |
| MC252 (Discoverer Enterprise) | 0 | 998.50 | 1.27 | 5.01 | 1578 | 300 | 50 | 30 |
| | 1:200 | 1009.18 | 1.37 | 3.06 | | | | |
| | 1:100 | 1085.54 | 1.48 | 1.22 | | | | |
| | 1:20 | 1998.60 | 4.76 | 0.39 | 3992 | 482 | 101 | 68 |
| MC252 (generic) | 0 | 857.35 | 1.24 | 4.42 | 1468 | 231 | 36 | 21 |
| | 1:200 | 877.78 | 1.25 | 3.56 | | | | |
| | 1:100 | 964.02 | 1.57 | 0.95 | | | | |
| | 1:20 | 1795.13 | 4.73 | 0.40 | 5093 | 511 | 113 | 67 |
| MESA | 0 | 757.84 | 1.19 | 18.14 | 1388 | 234 | 34 | 24 |
| | 1:200 | 806.76 | 1.22 | 11.97 | | | | |
| | 1:100 | 745.17 | 1.26 | 6.44 | | | | |
| | 1:20 | 1107.09 | 2.77 | 1.04 | 4088 | 439 | 85 | 62 |
| Sea Rose | 0 | 1145.29 | 1.28 | 9.80 | 1583 | 285 | 35 | 19 |
| | 1:200 | 1223.98 | 1.33 | 7.59 | | | | |
| | 1:100 | 1236.63 | 1.55 | 2.18 | | | | |
| | 1:20 | 1973.55 | 3.56 | 0.71 | 5903 | 601 | 120 | 70 |
| Terra Nova | 0 | 665.50 | 1.16 | 6.93 | 1038 | 168 | 18 | 11 |
| | 1:200 | 719.72 | 1.22 | 3.79 | | | | |
| | 1:100 | 821.24 | 1.37 | 1.47 | | | | |
| | 1:20 | 1380.34 | 3.76 | 0.40 | 5608 | 463 | 77 | 50 |

| Type II Oils | DOR | $F_{max}$[1] (RU) | IFE | FIR | Alkanes (µg/L) | 2-ring PAHs (µg/L) | 3-ring PAHs (µg/L) | 4-ring PAHs (µg/L) |
|---|---|---|---|---|---|---|---|---|
| Access Western Blend Dilbit | 0 | 39.58 | 1.02 | 11.41 | 93 | 15 | 4 | 10 |
| | 1:200 | 46.52 | 1.02 | 11.62 | | | | |
| | 1:100 | 49.84 | 1.03 | 8.54 | | | | |
| | 1:20 | 60.19 | 1.08 | 1.13 | 258 | 40 | 17 | 37 |
| Belridge Heavy | 0 | 118.69 | 1.07 | 4.90 | 42 | 31 | 21 | 30 |
| | 1:200 | 161.75 | 1.08 | 5.22 | | | | |
| | 1:100 | 140.96 | 1.07 | 4.62 | | | | |
| | 1:20 | 147.09 | 1.12 | 3.30 | 44 | 49 | 35 | 52 |
| Cold Lake Dilbit | 0 | 120.61 | 1.05 | 18.92 | 155 | 74 | 20 | 22 |
| | 1:200 | 120.65 | 1.05 | 17.33 | | | | |
| | 1:100 | 125.85 | 1.06 | 11.50 | | | | |
| | 1:20 | 133.15 | 1.17 | 1.92 | 368 | 160 | 50 | 57 |
| Heidrun | 0 | 902.69 | 1.28 | 4.50 | 382 | 337 | 55 | 43 |
| | 1:200 | 909.47 | 1.26 | 6.22 | | | | |
| | 1:100 | 964.31 | 1.33 | 3.74 | | | | |
| | 1:20 | 1098.90 | 2.19 | 0.77 | 684 | 524 | 96 | 79 |
| Hondo | 0 | 283.04 | 1.09 | 18.38 | 412 | 76 | 8 | 2 |
| | 1:200 | 312.27 | 1.08 | 15.38 | | | | |
| | 1:100 | 274.80 | 1.07 | 17.44 | | | | |
| | 1:20 | 288.01 | 1.07 | 16.33 | 319 | 67 | 7 | 1 |
| IFO-40 | 0 | 1173.91 | 1.20 | 27.94 | 1324 | 408 | 152 | 168 |
| | 1:200 | 1246.63 | 1.22 | 47.73 | | | | |
| | 1:100 | 1338.56 | 1.25 | 35.74 | | | | |
| | 1:20 | 1458.79 | 2.29 | 4.57 | 4354 | 1033 | 475 | 561 |
| IFO-120 | 0 | 3030.69 | 1.68 | 109.67 | 343 | 607 | 88 | 49 |
| | 1:200 | 2903.21 | 1.61 | 101.83 | | | | |
| | 1:10 | | | | | | | |

| | | | | | | | | |
|---|---|---|---|---|---|---|---|---|
| | 0 | | | | | | | |
| | 1:20 | 2527.73 | 1.67 | 34.32 | 840 | 885 | 212 | 118 |
| IFO-180 | 0 | 1263.05 | 1.22 | 33.67 | 866 | 410 | 235 | 320 |
| | 1:20 0 | 1394.42 | 1.23 | 36.08 | | | | |
| | 1:10 0 | 1703.55 | 2.37 | 36.31 | | | | |
| | 1:20 | 1532.99 | 1.63 | 12.19 | 2933 | 1189 | 797 | 1095 |
| IFO-300 | 0 | 720.55 | 1.11 | 61.26 | 446 | 216 | 79 | 188 |
| | 1:20 0 | 443.51 | 1.14 | 25.85 | | | | |
| | 1:10 0 | 465.91 | 1.07 | 45.70 | | | | |
| | 1:20 | 661.50 | 1.10 | 39.81 | 366 | 183 | 65 | 157 |
| Lago | 0 | 352.22 | 1.07 | 12.13 | 1289 | 114 | 32 | 18 |
| | 1:20 0 | 398.40 | 1.13 | 11.73 | | | | |
| | 1:10 0 | 367.75 | 1.12 | 8.88 | | | | |
| | 1:20 | 453.10 | 1.75 | 0.92 | 4221 | 258 | 88 | 51 |
| Santa Clara | 0 | 157.30 | 1.05 | 25.93 | 209 | 27 | 1 | 0 |
| | 1:20 0 | 147.55 | 1.05 | 22.73 | | | | |
| | 1:10 0 | 154.98 | 1.08 | 18.26 | | | | |
| | 1:20 | 169.39 | 1.12 | 6.97 | 1196 | 72 | 9 | 3 |
| Scotian Shelf Condensate | 0 | 946.52 | 1.15 | 40.62 | 447 | 125 | 2 | 0 |
| | 1:20 0 | 1408.59 | 1.44 | 53.68 | | | | |
| | 1:10 0 | 1487.16 | 1.53 | 58.06 | | | | |
| | 1:20 | 1337.98 | 1.50 | 47.65 | 1057 | 216 | 4 | 0 |
| Vasconia | 0 | 844.93 | 1.15 | 34.56 | 2550 | 317 | 98 | 59 |
| | 1:20 0 | 828.37 | 1.16 | 44.43 | | | | |
| | 1:10 0 | 835.62 | 1.17 | 34.09 | | | | |
| | 1:20 | 935.79 | 1.67 | 3.41 | 4402 | 467 | 164 | 95 |



ED_001324_00000913-00121

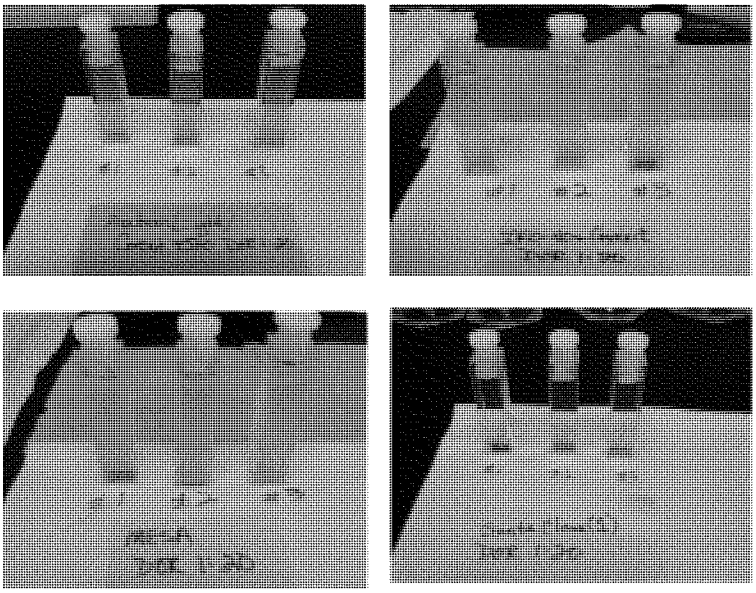



ED_001324_00000913-00122

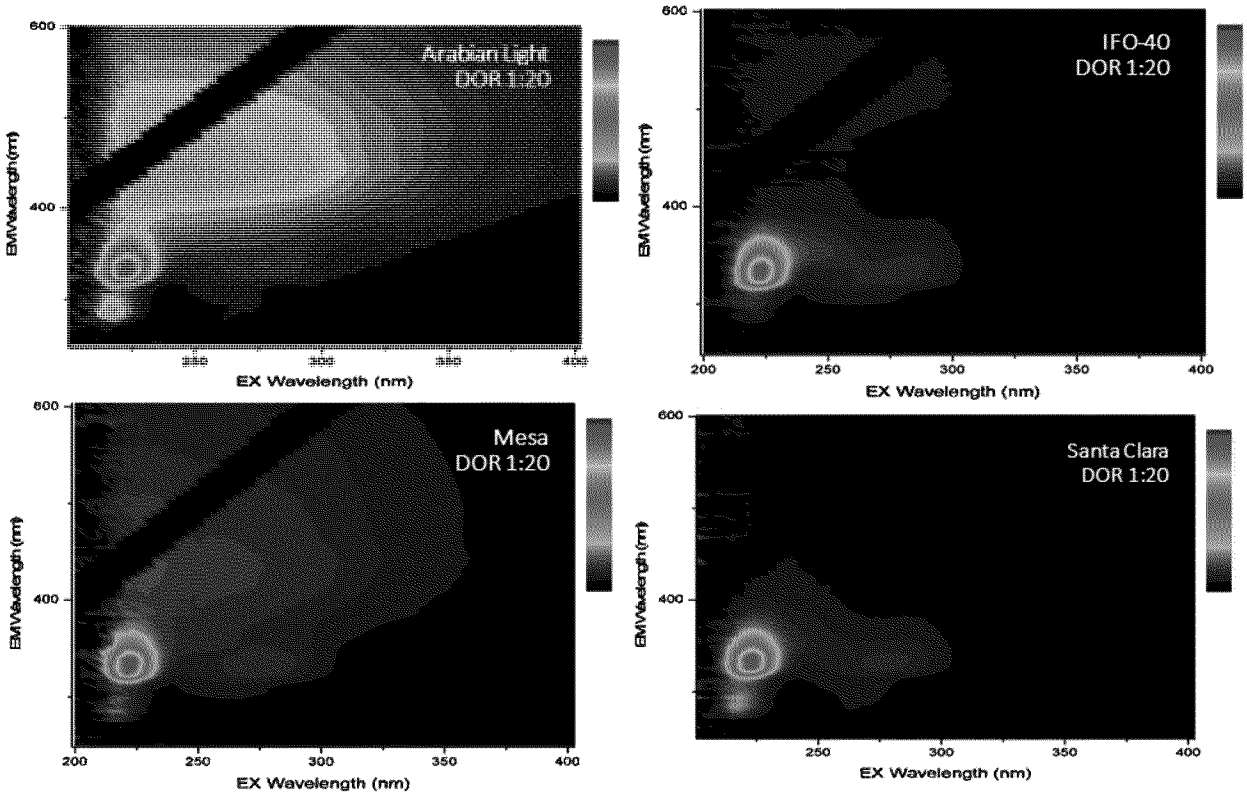


**Figure 44. Photographs of pre-analysis samples and corresponding example EEMs of Type I (left) and II (right) oils; DOR = 1:20 for Arabian Light (light oil, API gravity > 31.1°), Mesa (medium oil, API gravity 22.3 – 31.1°) and heavy oils (IFO 40 and Santa Clara, API gravity < 22.3°).**



ED_001324_00000913-00123

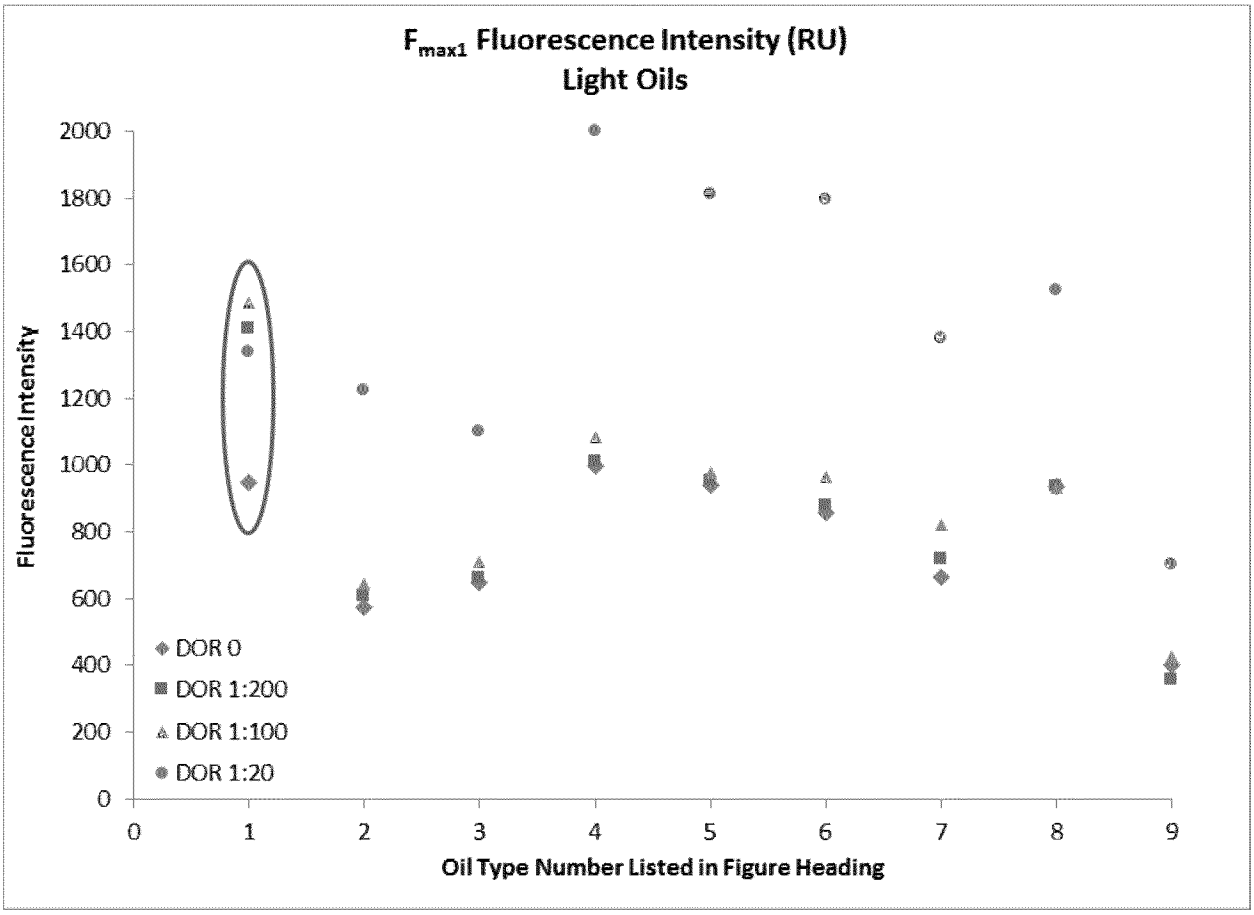


**Figure 45. $F_{max1}$ fluorescence for Light Oils (API gravity > 31°), in order of increasing density: 1. Scotian Shelf Condensate, 2. Federated, 3. Brent, 4. MC252—Discoverer Enterprise, 5. Hibernia, 6. MC252—generic, 7. Terra Nova, 8. Gullfaks, 9. Arabian Light. Note discrepancy in Scotian Shelf Condensate fluorescence pattern (circled) from that of all other Light Oils. It's particularly unusual that fluorescence intensity at highest DOR is lower than that at DORs 1:200 and 1:100.**



ED_001324_00000913-00124

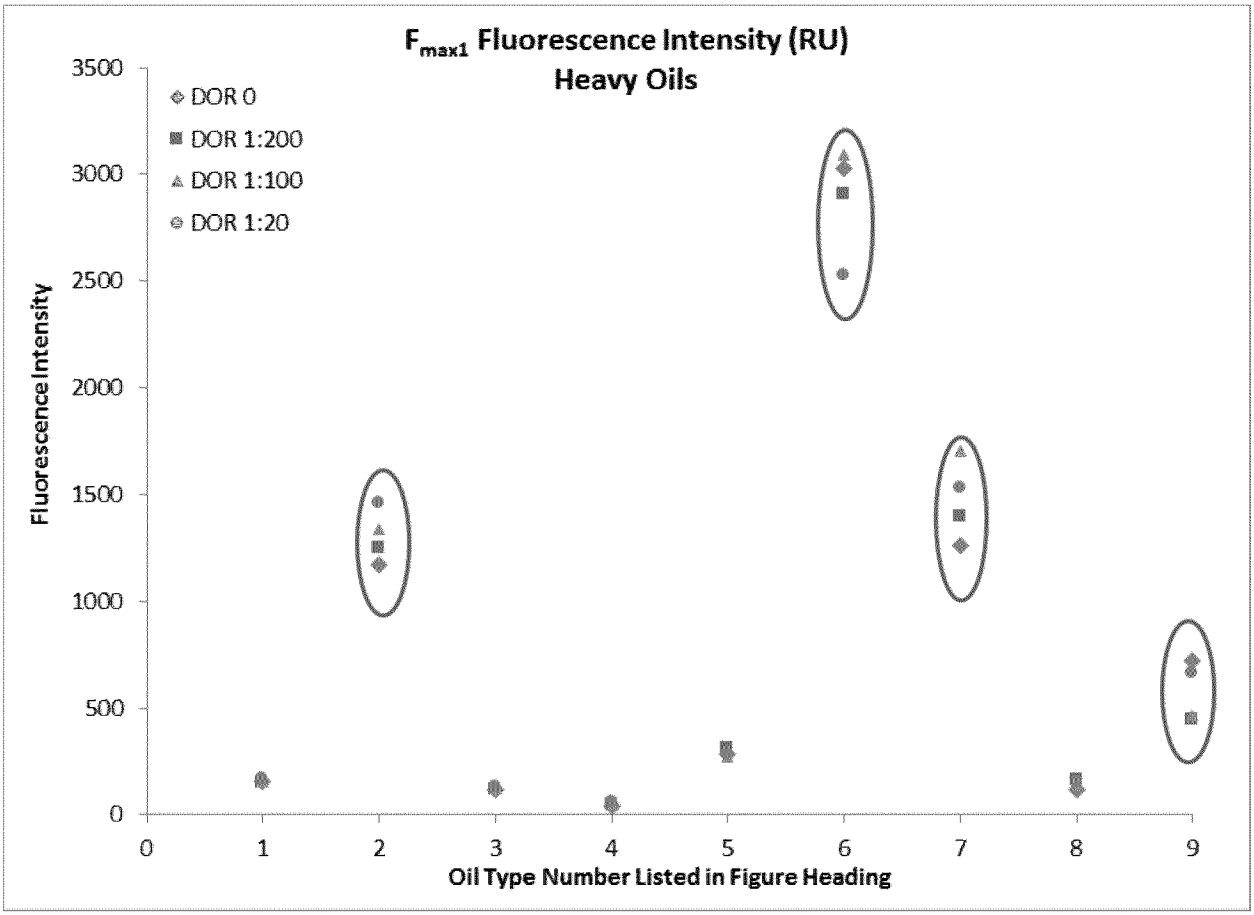


**Figure 46. $F_{max1}$ fluorescence for Heavy Oils (API gravity < 22.3°), in order of increasing density: 1. Santa Clara, 2. IFO 40, 3. Cold Lake Dilbit, 4. Access Western Blend Dilbit, 5. Hondo, 6. IFO 120, 7. IFO 180, 8. Belridge Heavy, 9. IFO 300. Note discrepancy in Intermediate Fuel Oils (circled) from that of all other Heavy Oils.**



ED_001324_00000913-00125

### B.3.2 Fluorescence as a Function of Chemistry

Samples of dispersed oil in artificial seawater (DOR 0 and DOR 1:20 for each oil type), extracted into methylene chloride were analyzed via GC-MS. Total alkanes, 2-ring, 3-ring, and 4-ring PAHs (see Table 10 for list of hydrocarbons in each class) were each plotted against $F_{max1}$, $F_{max2}$, $F_{max3}$, and $F_{max4}$ (Figures 47-50). Results showed highest correlation at DOR 0 between total 3-ring PAHs and fluorescence intensity at $F_{max3}$ and $F_{max4}$ (Figure 48) followed by that of 2-ring PAHs and fluorescence intensity at $F_{max1}$ and $F_{max2}$ (Figure 47) and between 4-ring PAHs and fluorescence intensity at $F_{max3}$ and $F_{max4}$ (Figure 48). It is important to note, however, that only 12 of the 25 oil types exhibited any $F_{max3}$ fluorescence at DOR 0.[2] These correlations support the fact that larger, more complex PAHs fluoresce at longer emission wavelengths.

For all oils at DOR 1:20, logarithmic relationships rather than linear relationships best modeled all correlations; however, overall these were weaker than those found at DOR 0. Highest correlation was observed between 2-ring PAHs and $F_{max3}$ intensity (Figure 50), with moderate correlations observed between 2-ring PAHs and fluorescence at $F_{max1}$ and between 2-ring PAHs and $F_{max2}$ fluorescence (Figure 49), and between 3-ring PAHs and $F_{max3}$ fluorescence (Figure 50). Only weak correlations were observed between 2-ring PAHs and fluorescence at $F_{max2}$ (Figure 49) and between 4-ring PAHs and $F_{max3}$ fluorescence (Figure 50). Clearly, full dispersion at DOR 1:20 results in widely varying changes in fluorescence intensity across all oil types.

[2] Oil types exhibiting Fmax3 fluorescence at DOR 0: Access Western Blend Dilbit, Alaska North Slope (both fresh and 10% weathered), Arabian Light, Brent, Federated, Gullfaks, Heidrun, Hibernia, MC252 (both Discoverer Enterprise and generic), and Terra Nova.



ED_001324_00000913-00126

**Table 10. Individual hydrocarbon compounds reported as Total Alkanes, Total 2-ring, 3-ring and 4-ring PAHs.**

| Total Alkanes: | Total 2-ring PAHs: | Total 3-ring PAHs | Total 4-ring PAHs: |
|---|---|---|---|
| n-decane | Naphthalene | phenanthrene | pyrene |
| undecane | Methylnaphthalene | anthracene | methylpyrene |
| dodecane | Dimethylnaphthalene | methylphenanthrene | dimethylpyrene |
| tridecane | Trimethylnaphthalene | dimethylphenanthrene | trimethylpyrene |
| tetradecane | tetramethylnaphthalene | trimethylphenanthrene | tetramethylpyrene |
| pentadecane | Acenaphthene | tetramethylphenanthrene | naphthobenzothiophene |
| hexadecane | Acenaphthylene | fluoranthene | methylnaphthobenzothiophene |
| heptadecane | Fluorene | | dimethylNBenzothiophene |
| 2,6,10,14-TMPdecane (pristine) | Methylfluorene | | trimethylNbenzothiophene |
| octadecane | Dimethylfluorene | | tetramethylNbenzothiophene |
| 2,6,10,14-TMHdecane (phytane) | Trimethylfluorene | | benz[a]anthracene |
| nonadecane | Dibenzothiophene | | chrysene |
| eicosane | methyldibenzothiophene | | methylchrysene |
| heneicosane | dimethyldibenzothiophene | | dimethylchrysene |
| docosane | trimethyldibenzothiophene | | trimethylchrysene |
| tricosane | tetramethyldibenzothiophene | | tetramethylchrysene |
| tetracosane | | | benzo[b]fluoranthene |
| pentacosane | | | benzo[k]fluoranthene |

| | | | |
|---|---|---|---|
| hexacosane | | | benzo[e]pyrene |
| heptacosane | | | perylene |
| octacosane | | | |
| n-nonacosane | | | |
| tricontane | | | |
| n-heneicontane | | | |
| dotriacontane | | | |
| tritriacontane | | | |
| tetratriacontane | | | |
| n-pentatriacontane | | | |
| 17α(H), 21β (H)-hopane | | | |
| 17β(H), 21α(H)-hopane | | | |



ED_001324_00000913-00128

The effect of DOR 1:20 on dissolved hydrocarbons can also be investigated by taking the ratio of total alkanes + PAHs at DOR 1:20 to total alkanes + PAHs at DOR 0 to yield the Chemical Dispersibility Ratio (CDR). The ratio ranges from between 0.8 for two heavy oils (Hondo and IFO 300) and 7.8 for Arabian Light. Although heavy oils tended to have lower CDRs and light oils tended to have higher ratios, oil density was not correlated with chemical dispersion For example, the heavy oil Santa Clara (API Gravity 22.1°) had the third highest CDR (5.4), while Scotian Shelf Condensate, by far the lightest oil (API Gravity 46.6°), had a CDR of only 2.2 (Figure 51 The effect of dispersion on fluorescence intensity can be similarly investigated by taking the ratio of $F_{max1}$ fluorescence intensity at DOR 1:20 to that at DOR 0, resulting in the Fluorescence Dispersibility Ratio (FDR). The FDR also shows a general increasing trend with increasing API Gravity, but only a moderate linear correlation ($R^2$ = 0.55). The relationship between CDR and FDR exhibited weak linear correlation (R2 = 0.17) (Figure 52).

All four Intermediate Fuel Oils (IFO 40, IFO 120, IFO 180, and IFO 300) as well as Scotian Shelf Condensate (SSC), showed fluorescence and chemistry anomalies that tended to skew overall results. With respect to SSC, all other light oils (API Gravity < 22.3°) exhibited increasing fluorescence intensity with increasing DOR, culminating in an increase at DOR 1:20; however, SSC showed a decrease in fluorescence intensity at DOR 1:20, dropping to below the level exhibited at DOR 1:200 (Figure 45). Additionally, SSC was the only light oil which exhibited no $F_{max3}$ fluorescence at any DOR. Chemically, SSC is unique, containing a high proportion of 2-ring to 3-ring PAHs—52.2 for DOR 0 and 58.6 for DOR 1:20. With the exception of Santa Clara, with a 2-ring to 3-ring ratio of 31.9 at DOR 0, all other oil types had a ratio of 10 or less at both DOR 0 and DOR 1:20. SSC also contained no 4-ring or 5-ring PAHs, unlike all other oils with the exception of DOR 0 Santa Clara. All Intermediate Fuel Oils fell into the heavy oil group (API Gravity > 31°), in which all other oils showed little to no increase in fluorescence intensity with increasing DOR as well as maximum $F_{max1}$ intensity of just 60-288 RU. The IFOs, however, showed far greater $F_{max1}$ intensity across the board (721-3031 RU) along with clear separation with increasing DOR. Like Scotian Shelf Condensate, IFO 120, IFO 180, and IFO 300 also exhibited a drop in $F_{max1}$ intensity at DOR 1:20; in fact, IFO 120 $F_{max1}$ at DOR 1:20 was

actually 17% lower than at DOR 0. These same three IFOs also had the highest overall concentration of PAHs, and all four IFOs were the only oils to contain any anthracene. For all oil types, total alkanes as a function of fluorescence intensity was found to be only loosely correlated, as total concentration increased overall in relation to fluorescence intensity with no clear relationship.



ED_001324_00000913-00130

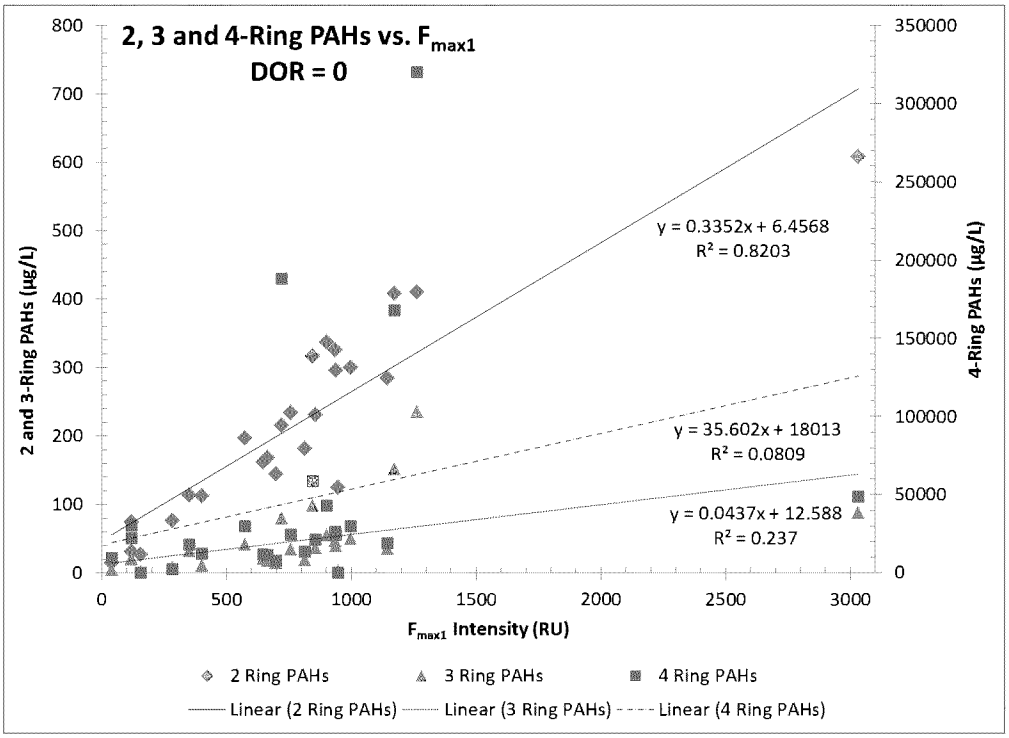


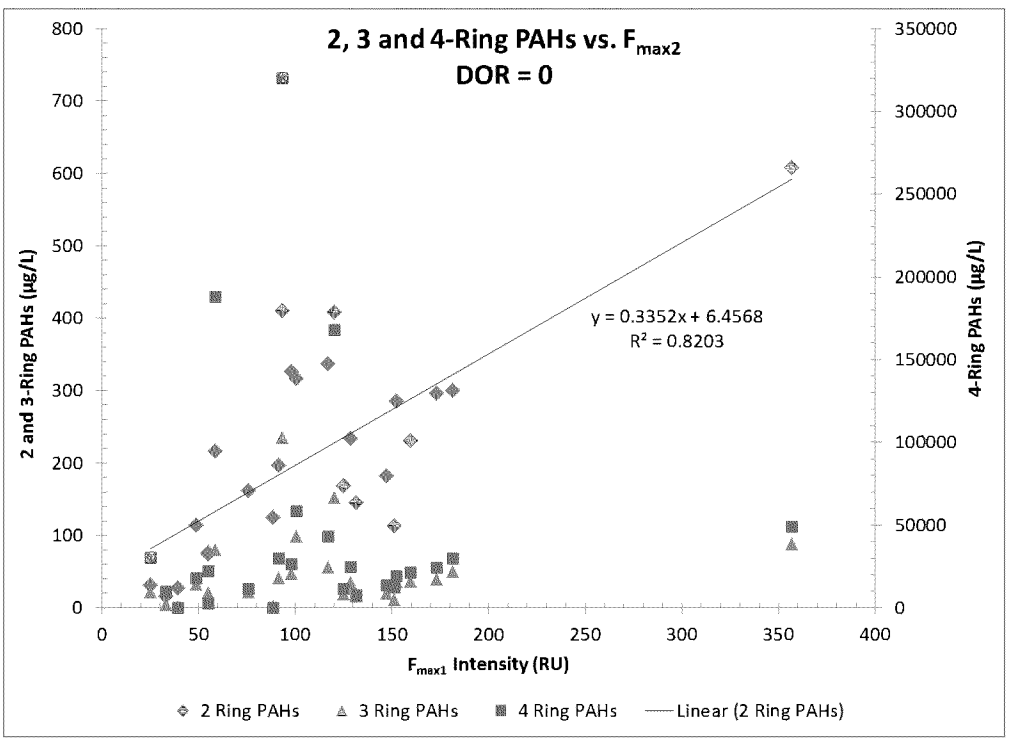


**Figure 47. For all oil types at DOR 0, total concentration of 2-ring, 3-ring, and 4-ring PAHs (µg/L) against fluorescence intensity (RU) at $F_{max1}$ (top), and against $F_{max2}$ (bottom). Strong linear correlation exists between 2-ring PAHs and $F_{max1}$ fluorescence, but little to no correlation between 3-ring or 4-ring PAHs and $F_{max1}$ fluorescence intensity (top). Strong linear correlation also exists between 2-ring PAHs and $F_{max2}$, but no correlation between 3-ring PAHs or 4-ring PAHs and $F_{max2}$ (bottom).**

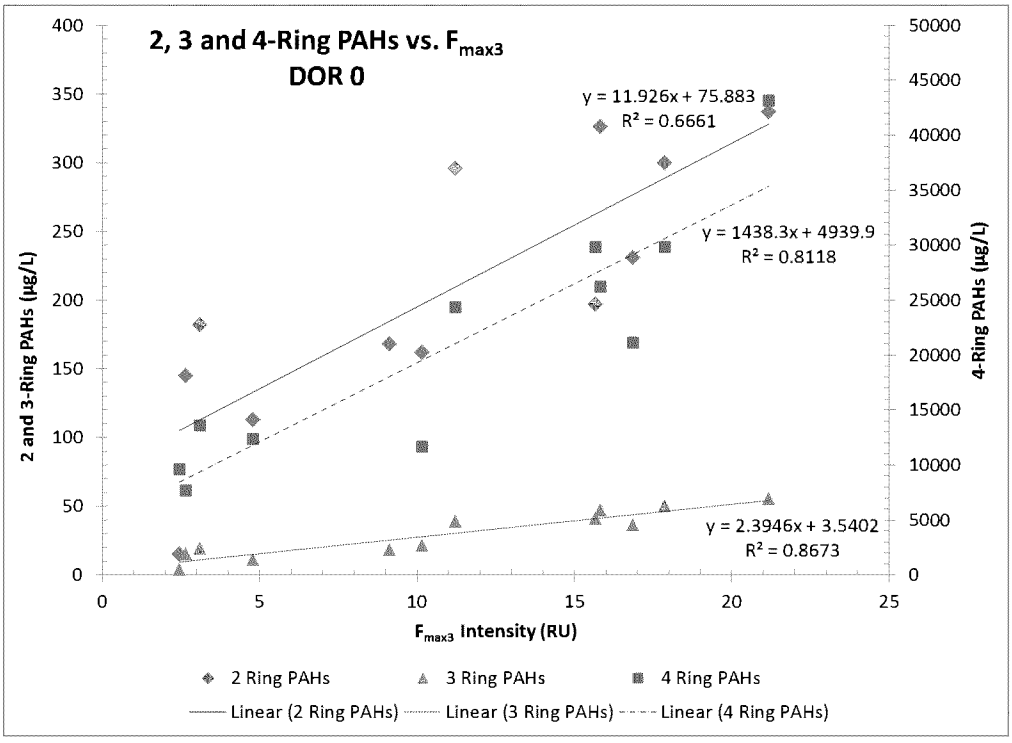


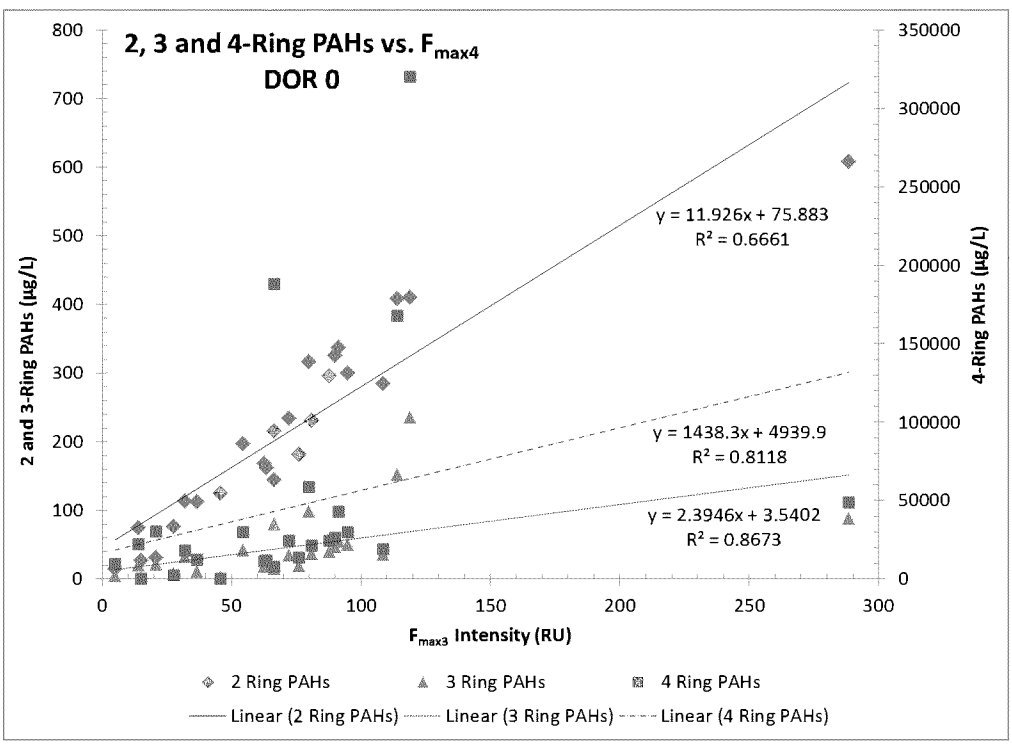


**Figure 48. For all oil types at DOR 0, total concentration of 2-ring, 3-ring, and 4-ring PAHs (µg/L) against fluorescence intensity (RU) at $F_{max3}$ (top), and against $F_{max4}$ (bottom). Strong linear correlation exists between 3-ring and 4-ring PAHs and both $F_{max3}$ and $F_{max4}$ fluorescence; however, only moderate correlation exists between 2-ring PAHs and $F_{max3}$ and $F_{max4}$ fluorescence intensity.**

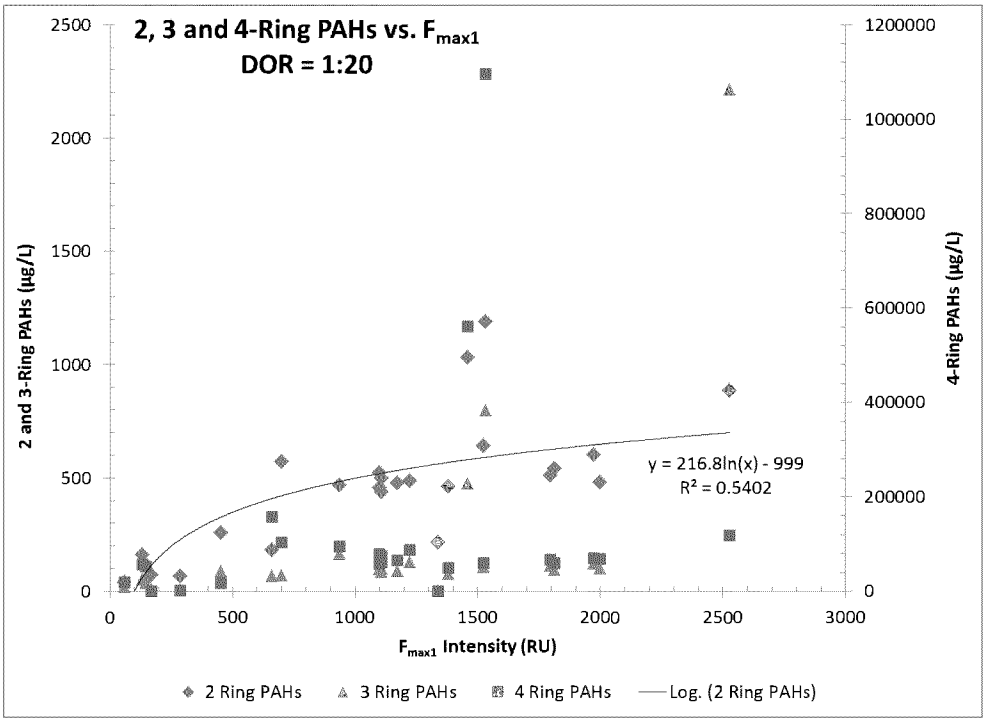


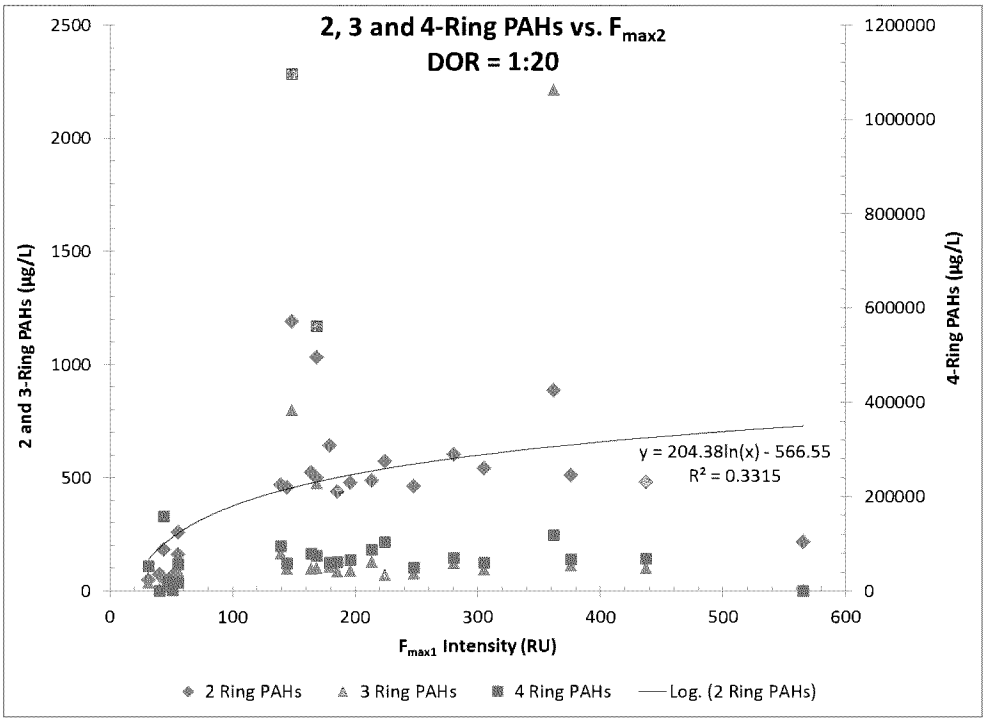


**Figure 49. For all oil types at DOR 1:20, total concentration of 2-ring, 3-ring, and 4-ring PAHs (µg/L) against fluorescence intensity (RU) at $F_{max1}$ (top), and against $F_{max2}$ (bottom). A moderate logarithmic correlation is exhibited between 2-ring PAHs and fluorescence intensity (RU) at $F_{max1}$ and a weaker correlation between 2-ring PAHs and $F_{max2}$, but no correlation exists between 3-ring or 4-ring PAHs and fluorescence intensity at either $F_{max1}$ or $F_{max2}$.**

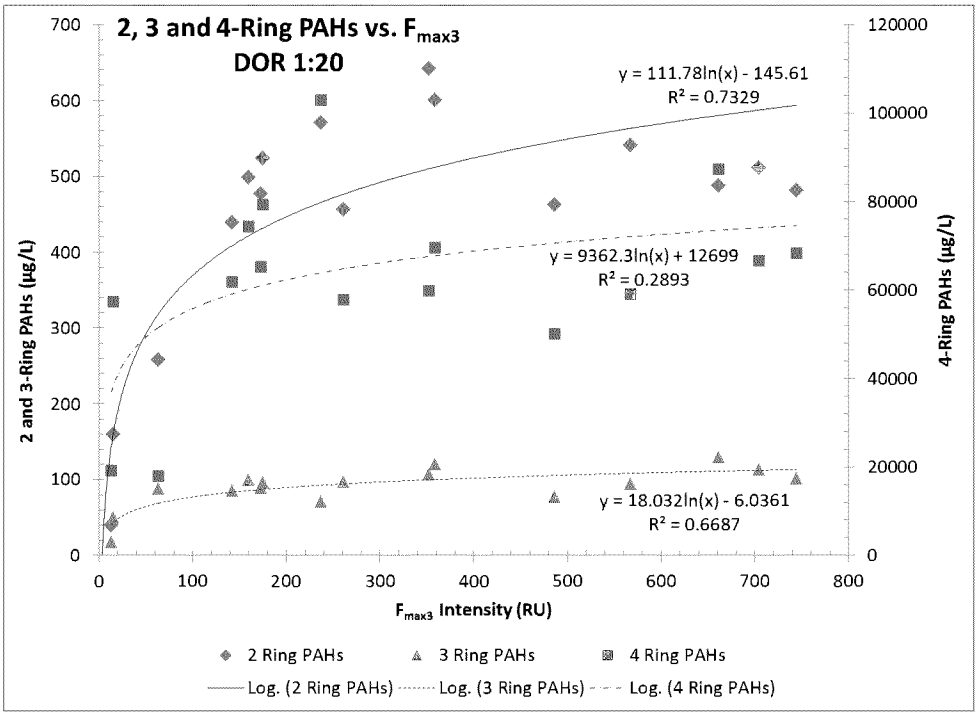


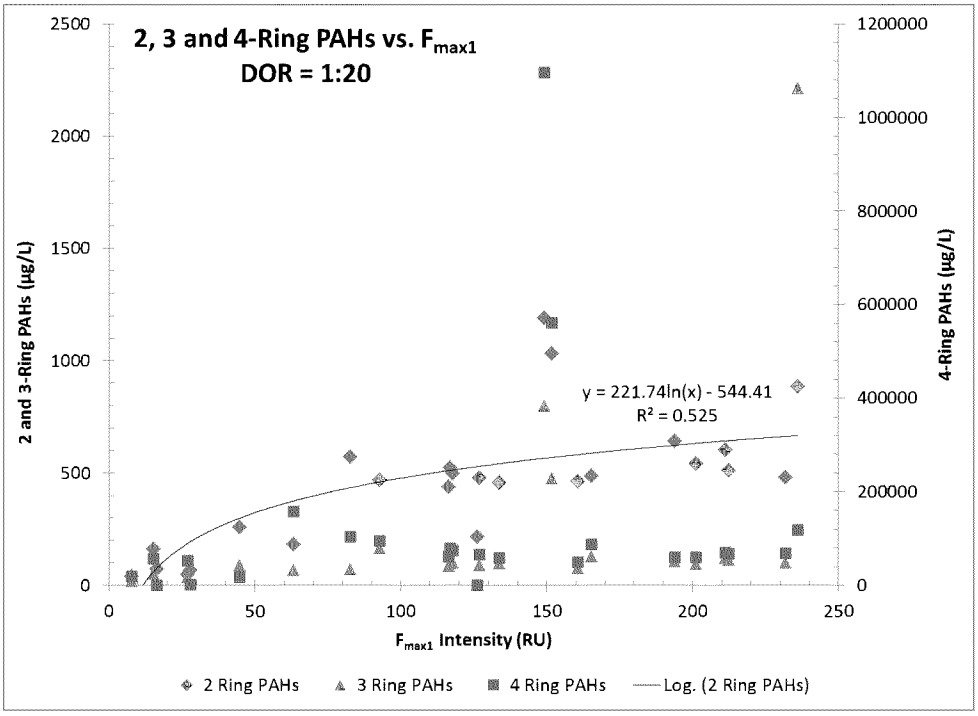


**Figure 50. For all oil types at DOR 1:20, total concentration of 2-ring, 3-ring, and 4-ring PAHs (µg/L) against fluorescence intensity (RU) at $F_{max3}$ (top), and against $F_{max4}$ (bottom). A strong logarithmic correlation is exhibited between 2-ring PAHs and fluorescence intensity at $F_{max3}$. Moderate correlations exist between 3-ring PAHs and $F_{max3}$ as well as between 2-ring PAHs and $F_{max4}$. However, only a weak logarithmic correlation exists between 4-ring PAHs and fluorescence intensity at $F_{max3}$, and there is no correlation between 3-ring or 4-ring PAHs and $F_{max4}$.**

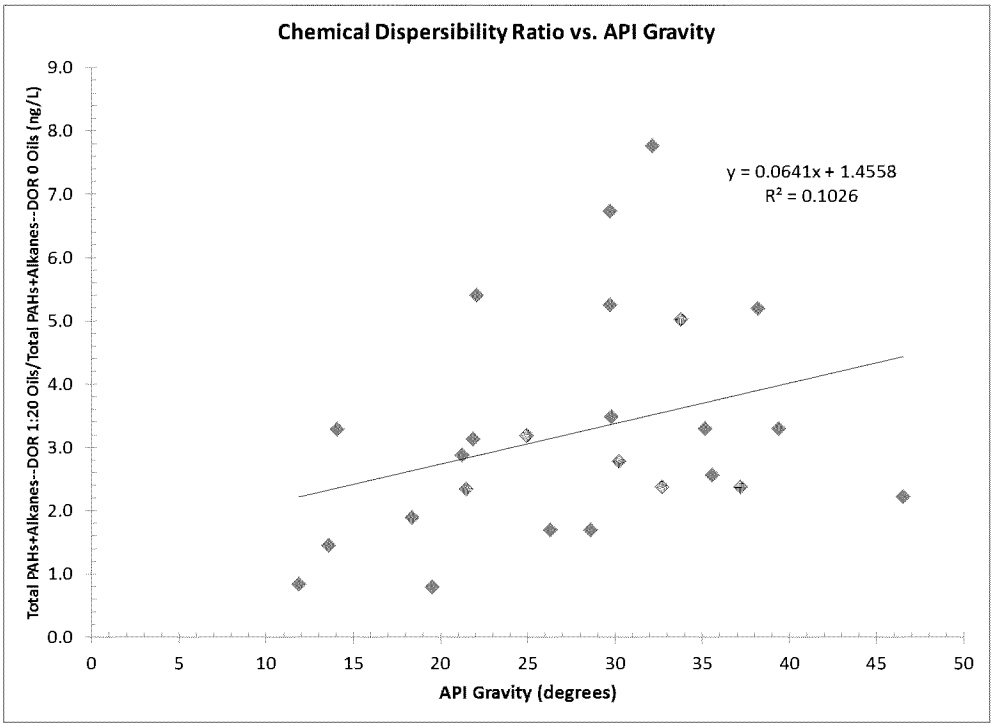


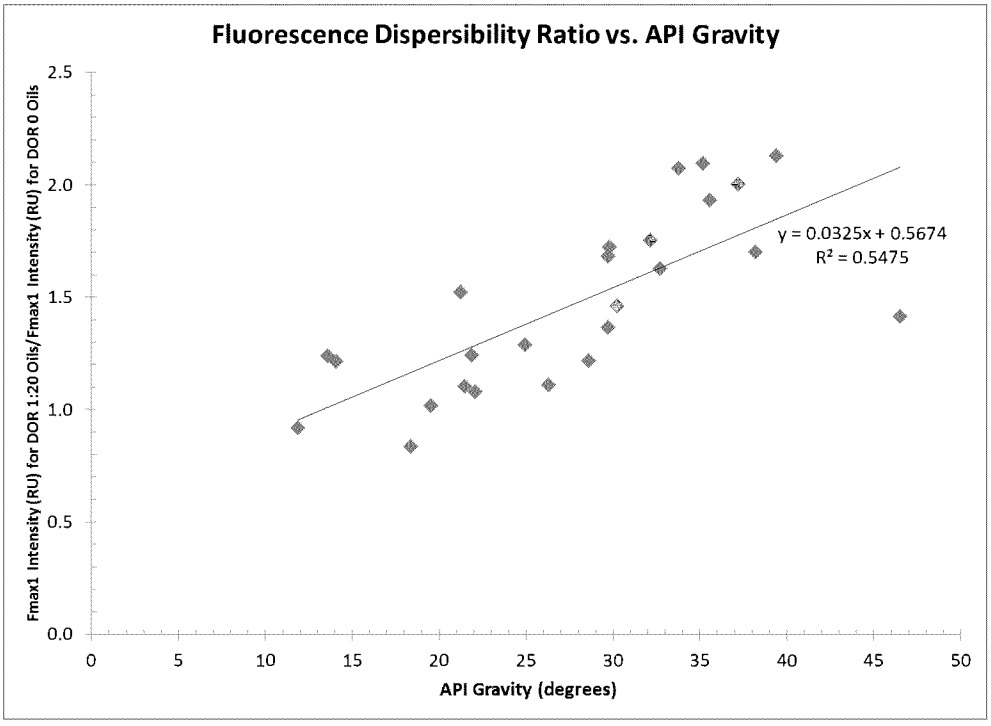


**Figure 51. Chemical Dispersibility Ratio (CDR) vs. decreasing oil density (top) and Fluorescence Dispersibility Ratio (FDR) vs. decreasing oil density (bottom) show only a weak correlation between chemistry and oil density, and a moderate correlation between fluorescence and oil density. With the removal of the data point for Scotian Shelf Condensation, correlation between fluorescence and oil density improves to $R^2$ = 0.71.**

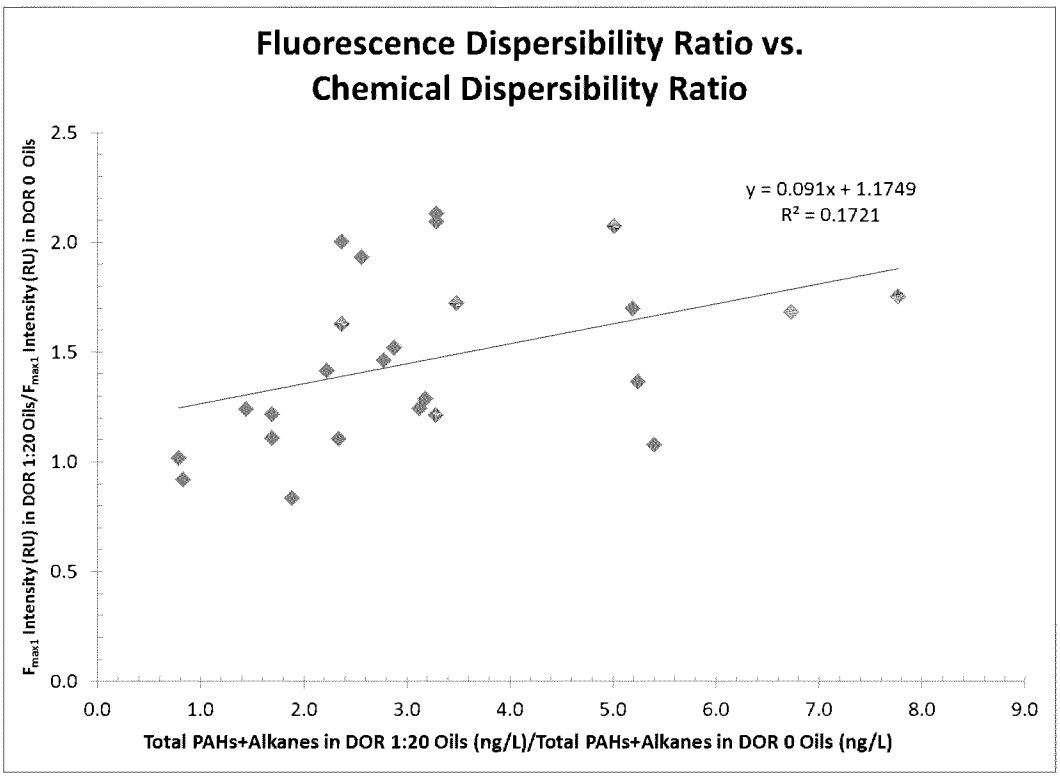


**Figure 52. Fluorescence Dispersibility Ratio (FDR) vs. Chemical Dispersibility Ratio (CDR) shows weak correlation between these two ratios.**



ED_001324_00000913-00136

### B.3.3 Flume Tank and Baffled Flask EEM Comparison

In addition to the EEMs generated from the BFT of 25 oil types, EEMS were also generated from the discrete sample collection during the flume tank experiments using South Louisiana Crude oil (SLC) in Task A of this project report. Samples for EEM analysis were collected and immediately analyzed on the same Horiba Aqualog at DFO using identical analysis protocols and data processing. A comparison of SLC MC252 EEMs for varying DOR from the BFT (left) and the flume tank (right) experiments are illustrated in Figure 53. Note that that the contour coloring for the peaks is identical between experiments, but the baseline color varied, where black was used for the BFT EEMs and blue used for tank EEMs, but the appearance of the blue color this is not to be confused with the presence of higher fluorescence in regions away from the peak fluorescence. Fluorescence Intensity Ratios (FIR) were calculated for the tank EEMs and found to be between 7.1 and 9.1 for DOR = 0, 1.3 and 4.3 for DOR = 1:100 and 0.6 and 0.8 for DOR = 1:20. This is follows the findings of Bugden et al., 2008 where a decrease in FIR is observed with the addition of dispersant. It is also consistent with the BFT EEMs which show a 4.9 for DOR = 0 and 0.4 for DOR = 1:20 (Supplemental Table A). These results indicate that FIR can be an indicator of dispersion effectiveness for SLC oil.



ED_001324_00000913-00137

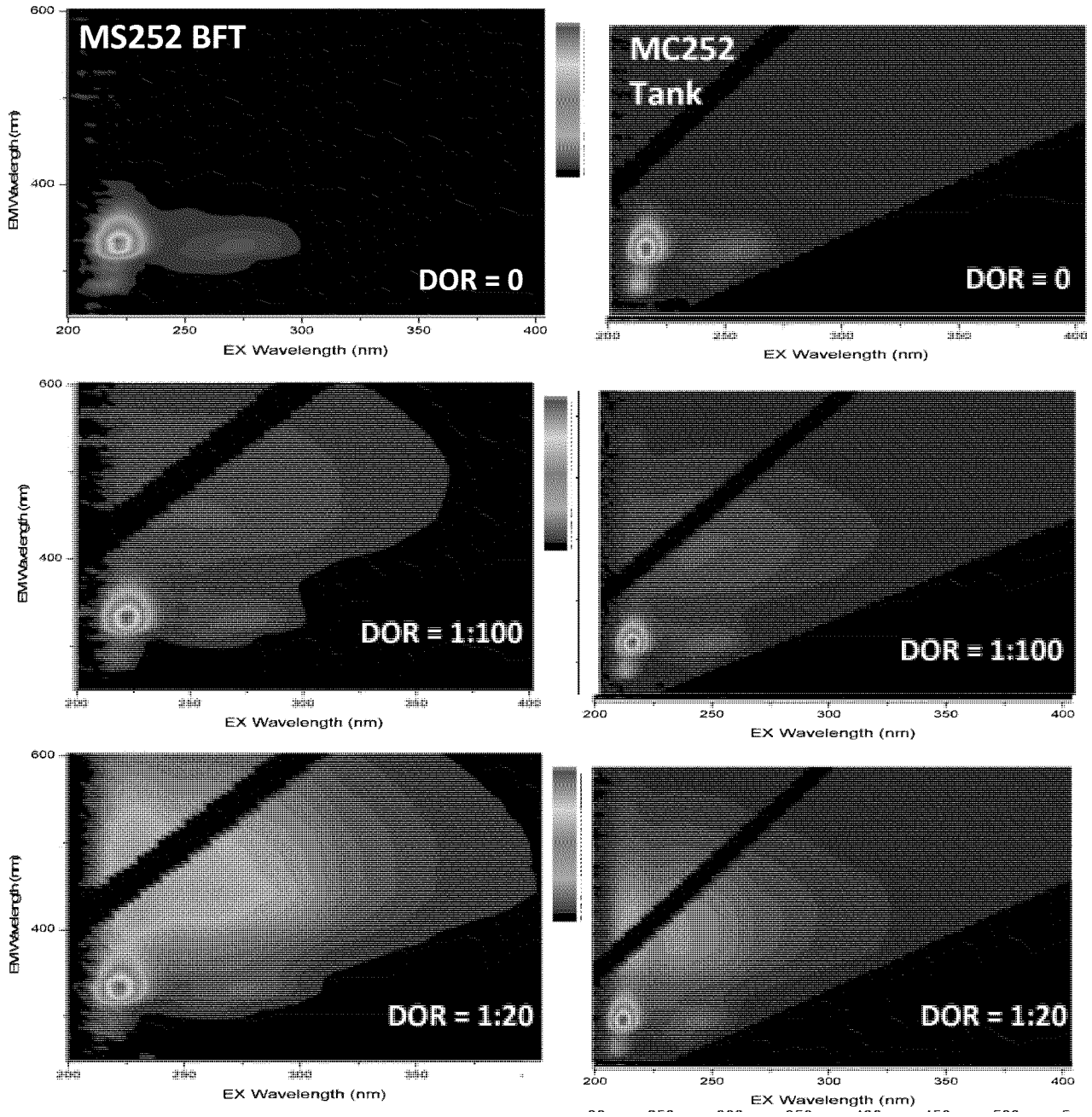


**Figure 53. South Louisiana Crude MC252 EEMS from BFT (left panels) and tank experiments (right Panels) for DOR = 0, 1:100 and 1:20.**

### B.3.4 PARAFAC Modeling

Originally designed to model complexity in the field of psychometrics (Carroll and Chang, 1970; Harshman, 1970), parallel factor analysis (PARAFAC, also known as canonical decomposition or CANDECOMP) was first employed in the analysis of fluorescence data within the next ten years (Appellof and Davidson, 1981). Over the past twenty years, PARAFAC has been widely embraced by chemometricians and used to tease apart the overlapping fluorescence components of complex chemical mixtures containing fluorescent substances ranging from proteins and pigments to pesticides and PAHs (Andersen and Bro, 2003). More recently, PARAFAC analysis has been used in the analysis of the fate and transport of dispersed oil from the Deepwater Horizon Oil Spill (Mendoza, et al., 2013; Zhou, et al., 2003).

Presented with hundreds of complex fluorescence EEM data sets containing samples, excitation, and emissions; PARAFAC analysis can reduce this to data sets containing samples and intensity at a few important wavelength pairs (Murphy et al., 2014). In the past, this information gathering was often done via time-consuming "peak-picking" whereby EEMs were visually inspected for apparent $F_{max}$ location, then fluorescence intensity data at that excitation/emission point was copied and pasted into a spreadsheet for further analysis. PARAFAC provides the capability to turn that somewhat qualitative task into a more quantitative exercise; however, careful preparation of the data is critical in order to obtain a meaningful outcome. PARAFAC analysis also allows the consideration of minor fluorescence peaks, which may have been overwhelmed by high-intensity major peaks, but may be no less important in the analysis of EEM results. More importantly, PARAFAC analysis allows for direct comparison to chemical composition upon successful modelling of an EEM data set (Murphy, et al., 2014). The steps that must be undertaken for successful PARAFAC analysis are: (1) assembling the dataset; (2) preprocessing to correct biases, remove scatter and normalize; (3) exploring the dataset to remove possible outliers and develop preliminary models; (4) validating the model by determining the proper number of components and evaluating model fit; (5) interpreting results (Murphy, et al., 2013).

In order to identify connections between the fluorescence profiles and underlying chemical



ED_001324_00000913-00139

complexity of the 25 oil types in the BFT analysis (Figure 53), PARAFAC analysis was performed on the fluorescence data. The PLS Toolbox (Eigenvector, Inc.) was used within MATLAB (MathWorks, Inc. 2014b) to accomplish this task. After importing raw data and assembling datasets, three constraints were applied to all samples: normalization, EEM filtering, and non-negativity. Normalization was conducted to compensate for the wide variation in fluorescence intensity across oil types ($F_{max1}$ = 39.6 RU for Access Western Blend Dilbit to $F_{max1}$ = 3090.2 RU for IFO 120) in order to prevent samples with high fluorescence intensity values from skewing the model. Further, normalization of maximum intensity to 1 (inf-Norm) was chosen rather than normalization of the entire area of fluorescence (1-Norm) to preserve differences in spectral shape. EEM filtering was applied in order to remove artifacts of the fluorescence analysis process known as first and second order Rayleigh scatter. This was accomplished by interpolating data across those regions (12 nm for first order Rayleigh and 24 nm for second order Rayleigh); zero values were also assigned to sub-Rayleigh wavelengths since fluorescence emission takes place at wavelengths above excitation due to Stokes shift. Raman scatter, the other light-related artifact which must be removed before PARAFAC analysis can be performed, was accomplished as sample analysis was done by subtracting that day's sample blank from each sample. Upon running several PARAFAC test models using 4, 5, 6 and 7-components on a dataset containing the DOR 0 sample from flask #1 of all 25 oil types, data between excitation at 200 nm and 212 nm was excluded. The inherent "noise" typically found at excitation < 240 nm, related to the low intensity of xenon lamps in that region, led to this decision. Excluding data at excitation and emission wavelengths above 680 nm was also employed in order to improve processing results since no fluorescence information of value was contained in that region.

The biggest challenge in PARAFAC modelling is in determining the most appropriate number of component factors. While it is important to ensure separation of all individual factors, it is also critical not to select too many components in order to avoid over-fitting the data. Several ways of doing this are suggested in the PARAFAC tutorial (Bro, 1997): comparison of the resulting factor profiles with background knowledge of expected components, consideration of the



ED_001324_00000913-00140

residuals, and split half validation of the model. The latter has also been recommended by other researchers (Harshman and Lundy, 1994; Murphy, et al., 2013). Split half analysis is accomplished by dividing the data into two independent subsets and applying the model to each of the subsets. In theory, if the correct number of components has been selected, the two halves of the data should each fit the model well; however, Murphy cautions that a relatively large data set is necessary in order for this to hold true (2013). Smilde, et al., (2004) also caution that some phenomenon observed within a subset of data may not match the overall model, but instead may just be present in that particular random half of the dataset. Thus, it could be anticipated that split half validation will work better with samples within oil weight subdivisions than with the dataset containing all 25 oil types as a whole. Bro and Kiers (2003) have also advised using core consistency of the model to validate that the correct number of components have been selected. All of these methods were employed for the following analyses by first noting the percentage of data fit by the model, next checking the core consistency of the model, then inspecting residuals, inspecting the loadings for Mode 3 (excitation) and Mode 2 (emission), and inspecting EEMs of each component. Finally, split half analysis was done. In all cases, several models were run with different numbers of components to ensure selection of the most appropriate model.

DOR 0

Initially, a five-component model was fit to the dataset, followed by 4-, 6- and 7-component models. Best overall fit was obtained with the six-component model, which explained 99.504% of the data. Core consistency was 52%, and split half validation was 56.4% (Figure 54). Review of residuals showed they were minimal with random distribution, inspection of plots of Mode 2 and Mode 3 loadings (Figure 55), variation per component (Figure 56), as well as EEMs of individual components (Figure 57) all supported choice of the 6-factor model for best fit.



ED_001324_00000913-00141

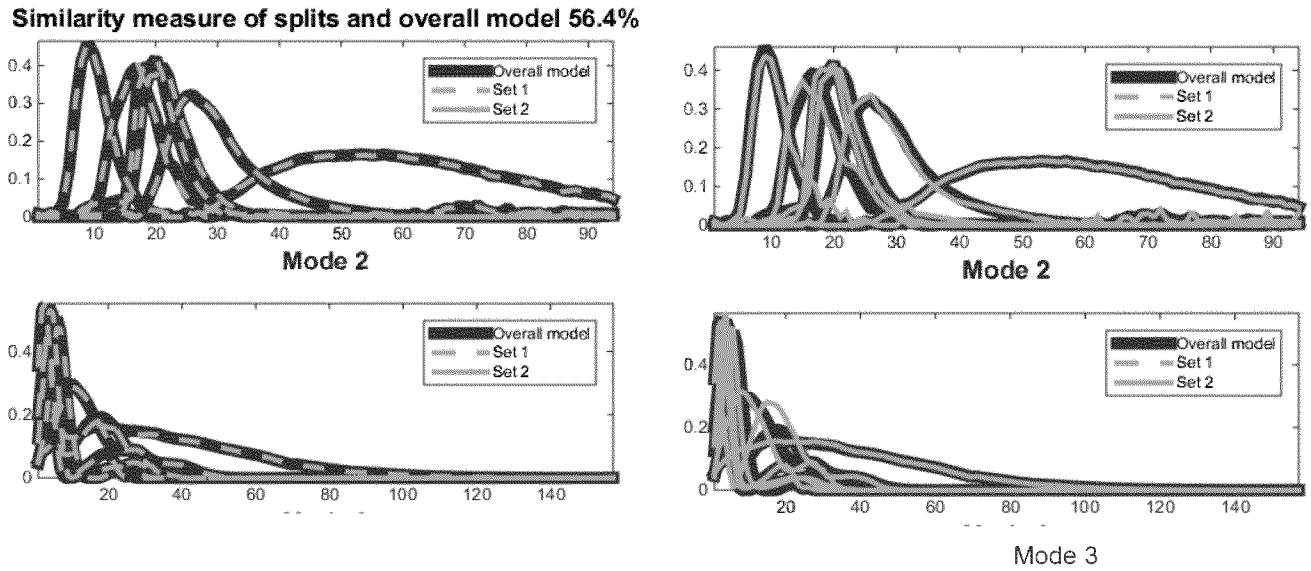


**Figure 54. Example of split half validation for the 6-component model of 25 oil types at DOR 0 showing individual fit of data splits (Set 1, left; and Set 2, right) compared to overall model for Mode 2 (top) and Mode 3 (bottom) loadings.**

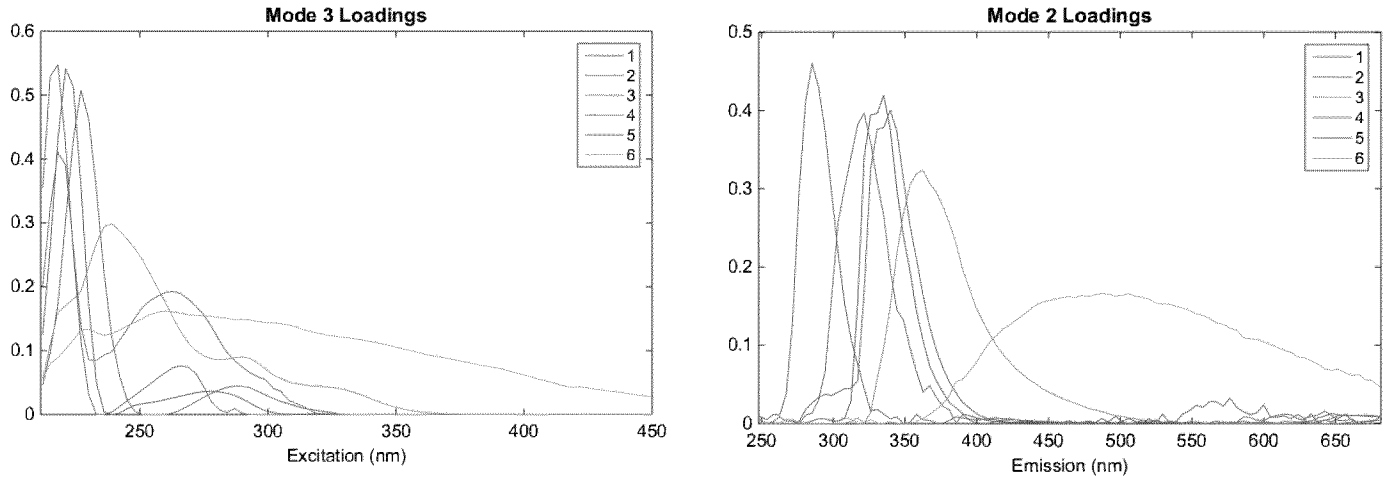


**Figure 55. Mode 3 Loadings (Excitation) and Mode 2 Loadings (Emission) for all 25 oil types—DOR0 using 6-component model. Note difference in x-axis scales. Although components are tightly spaced, all appear as separate and distinct peaks.**

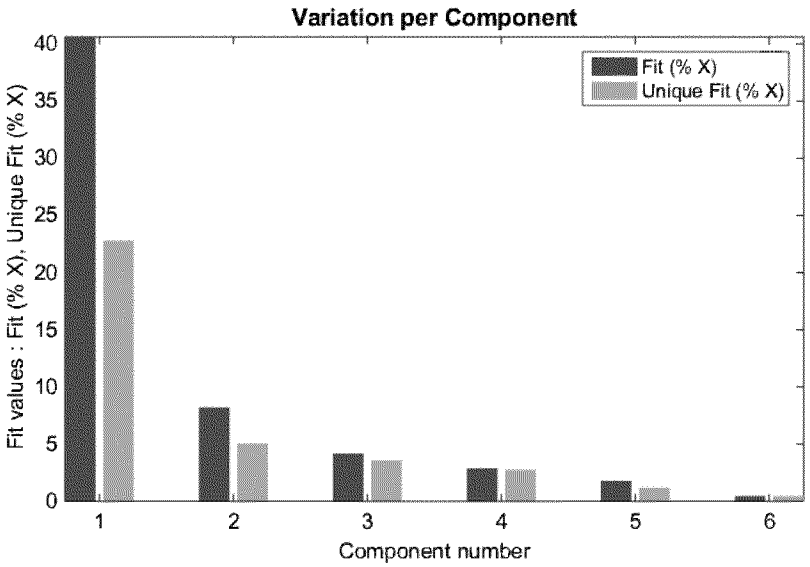


**Figure 56. Variation per Component shows Component 1 accounted for >20% to 40% (unique fit and fit) of the data, while Component 2-contributed 5-10% (unique fit and fit) and Components 3-6 accounted for 5% or less of the data, respectively. While Component 6 accounted for a very low percentage of the data, the 6-component model was still a better fit to the data than the 5-component model.**

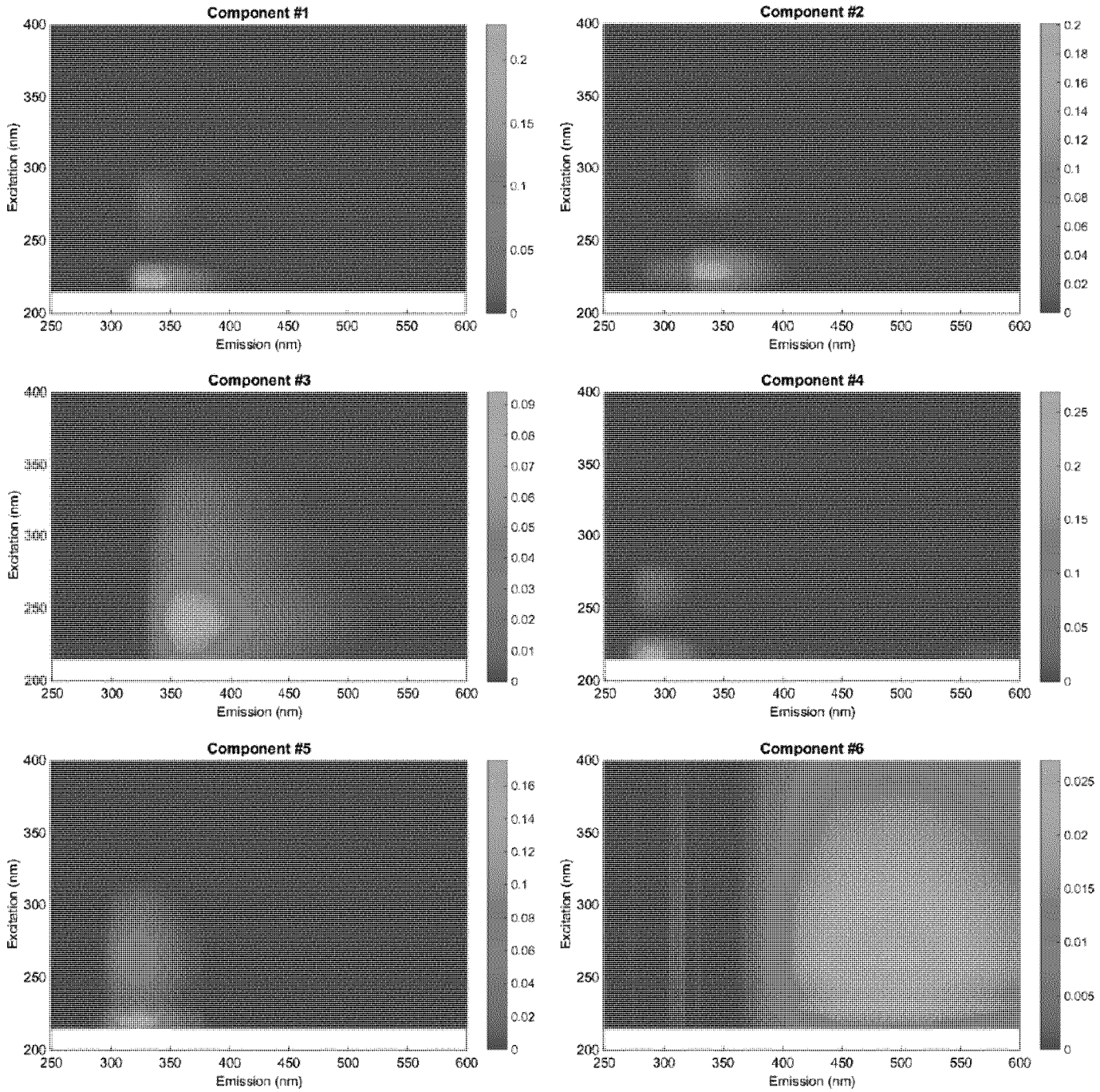


**Figure 57. EEM views of the six components of PARAFAC model for 25 oil types at DOR 0. Component #1: $F_{max}$ = Ex 224nm/Em 335nm; Component #2: $F_{max}$ = Ex 230nm/Em 340nm; Component #3: Fmax = Ex 239nm/Em 363nm; Component #4: Fmax = Ex 218nm/Em 290 nm; Component #5: Fmax = Ex 221nm/Em 322nm; Component #6: Fmax = Ex 260nm/Em 474-511nm.**

### DOR 1:100

A six-component model was fit to the dataset containing all 25 oil types at DOR 1:00 since that was the best fit for the DOR 0 dataset, followed by a 7-component model, which returned an error warning that two or more components may be fitting the same feature, as well as core consistency <0%. Finally, a 5-component model was fit to the dataset. Interestingly, for the DOR 1:100 dataset, the 5-component model proved to be the best fit, explaining 99.353% of the data with core consistency of 72% and split half validation of 75.8%. Residuals were minimal and randomly distributed, and visual inspection of loadings (Figure 58), variation per component (Figure 59) and component EEMs (Figure 60) led to acceptance of the 5-component model.



ED_001324_00000913-00146

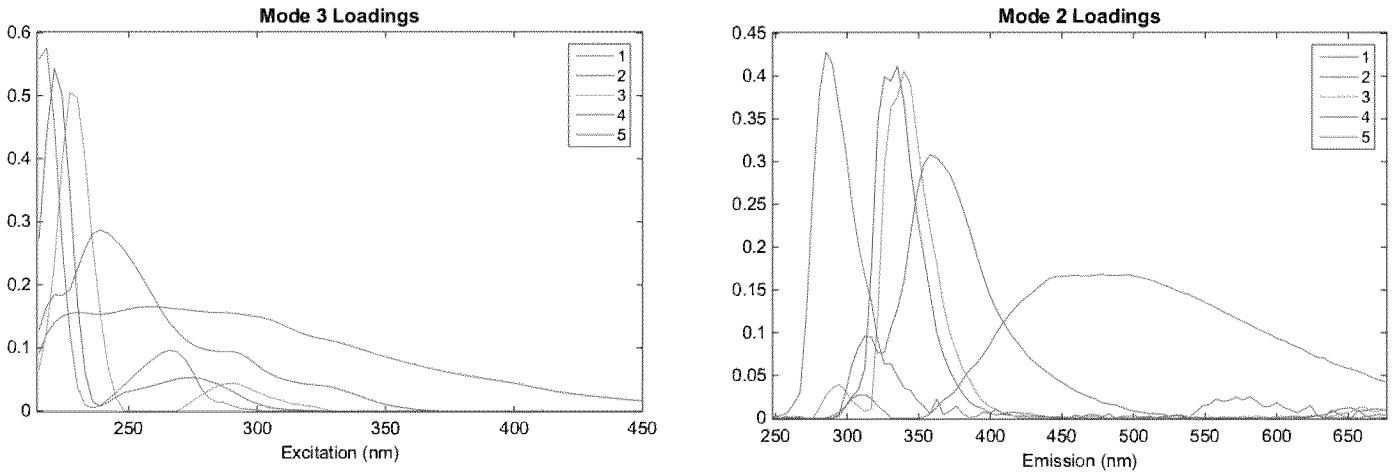


**Figure 58. Mode 3 Loadings (Excitation) and Mode 2 Loadings (Emission) for all 25 oil types—DOR 1:100 using 5-component model. Note difference in x-axis scales. Although components are tightly spaced, all appear as separate and distinct peaks.**



ED_001324_00000913-00147

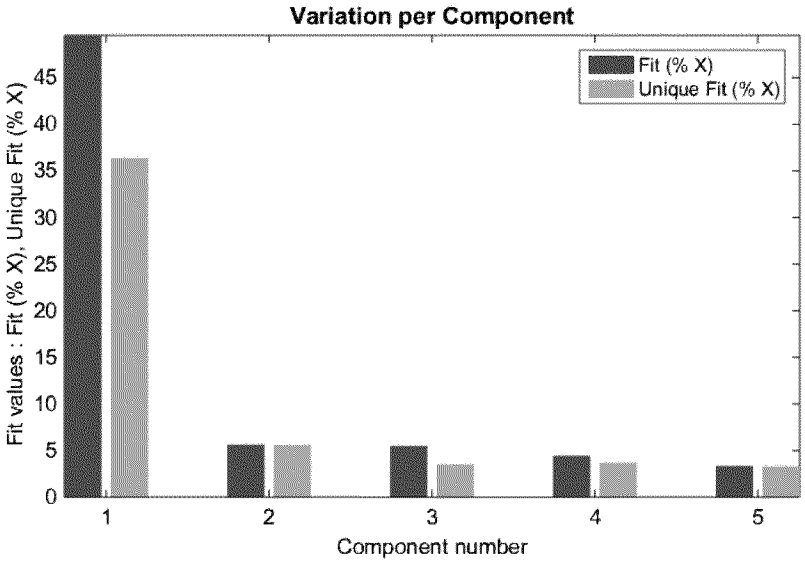


**Figure 59. Variation per Component shows Component 1 accounted for >35% to almost 50% (unique fit and fit) of the data, while Components 2-5 accounted for 5% or less of the data, respectively.**

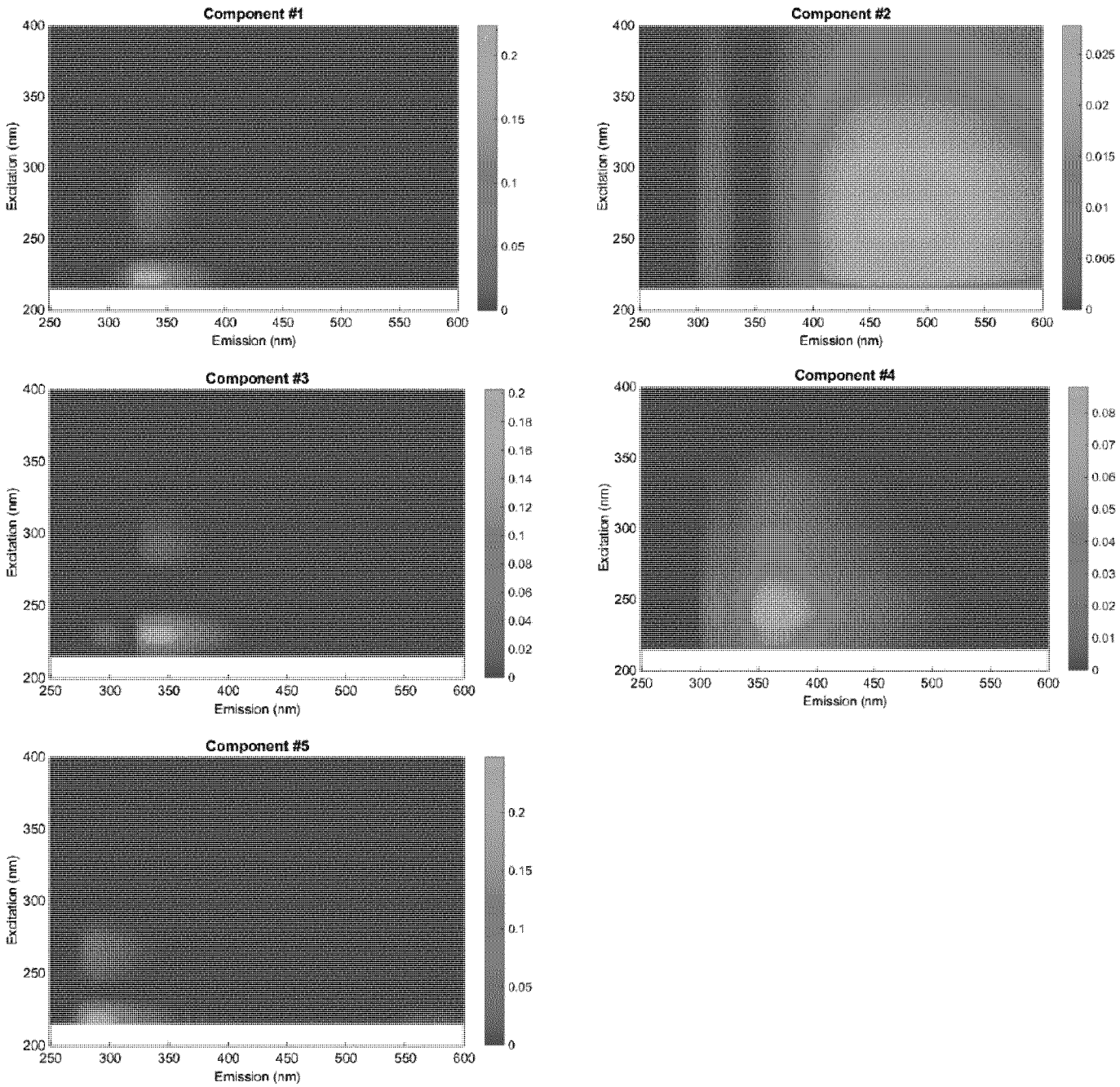


**Figure 60. EEM views of the five components of PARAFAC model for 25 oil types at DOR 1:100. Component #1: $F_{max}$ = Ex 224nm/Em 335nm; Component #2: $F_{max}$ = Ex 254-266nm/Em 455-501nm; Component #3: $F_{max}$ = Ex 230nm/Em 344nm; Component #4: $F_{max}$ = Ex 242nm/Em 363 nm; Component #5: $F_{max}$ = Ex 218nm/Em 290nm.**

DOR 1:20

Once again, a six-component was fit to the dataset containing all 25 oil types at DOR 1:20; however, an error message warning that two or more components may be fitting the same data was displayed, and the core consistency was <0%. Fitting a 5-component model to the data, however, resulted in 98.891% of the data explained by the model as well as core consistency of 84% and a split half validation of 84%. Overall, residuals were minimal and randomly distributed; however, residuals appeared to occur at somewhat higher wavelengths than at other DORs. Visual inspection of loadings (Figure 60), variation per component (Figure 62), and component EEMS (Figure 63) led to final acceptance of the 5-component model.



ED_001324_00000913-00150

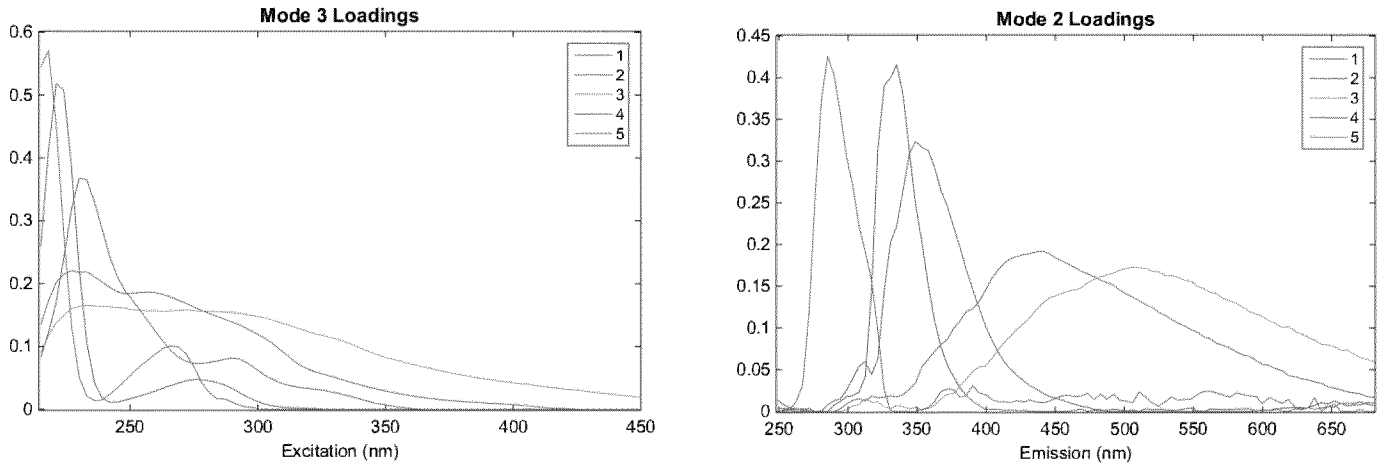


**Figure 61. Mode 3 Loadings (Excitation) and Mode 2 Loadings (Emission) for all 25 oil types—DOR 1:20 using 5-component model. Note difference in x-axis scales. Effect of full dispersion appears to broaden and shift emission peaks to longer wavelengths.**

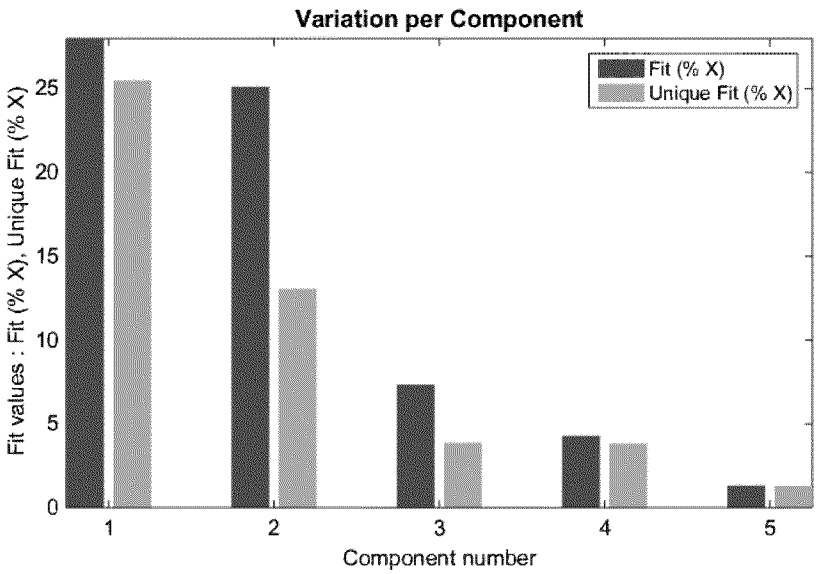


**Figure 62. Variation per Component shows Component 1 accounted for 25 to 30% of the data (unique fit and fit) while Component 2 has increased to >10% to 25% (unique fit and fit) of the data. Contribution from Component 3 and 4 have increased, as well.**



ED_001324_00000913-00151

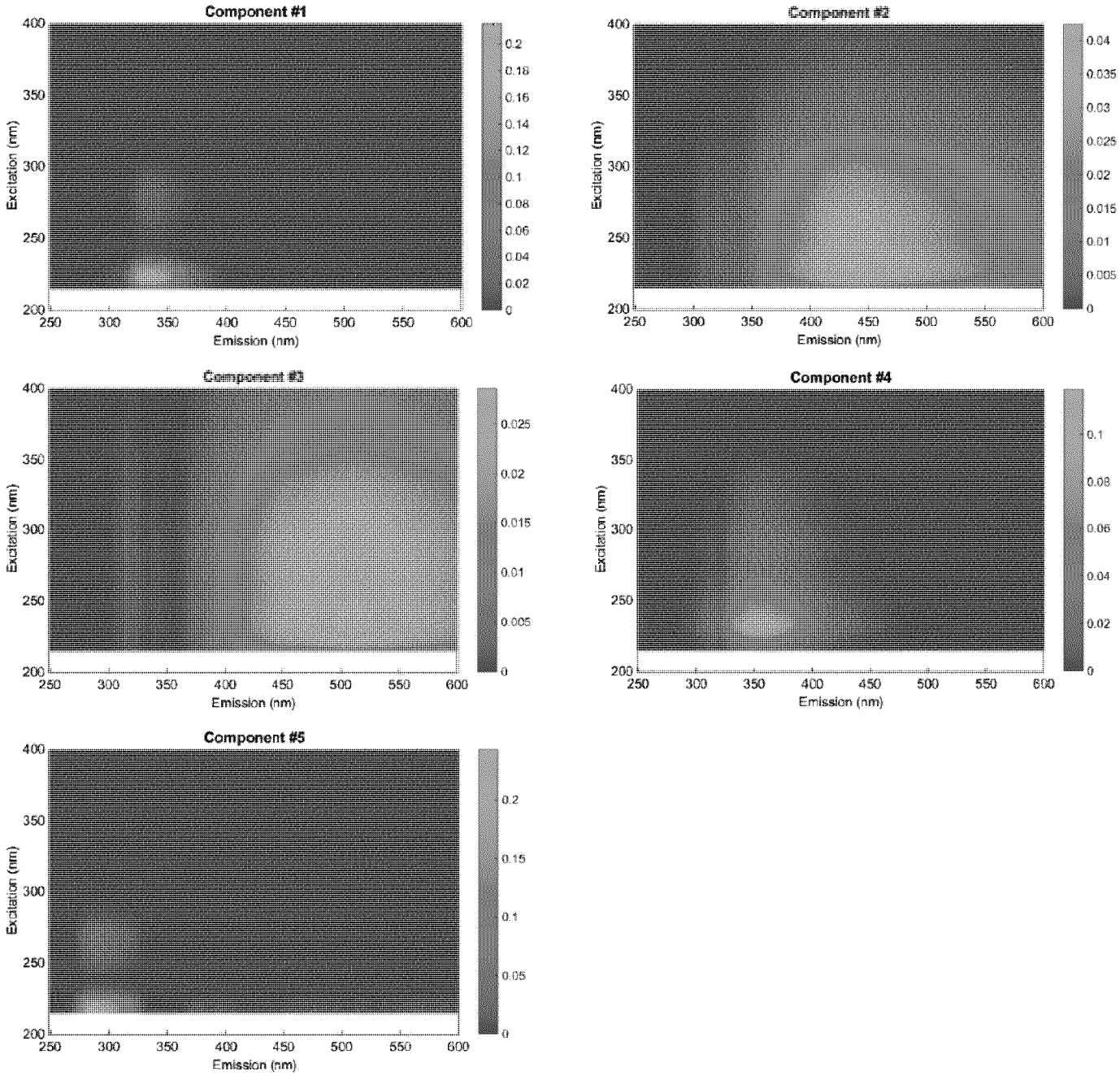


**Figure 63. EEM views of the five components of PARAFAC model for 25 oil types at DOR 1:20. Component #1: $F_{max}$ = Ex 224nm/Em 335nm; Component #2: $F_{max}$ = Ex 233-266nm/Em 432-450nm; Component #3: $F_{max}$ = Ex 230-242nm/Em 501-520nm; Component #4: $F_{max}$ = Ex 233nm/Em 349nm; Component #5: $F_{max}$ = Ex 218nm/Em 290nm.**

# PARAFAC Summary

PARAFAC analysis of EEM datasets for the 25 oil types at DOR 0, DOR 1:100 and DOR 1:20 show interesting changes in fluorescence intensity with increasing dispersion. However, we see a decrease in distinct components from six at DOR 0 to five at DOR 1:100 and 1:20. From analysis of plots of Mode 3 (Excitation) and Mode 2 (Emission) Loadings, it appears that increased dispersion results in a broadening and shift to longer emission wavelengths as well as in a larger contribution of fluorescence intensity at higher wavelengths. Upon examination of the EEMs of each component, several other patterns emerge. Even with the minimal dispersion at DOR 1:100, contribution to the overall model from a broad fluorescence peak which provided the least contribution to the overall model at DOR 0--Component #6—became second in importance at DOR 1:100, albeit with a contribution to the model of only about 5%. Upon full dispersion at DOR 1:20, this broad, high-wavelength peak retained importance to the model of approximately 5-7%; however, another broad, but slightly lower wavelength peak appeared as Component #2 with 12-25% contribution to the overall model. Throughout the entire analysis, Component #1 at Ex 224nm/Em 335nm remained the most important contribution to the model, which confirms this fluorescence region as the best target for detecting oil in the marine environment. However, since the region represented by Component #2 in the DOR 1:20 dataset becomes a major contribution to the model only upon effective dispersion, the FIR ratio (Bugden et al., 2008) can be used to track this important parameter.

The MC252 oil samples used for these analyses, both ones collected onboard the Discoverer Enterprise during DWH and the generic version provided by BP, are classified as light, sweet crude based on density and sulfur content. Overall, oil types range from light to heavy due to the proportion of n-alkanes and cyclo-alkanes vs. aromatic hydrocarbon compounds, while sulfur content determines the rank of sweet (<1%) vs. sour (>1%). These characteristics arise from kerogen source and reservoir maturity (Tissot and Welty, 1978). The 25 oils analyzed in the BFT cover a wide range of light to heavy oil types, as well as a range of sulfur content. Oil fluorescence phenomena arise from the presence of π-bonding in C=C bonds, leading to highest fluorescence intensity from polycyclic aromatic hydrocarbons (Ryder, 2005), with fluorescence



ED_001324_00000913-00153

intensity tending to increase with increasing molecular weight (Mendoza, et al., 2013). However, the presence of fluorescence quenching species, as well as energy transfer between complex molecules, complicates the isolation of compound-specific fluorescence in crude oil analysis. Fluorescence research has shown that heavy oils generally have broad, weak fluorescence while lighter oils have narrower, more intense emission bands (Steffens and Landulfo, 2010). Due to the hundreds, if not thousands, of complex hydrocarbons present in crude oils, characterization of fluorescence arising from specific PAH molecules would not be useful. However, PARAFAC analysis of these 25 oil types has shown that it is possible to use fluorescence characterization in specific wavelength regions for detect ion of non-dispersed vs. dispersed oil across a wide variety of oil types.

The well depth of the MC252 oil source is by far the deepest of all our 25 oil type sources (approximately 1600 m); however, a number of other oil types were sourced from offshore well locations. These include the light oils Brent and Gullfaks from the North Sea (140-230 m water depth) as well as Hibernia, Scotian Shelf Condensate and Terra Nova from offshore eastern Canada (12-100 m water depth). Intermediate weight oils Heidrun from the Norwegian Sea (350 m water depth) and Sea Rose from off the coast of Newfoundland, Canada (100 m water depth) as well as the heavy oil Hondo from offshore California (260 m water depth) were also included in this study. The intermediate weight Alaskan North Shore, both fresh and 10% weathered, would be representative of oil which may be sourced from offshore Alaska in the future. Additionally, with the presence of approximately 3,000 platforms in the U.S. Gulf of Mexico (BOEM, 2016), understanding the characterization of non-dispersed and dispersed MC252 oil will certainly aid in preparedness for the possibility of future oil spill events in that region.



ED_001324_00000913-00154

# References

Alliance for Coastal Technologies Report (2008) Hydrocarbon sensors for oil spill prevention and response. Ref # [UMCES]CBL08-095, 28 pp.

Andersen, C. M., R. Bro (2003) Practical aspects of PARAFAC modeling of fluorescence excitation-emission data. J. Chemom., 17:200-217.

Appellof, C.J., and E.R. Davidson (1981) Strategies for Analyzing Data from Video Fluorometric Monitoring of Liquid Chromatographic Effluents. J. Anal. Chem. 53:2053-2056.

Bahram, M., et al. (2006). "Handling of Rayleigh and Raman scatter for PARAFAC modeling of fluorescence data using interpolation." Journal of Chemometrics 20(3-4): 99-105.

Bieroza, M., A. Baker, J. Bridgeman (2010) Classification and calibration of organic matter fluorescence data with multiway analysis methods and artificial neural networks: an operational tool for improved drinking water treatment. Envirometrics, 22: 256-270.

Boehme, J.R., PG. Coble, R.N. Conmy (2004) Examining CDOM fluorescence variability using principal component analysis: seasonal and regional modeling of three-dimensional fluorescence in the Gulf of Mexico. Marine Chemistry, 89:3-14.

Bro, R. (1997) PARAFAC. Tutorial and applications. Chemometrics and Intelligent Laboratory Systems. 38:149-171.

Bro, R., and H.A.L. Kiers (2003) A new efficient method for determining the number of components in PARAFAC models. J. Chemometrics 17:274-286.

Bugden, J.B.C., C.W. Yeung, P.E. Kepkay, K. Lee (2008) Application of ultraviolet fluorometry and EEMS to fingerprint oil and chemically dispersed oil in seawater. Marine Pollution Bulletin, 56(4): 677-85.

CRRC Report (2010) Coastal Response Research Center Deepwater Horizon Dispersant USE Meeting Report, May 26-27, 2010, 108 pp.

Carroll, J.D. and J.-J. Chang (1970) Analysis of Individual Differences in Multidimensional Scaling via an N-Way Generalization of "Eckart-Young" Decomposition. Psychometrika 35:283-319.

Christensen, A.B. Hansen, J. Mortensen, O. Andersen (2005) Characterization and matching of oil samples using fluorescence and PARAFAC. Anal. Chem., 77:2210-17.

Coble, P.G. (1996) Characterization of marine and terrestrial DOM in seawater using EEM spectroscopy. Mar. Chem., 51: 325-346.

Coble, P.G. (2014) Aquatic Organic Matter Fluorescence. In Aquatic Organic Matter Fluorescence. Coble, P.G., Lead, L., Baker, A., Reynolds, D.M. and Spencer, R.G.M., Eds., Cambridge University Press, pp. 75-122.

Cole, M.G., T. King, K. Lee (2007) Analytical technique for extracting hydrocarbons from water using sample container as extraction vessel in combination with a roller apparatus. Anal. Chem., 77: 2210-17.

Conmy, R.N., P.G. Coble and C.E. Del Castillo (2004) Calibration and performance of the WetLabs' SAFIre

*in situ* fluorometer using seawater. Contin. Shelf Res., 24: 431-42.

Conmy, R. N., et al. (2014a) Submersible Optical Sensors Exposed to Chemically Dispersed Crude Oil: Wave Tank Simulations for Improved Oil Spill Monitoring. Environ Sci Technol 48(3): 1803-1810.

Conmy, R.N., C.E. Del Castillo, B. Downing, R.F. Chen (2014b) Calibrations and Quality Control of *In situ* Sensors. In: Fluorescence Applications in Aquatic Science. Eds: A. Baker & P.G. Coble, Cambridge Univ. Press, 31 pp.

Fingas, M. (2011) Introduction to Oil Chemistry and Properties. In Oil Spill Science and Technology; Fingas, M., Eds; Elsevier. pp. 51-59.

Frank, U. (1978) A Review of Fluorescence Spectroscopic Methods for Oil Spill Source Identification. Toxicological and Environment Chemistry Rev., 2:163-185.

Fuller, C.B., J.S. Bonner, C.A. Page, G. Arrambide, M.C. Sterling, Jr., T. Ojo (2003) Field instruments for real time in-situ crude oil concentration measurements. A Conrad Blucher Institute, Texas A&M Corpus Christi Report, 10 pp.

Harshman, R.A. (1970) Foundations of the PARAFAC procedure: Models and conditions for an "explanatory" multimodal factor analysis. UCLA Working Papers in Phonetics 16:1-84.

Harshman, R.A. and M.E. Lundy (1994) PARAFAC: Parallel factor analysis. Computational Statistics & Data Analysis 18:39-72.

Johansen, O., et al. (2013) Droplet breakup in subsea oil releases - Part 2: Predictions of droplet size distributions with and without injection of chemical dispersants. Marine Pollution Bulletin 73(1): 327-335.

Joint Analysis Group Report (2010) Review of Data to Examine Subsurface Oil in the Vicinity of DWH MC-252, May 19-June 19, 2010; 29 pp.

Kepkay, P., W. Young, J.B.C. Bugden, Z. Li, K. Lee (2008) Ultraviolet fluorescence spectroscopy (UVFS): A new means of determining the effectiveness of chemical dispersants on oil spills. International Oil Spill Conference. API, Washington D.C., Savannah, GA, pp. 639-44.

King, T.L., B. Robinson, C. McIntyre, P. Toole, S. Ryan, F. Saleh, M.C. Boufadel, K. Lee (2015) Fate of surface spills of cold lake blend diluted bitumen treated with dispersant and mineral fines in a wave tank. In: Environmental Engineering Science, Vol. 32, No. 3, 01.03.2015, p. 250-261.

Lee, K., Li, Z., Boufadel, M.C., Venosa, A.D. and Scott Miles, M. (2009) Wave tank studies on dispersant effectiveness as a function of energy dissipation rate and particle size distribution. Final report submitted to NOAA/CRRC/UNH. Pp67+ appendix.

Li, Z., Lee, K., King, T., Boufadel, M.C. and Venosa, A.D., (2008) Oil droplet size distribution as a function of energy dissipation rate in an experimental wave tank 2008 International Oil Spill Conference. Americal Petroleum Institute, Washington D.C., Savannah, GA, pp. 621-626.

Li, Z., Lee, K., King, T., Boufadel, M.C. and Venosa, A.D., (2009a) Evaluating Chemical Dispersant Efficacy in an Experimental Wave Tank: 2, Significant Factors Determining *In Situ* Oil Droplet Size Distribution. Environmental Engineering Science, 26(9): 1407-1418.

Li, Z., Lee, K., King, T., Boufadel, M.C. and Venosa, A.D., (2009b) Evaluating crude oil chemical dispersion efficacy in a flow-through wave tank under regular non-breaking wave and breaking wave conditions. Marine Pollution Bulletin, 58: 735-744.

Li, Z., Lee, K., King, T., Boufadel, M.C. and Venosa, A.D., (2010) Effects of temperature and wave conditions on chemical dispersion efficacy of heavy fuel oil in an experimental flow-through wave tank. Marine Pollution Bulletin, In Press, Corrected Proof.

Li, Z., K. Lee, T. King, P.E. Kepkay, O. Mikkelsen, C. Pottsmith (2011) Monitoring dispersed oil droplet size distribution at the GOM Deepwater Horizon spill site. International Oil spill Conference Proceedings, March 2011.

Masutani, S.M., E.E. Adams (2000) Experimental Study of Multiphase Plumes with Application to Deep Ocean Oil Spills," Final Report to U.S. Dept. of the Interior, Minerals Management Service, Contract No., 1435-01-98-CT-30946.

Mendoza, W.G., D.D. Riemer, R.G. Zika (2013) Application of fluorescence and PARAFAC to assess vertical distribution of subsurface hydrocarbons and dispersant during the Deepwater Horizon oil spill. Environmental Science Processes & Impacts 15:1017-1030.

Murphy, K. R., et al. (2010). "Measurement of Dissolved Organic Matter Fluorescence in Aquatic Environments: An Interlaboratory Comparison." Environ Sci Technol 44(24): 9405-9412.

Murphy, K. R., C.A. Stedmon, D. Graeber, R. Bro (2013) Fluorescence Spectroscopy and mutli-way techniques, PARAFAC. Anal. Methods, 5: 6557-6566.

Murphy, K.R., Bro, R., Stedmon, C.A. (2014) Chemometric Analysis of Organic Matter Fluorescence. In: Aquatic Organic Matter Fluorescence. Eds: Coble, P.G., Lead, J., Baker, A., Reynolds, D.M., Spencer, R.G.M. Cambridge University Press, pp.339-375.

NOAA Technical Report NOS OR&R 25 (2010): Joint Analysis Group, Deepwater Horizon Oil Spill: Review of Preliminary Data to Examine Subsurface Oil in the Vicinity of MC252, May 19 – June 19, 2010, 168 pp.

Oil Budget Calculator (2010) NOAA Report Oil Budget Calculator: Deepwater Horizon, Federal Interagency Solutions Group, 217 pp.

NRC Report (2005) National Research Council Oil Spill Dispersants: Efficacy and Effects, Washington, DC, 400 pp.

Priaro, M. (2014) A Bitumen and Dilbit Primer. https://www.behance.net/gallery/16654901/A-BITUMEN-AND-DILBIT-PRIMER (accessed June 10, 2016).

Rosin, P., E. Rammler (1933) The Laws Governing the Fineness of Powdered Coal. J. Institute of Fuel, 7, 29-36.

Ryder, A.G. (2005) Analysis of Crude Petroleum Oils Using Fluorescence Spectroscopy. Reviews in Fluorescence 2005 pp. 169-198.

Smilde, A., Bro, R., Geladi, P. (2004) Validation and Diagnostics. In: Multi-way Analysis with Applications in the Chemical Sciences. John Wiley & Sons, Ltd. Pp. 145-173

Stedmon, C.A., S. Markager, R. Bro (2003) Tracing dissolved organic matter in aquatic environments using a new approach to fluorescence spectroscopy. Mar. Chem., 82: 239-54.

Stedmon, C.A., R. Bro (2003) Characterizing dissolved organic matter fluorescence with parallel factor analysis: a tutorial. Limnol. Oceanogr. Methods, 6: 572-579.

Steffens, J., Landulfo, E., Courrol, L.C., Guardani, R. (2011) Application of Fluorescence to the Study of Crude Petroleum. J. Fluoresc. 21:859-864.

Tissot, B.P. and D.H. Welty (1978) Classification of Crude Oils. In: Petroleum Formation and Occurrence. Springer-Verlag, pp. 369-377.

Venosa, A.D., D.W. King, G.A. Sorial (2002a) The Baffled Flask Test for Dispersant Effectiveness: A Round Robin Evaluation of Reproducibility and Repeatability. Spill Science &Technology Bulletin, 7(5-6): 299-308.

Venosa, A.D., K. Lee, M.T. Suidan, S. Garcia-Blanco, S. Cobanli, M. Moteleb, J.R. Haines, G. Tremblay, M. Hazelwood (2002b) Bioremediation and Biorestoration of a Crude Oil-Contaminated Freshwater Wetland on the St. Lawrence River. Bioremediation Journal,6(3):261-281.

Wickley-Olsen, E., Boufadel, M.C., King, T., Li, Z., Lee, K., Venosa, A.D. (2007) Regular and breaking waves in wave tank for dispersion effectiveness testing. In: Proceedings of the 30th Arctic and Marine Oil spill Program (AMOP) Technical Seminar, Edmonton, AB, Canada. Environment Canada, Ottawa, Ontario, Canada, pp. 161–187.

Zepp, R. G., et al. (2004). "Dissolved organic fluorophores in southeastern US coastal waters: correction method for eliminating Rayleigh and Raman scattering peaks in excitation-emission matrices." Marine Chemistry 89(1-4): 15-3.

Zhao, L., et al. (2014). "Evolution of droplets in subsea oil and gas blowouts: Development and validation of the numerical model VDROP-J." Marine Pollution Bulletin 83(1): 58-69.

Zhou, Z, Guo, L., Shiller, A.M., Lohrenz, S.E., Asper, V.L., Osburn, C.L. (2003) Characterization of oil components from the Deepwater Horizon oil spill in the Gulf of Mexico using fluorescence EEM and PARAFAC techniques. Marine Chemistry 148:10-21.



ED_001324_00000913-00158

# Appendices (Separate Document)

APPENDIX A – Experiment Logs

APPENDIX B – Analytical Chemistry Results

APPENDIX C – Jet Release LISST Oil Droplet Size Distribution Histograms

APPENDIX D – Jet Release LISST Oil Droplet Size Distribution Time Series Contours

APPENDIX E – Submersible Fluorescence Time Series

APPENDIX F – Excitation Emission Matrix Contours

APPENDIX G – VDROP-J and JETLAG Numerical Plume Modeling Report

APPENDIX H – Weber Number Scaling Numerical Plume Modeling Report

**To:** conmy.robyn@gmail.com[conmy.robyn@gmail.com]
**From:** Conmy, Robyn
**Sent:** Tue 2/21/2017 7:51:06 PM
**Subject:** FW: back
IOSC 2017 Poster - B Robinson.pdf

<>/<>/<>/<>/<>/<>/<>/<>/<>/<>/<>/<>/<>/<>/<>/<>/<>

Robyn N. Conmy, Ph.D.

Research Ecologist

USEPA/NRMRL/LRPCD

26 West MLK Drive

Cincinnati, Ohio 45268

513-569-7090 (office)

513-431-1970 (EPA mobile)

727-692-5333 (Personal mobile)

conmy.robyn@epa.gov

**From:** Robinson, Brian [mailto:Brian.Robinson@dfo-mpo.gc.ca]
**Sent:** Tuesday, February 21, 2017 2:37 PM
**To:** Conmy, Robyn <Conmy.Robyn@epa.gov>; Michel Boufadel <boufadel@gmail.com>; King, Thomas L <Tom.King@dfo-mpo.gc.ca>
**Subject:** RE: back

Hi Robyn,

You caught me right in the middle of writing an email with the data!

I'm happy to report that we have all of the hypersaline data processed and chemistry samples

analyzed. I apologize for the delay in compiling this. The link below should lead to an archive file that can be downloaded.

https://drive.google.com/open?id=0BxtdKWaxXZP2ZU12aXFBNnF2Rmc

This includes:

- Raw and processed LISST data from two instruments (close to the oil release as well as farther downstream)

- Raw and processed data from the fluorometers (Turner, Chelsea, ECO) using manufacturer calibration curves

- Raw data from the SeaOWL – This data will need some work additional work in order to process, since there are many data streams

- Water column chemistry data – BTEX and TPH

I'm in the process of compiling a summary of the experimental methods that were used for these experiments, as well as my first pass at interpreting the data. I will share this as soon as I have a draft ready. In addition, I have completed a first draft of the IOSC poster which is attached. In summary, it would appear as though higher salinities did not have a significant effect on the DSD in our tank.

If you have any specific questions at this point, please let me know.

Brian

**From:** Conmy, Robyn [mailto:Conmy.Robyn@epa.gov]
**Sent:** February-21-17 3:16 PM
**To:** Michel Boufadel; King, Thomas L; Robinson, Brian
**Subject:** RE: back

Brian and Tom,

Is the hypersaline data ready to send to Michel? It was great to see Ken Lee at GoMRI 2 weeks ago, but sad that you weren't also in attendance.

Cheers,

Robyn

<>/<>/<>/<>/<>/<>/<>/<>/<>/<>/<>/<>/<>/<>/<>/<>

Robyn N. Conmy, Ph.D.

Research Ecologist

USEPA/NRMRL/LRPCD

26 West MLK Drive

Cincinnati, Ohio 45268

513-569-7090 (office)

513-431-1970 (EPA mobile)

727-692-5333 (Personal mobile)

conmy.robyn@epa.gov

**From:** Michel Boufadel [mailto:boufadel@gmail.com]
**Sent:** Friday, February 17, 2017 5:54 PM
**To:** Conmy, Robyn <Conmy.Robyn@epa.gov>
**Subject:** back

Hi Robyn,

I hope you return back home went well. I also hope we have some updates on the brine project.

Thank you,

Michel

--

Michel C. Boufadel, PhD, PE, BCEE, F. ASCE, D.WRE, P.Hydro.
Director, Center for Natural Resources Development and Protection (NRDP)

Professor, John A. Reif, Jr. Dept. Civil and Environmental Engineering

The New Jersey Institute of Technology

Room 435 Colton Hall

323 MLK Blvd, Newark, NJ 07102-1824

Ph: 973-596-6079

email: boufadel@gmail.com

http://nrdp.njit.edu

# Oil plume simulations: Tracking oil droplet size distribution and fluorescence within high-pressure release jets

**R.N. Conmy**[1], **B. Robinson** [2], **T. King** [2], **M. Boufadel**[3], **S. Ryan**[2], **C. McIntyre**[2], **M. I. Abercrombie**[4], **K. Lee** [2,5]

[1]U.S. Environmental Protection Agency, Office of Research and Development, 26 MLK Drive West, Cincinnati, OH 45255, USA

[2] Bedford Institute of Oceanography, Fisheries and Oceans Canada, 1 Challenger Dr, Dartmouth, NS, B2Y 4A2, Canada

[3] New Jersey Institute of Technology, Department of Civil and Environmental Engineering, University Heights, Newark, NJ 07102, USA

[4]University of South Florida, College of Marine Science, 140 7th Ave South, St. Petersburg, FL 33701, USA

[5] Commonwealth Scientific and Industrial Research Organisation, Oceans and Atmosphere Flagship, PO Box 1130, Bentley WA 6102, Australia

## ABSTRACT

Optical measurements have been used during oil spill response for more than three decades to determine oil presence in slicks and plumes. Oil surveillance approaches range from simple (human eyeball) to the sophisticated (sensors on AUVs, aircraft, satellites). *In situ* fluorometers and particle size analyzers were deployed during the Deepwater Horizon (DWH) Gulf of Mexico oil spill to track shallow and deep subsea plumes. Uncertainties regarding instrument specifications and capabilities during DWH necessitated performance testing of sensors exposed to simulated, dispersed oil plumes. Seventy two wave tank experiments were conducted at the Bedford Institute of Oceanography. Simulated were oil releases with varying parameters such as oil release rate, oil temperature (reservoir temp ~ 80 °C), water temperature (<8 °C and >15 °C), oil type, dispersant type (Corexit 9500 and Finasol OSR52) and dispersant



ED_001324_00000917-00001

to oil ratio (DOR). Plumes of Alaskan North Slope Crude, South Louisiana Crude and IFO-120 oils were tracked using *in situ* fluorescence, droplet size distribution (DSD), total petroleum hydrocarbons (TPH) and benzene-toluene-ethylbenzene-xylene (BTEX). Results offer valuable information on the behavior and dispersibility of oils over a range of viscosity, DOR and environmental conditions. Findings have implications for fate and transport models, where DSD, chemistry and fluorescence are all impacted by release variables. This research was supported by the Bureau of Safety and Environmental Enforcement.

## INTRODUCTION

The 2010 *Deepwater Horizon* (DWH) oil spill highlighted the pressing need for a better understanding of the interaction of chemical dispersants and crude oil at ocean depth. Early in the blowout release, partial emulsification of oil and heterogeneous slicks were observed as it rose to the surface from 1500-m depth (JAG report, 2010). As a countermeasure, Sub-Sea Dispersant Injection (SSDI) was used, where dispersants were injected directly at the release point as a possible means to increase dispersion efficiency and to potentially reduce the amount of dispersant needed if applied at the air-sea interface (CRRC Report, 2010). Potential advantages of this application during a continuous oil release included the fact that the fresh (unweathered) oil was considered well suited for dispersion, operators were able to inject the dispersant directly into the oil stream thereby maximizing dispersant/oil contact, sufficient control of DOR (Dispersant-to-Oil Ratio) could be maintained, injection may minimize the need for surface application because of reduced oil surfacing, and optimized subsurface application would likely promote formation of smaller and stable oil droplets, enhancing biodegradation (Lee et al., 2009). The Unified Area Command (UAC) coordinated a large-scale environmental



ED_001324_00000917-00002

monitoring program to track and characterize dispersed subsurface oil plumes based on field data and transport modeling outputs. Oil Droplet Size Distribution (DSD) and fluorescence intensity from submersible sensors were used as an indication of Dispersion Effectiveness (DE) onboard vessels, where concentrations were monitored to evaluate oil dispersion (presence of small droplets $\leq 70$ μm) based on previous studies for surface dispersant applications (Li et al., 2009a). Monitoring provided sound evidence of the presence of oil-bearing small particles both in surface waters and in the subsurface plume (JAG Report, 2010). SSDI correlated with a higher proportion of low molecular weight compounds in subsea waters compared to surface, suggesting that SSDI may have promoted the formation of small oil droplets in the deep sea and thus would have the potential for enhancing the weathering and dissolution of oil in the water column.

Uncertainties still exist, however, regarding the effectiveness of this application. For example, assumptions of the optimal DOR are based on empirical data mostly obtained from bench-scale experiments designed for testing at standard temperatures and pressures (STP), whereas conditions at a wellhead on the ocean floor or anywhere along a riser could be significantly different. Hence, DOR for direct injection needs to be better understood. Although theoretical analyses and experiments suggest that oil jet breakup is insensitive to the absolute value of hydrostatic pressure for incompressible liquid-liquid systems (Masutani and Adams 2000), the effects of several ambient environmental factors on SSDI, including high release pressure, high oil temperature, low water temperature, and the presence of methane and suspended sediments in the oil plume and/or surrounding water column remain to be clarified. Improved understanding on the influence of these factors and the interaction of oil and chemical



ED_001324_00000917-00003

dispersant under a range of turbulent regimes at depth is required for informed decision-making for future SSDI use.

For evaluating DE, standard laboratory tests are inherently limited in simulating operational performance under realistic environmental conditions in part due to space constraints that are critical for transport and dilution efficiency (NRC, 2005). Meso-scale tanks capable of generating waves and flume flows to simulate ocean conditions help to address this issue. One such tank facility at the Bedford Institute of Oceanography (BIO; Dartmouth, Nova Scotia) has been used previously to assess chemical dispersant effectiveness for various oil types as a function of energy dissipation rate and particle size distribution (Li et al. 2009b) and demonstrated that the effectiveness of a dispersant is strongly dependent on wave conditions, dispersant type, and oil type (Wickley-Olsen et al. 2007; Li et al. 2008; Lee et al. 2009). A strong correlation has been established between dispersion effectiveness and *in situ* DSD within the hydrodynamic regime, particularly energy dissipation rate, under a variety of wave conditions (Li et al. 2008; Li et al. 2009b), where flume mode can simulate the effects of underwater currents on dispersion and dilution of oil (Li et al. 2009a; Li et al. 2010). Experiments have also shown the reliability of fluorescence intensity as a proxy for oil concentration within oil dispersions (Conmy et al., 2014).

Presented here are results from a series of high pressure jet releases of oil within the BIO flume tank to assess the operational performance of SSDI. DSD and fluorescence intensity were used as a proxy for dispersion efficiency for treatments with (chemically-enhanced dispersion) and without (physical dispersion) chemical dispersants. The objective of this work was to evaluate the effects of water temperature and dispersant-to-oil ratio on DE of three oils at high



ED_001324_00000917-00004

reservoir temperatures. Findings help (1) to determine the applicability of existing *in situ* monitoring technologies for SSDI and (2) inform efforts to integrate DSD into deepwater blowout plume formation models that enable prediction of the dispersed oil droplets under high-flow subsurface release velocities. DWH spill monitoring program DSD and fluorescence data played a significant role in supporting emergency response operations, fate and transport modeling, and impact assessment. Findings from this study have implications for efforts in support of future deep-water spill preparedness.

## METHODS

***Flume Tank Description*** - Oil dispersion experiments were conducted using Alaska North Slope crude oil (ANS), South Louisiana Crude (SLC) and Intermediate Fuel Oil 120 (IFO 120) with Corexit 9500 and Finasol OSR 52 chemical dispersants in the 32m long flow-through carbon steel flume tank (31,000 L) at BIO. Seawater was pulled from the Bedford Basin (50cm below surface) via two smaller centrifugal pumps (110 gpm), and filtered through high-flow polypropylene bag filters (5 and 25 μm) to a fiberglass holding tank (25,000 L) that supplies seawater for the system to ensure that a constant flow rate is maintained. Two high-flow centrifugal pumps (600 gpm) provided flow to generate horizontal water currents in the tank, where flow gauges on influent and effluent pipes were monitored and valve adjustments made to obtain a balanced flow rate throughout experiments. Water current velocities were measured in the tank using an ADV (Nortek Vectrino) to maintain consistent horizontal water current velocities (3.5 cm/s) at all measured depths. At the completion of experiments, oil absorbent pads removed oil from the water surface. Effluent wastewater was filtered over layers of polypropylene PomPom Oil-Mops to remove insoluble oil from the water prior to discharging, where effluent samples were collected and PomPom's were changed if oil concentrations exceed



ED_001324_00000917-00005

the minimum guidelines (10 ppm) for wastewater discharge in Canada.

***Subsurface Oil Injection System*** - A custom subsurface oil injection system was used to generate dispersed oil plumes in the tank (Figure 1), consisting of a 2 L stainless steel pressure vessel and a series of valves and pressure gauges, fastened to the outer wall of the tank. Inside the tank, a fitting connects the outer assembly to a nozzle (2.4 mm), which extends mid-width perpendicular to the tank wall (9 m downstream from the influent pipe) and is angled at the tip to direct the discharge plume downstream and use horizontal length of the tank to capture the plume movement. For each experiment, oil or oil/dispersant premix is added to the pressure vessel in order to reduce the influence of any additional confounding factor of mixing effectiveness. Copper coil within the pressure vessel connects to a water bath to permit oil heating to 80°C, and then pressurized (40 psi for ANS and SLC; 60 psi for IFO 120) with compressed Nitrogen. A ball valve connected to the vessel controls the oil release through the subsurface nozzle into the tank. Release time and total volume (determined by mass) of oil injected are recorded. After each experiment, the subsurface injector system was cleaned by flushing with toluene, acetone and fresh water.

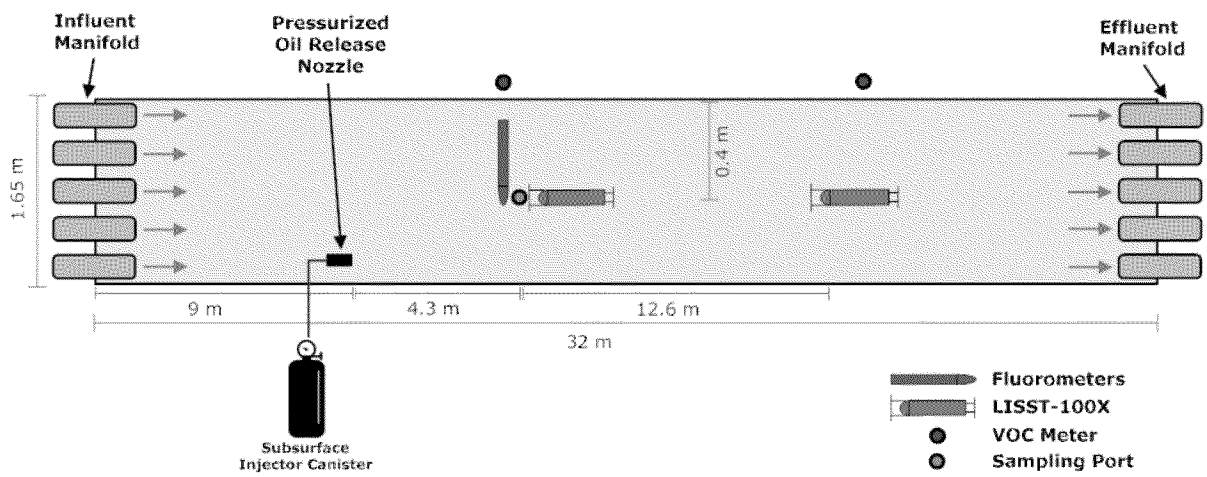

**Figure 1. Schematic diagram showing the location of the subsurface injector and *in situ* instrumentation submerged within the tank.**

***Submersible Sensor Deployment*** - Sensors were mounted on an aluminum frame located 4.3 m from the oil release point with their pressure windows and at a depth of 0.4 m. The instruments were attached to a crosspiece support bar, so that they were all located the same distance downstream from the oil release point with the pressure window pointed directly towards the bottom of the tank. Data acquisition systems were used to control and collect data with real-time displays from the *in situ* fluorometers. A total of six *in situ* hydrocarbon fluorometers were evaluated during this study; Chelsea Technologies Group UV Aquatrackas - Refined and Crude models, Turner Designs Group Cyclops - Fine and Crude models, Sea Bird – Wet Labs Inc ECO-FLU, and GmBH Trios. Sampling rates and units of signal intensity varied for each instrument with one reading every 5 seconds for GmBH (μg/L PAH), every 3 seconds for Cyclops (auto-gain feature; mV), and every 1 second for the ECO and Aquatrackas (μg/L QSDE, μg/L perylene and μg/L carbazole, respectively. Oil droplet size was measured *in situ* using two LISST-100X (Laser *in-situ* Scattering and Transmissometry) particle size analyzers (Sequoia Scientific, Inc), measuring particle size from 2.5 – 500 μm. The first LISST (upstream LISST) was located immediately after the fluorometer package support frame at a distance of 5.1 m from the oil release point and the second LISST (downstream LISST) was located at 16.9 m from the oil release point and both at a depth of 0.4 m (Figure 1). Placement was informed by the numerical modeling efforts conducted previously in the tank to maximize oil droplet detection without saturating the instrument. Real-time data was provided by LISST-SOP data acquisition software (ver. 5) with a sample acquisition rate of one measurement every 3 seconds.



ED_001324_00000917-00007

Underwater video of oil droplets and the transport of the plume were captured using a GoPro Hero4 digital camera, as well as a Sony RX100 III digital camera with underwater housing.

***Submersible Sensor Data Processing*** - LISST data files were processed using a statistically-based quality control script written using the R statistical package. This script identifies and removes "Over Range" samples (defined as 0 μL/L) and outliers. Outliers are defined as any reading that is greater than the moving mean (5 data points before and after the targeted time point) of the dataset multiplied by four times the standard deviation (over the same interval as the moving mean). Due to the potential for one or more extreme outliers to skew both the moving mean and standard deviation calculations for points around them, this outlier detection routine is run iteratively, excluding previously flagged points, until no more outliers are detected. The script then calculates the Total Particle Concentration (TPC), Volume Mean Diameter (VMD), and Particle Size Concentration (PSC). It then detects the plume curve (if present) and time-normalizes the data based on that location. Data are presented as Droplet Size Distribution (DSD). Plots presented include data 2 minutes before and 8 minutes after the start of the plume curve. Data from the Downstream LISST were normalized so that the plume began at t = 5 min in order to visually convey that the plume was detected in the tank roughly 3 min after detection by the LISST further upstream near point of injection release. Similar to the LISST data, a script was used to detect outliers in the fluorometry data. Curve detection was performed and the data was time-normalized to include 2 minutes of data before, and 8 minutes of data after the start of the plume curve. The baseline of the plume curve was calculated using data points observed in the first minute preceding the start of the curve and this baseline was subtracted from the data. Finally, factory calibration factors were applied to the data.

***Experimental Design*** -. Seawater temperature and salinity in the tank were recorded



ED_001324_00000917-00008

using a handheld probe (YSI Incorporated, Yellow Springs, OH). Prior to experiments, the tank was operated in recirculation mode (10 minutes) to allow current flow to stabilize. Five minutes prior to oil injection, data-logging on all instruments was started and background seawater samples were collected. After oil injection, the real-time readout of the fluorometer signal was monitored for the first spike in signal intensity (usually after 2 minutes), and bottle chemistry sample collection began. The experiments ran for 12 minutes and the tank was cleaned using Big Orange Degreaser, to prevent any potential contamination between experiments. Instrument windows were cleaned using disposable alcohol wipes. Water samples were returned to the lab and stored at 4°C.

***Discrete Chemistry Samples*** - Water samples for chemical analysis were collected at various time points throughout the experiments. Three ¼" stainless steel tubes were attached to the aluminum fluorometer frame, so that the end of the tube was located at the same depth as the instrument pressure windows (0.4 m). These were attached via silicon tubing to a digital peristaltic pump with a 120 mL/min flow rate. Samples were analyzed for Total Petroleum Hydrocarbon (TPH) using a method developed by DFO in-house (Cole et al., 2007; King et al., 2015) for Gas Chromatograph (GC) - Flame Ionization Detector (FID) analysis. An eight point calibration was generated using standards prepared from the appropriate crude oil stock that was used to generate the TPH samples (e.g. ANS, IFO 120 and SLC). Peak quantification was performed using relative response factors. Samples were analyzed for benzene, toluene, ethylbenzene and xylene (BTEX) using EPA Method 8240 (purge and trap), modified by running a GC - Mass Spectrometer (MS) in selected ion monitoring mode to include ethylbenzene. BTEX standards were prepared in 40 mL purge and trap vials; and samples and standards were analyzed using this method, along with sample blanks and duplicate samples.



ED_001324_00000917-00009

TPH and BTEX results are not shown here in detail but can be found in the EPA 600/F-16/250 Report (2016).

## RESULTS & DISCUSSION

A total of 72 experiments were conducted in replicate, where water ranged in temperature from 4.9 - 20.3 °C, with 11 °C serving as the cut off between warm and cold water tests. Previous experiments within the BIO flume tank facility have assessed dispersion effectiveness as a function of energy dissipation rate and particle size distribution (Li et al. 2009a) and demonstrated that DE is strongly dependent on wave conditions, dispersant type, and oil type (Lee et al. 2009) and highly correlated with *in-situ* droplet size distribution (Li et al. 2008; Li et al. 2009a). Here, DE was evaluated via response monitoring tools (fluorescence and particle size analyzers) during high-pressure subsurface injection experiments.

***Dispersant-to-Oil Ratio (DOR) Effects***- Addition of either Corexit 9500 or Finasol OSR 52 chemical dispersants to Alaskan North Slope (ANS), IFO 120 and South Louisiana Crude (SLC) oils resulted in a decrease in the Volume Mean Diameter (VMD) and shifted the Droplet Size Distribution (DSD) to smaller droplets for warm water treatments (Figure 2). For ANS, dispersions created without chemical dispersants or Dispersant-to-oil ratio (DOR) = 1:100 yielded VMD larger than 70 μm and exhibited unimodal DSD. Dispersions created with DOR = 1:20 yielded VMD between < 70 μm size range with a bimodal distribution. SLC oil was more dispersible compared to ANS for treatments with and without chemical dispersant. Bimodal distribution was observed during DOR = 1:20 and some DOR = 1:100 experiments indicating that the jet release of this particular oil into warm water produced smaller droplets than the ANS. During the DWH spill, droplets ≤ 70μm were considered small enough to remain in suspension



ED_001324_00000917-00010

and were monitored as a proxy for evaluating oil dispersion efficiency. This suggests that produced SLC droplets from a DOR = 1:20 or 1:100 dispersant injection, and ANS droplets at DOR = 1:20 would likely remain dispersed in the presence of mixing energy given the larger proportion of small droplet sizes observed. In general, Corexit 9500 produced slightly smaller droplets compared to Finasol OSR 52 for warm water treatments. The addition of Corexit 9500 or Finasol OSR 52 to IFO 120 during warm temperature experiments resulted in a shift in DSD and a decrease in VMD; however bimodal distribution was not achieved and even DOR = 1:20 did not yield VMD less than 70 μm in most cases. This suggests that dispersant addition to this oil at warm temperatures would not yield droplet sizes that would likely remain in suspension.

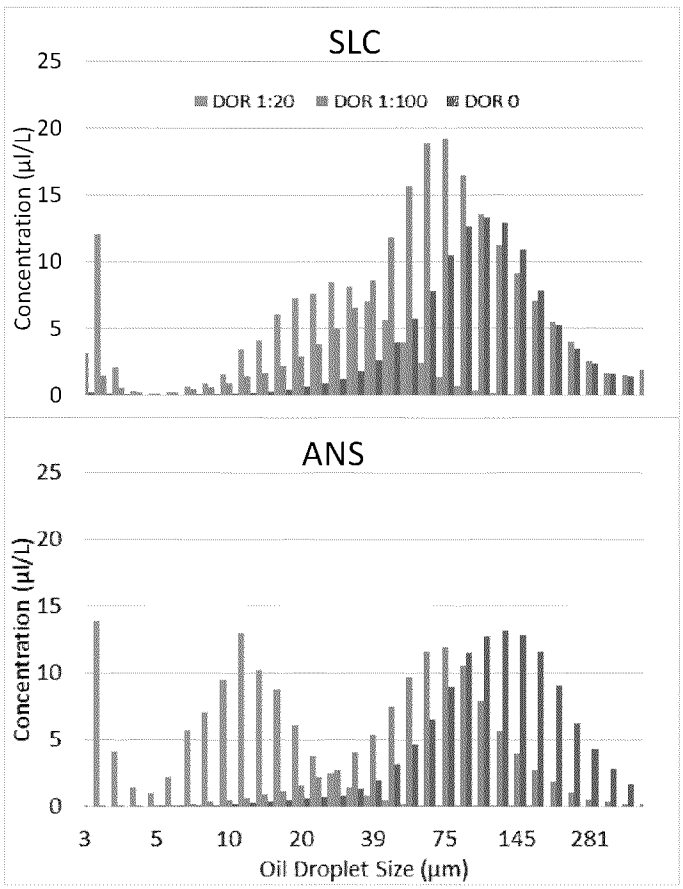

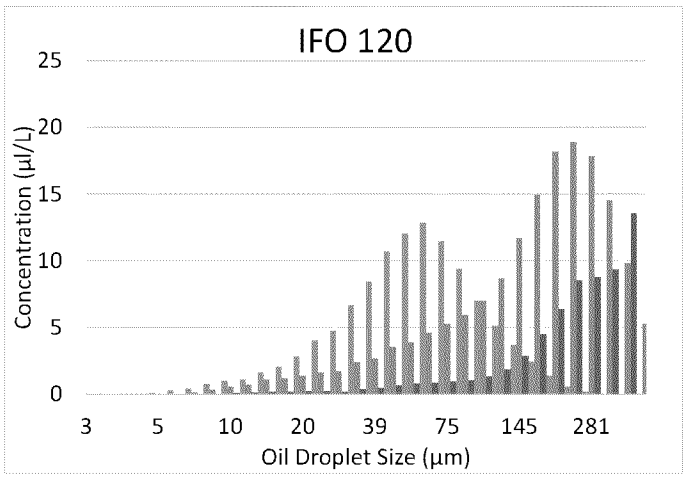


**Figure 2. LISST DSD for SLC, ANS and IFO 120 with Corexit 9500 at three DOR treatments in warm water. Histograms represent averages obtained at the 2 minute time stamp during each experiment.**

***Water Temperature Effects*** - For ANS, dispersion with < 70 µm droplet VMD was observed for the DOR = 1:20 treatments at both cold and warm water temperatures (Figure 3). Water temperature did not appear to influence the DSD or VMD for this lighter crude oil. However, a temperature effect was observed on the Total Particle Concentration (TPC), where lower temperatures were coincident with fewer particles dispersed within the plume for a given volume of oil injected. This may be due to enhanced density differences between the oil and water at colder temperatures, thus quicker rise time of the produced droplets. For the addition of Corexit 9500 or Finasol OSR 52 to IFO 120 at cold water temperatures, smaller droplet sizes were not observed, where DOR = 1:20 remained above 200 µm. This suggests that dispersant addition to this oil at cold temperatures would not yield droplet sizes that would likely remain in suspension.

ANS IFO 120

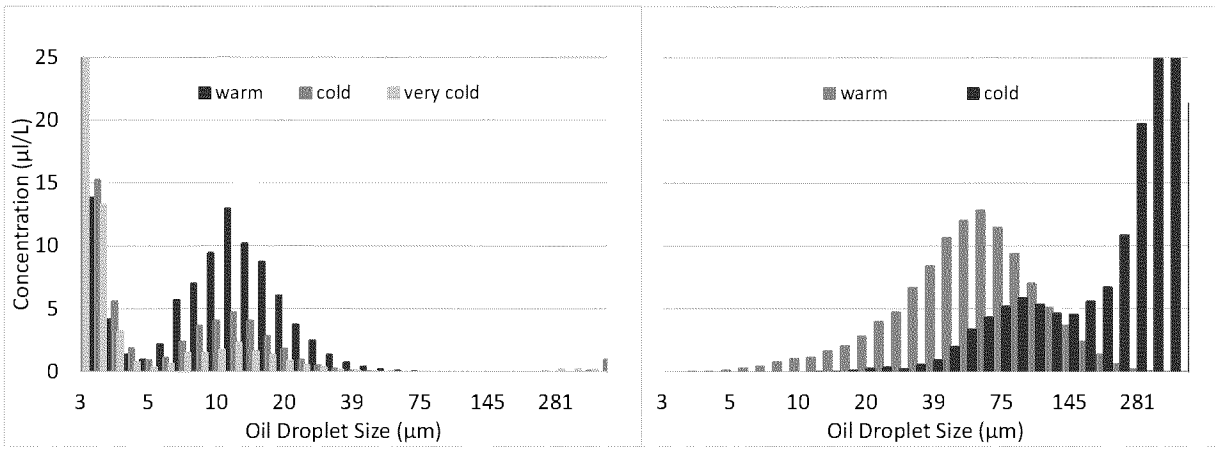


**Figure 3. LISST DSD for ANS and IFO 120 with Corexit 9500 at DOR = 1:20 and varying water temperature.**

For experiments conducted at water temperatures < 5 °C, the LISST particle size analyzer yielded unexpected DSD where even a unimodal distribution was not measured. Chemistry and *in situ* fluorescence data indicate that the oil was in fact dispersed adequately. This suggests potential operational problems < 5 °C, even though it is within the operating temperature (manufacturer manual). Additional testing of cold water temperature limits is recommended.

***Upstream and Downstream Particle Fractionation*** - Histograms representing the particle concentration for a given size class from the upstream and downstream LISSTs suggest dilution and fractionation of particles within the plume. The downstream LISST positioned further from the jet release serves as an indication of plume evolution through the tank. For all oil and DOR treatments, dilution in particles (decrease in TPC) within the plume expectedly occurred. Also evident is a shift to smaller particles for all DOR treatments as the plume moves through the tank, where size fractionation was dependent on DOR treatment (Figure 4). Physical dispersion (DOR 0) treatments for lighter oils were found to have the largest shift in

DSD and VMD between the upstream and downstream LISSTs suggesting the largest effect of particle fractionation in the plume. Where the decrease in TPC suggests plume dilution in the tank, the DSD shift to smaller particles suggests that within each experiment larger droplets were removed from the plume within 6 minutes of the oil release, most likely rising to the surface of the tank. The effect was least observed in the DOR 1:20 treatments where dilution occurred but the presence of smaller droplets (with lower rise times) at the point of release most likely didn't allow for fractionation. The effects of fractionation were observed in warm and cold treatments.

Time series particle size data allows for evaluating plume dynamics over the duration of the experiments. Figure 5 depicts time series contour plots of the plume, where colored contours represent the particle concentration (normalized to max value for comparison purposes) for given droplet sizes through time. These plots allow for ascertaining how the DSD shifts over the duration of the release as the plume moves in the horizontal direction in the tank. For ANS, data suggest that the leading edge of the plume, as detected by the upstream LISST, exhibited a wide range in DSD during the first few minutes after release. As the plume advances down the tank, the DSD becomes narrower with a shift in the VMD for the DOR = 1:100 and 0 treatments. DSD remained similar for the DOR = 1:20 treatment. Warm and cold water treatments exhibit similar trends.



ED_001324_00000917-00014

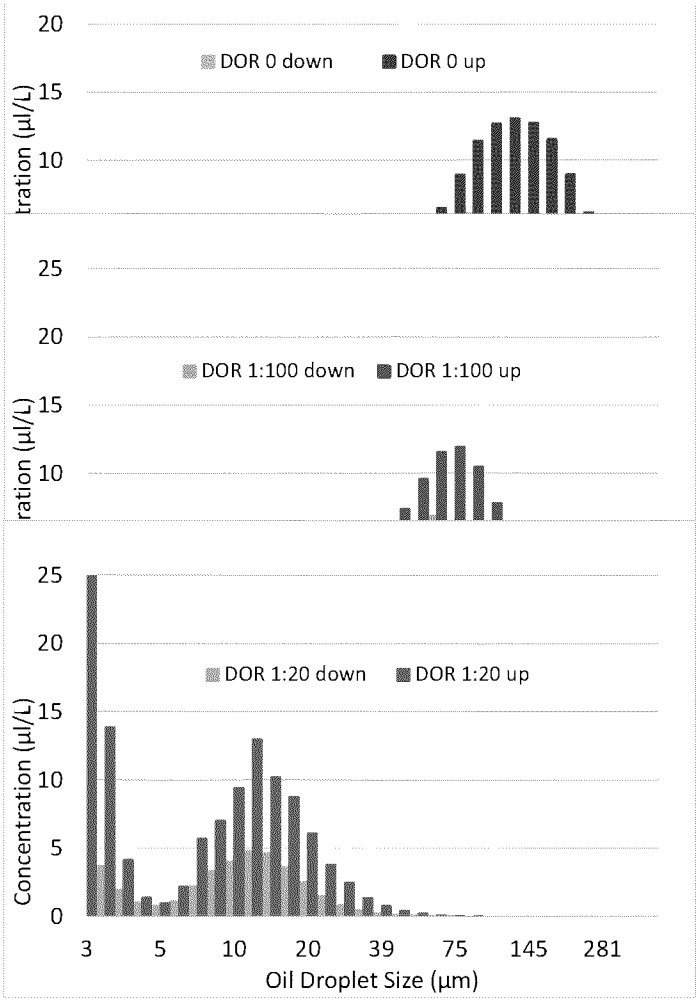


**Figure 4. Upstream and downstream LISST Droplet Size Distribution and particle concentration for ANS with Corexit 9500 during warm water treatments.**

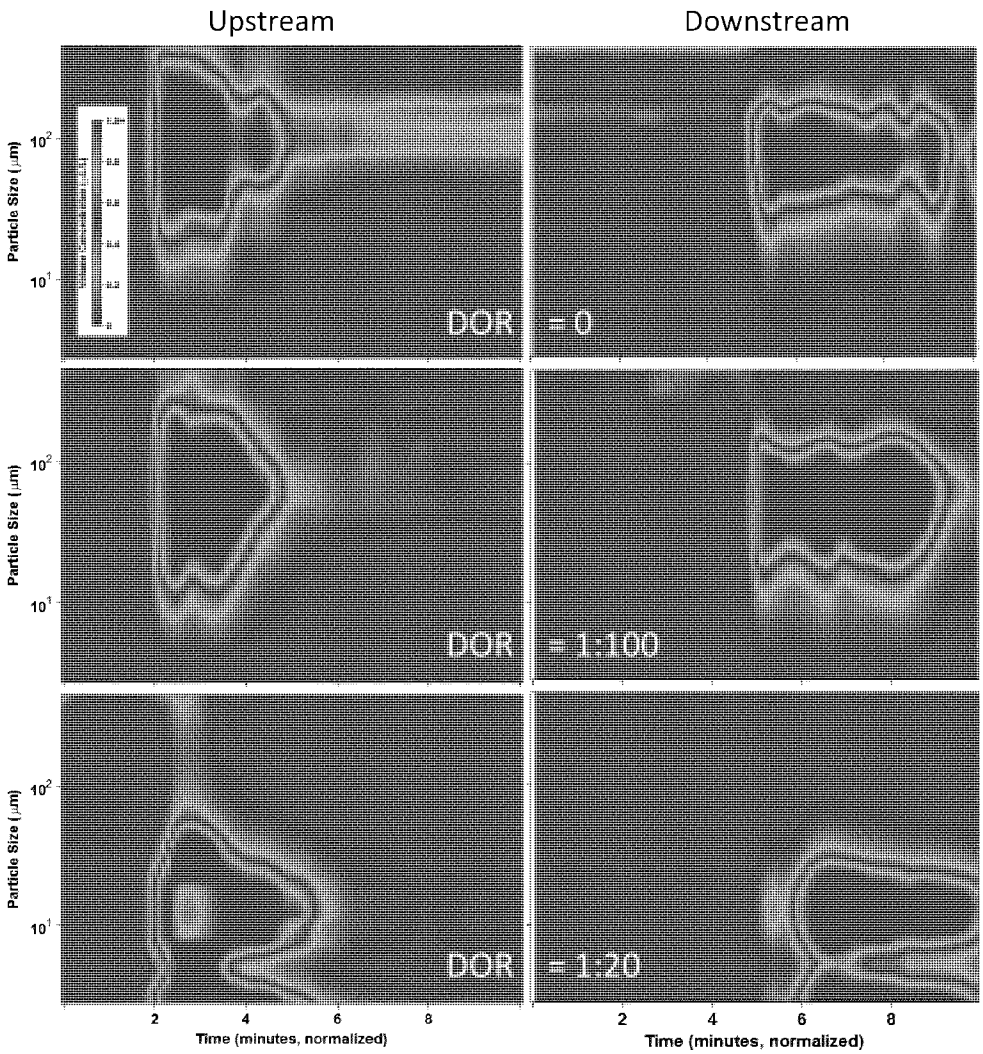


**Figure 5. Time series contours of droplet size distribution and particle concentration from the upstream (left panels) and downstream (right panels) LISSTs for ANS with Corexit 9500 during warm water treatments.**

***<u>Plume Fluorescence Intensity</u>*** – In addition to the plume transport of particles (oil droplets), dissolved hydrocarbons were also measured via discrete samples and by proxy using fluorescence intensity. The reliability of *in situ* fluorescence measurements as a proxy for oil concentration within physically and chemically dispersed oil has been demonstrated previously

within the tank (Conmy et al., 2014). Here, *in situ* fluorescence serves as a good proxy for oil concentration during the subsurface injection experiments. However, heterogeneity of the produced plumes and the short time scale of experiments (~10 min) led to difficulties in correlations between the plume particle size analyses and chemistry results. This is in part due to discrete samples representing 15 second averages as opposed to instantaneous measures given by fluorometers and particle size analyzers. Thus, although general trends were similar, exact matchups between *in situ* data streams and discrete samples proved to be challenging (Figure 6). Given the experimental design, fluorescence was found to be better suited for correlation with total particle concentration (Figure 7). Depicted are the in situ fluorescence and TPC data during a warm water experiment of ANS with (left) and without (right) Corexit 9500. When exposed to dispersant, fluorescence estimates of dissolved hydrocarbons was higher compared to oil alone treatments, and signal persisted for longer periods of time. Whereas a sharper decay in the fluorescence intensity and the TPH values were observed for the physically dispersed oil.

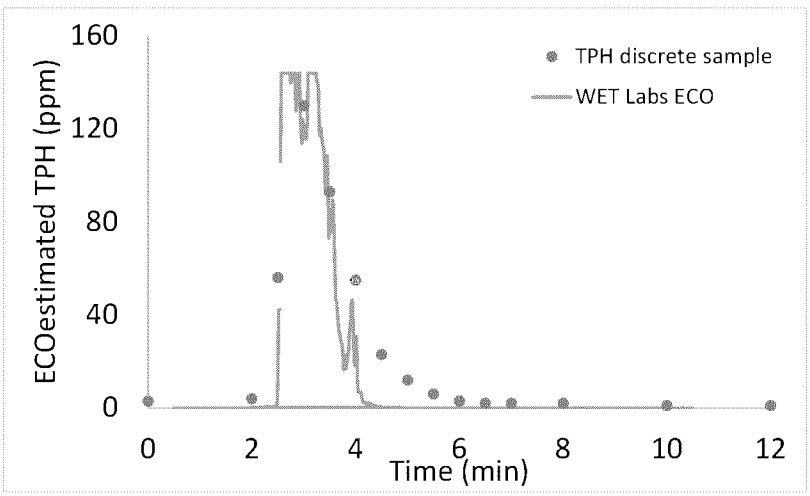


**Figure 6. Fluorescence intensity and TPH samples for a warm water treatment using SLC**

**at DOR = 1:20.**

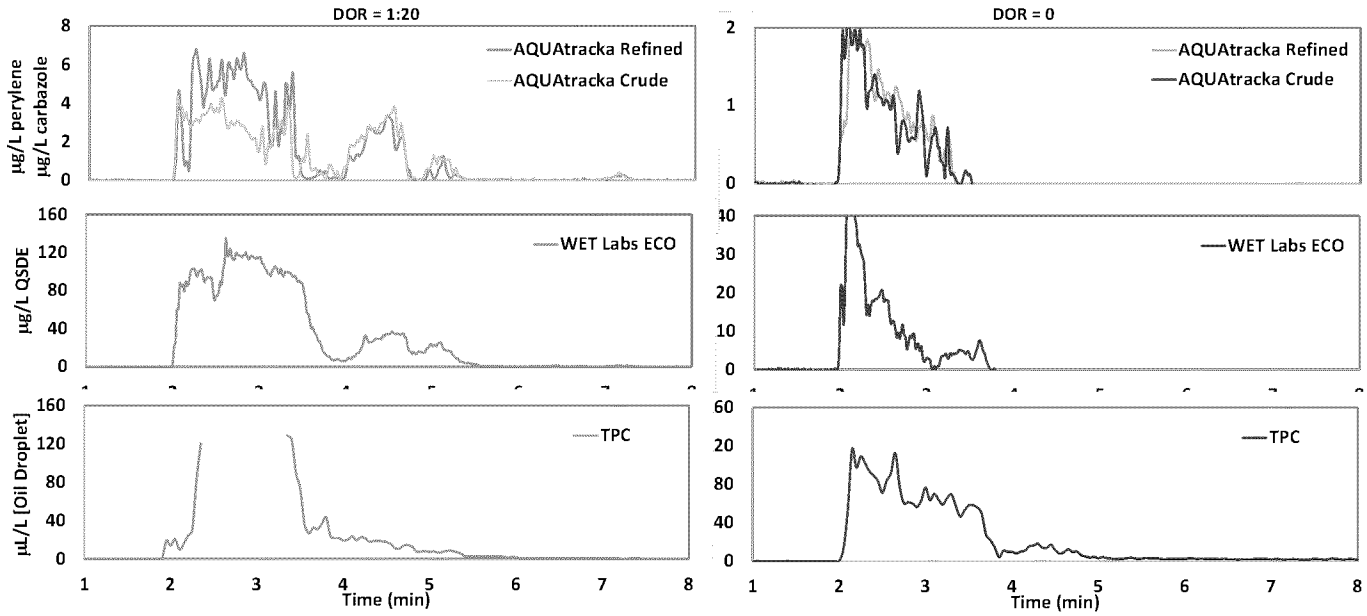


**Figure 7. Fluorescence intensity and TPC as a function of time for ANS warm water treatment.**

## CONCLUSIONS

*In situ* oil droplet size distribution, particle concentration and fluorescence data from this study are essential for better understanding dispersion effectiveness and for refining droplet formation and trajectory models, such as modified Weber Number technique (Johansen et al., 2013) and the VDROP-J model (Zhou et al., 2014). Thus, findings from this study have implications for predicting the behavior of oil and plume formation, decision-making pertaining to SSDI as a countermeasure, and assessing the transport and fate of slicks and subsurface plumes in support of emergency response operations during any future deepwater spills.

## REFERENCES


Conmy, R. N., et al. (2014) Submersible Optical Sensors Exposed to Chemically Dispersed Crude Oil: Wave Tank Simulations for Improved Oil Spill Monitoring. Environ. Sci. Technol. 48(3): 1803-1810.

Cole, M.G., T. King, K. Lee (2007) Analytical technique for extracting hydrocarbons from water using sample container as extraction vessel in combination with a roller apparatus. Anal. Chem., 77: 2210-17.

CRRC Report (2010) Coastal Response Research Center Deepwater Horizon Dispersant USE Meeting Report, May 26-27, 2010, 108 pp.

EPA 600/F-16/250 Federal Report (2016) Dispersant Effectiveness, In-Situ Droplet Size Distribution and Numerical Modeling to Assess Subsurface Dispersant Injection as a Deepwater Blowout Oil Spill Response Option *and* Evaluation of Oil Fluorescence Characteristics to Improve Forensic Response Tools; IAA No. E12PG00037 for DOI BSEE, 144 pp.

Joint Analysis Group Report (2010) Review of Data to Examine Subsurface Oil in the Vicinity of DWH MC-252, May 19-June 19, 2010; 29 pp.

Johansen, O., et al. (2013) Droplet breakup in subsea oil releases - Part 2: Predictions of droplet size distributions with and without injection of chemical dispersants. Mar. Poll. Bull. 73(1): 327-335.

Lee, K., Li, Z., Boufadel, M.C., Venosa, A.D. and Scott Miles, M. (2009) Wave tank studies on




ED_001324_00000917-00019

dispersant effectiveness as a function of energy dissipation rate and particle size distribution. Final report submitted to NOAA/CRRC/UNH, 67 pp.

Li, Z., Lee, K., King, T., Boufadel, M.C. and Venosa, A.D., (2008) Oil droplet size distribution as a function of energy dissipation rate in an experimental wave tank 2008 International Oil Spill Conference. American Petroleum Institute, Washington D.C., Savannah, GA, pp. 621-626.

Li, Z., Lee, K., King, T., Boufadel, M.C. and Venosa, A.D., (2009a) Evaluating crude oil chemical dispersion efficacy in a flow-through wave tank under regular non-breaking wave and breaking wave conditions. Mar. Poll. Bull., 58: 735-744.

Li, Z., Lee, K., King, T., Boufadel, M.C. and Venosa, A.D., (2009b) Evaluating Chemical Dispersant Efficacy in an Experimental Wave Tank: 2, Significant Factors Determining *In Situ* Oil Droplet Size Distribution. Environ. Engin. Sci., 26(9): 1407-1418.

Li, Z., Lee, K., King, T., Boufadel, M.C. and Venosa, A.D., (2010) Effects of temperature and wave conditions on chemical dispersion efficacy of heavy fuel oil in an experimental flow-through wave tank. Mar. Poll. Bull., 60(9): 1550-9.

NRC Report (2005) National Research Council Oil Spill Dispersants: Efficacy and Effects, Washington, DC, 400 pp.

Wickley-Olsen, E., Boufadel, M.C., King, T., Li, Z., Lee, K., Venosa, A.D. (2007) Regular and breaking waves in wave tank for dispersion effectiveness testing. In: Proceedings of the 30th Arctic and Marine Oil spill Program (AMOP) Technical Seminar, Edmonton, AB, Canada. Environment Canada, Ottawa, Ontario, Canada, pp. 161–187.

Zhao, L., et al. (2014). Evolution of droplets in subsea oil and gas blowouts: Development and validation of the numerical model VDROP-J. Mar. Poll. Bull., 83(1): 58-69.



ED_001324_00000917-00020

**To:** Barron, Mace[Barron.Mace@epa.gov]
**From:** Conmy, Robyn
**Sent:** Fri 3/17/2017 12:44:55 PM
**Subject:** RE: any luck in tracking down more oil spill mitigating agents?

It's a light –medium Alaskan pipeline oil. In looking at it, it will most likely be similar to ANS, but hopefully not as like as Endicott was. I'm afraid that's all we know so far….

<>/<>/<>/<>/<>/<>/<>/<>/<>/<>/<>/<>/<>/<>/<>/<>

Robyn N. Conmy, Ph.D.

Research Ecologist

USEPA/NRMRL/LRPCD

26 West MLK Drive

Cincinnati, Ohio 45268

513-569-7090 (office)

513-431-1970 (EPA mobile)

727-692-5333 (Personal mobile)

conmy.robyn@epa.gov

**From:** Barron, Mace
**Sent:** Friday, March 17, 2017 8:40 AM
**To:** Conmy, Robyn <Conmy.Robyn@epa.gov>
**Subject:** RE: any luck in tracking down more oil spill mitigating agents?

What is the new oil to test?

**From:** Conmy, Robyn
**Sent:** Thursday, March 16, 2017 10:43 AM
**To:** Barron, Mace <Barron.Mace@epa.gov>; Wilson, Gregory <Wilson.Gregory@epa.gov>; Principe, Vanessa <Principe.Vanessa@epa.gov>
**Subject:** RE: any luck in tracking down more oil spill mitigating agents?

Hey Mace,

Here is what we are thinking ….

Phase 3 – We originally budgeted for testing 1 each of a SWA, solidifier and bioremediation agents. But instead, I would propose to conduct tests only with 1 SWA (Cytosol) and 1 solidifier (CI Agent or Gelco 200) and not running the bioremediation agent at this time. Instead we can reserve those funds for conducting a tox test with the new 3rd potential oil with and without oil that arrived this week. Thoughts?

Phase 2 – We originally budgeted for 4 dispersants and we have completed 3 (corexit, finasol, accel) with Dorado and Endicott. But instead of adding a 4th dispersant, I think it is best to test the new potential reference oil with and without corexit. Thoughts?

Swapping out the tests should be budgetary neutral considering that one-Phase 1 and one-Phase 2 test would be equal to the proposed Phase 2 tests of new oil with and without corexit.

Mace, can you provide volume budgets of product and oil? We can then ship to hydrosphere.

Robyn

<>/<>/<>/<>/<>/<>/<>/<>/<>/<>/<>/<>/<>/<>/<>/<>/<>/<>

Robyn N. Conmy, Ph.D.

Research Ecologist

USEPA/NRMRL/LRPCD

26 West MLK Drive

Cincinnati, Ohio 45268

513-569-7090 (office)

513-431-1970 (EPA mobile)

727-692-5333 (Personal mobile)

conmy.robyn@epa.gov

**From:** Barron, Mace
**Sent:** Wednesday, March 15, 2017 4:45 PM
**To:** Conmy, Robyn <Conmy.Robyn@epa.gov>; Wilson, Gregory <Wilson.Gregory@epa.gov>; Principe, Vanessa <Principe.Vanessa@epa.gov>
**Subject:** any luck in tracking down more oil spill mitigating agents?

The tox lab asked if we would be shipping anything to them? As a reminder:

phase 2) 2 oils+4 dispersants

*testing completed on dorado and Endicott, plus finasol, accel and corexit

**still need one more dispersant

Phase 3) other oil agents (e.g., oil eater II, etc)

*need to track some down!

**To:** Barron, Mace[Barron.Mace@epa.gov]
**From:** Conmy, Robyn
**Sent:** Thur 3/16/2017 5:04:24 PM
**Subject:** RE: any luck in tracking down more oil spill mitigating agents?

Oil and product volume estimates to send???

<>/<>/<>/<>/<>/<>/<>/<>/<>/<>/<>/<>/<>/<>/<>/<>

Robyn N. Conmy, Ph.D.

Research Ecologist

USEPA/NRMRL/LRPCD

26 West MLK Drive

Cincinnati, Ohio 45268

513-569-7090 (office)

513-431-1970 (EPA mobile)

727-692-5333 (Personal mobile)

conmy.robyn@epa.gov

**From:** Barron, Mace
**Sent:** Thursday, March 16, 2017 11:44 AM
**To:** Conmy, Robyn <Conmy.Robyn@epa.gov>; Wilson, Gregory <Wilson.Gregory@epa.gov>; Principe, Vanessa <Principe.Vanessa@epa.gov>
**Subject:** RE: any luck in tracking down more oil spill mitigating agents?

Yea, I think those are great ideas!

**From:** Conmy, Robyn
**Sent:** Thursday, March 16, 2017 10:43 AM

**To:** Barron, Mace <Barron.Mace@epa.gov>; Wilson, Gregory <Wilson.Gregory@epa.gov>; Principe, Vanessa <Principe.Vanessa@epa.gov>
**Subject:** RE: any luck in tracking down more oil spill mitigating agents?

Hey Mace,

Here is what we are thinking ....

Phase 3 – We originally budgeted for testing 1 each of a SWA, solidifier and bioremediation agents. But instead, I would propose to conduct tests only with 1 SWA (Cytosol) and 1 solidifier (CI Agent or Gelco 200) and not running the bioremediation agent at this time. Instead we can reserve those funds for conducting a tox test with the new 3rd potential oil with and without oil that arrived this week. Thoughts?

Phase 2 – We originally budgeted for 4 dispersants and we have completed 3 (corexit, finasol, accel) with Dorado and Endicott. But instead of adding a 4th dispersant, I think it is best to test the new potential reference oil with and without corexit. Thoughts?

Swapping out the tests should be budgetary neutral considering that one-Phase 1 and one-Phase 2 test would be equal to the proposed Phase 2 tests of new oil with and without corexit.

Mace, can you provide volume budgets of product and oil? We can then ship to hydrosphere.

Robyn

<>/<>/<>/<>/<>/<>/<>/<>/<>/<>/<>/<>/<>/<>/<>/<>/<>/<>

Robyn N. Conmy, Ph.D.

Research Ecologist

USEPA/NRMRL/LRPCD

26 West MLK Drive

Cincinnati, Ohio 45268

513-569-7090 (office)

513-431-1970 (EPA mobile)

727-692-5333 (Personal mobile)

conmy.robyn@epa.gov

**From:** Barron, Mace
**Sent:** Wednesday, March 15, 2017 4:45 PM
**To:** Conmy, Robyn <Conmy.Robyn@epa.gov>; Wilson, Gregory <Wilson.Gregory@epa.gov>; Principe, Vanessa <Principe.Vanessa@epa.gov>
**Subject:** any luck in tracking down more oil spill mitigating agents?

The tox lab asked if we would be shipping anything to them? As a reminder:

phase 2) 2 oils+4 dispersants

*testing completed on dorado and Endicott, plus finasol, accel and corexit

**still need one more dispersant

Phase 3) other oil agents (e.g., oil eater II, etc)

*need to track some down!

# Comparative Study to Determine the Biodegradability of Dispersants at Environmentally Relevant Concentrations

Yu Zhang[1], Mobing Zhuang[1], Pablo Campo[2], Ruta Suresh Deshpande[3], Devi Sundaravadivelu[3], Robyn N. Conmy[4] and Jorge W. Santo Domingo[4]

1. Department of Biomedical, Chemical and Environmental Engineering, University of Cincinnati, 2901 Woodside Drive, Cincinnati, OH 45221, USA
2. Cranfield Water Science Institute, Cranfield University, Cranfield MK43 0AL, UK
3. Pegasus Technical Services Inc., 46 E Hollister Street, Cincinnati, OH 45219, USA
4. U.S. Environmental Protection Agency, National Risk Management Risk Laboratory, 26 W. MLK Drive Cincinnati, OH 45268, USA

## ABSTRACT

Chemical dispersant agents reduce the interfacial tension between oil and water, and increase the surface area to volume ratio of oil droplets thus facilitating the biodegradation of spilled oil. Dispersants are composed of surface active molecules known as surfactants and various commercial products contain Dioctyl Sulfosuccinate (DOSS) as the active ingredient. Since previous laboratory studies including the BFT were conducted at oil and dispersant concentrations significantly higher (~0.7 g/L oil with DOR of 1:25) than those typically found in field conditions, experiments were conducted at low levels of oil and dispersant (28 μg/L oil with DOR of 1:25) in order to determine the degradation trends at environmentally relevant concentrations. Experiments were conducted using two crude oils (Alaskan North Slope and Endicott) and two dispersant products (Corexit 9500 and Finalsol OSR 52) to study the biodegradation of dispersants and dispersed oil and oil alone samples were used as controls. Two

oil degrading cultures, isolated from the surface (meso) and deep sea (cryo) of the Gulf of Mexico, were enriched on crude oil at 25 and 5 °C and were used as the inocula. The biodegradation experiments were performed at 5 °C for 56 days and at 25 °C for 48 days using sterile GP2 artificial seawater as the media. The time series concentration of DOSS, the primary surfactant in the dispersants was monitored using LC-MS/MS in addition to the oil concentration which was measured using GC-MS/MS. Although the initial concentration of DOSS in Finasol OSR 52 was 20% higher than in Corexit 9500, over 95% of the anionic surfactant fraction was metabolized for both types of dispersant products by the end of the experiment at 25 °C while it persisted at 5 °C. The effect of dispersant and oil type on microbial community structure was also analyzed using PCR analysis. Results indicated that the abundance of *Thalassospira* correlated well with hydrocarbon degradation trends. The results from this study significantly expands on our understanding of biodegradation of DOSS, dispersed, and non-dispersed oil and also provides information regarding bacterial community composition.

**Keywords:** biodegradation, oil spills, dispersant, crude oil, RNA

## INTRODUCTION

First generation chemical dispersants (industrial detergents) were primarily used in marine oil spills after the first major tanker catastrophe, the *Torrey Canyon* oil spill, in which large amount of alkylphenol surfactants were delivered to the contaminated area (Clayton, 1993; Committee on Effectiveness of Oil Spill Dispersants, 1989). The addition of dispersant lowered the interfacial tension between spilled oil and water, accelerated the breakdown of oil slicks, and prevented the resurfacing of small droplets (European Maritime Safety Agency, 2010). Moreover, discussions regarding dispersant utilization in deep-sea condition has come to the forefront after the GOM oil spill in 2010.

Corexit 9500, a well-known formula capable of dispersing heavy and weathered oils, is listed on the U.S. EPA National Contingency Plan Product Schedule and stockpiled around the world (Lessard and Demarco, 2010). Finasol OSR 52, another product that is widely stockpiled in Europe and European Free Trade Association countries, has not been completely evaluated for its toxicity and biodegradability. However, the pressing demand for deep-sea drilling requires continuing assessment of biodegradability of dispersants and dispersed oil (Zhuang et al. 2016).

In the aquatic environment, biodegradation is one of the predominant oil removal mechanisms in which bacteria utilize the spilled oil as a carbon source and thus degrade the oil components. While chemical dispersants increase the bioavailability of the oil to the microbes, the degradation of the dispersants themselves can be a challenge for the microbial community. Several studies assessed the biodegradation of C9500, while only Bergueiro-Lopez et al. (1997) examined the metabolism of Finasol OSR 52 by employing a mixture of bacteria called BIOLEN

IG 30. To date, the biodegradability of various crude oils dispersed with C9500 have been assessed in laboratory experiments, such as Prude Bay crude oil (Venosa and Holder, 2007), Macondo crude oil (Wang et al., 2016), and South Louisiana crude oil (Campo et al., 2013). Results varied due to the differences in oil properties and microbial community structure. Only a limited number of studies have been conducted where the biodegradability of dispersed Endicott crude oil was evaluated, and with only one publication evaluating the biodegradation by monitoring total petroleum hydrocarbon concentration under anaerobic conditions (Personna et al., 2014).

In order to characterize the biodegradation of DOSS and hydrocarbons, experiments were set up to study the degradation of two crude oils (ANS and Endicott), two dispersants (C9500 and Finasol) and three dispersed oils (ANS dispersed by C9500, ANS dispersed by Finasol and Endicott dispersed by C9500) under two temperature conditions which represented the surface (25 °C) and deep water (5 °C) environments, respectively.

## METHODS

### Cultures and Medium

Two mixed cultures of oil degrading bacteria were provided by EPA's Gulf Ecology Division at Gulf Breeze, FL. The mixed cultures were collected at a depth of 1240 m (cryo) and 5 m (meso) near the Macondo well at the GOM, enriched using crude oil and preserved in 10% glycerol until use. Sterilized GP2 artificial seawater was used as the media in this experiment and was prepared by dissolving several mineral salts in deionized water (Bidwell and Spotte, 1985).

**Treatments**

*Dispersed oil treatment:* The dispersed oil treatment was prepared in a 2 L baffled flask by adding the crude oil and the dispersant to 1.5 L of GP2 at a volumetric dispersant-to-oil ratio of 1:24 (10 μL dispersant: 240 μL oil). The baffled flask was shaken at 200rpm for 10-minutes, followed by a 10-minute settling period to allow the undispersed oil to rise to the top. After settling, 1 L of the dispersion was drained without disturbing the undispersed oil slick on the water surface. This procedure was repeated two more times which yielded 3 L of total dispersed oil and it was diluted into 12 L of GP2 (Panels A, B and C of Figure). Subsequently, a series of 250 mL silanized shaker flasks were filled with 100 mL aliquots of the dispersed oil.

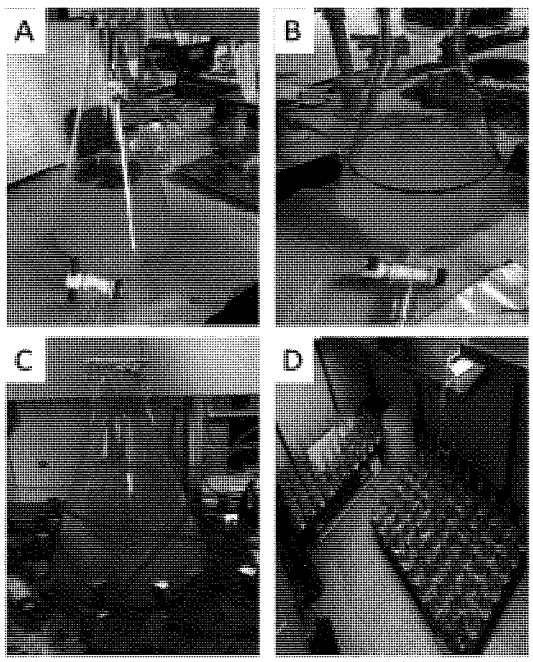


**Figure** Dispersed Oil Preparation (A, B and C) and Experiment Unit loading (D)

*Non-dispersed oil treatment:* To evaluate the biodegradation of crude oil alone,

approximately 4 μL crude oil was directly pipetted into each shake flask containing 100 mL sterile GP2. The final concentration of oil in the samples was approximately 28 μg/L, which was almost the same as the dispersed oil treatment.

*Dispersant alone treatment:* The dispersant alone treatments were prepared by spiking 20 μL of dispersant into 14 L of GP2 under continuous mixing, to yield a concentration similar to the dispersed oil treatment. After 30 minutes of continuously mixing, 100 mL of the solution was added into 250 mL silanized shaker flasks.

The dispersed oil, non-dispersed oil and dispersant alone treatments were then spiked with 0.5 mL of inoculum per flask with the cryo and meso cultures for the 5 and 25 °C experiments, respectively. After preparation, all the shaker flasks were placed on the orbital shakers in corresponding constant temperature rooms (5 or 25 °C) for the duration of the experiment (Panel D of Figure).

**Oil component and DOSS analysis**

DOSS and oil samples were prepared as described in Campo (2013). According to the ASTM D7730 Standard Method (ASTM D7730, 2011), DOSS was measured by using a 1200 series liquid chromatograph coupled with a 6410 tandem mass spectrometer (LC-MS/MS) from Agilent (Palo Alto, CA). Analysis of oil components was performed on an Agilent (Palo Alto, CA) 7890A GC coupled with an Agilent 7000 mass selective detector triple quadrupole and an Agilent 7693 series auto sampler. It was equipped with a DB-5 capillary column by J&W Scientific (30 m X 0.25 mm, and 0.25 μm film thickness) to achieved chromatographic separation of the alkanes and aromatics. A modified method based on EPA Method 8270D

(2007) was followed.

## RESULTS AND DISCUSSION

### Biodegradation of DOSS

Table 1 summarizes the initial concentration, biodegradation rates and removal extents of DOSS, the active anionic surfactant in C9500 and Finasol, with and without crude oils at 25 °C. Although the initial concentration of primary surfactant (DOSS) in Finasol was around 20% higher than in C9500, over 95% of the anionic surfactant fraction was metabolized for both types of dispersant products by the end of the experiment at 25 °C while it persisted at 5 °C. Thus, the low temperature condition greatly inhibited the microbial uptake of DOSS.

At 25 °C, biodegradation was fast in the replicates with or without ANS. 96% and 98% of DOSS were degraded for dispersant alone and dispersed oil treatment for two dispersants by the end of experiment, respectively. The presence of ANS remarkably favored the biodegradation first order rate of C9500 by approximately 2.4-fold, but no such effect was observed for the experiment with Finasol and ANS. Besides, DOSS uptake occurred after an acclimation period of 2 days, and removal extents surpassed 98% by day 48 in the presence of Endicott.

**Table 1** Summary of Biodegradability of Two Dispersants at 25 °C

| Treatments | Initial DOSS Concentration (μg/L) | Degradation rate ($d^{-1}$) | Removal extent (%) |
|---|---|---|---|
| C9500 alone | 203.97 ± 6.98 | - 0.07 ± 0.009 | 96 |
| C9500 + ANS | 228.16 ± 11.94 | - 0.16 ± 0.015 | 98 |
| Finasol Alone | 280.87 ± 21.19 | - 0.060 ± 0.008 | 96 |
| Finasol + ANS | 234.11 ± 5.38 | - 0.068 ± 0.006 | 98 |
| C9500 + Endicott | 206.96 ± 4.28 | - 0.077 ± 0.007 | 98 |

**Biodegradation of total alkanes**

Table 2 presents the hopane-normalized concentration of total alkanes in dispersed oils. All the targets compounds were normalized by hopane concentration since it was unchanged through the whole experiments in all the treatments. The initial hopane-normalized concentration for 5 °C was almost twice as that of 25 °C because of the oil present in the enrichments. This was confirmed by analyzing the cryo and meso biomass alone, without the addition of any oil. The biodegradation of total alkanes occurred without any lag phase at 25 °C, regardless of the type of dispersed oil, while a 4-day acclimation period was observed at 5 °C. Over 90% of the total alkanes was metabolized by the meso culture by the end of experiment in all the cases.

**Table 2** Biodegradability of Hopane-Normalized Total Alkanes in Dispersed Oils at 5 and 25 °C

| Temperature | Treatments | Initial Concentration (mg total Alkanes / mg Hopane) | Lag Phase Period (d) | Removal extent (%) |
|---|---|---|---|---|
| 25 °C | ANS + C9500 | 106.61 ± 3.64 | 0 | 92 |
| | ANS + Finasol | 113.17 ± 3.69 | 0 | 90 |
| | Endicott + C9500 | 142.91 ± 3.33 | 0 | 94 |
| 5 °C | ANS + C9500 | 209.79 ± 7.72 | 4 | 85 |
| | ANS + Finasol | 220.56 ± 4.30 | 4 | 93 |
| | Endicott + C9500 | 178.42 ± 1.77 | 4 | 94 |

At 5 °C, the presence of Finasol considerably favored the removal of alkanes than C9500 (93% vs. 85%) with ANS. Although, ANS and Endicott crude oil are both medium oil (Table 3), the percentage of total alkanes in Endicott is much higher than ANS crude oil, especially for light alkanes. The remove extent of dispersed Endicott is higher than that of dispersed ANS due to the easier metabolism of short chain alkanes.

**Table 3** Physical Properties of ANS and Endicott *

| Property | ANS | Endicott |
|---|---|---|
| Density, ρ (g/mL) | 0.8733 | 0.8838 |
| Dynamic Viscosity, μ (cP, at 15 °C) | 35 | 120 |
| Kinematic Viscosity, ν (cSt, at 15 °C) | 40 | 134 |
| API gravity | 28.24 | 23.00 |
| Total Alkanes Concentration (mg total Alkanes / mg Crude Oil) | 35.52 | 110.38 |
| of Total PAHs Concentration (mg total PAHs / mg Crude Oil) | 20.63 | 37.46 |

* General crude oil categories: Heavy (API < 22.3°), Medium (22.3° ≤ API < 31.1°), and Light (API ≥ 31.1°).
* Source: SL Ross Environmental Research, 2010.

**Biodegradation of total PAHs**

Table 4 presents total PAH degradation for all the dispersed oil treatments at two temperatures. Similar to alkanes, the hopane-normalized total PAH concentration at 5 °C was higher than at 25 °C because of the higher hopane content from the meso cultures. At 25 °C, a notable decline in total PAHs was observed after an acclimation period of 2 days, and, subsequently degraded up to 82% by day 48 in ANS + C9500 treatment. For the other two dispersed oils, PAHs persisted until the end of experiment. Such contrary and unexpected findings is explained in more detail under the microbial community structure section.

At 5 °C, a 12-day lag phase occurred before observable degradation ensued in dispersed ANS treatments, while the cryo culture began degrading PAHs after 32 days for dispersed Endicott. Similar to the alkanes, higher temperature considerably favored the biodegradation of ANS dispersed by C9500 by shortening the lag phase period. At the last sampling event, 21%,

28% and 15% of the initial loaded concentration persisted for ANS + C9500, ANS + Finasol and Endicott + C9500 treatment, respectively. Although Endicott contains more PAHs than ANS (as shown in Table 3), dispersed Endicott was easier to remove owing to the higher percentage of 2-ring compounds which biodegraded faster than 3- and 4- ring PAHs.

**Table 4** Biodegradability of Hopane-Normalized Total PAHs in Dispersed Oils at 5 and 25 °C

| Temperature | Treatments | Initial Concentration (mg total PAHs / mg Hopane) | Lag Phase Period (d) | Removal extent (%) |
|---|---|---|---|---|
| 25 °C | ANS + C9500 | 44.38 ± 1.54 | 2 | 82 |
| | ANS + Finasol | 61.08 ± 2.33 | 48 | 3 |
| | Endicott + C9500 | 53.81 ± 0.14 | 48 | 19 |
| 5 °C | ANS + C9500 | 51.17 ± 0 | 12 | 79 |
| | ANS + Finasol | 63.57 ± 2.25 | 12 | 71 |
| | Endicott + C9500 | 58.55 ± 0.38 | 32 | 85 |

**Microbial community structure**

As mentioned previously, meso cultures showed significant differences in PAHs uptake between ANS + C9500 and ANS + Finasol experiments which were performed under the same conditions, except for the dispersant product. PCR analysis of these bacterial consortia provided a clearer understanding of the microbial makeup and an in-depth explanation for the inconsistent result.

Table 5 displays the significant species in the active community including *Alcanivorax, Pseudoidiomarina* and *Thallassospira* which were abundant in the C9500 experiment but not in the Finasol experiment. In the active community, *Alcanivorax,* one of the predominant

hydrocarbon-degrading bacteria in the contaminated seawater, (Cappello et al, 2007; Harayama et al, 2004; Wang et al, 2014) increased from 0.74% to a maximum of 69.3% of total abundance in the C9500 experiment. *Alcanivorax* is a ubiquitous bacteria that was found in the GOM during the DWH oil spill (Kostka et al., 2016). However, the same species in the Finasol experiment was consistently lower at around 20%. Moreover, a similar trend was observed by comparing *Pseudoidiomarina* and *Thallassospira* (Moghadam et al., 2014). Hence, it is reasonable to infer this loss of active community could contribute to the unusual persistence of aromatics at 25 °C.

**Table 5** Significant active genes of meso cultures in ANS alone treatment of ANS + C9500 (A) and ANS + Finasol (B) experiments

| Species | Experiment | Initial Percentage (%) | Maximum Percentage (%) |
|---|---|---|---|
| *Alcanivorax* | A | 33.13 ± 15.19 | 69.34 ± 2.10 |
| | B | 10.74 ± 3.39 | 20.58 ± 6.51 |
| *Pseudoidiomarina* | A | 0.15 ± 0.15 | 21.88 ± 3.88 |
| | B | 12.75 ± 1.49 | 14.93 ± 1.22 |
| *Thallassospira* | A | 0.02 ± 0.03 | 26.28 ± 2.99 |
| | B | 3.92 ± 0.83 | 0.82 ± 0.69 |

## CONCLUSION

The goal of this work was to evaluate the effect of temperature on the biodegradability of dispersants and dispersed oils by using two oils (ANS crude oil and Endicott) and two dispersants (C9500 and Finasol OSR 52). This research not only evaluated the effect of dispersant type (Finasol and C9500) on ANS biodegradation, but also analyzed the biodegradation potential of two types of crude oil (ANS and Endicott) when dispersed with C9500.

DOSS disappeared promptly at 25 °C, while it persisted throughout the experiments at 5 °C. Additionally, the length of the acclimation period and removal extent were highly impacted by the addition of the dispersant. Similar to DOSS degradation, temperature affected the biodegradation of total alkanes significantly in both acclimation period and removal extent. Around 80% of the PAHs degraded at 5 °C whereas most PAHs persisted at 25 °C in ANS+Finasol and Endicott+C9500 treatment, which possibly resulted from the loss of several oil degrading microbial species such as *Alcanivorax, Pseudoidiomarina* and *Thallassospira.* Although the composition of Endicott considerably differs from ANS, especially the short chain paraffin and 2-ring PAHs, the degradation trends were similar to dispersed ANS, which indicated that the effect of C9500 on the two oils were similar. Since the PAHs persisted at 25 °C, and low activity of critical degrading species in meso cultures was observed, it is recommended that different cultures should be evaluated under the same test conditions in future experiments.

## ACKNOWLEDGEMENTS

We acknowledge Jan Kurtz and Diane Yates from EPA's Gulf Ecology Division (GED) at Gulf Breeze, FL, who collected the water samples in the GOM and performed the enrichments and provided them for the experiments. The research was a product of the U.S. Environmental Protection Agency's National Risk Management Research Laboratory (NRMRL) and was partially funded by EPA, NRMRL, Cincinnati, OH, under Pegasus Technical Services, Inc. Contract EP-C-11-006.

## REFERENCES

1. ASTM D7731-11e1, 2011. Standard test method for determination of

dipropyleneglycol monobutyl ether and ethylene glycol monobutyl ether in sea water by liquid chromatography/tandem mass spectrometry (LC/MS/MS). *ASTM International*, West Conshohocken, PA. *www.astm.org*

2. Bergueiro-Lopez J.R., Moreno-Garcia-Luengo S., Serra-Socias F., Fuertes- Perez A., Perez-Navarro-Gomez A., Morales-Correas N., Domingez-Laseca, F., 1997. FINASOL OSR 52 Active Components Biodegradation by Using the Biological Activator BIOLEN IG 30. *Spill Science & Technology Bulletin* 3(4), 269-272. doi: 10.1016/S1353-2561(97)00026-1
3. Bidwell J.P., and Spotte S., 1985. Artificial Seawaters: Formulas and Methods. Jones and Bartlett Publishers, Inc., Boston, Ma.
4. Campo P., Venosa A.D., Suidan M.T., 2013. Biodegradability of Corexit 9500 and Dispersed South Louisiana Crude Oil at 5 and 25 °C. *Environmental Science & Technolology* 47(4), 1960-1967. doi: 10.1021/es303881h
5. Cappello S., Denaro R, Genovese M., Giuliano P., Yakimov M.M., 2007. Predominant growth of Alcanivorax during experiments on "oil spill bioremediation" in mesocosms. *Microbiological Research* 162(2), 185-190. doi: http://dx.doi.org/10.1016/j.micres.2006.05.010
6. Clayton, John R., 1992. Oil Spill Dispersants: Mechanisms of Action and Laboratory Tests. 9-23.
7. Committee on Effectiveness of Oil Spill Dispersants, 1989. Using Oil Spill Dispersants on the Sea. 6-7.
8. European Maritime Safety Agency, 2010. Manual on the Applicability of Oil Spill Dispersants - Version 2. *www.emsa.europa.eu*
9. HarayamA S., Kasai Y., Hara A., 2004. Microbial communities in oil-contaminated seawater. *Current Opinion in Biotechnology* 15(3), 205-214. doi: http://dx.doi.org/10.1016/j.copbio.2004.04.002
10. Kostka, J. E., Prakash, O., et al., 2011. Hydrocarbon-degrading bacteria and the bacterial community response in Gulf of Mexico beach sands impacted by the Deepwater Horizon oil spill. *Applied and Environmental Microbiology* 77(22), 7962-7974.

doi: 10.1128/AEM.05402-11

11. Lessard P.R., Demarco G., 2000. The Significance of Oil Spill Dispersants. *Spill Science & Technolology Bulletin* 6(1), 59-68.
doi: http://dx.doi.org/10.1016/S1353-2561(99)00061-4

12. Moghadam M.S., Ebrahimipour G., Abtahi B., Ghassempour A., Hashtroudi M.S., 2014. Biodegradation of polycyclic aromatic hydrocarbons by a bacterial consortium enriched from mangrove sediments. *Journal of Environmental Health Science and Engineering* 12(1).
doi: 10.1186/s40201-014-0114-6

13. Personna Y.R., Boufadel M.C., Zhang S., 2014. Assessing weathered Endicott oil biodegradation in brackish water. *Marine Pollution Bulletin* 86, 102-110.
doi: http://dx.doi.org/10.1016/j.marpolbul.2014.07.037

14. SL Ross Environmental Research, 2010. Comparison of large scale (Ohmsett) and small scale dispersant effectiveness test results. *Report for U.S. Department of the Interior*, Minerals Management Service, Herndon, Va.

15. United State Environmental Protect Agency, 2007. Method 8270D Semivolatile Organic Compounds by Gas Chromatography/Mass Spectrometry (GC-MS). *https://www3.epa.gov/*

16. Venosa, A.D., Holder, E.L., 2007. Biodegradability of dispersed crude oil at two different temperatures. *Marine Pollution Bulletin* 54, 545-553.
doi: http://dx.doi.org/10.1016/j.marpolbul.2006.12.013

17. Wang J., Sandoval K., Ding Y., Stoeckel D.,1, Minard-Smithc A., Andersen G., Dubinsky E., Atlas R., Gardinali P., 2016. Biodegradation of dispersed Macondo crude oil by indigenous Gulf of Mexico microbial communities. *Science of the Total Environment* 557-558, 453-468.
doi: http://dx.doi.org/10.1016/j.scitotenv.2016.03.015

18. Wang W., Zhong R., Shan D., Shao Z., 2014. Indigenous oil-degrading bacteria in crude oil-contaminated seawater of the Yellow Sea, China. *Applied Microbiology and Biotechnology* 98(16), 7253-7269.
doi: 10.1007/s00253-014-5817-1

19. Zhuang M., Abulikemub G., Campo P., Platten W.E., Suidan M.T., Venosa A.D.,

Conmy R.N., 2016. Effect of dispersants on the biodegradation of South Louisiana crude oil at 5 and 25 °C. *Chemosphere* 144, 767-774.
doi: http://dx.doi.org/10.1016/j.chemosphere.2015.08.040

# Technical Manuscript Review Form

| | |
|---|---|
| **Title**<br>Comparative Study to Determine the Biodegradability of Dispersants at Environmentally Relevant Concentrations | **Author(s)**<br>Yu Zhang, Mobing Zhuang, Pablo Campo, Ruta Suresh Deshpande, and Robyn N. Conmy |
| **Date Review Requested** 01/24/2017 / **Date Review Required** 02/01/2017 | **Project Officer/Organization/Address**<br>Robyn Conmy<br>EPA ORD NRMRL -Land Remediation Pollution Control Division<br>26 W MLK, Cincinnati OH 45268 |
| **Type of Publication/Audience**<br>conference proceedings paper | **Reviewer/Organization/Address**<br>Fran Kremer<br>EPA ORD NRMRL-LRPCD<br>26 MLK Drive West, Cincinnati, OH |
| **Review Coordinator (e.g., PO, TIM, Supervisor)**<br>PO - Robyn Conmy<br>TIM - Kim McClellan<br>Supervisor - Joseph Schubauer-Berigan | |

**You are asked to review and comment on the attached manuscript. Feel free to make notations on the manuscript as well as in the comments section below, particularly regarding your recommendations for revisions. If you are unable to review the manuscript by the required date, please return it now. Your suggestions for alternate or additional reviewers will be welcomed.**

| SUMMARY RATING | | | RECOMMENDATIONS |
|---|---|---|---|
| Please rate the manuscript as follows: | Satisfactory | Unsatisfactory | |
| Content & Scope | ☑ | ☐ | G (1) ☐ Acceptable as is |
| Organization & Presentation | ☑ | ☐ | G (2) ☑ Acceptable after minor revisions |
| Quality of data & validity of analytical techniques | ☑ | ☐ | G (3) ☐ Acceptable after major revisions |
| Soundness of Conclusions | ☑ | ☐ | G (4) ☐ Not acceptable |
| Editorial Quality | ☑ | ☐ | If you have checked either 3 or 4, please specifically state reason(s) in the comments space below. |
| Other (specify) | ☐ | ☐ | |
| | ☐ | ☐ | |
| | ☐ | ☐ | Reviewer's Signature — Date 2/4/17 |

**Comments:**

Tech. Rev. Form EPA363

# Audit Trail for

## Technical Manuscript Review Form

**PDF Name:** TMRF_363.pdf
**Form Number:** EPA363
**Document Identifier:** EPA363-12250124123-RC

**To:** Mike Fulton - NOAA Federal[mike.fulton@noaa.gov]
**From:** Conmy, Robyn
**Sent:** Tue 4/12/2016 12:56:32 PM
**Subject:** RE: purchase fo finasol and corexit

Thanks Mike. This is our same contact, so I guess I will just keep trying to reach her. EPA is looking to procure a few gallons and will be doing toxicity testing. We will ask nicely and point out that the testing will be used to help with finalizing the NCP Subpart J language. If they still won't sell, we will look into if there is regulatory language that exists to help convince them to waive the waiver requirements. As you know, access to Nalco dispersants is quite a challenge for research.

Cheers,

Robyn

<>/<>/<>/<>/<>/<>/<>/<>/<>/<>/<>/<>/<>/<>/<>/<>

Robyn N. Conmy, Ph.D.

Research Ecologist

USEPA/NRMRL/LRPCD

26 West MLK Drive

Cincinnati, Ohio 45268

513-569-7090 (office)

513-431-1970 (EPA mobile)

727-692-5333 (Personal mobile)

conmy.robyn@epa.gov

**From:** Mike Fulton - NOAA Federal [mailto:mike.fulton@noaa.gov]
**Sent:** Tuesday, April 12, 2016 8:41 AM
**To:** Conmy, Robyn <Conmy.Robyn@epa.gov>
**Subject:** Re: purchase fo finasol and corexit

Hi Robyn,

See below contact info for NALCO. You may have more success if you can sign a waiver that you won't use for toxicity testing. Good luck.

Mike

Debby.Theriot@nalco.com

281 263 7709

On Tue, Apr 12, 2016 at 7:58 AM, Conmy, Robyn <Conmy.Robyn@epa.gov> wrote:

> Thanks Mike. I spoke to a contact at Total yesterday and we are getting some Finasol. Nalco hasn't responded to a voicemail as of yet, so your contact at Nalco could be a huge help.
>
> <>/<>/<>/<>/<>/<>/<>/<>/<>/<>/<>/<>/<>/<>/<>/<>/<>
>
> Robyn N. Conmy, Ph.D.
>
> Research Ecologist
>
> USEPA/NRMRL/LRPCD
>
> 26 West MLK Drive
>
> Cincinnati, Ohio 45268
>
> 513-569-7090 (office)
>
> 513-431-1970 (EPA mobile)
>
> 727-692-5333 (Personal mobile)
>
> conmy.robyn@epa.gov
>
> **From:** Mike Fulton - NOAA Federal [mailto:mike.fulton@noaa.gov]

**Sent:** Monday, April 11, 2016 5:00 PM
**To:** Conmy, Robyn <Conmy.Robyn@epa.gov>
**Subject:** Re: purchase fo finasol and corexit

Hi Robyn, Ultimately, We weren't able to get Corexit from Nalco, but I'll get you the contact info for both manufacturers.

On Monday, April 11, 2016, Conmy, Robyn <Conmy.Robyn@epa.gov> wrote:

Hi Mike,

Awhile back we had discussed NOAA's possible procurement of Corexit and Finasol for your toxicity work. Would you mind sharing the POC for Nalco and Total that were contacted in your hunt to procure the dispersants?

Thanks,

Robyn

<>/<>/<>/<>/<>/<>/<>/<>/<>/<>/<>/<>/<>/<>/<>/<>

Robyn N. Conmy, Ph.D.

Research Ecologist

USEPA/NRMRL/LRPCD

26 West MLK Drive

Cincinnati, Ohio 45268

513-569-7090 (office)

513-431-1970 (EPA mobile)

727-692-5333 (Personal mobile)

conmy.robyn@epa.gov

--

Dr. Michael H. Fulton-Estuaries and Land Use Branch Chief

Center for Coastal Environmental Health and

Biomolecular Research (CCEHBR)

USDOC/NOAA/NOS/NCCOS

219 Fort Johnson Road

Charleston, SC 29412-9110

voice: (843) 762-8576 fax: (843) 762-8700

e-mail: mike.fulton@noaa.gov

--

Dr. Michael H. Fulton-Estuaries and Land Use Branch Chief

Center for Coastal Environmental Health and

Biomolecular Research (CCEHBR)

USDOC/NOAA/NOS/NCCOS

219 Fort Johnson Road

Charleston, SC 29412-9110

voice: (843) 762-8576 fax: (843) 762-8700

e-mail: mike.fulton@noaa.gov

# DISPERSANT EFFECTIVENESS UNDER HIGH SALINITY CONDITIONS FOLLOWING A SUBSURFACE JET RELEASE OF OIL


**Brian Robinson, Thomas King, Scott Ryan**
Department of Fisheries and Oceans Canada
Bedford Institute of Oceanography, Dartmouth, Nova Scotia, Canada

**Robyn Conmy**
U.S. Environmental Protection Agency
Office of Research and Development, Cincinnati, Ohio, USA

**Michel Boufadel, Lin Zhao, Feng Gao**
Department of Civil and Environmental Engineering
New Jersey Institute of Technology, Newark, New Jersey, USA


## INTRODUCTION

Potential oil exploration and production activities in close proximity to hypersaline water bodies, such as brine channels in the Arctic or brine pools in the Gulf of Mexico (GoM), necessitates characterization of Dispersant Effectiveness (DE) at high salinities. The 2010 GoM Deepwater Horizon (DWH) oil spill was the largest and deepest oil release ever to be treated with chemical dispersants as the primary mitigation tool, demonstrating that dispersants could be injected directly into a high pressure oil blowout at a depth of 1500 m. Yet, if such a release were to occur into hypersaline waters, it is currently unknown whether dispersants would be an effective response tool, particularly during extreme mixing of brine with overlying seawater. To investigate the effect of hypersaline conditions on DE, a series of experiments were conducted using an underwater jet release of oil in a flume tank.

## DESCRIPTION OF FLUME TANK FACILITY

Subsurface injection experiments were conducted in a flume tank located at the Bedford Institute of Oceanography in Dartmouth, Nova Scotia, Canada. The tank has inner dimensions of 30 m x 2 m x 0.6 m (LxWxH) with an operational water volume of 30,000 L. All experiments were conducted using a natural supply of seawater that had been pumped through 5 µm and 25 µm bag filters.

The tank is equipped with a high flow seawater pumping system connected to a series of influent and effluent manifolds that are capable of generating horizontal water currents of up to 5 cm $s^{-1}$ in the tank.

The subsurface oil injector consists of a stainless steel pressure vessel that can hold up to 2 L of oil. Inside the pressure vessel was a coil of copper tubing that was connected to a circulating water bath which allowed for maintaining the oil temperature at 20°C. The pressure vessel was pressurized to 50 psi (ANS) or 90 psi (IFO) by connecting it to a tank of compressed nitrogen. A series of valves were used to connect the pressure vessel to an injector nozzle inside the tank. The nozzle had an orifice diameter of 2.4 mm and was oriented 20 cm off the bottom of the tank and pointed in a horizontal down current direction. Injection times ranged between 5-7 seconds resulting in a 350 g oil release.

The BIO wave tank and flume tank facility.

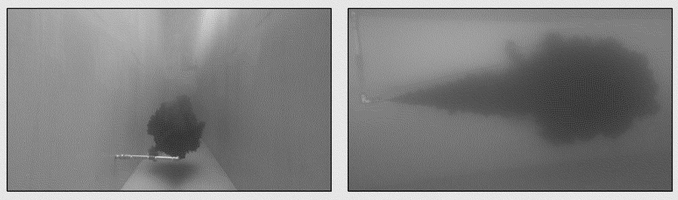

Underwater images of a subsurface oil injection experiment.

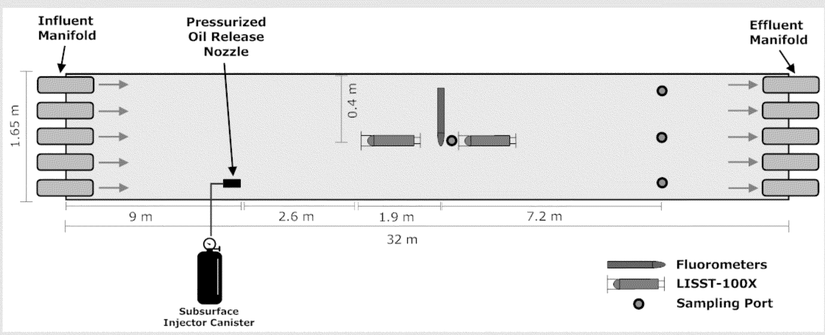


Figure 1: Cross section of the flume tank used in this study showing the high flow seawater manifold system (left) and the subsurface injection system and insitu instrument package (right).

## EXPERIMENTAL METHODS

A series of 10 subsurface injection flume tank experiments were conducted to evaluate the horizontal transport of subsurface oil droplets under four test salinities. Two different oil types were used – Alaska North Slope (ANS) crude and Intermediate Fuel Oil 120 (IFO). Each oil type was tested without dispersant treatment as well as with the dispersant Corexit 9500A at a dispersant-to-oil ratio (DOR) of 1:25. The experiments were conducted in the fall of 2016 and average water temperatures were 14.1°C for experiments with ANS and 9.5°C for experiments for experiments with IFO-120. A complete list of the experimental treatment conditions can be found in the table below.

To monitor the transport of dispersed oil in the tank, a series of insitu instruments were deployed at various locations in the tank. Oil droplet sizes between 2.5-500 µm were measured using two LISST-100X particle size analyzers (Sequoia Scientific) which were located 2.6 m and 4.5 m downstream of the subsurface oil release. Also deployed in the tank were a series of four commercially available hydrocarbon fluorometers (Turner Cyclops C7 Refined and Crude Optics, Chelsea UV Aquatracka Refined Optics, Wetlabs ECO) so that their response to dispersed oil resulting from a subsurface release could be evaluated. Discrete water samples were collected during each experiment for chemical analysis of BTEX (benzene, toluene, ethylebenzene and xylene) and TPH (Total Petroleum Hydrocarbons).

| | | Water Temp (°C) | Air Temp (°C) | Salinity (ppt) |
|---|---|---|---|---|
| **Experiment ID** | **Oil Type** | **(Avg)** | **(Avg)** | |
| SubHS-1, 2, 3, 4 | ANS Crude | 14.1±1.1 | 11.6±4.1 | 28, 50, 75, 100 |
| SubHS-7, 8, 9, 10 | ANS Crude | 9.5±0.6 | 7.7±1.6 | 28, 50, 75, 100 |

| | Viscosity @ Selected Temperatures cPoise | | Density @ 40°C g $ml^{-1}$ |
|---|---|---|---|
| | 15°C | 40°C | |
| ANS | 18.9 | 8.3 | 0.8600 |
| IFO-120 | 2481.5 | 240.3 | 0.9411 |

## REFERENCES


Conmy et al. 2013. Submersible Optical Sensors Exposed to Chemically Dispersed Crude Oil: Wave Tank Simulations for Improved Oil Spill Monitoring. Environmental Science and Technology, 48:1803-1810.

Li et al. 2016. Reynolds Number Scaling to Predict Droplet Size Distribution in Dispersed and Undispersed Subsurface Oil Releases. Marine Pollution Bulletin, 113:332-342.

Zhao et al. 2016. Underwater oil jet: Hydrodynamics and droplet size distribution. The Chemical Engineering Journal, 299:292-303


## DROPLET SIZE RESULTS

Data obtained from the LISST was used to generate the oil droplet size distribution (DSD) plots shown in Figure 2 below. The use of dispersants had the greatest impact on oil droplet sizes for both oil types. For the ANS crude oil experiments, without the use of dispersant the resulting oil droplet size had a D50 of 75 µm, while with Corexit 9500A at a DOR of 1:25 the D50 was reduced to 12 µm. For the IFO-120 experiments, the more viscous product resulted in overall larger droplets with dispersant having less of an effect compared to ANS. A D50 of 104 µm was obtained in IFO-120 experiments without the use of dispersant, while a D50 of 88 µm was obtained with the use of Corexit. Salinity appeared to have very little effect on the DSD for both oil types, with or without dispersant application.

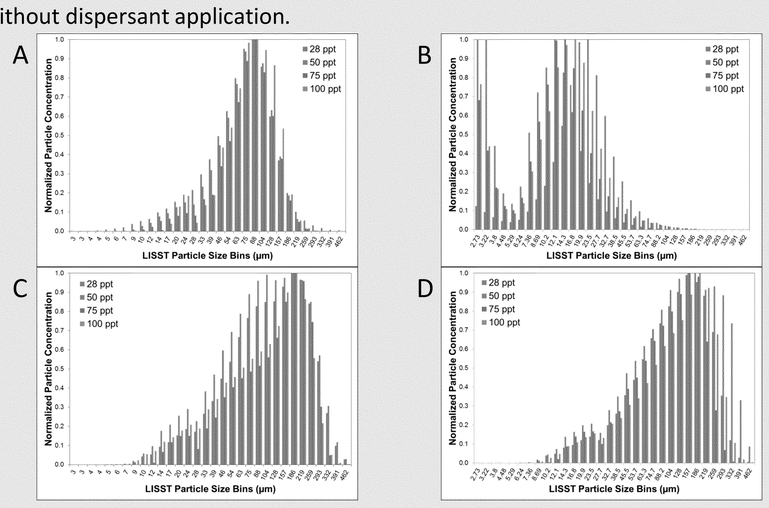


Figure 2: Droplet size distribution at four different test salinities for (A) ANS, (B) ANS+Corexit, (C) IFO, and (D) IFO+Corexit.

The impact of increased salinity on oil droplet buoyancy was calculated using Stokes Law. Based on the oil droplet rise velocities shown in Figure 3, droplets less 500 µm would remain submerged during the entire length of the experiment. The impact of salinity on oil droplet rise velocities would be more noticeable for larger droplets (i.e. 2mm or greater in diameter).

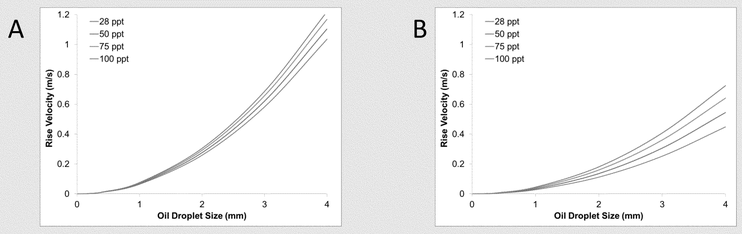


Figure 3: Droplet size rise velocities for (A) ANS Crude and (B) IFO-120 at four test salinities.

## WATER COLUMN HYDROCARBON RESULTS

The use of in-situ fluorometers during oil spill response is becoming increasingly common due to their relative ease of deployment and sensitivity to a range of petroleum hydrocarbons. However, there are numerous in-situ fluorometers available commercially, each using different optical properties and thus having varying responses to different crude oil types. An example of the realtime response from the four different hydrocarbon fluorometers deployed during these experiments is shown in Figure 4. All four instruments gave a higher signal response to ANS crude oil compared to IFO-120. In addition, experiments using ANS that had been dispersed with Corexit 9500 had on average twice the signal response compared to ANS oil alone. There was little difference in the intensity of the fluorometer response for IFO-120 with and without dispersant treatment. Measurement of water column hydrocarbon concentrations found that there were significant differences between the two oils (Table 1). For the volatile hydrocarbon (BTEX) results, the ANS crude generated concentrations that were approximately an order of magnitude greater than IFO-120. The use of dispersant also resulted in BTEX concentrations that were approximately double compared to experiments that did not use dispersant. Total oil concentrations (TPH) in the water column were also higher for both ANS and IFO-120 when treated with dispersant, while IFO-120 had slightly higher TPH concentrations for experiments both with and without dispersant compared to ANS.

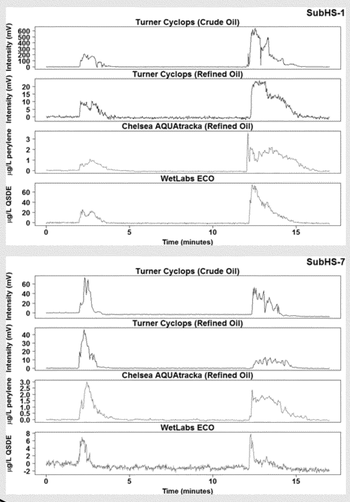


Figure 4 (Left) shows the insitu fluorometer response for ANS Crude (top) and IFO-120 (bottom). The first peak on each plot is for an oil injection without dispersant treatment, while the second peak is for oil and dispersant.

Table 1 (right) summarizes the average water column hydrocarbon chemistry results for BTEX and TPH analyses.

| BTEX (ppb) | | |
|---|---|---|
| | ANS | IFO-120 |
| No Dispersant | 195.0 | 37.3 |
| With Dispersant | 513.7 | 51.1 |

| TPH (ppm) | | |
|---|---|---|
| | ANS | IFO-120 |
| No Dispersant | 20.1 | 34.8 |
| With Dispersant | 33.3 | 37.9 |

## SUMMARY


A series of subsurface oil injection experiments were conducted to evaluate the effect of hypersaline conditions on dispersant effectiveness. Under the conditions used in this study, salinities of up to 100 ppt did not have a significant effect on crude oil dispersion. Higher salinities would have an impact on oil droplet rise velocities, although these effects were not observed in our shallow water test tank. In situ fluorometer response varied across the different instruments that were deployed. A stronger signal on all instruments for the ANS crude oil may have been a result of its chemical composition as well as the oil droplet size distribution generated by this oil.



ED_001324_00000947-00001

**IAA No. E12PG00037**

**Draft Final Report**

# Dispersant Effectiveness, In-Situ Droplet Size Distribution and Numerical Modeling to Assess Subsurface Dispersant Injection as a Deepwater Blowout Oil Spill Response Option

*and*

# Evaluation of Oil Fluorescence Characteristics to Improve Forensic Response Tools

*Submitted to:*

Bureau of Safety and Environmental Enforcement
Sterling, VA

*Submitted by:*

Robyn N. Conmy, Ph.D.
U.S. Environmental Protection Agency
National Risk Management Research Laboratory
Land Remediation and Pollution Control Division
26 W. Martin Luther King Drive
Cincinnati, OH 45268
*Tel: 513-569-7090, Fax: 513-569-7620
Email: conmy.robyn@epa.gov

Thomas King, M.Sc.; Brian Robinson; Scott Ryan; Youyu Lu;
Department of Fisheries and Oceans Canada
Center for Offshore Oil, Gas and Energy Research (COOGER)
1 Challenger Drive, Dartmouth, Nova Scotia, Canada B2Y 4A2
Tel: 902-426-4172
Tom.King@mar.dfo-mpo.gc.ca

September 30, 2015

**ACKNOWLEDGEMENTS**

The research presented in this report was funded by the Bureau of Safety and Environmental Enforcement (BSEE) through Interagency Agreement E12PG00037. Efforts were partially supported by the U.S. Environmental Protection Agency - Office of Research and Development (EPA ORD) and the Department of Fisheries Oceans Canada – Bedford Institute of Oceanography (DFO-BIO). This work was a highly collaborative effort and the authors would like to thank all of the contributors. The numerical modeling components are contributions by collaborators Dr. Michel Boufadel and Feng Gao (New Jersey Institute of Technology) and Dr. Haibo Niu and Linlu Weng (Dalhousie University). The high-resolution fluorescence component is a contribution of Mary Abercrombie (University of South Florida). A special thanks to all of the DFO and BDR Contracting staff who made the wave tank experiments possible: Patrick Toole, Claire McIntyre, Cody Sherren, Jennifer Mason, Peter Thamer, Gary Wohlgeschaffen, Susan Cobanli, and Rod Doane.

**DISCLAIMER**

This draft report contains scientific observations from a series of subsurface oil injection experiments and high resolution fluorescence analyses. Findings are subject to institutional review and are considered draft, thus the information provided here should not be parsed. Refrain from citing or posting until report is considered final. Upon review, approval does not signify that the contents reflect the views of the U.S. EPA, DFO Canada, or BSEE, nor does the mention of trade names or commercial products constitute endorsement or recommendation for use.



ED_001324_00000953-00002

# EXECUTIVE SUMMARY

This report summarizes two projects covered under an Interagency Agreement between the Bureau of Safety and Environmental Enforcement (BSEE) and the U.S. Environmental Protection Agency (EPA) in collaboration with the Bedford Institute of Oceanography, Department of Fisheries and Oceans Canada (BIO DFO), New Jersey Institute of Technology (NJIT) and Dalhousie University. Both projects dovetail together in addressing in differentiating physical from chemical dispersion effectiveness using oil and dispersant injection simulations within a wave tank for improving forensic response monitoring tools. This report is split into Tasks based upon the two projects funded by BSEE:

1) Dispersant Effectiveness, In-Situ Droplet Size Distribution and Numerical Modeling to Assess Subsurface Dispersant Injection as a Deepwater Blowout Oil Spill Response Option.
2) Evaluation of Oil Fluorescence Characteristics to Improve Forensic Response Tools.

***TASK A: Dispersant Effectiveness, In-Situ Droplet Size Distribution and Numerical Modeling to Assess Subsurface Dispersant Injection as a Deepwater Blowout Oil Spill Response Option.***

The main objectives of work under Task A were to evaluate high speed subsurface releases of physically and chemically dispersed oil using a flow-through wave tank / flume facility. This project addressed three issues: (1) performance evaluation of dispersants for subsurface injection into sub-sea blowouts, (2) tracking, modeling, and predicting the movement and spread of the deepwater plume and oil surfacing from deepwater blowouts, and (3) evaluating the influence of dispersant applications in reducing the concentration of volatile organic compounds emanating from the water surface. Oil dispersion experiments were conducted in the flow-through wave tank (flume) at the Department of Fisheries and Oceans Canada, Bedford Institute of Oceanography (DFO BIO), which is equipped with an underwater oil release system to simulate a deepwater blowout oil spill scenario. Subsea plume simulations were generated with a pressurized underwater oil release system adapted from existing technology developed by Masutani and Adams (2000). To mitigate wall effects and to generate



ED_001324_00000953-00003

oil droplets in the size range observed at depth during the Gulf of Mexico Deepwater Horizon (GoM DWH) oil spill, a high flow-rate of oil was released through a small diameter nozzle (2.4 mm). Although it is impossible to simulate in the tank the extreme hydrostatic pressures that exist at 1500 m water depth, underwater high-pressure release of crude oil can be simulated with and without dispersant addition.

A total of 48 core and 24 complimentary wave tank experiments were conducted to evaluate the effectiveness of dispersant injection and natural attenuation of the plume as a function of oil type (ANS pipeline blend for a light-medium crude, IFO-120 for a heavy refined product and South Louisiana Crude for a light crude), chemical dispersant type (Corexit 9500 and Finasol OSR 52), dispersant-to-oil ratio (DOR of 0, 1:25, 1:100, and 1:250; corresponding to DOR concentrations of 0, 4, 1, and 0.4%) and water temperature (< 10 ºC for low temperature and > 10 ºC for higher temperature). Experiments were conducted at a fixed current flow rate of 1 cm/s (~ 1/8$^{th}$ of deep water flow rates in the GoM), with low energy coherent wave conditions and 80 ºC oil temperature.

Time series dispersion effectiveness was evaluated by measuring dispersed oil concentrations from samples in the wave tank, and via *in situ* droplet size distribution analysis and fluorescence measurements. Discrete samples were collected from two different horizontal distances from the wave-maker end and at three vertical depths (near surface, middle, and near bottom) at several different time points. Samples were subdivided for oil chemistry analysis of Total Petroleum Hydrocarbons (TPH) and Benzene-Toluene-Ethylbenzene-Xylene (BTEX) via gas chromatography coupled to a flame ionization detector (GC/FID) and gas chromatography mass spectrometry (GC/MS), employed to quantify oil concentration and partitioning of hydrocarbon compounds in seawater.

The produced Droplet Size Distribution (DSD) was determined by using Laser *In-Situ* Scattering and Transmissometry instruments (LISST-100X, type C, size range: 2.5~500 µm; Sequoia Scientific Inc. Seattle, WA) to track the full range diameters of chemically and physically dispersed oil droplets. Physically dispersed oil droplets may be capable of recoalescing and rising to the surface under less energetic mixing conditions, where the LISST facilitates a



ED_001324_00000953-00004

comparison between natural (physical) and chemical dispersion efficiency of crude oil. All submersible sensors were operated with real-time data acquisition throughout each experiment. In situ fluorescence was monitored real-time using two Chelsea Technologies Group AquaTrackas (crude and refined oil types), one Sea Bird – Wet Labs Inc. ECO (gelbstoff type), two Turner Designs Inc. Cyclops (crude and refined oil types) and one GmBH Trios (hydrocarbon type) fluorometers. Many of the fluorescence sensors used in this study are the same models employed to track the subsea plume during the DWH oil spill and confirm dispersion effectiveness. Sensors used in this work are also ones named in the National Response Team (NRT) *Subsea Dispersant Monitoring and Assessment Interim Guidance* Document, that states "the Risk Plan should use a properly calibrated oil-specific fluorometer (e.g., Chelsea UV AQUAtracka, Turner Designs Cyclops, Wet Labs ECO, or equivalent oil-specific instrument) to enable ongoing improvements in sampling".

Also monitored during experiments was the level of Volatile Organic Carbon (VOC) above the air-water interface of the tank to evaluate concentrations from the perspective of worker safety. Correlations between in situ fluorescence data, droplet size distribution, total particle concentration, and oil chemistry serve as inputs to the modeling activities of this project.

Oil droplet size distribution data from this study is essential for the improvement of oil spill trajectory and ocean circulation modeling processes to predict the fate and transport of subsurface plumes and surface oil slick movement. This has implications for improving the community's understanding on the impacts of dispersant application at depth, ultimate fate of subsurface dispersed oil plumes and potential natural resource damages. Recent advancements in the use of numerical modelling have allowed for the prediction oil droplet sizes resulting from a subsurface release. Several different mathematical approaches have been used to determine how oil would behave flowing out of an orifice at high pressure. This includes the modified Weber Number technique (Johansen et al., 2013) and the VDROP model (Zhou et al., 2014) to predict oil droplet breakup taking into account oil viscosity and interfacial tension. However, there is a limited amount of large scale real world data to help validate the output of these models. This study provided the opportunity to further test these techniques



ED_001324_00000953-00005

through the use of several different oil types and treatment conditions. Results from the numerical modelling using data obtained from tank experiments are presented in Appendix G, with Part 1 using the modified Weber Number and Part 2 using VDROP. The premise for this research is that the evaluation and efficacy of chemical dispersants at depth will differ dramatically from conventional use of chemical dispersants for treating surface oil slicks, where mixing energy is provided mainly through naturally occurring surface waves and currents, especially breaking wave energy dissipation rates. Monitoring of DSD is essential in differentiating between chemically and physically dispersed oil. Tank observations using underwater injection experiments provide evidence of stable dispersion that may be expected during deepwater blowout scenarios. Naturally dispersed oil droplets may be capable of recoalescing and rising to the surface under less energetic mixing conditions without enhancement by chemical dispersant injection. The experimental results from this work demonstrate the dispersion of oil into small droplets and help to predict the likelihood of recoalescence and resurfacing of oil. Results of the project provide spill responders with critical information on the utility of subsurface dispersant application as an oil spill response option and the modeling capabilities that are available to predict oil trajectory during deep water blowouts. Both assist decision-making regarding countermeasures.

***TASK B: Evaluation of Oil Fluorescence Characteristics to Improve Forensic Response Tools.***

This project addresses the evaluation of oil fluorescence characteristics and sensor performance for improving response tools used in oil spill countermeasure decision-making. Fluorescence has long been used as 'one tool in the toolbox' for surface spills where visual confirmation is a component of response efforts. Recent oil and gas production in extremely remote locations brings an increased risk of spills in under-the-ice and/or deep-sea environments. For accidental releases in these environs, responders will be evermore reliant on submersible fluorometers for plume tracking when the human eye cannot be employed. As such, the oil spill community has identified the need for better characterization of spilled oil by fluorometers.



ED_001324_00000953-00006

Submersible fluorometers deployed during the 2010 Gulf of Mexico Deepwater Horizon (DWH) oil spill highlighted the challenges in ensuring selection of the optimum sensor configuration as fluorescence peaks occur over a wide nanometer range, vary in shape and wavelength position, are dependent on oil type due to chemical differences, and are affected by the addition of dispersants. This project addresses these concerns through the following objectives: (1) Characterization of oil optical properties as a function of oil type, dispersant-to-oil ratio (DOR) and concentration; (2)Generation of a comprehensive EEMs (Excitation Emission Matrix Spectroscopy) library that will be subjected to advanced statistical analyses for identification of wavelength regions best suited for oil detection; and (3) Evaluation of sensor performance through a series of experiments in a wave tank capable of static and flow-through operations, where sensor data will be validated with chemical and optical analyses.

A series of bench-scale dispersed oil-in-seawater experiments were conducted on 25 oils at 4 dispersant-to-oil ratios (DORs) using Corexit 9500 chemical dispersant. Analysis of the resulting 3D fluorescence excitation-emission matrix spectra (EEMs) shows oil-specific results as well as differing effects of dispersant and DORs. Results will enhance the identification of optimum detection wavelengths for oil in the marine environment as well as determination of the effectiveness of dispersant application. Samples were prepared using baffle flasks to physically disperse the oil within seawater. The effect of dispersant on oil-specific fluorescence is shown, where shifts in intensity and peak wavelengths were observed. Results were compared to chemistry results of oil components.

Results of the laboratory EEMS analysis were compared to EEMS collected under Task A of this project to compare the applicability of baffle flask fluorescence to large scale mixing experiments in the wave tank.

Given recent advances with in situ fluorometers, enabling lower UV-wavelength detection, these findings help to discern wavelength regions influenced by dispersed oil within seawater, improve the interpretation of fluorescence data, and inform decision-making by responders.



ED_001324_00000953-00007

Findings from this project will serve to improve confidence in field data, filling operational gaps and formulating operational guidelines.

Overall findings from both tasks of this project include:

1. Addition of either Corexit 9500 or Finasol OSR 52 chemical dispersants to Alaskan North Slope (ANS), IFO-120 and South Louisiana Crude (SLC) oils decreased the Volume Mean Diameter (VMD) and shifted the Droplet Size Distribution (DSD) to smaller droplets. In general, Corexit 9500 produced smaller droplets compared to Finasol OSR 52.
2. Dispersions created without chemical dispersants or Dispersant-to-oil ratio (DOR) = 1:200 yielded VMD larger than 70 µm and exhibited unimodal DSD. Dispersions created with DOR = 1:20 yielded VMD between 2.5 to 70 µm size range with a bimodal distribution. This suggests that produced droplets from a DOR = 1:20 dispersant injection would likely remain dispersed in the presence of mixing energy given the small droplet size observed.
3. Particle size analyses near the injection release (LISST Release) exhibited larger VMD compared to those generated further downstream from release in the tank (LISST Downstream) indicating a shift from larger to smaller droplets within the plume during the 10 minute experiments for ANS and SLC oils. This effect was not always observed with the heavier IFO-120 oil.
4. For ANS, adequate dispersion (< 70 um droplet VMD) was observed for the DOR = 1:20 treatments at both cold and water temperatures. Water temperature did not appear to influence the DSD or VMD for this lighter crude oil. However, a temperature effect was observed on the Total Particle Concentration (TPC), where lower temperatures were coincident with fewer particles dispersed within the plume for a given volume of oil injected.
5. The addition of Corexit 9500 or Finasol OSR 52 to IFO-120 during warm temperature experiments resulted in a shift in DSD and a decrease in VMD, however bimodal distribution was not achieved and even DOR = 1:20 did not yield VMB less than 70



ED_001324_00000953-00008

µm in most cases. A cold water temperatures, lower droplet sizes were not observed with the addition of dispersant, where DOR = 1:20 remained well above 200 µm. This suggests that dispersant addition to this oil at cold temperatures would not yield droplets that remain in suspension.

6. For experiments conducted at water temperatures less than 5 °C, particle size data from the LISST analyzers appears problematic, where even a unimodal distribution is not measured. Chemistry and in situ fluorescence data do not reflect any problems for these experiments. Although 5 °C is within the operating temperature of the LISST (manufacturer manual), additional testing of the cold water temperature limits of the sensor is recommended.
7. SLC oil was more dispersible compared to ANS for treatments with and without chemical dispersant. Bimodal distribution was observed during DOR = 1:20 and some DOR = 1:100 experiments indicating that the jet release of this particular oil into warm water produced smaller droplets than the ANS.
8. In situ fluorescence serves as a good proxy for oil concentration during the subsurface injection experiments. Given the experimental design, fluorescence is better suited for correlation with particle size analysis and concentration. Heterogeneity of the produced plumes and the short time scale of experiments (~10 min) led to difficulties in correlations between the plume particle size analyses and chemistry results. This is in part due to discrete samples representing 30 second averages as opposed to instantaneous measures given by fluorometers and particle size analyzers.
9. VOC air monitoring was conducted above the tank during experiments. The gas condensate exhibited the highest surface VOC concentrations, followed by ANS and SLC which exhibited similar values. Lowest concentrations were observed for IFO-120 experiments. High VOC concentrations in the air were usually accompanied by higher BTEX concentrations in the water. For all oils tested, the addition of chemical dispersants (DOR = 1:20) resulted in a reduction in VOC concentrations compared to experiments without dispersant near the jet release location.



ED_001324_00000953-00009

10. Fluorescence Excitation Emission Matrices (EEMs) were generated for 25 oil types under varying DOR, where two categories were found based on dispersiblity and light, medium and heavy oils were found in each category. Fluorescence peaks are chemistry dependent and were well correlated with Total Petroleum Hydrocarbon (TPH) and Benzene-Toluene-Ethylbenzene-Xylene (BTEX) concentrations. EEMs generated from tank and Baffle Flask Test (BFT) experiments were in agreement with respect to fluorescence peak position and Fluorescence Intensity Ratio (FIR) values as an indication of dispersion effectiveness.
11. Programs for jet hydrodynamics, the droplet size distribution, and the movement of oil droplets within the jet/plume were employed where developed models were calibrated to experimental data of oil jet released in a wave tank. The models VDROP-J and JETLAG were used to predict the streamwise velocity and the holdup along the centerline of the plume, where both models were in agreement, implying that VDROP-J is capable of predicting the average droplet size distribution in the plume. In the absence of dispersant, the model VDROP-J predicted the oil DSD measured by the LISST. In the presence of dispersant, the VDROP-J model captured the overall trend of the DSD, but was challenged in capturing the peak in droplet concentration observed for 5 microns. The observed peak is most likely due to tip-streaming, and VDROP-J does not yet have a module for this component.
12. The Modified Weber Number approach developed by SINTEF is a recent and promising approach for predicting DSD. Previously the method has been validated by solely a light crude oil. For this project, median droplet diameters ($d_{50}$) and the relative droplet size ($d_{50}/D$) were calculated based on the measured droplet sizes obtained from the tank experiments, and the relations between $d_{50}/D$ and modified Weber number, Reynolds number, and oil concentration were quantified. Results demonstrate that chemical dispersants play an important role in reducing the droplet size of ANS in both cold and warm temperatures and that dispersants are more effective in reducing droplet size ANS compared to IFO-120. A two-step Rosin-Rammler approach was found



ED_001324_00000953-00010

to better predict the droplet size distribution as indicated by higher regression coefficients.



ED_001324_00000953-00011

# TABLE OF CONTENTS

***TASK A - Dispersant Effectiveness, In-Situ Droplet Size Distribution and Numerical Modeling to Assess Subsurface Dispersant Injection as a Deepwater Blowout Oil Spill Response Option.***


**A.1 INTRODUCTION & RELEVANCE ..... 14**
**Objectives ..... 17**

**A.2 EXPERIMENTAL METHODS ..... 18**
**A.2.1 Flume Tank Description, Flow Calibration and Operation ..... 18**
**A.2.2 Waste Water Treatment ..... 21**
**A.2.3 Subsurface Oil Injection System ..... 21**
**A.2.4 Submersible Sensor Deployment ..... 25**
**A.2.5 VOC Air Monitoring ..... 26**
**A.2.6 Discrete Water Sample Collection ..... 27**
**A.2.7 Oil and Dispersant Samples ..... 28**
**A.2.8 Experimental Design – Core and Complimentary Experiments ..... 30**
**A.2.9 Submersible Sensor Calibration Experiments ..... 30**
**A.2.10 Submersible Fluorometer and LISST Data Processing ..... 32**
**A.2.11 Analytical Chemistry Analysis ..... 33**
**A.2.12 Numerical Modeling ..... 34**

**A.3 RESULTS & DISCUSSION ..... 35**
**A.3.1 ANS Dispersion Effectiveness ..... 35**
**A.3.2 IFO-120 Dispersion Effectiveness ..... 49**
**A.3.3 SLC Dispersion Effectiveness ..... 59**
**A.3.4 Gas Condensate Dispersion Effectiveness ..... 63**
**A.3.5 Tank Dilution Series Fluorescence Measurements ..... 66**
**A.3.6 VOC Air Monitoring ..... 71**
**A.3.7 VDROP-J and JETLAG Numerical Plume Modeling ..... 81**
**A.3.8 Weber Number Scaling Numerical Plume Modeling ..... 83**


***TASK B: Evaluation of Oil Fluorescence Characteristics to Improve Forensic Response Tools.***


**B.1 INTRODUCTION & RELEVANCE ..... 85**
**Objectives ..... 91**

**B.2 EXPERIMENTAL METHODS ..... 94**
**B.2.1 Sample Preparation ..... 94**
**B.2.2 Artificial Seawater Protocol ..... 94**
**B.2.3 Dispersed Oil in Seawater Protocol ..... 94**
**B.2.4 Spectrophotometric Analysis ..... 95**

**B.3 RESULTS & DISCUSSION ..... 99**
**B.3.1 Oil Fluorescence Properties ..... 99**
**B.3.2 Fluorescence as a Function of Chemistry ..... 109**
**B.3.3 Wave Tank & Baffle Flask EEM Comparison ..... 114**
**B.3.4 PARAFAC Modeling ..... 116**

***REFERENCES* ..... 155**

***APPENDICES (Separate Document)***
**APPENDIX A – Experiment Logs**
**APPENDIX B – Analytical Chemistry Results**
**APPENDIX C – Jet Release LISST Oil Droplet Size Distribution Histograms**
**APPENDIX D – Jet Release LISST Oil Droplet Size Distribution Time Series Contours**
**APPENDIX E – Submersible Fluorescence Time Series**
**APPENDIX F – Excitation Emission Matrix Contours**
**APPENDIX G – VDROP-J and JETLAG Numerical Plume Modeling Report**
**APPENDIX H – Weber Number Scaling Numerical Plume Modeling Report**



ED_001324_00000953-00013

# TASK A.1 INTRODUCTION & RELEVANCE

The 2010 Deepwater Horizon (DWH) oil spill in the Gulf of Mexico has highlighted the pressing need for a better understanding of the interaction of chemical dispersants and crude oil at ocean depth. Early in the blowout release, partial emulsification of oil was observed as it rose to the surface from 1500-m depth, and surface slicks were not continuous (Oil Budget Calculator). As a result, a decision was made to inject dispersants directly at the release point as a means to increase efficiency of dispersion, to reduce the amount of dispersant needed, and potentially reduce volatile organic compound (VOC) concentrations at the air-sea interface. Large quantities of chemical dispersant were applied via subsurface injection and traditional spraying from aircraft onto the surface oil slick (Oil Budget Calculator). At a decision-makers workshop to discuss the use of subsurface chemical dispersants as an oil spill response option, agreement was reached among spill response and research expert attendees on potential advantages of subsurface dispersant injection given the rate of continuous oil release and preliminary evidence of the dispersant efficacy from the DWH spill (CRRC 2010). Potential advantages of this application included the fact that the fresh (unweathered) oil was considered well suited for dispersion, operators were able to inject the dispersant directly into the oil stream thereby maximizing dispersant/oil contact, sufficient control of DOR (Dispersant-to-Oil Ratio) could be maintained, injection may minimize the need for surface dispersant application because of reduced oil surfacing and optimized subsurface application would likely promote formation of smaller, more stable droplets of oil, enhancing biodegradation (Lee et al., 2009).

As recommended by the interagency Unified Area Command (UAC) and on-site emergency spill response coordinators, a large-scale environmental monitoring program was implemented to detect and characterize dispersed oil based on field data and plume modeling outputs. This allowed for tracking the subsurface oil plume emanating from the blowout wellhead. Droplet Size Distribution (DSD) analysis using the LISST-100X Laser *in-situ* Scattering and Transmissometry System (Sequoia Scientific Inc. Seattle, WA) and fluorescence intensity from submersible fluorometers were used as an indication of Dispersion Effectiveness onboard the research vessels, where small particle (≤ 70 µm) concentrations were monitored to evaluate



ED_001324_00000953-00014

oil dispersion (Li et al., 2009b). Data analysis of the monitoring samples provided sound evidence of the presence of oil-bearing small particles both in surface waters and in the subsurface plume (Lee, 2010). Furthermore, a negative correlation between subsurface dispersant injection and low molecular weight compounds in surface waters was observed. In contrast, a strong positive correlation was observed in the subsurface. These results suggest that subsurface dispersant use may have stimulated *in situ* weathering of oil at depth in areas surrounding the wellhead and may have suppressed the rising of volatile and semi-volatile organic compounds to the surface layer (Li et al., 2011).

Although it appears likely that subsurface *in-situ* use of chemical dispersants at the release source may be effective for countering deepwater spill blow-out scenario, much uncertainty still exists in terms of the DE with this type of application. For example, assumptions of the optimal DOR are based on empirical data mostly obtained from bench-scale experimental protocols that have been designed for testing at standard temperatures and pressures (STP), whereas conditions at a wellhead on the ocean floor or anywhere along a riser beneath the ocean surface could be significantly different. Hence, DOR for direct injection needs to be better understood. Although theoretical analyses and experiments suggest that jet breakup of the oil is insensitive to the absolute value of system hydrostatic pressure for incompressible liquid-liquid systems (Masutani and Adams 2000), the effects of several ambient environmental factors on subsurface dispersant effectiveness, including high release pressure, high oil temperature, low water temperature, and the presence of methane and suspended sediments in the oil plume and/or surrounding water column remain to be clarified. Improved understanding on the influence of these factors on DE and the interaction of crude oil and chemical dispersant under a range of turbulent regimes at depth is required for informed decision-making for future subsurface dispersant use.

For evaluating chemical dispersion effectiveness, standard laboratory tests are inherently limited in simulating real field operational performance due to space constraints that are critical for transport and dilution efficiency (NRC 2005). To address the need to evaluate chemical dispersion effectiveness under more realistic oceanographic and environmental



ED_001324_00000953-00015

conditions, a meso-scale wave tank capable of generating breaking and regular non-breaking wave conditions is currently in operation at the Bedford Institute of Oceanography (BIO), Dartmouth, Nova Scotia. This tank facility has been used previously to characterize the tank hydrodynamics and the efficacy of several oil dispersant formulations on dispersion of different oil types, including fresh and weathered crude oils and heavy fuel oils (Figure 1) (Lee et al. 2009; Li et al. 2008; Wickley-Olsen et al. 2007). Mathematical modeling and experimental measurements have been used in the characterization of the fluid dynamics of the wave tank. In modeling, computer fluid dynamics software packages have been used to conduct numerical simulation of the fluid field and transport phenomena of the wave tank under both non-breaking and breaking wave conditions. Experimentally, wave gauges (WG-50) have been used to monitor wave profiling throughout the wave tank under various hydrodynamic conditions. Acoustic Doppler Velocimetry (ADV) has been employed to evaluate the *in situ* instantaneous three-dimensional velocity distribution, which is used to compute the velocity gradients and energy dissipation rates ($\varepsilon$) in the tank. Using this facility, previous experiments have assessed chemical dispersant effectiveness as a function of energy dissipation rate and particle size distribution (Li et al. 2009a) and demonstrated that the effectiveness of chemical dispersant is strongly dependent on wave conditions, dispersant type, and oil type (Lee et al. 2009). A strong correlation has been established between dispersion effectiveness and *in-situ* droplet size distribution within the hydrodynamic regime, particularly energy dissipation rate, under a variety of non-breaking wave and breaking wave conditions (Li et al. 2008; Li et al. 2009a). The wave tank has also been operated in flow-through mode to accommodate the effects of underwater currents on dispersion and dilution of oil (Li et al. 2009b; Li et al. 2010). Experiments have also shown the reliability of fluorescence measurements as a proxy for oil concentration within physically and chemically dispersed oil (Conmy et al., 2014). Experimental studies have also been conducted to demonstrate the feasibility of applying mineral fines to promote oil-mineral aggregate (OMA) formation and to facilitate physical and chemical dispersion of oil (Lee et al. 2009).

This report summarizes results from a project that addresses the operational performance of the subsurface injection of dispersants into deep water blowouts. Developed were methods



ED_001324_00000953-00016

focused on oil transport after dispersant injection by outfitting a new flow-through wave tank at the Department of Fisheries and Oceans Canada BIO facility with a new underwater high flow rate oil injection release system. In this way, the efficiency of chemical dispersion of deepwater oil blowouts can be quantitatively evaluated as a spill response option vis-à-vis physical dispersion (without dispersant addition). To this end, the **objectives** of this work were to:

1) Refine existing equipment, technologies, and methodologies for subsurface dispersant application assessment and monitoring by measuring dispersed oil concentration, fluorescence, and *in situ* oil droplet size distribution,
2) Evaluate effects of water temperature and dispersant on dispersion efficacy and dispersed oil droplet size distribution of oil at high temperatures,
3) Evaluate dispersion effectiveness (DE) as a function of oil type and dispersant-to-oil ratio (DOR) for deepwater blowout spill response,
4) Assess the effect of dispersant application on the VOC concentration in air above the air-sea interface of the wave tank,
5) Integrate droplet size distribution into deepwater blowout transport/behavior models to enable prediction of the dispersed oil droplets under high flow velocities in deepwater blowouts.

During the DWH spill, small droplet ($d \leq 70\mu m$) concentrations were monitored to aid in evaluating oil dispersion efficiency. The particle size and distribution data obtained from the field monitoring program during the DWH oil spill had a significant role in supporting emergency oil spill response operations, fate and transport modeling, and impact assessment. Findings from this study will have significant implications in further supporting emergency such operations, spill transport models and assessments for future deepwater spills.



ED_001324_00000953-00017

# TASK A.2 EXPERIMENTAL METHODS

## ***A.2.1 Flume Tank Description, Flow Calibration, and Operation***

Oil dispersion experiments were conducted in the flow-through wave tank at the Bedford Institute of Oceanography (BIO). The BIO flume tank is rectangular shaped with dimensions of 32 m in length x 2 m in height x 0.6 m in width. It was fabricated with carbon steel (3/16") and the interior and exterior surfaces are coated with a marine epoxy paint finish to reduce corrosion while operating under marine conditions. Two sets of manifolds consisting of five inflow and outflow pipes (each constructed of 4" PVC pipe and equipped with a ball valve so that the flow rate can be controlled) are fixed (1.1 m from the outer edges) at both ends of the tank (Figure 2). Two high flow pumps (Magnatex 3575 Series Centrifugal Pump, 3" suction, 4" discharge, 600 gpm, Houston, TX), one connected to the inflow manifold and the second located at the outflow manifold provide a flow-through system used to generate horizontal water currents in the tank. A fiberglass holding tank is used to supply seawater for the system to ensure that a constant flow rate is maintained.

Seawater was obtained from the Bedford Basin, which is directly adjacent to the tank. Two smaller pumps (5 HP Pacer S Series Centrifugal Pump, 110 gpm, Lancaster, PA) were used to pull seawater (~50 cm below the surface) through a 3" suction hose from the Basin. A foot valve was installed at the end of the hose to maintain prime water in the line between fillings. Prior to entering the tank, the seawater was filtered through high-flow polypropylene bag filters (5 µm and 25 µm, Atlantic Purification, Dartmouth, NS).

During normal operations, the flume tank (30,000 L) and holding tanks (25, 000 L) are filled with filtered seawater. A stainless steel baffle was mounted (~0.5 m) in front of the influent manifold to control current flow. Flow gauges on the influent and effluent lines were monitored and valve adjustments were made to obtain a balanced flow rate, and so that the operational volume was maintained throughout the experiment. Water current velocities were measured at various depths and locations in the tank using an ADV (Nortek Vectrino+,



ED_001324_00000953-00018

Boston, MA) and the flow rates adjusted until the horizontal water current velocities were consistent at all measured depths.

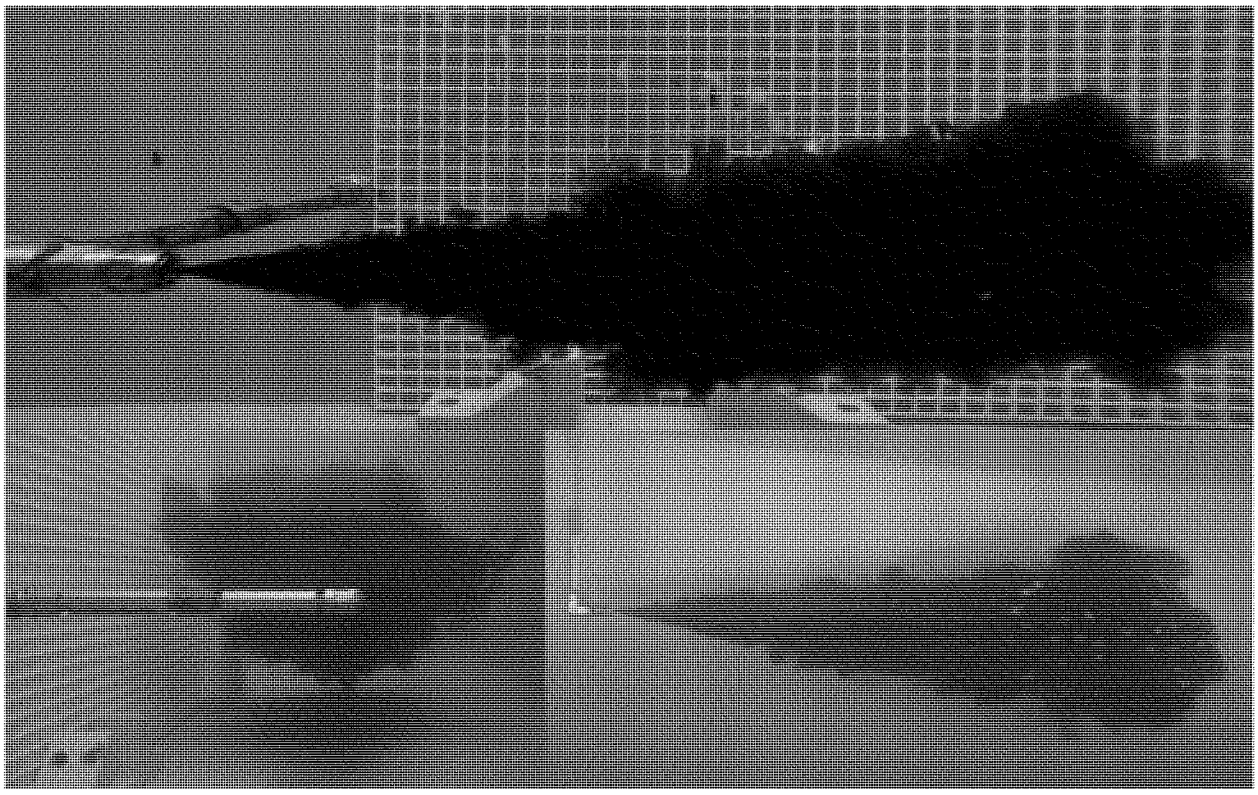

**Figure 1. Photos of subsurface oil injection at the BIO wave tank showing the formation of the subsurface oil plume.**



ED_001324_00000953-00019

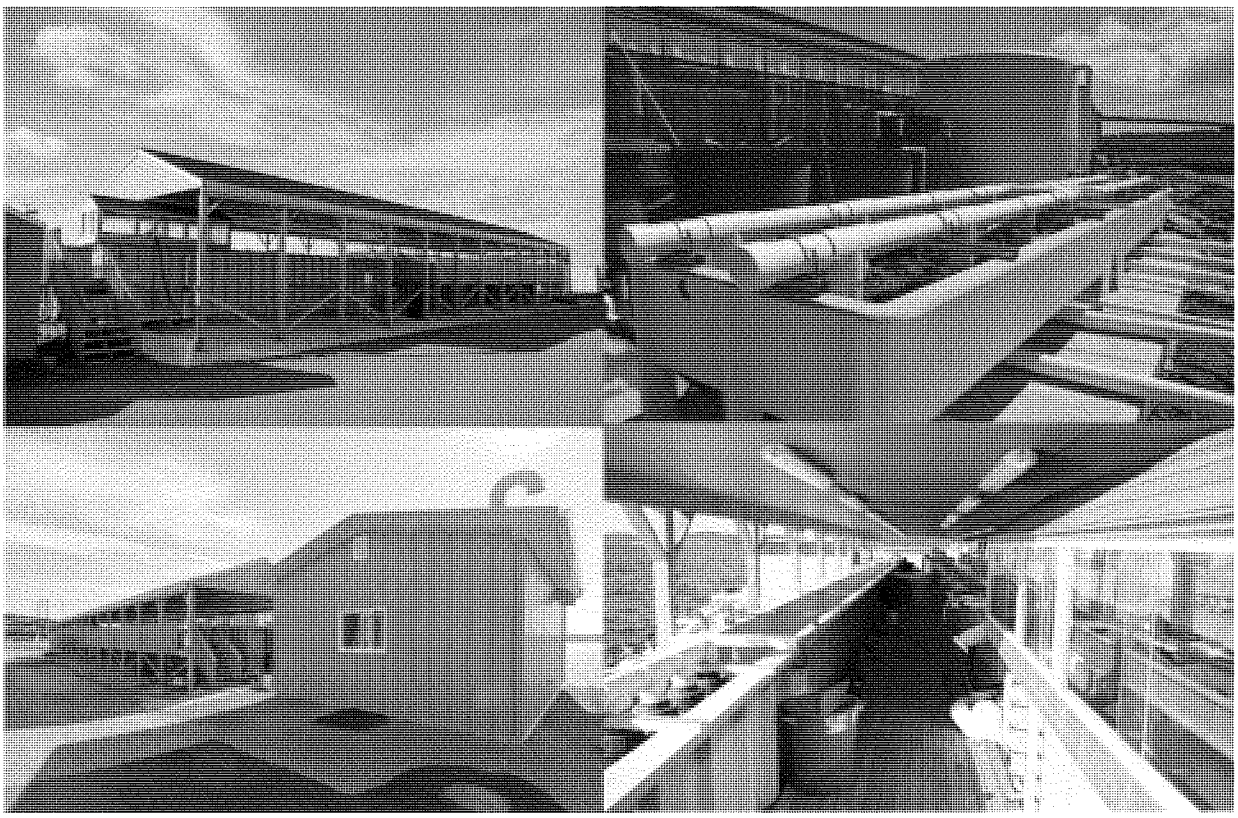

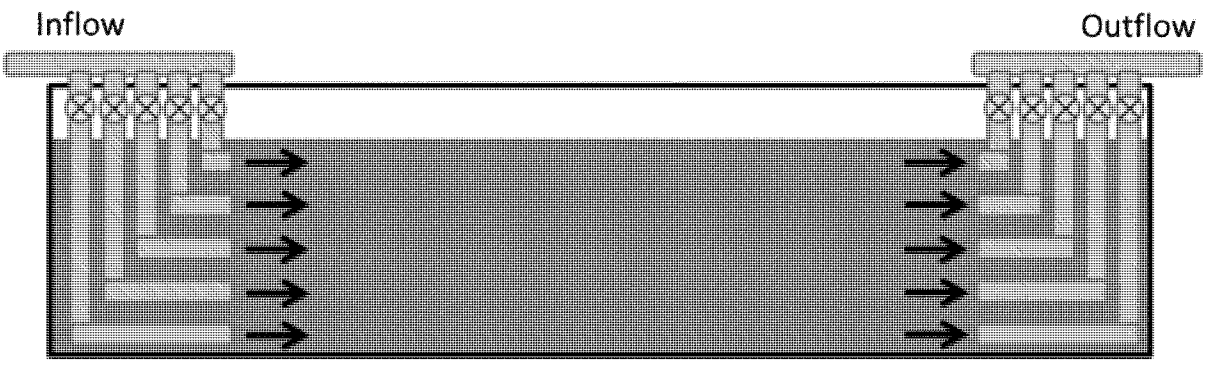


**Figure 2. Photo of the DFO BIO flume tank (top) and cross-section of the tank showing the high-flow manifolds used to generate horizontal water currents (not to scale).**



ED_001324_00000953-00020

### *A.2.2 Waste Water Treatment*

Oil absorbent pads (New Pig, Tipton, PA) are used to manually remove oil from the water surface. The remaining water in the tank is removed by pumping it through an effluent pipe that discharges the waste water over layers of polypropylene PomPom Oil-Mops (New Pig, Tipton, PA) that filter the waste water by removing any remaining insoluble oil prior to discharging it back into the Bedford Basin. Water samples are collected from the treated effluent and the PomPom's are changed if total petroleum hydrocarbon concentrations exceed the minimum guidelines (10 ppm) for wastewater discharge in Canada.

### *A.2.3 Subsurface Oil Injection System*

A custom (engineered in-house) subsurface oil injection system was used to generate dispersed oil plumes in the tank (Figure 3). Briefly, the system consists of a 2 L stainless steel pressure vessel that rests in a support rack. A series of valves and pressure gauges are connected to the pressure vessel. The assembled system is fastened to the outer wall of the tank by way of a quick connect bulkhead fitting. From the same location inside the tank, the fitting connects the outer assembly to a nozzle (2.4 mm inner diameter), which extends mid-width perpendicular to the tank wall (20 cm off the bottom and 9 m downstream from the inflow manifold) and is angled at the tip, so as to direct the discharge plume downstream.

For each experiment, oil or oil/dispersant premix is added to the pressure vessel (Figure 4A). Inside the pressure vessel is a copper coil that is connected to a water bath to permit the oil to be heated to 80°C, which takes 30 minutes. The vessel is then pressurized (40 psi for ANS, SLC and Condensate; 60 psi for IFO-120) with compressed Nitrogen. A ball valve connected to the pressure vessel is manually opened and oil is released through the subsurface nozzle into the flume tank (Figure 4B). The release time and total volume (determined by mass) of oil injected are recorded. After each experiment, the entire subsurface injector system was cleaned by flushing with toluene, acetone and fresh water prior to next experiment.



ED_001324_00000953-00021

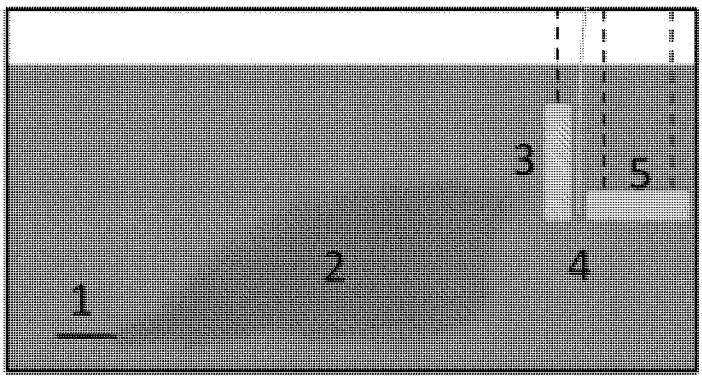


1. Subsurface Injection Nozzle
2. Oil Plume
3. Insitu fluorometers
4. Water sampling port
5. LISST

**Figure 3. Schematic diagram showing the location of the subsurface injector and in situ instrumentation submerged within the tank.**



ED_001324_00000953-00022

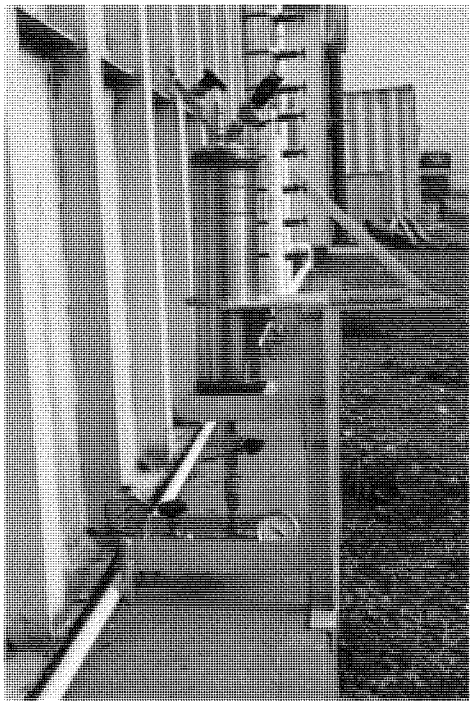

**Figure 4A. Photo of the pressure vessel used to hold the oil for the subsurface release.**



ED_001324_00000953-00023

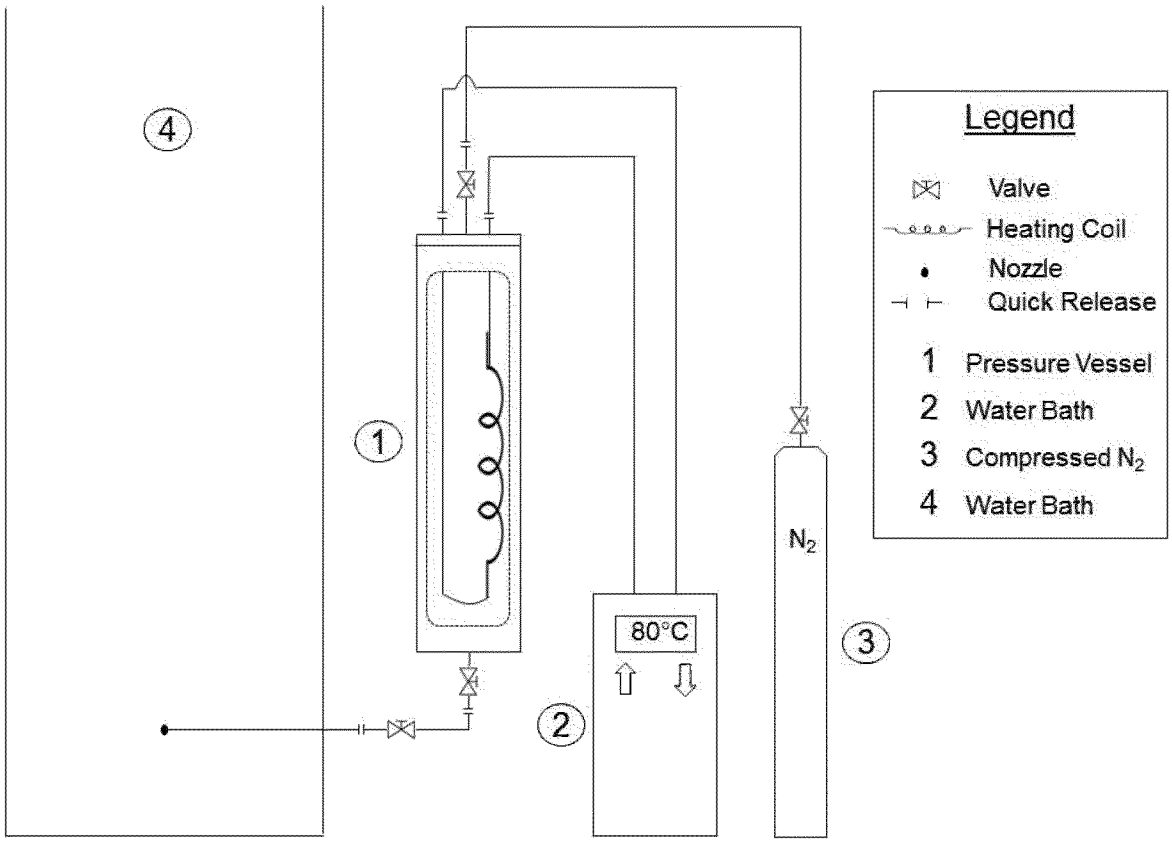


**Figure 4B. Schematic diagram of the subsurface oil release system.**



ED_001324_00000953-00024

### *A.2.4 Submersible Sensor Deployment*

*Fluorescence* - A total of six hydrocarbon fluorometers were evaluated during this study (Table 1). The fluorometers were mounted on an aluminum frame located 4.3 m from the oil release point and at a depth of 0.4 m. The instruments were attached to a crosspiece support bar, so that they were all located the same distance downstream from the oil release point with the UV window pointed directly down at the bottom of the tank.

**Table 1. List of hydrocarbon fluorometers used in this study.**

| Instrument | Excitation/Emission wavelengths |
|---|---|
| Chelsea UV AQUAtracka (Refined) | 239/360nm |
| Chelsea UV AQUAtracka (Crude) | 239/440nm |
| Turner Designs Cyclops (Fine Oil) | 254/350nm |
| Turner Designs Cyclops (Crude Oil) | 365/510nm |
| Sea Bird – WET Labs ECO-FLU | 370/460nm |
| GmbH Trios | 254/360nm |

Several different data acquisition systems were used to control and collect data from the in situ fluorometers. The GmBH Trios was operated by the manufacturer's power supply and data acquisition system using the MSDA_DE software, which provided a real-time display of the signal intensity in calibrated units of µg/L PAH. The sampling rate was set at one reading every five seconds and raw data was saved as a .csv file. The two Turner instruments were connected to a Databank Handheld Datalogger (Turner Designs, Sunnyvale, CA), which powered both instruments and recorded data at a sampling rate of 1 reading every 3 seconds. The datalogger auto-gain feature cycles through settings of 1x, 10x, and 100x depending on the signal intensity. Raw data was recorded as signal intensity in mV and was offloaded from the



ED_001324_00000953-00025

datalogger via USB connection to a laptop and saved as a .txt file. The Sea Bird - WET Labs and Chelsea instruments were connected to a custom-built power supply and data acquisition system (Pace Scientific XR5-SE datalogger; Mooresville, NC), which collected data from the instruments at a sampling rate of one reading per second. The signal was recorded internally on the datalogger and then sent via wireless connection to a laptop in real-time display. Raw data was recorded as signal intensity in mV and offloaded as a .txt file.

*Particle Size Analysis* - Oil droplet size was measured in situ using two LISST-100X particle size analyzers (Sequoia Scientific, Seattle, WA). The instrument measures particle sizes in the range of 2.5 – 500 µm in 32 logarithmically spaced bins. The first LISST was located immediately after the aluminum frame supporting the fluorometer package at a distance of 5.1 m from the oil release point and the second LISST was located at 16.9 m from the oil release point and both at a depth of 0.4 m. Both instruments were connected via a 20 m cable to laptops running the LISST-SOP data acquisition software (v5). Prior to the start of each experiment, a background scatter file of the seawater quality in the tank was generated and used later to subtract from the final experimental data file. The instruments were operated in real-time mode with a sample acquisition rate of one measurement every three seconds.

*Supplemental Measures* - Weather conditions (air temperature, wind speed, wind direction, humidity, rainfall) for all experiments were recorded using a Vantage VUE Weather station (Davis Instruments, Hayward, CA). Water temperature and salinity were measured using a YSI handheld probe. Underwater video of oil droplets and the transport of the plume were captured using a GoPro Hero4 digital camera, as well as a Sony RX100 III digital camera with underwater housing.

### ***A.2.5 VOC Air Monitoring***

Surface volatile organic compound (VOC) concentrations were monitored using handheld ToxiRAE Pro PID portable gas detectors (RAE Systems, San Jose, CA). Two detectors were used for each experiment, and they were positioned 0.4 m above the water surface at distances of



ED_001324_00000953-00026

5.1 and 16.9 m from the oil release point. The detectors were calibrated using a certified 25 ppm benzene calibration gas (AirLiquide, Dartmouth, NS) according to the manufacturer's recommended procedure. Instrument drift was checked periodically against the calibration gas and recalibrated if necessary. During the experiments, the handheld meters were set to datalogging mode, which recorded VOC concentrations as ppm of Benzene every three seconds. This data was offloaded and saved as a .txt file for processing.

### ***A.2.6 Discrete Water Sample Collection***

Water samples for chemical analysis were collected at various time points throughout the experiments (Table 2). Three ¼" stainless steel tubes were attached to the aluminum fluorometer frame, so that the end of the tube was located at the same depth as the instruments (0.4 m). These were attached via peroxide cured silicon tubing (Cole Parmer, Vernon Hills, IL) to a Masterflex L/S multi-channel digital peristaltic pump (Cole Parmer, Vernon Hills, IL) which flowed to a three-way valve system. When the valve was set to bypass mode, the water in the lines were continuously primed and flowing and it could instantaneously be switched to sample mode to permit sample collection. The pump flow rate was set to approximately 120 mL/min, and all tubing was flushed with clean seawater for 5 minutes prior to the start of any experiment. Tubing was replaced on an as needed basis. Water samples from the effluent manifolds were also collected through a 1" sampling valve at the exit of effluent pipe, which represented a depth integrated water sample prior to it entering the treatment system.

### ***A.2.7 Oil and Dispersant Samples***

Four different hydrocarbon products were tested in this study: Two crude oils, a fuel oil, and a gas condensate. Samples of Alaska North Slope crude oil (ANS) and Intermediate Fuel Oil 120 (IFO-120) were obtained from BSEE. Sweet Louisiana Crude was obtained from NOAA. Gas Condensate was obtained from Exxon Mobil and originated from the Sable Offshore Energy Project. Physical properties of the samples (Table 3) were measured using an Anton Paar SVM



ED_001324_00000953-00027

3000 Stabinger Viscometer (Anton Paar, Saint Laurent, QC). Supplies of chemical dispersants (Corexit 9500 and Finasol OSR 52) were purchased from the manufacturers.

**Table 2. Protocol for collection of water samples for the core and complimentary experiments.**

| Time | TPH (Tank) | TPH (Effluent) | BTEX (Tank) | BTEX (Effluent) | Fluorometry (Tank) | Fluorometry (Effluent) |
|---|---|---|---|---|---|---|
| Background | X | | X | | X | |
| T = 0 | X | X | X | | | |
| T = 0.5 | X | | | | | |
| T = 1.0 | X | | X | | X | |
| T = 1.5 | X | | | | | |
| T = 2.0 | X | X | X | | X | |
| T = 2.5 | X | | | | | |
| T = 3.0 | X | | X | | | |
| T = 3.5 | X | | | | | |
| T = 4.0 | X | X | X | X | | |
| T = 4.5 | X | | | | | |
| T = 5.0 | X | | X | X | | |
| T = 6.0 | X | X | X | X | | |
| T = 8.0 | X | X | X | X | | X |
| T = 10.0 | X | X | X | X | | |
| T = 12.0 | X | X | X | X | | |
| Total # Samples/Expt | 16 | 7 | 11 | 5 | 3 | 1 |
| Total # of Samples Analyzed | TPH – 1725<br>BTEX – 1200<br>Fluorometry – 300 | | | | | |



ED_001324_00000953-00028

**Table 3. Physical property measurements of the oils used in this study.**

| Oil Type | Measurement Temperature (°C) | Density (g/mL) | Kinematic Viscosity (centistokes) |
|---|---|---|---|
| Alaska North Slope (ANS) | 50 | 0.8529 | 6.4 |
| | 40 | 0.8600 | 8.3 |
| | 25 | 0.8704 | 13.1 |
| | 15 | 0.8777 | 18.9 |
| Intermediate Fuel Oil (IFO-120) | 50 | 0.9345 | 134.0 |
| | 40 | 0.9411 | 240.3 |
| | 25 | 0.9515 | 781.4 |
| | 15 | 0.9587 | 2481.5 |
| Gas Condensate (CND) | 50 | 0.7247 | 0.4 |
| | 15 | 0.7466 | 0.5 |
| Sweet Louisiana Crude (SLC) | 50 | 0.8219 | 3.2 |
| | 40 | 0.8291 | 4.0 |
| | 25 | 0.8733 | 5.8 |
| | 15 | 0.8473 | 8.2 |



ED_001324_00000953-00029

### *A.2.8 Experimental Design – Core and Complimentary Experiments*

Both the flume tank and holding tanks were filled with filtered seawater as described above. Seawater temperature and salinity were recorded using a handheld probe (YSI Incorporated, Yellow Springs, OH). After the flume tank was filled, the in situ instrumentations including the fluorometers, LISSTs, and VOC meters were positioned in desired locations as indicated previously. The subsurface oil release system was filled with oil or oil/dispersant premix, which was heated to operating temperature. The water supply lines leading to the high flow pumps were primed and the inflow and outflow pumps were started. The system was run in recirculation mode for 10 minutes to allow current flow to stabilize in the flume tank. At a set time point prior to oil injection (5 minutes), data-logging on all instruments was started and background seawater samples were collected. After the oil was injected into the tank, the real-time readout of the fluorometer signal was monitored. Once the first spike in signal intensity was observed (usually after 2 minutes based on the fluorometer signal readout), a stopwatch was started and the first chemistry samples were collected. At this point the high flow system was switched from recirculation mode to flow through, which diverted the water flow into the effluent treatment system instead of returning it to the holding tank. The experiment ran for 12 minutes, at which point the high flow pumps were turned off and the instrument data acquisition was stopped. The tank was cleaned and drained as described above. Oil stuck to the sides of the tank or on instruments was cleaned using Big Orange Degreaser (Zep Superior Solutions, Atlanta, GA). Instrument windows were cleaned using disposable alcohol wipes (Bausch and Lomb, Vaughan, ON). Water samples were returned to the lab and stored at 4°C.

### *A.2.9 Submersible Sensor Calibration Experiments*

The calibration experimental setup was similar to the core and complimentary experiments, except that the oil was added in a step-wise fashion to the flume tank as shown in Table 4. Calibration experiments were conducted in such a way so as to create a series of known concentrations of dispersed oil in the flume tank. Predetermined amounts of oil and dispersant premix were added to the tank (Alaska North Slope crude was used at a DOR of 1:20) using the subsurface injector, while the high flow system was operated in recirculation mode.



ED_001324_00000953-00030

The flume tank was operated in recirculation mode and oil injections occurred every 45 minutes, which provided a sufficient time for the dispersed oil concentrations to stabilize in the tank (previous testing of this system showed that hydrocarbon concentrations in the tank are homogenous after 45 minutes of recirculation). The currents created by the high flow system provided sufficient mixing energy so as to allow droplets generated by the subsurface injector to remain dispersed in the water column. In situ instrumentation was located at the same locations as all other experiments. Water samples were collected at 45 minute time intervals after each oil addition.

Upon reaching homogeneity in the tank (i.e. 45 minutes after each oil addition), the average fluorometric intensity signal collected over a 4 minute time period was calculated. Fluorometers were calibrated to manufacturer suggested units using factors provided. Triplicate water sample analysis results for TPH and BTEX were averaged that correspond with the same time points. Fluorescence and chemistry averages were regressed to generate calibration curves of TPH and BTEX vs signal intensity for oil additions ranging from 1 to 18 ppm. Higher variability at low concentrations resulted in the exclusion of some data points in the regression calculation.

**Table 4. Step-wise sensor calibration experiment parameters.**

| Oil Addition # | Mass of Oil Added for each Addition (g) | Cumulative Oil Concentration in Tank (mg/L) |
|---|---|---|
| 1 | 9.45 | 0.3 |
| 2 | 9.45 | 0.6 |
| 3 | 12.6 | 1 |
| 4 | 63 | 3 |
| 5 | 94.5 | 6 |
| 6 | 189 | 12 |
| 7 | 189 | 18 |



ED_001324_00000953-00031

### ***A.2.10 Submersible Fluorometer and LISST Data Processing***

Raw LISST data files were processed using a statistically based quality control script written using the R statistical package. In summary, this script identifies and removes "Over Range" samples (defined as 0 µL/L across all particle size bins) and outliers. Outliers are defined as any reading that is greater than the moving mean (5 data points before and after the targeted time point) of the dataset multiplied by four times the standard deviation (over the same interval as the moving mean). Due to the potential for one or more extreme outliers to skew both the moving mean and standard deviation calculations for points around them, this outlier detection routine is run iteratively, excluding previously flagged points, until no more outliers are detected. Once these QC steps have been performed the script calculates a number of parameters from the data such as Total Particle Concentration (TPC), Volume Mean Diameter (VMD), and Particle Size Concentration (PSC). It then goes on to detect the plume curve (if present) and time-normalizes the data based on that location. Plots presented include data 2 minute before and 8 minutes after the start of the plume curve. Data form the Downstream LISST were normalized so that the plume began at t = 5 min in order to visually convey that the plume was detected in the tank roughly 3 min after detection by the LISST further upstream near point of injection release.

Similar to the LISST data, a script was used to detect outliers in data collected from the in situ fluorometers. Curve detection was then performed and the data was time-normalized to include 2 minutes of data before, and 8 minutes of data after the start of the plume curve. The baseline of the plume curve was then calculated using data points observed in the first minute preceding the start of the curve and this baseline was subtracted from the data. Finally, factory calibration factors were applied to the data values for each instrument before plotting.

### ***A.2.11 Analytical Chemistry Analysis***

*Total Petroleum Hydrocarbon (TPH) Analysis* -The method used for extraction and processing of TPH samples was developed by DFO in-house (Cole et al., 2007; King et al., 2015). Water samples were collected in pre-weighed 125 mL amber glass bottles and filled to approximately



ED_001324_00000953-00032

90 mL. Sample bottles were weighed and a mass difference was used to determine the total volume of the collected water sample. The samples were immediately stored at 4°C until ready for further processing. Within 24 hrs of collection, 10.0 mL of dichloromethane (DCM) was added to each sample. The samples were shaken by hand for 30 seconds, and then placed on a Wheaton R2P roller (Wheaton, Millville, NJ) set at 9 rpm. After 18 hours on the roller, a Pasteur pipette was used to transfer the DCM solvent layer into a pre-weighed 15 mL graduated centrifuge tube. The solvent was then evaporated under a gentle stream of nitrogen using an N-Evap (Organomation, Berlin, MA) and topped up with DCM to a final volume of 1.00 mL. The solvent extract was transferred into an auto-sampler vial and stored at -20°C for GC-FID analysis.

Sample extracts (1 µL) are injected using an Agilent 7683 auto-sampler into an Agilent 7890B GC, using splitless injection which is set to oven track mode (2°C higher than the oven temperature program). The column used for separations is a Supelco MDN-5s 30 m × 250 µm × 0.25 µm (length × i.d. × film thickness). Hydrogen is used as a carrier gas with a flow rate of 3.0 mL/min. The GC oven is programmed to an initial oven temperature of 35°C, held for 2 min, followed by an increase to 320°C at 20°C/min, and held at 320°C for 10 min, with a total run time of 26.25 min. The GC flame ionization detector (FID) is operated at 320°C with the hydrogen flow set at 30 mL/min and the air flow set at 400 mL/min. An eight point calibration is generated using standards prepared from the appropriate crude oil stock that was used to generate the TPH samples (e.g. ANS, IFO-120, SLC or Gas Condensate). Peak quantification is performed using relative response factors. Routinely the method of extraction was tested for efficiency by a spike and recovery study. Typically, a mean percent recovery of >90% was calculated from filtered seawater spiked with crude oil. Lab and field blanks were incorporated in the method.

*BTEX Analysis* - EPA Method 8240 (purge and trap) was modified by running a gas chromatograph/mass spectrometer in selected ion monitoring mode to include ethylbenzene. To summarize, water samples for BTEX (benzene, toluene, ethylbenzene and [m,p & o] xylene)



ED_001324_00000953-00033

analysis were collected in 40 mL purge and trap vials. The vials were spiked with 40 µL of 6N HCl to serve as a preservative, so that they can be stored at 4°C for up to 14 days.

The purge and trap system was a Teledyne Tekmar Stratum PTC purge and trap concentrator equipped with a Tenax/silica gel/charcoal trap. The auto-sampler was a Teledyne Tekmar Aquatek 70-vial unit. The auto-sampler transferred a 5 mL aliquot of sample into the purge and trap chamber, where it was purged with helium for 11 minutes. During this process, the volatiles were trapped on the Tenax trap and then desorbed at 225°C for 2 min. The desorbed gases enter a heated transfer line connected to the Agilent 6890 GC injector and subsequently proceed to the GC column (Supelco MDN-5s 30 m × 250 µm × 0.25 µm length × i.d. × film thickness).

The GC oven was programmed at an initial oven temperature of 50ºC, held for 8 min, followed by an increase to 280ºC at 40ºC/min, and held at 280ºC for 2 min, for a total run time of 18 min. The gases exiting the GC column were detected by an Agilent 5973 mass selective detector (MS) used in selective ion mode (SIM) monitoring for six ions: 77, 78, 91, 92, 105 and 106 amu. BTEX standards were prepared in 40 mL purge and trap vials. Samples and standards were analyzed using this method, along with sample blanks and duplicate samples.

### ***A.2.12 Numerical Modeling Methods***

Refer to Appendices G and H for numerical modeling components.



ED_001324_00000953-00034

# TASK A.3 RESULTS

The overarching objective for this project was to evaluate the operational performance of the subsurface injection of dispersants into deepwater blowouts. Presented here are the results from a series of wave tank subsurface injection experiments where dispersion effectiveness was evaluated via response monitoring tools (fluorescence and particle size analyzers), discrete sample chemistry and VOC monitors. The logs for all experiments conducted can be found in Appendix A. Corresponding chemistry results for each experiment are tabulated in Appendix B.

## ***A.3.1 ANS Dispersion Effectiveness***

Injection experiments were conducted using Alaskan North Slope (ANS) crude oil, chemically dispersed with Corexit and Finasol. Regardless of warm ($\geq$ 11°C) or cold ($\leq$ 10°C) water temperatures, the addition of dispersant lowers the VMD and shifts the DSD to smaller droplets within the plume. An example of this trend is shown in Figures 5 and 6). Note that LISST histogram plots have constrained Y-axes, thus lines which extend slightly above the top of the plot area represent values which were truncated. Plots for triplicate experiments for each treatment are shown in Appendices C and D. All plots represent data from the LISST positioned closest to the jet release (denoted as Jet Release LISST throughout the document) and in close proximity to the submersible fluorometers. Histograms represent the particle concentration for a given size class (Y axes). Contour plots represent the 10 minute time series of the plume, where colored contours represent the particle concentration (normalized to max value for sake of comparison) and X axes represent the droplet sizes in µm. These contours allow for ascertaining how the DSD shifts over the duration of the release. A second LISST positioned further downstream of release (denoted as Downstream LISST throughout the document) allows for comparing the evolution of the plume in space and time since release of the plume. For warm temperature experiments, there is slight decrease in VMD for DOR = 1:200 and 1:100 compared to the no-dispersant treatment (DOR = 0), in this case ~130 µm down to ~80 µm (exact numbers are within text of the figures). A large shift in DSD is observed for the DOR 1:20 treatment, where VMD is ~ 10 µm. The cold



ED_001324_00000953-00035

water treatments exhibit this same trend, where VMD is ~ 10 µm for the DOR = 1:20 treatment (Figure 6). In situ submersible fluorescence from multiple fluorometers was recorded during experiments. Example time series for each dispersant and temperature treatment are shown in Figure 7 and illustrate the impact of dispersant at DOR = 1:20 on the plume. With the no or little dispersant treatments, the plumes tend to exhibit a spike in fluorescence shortly after release (within 2 min), and then a sharp decline in signal that is brought to extinction by 4 minutes. For DOR = 1:20, however, the signal remains elevated and with variability for up to 6 minutes. This indicates that more oil is remaining submerged in the plume for a longer time period. Time series fluorescence plots for triplicate experiments for each treatment are shown in Appendix E.

The Downstream LISST positioned further from the jet release and the fluorometers serves as an indication of plume evolution through the tank. Plots of the Downstream LISST DSD and VMD all dispersant treatments for warm and cold water experiments are shown in Figures 8 and 9, respectively. Comparing these to the LISST results near the release illustrates the decrease in Total Particle Concentration (TPC; represents the maximum concentration for the entire plume) as the plume disperses through the tank (note the change of Y axis scale). Also evident is a shift to smaller particles for all DOR treatments as the plume moves through the tank. Where the decrease in TPC suggests plume dilution in the tank, the DSD shift to smaller particles suggests that larger droplets were removed from the plume within 6 minutes of the oil release, most likely rising to the surface of the tank.

Warm water experiments conducted with ANS and Finasol OSR 52 dispersant also yield a shift in DSD towards smaller VMD for DOR = 1:20 (Figure 10). However the shift is smaller than that observed with Corexit 9500, with lowest VMD on the order of ~50-60 µm. DOR = 1:200 and 1:100 treatments exhibited spikes in fluorescence signal that taper off within 3 minutes of oil release (Figure 11). Fluorescence for DOR = 1:20 treatments trailed off at 4 minutes which is quicker than that for treatments with Corexit 9500. The Downstream LISST



ED_001324_00000953-00036

exhibited a similar shift in DSD and TPC that was observed with Corexit 9500 treatments (Figures 12 and 13).

Water temperatures for experiments ranged between 5.4 – 20.8 °C. In general there was no clear trend on influence of temperature on DSD, VMD fluorescence intensity, or oil concentrations for the time series for DOR = 0, 1:200 or 1:100 treatments. This suggests that water temperature has little effect on the dispersibility of ANS (80 °C oil temperature) when released as a jet with little or no exposure to chemical dispersant. In contrast, DOR = 1:20 experiments showed a decrease in total particle concentration (TPC) with decreasing temperature even though no effect was observed on DSD. Figure 14 shows three examples of this effect, where TPC values for each DOR = 1:20 experiment are strongly correlated with temperature (Figure 15). It is important to note that for all treatments using ANS, the experiment with the lowest temperature (SubANS-10R; 5.4 °C) exhibited anomalous dispersion compared to the other DOR = 1:200 treatments (Appendices C and D). Because this occurred in only one experiment out of 33 experiments with ANS, it is difficult to surmise a cause for this other than an improper jet release of oil.



ED_001324_00000953-00037

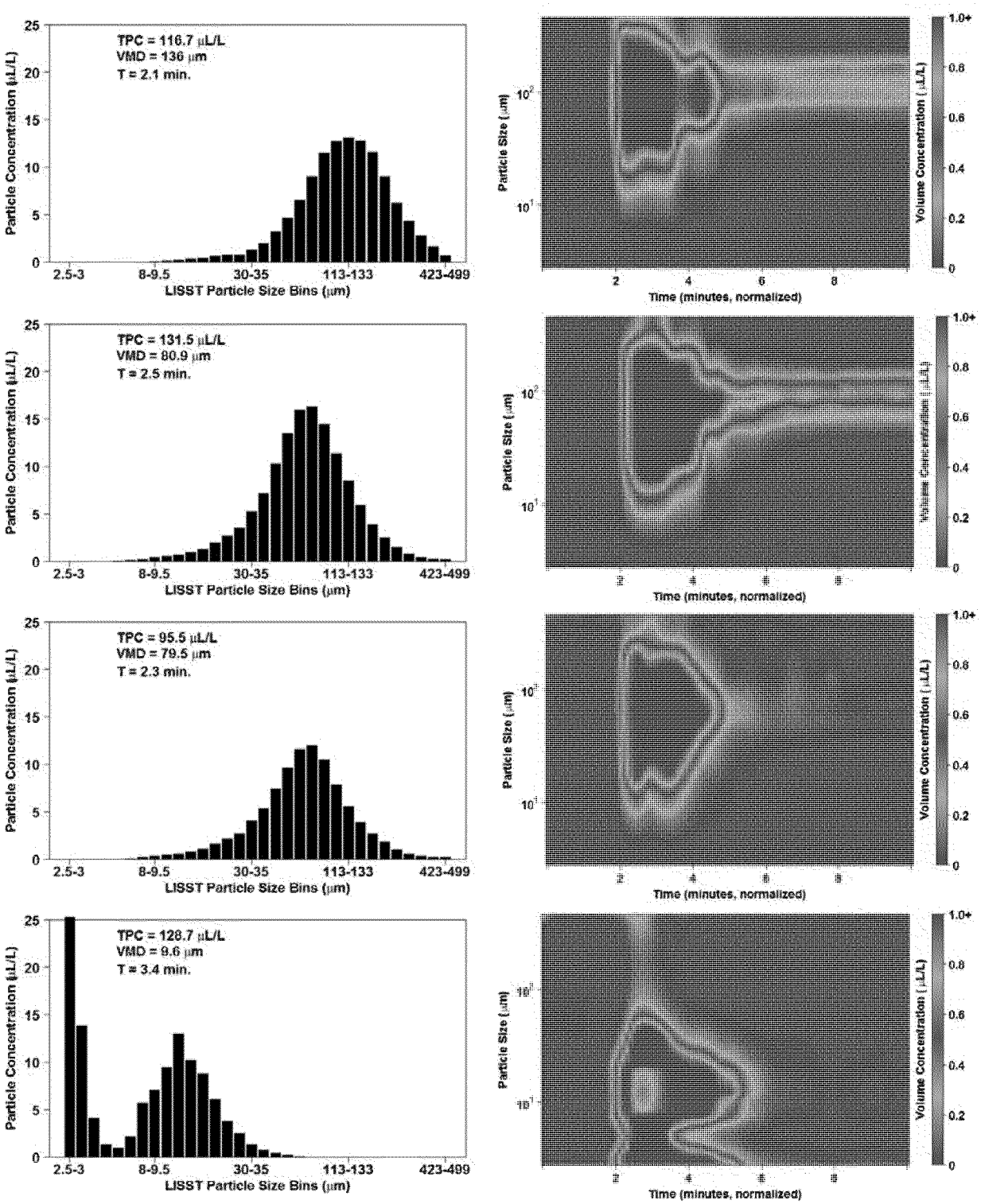


**Figure 5. LISST DSD and VMD (left panels) and time series of concentration and particle size (right panels) for ANS and Corexit 9500 warm water treatments. From top to bottom, DOR = 0, 1:200, 1:100, 1:20.**



ED_001324_00000953-00038

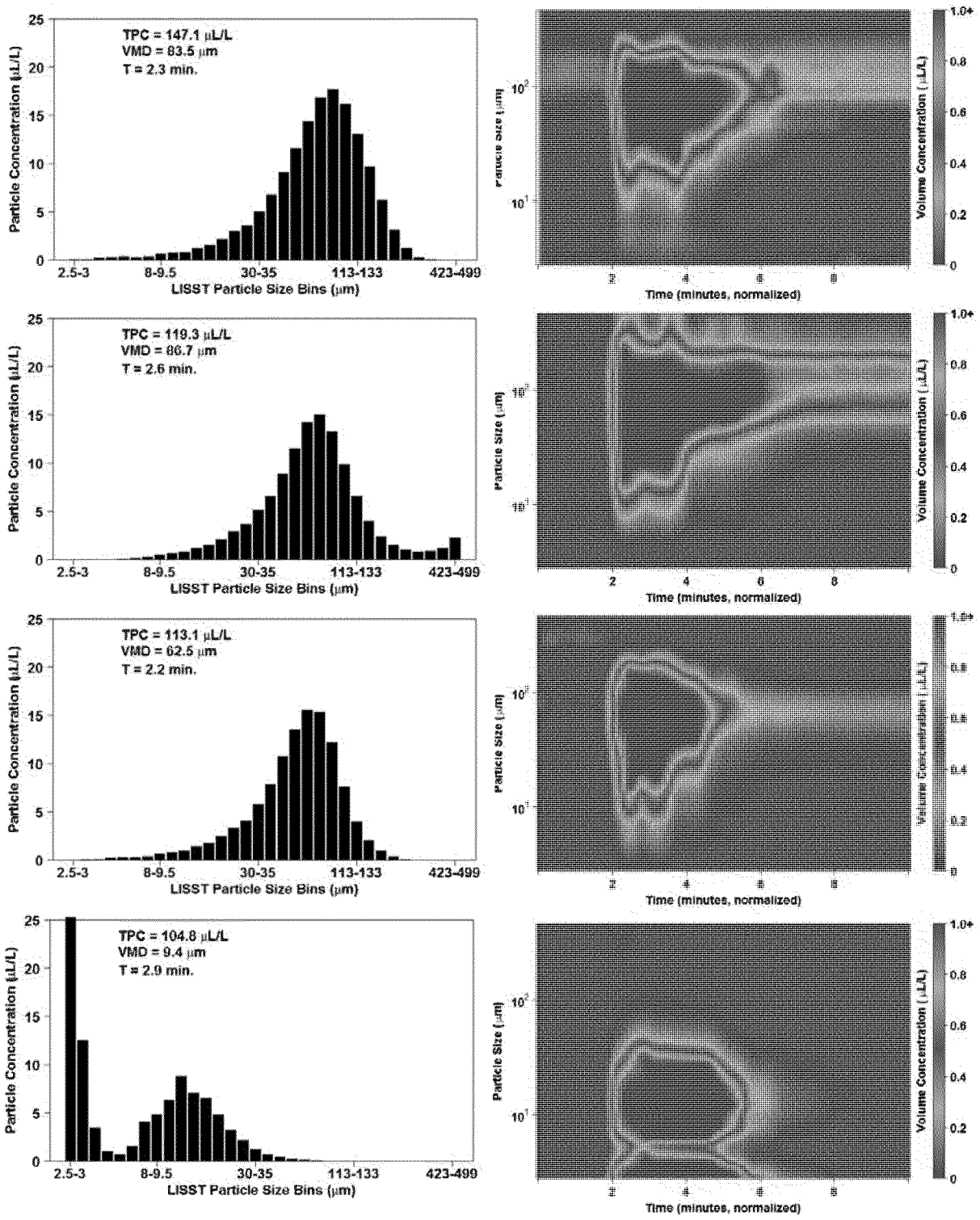


**Figure 6. LISST DSD and VMD (left panels) and time series of concentration and particle size (right panels) for ANS and Corexit 9500 cold water treatments. From top to bottom, DOR = 0, 1:200, 1:100, 1:20.**



ED_001324_00000953-00039

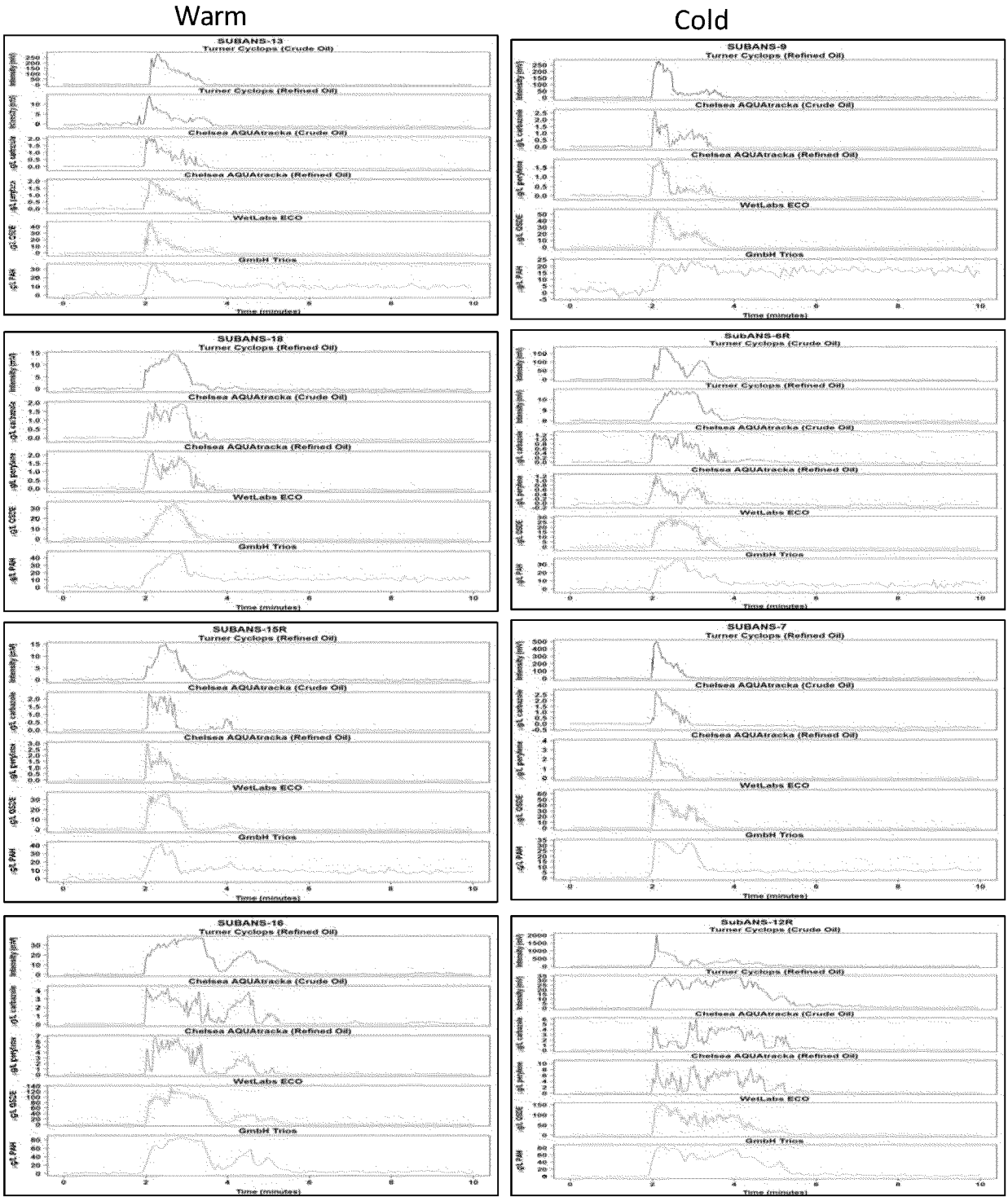


**Figure 7. In situ submersible fluorescence time series of sub-injection plume of ANS and Corexit 9500 warm water (left panels) and cold water (right panels) treatments. From top to bottom, DOR = 0, 1:200, 1:100, 1:20.**



ED_001324_00000953-00040

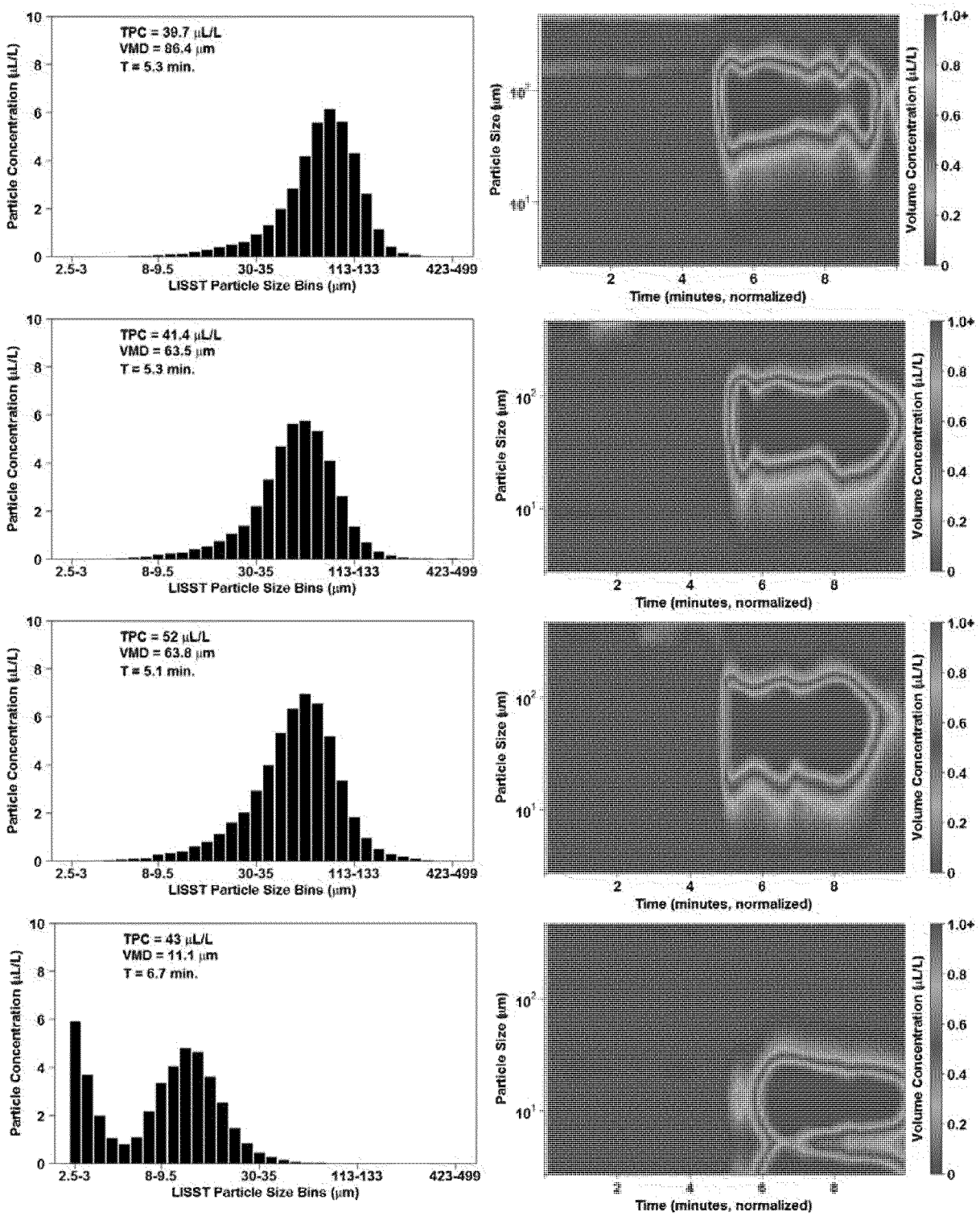


**Figure 8. Downstream LISST DSD and VMD (left panels) and time series of concentration and particle size (right panels) for ANS and Corexit 9500 warm water treatments. From top to bottom, DOR = 0, 1:200, 1:100, 1:20.**



ED_001324_00000953-00041

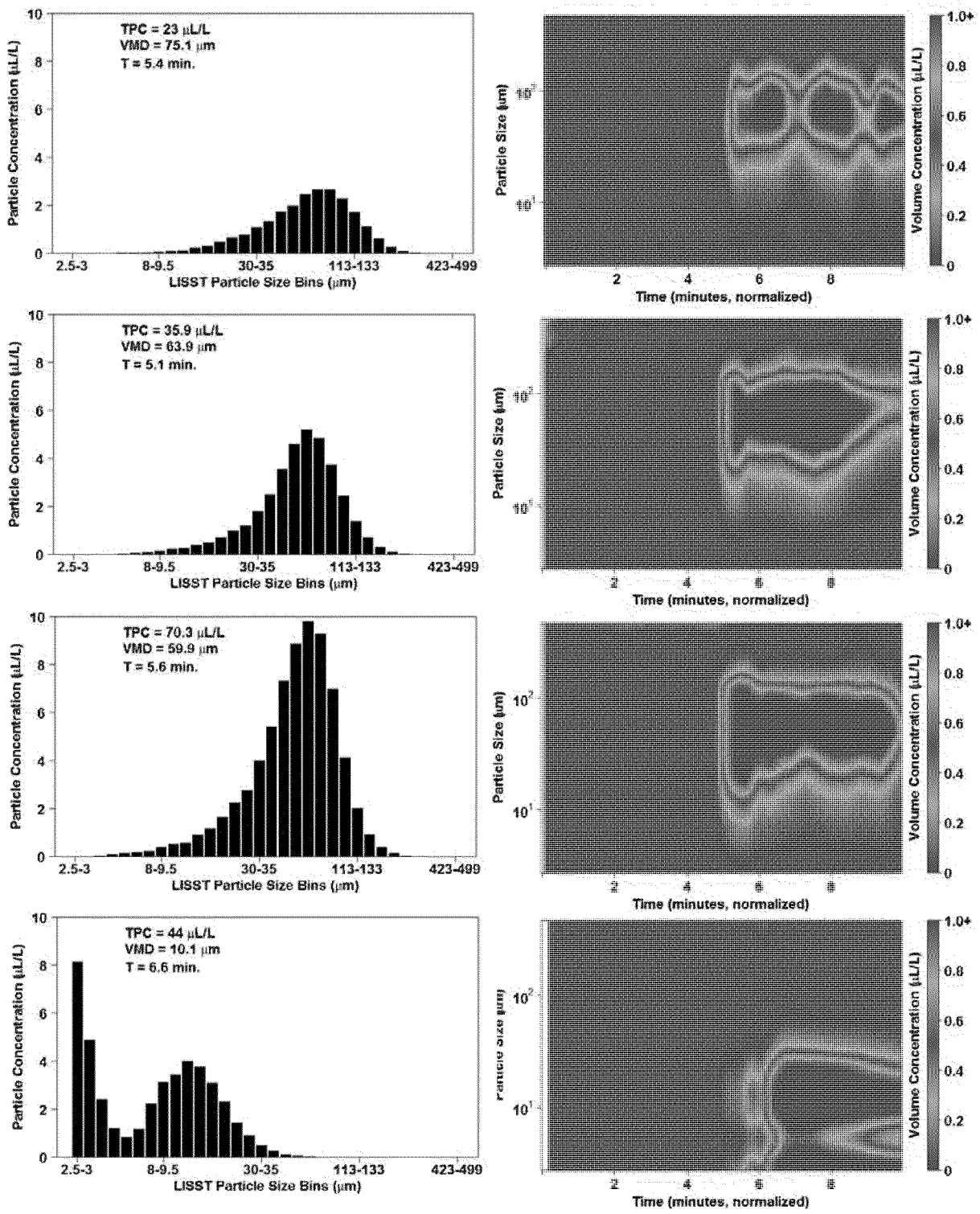


**Figure 9 Downstream LISST DSD and VMD (left panels) and time series of concentration and particle size (right panels) for ANS and Corexit 9500 cold water treatments. From top to bottom, DOR = 0, 1:200, 1:100, 1:20.**



ED_001324_00000953-00042

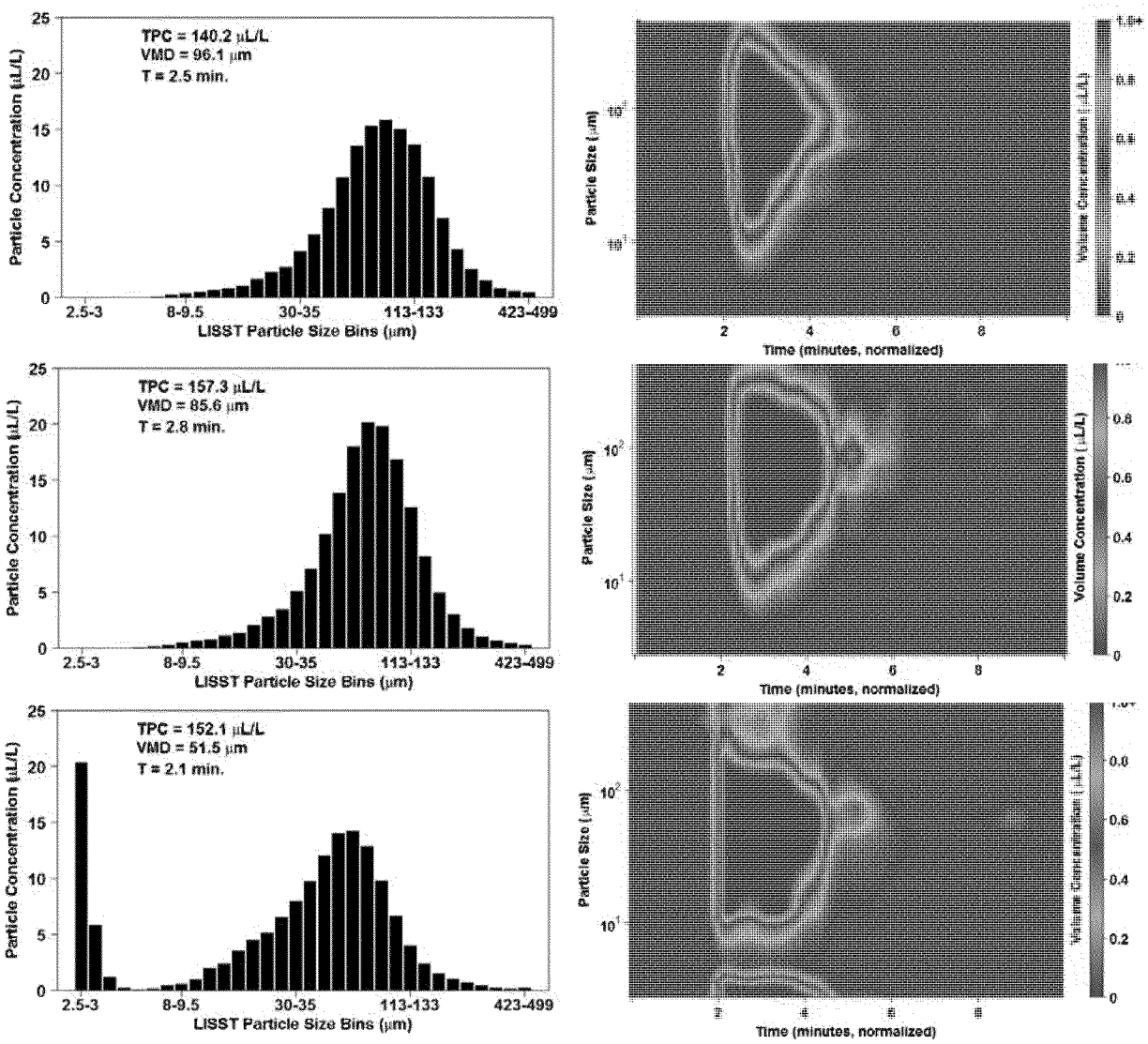


**Figure 10. LISST DSD and VMD (left panels) and time series of concentration and particle size (right panels) for ANS and Finasol OSR 52 warm water treatments. From top to bottom, DOR = 1:200, 1:100, 1:20.**



ED_001324_00000953-00043

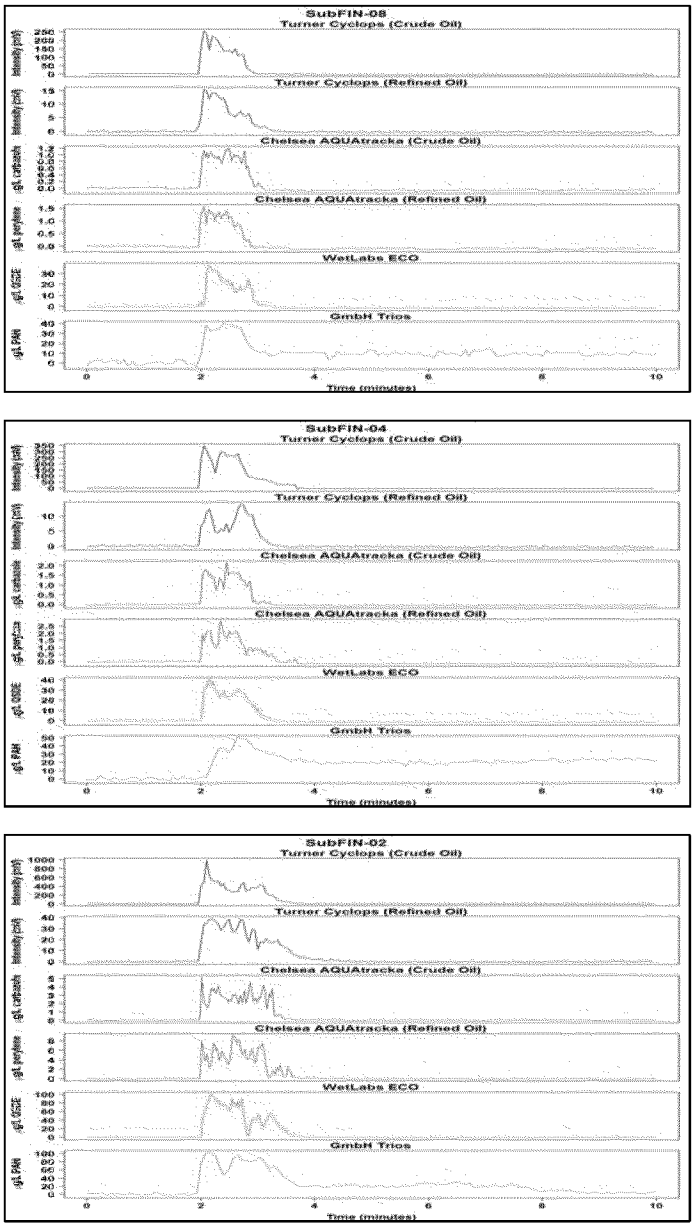


**Figure 11. In situ submersible fluorescence time series of sub-injection plume of ANS and Finasol OSR 52 warm water treatments. From top to bottom, DOR = 1:200, 1:100, 1:20.**

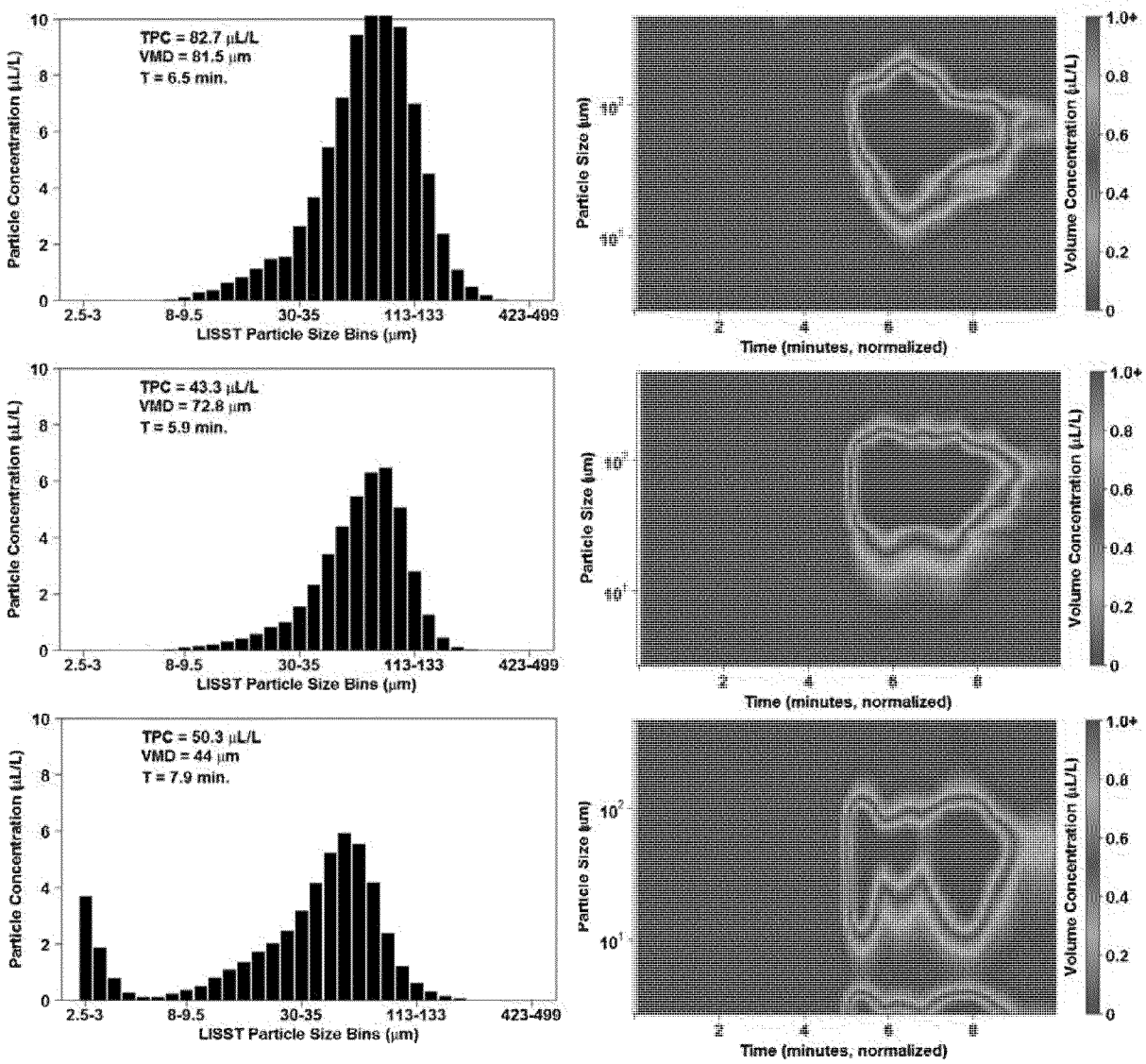


**Figure 12. Downstream LISST DSD and VMD (left panels) and time series of concentration and particle size (right panels) for ANS and Finasol OSR 52 warm water treatments. From top to bottom, DOR = 1:200, 1:100, 1:20.**



ED_001324_00000953-00045

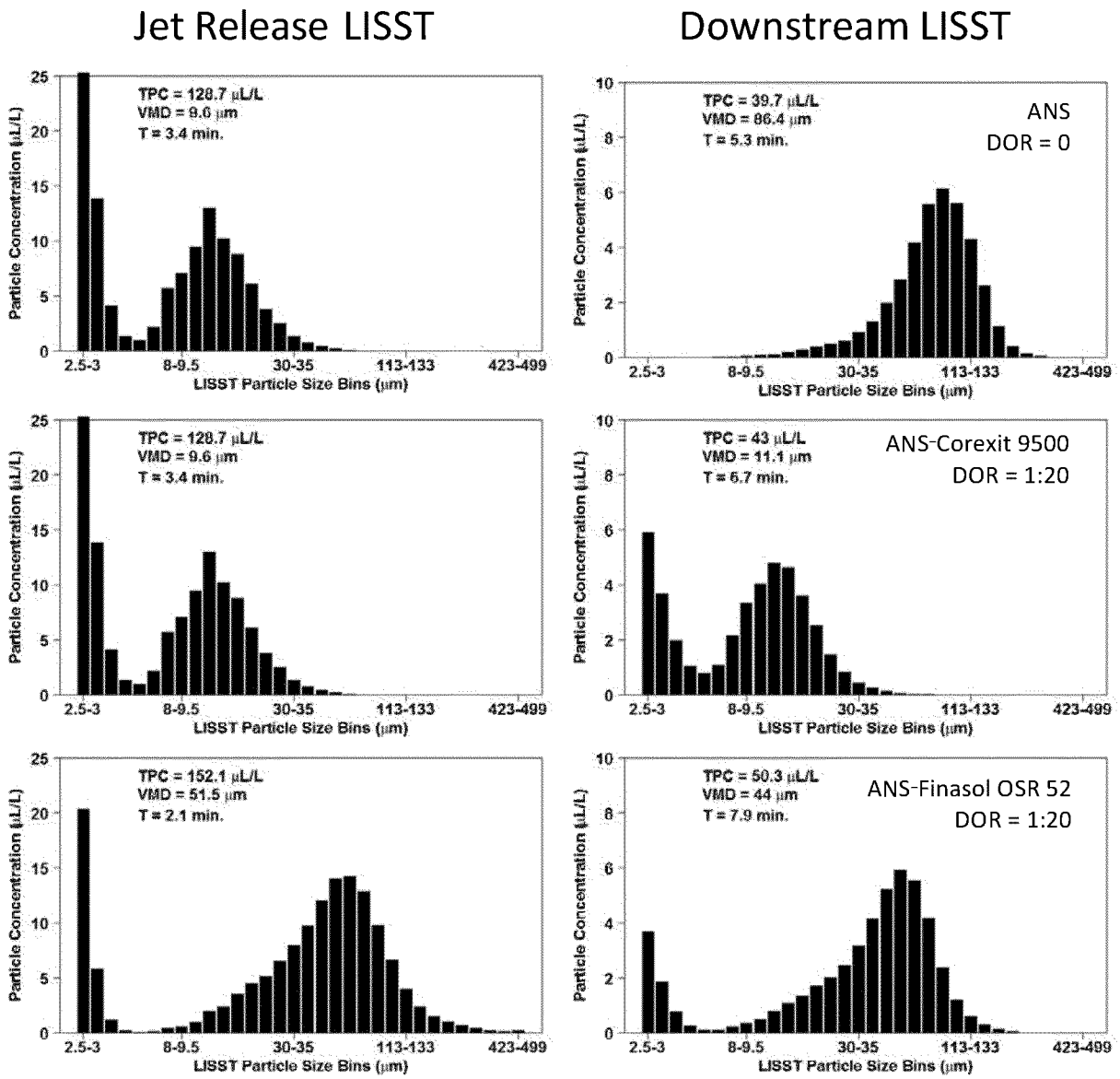


**Figure 13. LISST DSD with TPC for ANS with Corexit 9500 and Finasol OSR 52 treatments. DOR = 0 (top panel); DOR = 1:20 experiments are middle and bottom panels.**

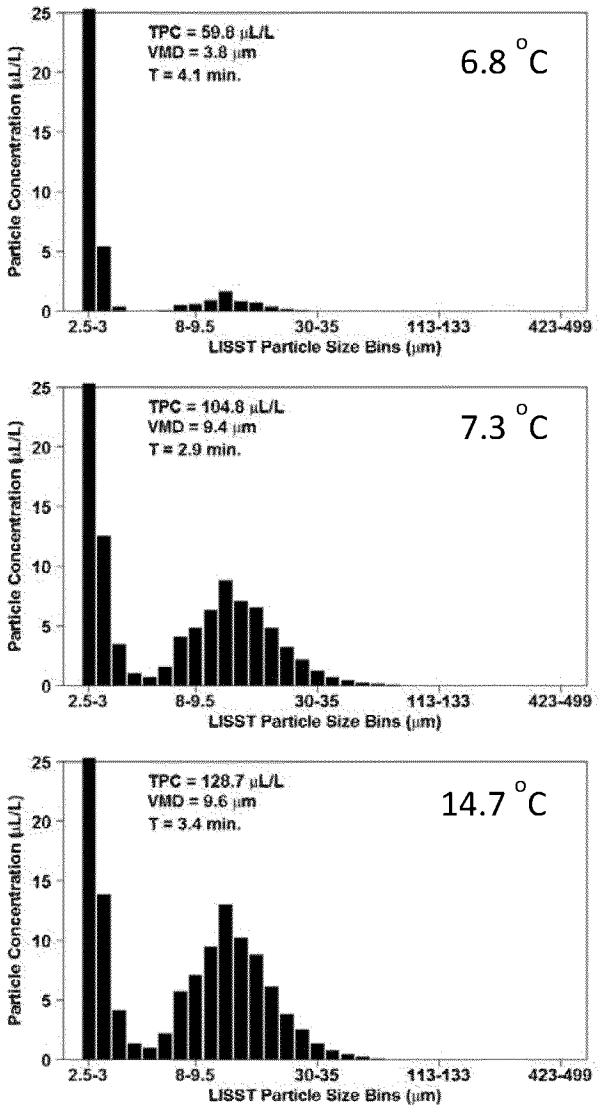


**Figure 14. LISST DSD with TPC (Total Particle Concentration) for DOR = 1:20 experiments of ANS and Corexit 9500 treatments. Water temperatures increase from top to bottom panels.**



ED_001324_00000953-00047

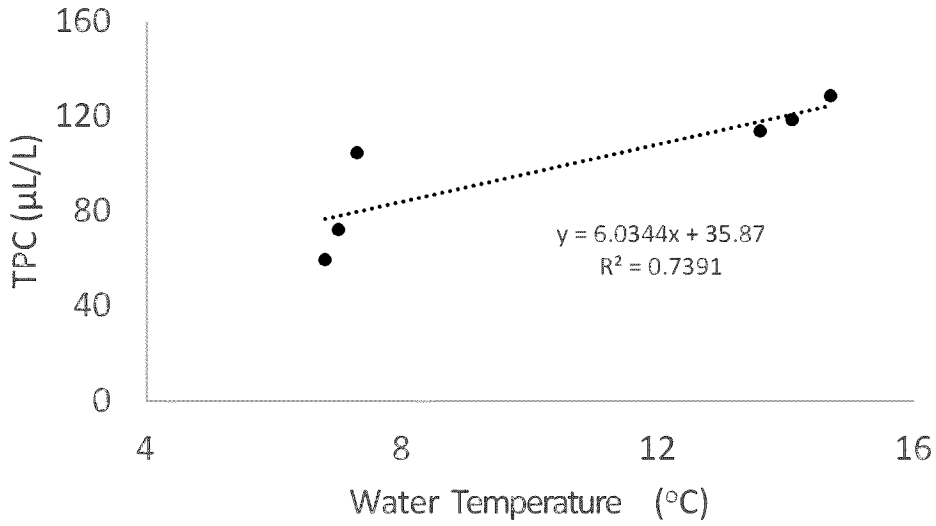


**Figure 15. LISST TPC (Total Particle Concentration) for DOR = 1:20 experiments of ANS and Corexit 9500 treatments as a function of water temperature.**



ED_001324_00000953-00048

### *A.3.2 IFO-120 Dispersion Effectiveness*

Injection experiments were conducted using Intermediate Fuel Oil (IFO-120), chemically dispersed with Corexit 9500 and Finasol OSR 52. For warm water experiments, temperatures ranged between 13.5 – 16 °C for treatments with Corexit 9500 and between 17.5 – 20.3 °C for treatments with Finasol OSR 52. In the DOR = 0, 1:200 and 1:100 treatments using Corexit 9500, VMD typically remained > 200 µm Figure 16. VMD values were smaller for DOR = 1:20 treatments (~66-120 µm), indicating a shift in DSD, but to a lesser extent than the shift observed for ANS experiments. Fluorescence data exhibited scatter and noise in the signal for all but the DOR = 1:20 treatments. Appendix E. A similar trend in DSD, VMD and fluorescence signal was observed for IFO-120 exposed to Finasol OSR 52 at warm temperatures (Figure 17), where DOR = 1:200, 1:100 and 1:20 exhibited VMD values of 376.5, 209.5 and 125.8 µm, respectively. Unlike experiments with ANS, which is less viscous and dense, IFO-120 exposed to dispersant tended to result in larger oil droplets for a given amount of dispersant added. Comparing the results of IFO-120 with the two dispersants is challenging because no triplicate experiments were conducted for Finasol OSR 52 treatments. But in general, from the data collected, it appears as though Finasol OSR 52 yields higher VMD for a given DOR compared to Corexit 9500 at warm temperatures. As with the ANS, the Downstream LISST measured a decrease in TPC and shift to smaller droplet sizes as the plume moved through the tank for all treatments, but to a lesser extent with DOR = 1:20 (Figures 18, 19 and 20).

For cold water experiments using IFO-120 exposed to Corexit 9500, temperatures ranged between (4.9 – 7.5 °C). At these colder temperatures a shift in DSD and VMD was not as apparent (Figure 21). For DOR = 0, 1:200 and 1:100 VMD typically remained > 223 µm but was as high as 344 µm. The DOR = 1:20 treatment exhibited VMD of178-327 µm, suggesting that this oil was not well dispersed at cold temperatures. Fluorescence time series data were noisy for all experiments except the DOR = 1:20 (Appendix E). The Downstream LISST recorded extremely low particle concentrations further suggesting poor dispersion (Figure 22). During the IFO-120 cold water treatments, one experiment resulted in an anomalous DSD histogram that was similar to one observed during one of the ANS experiments (Figure



ED_001324_00000953-00049

23). In both cases, the experiments were conducted at the coldest temperatures during the course of this study (4.9 and 5 °C). Suspected as a possible cause may be the LISST instrument itself. The manual reports that the lower operating temperature for the LISTT-100X is -10 °C. However, the data suggests that our particular unit may have experienced some complications at low temperatures. This is supported by the fact that the fluorescence signal and chemistry data for these experiments indicate no anomalies. Further testing would be needed to confirm the effect of low temperatures on particle size analysis results using our instrument to rule out any potential issues with operating at temperatures between 5 and -10 °C.

One thing to note with the IFO-120 cold water experiments is that a few of the treatments were conducted at temperatures of ~12 °C, which overlaps with the temperatures of the warm water group. This was the result of erratic weather patterns that at times were difficult to work around. Thus, when interpreting the data, caution must be exercised for these particular experiments (refer to Appendix A for temperature log), and for the interpretation in this section, they were excluded as they do not represent cold conditions.



ED_001324_00000953-00050

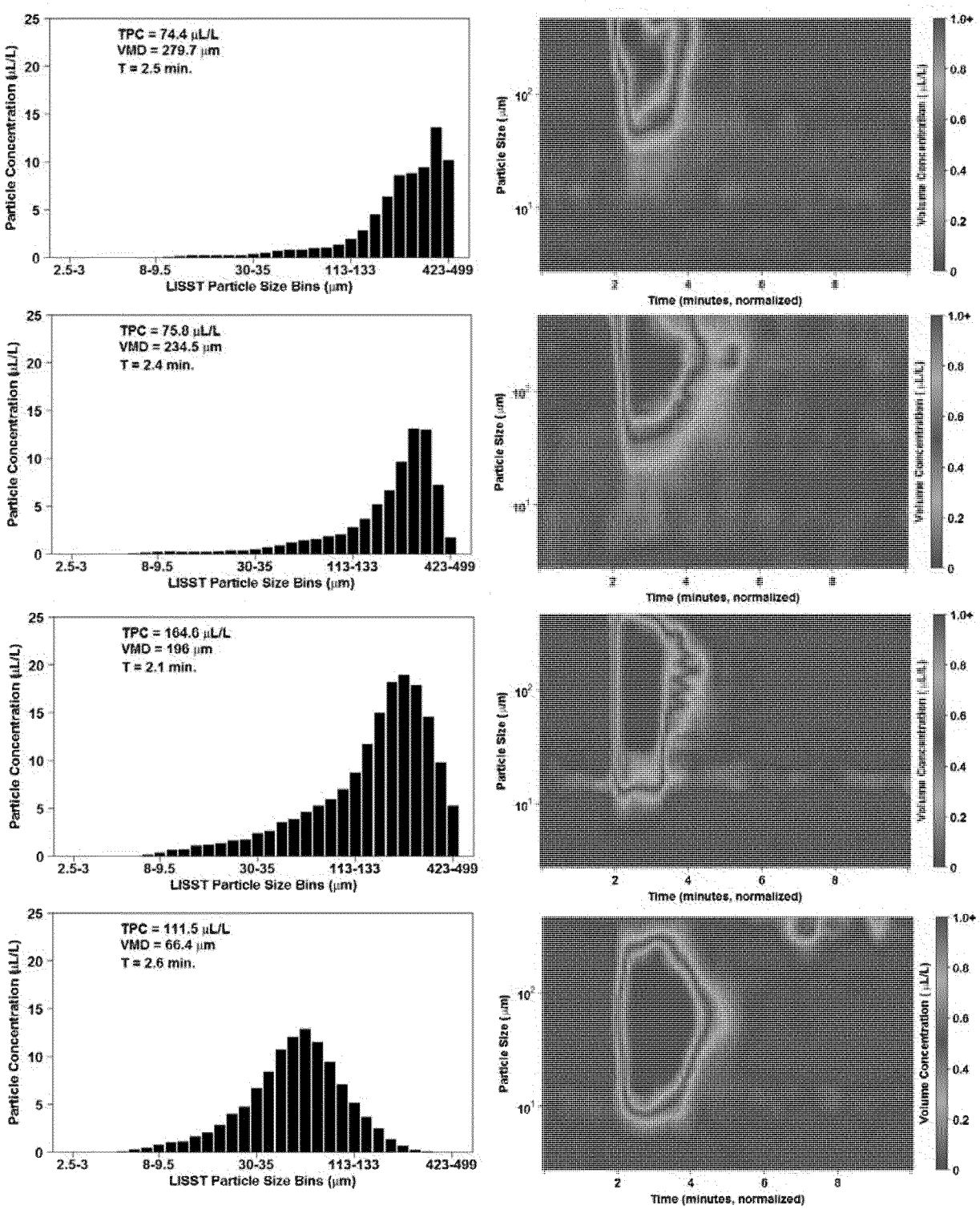


**Figure 16. LISST DSD and VMD (left panels) and time series of concentration and particle size (right panels) for IFO-120 and Corexit 9500 warm water treatments. From top to bottom, DOR = 0, 1:200, 1:100, 1:20.**



ED_001324_00000953-00051

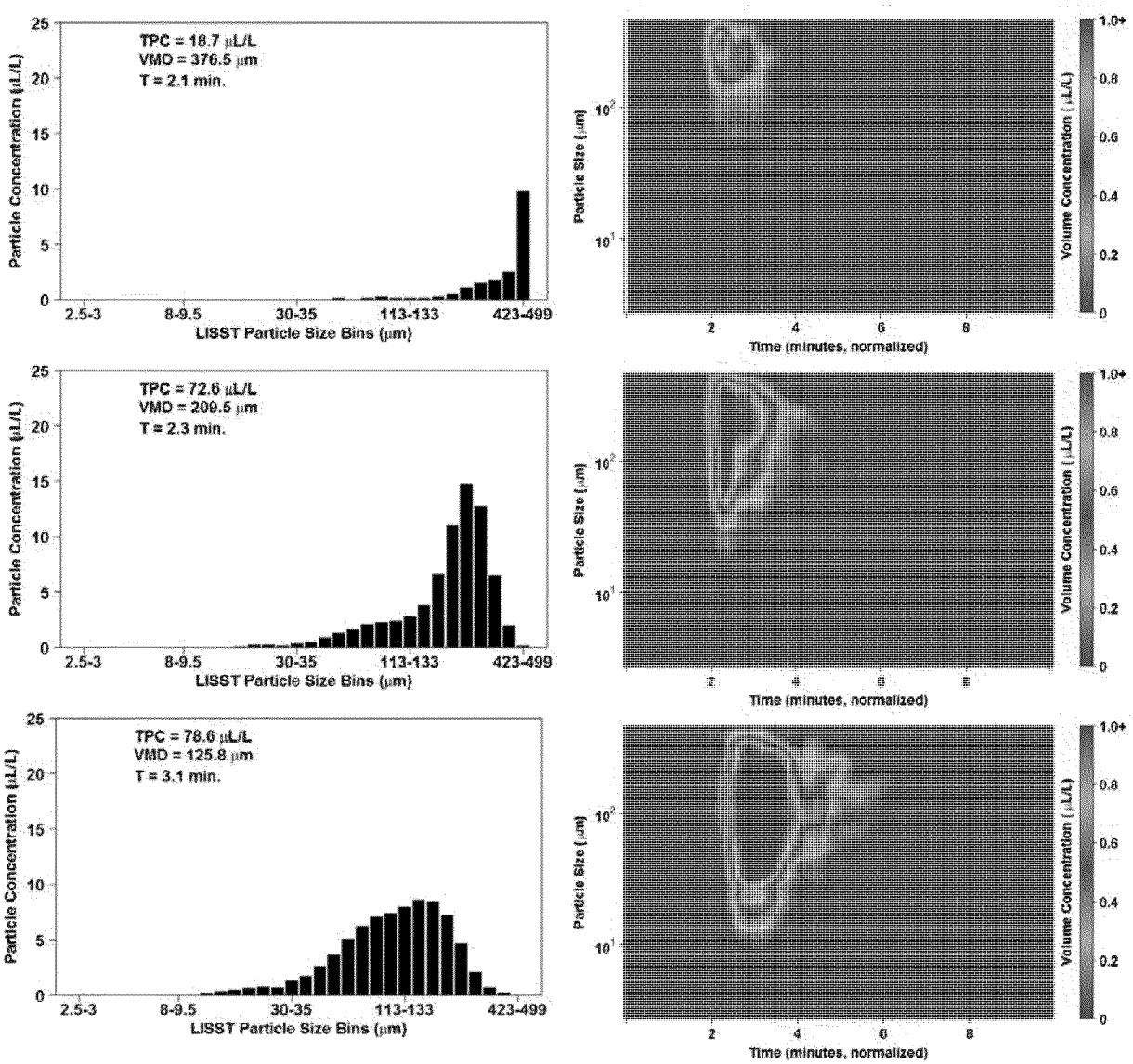


**Figure 17. LISST DSD and VMD (left panels) and time series of concentration and particle size (right panels) for IFO-120 and Finasol OSR 52 warm water treatments. From top to bottom, DOR = 1:200, 1:100, 1:20.**



ED_001324_00000953-00052

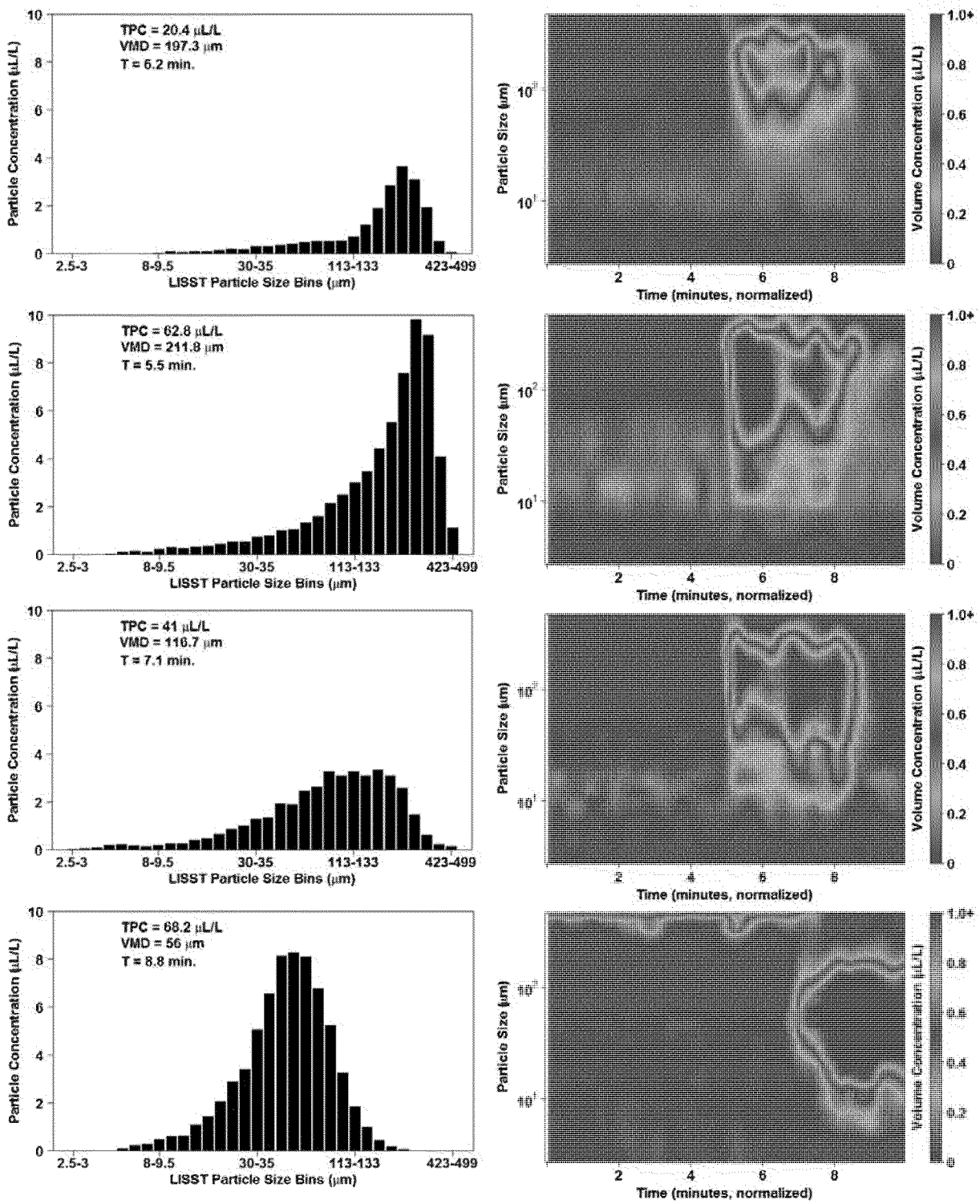


**Figure 18. Downstream LISST DSD and VMD (left panels) and time series of concentration and particle size (right panels) for IFO-120 and Corexit 9500 warm water treatments. From top to bottom, DOR = 0, 1:200, 1:100, 1:20.**



ED_001324_00000953-00053

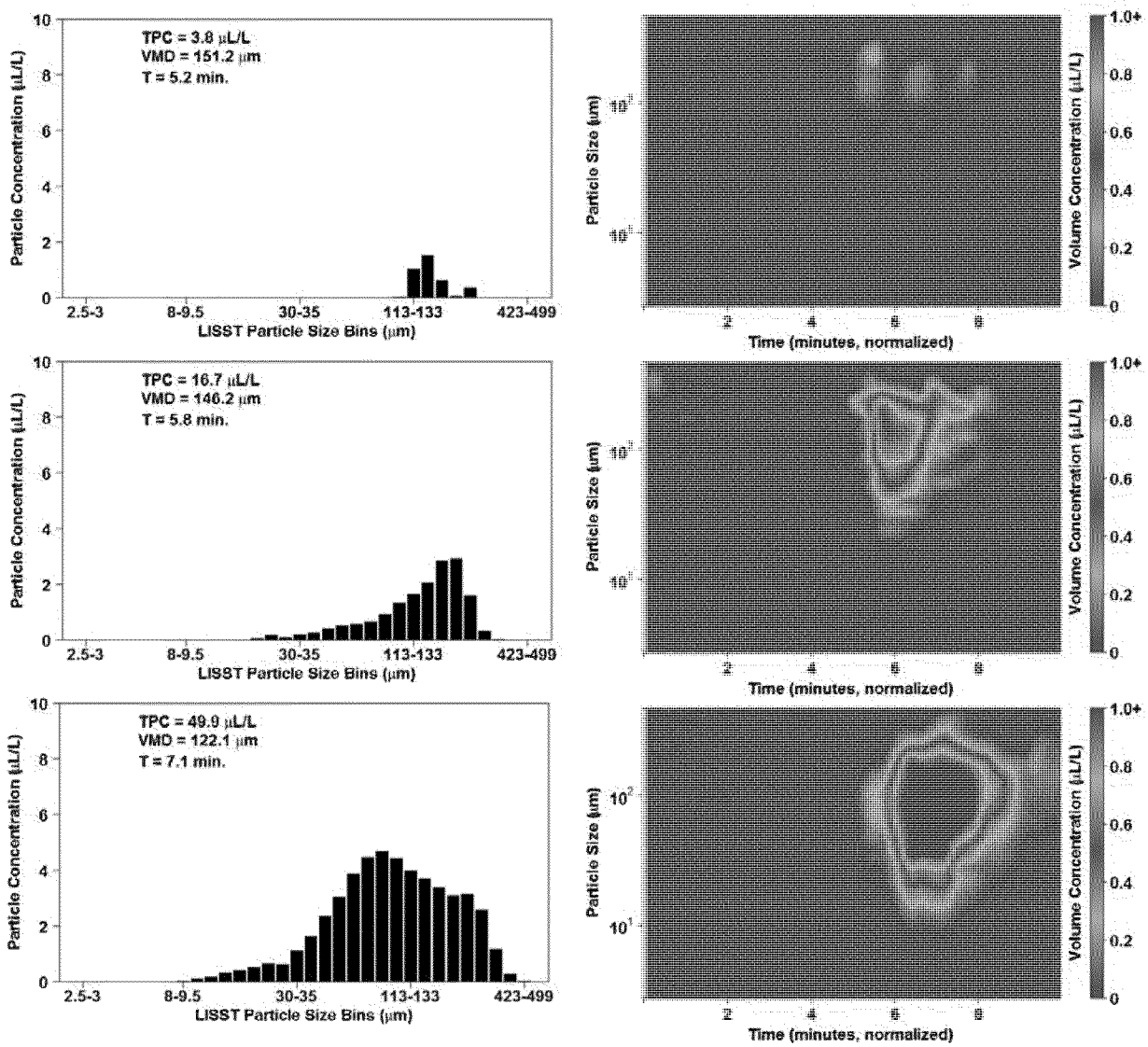


**Figure 19. Downstream LISST DSD and VMD (left panels) and time series of concentration and particle size (right panels) for IFO-120 and Finasol OSR 52 warm water treatments. From top to bottom, DOR = 0, 1:200, 1:100, 1:20.**



ED_001324_00000953-00054

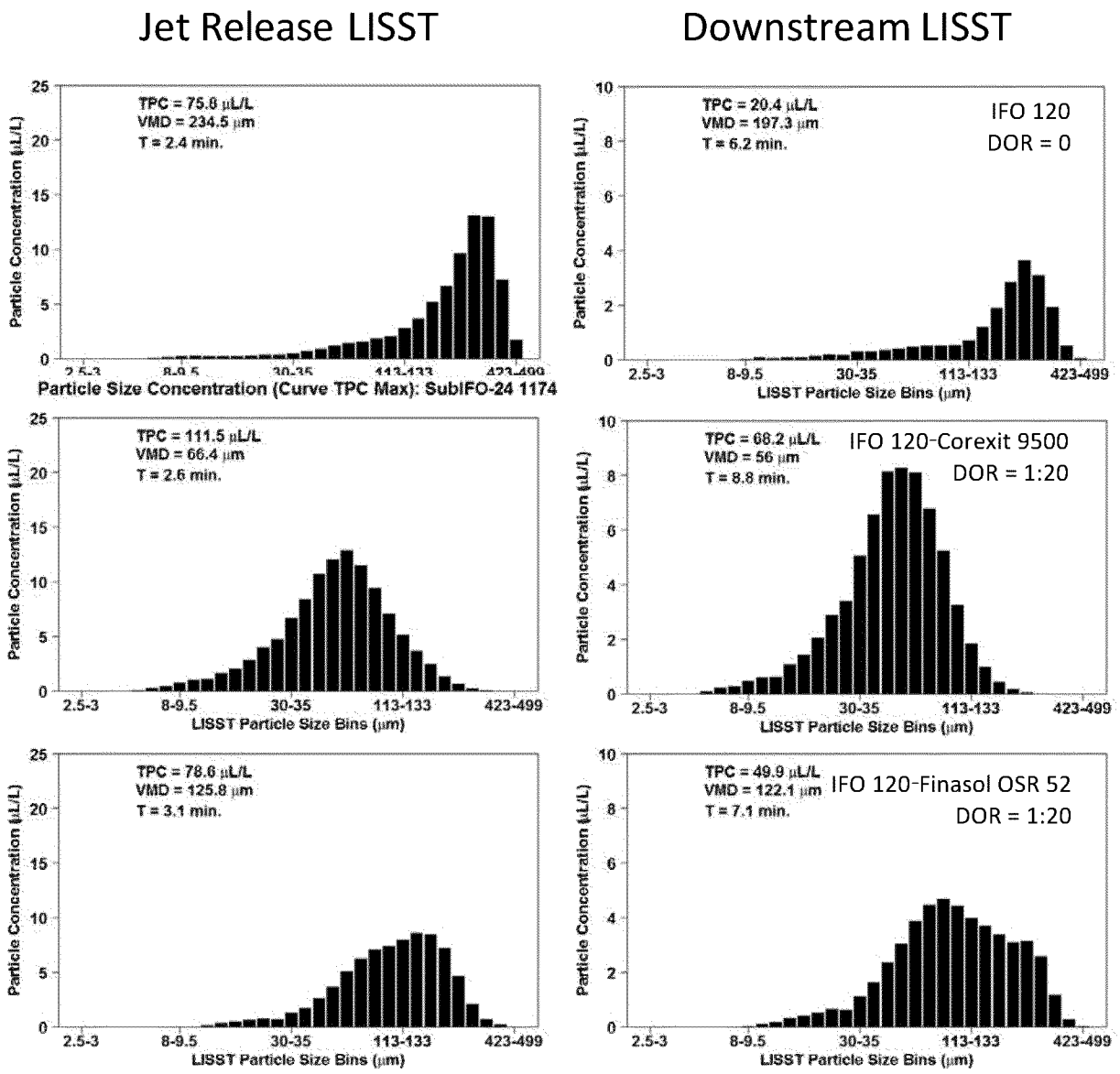


**Figure 20. LISST DSD with TPC for IFO-120 with Corexit 9500 and Finasol OSR 52 treatments at warm temperatures. DOR = 0 (top panel); DOR = 1:20 experiments are middle and bottom panels.**



ED_001324_00000953-00055

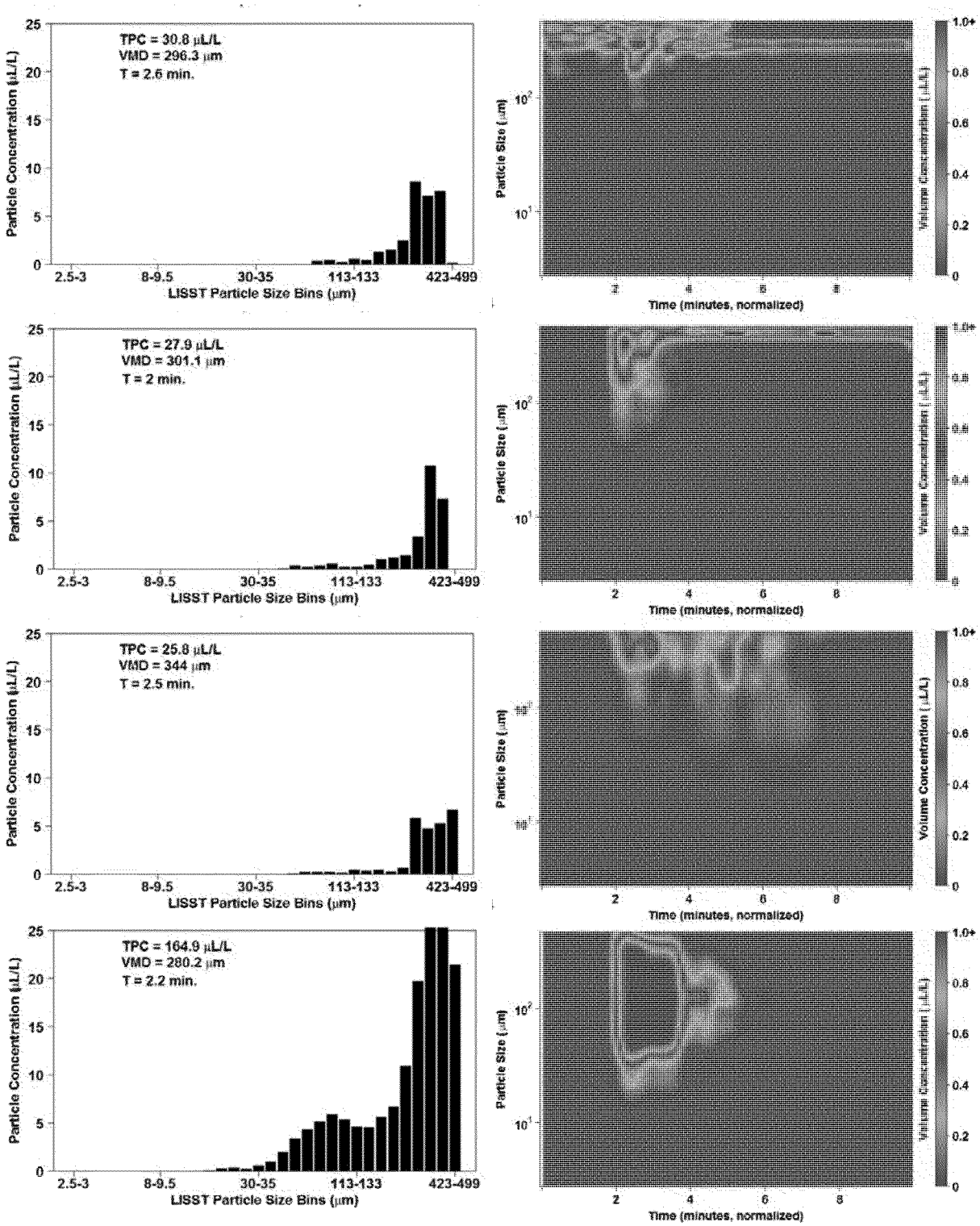


**Figure 21. LISST DSD and VMD (left panels) and time series of concentration and particle size (right panels) for IFO-120 and Corexit 9500 cold water treatments. From top to bottom, DOR = 0, 1:200, 1:100, 1:20.**



ED_001324_00000953-00056

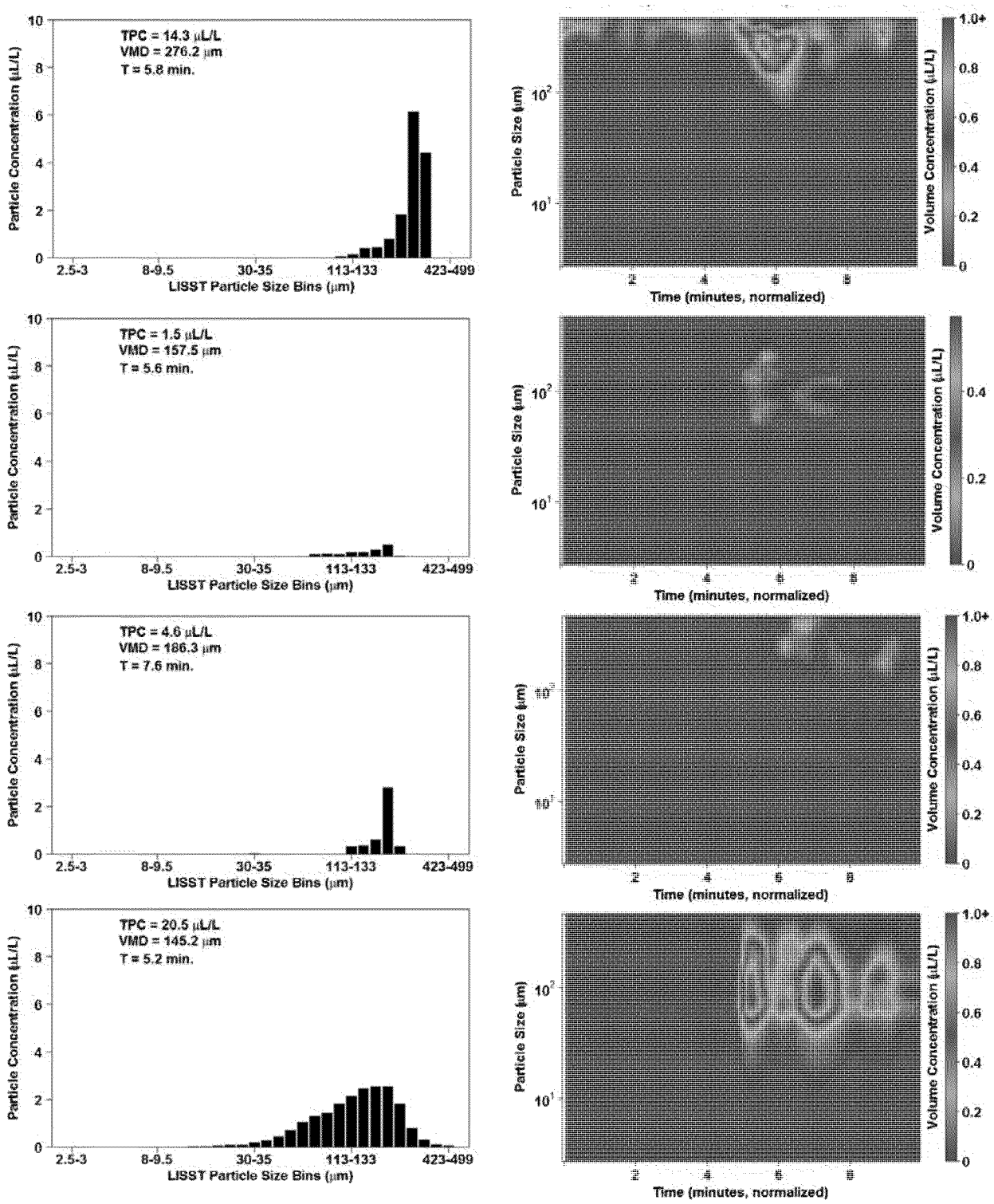


**Figure 22. Downstream LISST DSD and VMD (left panels) and time series of concentration and particle size (right panels) for IFO-120 and Corexit 9500 cold water treatments. From top to bottom, DOR = 0, 1:200, 1:100, 1:20.**



ED_001324_00000953-00057

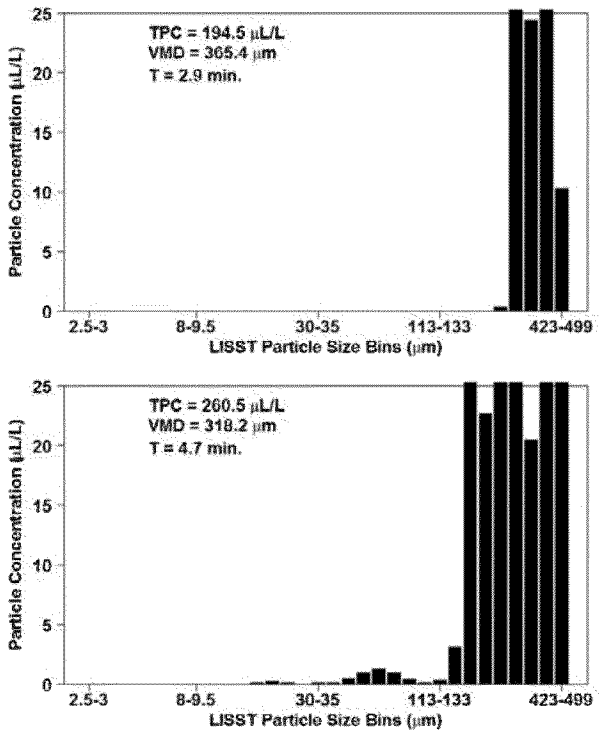


**Figure 23. LISST DSD and VMD for IFO-120 (top; DOR = 1:100) and ANS (bottom; DOR = 1:200) with Corexit 9500 during cold water treatments.**



ED_001324_00000953-00058

### *A.3.3 SLC Dispersion Effectiveness*

South Louisiana Crude (SLC) oil treated with Corexit 9500 experiments were conducted for warm water conditions (16.6 – 19.6 °C (temperature range) to compare dispersion between ANS and SLC. Experiments with SLC yielded higher TPC values compared to ANS results, most likely the result of slightly larger amounts of oil added to the pressure canister (~25-50 g), so comparisons shouldn't be made regarding TPC. The observed VMD of physically-dispersed SLC oil (neat; DOR = 0; ~123-148 µm) was found to be less than that of ANS (>200 µm). The addition of dispersant yielded a shift in DSD and VMD to smaller particles, where DOR = 1:200 and 1:100 exhibited diameters of ~91-108 µm, and DOR = 1:20 ranged between ~15 -21 µm, as depicted in Figure 24. The Downstream LISST results indicate smaller droplet size as the plume moves through the tank and a decrease in TPC, further demonstrating this trend for all oils (Figure 25). The fluorescence data indicates a strong signal with little scatter for up to 4 min in these treatments (Figure 26; Appendix E). Using these results, comparisons can be made to results of SLC with Corexit 9500 from surface plume simulations (pour in) from Conmy et al., 2014b (and unpublished data) from those experiments. No apparent differences between DSD and VMD for DOR = 0 treatments were found. For DOR = 1:20 VMD values are similar, however, the range of droplet diameters for surface simulations is larger with particles up to 200 µm. In subsurface injection jet experiments, that range of diameters is narrower, where particles > 100 µm were not observed. This suggests that the combination of chemical dispersant, elevated turbulence mixing from the jet release and higher oil temperature of 80 °C yielded smaller droplets. To discern the dominant factor controlling the difference, additional testing would need to be conducted.



ED_001324_00000953-00059

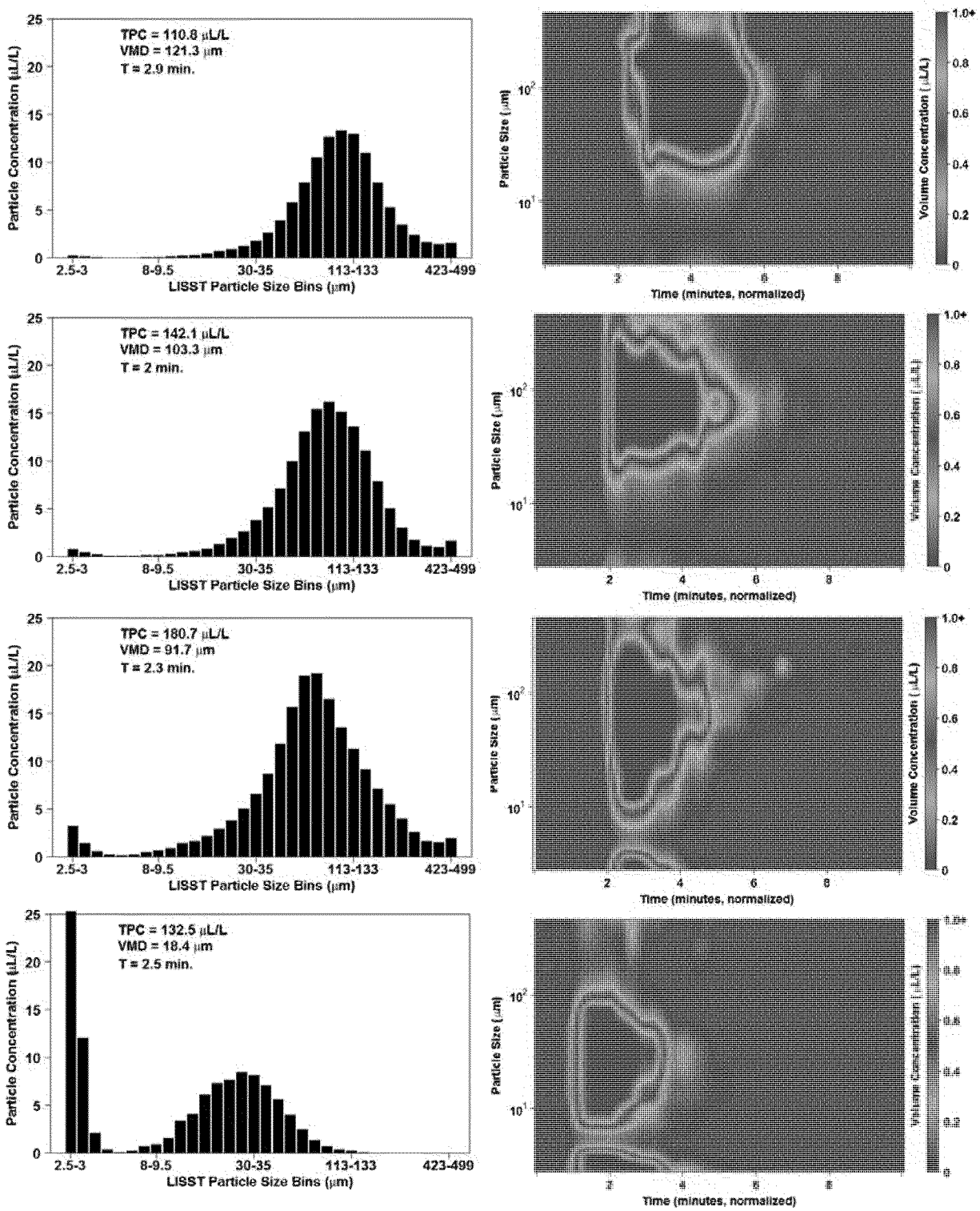


**Figure 24. LISST DSD and VMD (left panels) and time series of concentration and particle size (right panels) for SLC and Corexit 9500 warm water treatments. From top to bottom, DOR = 0, 1:200, 1:100, 1:20.**



ED_001324_00000953-00060

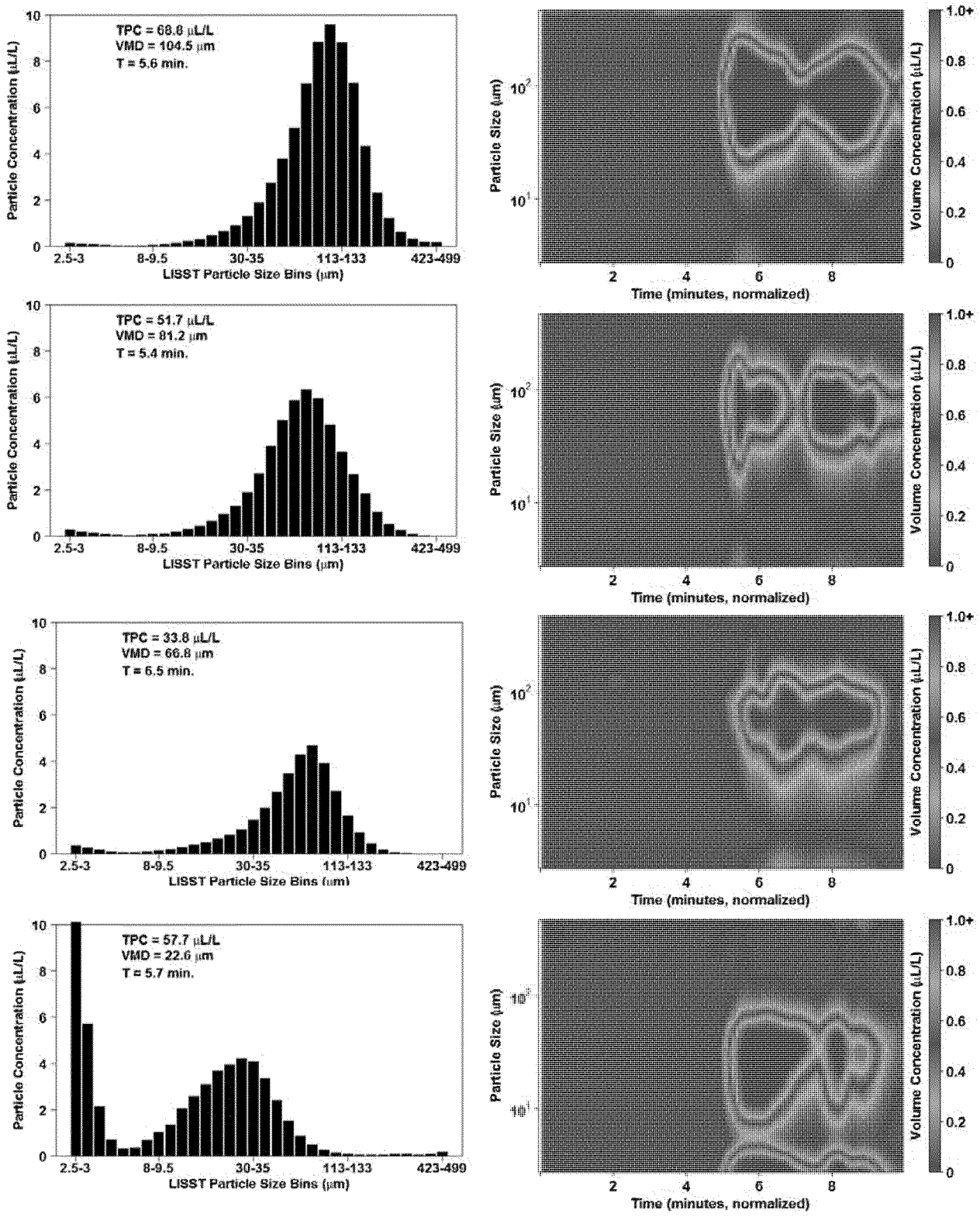


**Figure 25. Downstream LISST DSD and VMD (left panels) and time series of concentration and particle size (right panels) for SLC and Corexit 9500 warm water treatments. From top to bottom, DOR = 0, 1:200, 1:100, 1:20.**



ED_001324_00000953-00061

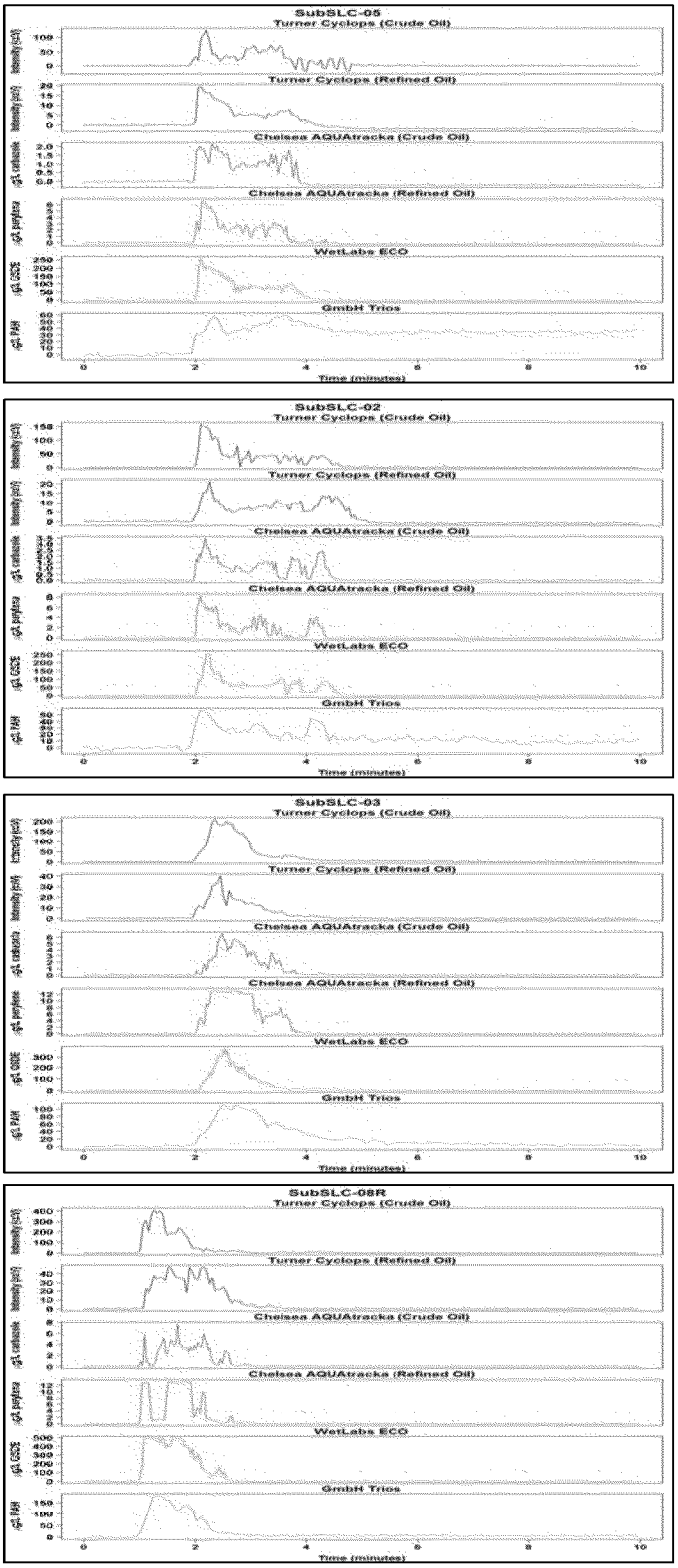


**Figure 26. In situ submersible fluorescence time series of sub-injection plume of SLC and Corexit 9500 warm water treatments. From top to bottom, DOR = 0, 1:200, 1:100, 1:20.**

### *A.3.4 Gas Condensate Dispersion Effectiveness*

Injection experiments were conducted with Gas Condensate Corexit 9500 for warm water conditions (10 – 12 °C temperature range) and DOR = 0 and 1:20 only. The VMD for Gas Condensate with no dispersant added ranged between ~150 – 215 µm (Figure 27). With the addition of dispersant , VMD for the triplicates were 60.4, 68.2 and 170.4 µm suggesting that dispersant at DOR = 1:20 shifts the DSD to smaller particles for most experiments. The corresponding fluorescence data for these treatments indicate a strong signal with little scatter for up to 3 min in both treatments (Figure 28; Appendix E).



ED_001324_00000953-00063

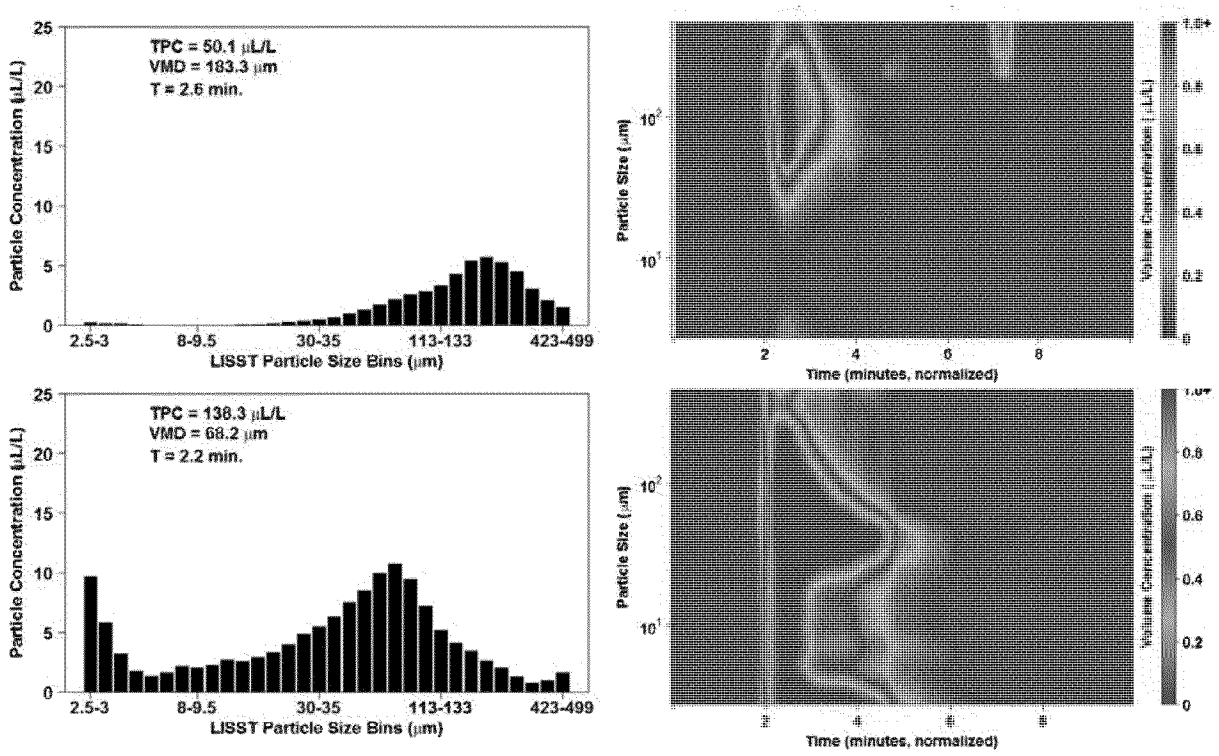


**Figure 27. LISST DSD and VMD (left panels) and time series of concentration and particle size (right panels) for Gas Condensate and Corexit 9500 warm water treatments. Top panels are DOR = 0 and bottom panels are DOR = 1:20.**



ED_001324_00000953-00064

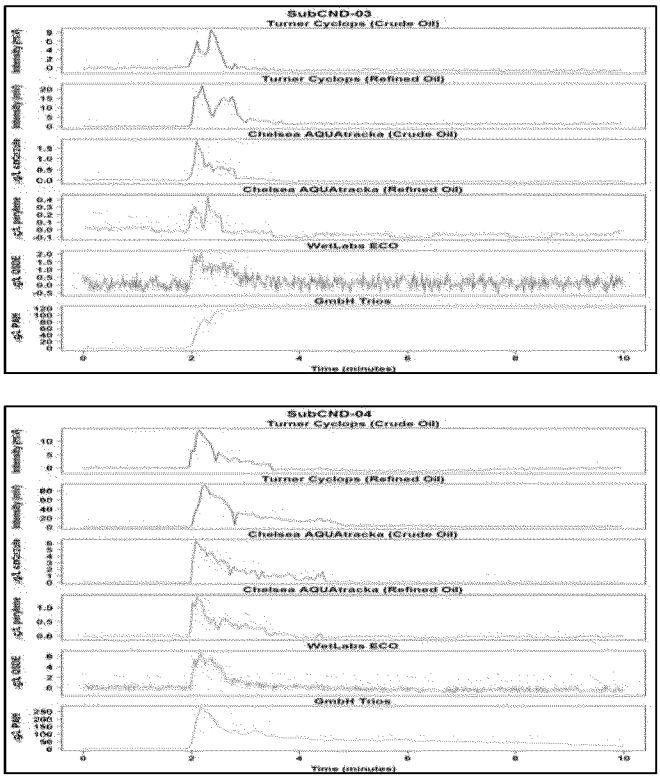


**Figure 28. In situ submersible fluorescence time series of sub-injection plume of Gas Condensate and Corexit 9500 warm water treatments. Top panels are DOR = 0 and bottom panels are DOR = 1:20.**



ED_001324_00000953-00065

### *A.3.5 Tank Dilution Series Fluorescence Measurements*

Submersible fluorescence results are presented in units recommended by manufacturers and using calibration factors provided by the manufacturers. Efforts were made to correlate the fluorescence intensity with TPH and / or BTEX concentration but were not possible due to issues inherent with the discrete sample collection. In order to fill bottles for chemical analysis, a 30 second time period was needed. Due to the short time period of the experiments and the heterogeneity of the plume concentration through time (evident from the fluorescence time series), oil concentrations within the bottles represent an average over a 30 second time period that cannot be aligned with the time series data which is generated on the time scale of seconds. Given this fact, a dilution series within the tank using ANS was conducted to provide a calibration curve for fluorometers to a known concentration of oil in a homogeneous tank akin to Conmy et al., 2014a. Calibration regression results for all submersible fluorometers can be found in Figures 29 and 30 for TPH and BTEX, respectively and regression equations are tabulated in Table5. Strong correlations between oil concentration and fluorescence intensity were observed, suggesting that fluorescence signal can serve as a robust proxy for TPH or BTEX at specific time points within the tank. This is an advantage as the fluorescence is well correlated with TPC time series and employing this type of calibration will provide for chemistry estimates that can be correlated with particle / oil droplet concentrations at fine time scales within the tank during experiments. For example, comparing the TPC and fluorescence signature for ANS with and without dispersant illustrates the differences in the oil droplets and dissolved oil during injection experiments and the utility of monitoring both to understanding plume dynamics Figure 31.



ED_001324_00000953-00066

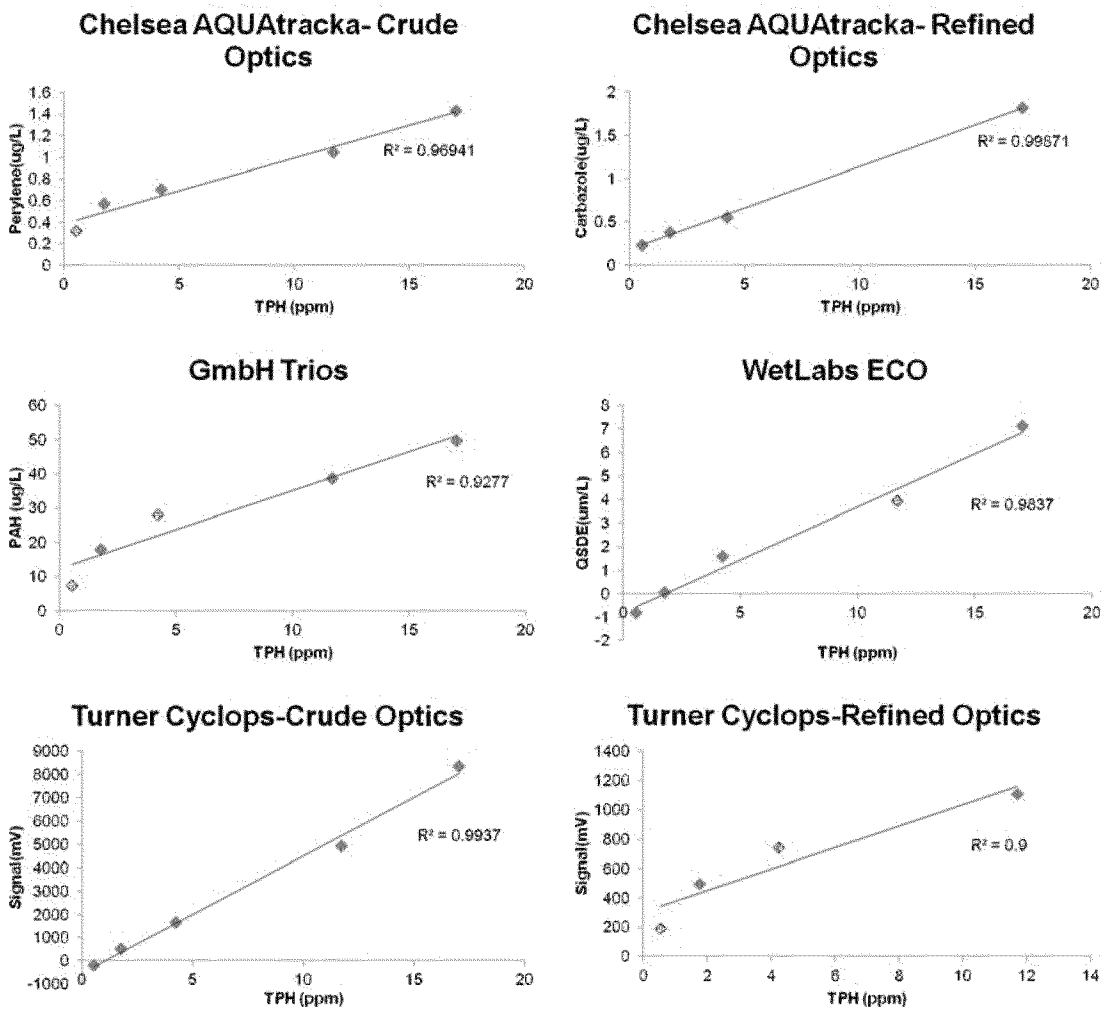


**Figure 29. Calibration lines for fluorometer response vs TPH concentrations.**



ED_001324_00000953-00067

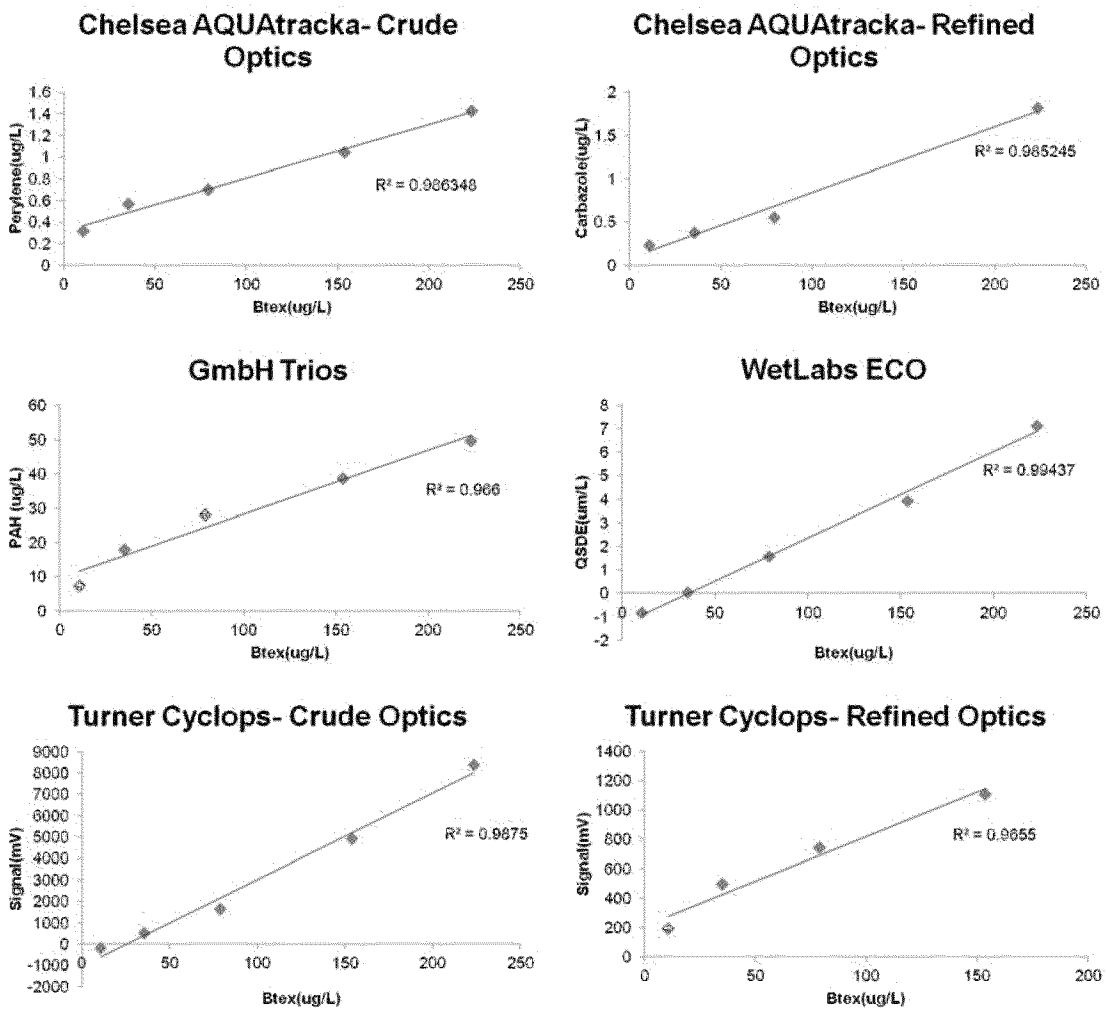


**Figure 30. Calibration lines for fluorometer response vs BTEX concentrations.**



ED_001324_00000953-00068

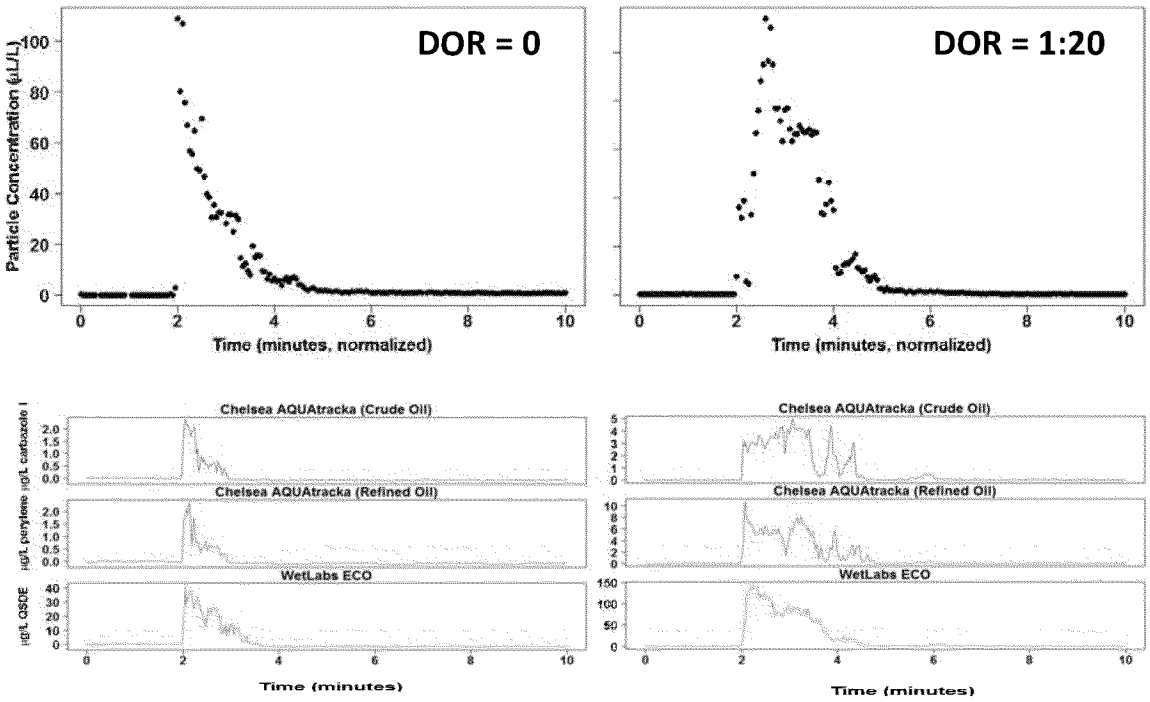


**Figure 31. Total Particle Concentration and fluorescence time series for ANS crude oil with Corexit 9500 dispersant.**



ED_001324_00000953-00069

**Table 5. Calibration equations for the submersible fluorometers. Data in this report have fluorescence signal in the manufacturer recommended units.**

| Instrument | Factory Calibration Standard (units) | TPH Calibration Equation | BTEX Calibration Equation |
|---|---|---|---|
| Chelsea Aquatracka (Crude Optics) | Perylene (ug/L) | [TPH] = ([Perylene]-0.3834)/0.06051 | [BTEX] = ([Perylene]-0.3165)/0.004922 |
| Chelsea Aquatracka (Refined Optics) | Carbazole (ug/L) | [TPH] = ([Carbazole]-0.1804)/0.09575 | [BTEX] = ([Carbazole]-0.08487)/0.007584 |
| GmbH Trios | PAH (ug/L) | [TPH] = ([PAH]-12.288)/2.2733 | [BTEX] = ([PAH]-9.559)/0.1871 |
| Turner Cyclops (Crude Optics) | Signal (mV) | [TPH] = (Signal+320.26)/503.94 | [BTEX] = (Signal+1152.2)/42.429 |
| Turner Cyclops (Refined Optics) | Signal (mV) | [TPH] = (Signal-299.29)/73.339 | [BTEX] = (Signal-212.05)/6.0593 |
| Wetlabs ECO | QSDE (uM/L) | [TPH] = (QSDE-0.2102)/0.4362 | [BTEX] = (QSDE+0.5403)/0.03697 |



ED_001324_00000953-00070

### *A.3.6 VOC Air Monitoring*

For all experiments, the Volatile Organic Compounds (VOC) measurements exhibited higher variability compared to the in water sensor measurements. Despite the fact that a wind screen was installed at the tank facility, the effects of wind were not completely eliminated. The observed variability is likely caused by differences in wind speed and direction both between the triplicate experiments (typically run on the same day), and between the different treatments (which were run over days/weeks). The VOC meters were installed with the air intakes pointing down and were 0.4 m above the water surface at the top edge of the tank. This positioning helped to reduce the effects of wind, given that the tank walls acted as an additional wind blocker.

Two VOC meters were deployed above the tank, but only results from the VOC meter closest to the oil release are presented here (Jet Release VOC meter; the VOC meter directly above the fluorometer rack). Results from the second VOC meter (Downstream VOC meter) installed 11.8 m farther downstream are more variable, both in concentrations between triplicate runs and in the time it takes for airborne VOC concentrations to reach the meter. In general, readings from the second meter showed a broader plume with a lower peak VOC concentration. Due to an instrument failure, approximately 17 experiments are missing data from the Downstream VOC meter. All results from Jet Release VOC meter are presented in Figures 32-39. Note that the Y-axis scale differs depending on the oil type (20 ppm for IFO, 45 ppm for ANS & SLC, 250 ppm for Gas Condensate).

Of the four different hydrocarbon products tested, experiments using the gas condensate exhibited the highest surface VOC concentrations, followed by ANS and SLC which exhibited similar values. The lowest concentrations were observed for IFO-120 experiments. Higher concentrations of VOC in the air were usually accompanied by higher BTEX concentrations in the water for each oil type (analytical chemistry results in Appendix B). The chemistry results from the water column (effluent) samples help to verify the findings from the VOC meters. In general, the measured concentrations of BTEX in the effluent water samples were higher for experiments using dispersant compared to the untreated experiments. The effluent port in the



ED_001324_00000953-00071

flume tank during normal operation produces a depth integrated water sample which does not draw off the water surface. Therefore, oil that rises to the surface is not drawn into the effluent, and so this can be used as a measure of how much oil was effectively dispersed into the water column. Regardless of the oil product tested, the use of chemical dispersants at a DOR = 1:20 resulted in a significant reduction in VOC concentrations compared to corresponding experiments without dispersant, summarized in Table 6. A general trend was also observed where increasing the DOR resulted in lower surface VOC concentrations near the jet release location. Due to wind effects mentioned previously, trends in VOC concentrations above the plume further down the tank could not be established.

**Table 6. Summary of peak VOC concentrations at the various treatment conditions tested in this study. Values shown for ANS and IFO-120 are from the warm water season experiments.**

| | Avg. Peak VOC Concentration (ppm benzene), n = 3 | | | |
|---|---|---|---|---|
| Oil Type | No Dispersant | DOR 1:200 | DOR 1:100 | DOR 1:20 |
| ANS (Corexit 9500) | 23.07 | 13.27 | 12.43 | 0.13 |
| ANS (Finasol OSR 52) | 23.07 | 16.56 | 7.17 | 2.9 |
| IFO-120 | 1.00 | 0.90 | 7.37 | 0.17 |
| Condensate | 121.23 | -- | -- | 19.73 |
| SLC | 28.53 | 27.5 | 16.75 | 1.53 |



ED_001324_00000953-00072

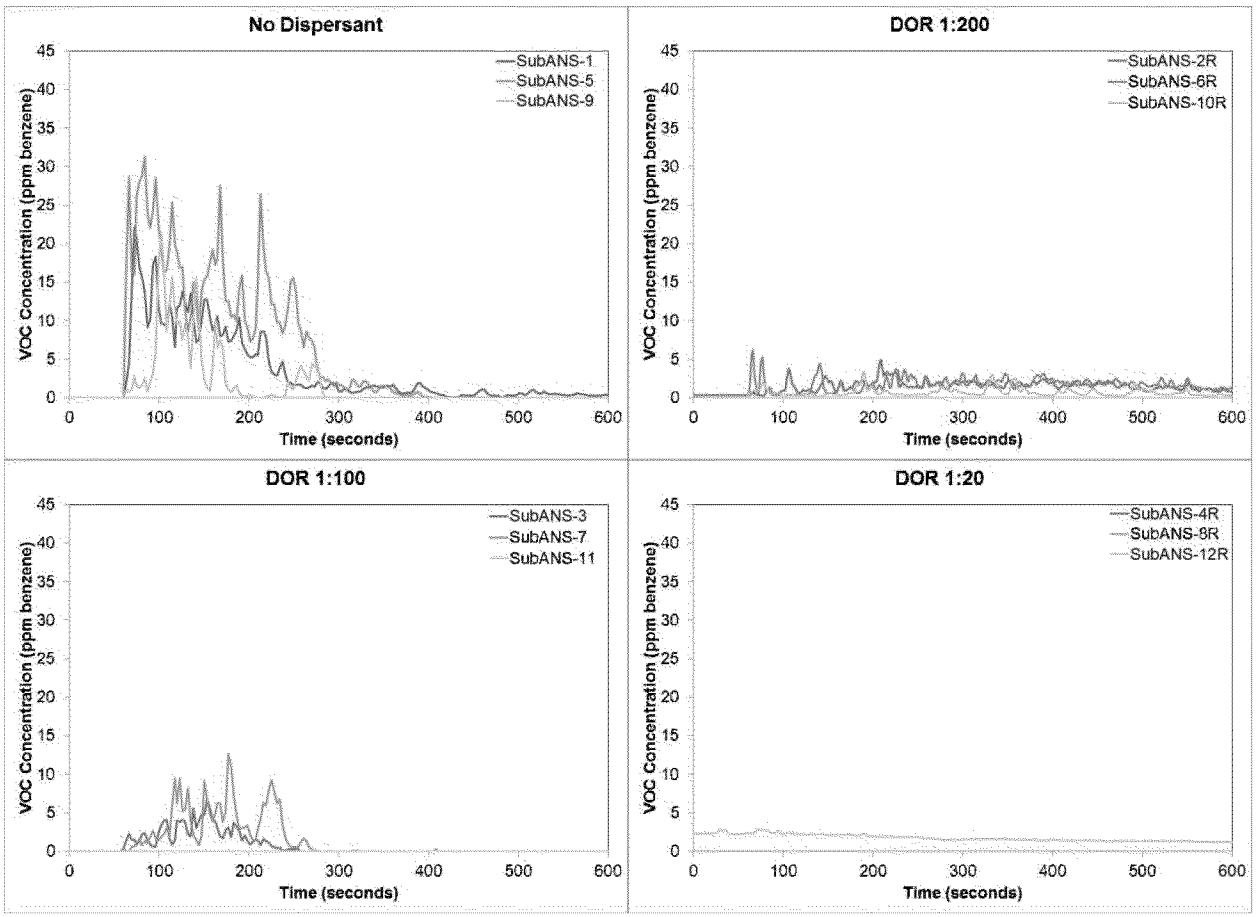


**Figure 32. VOC results for subsurface injection experiments (cold water season) using Alaska North Slope crude oil and four treatment conditions (no dispersant, DOR 1:200, DOR 1:100, DOR 1:20).**



ED_001324_00000953-00073

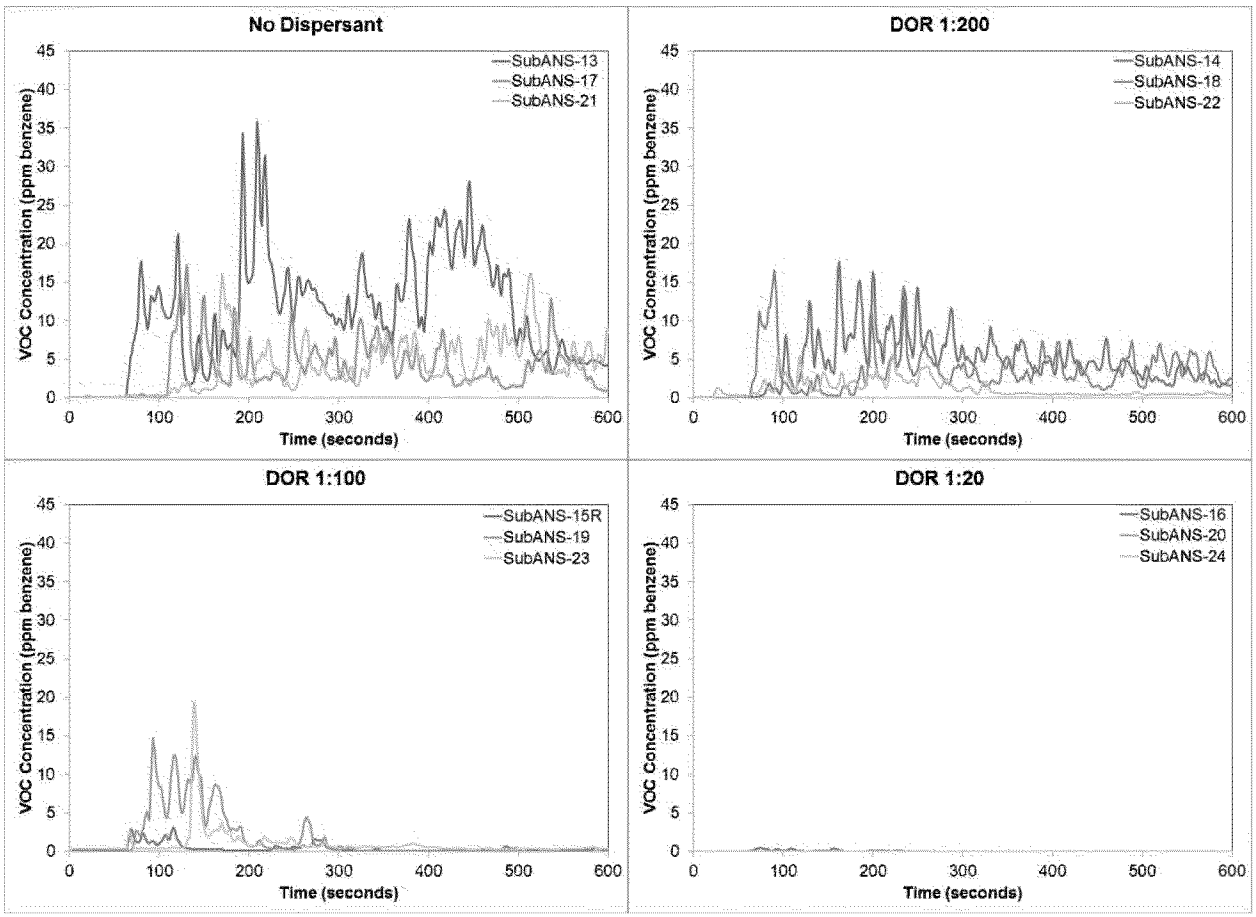


**Figure 33. VOC results for subsurface injection experiments (warm water season) using Alaska North Slope crude oil and four treatment conditions (no dispersant, DOR 1:200, DOR 1:100, DOR 1:20). Corexit 9500 was used as the treating agent.**



ED_001324_00000953-00074

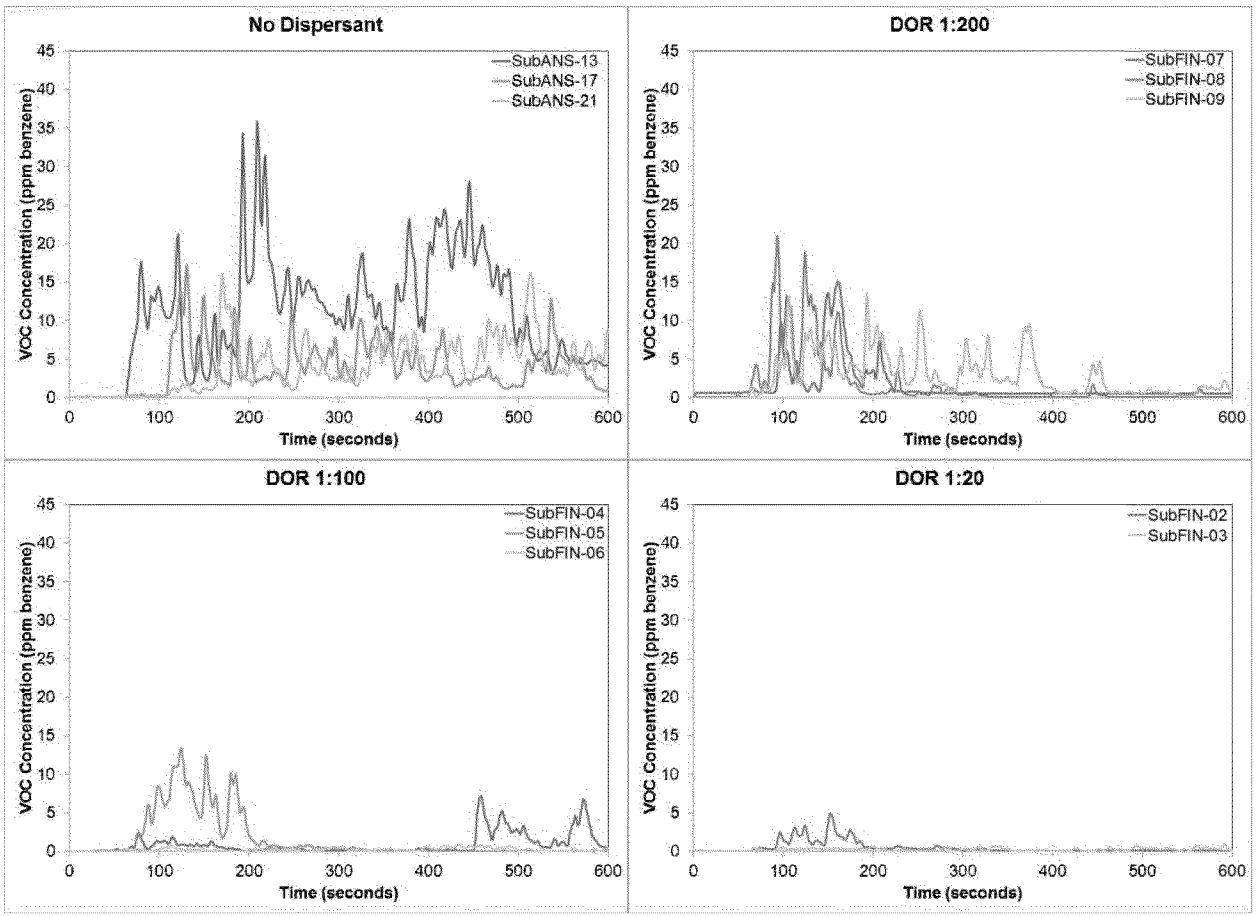


**Figure 34. VOC results for subsurface injection experiments (warm water season) using Alaska North Slope crude oil and four treatment conditions (no dispersant, DOR 1:200, DOR 1:100, DOR 1:20). Finasol OSR 52 was used as the treating agent.**



ED_001324_00000953-00075

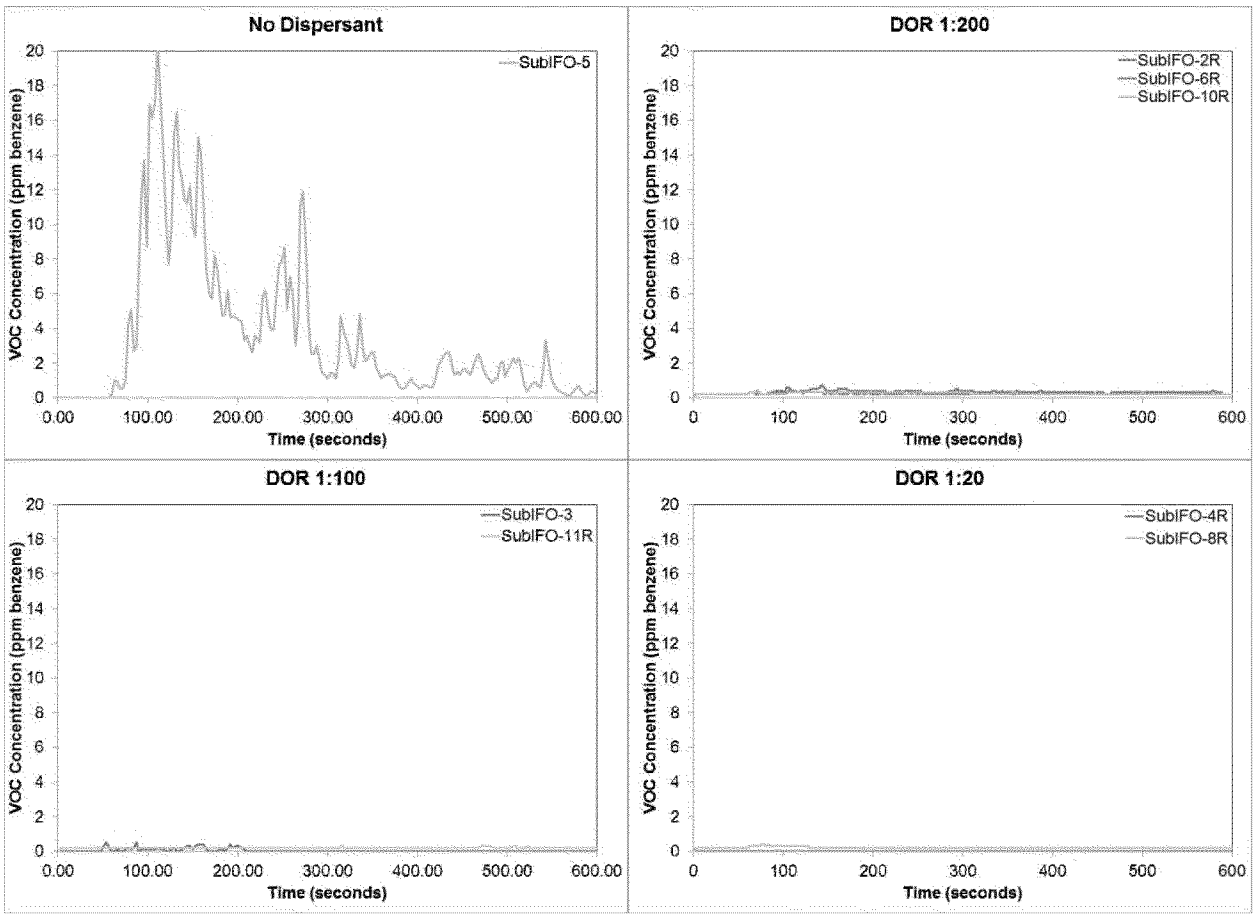


**Figure 35. VOC results for subsurface injection experiments (cold water season) using IFO-120 and four treatment conditions (no dispersant, DOR 1:200, DOR 1:100, DOR 1:20). Corexit 9500 was used as the treating agent.**



ED_001324_00000953-00076

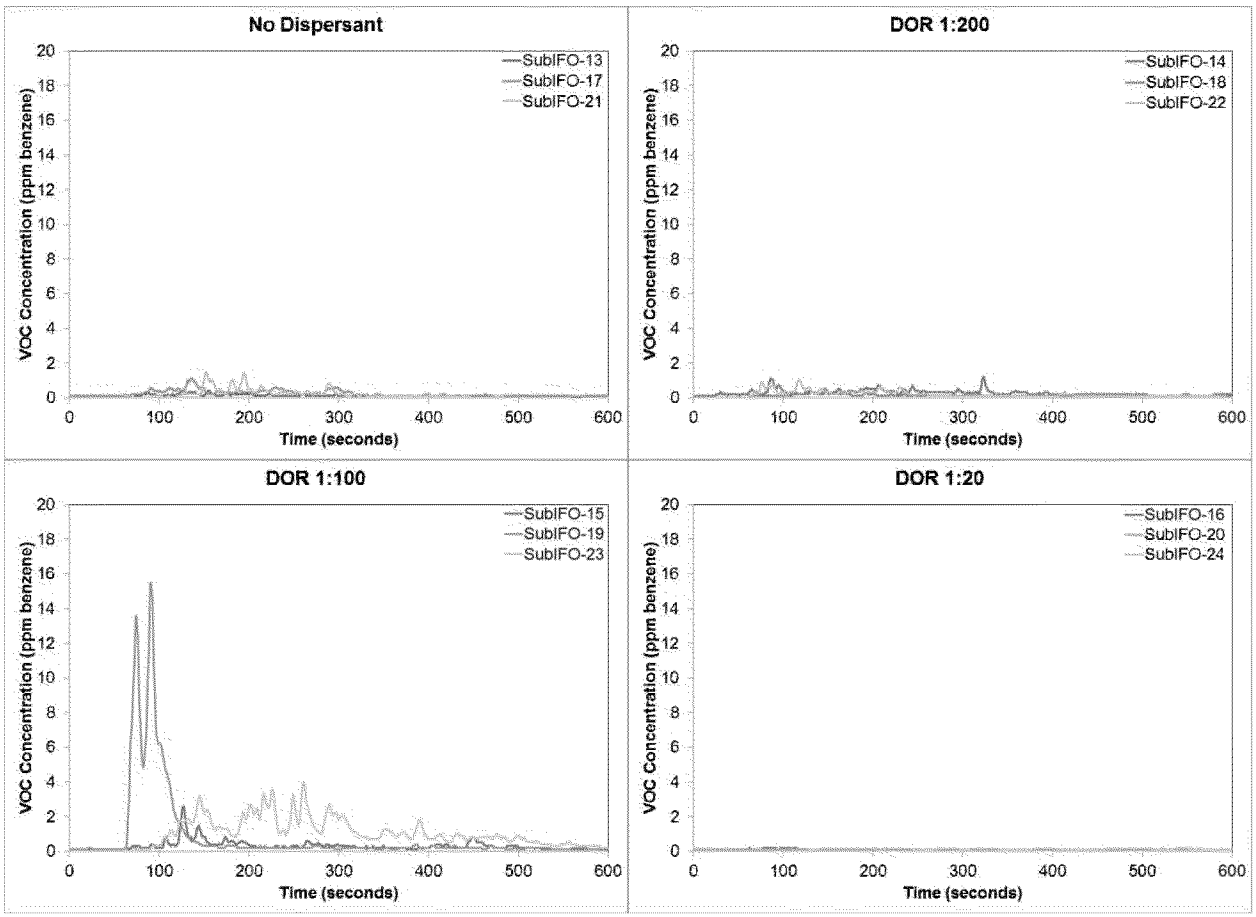


**Figure 36. VOC results for subsurface injection experiments (warm water season) using IFO-120 and four treatment conditions (no dispersant, DOR 1:200, DOR 1:100, DOR 1:20). Corexit 9500 was used as the treating agent.**



ED_001324_00000953-00077

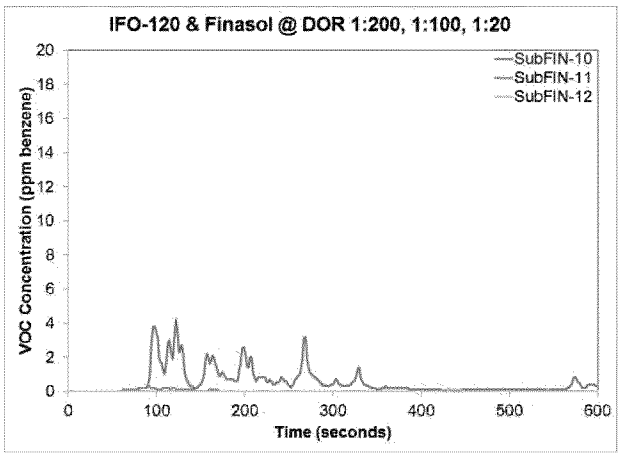


**Figure 37. VOC results for subsurface injection experiments (warm water season) using IFO-120 and three treatment conditions (DOR 1:200, DOR 1:100, DOR 1:20). Finasol OSR 52 was used as the treating agent (note – these treatments were not tested in triplicate).**



ED_001324_00000953-00078

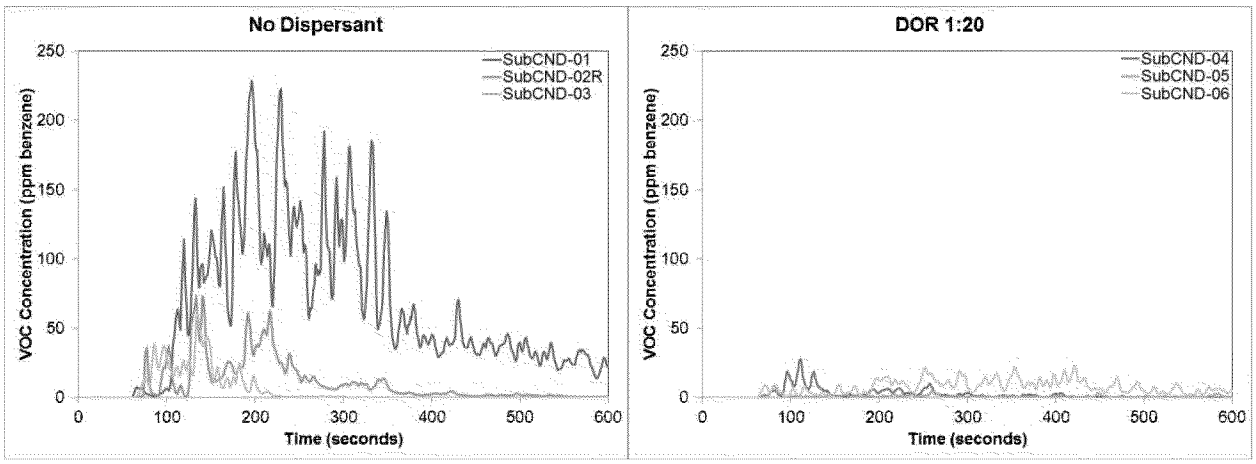


**Figure 38. VOC results for subsurface injection experiments using gas condensate and two treatment conditions (no dispersant, DOR 1:20). Corexit 9500 was used as the treating agent.**



ED_001324_00000953-00079

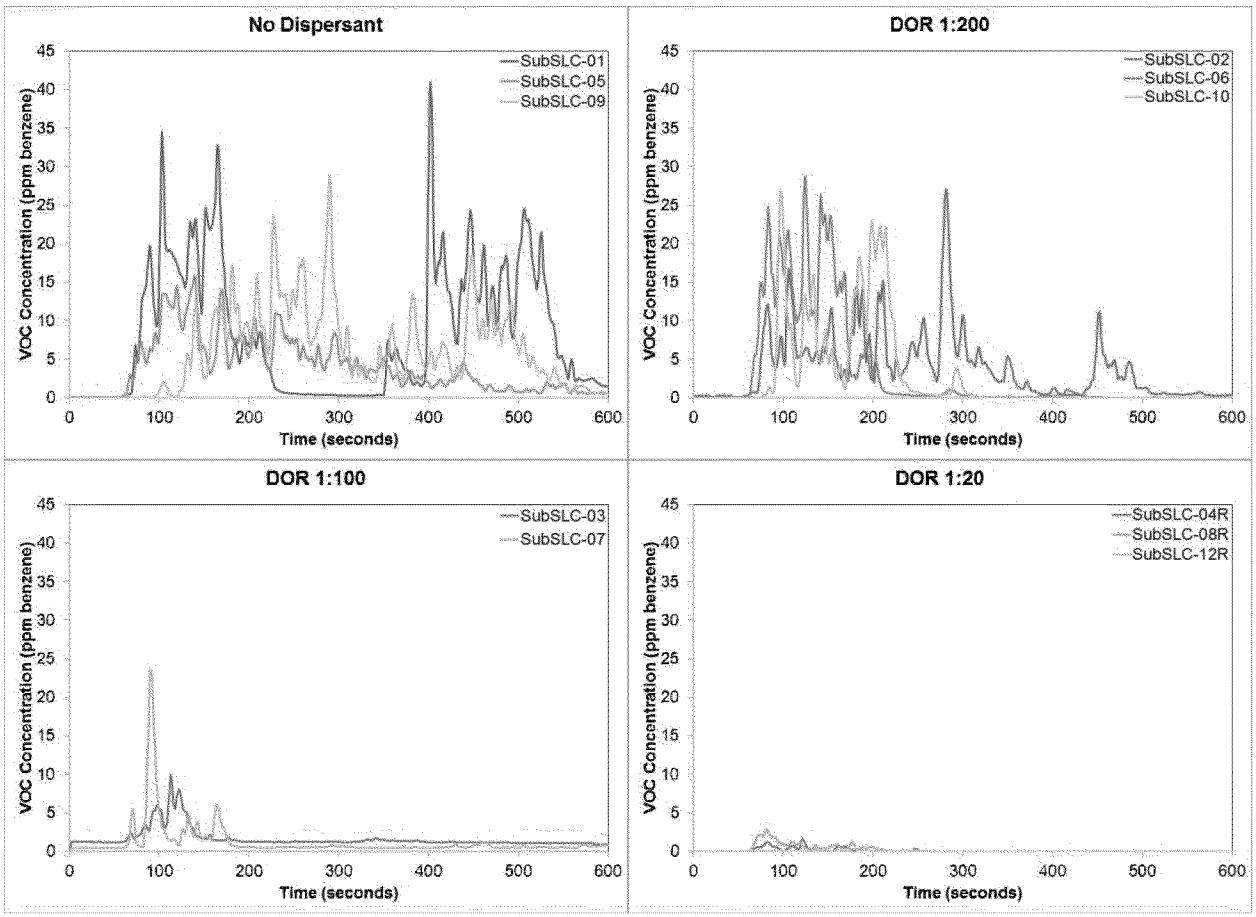


**Figure 39. VOC results for subsurface injection experiments using Sweet Louisiana Crude oil and four treatment conditions (no dispersant, DOR 1:200, DOR 1:100, DOR 1:20). Corexit 9500 was used as the treating agent.**



ED_001324_00000953-00080

### *A.3.7 VDROP-J and JETLAG Numerical Plume Modeling*

Refer to Appendix G for detailed summary of the VROP-J and JETLAG numerical modeling component along with figures. Modeling the movement of oil released underwater is a challenging task due to limitations in measuring hydrodynamics in an oil-water system. Computational Fluid Dynamics (CFD) models are capable of reproducing the hydrodynamics provided they have sufficient resolution. However, CFD models cannot predict the droplet size distribution. For this reason, we used in this work a suite of programs to understand jet hydrodynamics, the droplet size distribution, and the movement of oil droplets within the jet/plume. The developed models were calibrated to experimental data of oil jet released underwater in the Bedford Institute of Oceanography tank. Based on the properties of the jet (mass flow rate 3.8 L/min through a 2.4 mm orifice), the regime of the jet is atomization, which indicates that the jet would break into small droplets. The models VDROP-J and JETLAG were used to predict the streamwise velocity and the holdup (volume of oil divided by the total volume of fluids in a control volume) along the centerline of the plume, where both models were in agreement. This implies that VDROP-J is adequate to predict the average droplet size distribution in the plume. In the absence of dispersant, the model VDROP-J predicted oil DSD that is very close to that measured by the LISST instrument. However, In the presence of dispersant premixed with the oil, the VDROP-J model captured the overall trend of the DSD, but could not capture the peak in droplet concentration observed at 5 µm. The observed peak is most likely due to tip-streaming, and VDROP-J does not have such a module at this time but is considered for future development.

The computational fluid dynamics (CFD) program Fluent (www.ansys.com) was used to model the hydrodynamics of the horizontal jet experiments. The standard $k$ □□ model was used to model turbulence and the Volume of Fluid (VOF) was used to model the two phases (oil and water). The profiles of the holdup (ratio of oil volume to total volume), velocity magnitude, eddy diffusivity and turbulent dissipation rate were presented. Findings indicate that the holdup drops sharply to a few percent with 0.50 m from the source, suggesting the presence of water entrainment into the plume. A significant reduction in the energy dissipation rate was also found, by orders of magnitude along the centerline, starting from $10^4$ watt/kg to $10^{-4}$



ED_001324_00000953-00081

watt/kg. Both holdup and energy dissipation values have important consequences on oil droplet breakup and coalescence. The plume exhibited a core of high velocity and high mixing, while the edge of the plume had more or less violent conditions, which is probably due to the entrained water squishing the edges of the plume. The velocity and eddy diffusivity are needed to predict the movement of individual oil droplets. The shape of the plume was circular near the orifice, but became oblate horizontally at a centerline distance of 2.0 m, which is due to both the buoyancy of the whole plume and its inertia. This suggests that the narrow width of the tank (0.60 m) did not affect the jet hydrodynamics (otherwise the jet would be elongated in the vertical). The width of the tank had an effect on the jet dynamics only near the surface as the plume became elongated along the tank near the surface.

Our CFD approach has its limitations as it smooths out the edge of the oil jet/plume, and thus does not allow for the formation of large eddies around the plume. Here, large eddy simulations (LES) were used to capture the large eddies where the movement of individual oil droplets employed a lagrangian approach. Water velocity and the eddy diffusivity were used to transport oil droplets, and the effect of individual oil droplet buoyancy and inertia were accounted for. Accounting for the inertia of oil droplets has not been done previously in the oil spill literature. Neglecting the inertia of the droplets results in overestimates of their rise rate as the inertia from a horizontal jet tends to propel the droplet more horizontally, and thus their rise gets delayed also by turbulent mixing. Results suggest that oil droplets with a diameter less than 100 µm would mix uniformly in the plume, while those close to 500 µm would tend to be above the centerline of the plume. This indicates that, when measuring the droplet size distribution using the LISST, the placement of the LISST would not affect the reading of droplets that are less than 100 microns. But the LISST needs to be placed judicially to capture particles that are 300 to 500 µm, otherwise LISST placement below the centerline would underestimate the actual droplets in that range. In contrast, LISST placement above the centerline does not allow for surmising that the concentration values represent the whole cross section of the plume.



ED_001324_00000953-00082

### *A.3.8 Weber Number Scaling Numerical Plume Modeling*

Refer to Appendix H for detailed summary of the Weber Number Scaling numerical modeling component. During the Deepwater Horizon oil spill, modeling activities for predicting oil droplet size distribution formed in subsea oil blowouts was critical given their direct influence on the fate and transport of oil in the marine environment. The community's knowledge on droplet size distributions and our capability to predict the distributions are still limited. A recent and promising approach for predicting DSD is the Modified Weber Number approach developed by SINTEF. Thus far, this method has been based on experimental results, validated by a light crude oil (Oseberg Blend crude oil). Here, this approach is validated over a range of oil types using a series of experimental studies was conducted with a subsurface release of Intermediate IFO-120 and ANS crude oils in the DFO horizontal flow tank.

Based on the measured droplet sizes obtained from the tank experiments, corresponding median droplet diameters ($d_{50}$) and the relative droplet size ($d_{50}/D$) were calculated. Accordingly, the relations between $d_{50}/D$ and modified Weber number, Reynolds number, and oil concentration were quantified. With regression analyses, the empirical coefficients for the prediction of droplets size distribution based on the modified Weber number were determined for a certain type of oil (e.g., IFO-120 and ANS). The results indicated that chemical dispersants play an important role in reducing the droplet size of ANS in both cold and warm temperatures. The effectiveness of dispersant in reducing droplet size is higher for ANS compared to IFO-120. There may be thresholds for the dose of chemical dispersant to some oils (e.g., IFO-120) but further data analyses are needed to confirm this. There may also be over dose of dispersant to some oils (e.g., ANS) when the DOR is high, eventually affecting the droplet size distribution. Furthermore, the data indicate that the distributions of the data with $d/d_{50} <= 1$ and $d/d_{50} > 1$ are significantly varied. Therefore, a two-step Rosin-Rammler approach was introduced to more accurately predict the droplet size distribution. The regression coefficients for the two-step Rosin-Rammler are higher compared to the single step in most cases, indicating the advantage of the proposed two-step Rosin-Rammler approach. It should also be noted that the measured IFT for the IFO-120 and ANS with different DORs appear to be significantly



ED_001324_00000953-00083

different compared to the measured results from SINTEF for the modified Weber number approach, possibly due to the characteristics of different oils.



ED_001324_00000953-00084

# TASK B.1 INTRODUCTION & RELEVANCE

Results presented in Task B are contribution of Mary Abercrombie of the University of South Florida and are a portion of her dissertation efforts.

BSEE's *Remote Sensing & Surveillance of Oil Spills* webpage states that "In remote sensing, a sensor other than human vision or conventional photography is used to detect or map oil spills". Thus, although remote sensing of oil spills is traditionally linked to detection of oil on the sea surface from above, the scope of the technology can be extended to include the detection of oil in the deep-sea and/or under-the-ice conditions using various sensors, as vision cannot be used within the water column. As demonstrated during the 2010 Gulf of Mexico Deepwater Horizon (DWH) oil spill, oil detection by fluorescence enabled responders to discern trajectory of plumes and assess effectiveness of dispersant countermeasures (ACT, 2008; Joint Analysis Group Report, 2010). The information supported both Net Environmental Benefit Analyses (NEBA) to ensure minimal impacts on threatened coastal resources and human health from the application of spill countermeasures, and subsequent Natural Resource Damage Assessments (NRDA). To advance the application of this methodology, this project evaluated fluorescence characteristics of various oils with and without dispersants to aid in the selection and refinement of *in situ* sensors for use in oil spill response operations.

The overall objective of this work was to translate oil fluorescence R&D into operational tools for spill response. Tabulating information on the optimum fluorescence wavelengths for oil detection as a function of oil type and DOR assists responders selecting sensors and establishing Best Practices for rapid decision making during spill response. The results of this project are timely and can be used in conjunction with the National Response Team (NRT) interim guidance document, *Subsea Dispersant Monitoring and Assessment Interim Guidance,* for incident-specific decisions concerning monitoring subsea dispersant use. It specifically calls upon using oil-specific submersible fluorometers with laboratory and on-board ship analyses using fixed wavelength and scanning spectrofluorometers to enable improvements to monitoring sampling during dispersant application. Findings from this project provide additional scientific information required for the production of future sanctioned operational guidance documents.

*Fluorescence characteristics* - All fluorophores (molecules that fluoresce) have characteristic wavelengths for maximum absorption of light and characteristic wavelengths at which they emit light as fluorescence. Absorption and fluorescence can occur at either narrow or wide wavelength ranges depending on the chemistry and complexity of the fluorophores. A variety of naturally occurring fluorescent compounds occur in the ocean, from ones with narrow wavelength ranges with sharp fluorescence peak maxima (pigments, proteins) to complex compounds with wide diffuse peaks over long wavelength ranges, such as the ubiquitous Colored Dissolved Organic Matter (CDOM) or petroleum oils.

Fluorescence characteristics of complex mixtures can overlap if structurally similar compounds are shared. Such is the case with CDOM and the aromatic fraction of crude oils. Both are comprised of a variety of organic molecules and both exhibit complex, three-dimensional excitation and emission (EEM) spectra. In general, crude oils have a broad excitation peak centered in the ultraviolet spectrum (< 300 nm) and two emission peaks, one centered in the ultraviolet spectrum around 350 nm and a much larger and broader peak in the visible around 445 nm Bugden et al., 2008). These peaks result from the single ring benzene derivatives and the "polynuclear aromatic" fraction that are particularly susceptible to UV excitation wavelengths. EEMs exhibit distinct fingerprints for different oils as illustrated by previous studies (Bugden et al., 2008; Kepkay et al., 2008).

*DWH in situ oil fluorescence* - Deployment of submersible fluorometers during the DWH oil spill response illustrated the utility of this forensic tool that enabled large-scale monitoring of oil concentrations to a depth of 1600 m. Co-deployment of the fluorometers alongside other response sensors [Conductivity-Temperature-Depth (CTD), Dissolved Oxygen (DO), Laser *In-Situ* Scattering and Transmissometry (LISST)] from multiple platforms including Autonomous Underwater Vehicles (AUVs) and profilers with real-time capabilities improved our understanding of the processes influencing the fate and behavior of the oil in the presence and absence of chemical dispersants. Added to this, extensive water column sampling also involved discrete sample collection for oil particle concentration and size, Total Petroleum Hydrocarbons (TPH), Volatile Organic Carbon (VOC) and other physical, chemical, biological factors. To date the in-



ED_001324_00000953-00086

depth reviews by the Joint Analysis Group (JAG) charged with data analysis have found that of all the variables measured, the most highly correlated in the subsea plume are *in situ* DO and oil fluorescence intensity (Joint Analysis Group Report, 2010). Such a correlation is not unexpected as laboratory tests show that enhanced oxygen utilization can result from microbial respiration in the presence of oil compounds (Venosa et al., 2002b). Beyond the underlying biochemical mechanisms however, likelihood of correlation is increased based on the fact that variables measured *in situ* at high sampling rates are better to capture plume heterogeneity. Hence, the utility of *in situ* fluorescence as a tool was ascertained early in the response due to such correlations, the high temporal and spatial resolution provided by the sensors, and also the advantages afforded by real-time capability compared to discrete analyses.

However, the multitude of submersible fluorometers used in the DWH response called to attention differences in the sensitivity and analytical capability of the instruments used due to differences in configuration of excitation and emission wavelengths, methods of calibration, sensitivity, and correlation to oil concentration (Figure 40, Table7). Many are not customized to capture oil fluorescence peak maxima, rather only a fraction of the signal (Fuller et al., 2003; Conmy et al., 2004 Conmy et al., 2014b). Furthermore, the ability of any fluorescence sensor (laboratory or submersible) to detect oil is function of (1) how well the sensor matches the excitation and emission wavelengths of the oil (including bandwidth of the wavelength filters or bandpasses from gratings, (2) the power of the light source, and (3) the sensitivity of the detector.

When tracking in the subsea became necessary early in the response, fluorometers used for detection of CDOM (i.e., WET Labs ECO series) were deployed on the vertical profilers as they were widely available, were capable of full ocean depth deployment and had been previously shown to detect oil in water (Wet Labs, Inc. website, www.wetlabs.com). These sensors typically have light sources that excite at wavelengths slightly longer than peak absorption by hydrocarbons and detect emission in the visible. They employ filters centered on excitation (Ex) and emission (Em) wavelengths at 370 and 460 nm ($ExEm_{370/460nm}$). Although the center wavelength of the filters does not capture the peak of the oil fluorescence signal, the wide bandwidth of the emission filters (120 nm Full Width at Half Max) and the broad nature of the



ED_001324_00000953-00087

fluorescence peaks means that CDOM sensors are capable of detecting a portion of the visible fluorescence signal. CDOM fluorometers were used to detect oil during the response in part because of their accessibility, but also because these sensors capture some portion of the oil fluorescence peak that occurs at the longer UV wavelengths where CDOM peaks also exist.

To quell questions regarding the ability of the ECO CDOM fluorometer to detect oil in the subsea plume, calibration tests were conducted at Louisiana State University (LSU) using Mississippi Canyon 252 (MC252) source oil. They provided a means to convert raw fluorescence data to Quinine Sulfate Dihydrate Equivalents (QSDE, the standard typically used for CDOM) to ppm of oil (JAG report, 2010). The calibrations were conducted in flasks on orbital shakers at 90 revolutions per minute (rpm), where oil concentrations ranged between 1-50 ppm. Dispersant (Corexit 9500) was added at a DOR of 1:2.5 and 1:25. The response of the fluorometer was linear with respect to oil but varied as a function of DOR, with a quenching of fluorescence in the presence of more dispersant per unit oil. Results of this test indicated that the ECO sensor was a sufficient proxy for oil concentrations greater than 1 ppm. However, as the response continued and after the well was capped, oil concentrations in the subsea plume decreased as well as the magnitude of the fluorescence anomaly. Concern was raised that a fluorometer with higher sensitivity for oil (one with a hydrocarbon-specific configuration) was needed. At that time, Chelsea UV Aquatrackas ($ExEm_{239/360nm}$) were deployed to track the plume in the far field of the response geographic region with the expectation (and subsequent confirmation) that it would detect fluorescence signal at lower oil concentrations.



ED_001324_00000953-00088

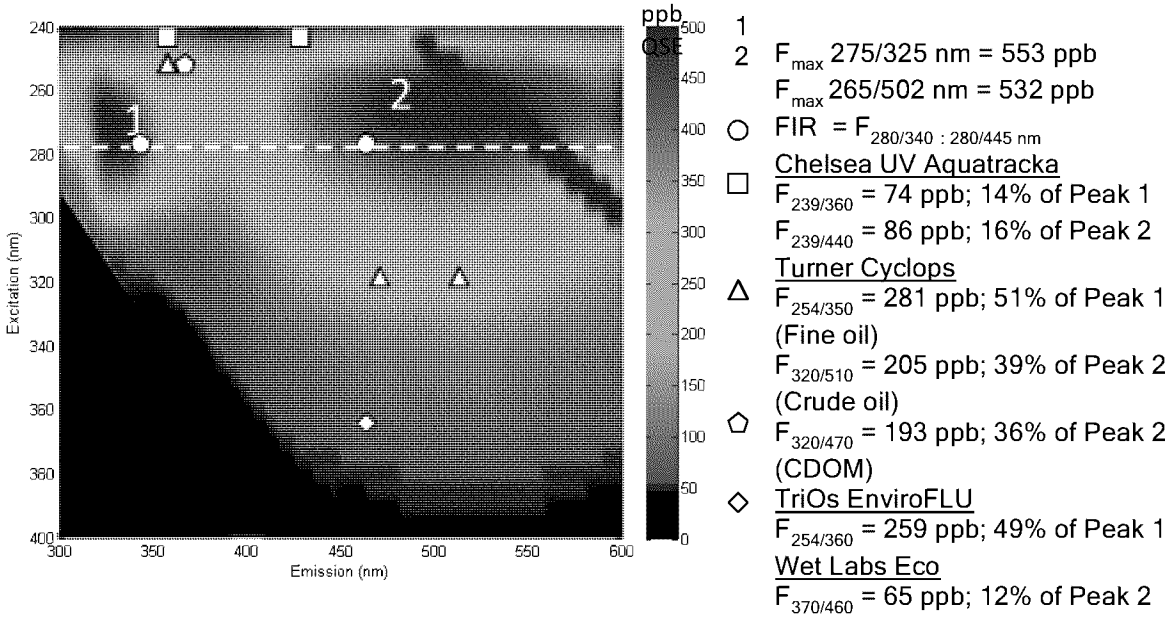


**Figure 40. Fluorescence peaks of S. Louisiana sweet crude dispersed in water. Symbols represent Fluorescence Intensity Ratio (FIR) locations and the Center Wavelength (CWL) reported by sensor manufacturers. Bandwidths (BW) are not shown.**

**Table 7. Sensor specifications as listed from manufacturers. Wavelengths listed as Center Wavelengths (CWL) with Full width at Half Max (FWHM) and Bandwidth (BW). Standards used are QS (Quinine Sulfate Dihydrate), NDD Salt (Napthalene Disulfonic Disodium) and PTSA Salt (Pyrenetetrasulfonic Acid Tetrasodium) (From Conmy et al., 2014b).**

| Manufacturer | Instrument | Light source | Excitation □ (nm) | Emission □ (nm) | Detector | Dynamic Range |
|---|---|---|---|---|---|---|
| Chelsea Technologies Group | UV AQUAtracka | Xenonlamp | 239 CWL | 360 CWL | PMT | 0.001- 10 µg/LCarbazole |
| | UV AQUAtracka | Xenonlamp | 239 CWL | 440 CWL | PMT | 0.001 - 10 µg/LPerylene |
| SeapointSensors | SUVF | LED | 370, 12 FWHM | 440, 40 FWHM | Photodiode | 0.1 - 1500 µg/LQS |
| TriOS, GmbH | EnviroFLU-HC,DS | Xenonlamp | 254, 25 FWHM | 360, 50 FWHM | Photodiode | 0 - 5000 ppb Phenanthren |
| Turner Designs | Cyclops(Fine oil) | LED | 254, 40 nmBP | 350, 50 nmBP | Photodiode | 0 - 10,000 ppb NDD Salt |
| | Cyclops(Crude oil) | LED | 320, 130 nmBP | 510, 180 nmBP | Photodiode | 0 - 2700 ppb PTSA Salt |
| | Cyclops(CDOM) | LED | 320, 130 nmBP | 470, 60 nmBP | Photodiode | 0 - 2500 ppb QS |
| WetLabs | WetStar | LED | 370, 10 FWHM | 460, 120 FWHM | Photodiode | 0.100 - 1000 ppb QS |
| | ECO-FLU, triplet,puck | LED | 370, 10 FWHM | 460, 120 FWHM | Photodiode | 0.01 - 500 ppb QS |

*Post-DWH response sensor tank testing* -To address persisting uncertainties regarding sensor performance in the subsea, a team of scientists conducted experiments in May 2011 to study the dynamic range, sensitivity, and response *of in situ* fluorometers to changing excitation or emission properties of fresh and weathered MC252 oil (NOAA Science Box Award, PI: Michelle Wood; Co-PI's from EPA, NOAA, University of South Florida). The experiment was conducted within the flow-through wave tank at the Bedford Institute of Oceanography's (BIO) Center for Offshore Oil and Gas Environmental Research in Dartmouth, Nova Scotia, taking into consideration environmental factors such as wave energy and ocean currents. Experiments included the stepwise addition of oil and dispersant (DOR of 1:25; 0.3 - 12 ppm of oil to the wave tank while collecting *in situ* fluorescence and droplet-size distribution data, as well as coincident discrete samples for chemistry and EEM analyses. The wave tank was operated in static mode and each addition of oil and dispersant was allowed to homogenize prior to collecting discrete samples and coincident sensor measurements to calculate the least linear squares regressions. Results indicated that all sensors tested were responsive to changes in MC252 oil concentration



ED_001324_00000953-00090

regardless of wavelength configuration. Linear response of the WET Labs ECO, Turner Designs Cyclops and the Chelsea Technologies Group AQUAtrackas sensors as a function of oil concentration was observed, where lowest concentrations were not below the detection limit of any sensor tested (Conmy et al., 2014a). Results demonstrated that all sensors exhibited a wide dynamic range of detection for MC 252 oil and were capable of detecting oil at the lowest concentration (approximately 300 ppb oil), which is significantly lower than the LSU calibration study (1 ppm) and a common misconception during the response. Differences in the detection limit between the studies may be explained by differences in the design, scale and the amount of physical dispersion of the tests, where the tank can provide mixing energies similar to those found in the field.

The 2011 study findings answered critical questions about sensor performance to detecting MC252 oil. However, the experiment highlighted the need for future studies to evaluate sensor performance using a variety of DORs and for multiple oil types. Evident from the DWH spill and post-spill research was that further R&D is needed to transfer knowledge gained through laboratory 3-D Excitation Emission Matrix (EEM) Spectroscopy into practical information for fluorescence tools used during spill response. Fluorescent properties are oil specific and investigating variations in EEMs as function of oil type and dispersant-to-oil ratios better prepares the community in identifying sensors for response options. To that end, the objectives of this project were to:

I. Generate a comprehensive EEMs database, building upon existing data at the Department of Fisheries and Oceans Canada, to provide fluorescence peak information as a function of oil type, weathering state, concentration and Dispersant-to-Oil Ratios (DORs).
II. Critically examine the database using advanced statistical methods and models to identify wavelengths best suited for oil monitoring during dispersant application and degradation.



ED_001324_00000953-00091

III. Conduct wave tank experiments to determine submersible sensors capable of providing data comparable to scanning and/or fixed wavelength laboratory fluorometers for rapid deployment during response efforts.

Through this project, a comprehensive EEMs library database was generated covering a wide variety of oils from light to heavy fuel and crude oils and diluted bitumen. Varying DORs (1:25, 1:100, 1:250, 0) and oil concentrations were evaluated as the presence of dispersant alters EEM fingerprints. EEMs were subjected to advanced statistical analyses and models to identify wavelengths best suited for oil monitoring during dispersant application and biodegradation. Fluorescence is a non-destructive characterization tool that is routinely used to examine complex organic mixtures (foods, wine, medical compounds, aquatic organic matter, oils). Unlike single compound solutions, they exhibit broad, diffuse peaks that result from overlapping smaller peaks with similar chemistry. Although EEMs can be a substantial source of information on chemical composition and variability amongst samples, the high-dimensionality (intensity by emission by excitation) and nonlinearity of the data equates to difficulties in data interpretation and extraction of practical information as a characterization tool (Bieroza et al., 2010). Therefore, it is difficult to determine which underlying chemical components are responsible for which portion of the fluorescence fingerprint. Combining standard techniques for EEM analysis such ads assessment of particular fluorescence peak features such as peak height and wavelength position via 'peak picking' with Parallel Factor Analysis (PARAFAC) modeling results in a more comprehensive understanding of the chemical constituents. The use of advanced multivariate analyses such as PARAFAC and has gained popularity as an effective means to deconvolve complex, broad peaks into their underlying smaller components (Stedmon et al., 2003; Boehme et al., 2004; Christensen et al., 2005; Stedmon and Bro, 2008). Here, we will process EEMs data with scripts in the N-way toolbox for Matlab (Andersen and Bro, 2000) and use the algorithms to isolate wavelengths to best characterize an oil type. An excellent review of these chemometric techniques and applications is provided in Bieroza et al., 2010. This approach will allow for comparing oil in water mixtures for similarities and contrasting features.



ED_001324_00000953-00092

Results were evaluated for the Fluorescence Intensity Ratio (FIR) technique (Bugden et al. 2008; Kepkay et al. 2008). The latter calculates the ratio at $ExEm_{280/340nm}$ to $ExEm_{280/445nm}$ as an indicator of oil dispersion. Previous studies at DFO COOGER have shown that dispersed oil fluoresces over two peaks centered on emission wavelengths of 340 nm and 445 nm, at excitation wavelength 280 nm, and that chemical dispersion enhances the emission intensity at 450 nm (Bugden et al. 2008; Kepkay et al. 2008). Postulated is that the fluorescence intensity at $ExEm_{280/340nm}$ represents the dispersion of lower molecular weight aromatic hydrocarbons, while intensity at $ExEm_{280/445nm}$ corresponds to higher molecular weight aromatic compounds.

Finally our work addresses the disconnect that exists between fluorescence research conducted in laboratories and the collection of fluorescence data from submersible sensors. By conducting laboratory-based and tank-based experiments on the same oil type and DOR, comparisons between EEMs can be made across scales. This helps to determine how well the in situ sensors are aligned in detecting dispersed oil.



ED_001324_00000953-00093

# TASK B.2 EXPERIMENTAL METHODS

***B.2.1 Sample Preparation*** - Twenty-five oil samples from the DFO and EPA stockpiles were used for spectrofluorometric testing, where oil characteristics were tabulated for the test oils based on an extensive literature search (Table 8; Supplemental Material A). All glassware used in this study was cleaned to ensure highest analytical integrity including solvent rinsing, deionized water rinsing and baking in muffle furnace at 450˚C where appropriate. Samples were stored in 125mL amber glass bottles with PTFE-lined caps (Figure 41).

***B.2.2 Artificial Seawater Protocol*** - Artificial seawater was used for DOR mixing to avoid interference of fluorophores found in natural seawater with oil fluorescence signal. Fresh artificial seawater was made to salinity ≈28 ppt and was prepared in 1 L quantity at the beginning of each experiment by adding Tropic Marin® salts (Appendix A) to 1 L ultrapure water dispensed from a Millipore Milli-Q unit (≤ 4 ppb DOM) into a 1.5 L glass beaker, covering the beaker with aluminum foil, and stirring with a magnetic stir-bar on electric stir plate for 20 minutes at room temperature (~24°C).

***B.2.3 Dispersed Oil in Seawater Protocol*** - A series of dispersed-oil-in-seawater experiments were performed using baffled trypsinizing flasks (baffle flasks) with artificial seawater, MC252 oil and Corexit 9500 chemical dispersant (Venosa et al., 2002a). Four petroleum oil / dispersant solutions were prepared for each oil type at the following DORs: 0, 1:20, 1:100, and 1:200. Oil was pipetted into an 8.6 ml amber vial, followed by addition of the appropriate amount of Corexit 9500 chemical dispersant into the vial. Teflon-lined capped vials were shaken by hand for 60 seconds and 10 µL of dispersed oil mixture was pipetted (Eppendorf positive displacement micropipettes, 1-20 µL) into 100 mL artificial seawater contained in each of three replicate flasks. Flasks were covered with parafilm and placed on a New Brunswick Scientific Innova 2100 platform shaker (orbit = 1.9 cm) for 12 minutes at 200 rpm. Approximately 3.5mL of the resulting dispersed-oil-in-seawater was immediately dispensed through a spigot near the bottom of each flask into three 4.0-mL UV-grade quartz cuvettes, which were immediately covered with Teflon stoppers to prevent evasion of volatile components during fluorescence analyses (Figure 42).



ED_001324_00000953-00094

After removal of spectrophotometric samples, additional volumes of sample were removed from the baffle flasks for extraction of total petroleum hydrocarbons (TPH) by methylene chloride. TPH analysis follows the same Gas Chromatography-Mass Spectrometry (GC-MS) method as in Task A of this project.

***B.2.4 Spectrophotometric Analysis*** - A Horiba Scientific AquaLog spectrofluorometer was used to analyze the 25 oil types with varying DOR. A series of analyses were initially performed while varying the instrument's settings (excitation and emission increments, gain setting, integration time) in order to determine optimal settings for the entire experimental protocol. Excitation-Emission Matrices (EEMs) were generated using the following instrument parameters: 200 – 800 nm excitation (3 nm increments), 249 – 828 nm emission range (CCD detector at 534 nm 8 pixel increments), medium gain setting and integration time of 0.1 sec. A quinine sulfate dehydrate dilution series was created consisting of: 0.5N H2SO4 solvent; 100ppm 1° solution; 100ppb 2° solution; 1,3,5,10 and 20ppb quinine sulfate solutions. Dilutions were analyzed for fluorescence and used for cross-calibration with instrument software built-in quinine sulfate tool to convert results into Quinine Sulfate Equivalents (QSE) and demonstrate linearity of fluorescence in a dilution series. All data processing and spectral corrections follow the manufacturer's manual. Dilution series with oil concentrations between 1 – 500 ppb were also generated to determine lower detection limits for oils. EEMs are presented in Raman Units (RU).



ED_001324_00000953-00095

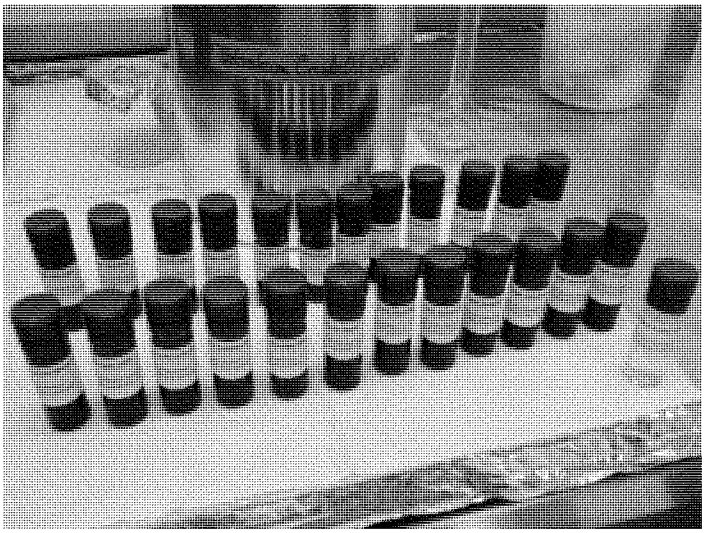

**Figure 41. Twenty-five oil samples stored in glass bottles.**



ED_001324_00000953-00096

Table 8. List of oil samples used for EEM analyses.

| | | |
|---|---|---|
| Lago | Santa Clara | Heidrun |
| Federated | Hondo | Arabian Light |
| Gullfaks | Belridge Heavy | Scotian Shelf Condensate |
| Brent | Cold Lake Dilbit | Medium South American (MESA) |
| IFO-40 | Access Western Blend Dilbit | Alaska North Slope (ANS) |
| IFO-120 | Hibernia | ANS (10% Weathered) |
| IFO-180 | Sea Rose | Mississippi Canyon Block 252 (MC252) (generic) |
| IFO-300 | Terra Nova | MC252 (Discoverer Enterprise) |
| Vasconia | | |



ED_001324_00000953-00097

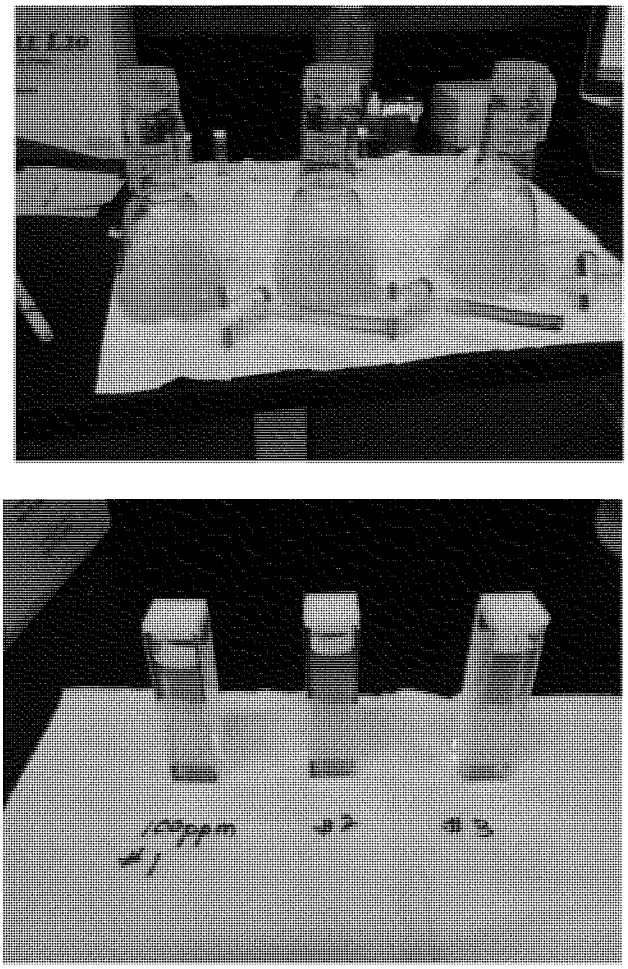

**Figure 42. Trypsinizing baffle flasks containing dispersed oil in artificial seawater (left) and corresponding samples removed from each flask, ready for spectrofluorometric analysis.**



ED_001324_00000953-00098

# TASK B.3 RESULTS & DISCUSSION

## ***B.3.1 Oil Fluorescence Properties***

Four characteristic excitation/emission (Ex/Em) peak locations were identified: $F_{max1}$ – $F_{max4}$ for all 25 oil types at four DORs (Figure 43). The highest intensity peak ($F_{max1}$) occurred, without exception, at Ex 221-239 nm/Em 335-344 nm and was paired with a blue-shifted, lower intensity peak ($F_{max2}$) at Ex 215-221 nm/Em 285-308 nm in all oil types. A third broad, low-intensity peak ($F_{max3}$) was observed at Ex 215-305 nm/Em 418-571 nm, but appeared in only 68% of oil types. A fourth region of broad, low-intensity fluorescence ($F_{max4}$) was identified at Ex 269-291 nm/Em 326-353 nm in all oil types. In addition to maximum fluorescence intensity (in RU), full width at half maximum (FWHM) was recorded for all peaks. Further, fluorescence intensity at Ex/Em 281/340 and 281/450 nm was recorded to enable calculation of the FIR for all samples. Optimum settings for signal collection on the HORIBA AquaLog necessitated excitation at 3 nm intervals, which accounts for the 1 nm discrepancy from the published FIR wavelengths (Bugden, et al. 2008). Finally, fluorescence intensity at the specified Ex/Em wavelength settings of five off-the-shelf in situ fluorometers (Conmy et al., 2014b), which were all employed in the response to the DWH spill, was recorded. Those wavelengths were also adjusted slightly to compensate for signal collection intervals on the HORIBA AquaLog. Selected results are presented in Table 9 along with results of chemical analyses, and complete fluorescence results are included as a Supplemental Table A. EEM contour 'fingerprint' plots for all oils are presented in Appendix F and illustrate the effect of dispersant on the fluorescence properties.

Intensity of $F_{max1}$ was consistently strong across oil types, with no ambiguity in peak location. The observed Ex/Em range of significant fluorescence intensity was fairly narrow with FWHM of only 37-50 nm, and little to no change in peak location with increasing DOR. However, ten oil types displayed a slight increase (approximately 4.5 nm) in FWHM with maximum dispersion (DOR 1:20). The impact of applying the Inner Filter Effect correction tool (IFE) to fluorescence intensity was also calculated for $F_{max1}$. This correction utilizes the measured absorbance of the sample to correct for fluorescence emitted by fluorophores within the sample, but re-absorbed within the sample itself. If note is that application of the IFE resulted in only a small magnification of the fluorescence signal at DORs 0, 1:200 and 1:100 for all oil types; however, there was a clear



ED_001324_00000953-00099

delineation between two categories of oil types at DOR 1:20: Oil Type I, with IFE effect > 2.5 and Oil Type II, with IFE effect < 2.5 (Table 9). Example EEMs of each type are shown in Figure 44 to illustrate the difference in fluorescence between the types regardless of being a light or heavy crude oil.

Due to variation from laboratory to laboratory, and even differences in instrument to instrument performance from the same manufacturer, it is necessary to convert fluorescence intensity "raw counts" to a standardized unit for useful reporting purposes. Traditionally, the fluorescence community has utilized a dilution series of quinine sulfate dihydrate in weak acid to convert instrument output to Quinine Sulfate Equivalents (QSE) (Coble, 1996). However, in recent years the alternate method of reporting in Raman Units (RU) has gained favor (Murphy et al., 2010). Due to inherent properties of water molecules, the Raman scatter peak is a reliable feature which can be used through collecting a scan of ultra-pure water at the beginning of each day, and then using the ratio of raw counts to the area under the curve of the Raman peak (approximately 381-426 nm) to convert fluorescence to RU. As the Quinine Sulfate SRM is no longer available from NIST, we will report results in RU and offer a conversion factor to QSE using the highest quality quinine sulfate dehydrate readily available.

Overall, $F_{max1}$ intensity ranged from a minimum of 39.58 RU (Access Western Blend Dilbit DOR 0) to 3090.23 RU (IFO-120 DOR 1:100). Since all of the Intermediate Fuel Oils and the Scotian Shelf Condensate showed unusual fluorescence profiles which tended to skew our results, these will be eliminated them from the remaining discussion. $F_{max1}$ intensity within Type I oils ranged from 357.62 RU (Arabian Light DOR 1:200) to 1998.60 RU (MC252 Discoverer Enterprise DOR 1:20), while the range in Type II Oils was the overall low of 39.58 previously mentioned to a high of 1098.90 (Heidrun DOR 1:20).

While the excitation wavelength of maximum intensity for $F_{max2}$ remained relatively consistent, the emission wavelength varied within, as well as among, oil types. The occurrence of double and triple peaks, as well as minor sub-peaks, within the $F_{max2}$ region was fairly common. It was sometimes difficult to distinguish the $F_{max2}$ peak from the shoulder of a very strong $F_{max1}$ peak, especially at higher DORs. For this reason, determination of the true FWHM was sometimes



ED_001324_00000953-00100

problematic. For $F_{max2}$ intensity, Type I Oils ranged from 63.95 RU (Brent DOR 1:200) to 437.32 RU (MC252 Discoverer Enterprise DOR 1:20), and Type II Oils ranged from 25.07 RU (Belridge Heavy DOR 0) to 164.07 RU (Heidrun DOR 1:20).

For oil types exhibiting an $F_{max3}$ peak, it was most apparent at the highest DOR (1:20), where some oils exhibited a strong $F_{max3}$ peak across all DORs (e.g., Brent, Federated). However, for those oils the $F_{max3}$ peak at DOR 1:20 was significantly blue shifted from the $F_{max3}$ location observed at lower DORs. FWHM of the $F_{max3}$ peak was much greater than that of any other peak (145-283 nm), with the exception of the three lower DORs of Access Western Blend Dilbit (52-56 nm). Identification of highest $F_{max3}$ intensity proved somewhat problematic as it tended to lie in the second order Rayleigh region, a band of high intensity light resulting from scattering by water molecules. The edge of highest intensity could also lie in this region, so determination of the true FWHM was also problematic for many oil types. Traditionally, second order Rayleigh is eliminated by simply masking this region (10-12 nm). Although algorithms have been developed to model the character of fluorescence peaks lying within (Zepp, et al. 2004; Bahram, et al. 2006), assumptions about the linearity of fluorescence must be made, and the true signal behavior cannot be known. For this reason, as our goal was to identify signals which could also be detected by in situ instruments, the decision was made to identify the maximum fluorescence intensity lying outside of the second order Rayleigh region rather than to try to interpolate the data.

As previously mentioned, $F_{max3}$ intensity was not always present, and it was observed far more often in Type I Oils with a range of 2.64 RU (Arabian Light DOR 1:200) to 744.69 (MC252 Discoverer Enterprise DOR 1:20). Only four of the Type II Oils exhibited $F_{max3}$ peaks and these ranged from 2.45 RU (Access Western Blend Dilbit DOR 0) to 174.93 RU (Heidrun DOR 1:20).

As with $F_{max2}$, the $F_{max4}$ region sometimes contained double peaks. Unique spectral shapes for this region were also observed, especially in higher-density oils such as Access Western Blend Dilbit, Belridge Heavy, and Cold Lake Dilbit. FWHM ranged from 27 nm to 73 nm, for all oil types but one. The exception was Access Western Blend Dilbit, with FWHM of 77-110. Intensity at $F_{max4}$ ranged from 33.53 RU (Arabian Light DOR 1:200) to 231.86 RU (MC252 Discoverer Enterprise



ED_001324_00000953-00101

DOR 1:20) in Type I Oils and from 4.93 RU (Access Western Blend Dilbit DOR 0) to 116.97 RU (Heidrun DOR 1:20) in Type II Oils.

Results of the concentration dilution series showed that the HORIBA AquaLog was consistently capable of detecting dispersed oil in artificial seawater in the three oil types tested (Alaska North Slope, IFO-120, and MC252 Discoverer Enterprise) at all four DORs down to at least 50 ppb. However, detecting dispersed oil below 100 ppb necessitated increasing the integration time to 10 sec. per scan in order to collect sufficient data, which resulted in a total analysis time of approximately 30 minutes for each sample. Since the HORIBA AquaLog scans from high to low wavelengths and much of the fluorescence signal from petroleum resides at in the UV region, photobleaching of the sample as well as temperature effects certainly may have impacted these results.



ED_001324_00000953-00102

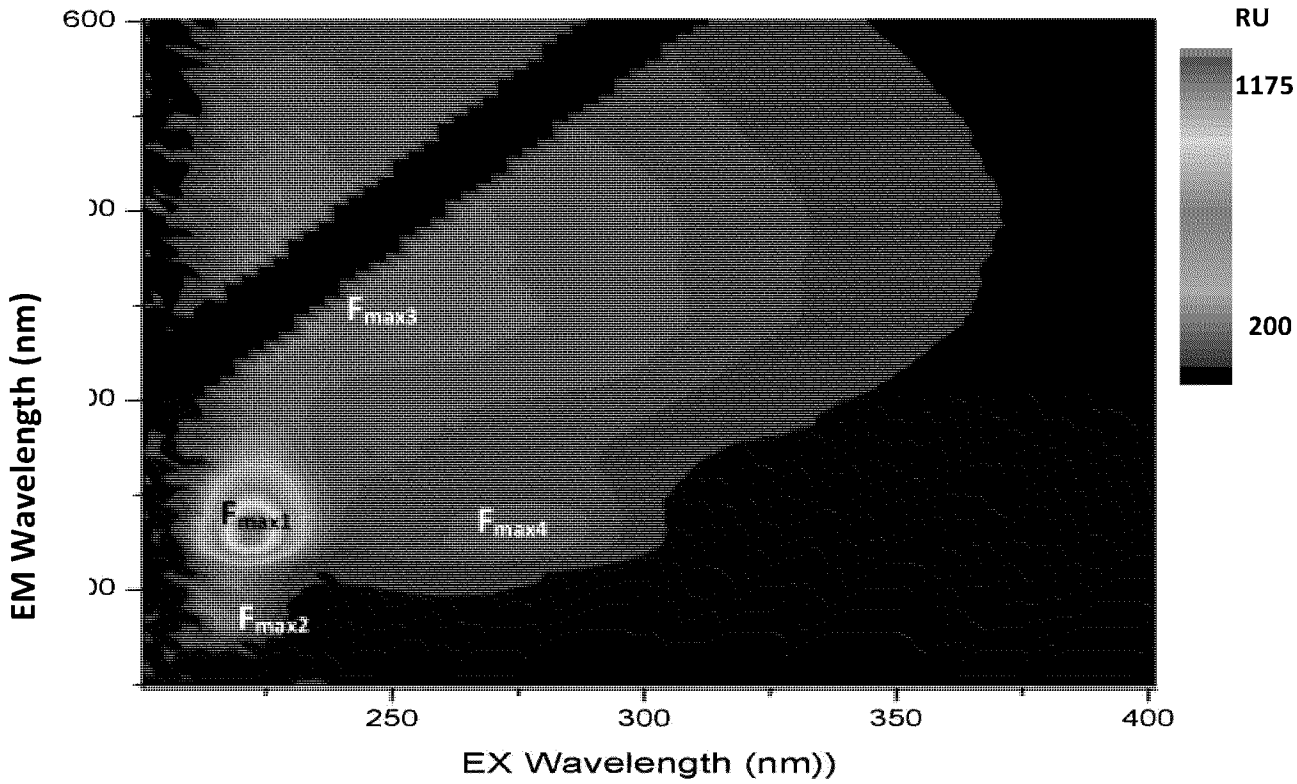


**Figure 43. Alaska North Slope dispersed oil in artificial seawater at DOR 1:20 with locations of $F_{max1}$, $F_{max2}$, $F_{max3}$ and $F_{max4}$ indicated. Note that maximum fluorescence intensity at $F_{max3}$ is mostly obscured by masking of second order Rayleigh scattering.**



ED_001324_00000953-00103

**Table 9. Fluorescence and chemical characteristics of EEMs. For full table of fluorescence properties, refer to Supplemental Table A.**

| **Type I Oils** | DOR | $F_{max}$[1] (RU) | FIR | Alkanes (µg/L) | 2-3 rings (µg/L) | 4-5 rings (µg/L) | **Type II Oils** | DOR | $F_{max}$[1] (RU) | FIR | Alkanes (µg/L) | 2-3 rings (µg/L) | 4-5 rings (µg/L) |
|---|---|---|---|---|---|---|---|---|---|---|---|---|---|
| Alaska North Slope | 0 | 697.07 | 21.59 | 375 | 160 | 8 | Access Western Blend Dilbit | 0 | 39.58 | 12.24 | 93 | 19 | 10 |
| | 1:200 | 715.01 | 37.73 | | | | | 1:200 | 46.52 | 14.20 | | | |
| | 1:100 | 839.60 | 6.87 | | | | | 1:100 | 49.84 | 8.97 | | | |
| | 1:20 | 1171.63 | 0.88 | 3019 | 566 | 65 | | 1:20 | 60.19 | 1.15 | 258 | 57 | 38 |
| Alaska North Slope (10% weathered) | 0 | 812.97 | 22.75 | 545 | 201 | 14 | Belridge Heavy | 0 | 118.69 | 5.31 | 42 | 52 | 30 |
| | 1:200 | 831.70 | 21.86 | | | | | 1:200 | 161.75 | 5.65 | | | |
| | 1:100 | 828.06 | 8.98 | | | | | 1:100 | 140.96 | 4.93 | | | |
| | 1:20 | 1109.51 | 0.93 | 3312 | 598 | 74 | | 1:20 | 147.09 | 3.51 | 44 | 84 | 52 |
| Arabian Light | 0 | 400.42 | 7.90 | 733 | 124 | 12 | Cold Lake Dilbit | 0 | 120.61 | 20.72 | 155 | 94 | 23 |
| | 1:200 | 357.62 | 12.06 | | | | | 1:200 | 120.65 | 18.01 | | | |
| | 1:100 | 426.82 | 2.68 | | | | | 1:100 | 125.85 | 13.11 | | | |
| | 1:20 | 701.75 | 0.39 | 6004 | 642 | 103 | | 1:20 | 133.15 | 1.94 | 368 | 210 | 58 |
| Brent | 0 | 646.18 | 7.78 | 1068 | 183 | 12 | Heidrun | 0 | 902.69 | 4.61 | 382 | 392 | 43 |
| | 1:200 | 660.37 | 6.88 | | | | | 1:200 | 909.47 | 6.32 | | | |



ED_001324_00000953-00104

| | | | | | | | | | | | | | |
|---|---|---|---|---|---|---|---|---|---|---|---|---|---|
| | 1:100 | 708.16 | 2.03 | | | | | 1:100 | 964.31 | 3.80 | | | |
| | 1:20 | 1098.42 | 0.69 | 5954 | 553 | 59 | | 1:20 | 1098.90 | 0.80 | 684 | 620 | 82 |
| Federated | 0 | 574.35 | 3.72 | 1921 | 238 | 30 | Hondo | 0 | 283.04 | 21.99 | 412 | 84 | 3 |
| | 1:200 | 607.97 | 2.06 | | | | | 1:200 | 312.27 | 18.73 | | | |
| | 1:100 | 645.28 | 0.97 | | | | | 1:100 | 274.80 | 20.66 | | | |
| | 1:20 | 1223.17 | 0.37 | 6501 | 617 | 87 | | 1:20 | 288.01 | 17.01 | 319 | 74 | 1 |
| Gullfaks | 0 | 937.00 | 5.86 | 762 | 373 | 26 | IFO-40 | 0 | 1173.91 | 33.15 | 1324 | 560 | 172 |
| | 1:200 | 934.42 | 5.64 | | | | | 1:200 | 1246.63 | 59.63 | | | |
| | 1:100 | 933.08 | 3.30 | | | | | 1:100 | 1338.56 | 42.94 | | | |
| | 1:20 | 1524.21 | 0.69 | 1943 | 749 | 61 | | 1:20 | 1458.79 | 4.40 | 4354 | 1508 | 570 |
| Hibernia | 0 | 938.08 | 7.46 | 2289 | 335 | 24 | IFO-120 | 0 | 3030.69 | 117.26 | 343 | 696 | 51 |
| | 1:200 | 951.49 | 3.22 | | | | | 1:200 | 2903.21 | 334.13 | | | |
| | 1:100 | 978.62 | 1.66 | | | | | 1:100 | 3090.23 | 88.73 | | | |
| | 1:20 | 1812.41 | 0.50 | 6095 | 635 | 59 | | 1:20 | 2527.73 | 42.66 | 840 | 3097 | 122 |
| | 0 | 998.50 | 4.97 | 1578 | 350 | 30 | IFO-180 | 0 | 1263.05 | 38.88 | 866 | 645 | 326 |
| | 1:200 | 1009.18 | 3.07 | | | | | 1:200 | 1394.42 | 42.40 | | | |



ED_001324_00000953-00105

| | | | | | | | | | | | | | |
|---|---|---|---|---|---|---|---|---|---|---|---|---|---|
| Hibernia | 0 | 938.08 | 7.46 | 2289 | 335 | 24 | IFO-120 | 0 | 3030.69 | 117.26 | 343 | 696 | 51 |
| | 1:200 | 951.49 | 3.22 | | | | | 1:200 | 2903.21 | 334.13 | | | |
| | 1:100 | 978.62 | 1.66 | | | | | 1:100 | 3090.23 | 88.73 | | | |
| | 1:20 | 1812.41 | 0.50 | 6095 | 635 | 59 | | 1:20 | 2527.73 | 42.66 | 840 | 3097 | 122 |
| MC252 (Discoverer Enterprise) | 1:100 | 1085.54 | 1.23 | | | | | 1:100 | 1703.55 | 5.76 | | | |
| | 1:20 | 1998.60 | 0.39 | 3992 | 583 | 69 | | 1:20 | 1532.99 | 12.28 | 2933 | 1986 | 1109 |
| MC252 (generic) | 0 | 857.35 | 4.81 | 1468 | 267 | 21 | IFO-300 | 0 | 720.55 | 65.84 | 446 | 295 | 192 |
| | 1:200 | 877.78 | 3.11 | | | | | 1:200 | 443.51 | 48.50 | | | |
| | 1:100 | 964.02 | 0.97 | | | | | 1:100 | 465.91 | 75.70 | | | |
| | 1:20 | 1795.13 | 0.41 | 5093 | 624 | 68 | | 1:20 | 661.50 | 43.02 | 366 | 248 | 162 |
| MESA | 0 | 757.84 | 20.04 | 1388 | 268 | 24 | Lago | 0 | 352.22 | 12.53 | 1289 | 146 | 18 |
| | 1:200 | 806.76 | 12.21 | | | | | 1:200 | 398.40 | 11.30 | | | |
| | 1:100 | 745.17 | 6.33 | | | | | 1:100 | 367.75 | 9.10 | | | |
| | 1:20 | 1107.09 | 1.09 | 4088 | 524 | 62 | | 1:20 | 453.10 | 0.93 | 4221 | 346 | 52 |
| Sea Rose | 0 | 1145.29 | 10.65 | 1583 | 320 | 19 | Santa Clara | 0 | 157.30 | 23.17 | 209 | 28 | 0 |
| | 1:200 | 1223.98 | 7.40 | | | | | 1:200 | 147.55 | 27.03 | | | |
| | 1:100 | 1236.63 | 2.16 | | | | | 1:100 | 154.98 | 19.29 | | | |



ED_001324_00000953-00106

| | | | | | | | | | | | | | |
|---|---|---|---|---|---|---|---|---|---|---|---|---|---|
| Hibernia | 0 | 938.08 | 7.46 | 2289 | 335 | 24 | IFO-120 | 0 | 3030.69 | 117.26 | 343 | 696 | 51 |
| | 1:200 | 951.49 | 3.22 | | | | | 1:200 | 2903.21 | 334.13 | | | |
| | 1:100 | 978.62 | 1.66 | | | | | 1:100 | 3090.23 | 88.73 | | | |
| | 1:20 | 1812.41 | 0.50 | 6095 | 635 | 59 | | 1:20 | 2527.73 | 42.66 | 840 | 3097 | 122 |
| | 1:20 | 1973.55 | 0.72 | 5903 | 721 | 70 | | 1:20 | 169.39 | 7.39 | 1196 | 81 | 3 |
| Terra Nova | 0 | 665.50 | 6.81 | 1038 | 186 | 11 | Scotian Shelf Condensate | 0 | 946.52 | 43.40 | 447 | 127 | 0 |
| | 1:200 | 719.72 | 3.96 | | | | | 1:200 | 1408.59 | 51.61 | | | |
| | 1:100 | 821.24 | 1.47 | | | | | 1:100 | 1487.16 | 49.14 | | | |
| | 1:20 | 1380.34 | 0.40 | 5608 | 540 | 50 | | 1:20 | 1337.98 | 51.42 | 1057 | 220 | 0 |
| | | | | | | | Vasconia | 0 | 844.93 | 34.44 | 2550 | 415 | 59 |
| | | | | | | | | 1:200 | 828.37 | 53.23 | | | |
| | | | | | | | | 1:100 | 835.62 | 29.32 | | | |
| | | | | | | | | 1:20 | 935.79 | 3.64 | 4402 | 631 | 96 |



ED_001324_00000953-00107

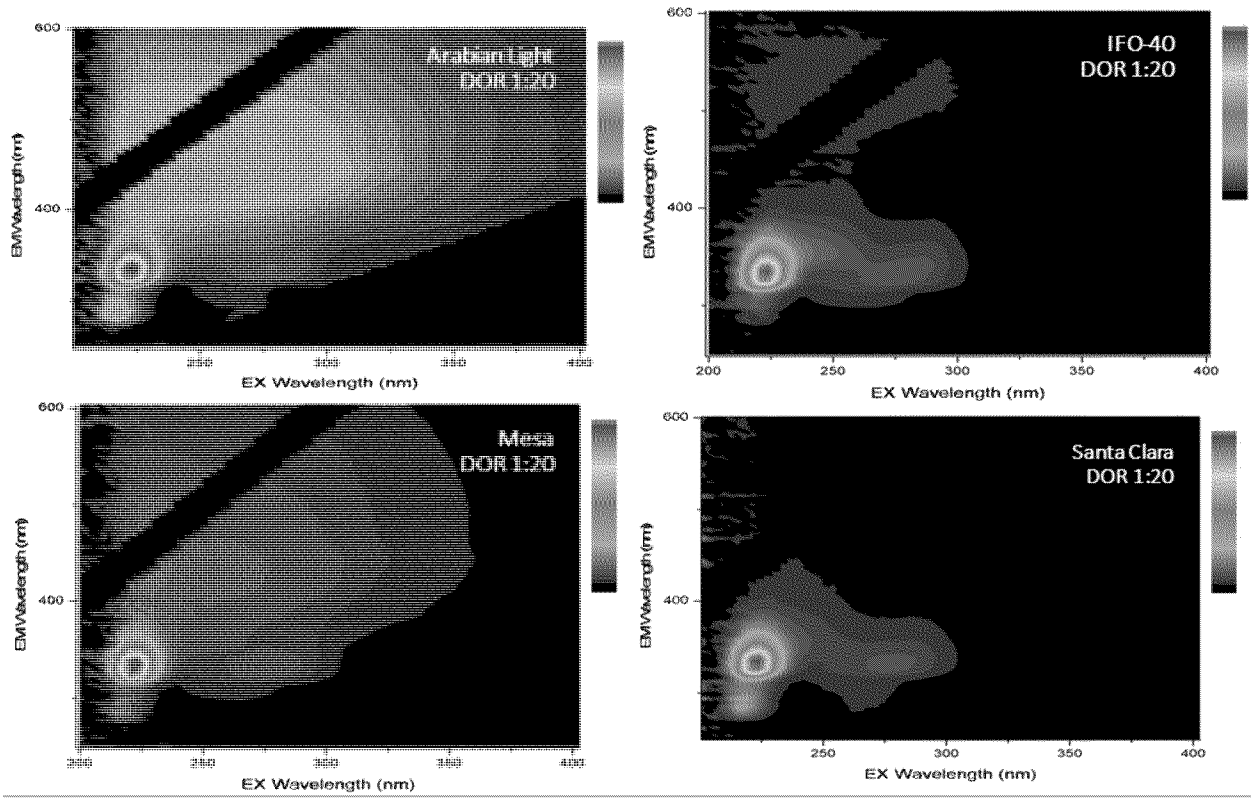


**Figure 44. Example EEMs of Type I and II oils for DOR = 1:20. Arabian Light and IFO-40 are light oils. Mesa and Santa Clara are medium oils.**



ED_001324_00000953-00108

### ***B.3.2 Fluorescence as a Function of Chemistry***

Samples of dispersed oil in artificial seawater (DOR 0 and DOR 1:20 for each oil type), extracted into methylene chloride were analyzed via GC-MS. Total 2-3 ring benzenes, total 4-5 ring benzenes, and total alkanes were all plotted against $F_{max1}$, $F_{max2}$, $F_{max3}$, and $F_{max4}$. Results showed best correlation between total 2-3 ring benzenes and fluorescence intensity. Both $F_{max1}$ and $F_{max4}$ had the best overall fit, with less well-correlated results for total 2-3 ring benzenes with $F_{max2}$ and $F_{max3}$, perhaps due to the confounding presence of double peaks and sub-peaks in the latter two. A linear relationship was found between concentration of total 2-3 ring benzenes and fluorescence intensity ($F_{max1}$ and $F_{max4}$) at DOR 0, while a logarithmic relationship best modeled the fit at DOR 1:20 (Figures 45-48).

With respect to the chemistry - fluorescence intensity relationship, all four Intermediate Fuel Oils (IFO-40, IFO-120, IFO-180, and IFO-300) as well as Scotian Shelf Condensate, were anomalous and thus were eliminated from these analyses. Three of the four Intermediate Fuel Oils had the highest concentration of benzene ring compounds (IFO-40, 120 and 180), and all four IFO types were the only oils to contain the coal-tar derivative anthracene, perhaps partially responsible for these anomalous results. Total alkanes as a function of fluorescence intensity was found to be loosely correlated, as total concentration increased overall in relation to fluorescence intensity with no clear relationship.



ED_001324_00000953-00109

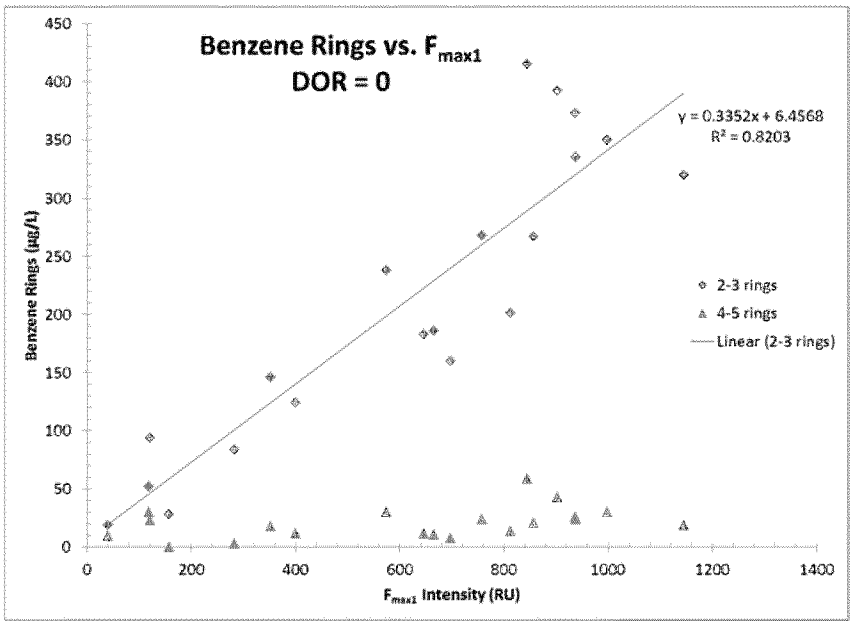


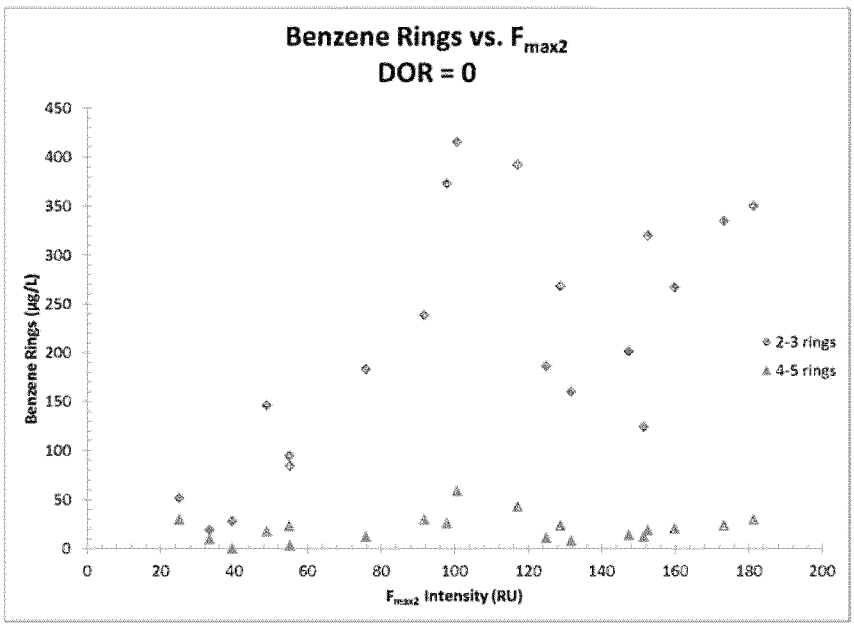


**Figure 45. For all oil types at DOR0, total concentration of 2-3 ring benzene and 4-5 ring benzene compounds (µg/L) against fluorescence intensity (RU) at $F_{max1}$ (top) and $F_{max2}$ (bottom). A linear correlation exists between 2-3 ring benzenes and fluorescence intensity at $F_{max1}$; however, there is only a general linear correlation between 2-3 ring benzenes and fluorescence intensity at $F_{max2}$ and no correlation at all between 4-5 ring benzenes and fluorescence intensity at either peak.**



ED_001324_00000953-00110

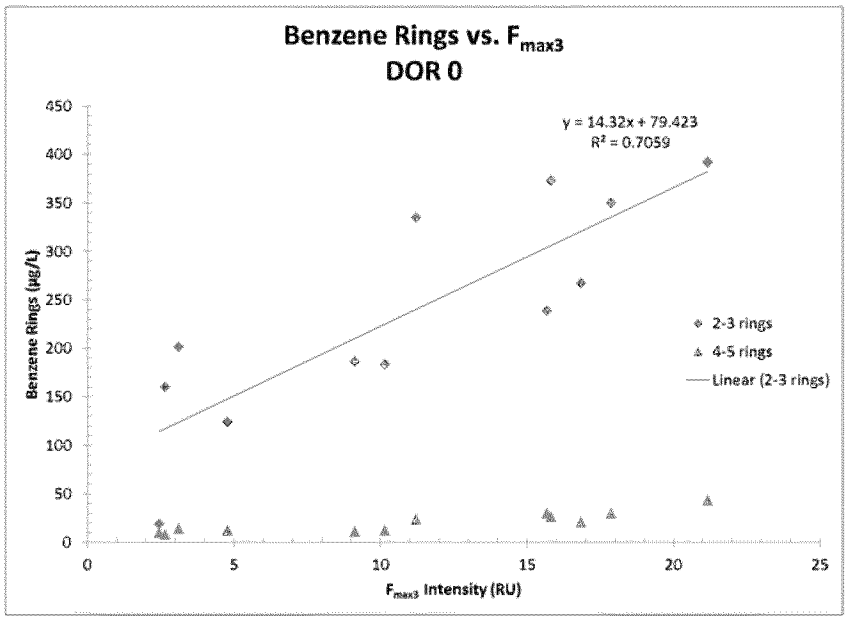


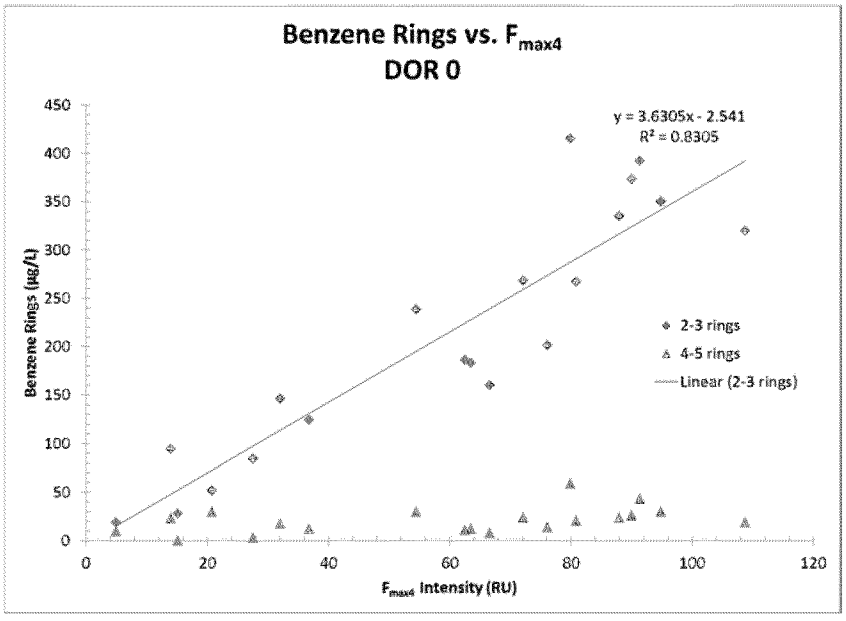


**Figure 46. For all oil types at DOR0, total concentration of 2-3 ring benzene and 4-5 ring benzene compounds (µg/L) against fluorescence intensity (RU) at $F_{max3}$ (top) and $F_{max4}$ (bottom). A linear correlation exists between 2-3 ring benzenes and fluorescence intensity at both $F_{max3}$ and $F_{max4}$; however, no correlation exists between 4-5 ring benzenes and fluorescence intensity at either peak.**



ED_001324_00000953-00111

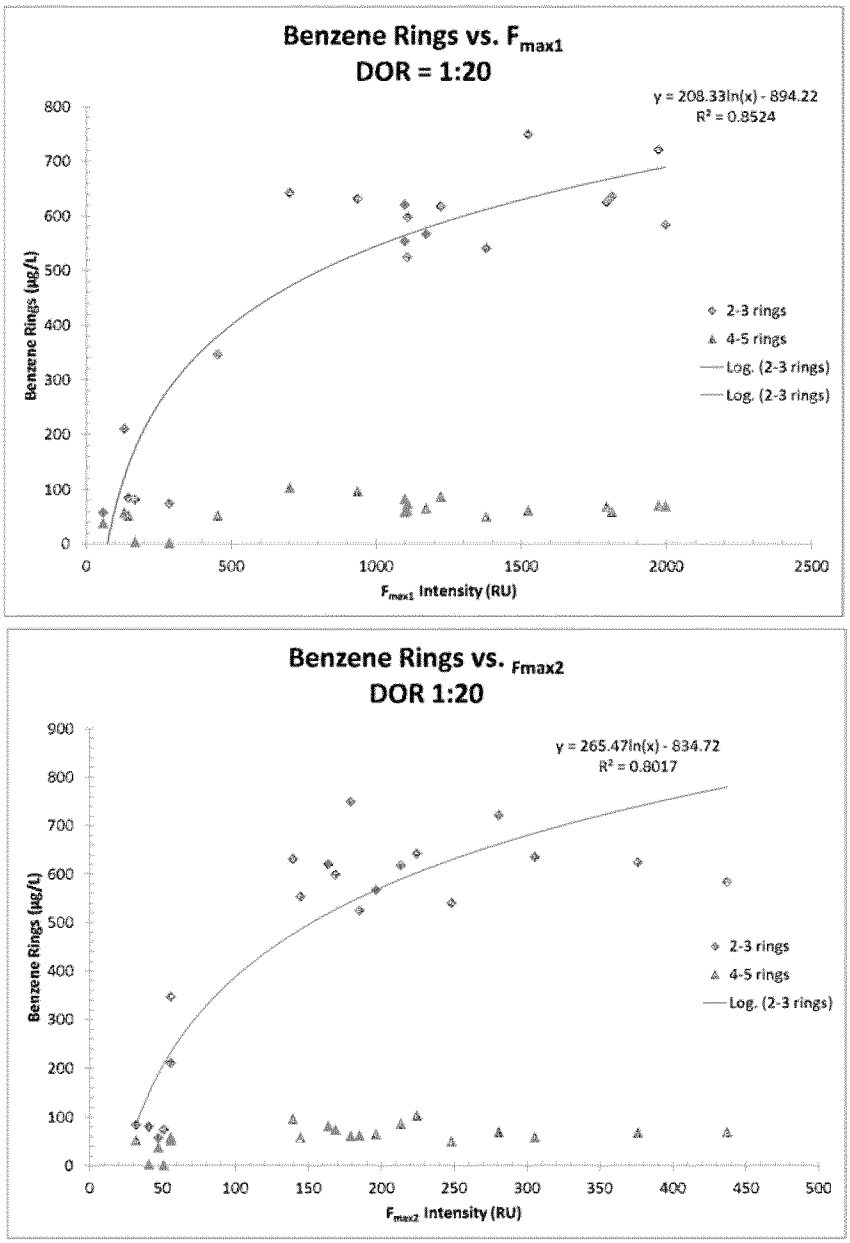


**Figure 47. For all oil types at DOR1:20, total concentration of 2-3 ring benzene and 4-5 ring benzene compounds (µg/L) against fluorescence intensity (RU) at $F_{max1}$ (top) and $F_{max2}$ (bottom). An apparent logarithmic correlation exists between 2-3 ring benzenes and fluorescence intensity at both $F_{max1}$ and $F_{max2}$; however, there no correlation between 4-5 ring benzenes and fluorescence intensity at either peak.**

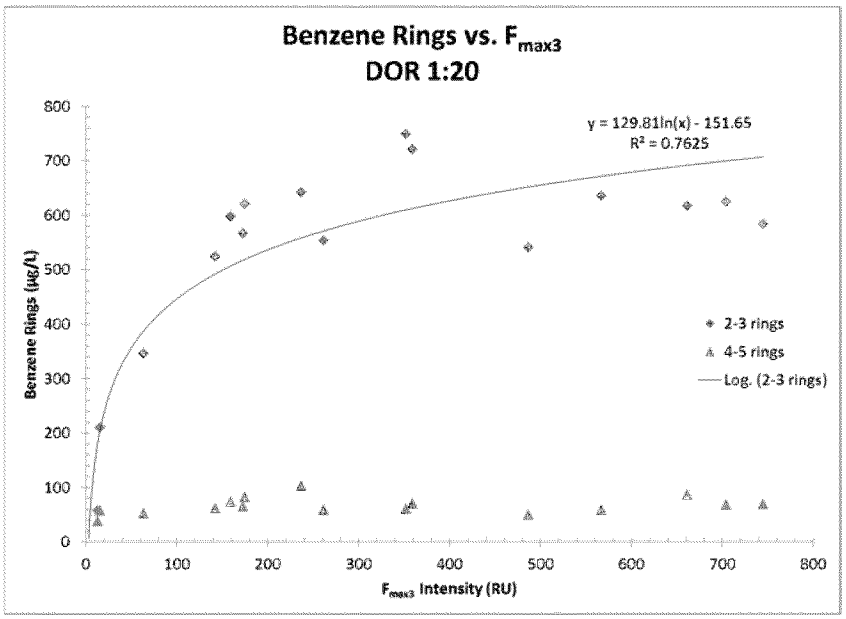


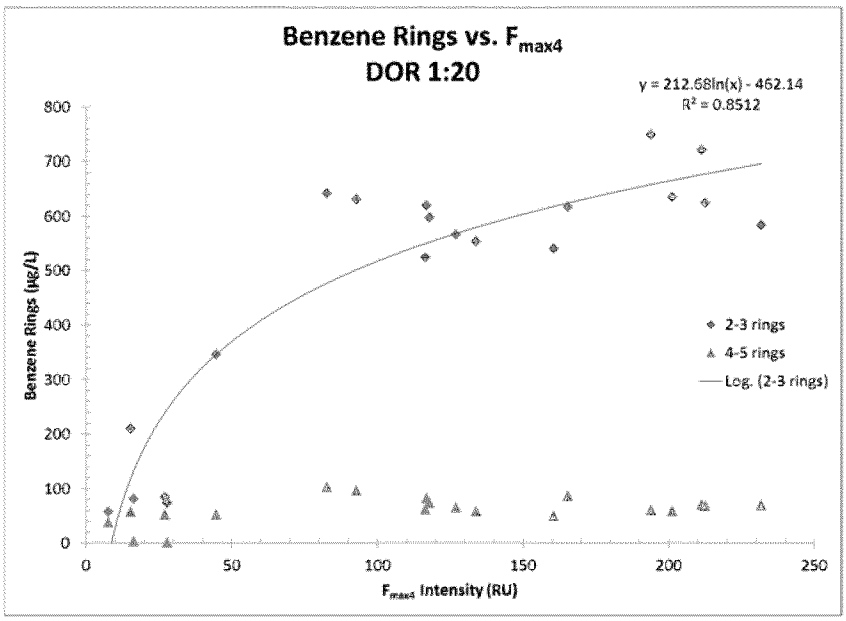


**Figure 48. For all oil types at DOR1:20, total concentration of 2-3 ring benzene and 4-5 ring benzene compounds (µg/L) against fluorescence intensity (RU) at Fmax3 (top) and Fmax4 (bottom). An apparent linear correlation exists between 2-3 ring benzenes and fluorescence intensity at both Fmax3 and Fmax4; however, no correlation exists between 4-5 ring benzenes and fluorescence intensity at either peak.**

### ***B.3.3 Wave Tank and Baffle Flask EEM Comparison***

In addition to the EEMs generated from the BFT of 25 oil types, EEMS were also generated from the discrete sample collection during the wave tank experiments using South Louisiana Crude oil (SLC) in Task A of this project. Samples for EEM analysis were collected and immediately analyzed on the same Horiba Aqualog at DFO using identical analysis protocols and data processing. A comparison of SLC MC252 EEMs for varying DOR from the BFT (left) and the wave tank (right) experiments are illustrated in Figure 49. Note that that the contour coloring for the peaks is identical between experiments, but the baseline color varied, where black was used for the BFT EEMs and blue used for tank EEMs, but the appearance of the blue color this is not to be confused with the presence of higher fluorescence in regions away from the peak fluorescence. Fluorescence Intensity Ratios (FIR) were calculated for the tank EEMs and found to be between 7.1 and 9.1 for DOR = 0, 1.3 and 4.3 for DOR = 1:100 and 0.6 and 0.8 for DOR = 1:20. This is follows the findings of Bugden et al., 2008 where a decrease in FIR is observed with the addition of dispersant. It is also consistent with the BFT EEMs which show a 4.9 for DOR = 0 and 0.4 for DOR = 1:20 (Supplemental Table A). These results indicate that FIR is a robust means of confirming dispersion effectiveness for SLC oil.



ED_001324_00000953-00114

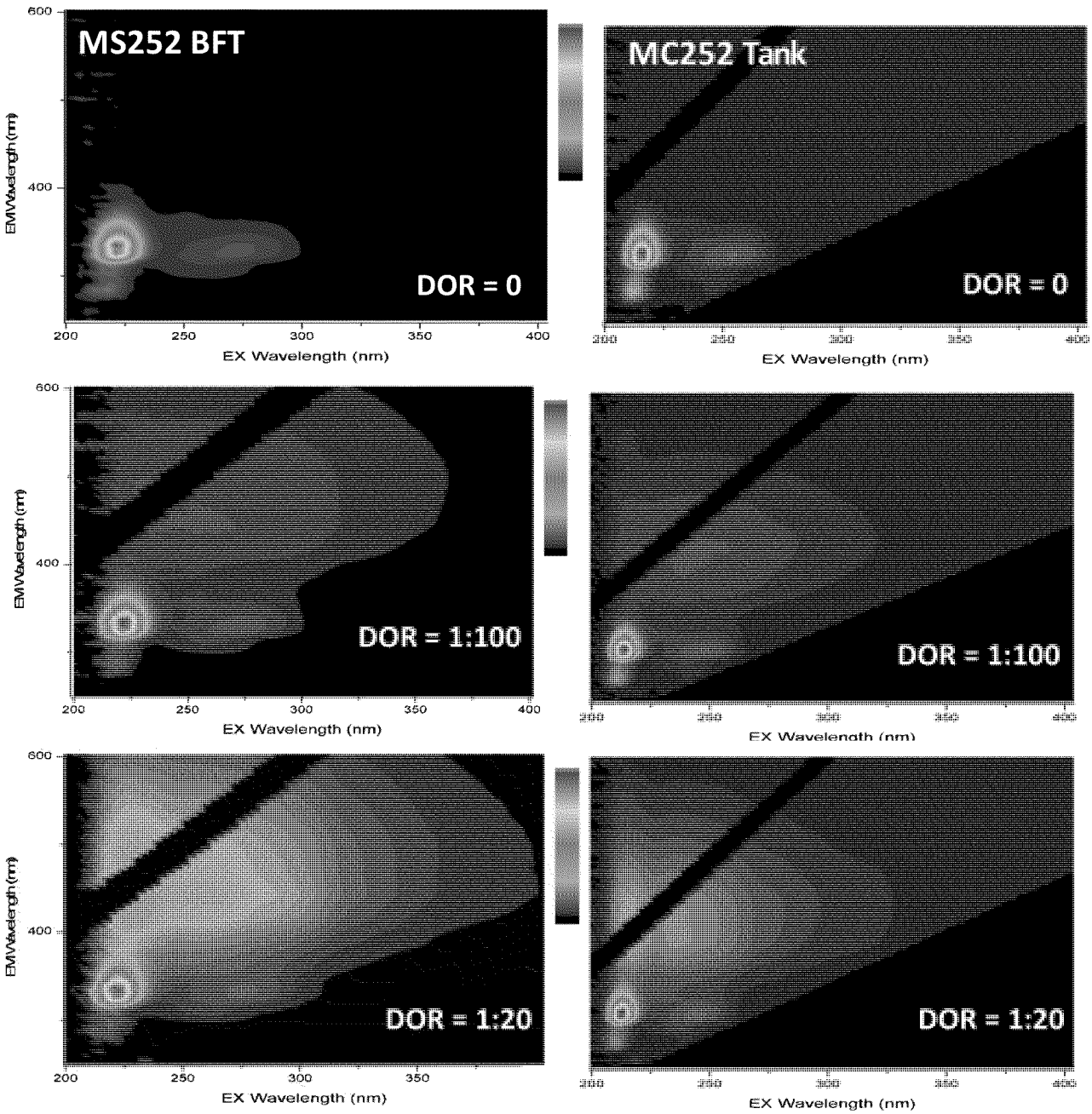


**Figure 49. South Louisiana Crude MC252 EEMS from BFT (left panels) and tank experiments (right Panels) for DOR = 0, 1:100 and 1:20.**



ED_001324_00000953-00115

### ***B.3.4 PARAFAC Modeling***

***DOR = 0***

PARAFAC modelling was performed using SOLO software (Eigenvector, Inc.) after importing the flask #1 sample file of each of 22 oil types from the baffle flask experiments for DOR = 0 (Table 10). IFO-120, IFO-300 and Scotian Shelf Condensate were not included due to anomalous fluorescence profiles; however, IFO-40 and IFO-180 were retained for these analyses. A five-factor model was fit to the dataset without application of any pre-processing options, then with application of constraints for non-negativity, EEM filtering (12nm First Order Rayleigh and 24nm Second Order Rayleigh), and normalization methods 1-Norm (area = 1) and inf-Norm (maximum = 1). The initial 5-factor model without any constraints explained 97.623% of the data, core consistency was high (92%), and residuals were low and randomly distributed; however, split half analysis showed 0% similarity between the splits and overall model. Further, Mode 2 (emission) factors 4 and 5 contained significant negative regions, factor 4 appeared to be modelling only noise, and factor 5 contained two significant and equal peaks, all indications of poor fit. Application of the non-negativity constraint and re-running the 5-factor model resulted in a slight reduction in percentage of data explained by the model (96.544%), and a slight reduction in core consistency (88%). Split half analysis resulted in only 0.8% agreement between splits and the overall model, while factor 4 now contained the two significant and equal peaks seen previously in factor 5, and factor 5 now appeared to be modelling only noise. Addition of EEM filtering as well as non-negativity to a third PARAFAC analysis resulted in a very slight increase to 96.717% of the data explained by the model and an increase in core consistency to 91%, but split half analysis dropped to 0% agreement between splits and the overall model; aforementioned problems with Mode 2 factors 4 and 5 remained as well. Application of 1-Norm (area = 1) normalization constraint along with non-negativity and EEM filtering and re-running the 5-factor model provided nearly identical results, with 96.876% of data explained, 87% core consistency, and the same problems with Mode 2 factors 4 and 5; however, split half analysis improved slightly to 4.6%. Changing the normalization method to inf-Norm (maximum = 1) method and re-running the 5-factor model resulted in 95.55% of data explained by the model and 81% core consistency, but problems with Mode 2 factors 4 and 5 remained. Split half analysis again resulted in 0%



ED_001324_00000953-00116

similarity between splits and the overall model. In order to find the optimal number of factors to fit the data, 4-factor models were run with non-negativity, EEM filtering, and each type of normalization applied separately, followed by 3-factor models taken through the same process. The 3-factor model with application of non-negativity, EEM filtering and normalization proved best overall. Both methods of normalization gave results within 1-3% on all measures of goodness of model fit; however, the model using the inf-Norm (maximum = 1) normalization method was selected as the more conservative method, preserving differences in spectral shape among oil types. The 3-factor model represented 95.067% of the data with 93% core consistency, good variation per component, and low, randomly distributed residuals. The split half analysis showed 75.2% similarity between splits and the overall model.



ED_001324_00000953-00117

**Table 10. Oil Types used for PARAFAC Analysis**

| Type I | Type II |
|---|---|
| ANS | Access Western Blend Dilbit |
| ANS 10% weathered | Belridge Heavy |
| Arabian Light | Cold Lake Dilbit |
| Brent | Heidrun |
| Federated | Hondo |
| Gullfaks | IFO-40 |
| Hibernia | IFO-180 |
| MC252 – Discoverer Enterprise | Lago |
| MC252 – generic | Santa Clara |
| MESA | Vasconia |
| Sea Rose | |
| Terra Nova | |

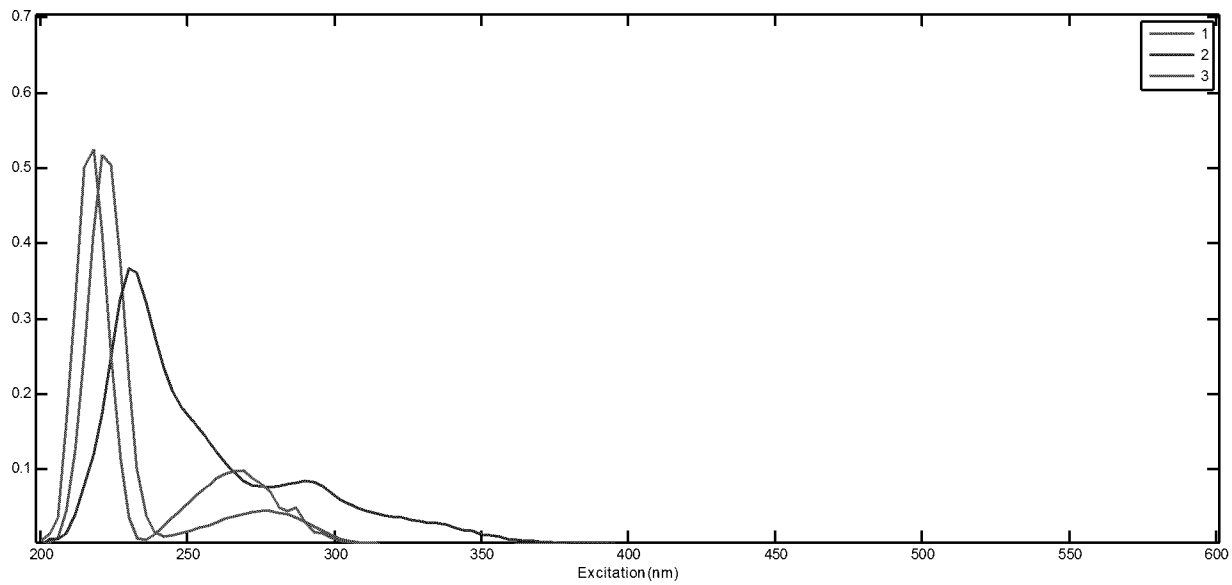


**Figure 50. Graph of loadings for Mode 3 - excitation for all 22 oils at DOR = 0 resulting from 3-factor PARAFAC model.**



ED_001324_00000953-00118

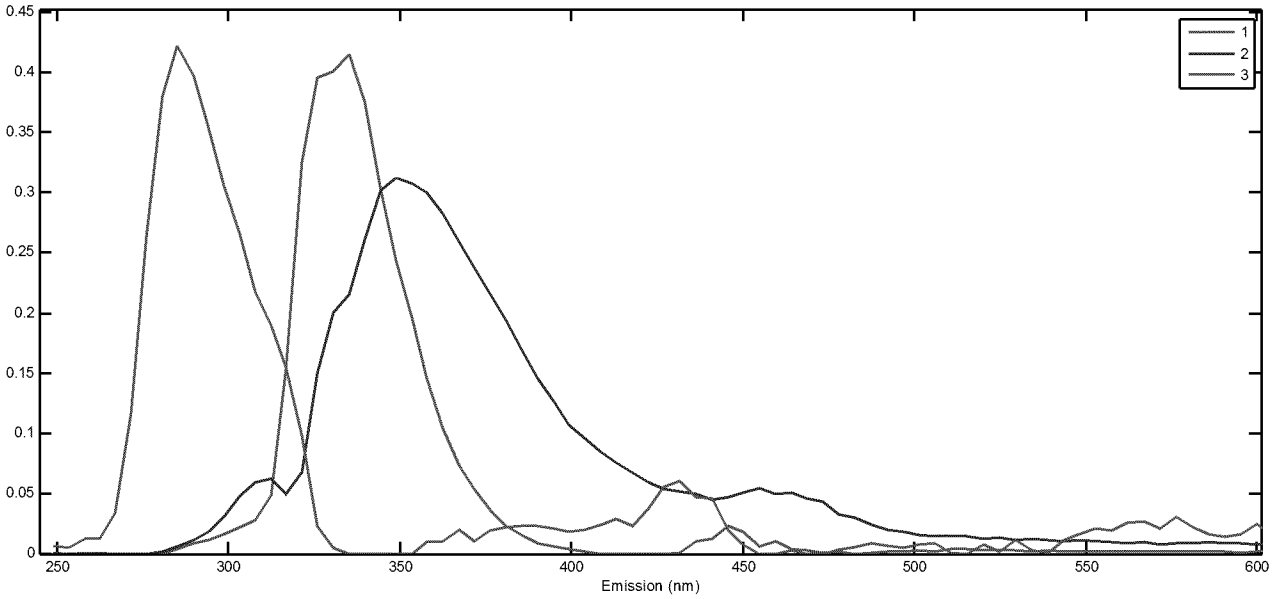


**Figure 51. Graph of loadings for Mode 2 - emission for all 22 oils at DOR = 0 resulting from 3-factor PARAFAC model.**

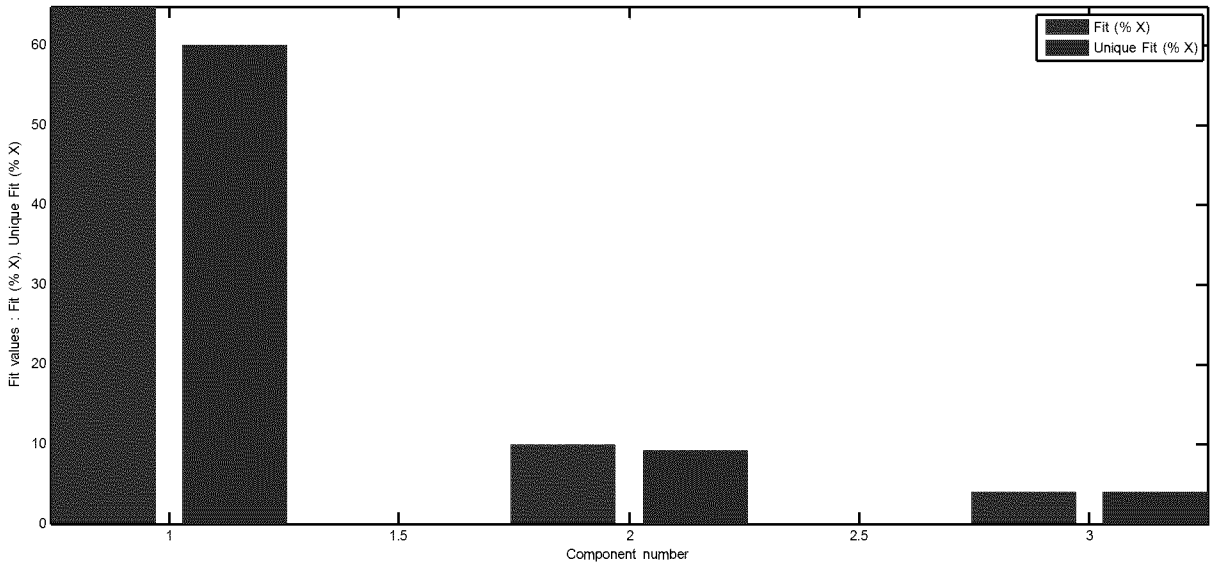


**Figure 52. Fit (% X) vs. unique fit (% X) for 3-factor PARAFAC model run on all 22 oil types at DOR = 0.**



ED_001324_00000953-00119

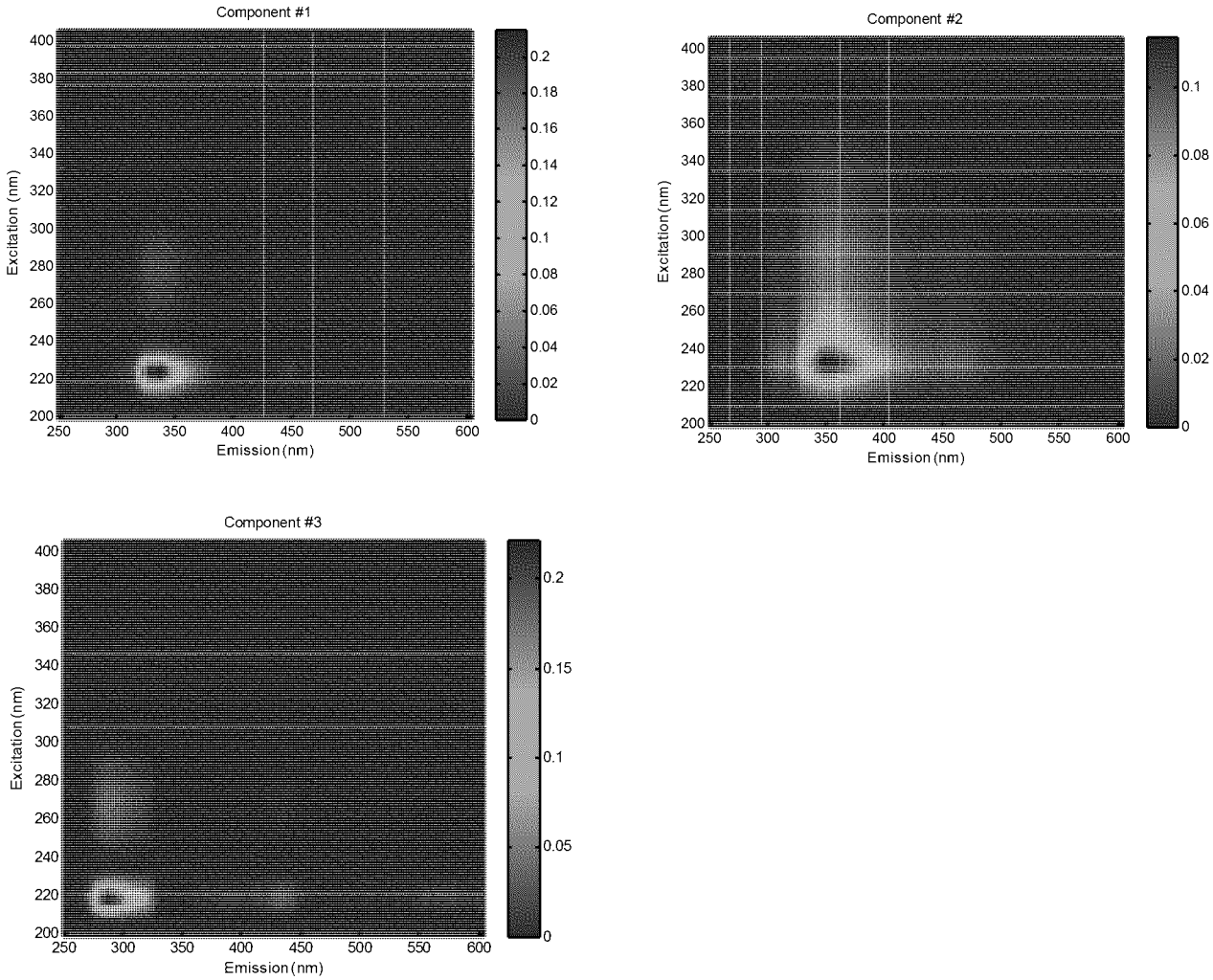


**Figure 53. EEM views of factor 1 with Fmax at Ex/Em = 224/340nm (top left), factor 2 with Fmax at Ex/Em = 233/353nm (top right), and factor 3 with Fmax at ex/em = 218/290 (bottom).**



ED_001324_00000953-00120

***DOR = 1:100***

Sample files from the DOR = 1:100 baffle flask experiments (flask #1) were uploaded, and a five-factor PARAFAC model was performed using the previously determined optimal combination of pre-processing constraints—non-negativity, EEM filtering (12 and 24 nm for First and Second Order Rayleigh, respectively), and inf-Norm normalization. Core consistency was high (93%) and the model explained 96.726% of the data; however, variation per component was very low for factor 5, and the loadings for Mode 2 (emission) showed factor 5 appeared to be modelling noise. Split half analysis showed similarity between splits and overall model of only 5.8%. Re-running the model with six factors resulted in a slight improvement to 96.855% of the data explained and good core consistency of 89%; however, both factors 5 and 6 appeared to be modelling noise and had low variation per component. Split half analysis failed, with 0% similarity between splits and the overall model. A four-factor model resulted in 96.569% of the data explained by the model and core consistency of 96%. Variation per component was good for all four factors, and loadings for Modes 2 and 3 contained only appropriately-shaped emission and excitation curves, respectively. Residuals were low and randomly distributed. Split half analysis was excellent, with similarity between splits and overall model of 83.5%.



ED_001324_00000953-00121

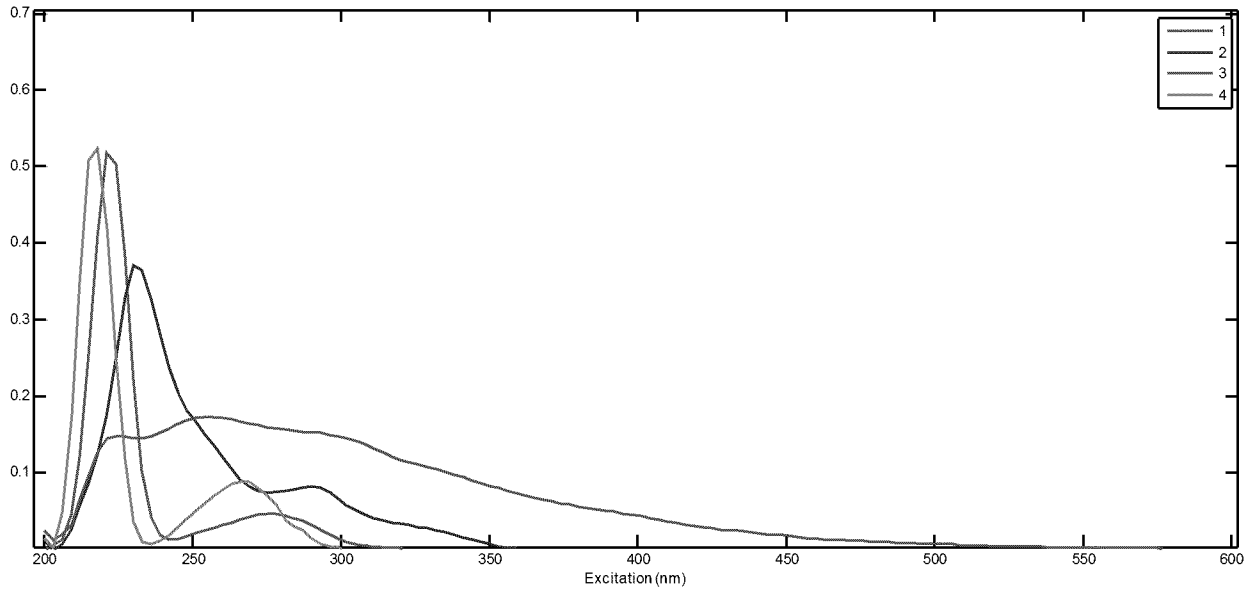


**Figure 54. Graph of loadings for Mode 3 - excitation for all 22 oils at DOR = 1:100 resulting from 4-factor PARAFAC model.**



ED_001324_00000953-00122

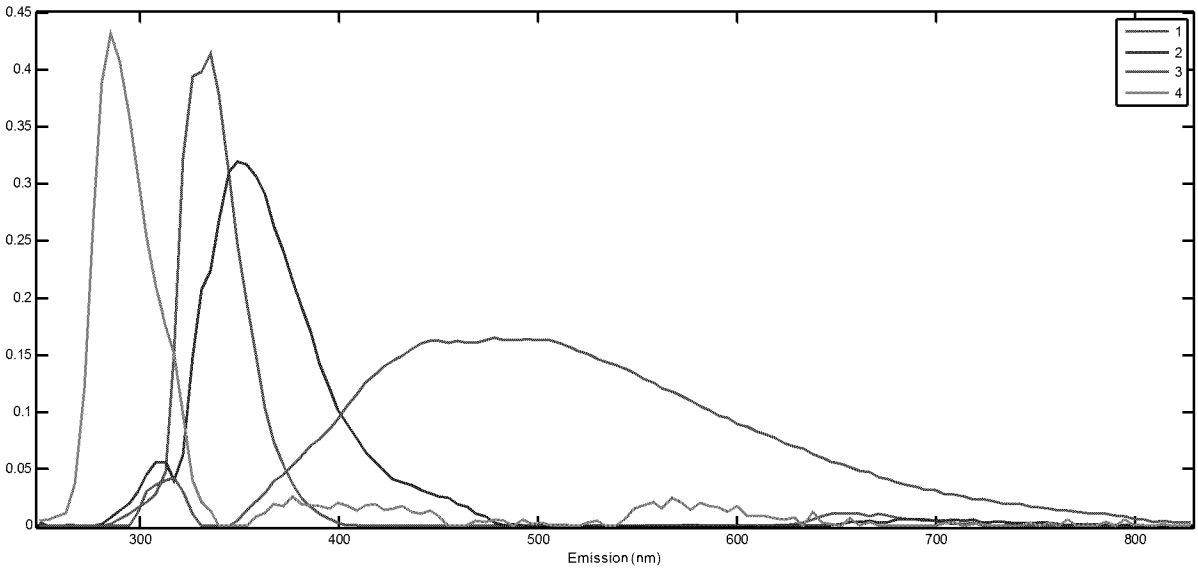


**Figure 55. Graph of loadings for Mode 2 - emission for all 22 oils at DOR = 1:100 resulting from 4-factor PARAFAC model.**

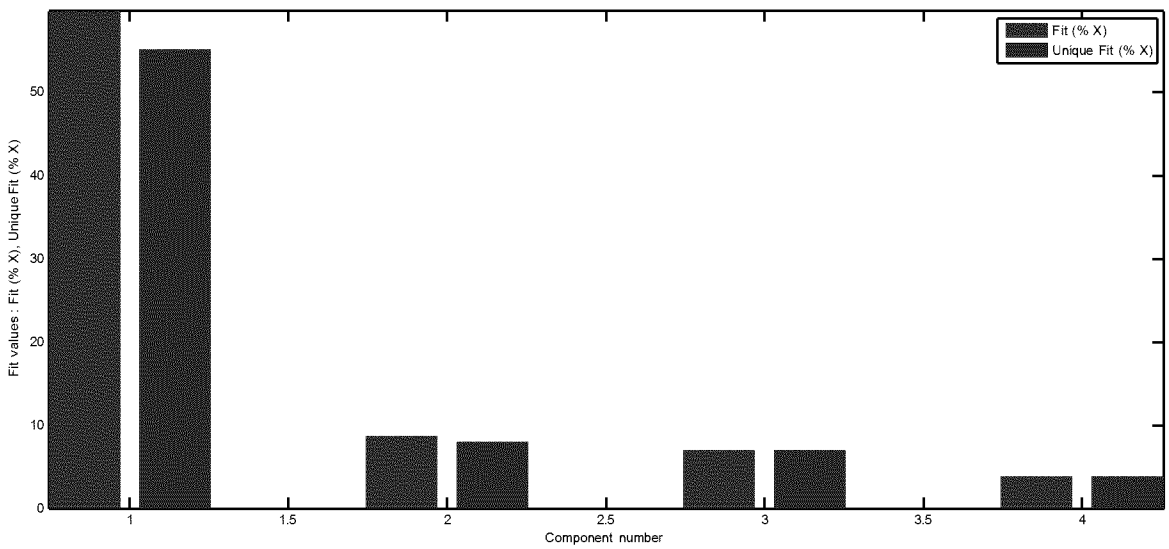


**Figure 56. Fit (% X) vs. unique fit (% X) for 4-factor PARAFAC model run on all 22 oil types at DOR = 1:100.**



ED_001324_00000953-00123

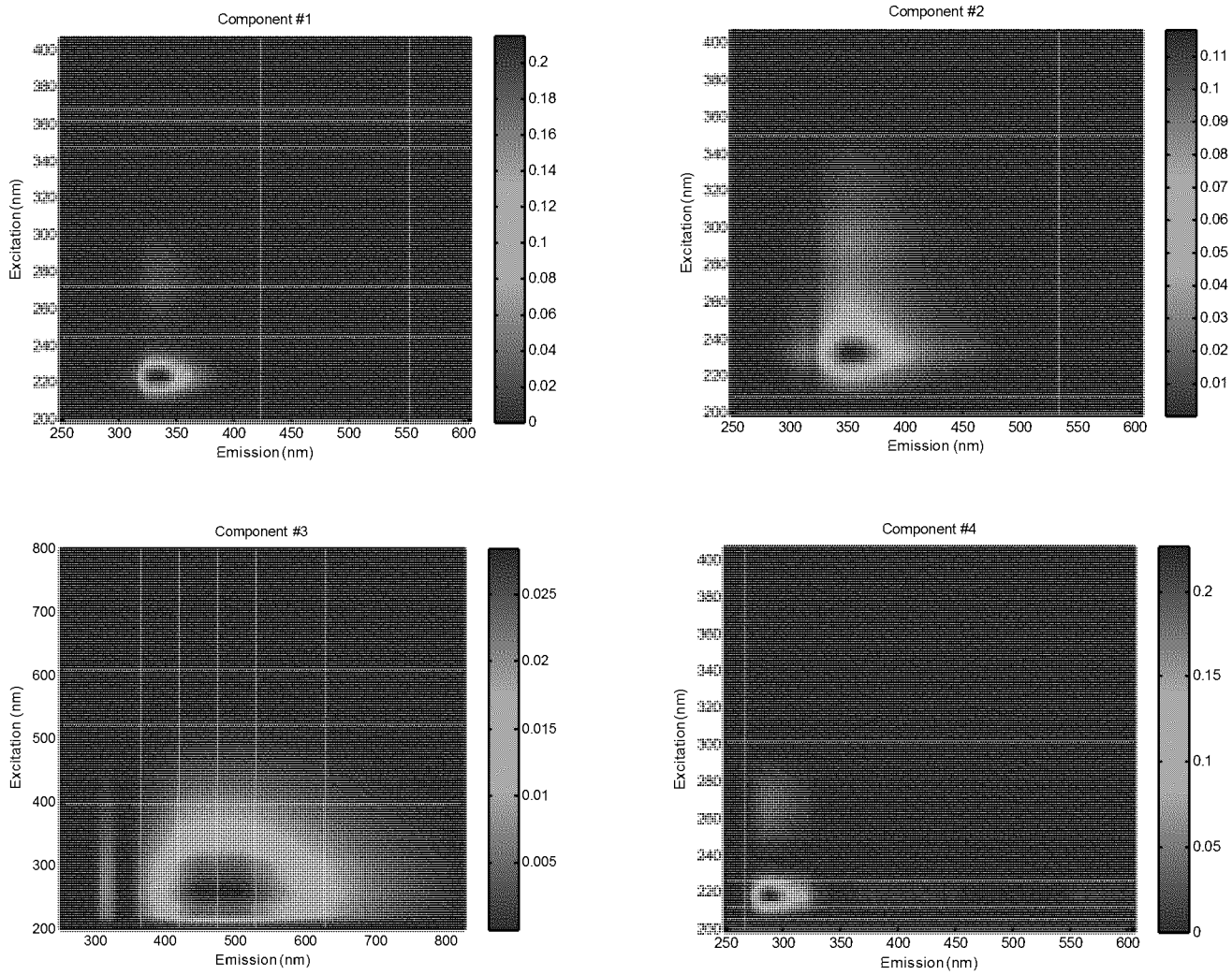


**Figure 57. EEM view of factor 1 with Fmax at Ex/Em = 221/335nm (top left), factor 2 with Fmax at Ex/Em = 230/349 nm (top right), factor 3 with Fmax at Ex/Em = 254/445-506 nm (bottom left), and factor 4 with Fmax at Ex/Em = 218/285 nm (bottom right).**



ED_001324_00000953-00124

***DOR = 1:20***

Sample files from flask #1 of the DOR = 1:20 baffle flask experiments were loaded, and based on results obtained in previous analyses, a five-factor model with non-negativity, EEM filtering (12 and 24nm First and Second Order Rayleigh, respectively), and inf-Norm normalization constraints was performed. Results showed 95.797% of the data was explained by the model with 87% core consistency and good variation per component; however, the relative percent difference between fit and unique fit for factor 1 was 55%. Residuals were low and randomly distributed and loadings for Mode 2 and 3 appeared to be valid emission and excitation curves. Unfortunately, split half analysis was 0% between splits and the overall model. In order to obtain better results, a six-factor model was performed; however, split half analysis was still 0%. Stepping through individual sample residuals showed an anomalously high negative peak in Arabian Light sample, so the data was reloaded with the sample file from baffle flask #2 for that oil type and a new five-factor model run. Results obtained showed 95.999% of the data explained by the model with 86% core consistency; however, split half analysis was still just 0.1%. Repeating the six-factor model with the new sample set resulted in 96.143% of data explained by the model and 87% core consistency; split half analysis revealed a 5.5% similarity between splits and the overall model. Running a seven-factor model resulted in an error message of <0% core consistency due to two or more components fitting the same feature. A four-factor model explained 95.567% of the model with 94% core consistency. Split half analysis resulted in 40.3% similarity between splits and overall model; however, visual inspection of the splits showed one peak significantly shifted and transformed from the model curve in split 2. These results indicate that it may be impossible to represent all 22 types of oil with one PARAFAC model. Visual inspection of the loadings for Mode 2 from the six-factor model suggest that there may be two underlying types, each with three factors, since there are three pairs of similar curves.



ED_001324_00000953-00125

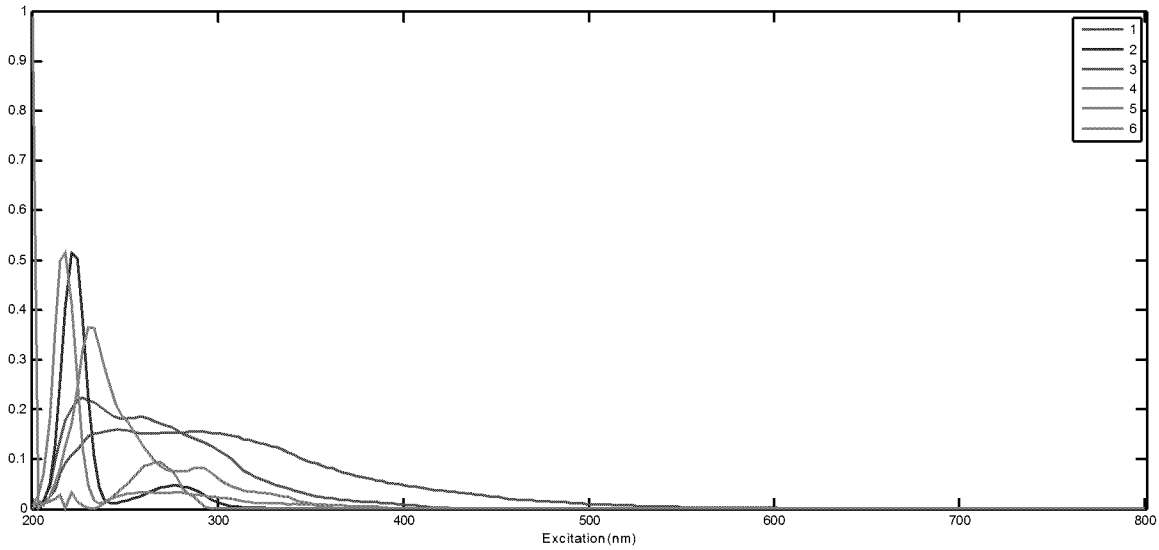


**Figure 58. Mode 3 loadings - Excitation for six-factor PARAFAC model on all 22 oil types at DOR 1:20.**



ED_001324_00000953-00126

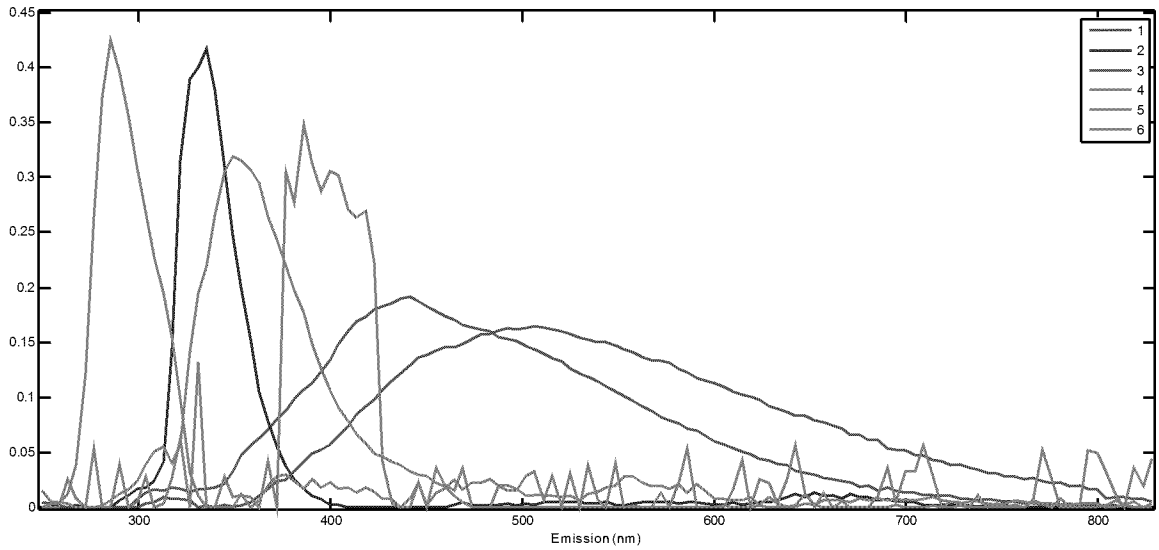


**Figure 59. Mode 2 loadings - Emission for six-factor PARAFAC model of all 22 oil types at DOR = 1:20.**

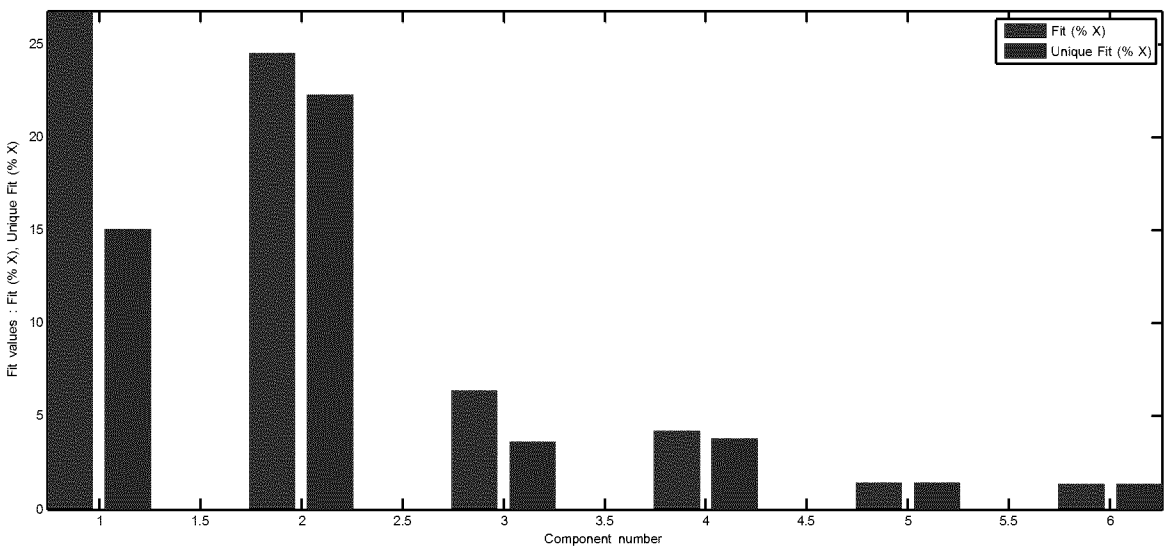


**Figure 60. Fit (% X) vs. unique fit (% X) for six-factor PARAFAC model on all 22 oil types at DOR = 1:20.**



ED_001324_00000953-00127

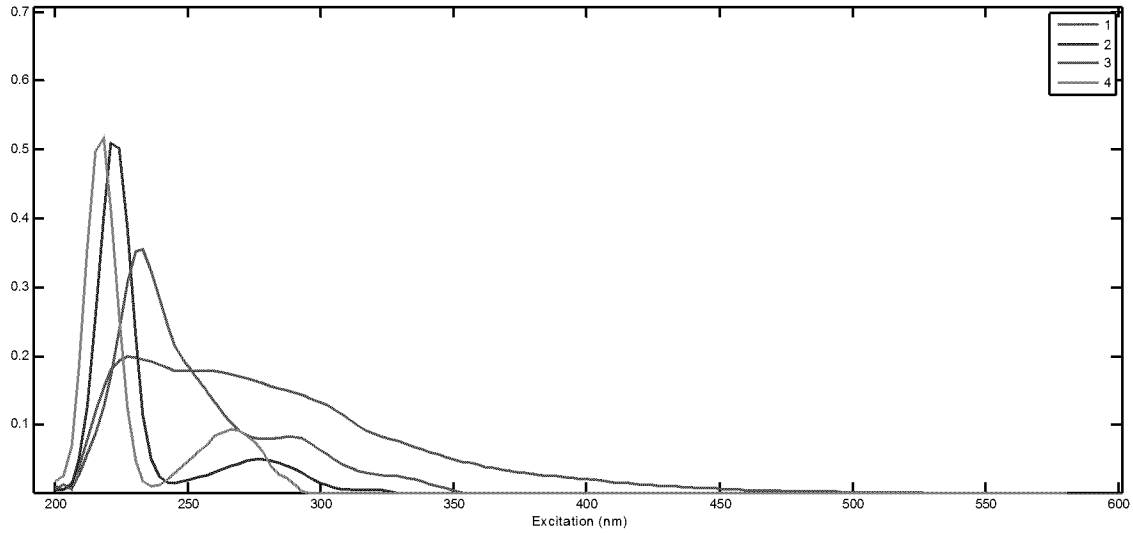


**Figure 61. Mode 3 loadings – Excitation for five-factor PARAFAC model of all 22 oil types at DOR = 1:20.**

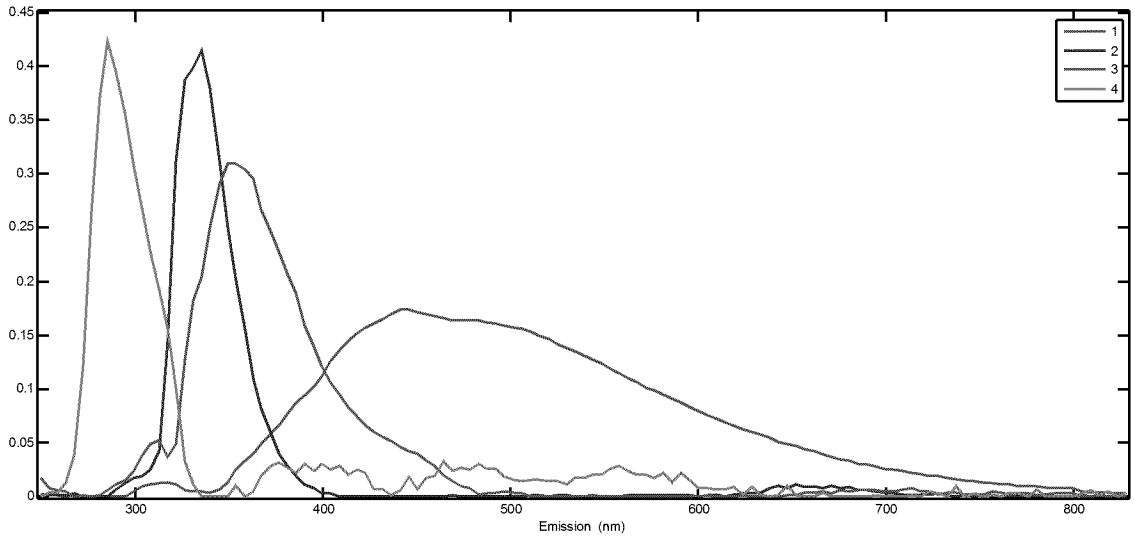


**Figure 62. Mode 2 loadings – Emission for five-factor PARAFAC model of all 22 oil types at DOR = 1:20.**



ED_001324_00000953-00128

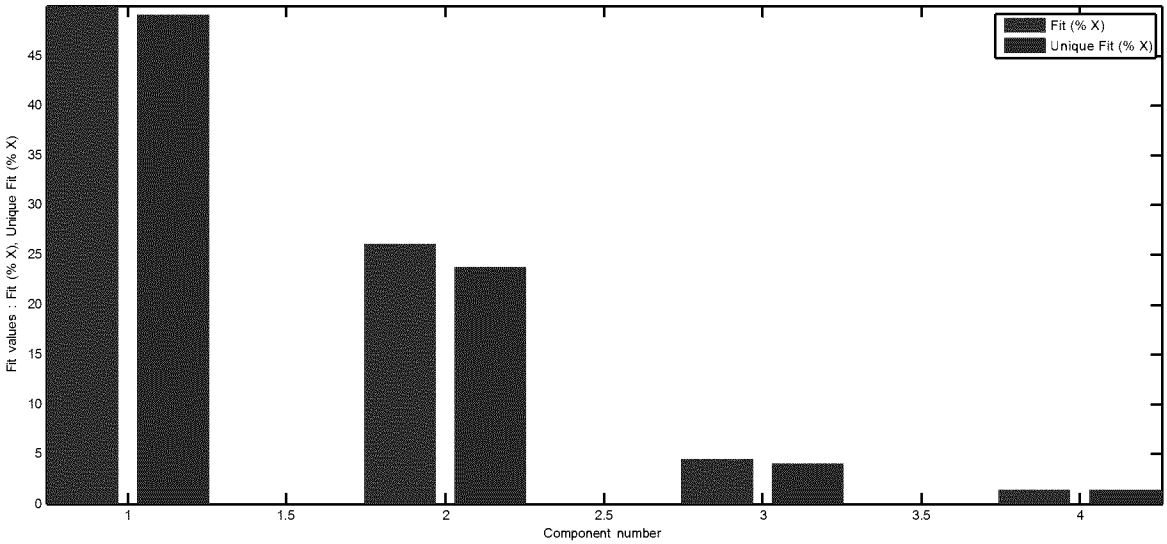


**Figure 63. Fit (% X) vs. unique fit (% X) for five-factor PARAFAC model on all 22 oil types at DOR = 1:20.**

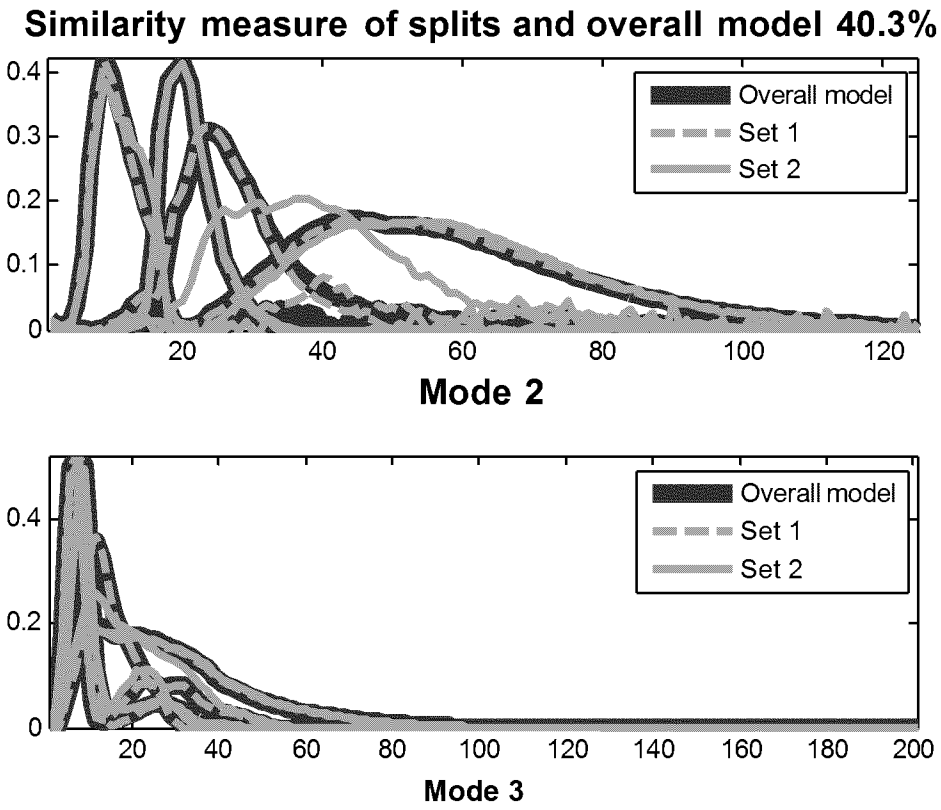


**Figure 64. Similarity measure of split halves and overall model for 5-factor model.**

***DOR = 1:20, Oil Type I & II Comparison***

The 22 types of oil can be grouped by the tendency for $F_{max}$ fluorescence intensity to markedly increase with increased DOR (Type I), and those with little to no increase in $F_{max}$ fluorescence intensity with increasing DOR (Type II). Since it was not possible to determine a definitive number of component factors using all 22 sample files from the DOR = 1:20 baffle flask experiments, PARAFAC analysis was performed separately on Type I and Type II oil samples.

**Type I Oils**

A four-factor model with the optimal pre-processing constraints of non-negativity, EEM filtering (12 and 24nm for First and Second Order Rayleigh, respectively), and info-Norm constraints was run on the twelve Type I oil samples (Table 3) by loading the DOR = 1:20 dataset and excluding Type II samples. Results showed the model explained 95.898% of the data with 95% core consistency and low, randomly distributed residuals; however, the relative percent difference between fit and unique fit was high at 60% and 62% for factors 1 and 3, respectively. Factor 4 represented only 1.1% of the data and appeared to be modelling only noise from the graph of loadings for Mode 2 (emission). Split half analysis showed a 0% similarity between splits and the overall model. Re-running the model with three factors explained 95.702% of the data with 95% core consistency. Variation per component was problematic for factors 2 and 3, with relative percent difference between fit and unique fit of 61% and 62%, respectively. Further, in the graph of loadings for Mode 2 (emission) factor 3 appeared nearly identical to factor 2, just shifted to a slightly longer wavelength. Split half analysis was slightly improved over the four-factor model, with a 28.4% similarity between splits and model. Finally, re-running the model with two factors resulted in the best result with 94.967% of the data explained, 100% core consistency and good variation per component. Split half analysis showed an excellent 96.3% similarity between splits and the overall model. The graphs of loadings for Mode 2 and 3 appear to be reasonable emission and excitation spectra, respectively. Noted, however, is the appearance of minor double peaks in emission spectra at 308 nm for factor 1 and 294 nm for factor 2.



ED_001324_00000953-00130

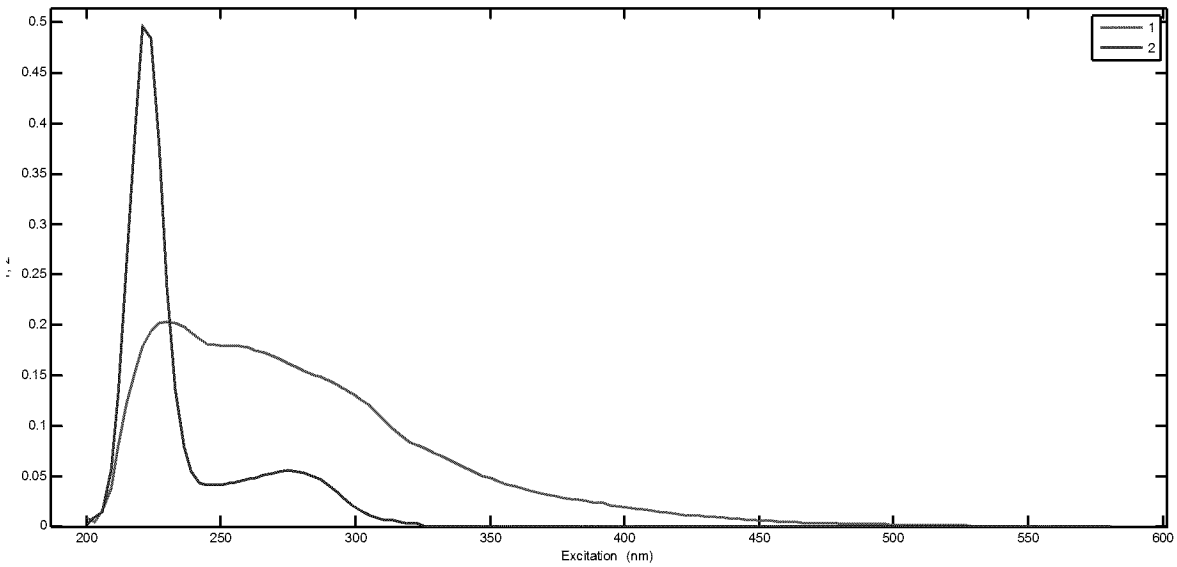


**Figure 65. Mode 3 loadings - Excitation for two-factor PARAFAC model of Type I oils at DOR = 1:20.**

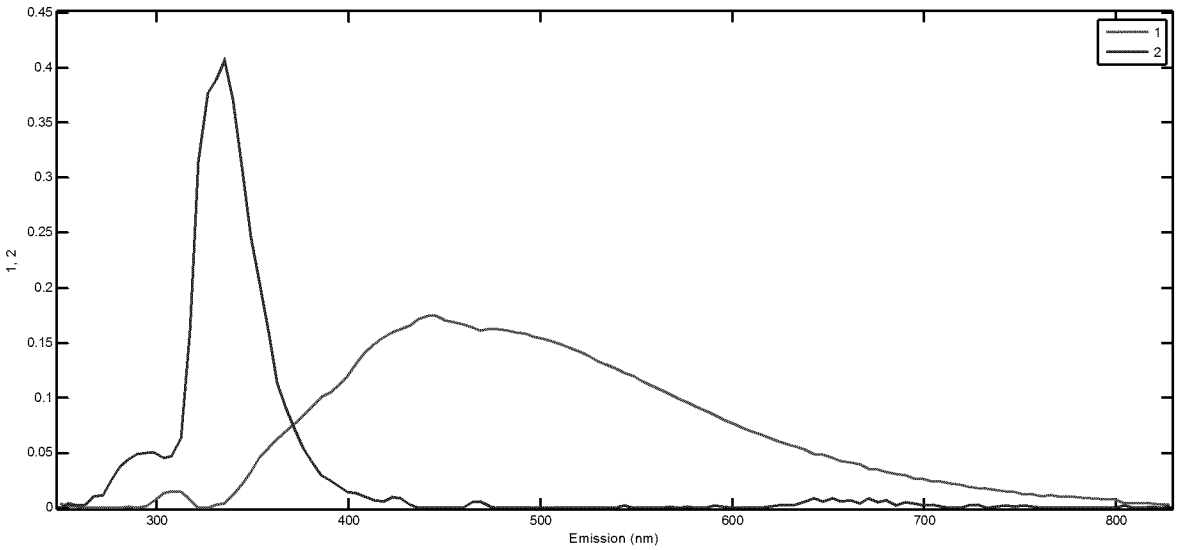


**Figure 66. Mode 2 loadings - Emission for two-factor PARAFAC model of Type I oils at DOR = 1:20.**



ED_001324_00000953-00131

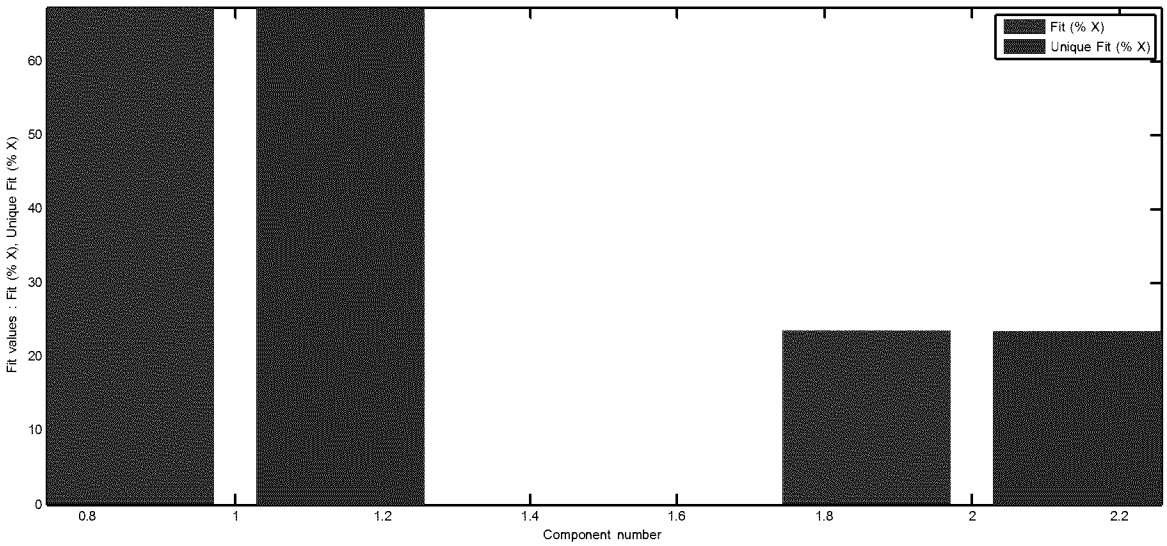


**Figure 67. Fit (% X) vs. unique fit (% X) for two-factor PARAFAC model of Type I oils at DOR = 1:20.**



ED_001324_00000953-00132

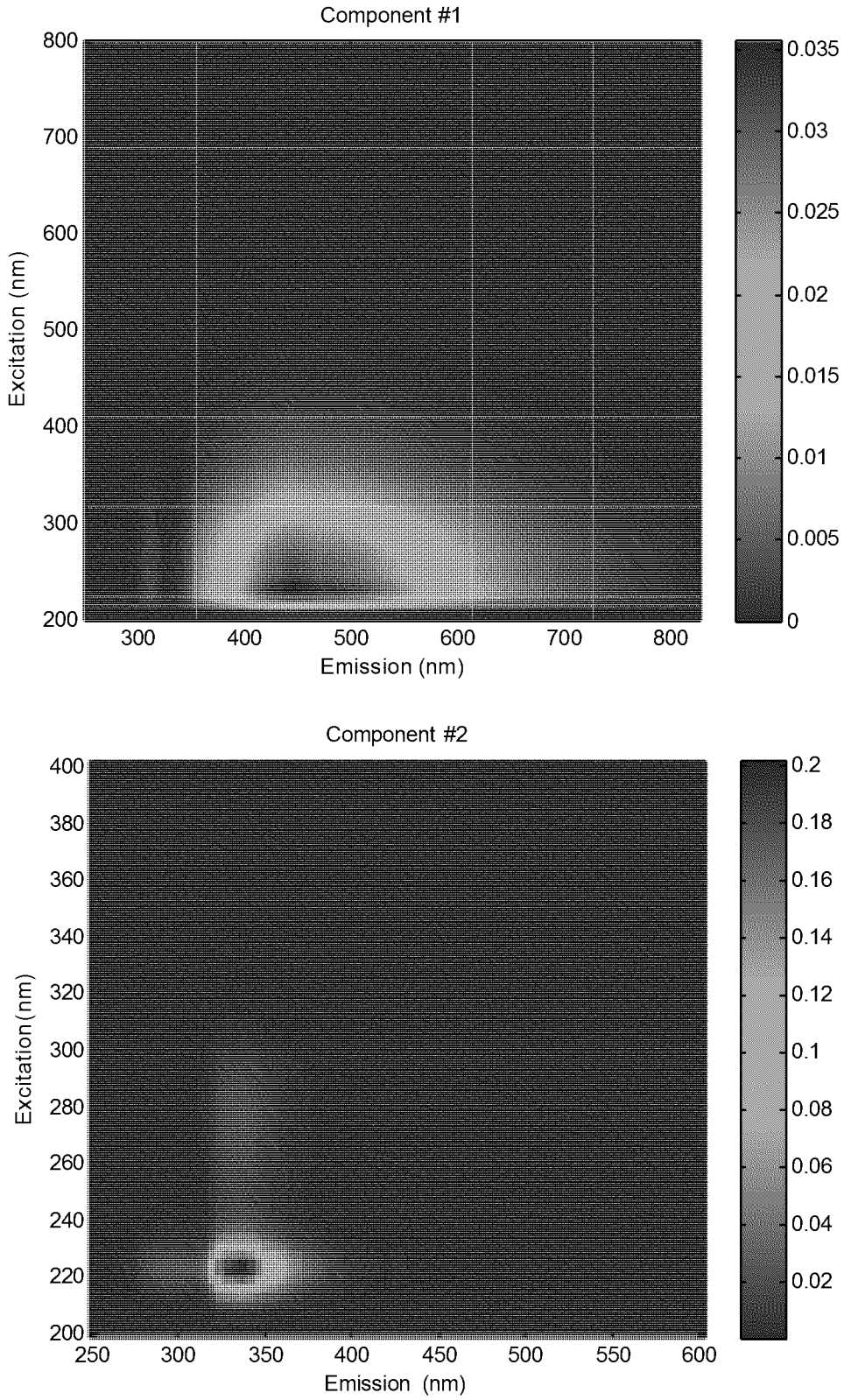


**Figure 68. EEM view of factor 1 with $F_{max}$ at Ex/Em = 230/445 nm (above), and factor 2 with $F_{max}$ at Ex/Em = 221/335 nm (below)**



ED_001324_00000953-00133

**Type II Oils**

To initiate PARAFAC analysis with the group of ten Type II oil samples (Table 3), the same four-factor model with aforementioned three optimal constraints was performed. The model explained 95.862% of the data with 91% core consistency and low, randomly distributed residuals. Variation per component was good for all four factors. The graph of loadings for Mode 2 (emission) had the appearance of true emission profiles for factors 1-3; however, factor 4 contained a significant, broad double peak. Split half analysis resulted in a similarity measure of only 22.8% between splits and the overall model. Increasing the number of factors to five and re-running the model in an attempt to separate the two peaks noted in emission factor 4 did not appreciably improve results, with 96.132% of the data explained by the model and 90% core consistency. Variation per component showed factor 5 accounted for less than 1% of the data, and split half analysis yielded 0.3% similarity between splits and the overall model. Re-running the model with three factors resulted in the best result with 93.322% of the data explained by the model, 94% core consistency and good variation per component. Split half analysis showed 87.9% similarity between the splits and the overall model. Noted once again is the appearance of minor double peaks in emission spectra at 290 nm for factor 1, 303 nm for factor 2, and 312 nm for factor 3.

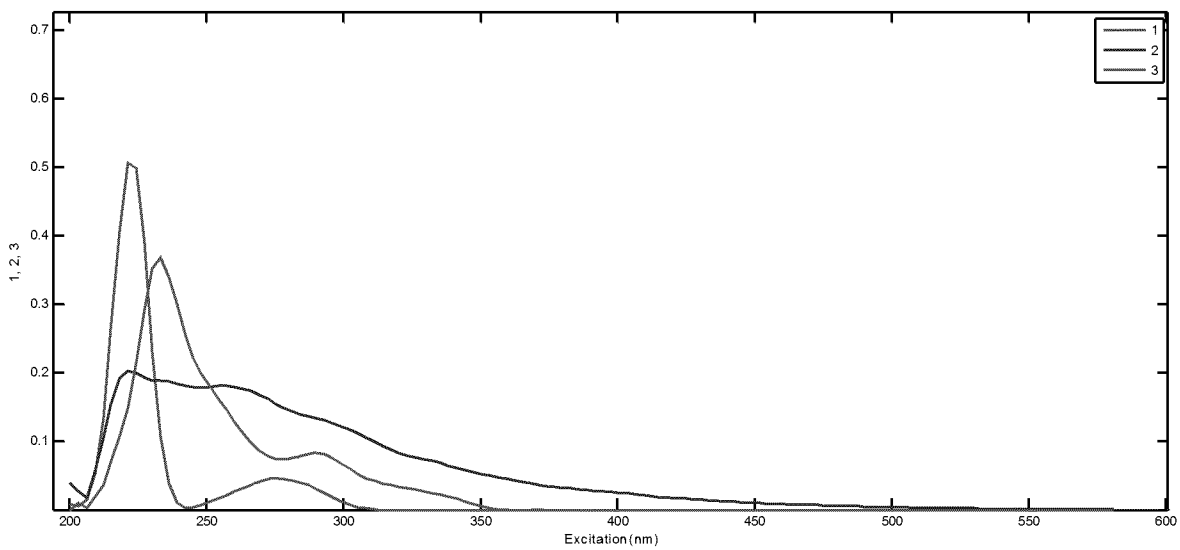


**Figure 69. Mode 3 loadings - Excitation for three-factor PARAFAC model of Type II oils at DOR = 1:20.**

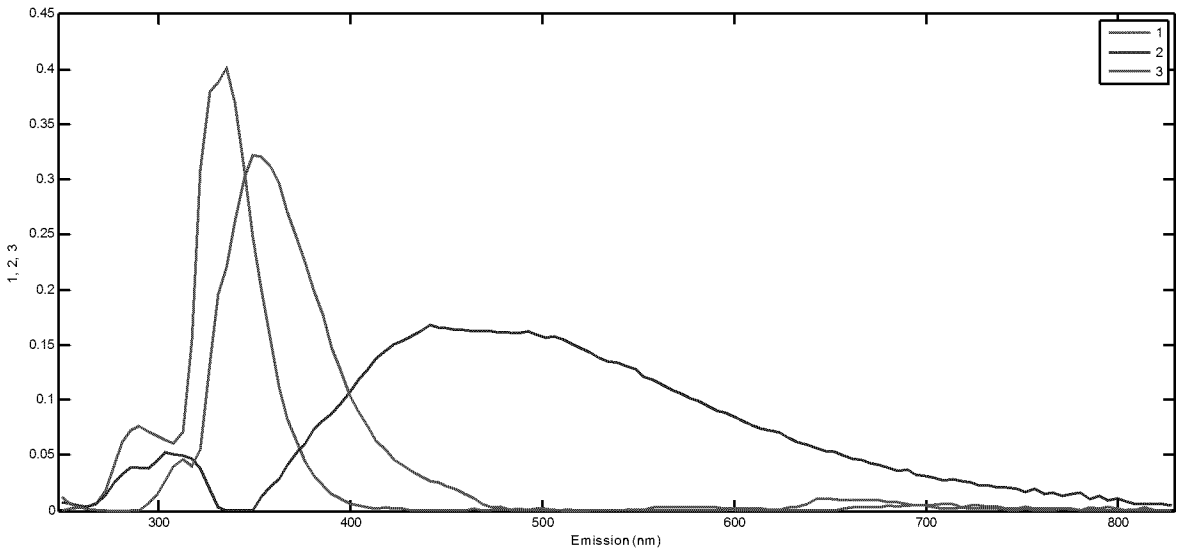


**Figure 70. Mode 2 loadings - Emission for three-factor PARAFAC model of Type II oils at DOR = 1:20.**

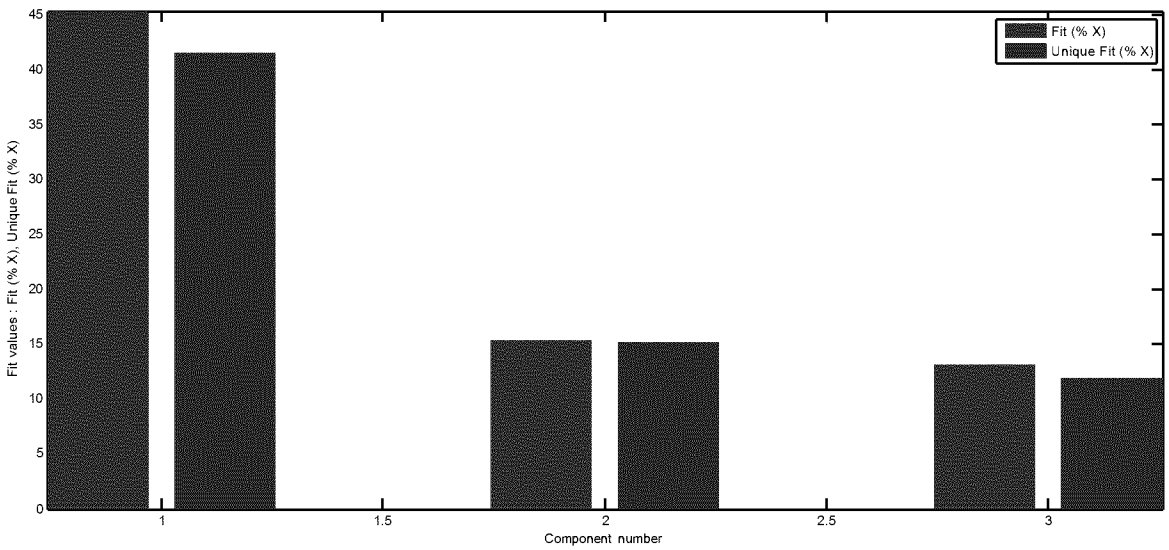


**Figure 71. Fit (% X) vs. unique fit (% X) for three-factor PARAFAC model of Type II oils at DOR = 1:20.**



ED_001324_00000953-00135

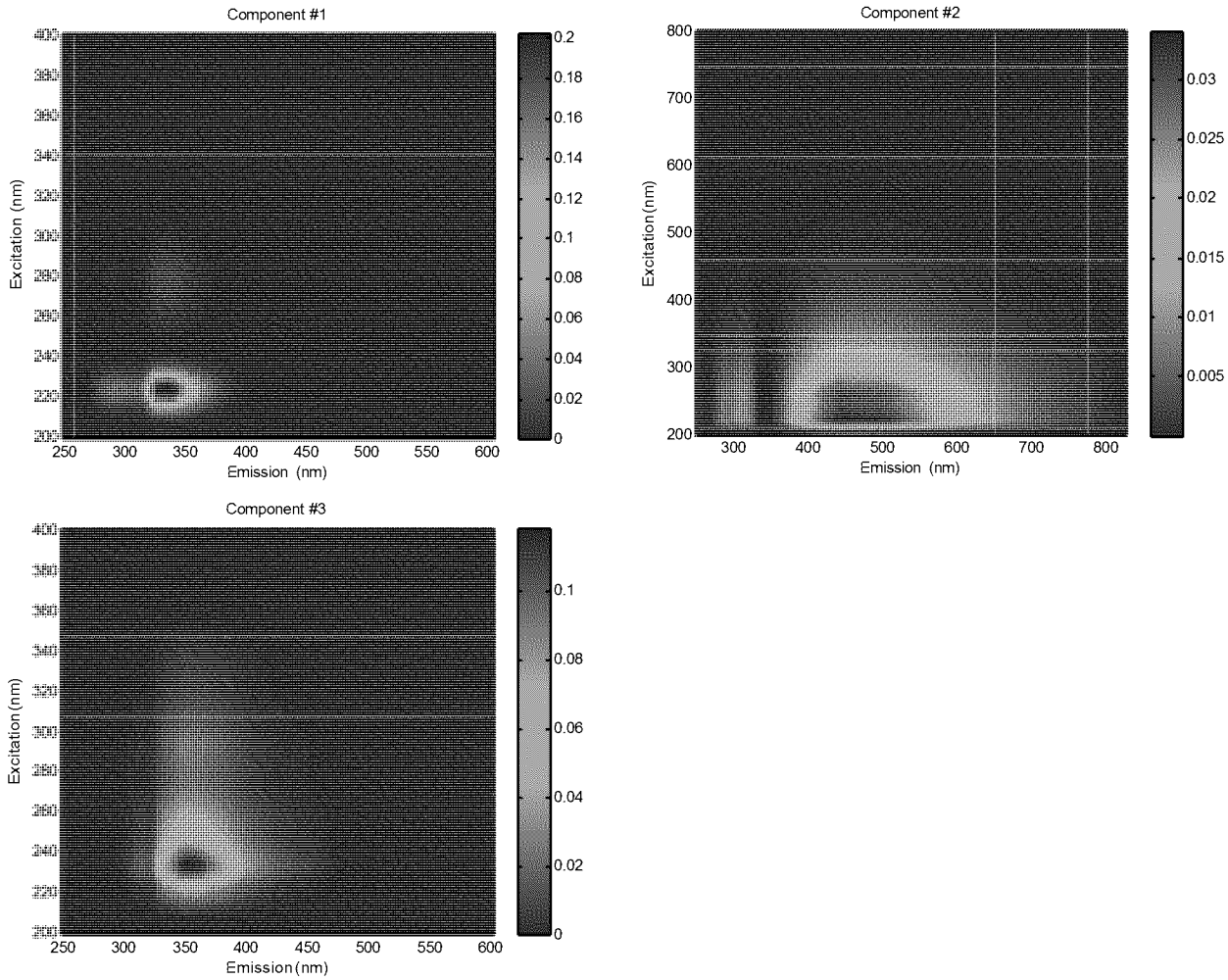


**Figure 72. EEM view of factor 1 with Fmax at Ex/Em = 221/335 nm (top left), factor 2 with Fmax at Ex/Em = 221/492 nm (top right), and factor 3 with Fmax at Ex/Em = 233/349 nm (bottom left).**



ED_001324_00000953-00136

***DOR = 1:100, Oil Type I & II Comparison***

**Type I Oils**

Given the success with splitting samples into Type I and II groupings and improving the PARAFAC analysis in resolving difficulties in factor identification with DOR = 1:20 oil samples, this procedure was performed with DOR = 1:100 and DOR = 0 oil samples, as well. First analysis of the twelve Type I oil samples at this DOR was done using a three-factor PARAFAC model with the same three pre-processing constraints previously applied. The DOR = 1:100 dataset was loaded, and Type II oil samples were excluded from analysis. Results showed 97.795% of the data explained by the model with 88% core consistency. Variation per component was good, but fit vs. unique fit for factors 1 and 3 had a relative percent difference of 51%. Visual inspection of loadings graphs showed Mode 2 (emission) factors 1 and 3 were almost completely overlapping, the only difference being a minor double peak at 285 nm on factor 3. Similarity between splits and overall model was only 0.3%. Increasing the number of factors to four and re-running the model resulted in a slight increase in the data explained (98.216%); however core consistency dropped to 78%. Variation per component was essentially unchanged for components 1, 2 and 3, and less than 3% of the data was explained by factor 4. Split half analysis similarity between splits and the overall model was 0%. Dropping the number of factors to two and re-running the model resulted in 96.985% of the data explained by the model and 100% core consistency. Variation per component was good; however, over 75% of the fit was modelled by factor 1. Loading curves for both Mode 2 and Mode 3 looked very much like those for Type I oils at DOR = 1:20. Split half analysis resulted in only 22.6% similarity between splits and the model. The graph of data Set 2 and the model correlated nicely; however, the graph showed for data Set 1, factor 2 was not well correlated with the model in either Mode 2 (emission) or Mode 3 (excitation). Separation of oils into further sub-types may help to achieve a representative PARAFAC model.



ED_001324_00000953-00137

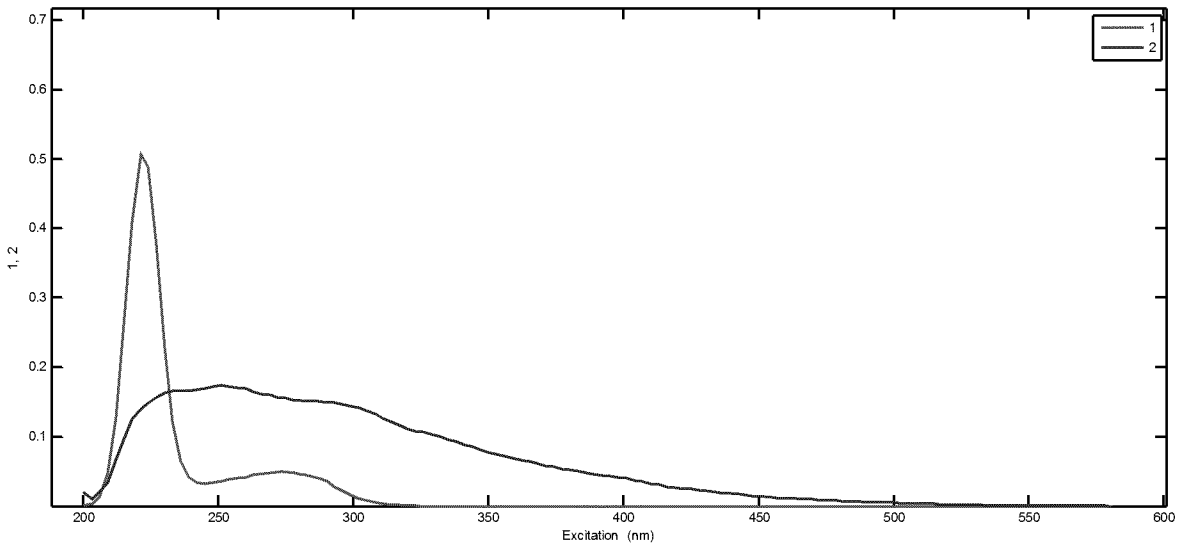


**Figure 73. Mode 3 loadings - Excitation for two-factor PARAFAC model of Type I oils at DOR = 1:100.**

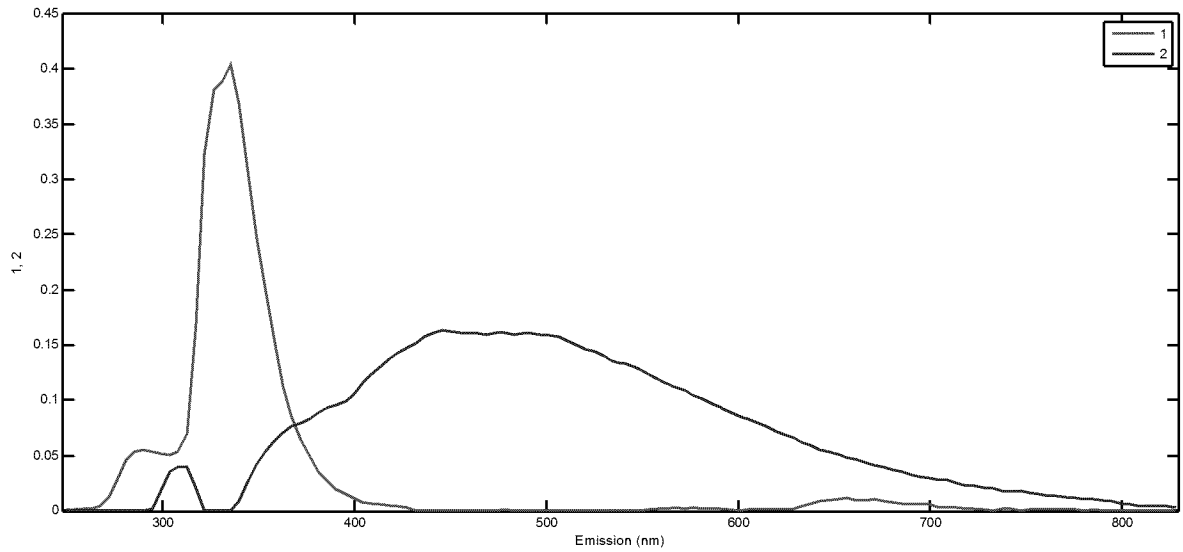


**Figure 74. Mode 2 loadings - Emission for two-factor PARAFAC model of Type I oils at DOR = 1:100.**



ED_001324_00000953-00138

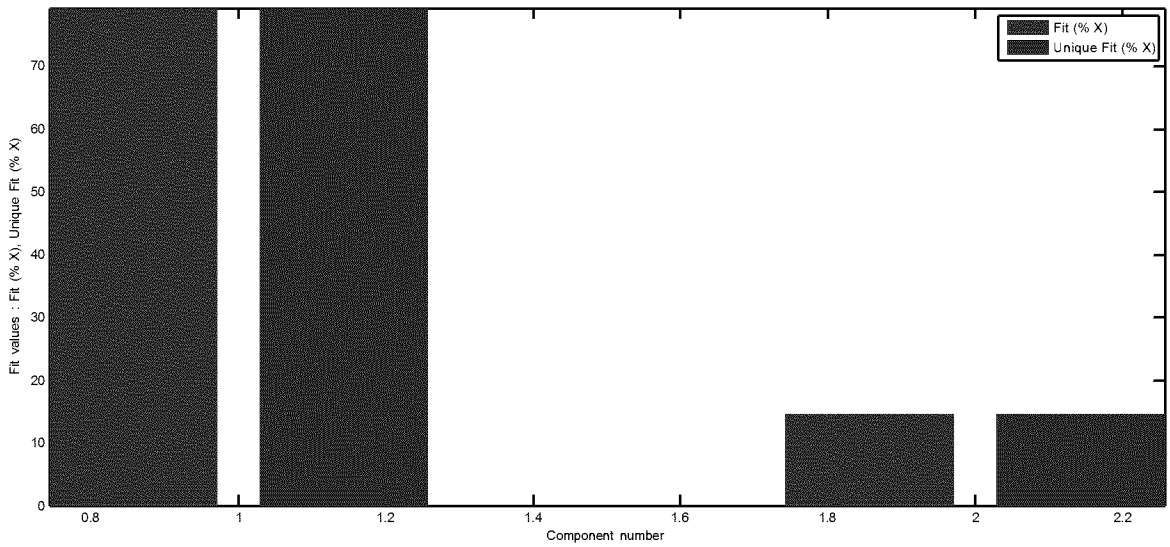


**Figure 75. Fit (% X) vs. unique fit (% X) for two-factor PARAFAC model of Type I oils at DOR = 1:100.**

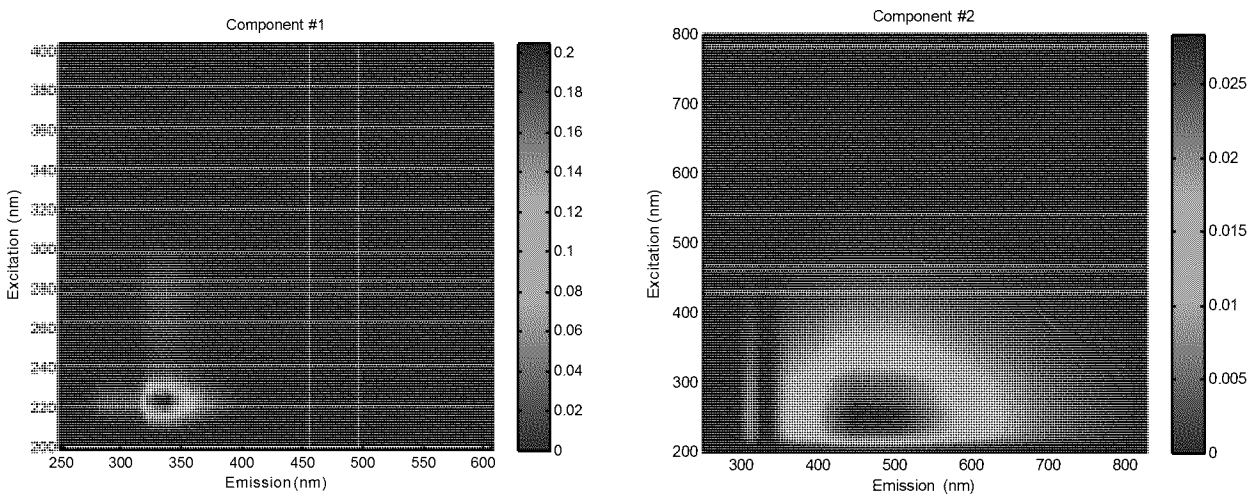


**Figure 76. EEM view of factor 1 with $F_{max}$ at Ex/Em = 221/335 nm (above), and factor 2 with $F_{max}$ at Ex/Em = 251/445-500 nm (below).**



ED_001324_00000953-00139

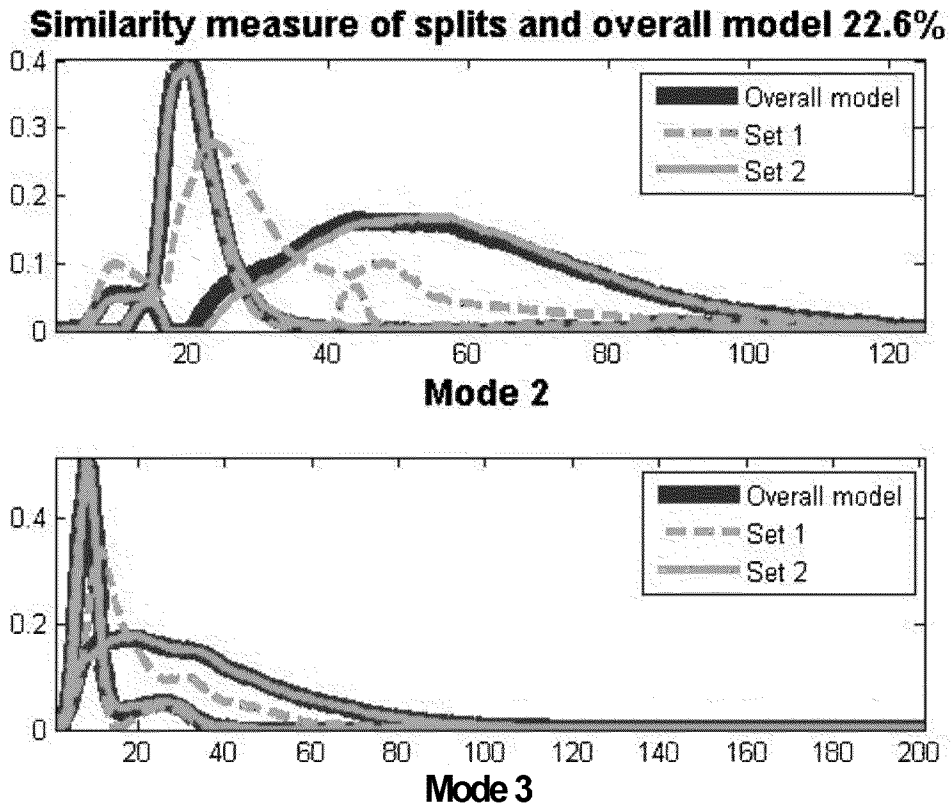


**Figure 77. Similarity measure of split halves and overall model for 2-factor model.**

**Type II Oils**

Based on results of PARAFAC modelling performed on DOR = 1:20 Type II oils, a three-factor model with the same previously applied pre-processing constraints was run on the DOR = 1:100 Type II oil samples. The model explained 94.705% of the data, and core consistency was 95%. Variation per component was very good, and loadings for both Mode 2 and 3 appeared to model reasonable emission and excitation spectra. Split half analysis had a somewhat low similarity of 62.7% between splits and the overall model. To find a better fit, a four-factor model was performed, and results showed a slight increase to 95.315% of data explained by the model, but a reduction to 56% in core consistency, and split half analysis similarity was only 1.8% between splits and the model. A two-factor model was then performed, resulting in 90.958% of the data explained by the model and core consistency of 100%. Split half analysis yielded similarity of 70.5% between splits and the overall model. While split half analysis was somewhat better for the two-factor model, the three-factor model represented a better percentage of the data while retaining high core consistency. It is clear from viewing the loadings graphs and EEM view of components that the three-factor model is capturing a true third component.

**Two-factor Model**

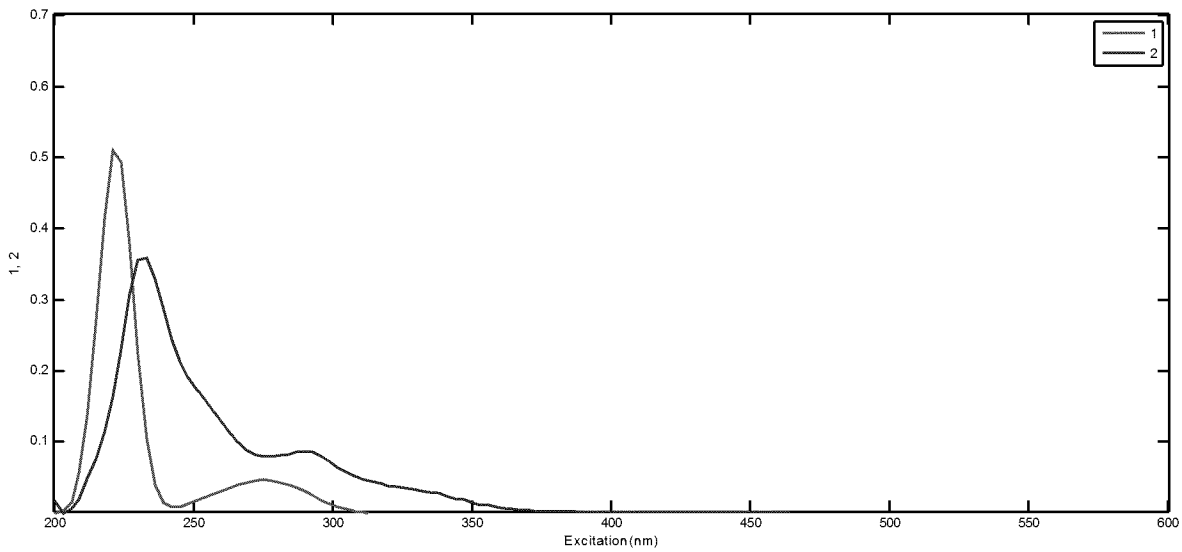


**Figure 78. Mode 3 loadings - Excitation for two-factor PARAFAC model of Type II oils at DOR = 1:100.**



ED_001324_00000953-00141

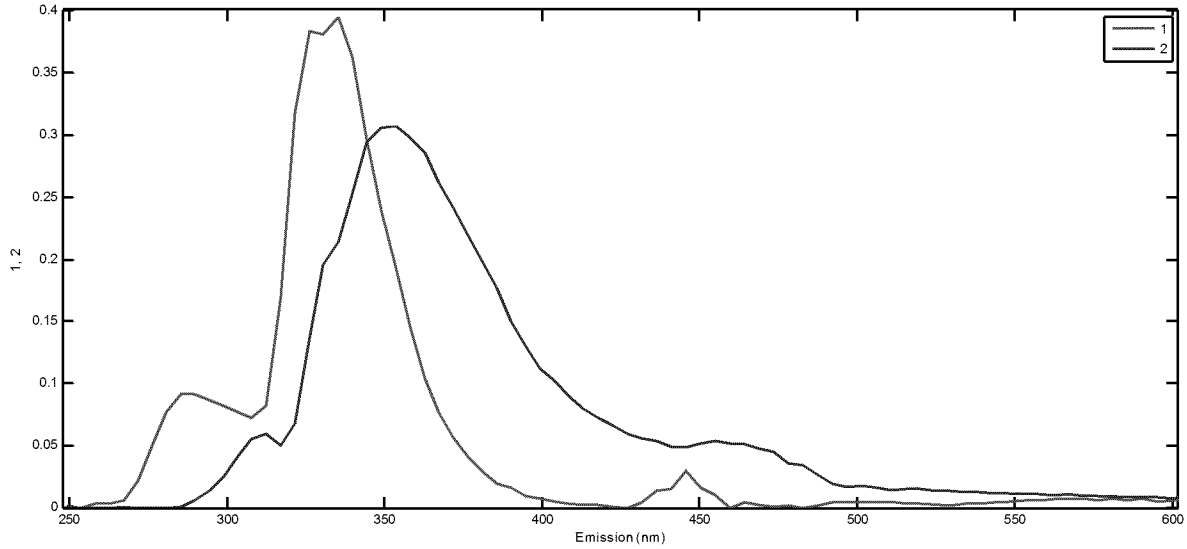


**Figure 79. Mode 2 loadings - Emission for two-factor PARAFAC model of Type II oils at DOR = 1:100.**

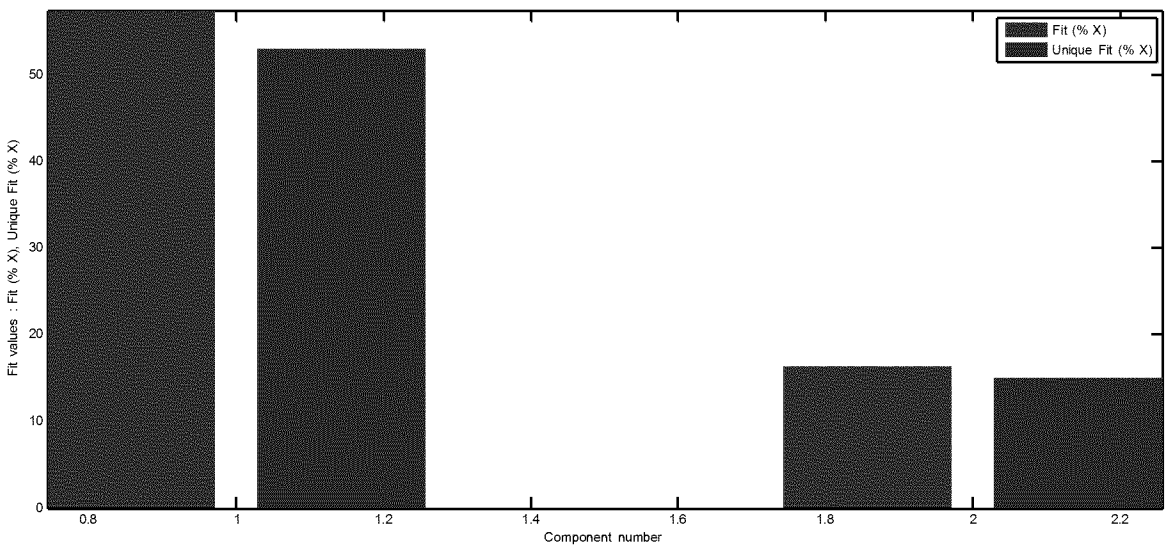


**Figure 80. Fit (% X) vs. unique fit (% X) for two-factor PARAFAC model of Type II oils at DOR = 1:100.**



ED_001324_00000953-00142

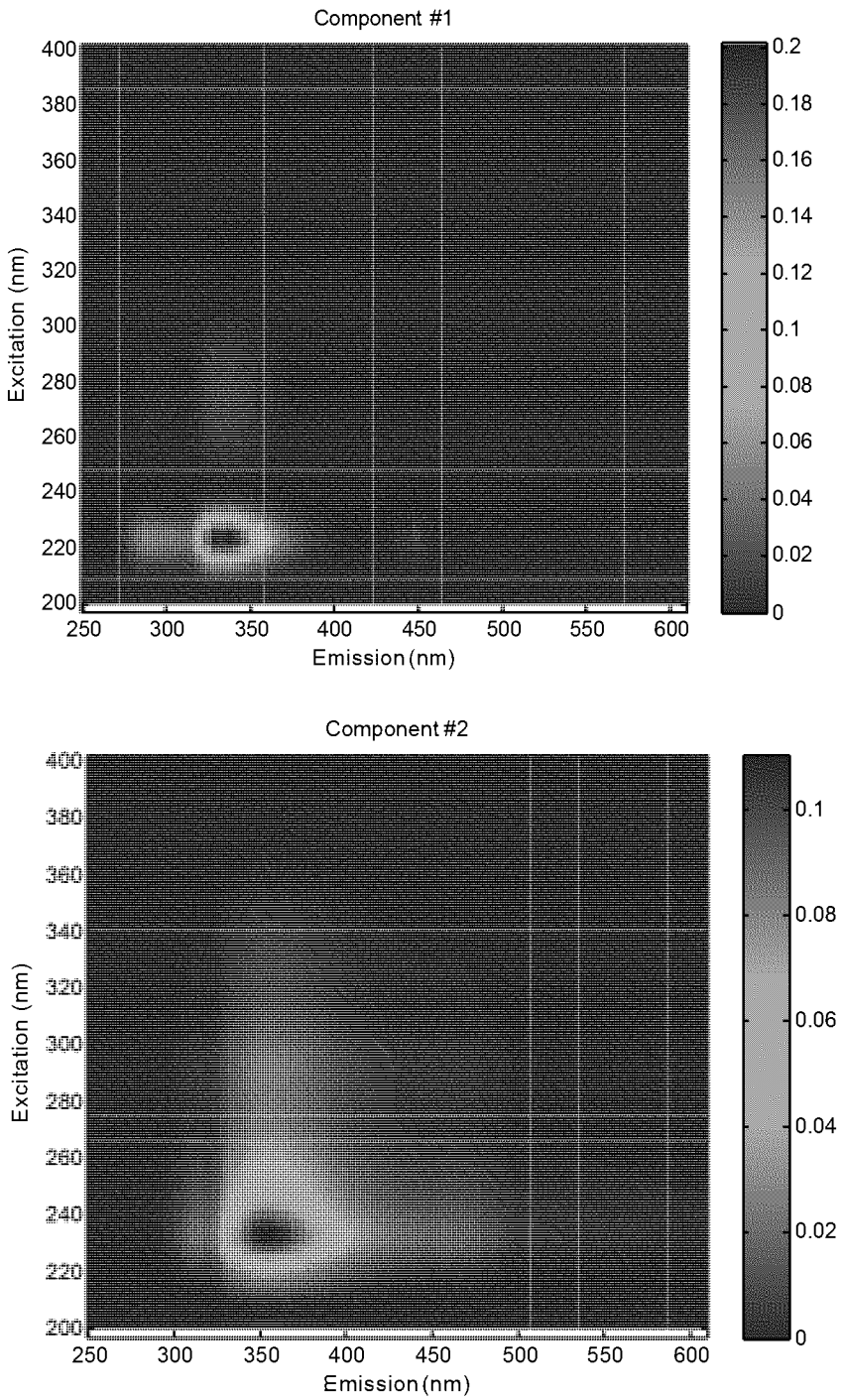


**Figure 81. EEM view of factor 1 with $F_{max}$ at Ex/Em = 221/335 nm (above), and factor 2 with $F_{max}$ at Ex/Em = 233/353 nm (below).**



ED_001324_00000953-00143

## Three-factor Model

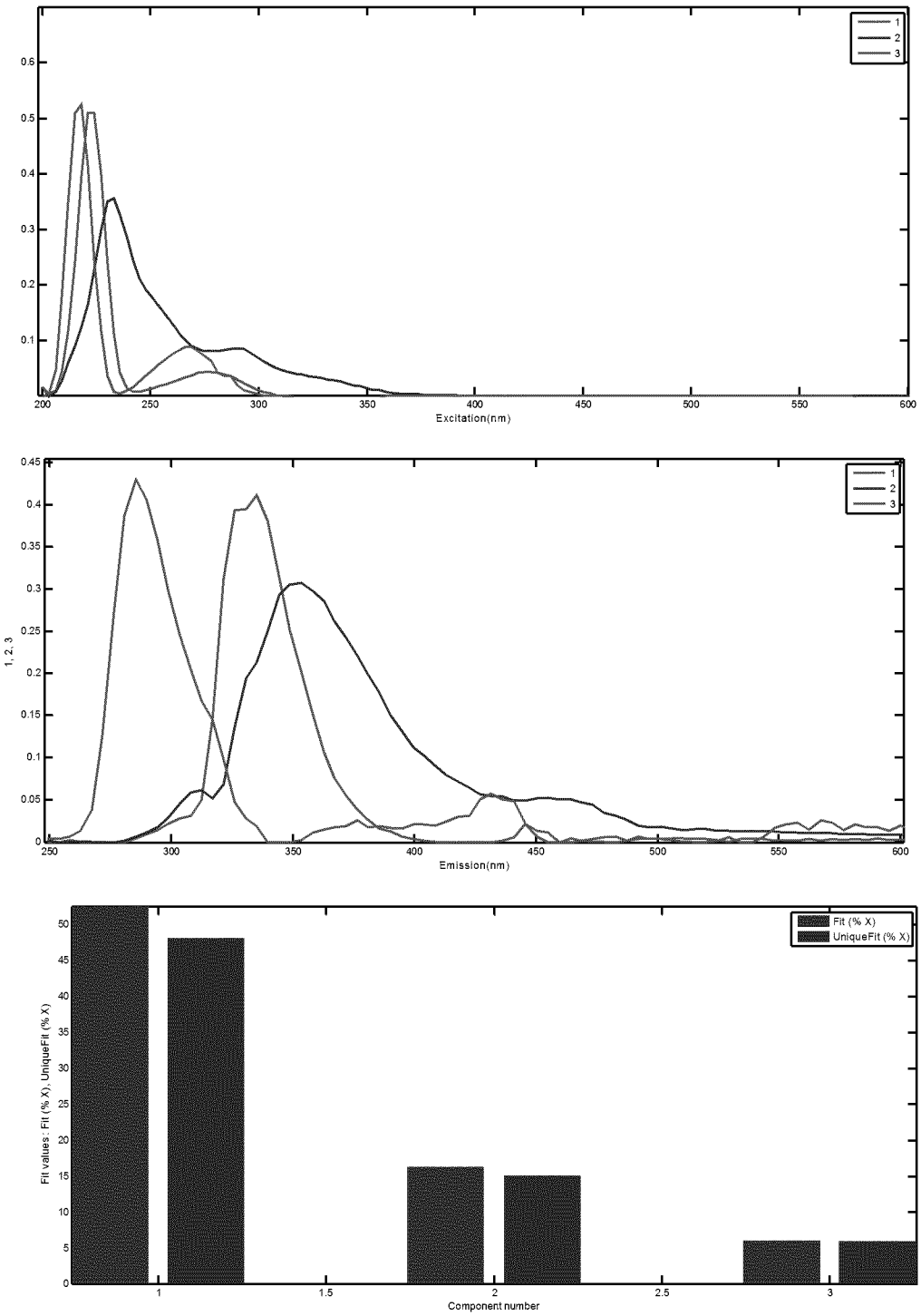


**Figure 82. Mode 3 loadings - Excitation (top) and Mode 2 loadings - Emission (middle) for three-factor PARAFAC model of Type II oils at DOR = 1:100. Fit (% X) vs. unique fit (% X) for three-factor PARAFAC model of Type II oils at DOR = 1:100 (bottom).**



ED_001324_00000953-00144

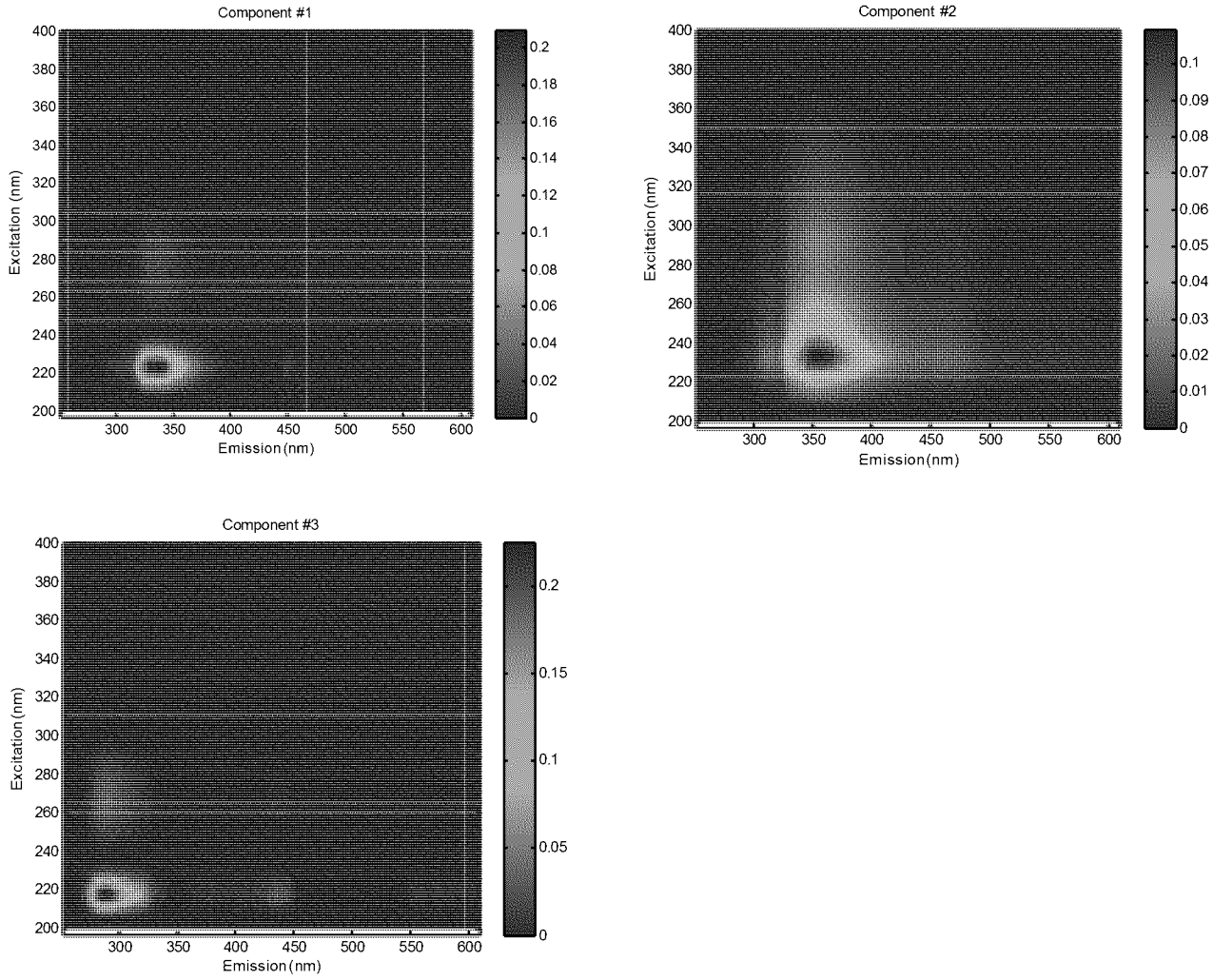


**Figure 83. EEM view of factor 1 with Fmax at Ex/Em = 221/335 nm (top left), factor 2 with Fmax at Ex/Em = 233/353 nm (top right), and factor 3 with Fmax at Ex/Em = 218/285 nm (bottom left).**



ED_001324_00000953-00145

**DOR = 0 – Type I Oils**

To begin the analysis of Type I oil samples, the DOR = 0 dataset was loaded, and Type II oil sample files were excluded. A three-factor PARAFAC model with the previously selected pre-processing constraints was performed. Results explained 94.435% of the data, but core consistency was only 19%. Variation per component was not optimal, with a relative percent difference of 42% between fit and unique fit in both factors 1 and 2. While fit vs. unique fit for factor 3 was good, it only accounted for 2.4% of the model. Split half analysis resulted in similarity of 0.8% between the splits and the model. Re-running the model with four factors resulted in 94.673% of the data explained by the model and core consistency of only 33%. Variation per component was similar to that obtained with the three-factor model; however, the addition of factor 4 represented less than half of one percent of the data. Split half analysis yielded 0% similarity between splits and the overall model. Dropping the number of factors to two and running the model again resulted in 93.55% of the data explained by the model and 100% core consistency. Variation per component showed close to 90% of the data was modelled by factor 1 and less than 2% by factor 2. In addition, factor 2 displayed two separate and equal peaks in loadings for Mode 2 (emission), indicating a poor fit. Split half analysis resulted in 0.3% similarity between the splits and the overall model. It appears impossible to arrive at a satisfactory PARAFAC model for all Type I oils collectively; perhaps splitting these samples into at least two subgroups would improve resolution.

**DOR = 0 – Type II Oils**

Type I oil samples were then excluded from the DOR = 0 dataset, and a three-factor PARAFAC model with the previously selected pre-processing constraints was run on the Type II oil sample files. Results showed that 96.213% of the data was explained by the model, with 94% core consistency. Variation per component was good with only 7-8% relative percent difference between fit and unique fit in factors 1 and 2, and less than 1% difference in factor 3. Split half analysis showed 68% agreement between splits and the overall model. Four-factor and two-factor models, with the same constraints, were also run in an attempt to improve goodness-of-fit. The four-factor model resulted in 96.471% of the data explained by the model and 93% core



ED_001324_00000953-00146

consistency, but split half similarity between splits and overall model was only 0.1%. The two-factor model resulted in a drop in data explained by the model to 92.807% and an increase in core consistency to 100%. However, split half similarity between splits and model was 0.7%. Therefore, the three-factor model was selected as best overall. It was noted that the graphs of loadings and EEM views of factors were almost identical to those obtained with the three-factor PARAFAC model for all 22 oils at DOR = 0.



ED_001324_00000953-00147

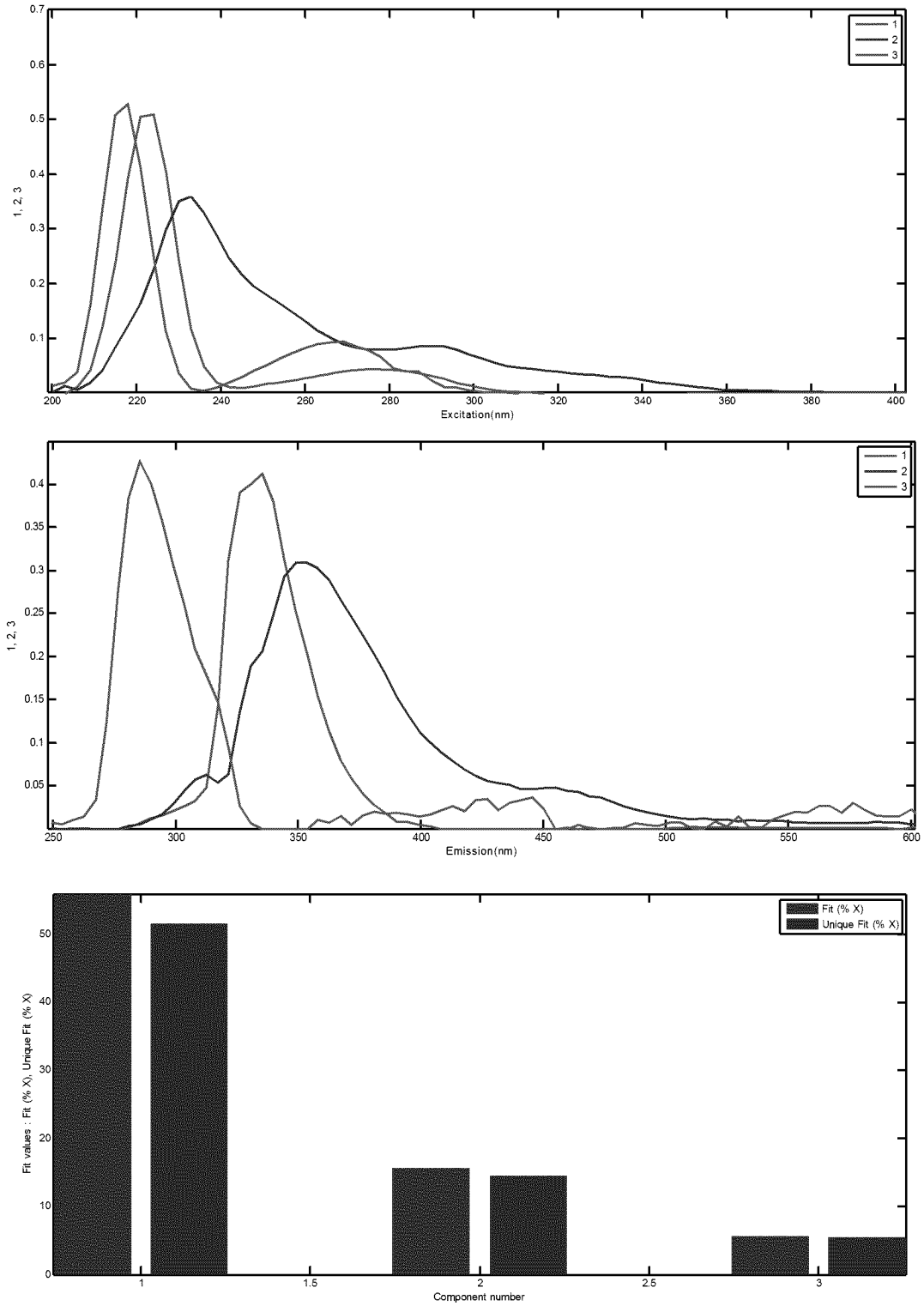


**Figure 84. Mode 3 loadings -excitation (top), Mode 2 loadings – emission (middle) and fit (% X) vs. unique fit (% X) (bottom) for three-factor PARAFAC model of Type II oils at DOR = 0.**

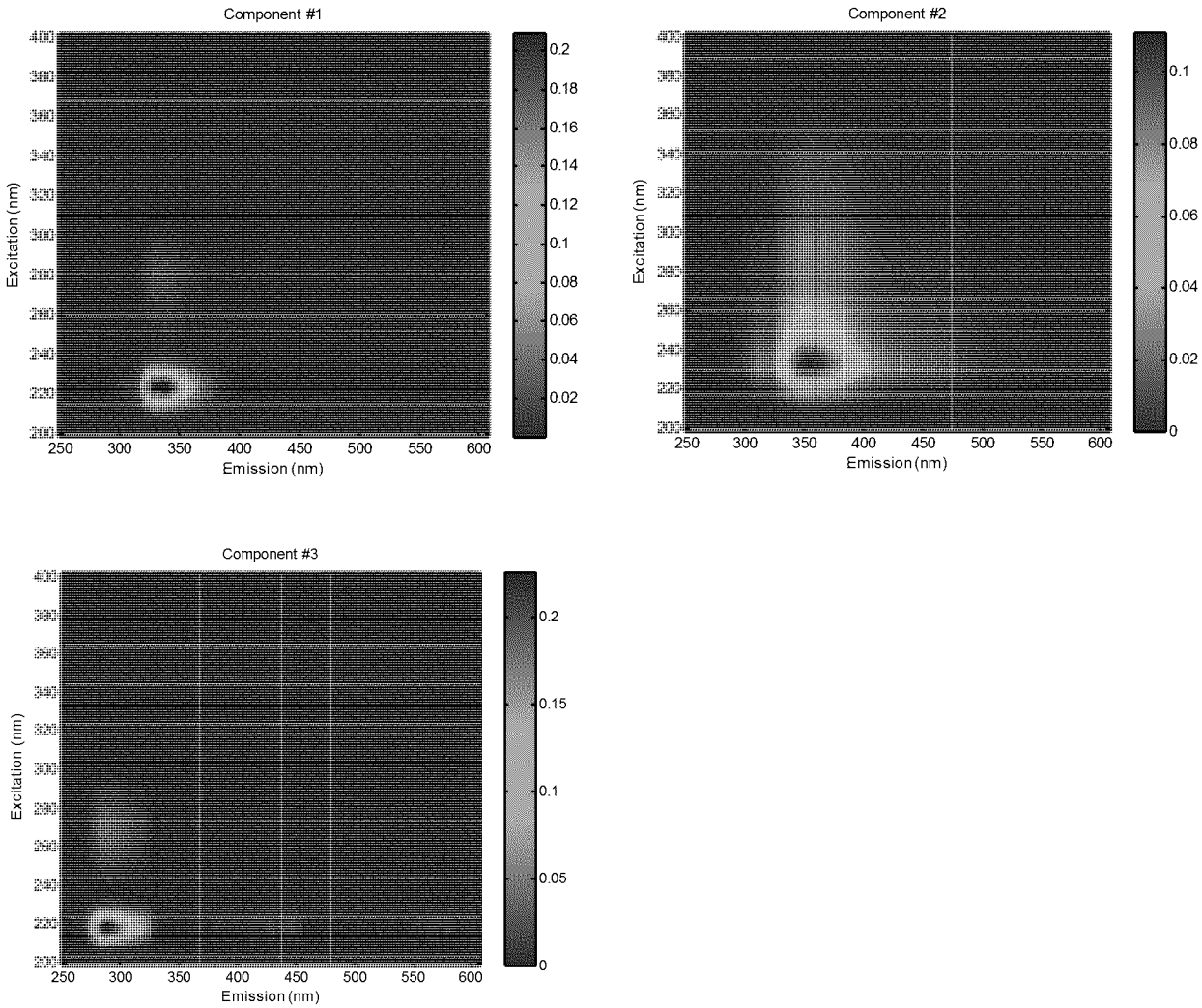


**Figure 85. EEM view of factor 1 with Fmax at Ex/Em = 224/335 nm (top left), factor 2 with Fmax at Ex/Em = 233/353 nm (top right), and factor 3 with Fmax at Ex/Em = 218/285 nm (bottom left).**



ED_001324_00000953-00149

**PAHs and Proteins**

A four-factor PARAFAC model was run with non-negativity, EEM filtering (12nm First Order Rayleigh, 24nm Second Order Rayleigh), and inf-Norm normalization (maximum = 1). An error message was displayed indicating that two or more components could be fitting the same feature, and core consistency was <0%. Although variation per component was good, only 69.228% of data was explained by the model, sample 1 residuals were high, and Mode 1 Loadings showed samples 3 and 4 (pyrene and phenanthrene) clearly overlapping.

**Table 11. Polycyclic Aromatic Hydrocarbons (PAHs) in dichloromethane, further dissolved in artificial seawater.**

| PAH | Original concentration | Amount added to seawater | Final concentration |
|---|---|---|---|
| Fluorene | 1000µL/mL | 10 µL | 1.0 mg/L |
| Phenanthrene | 129.26 µg/mL | 10 µL | 2.9 µg/L |
| Anthracene | 10 ppm | 20 µL | 0.2 µg/L |
| Pyrene | 10mg/mL | 20 µL | 2.0 mg/L |



ED_001324_00000953-00150

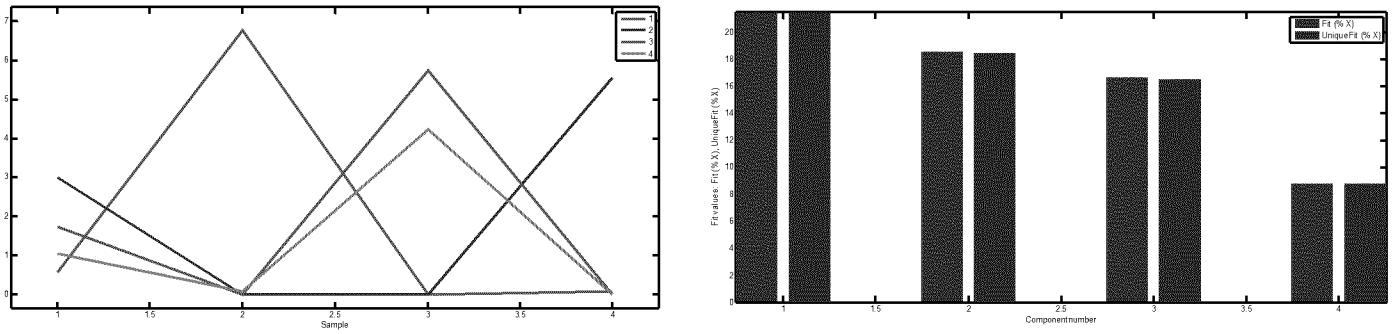


**Figure 86. Mode 1 loadings (left), and Fit (% X) vs. unique fit (% X) (right), for PAHs.**

Results of a three-component model had core consistency of 94%; however, only 61.709% of the data was explained by the model, and Mode 2 factor 3 appeared to be modelling noise. A two-component model explained only 53.476% of the data; however, core consistency was 100% and both Mode 2 emission factors appeared to be valid emission spectra.

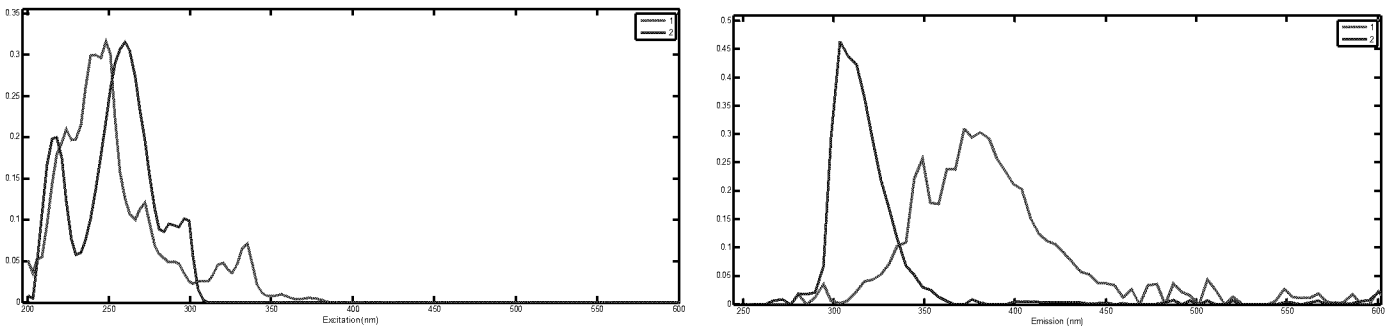


**Figure 87. Mode 3 loadings - Excitation (left) and Mode 2 loadings - Emission (right) for two-factor PARAFAC model of PAHs.**

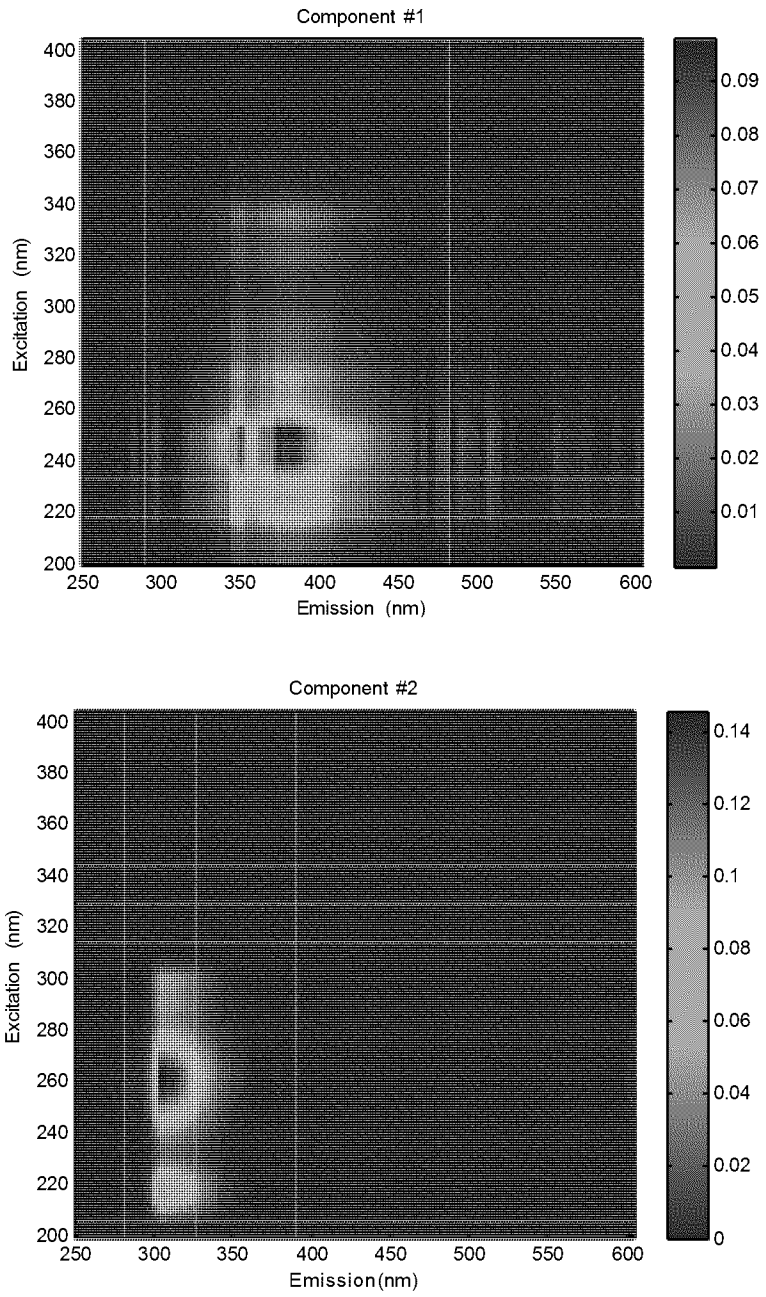


**Figure 88. EEM view of factor 1 with $F_{max}$ at Ex/Em = 251/376 nm (above), and factor 2 with $F_{max}$ at Ex/Em = 263/308 nm (below).**

Sample files of two proteins—tyrosine and tryptophan, 1ppm in artificial seawater, were also imported into SOLO, and a two-factor PARAFAC model was performed. Results showed that 99.213% of the data was explained by the model and core consistency was 100% with excellent variation per component and low, randomly distributed residuals. Loadings for Mode 2 (emission) and Mode 3 (excitation) show realistic spectra for these two proteins.

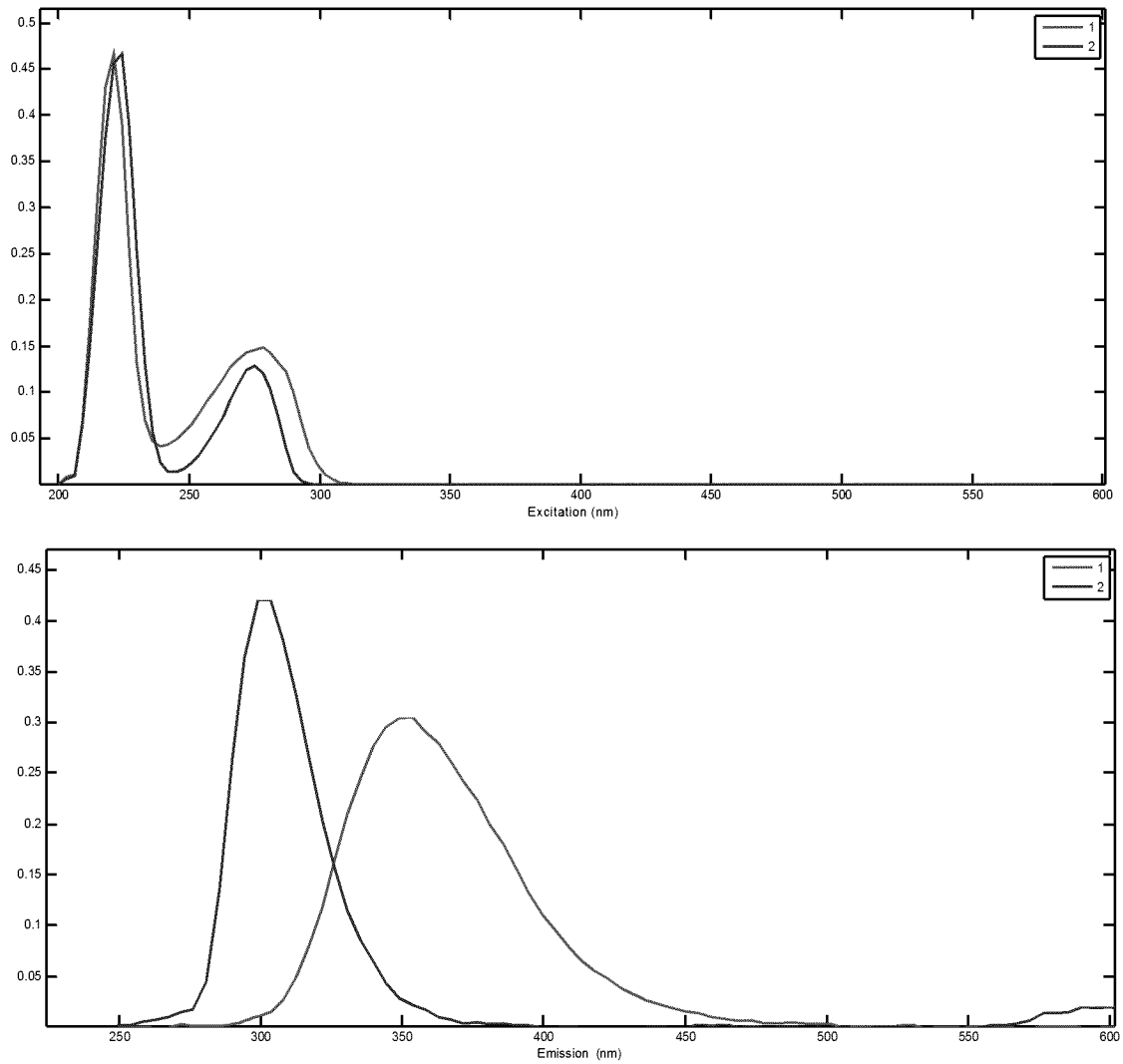


**Figure 89. Mode 3 loadings - Excitation (above) and Mode 2 loadings - Emission (below) for two-factor PARAFAC model of proteins.**



ED_001324_00000953-00153

Comparing the results of PARAFAC analysis on PAHs with that on naturally-occurring proteins illustrates the complexity of the fluorescence signals displayed by PAHs vs. the strong, clear signals arising from proteins. Ideally, PARAFAC modelling of aqueous organic fluorophores would show little overlap between excitation and emission spectra and have a single emission peak (Murphy,et al. 2013); however, the molecular complexity of PAHs leads to convoluted fluorescence signals which creates a challenge for PARAFAC decomposition into component factors.

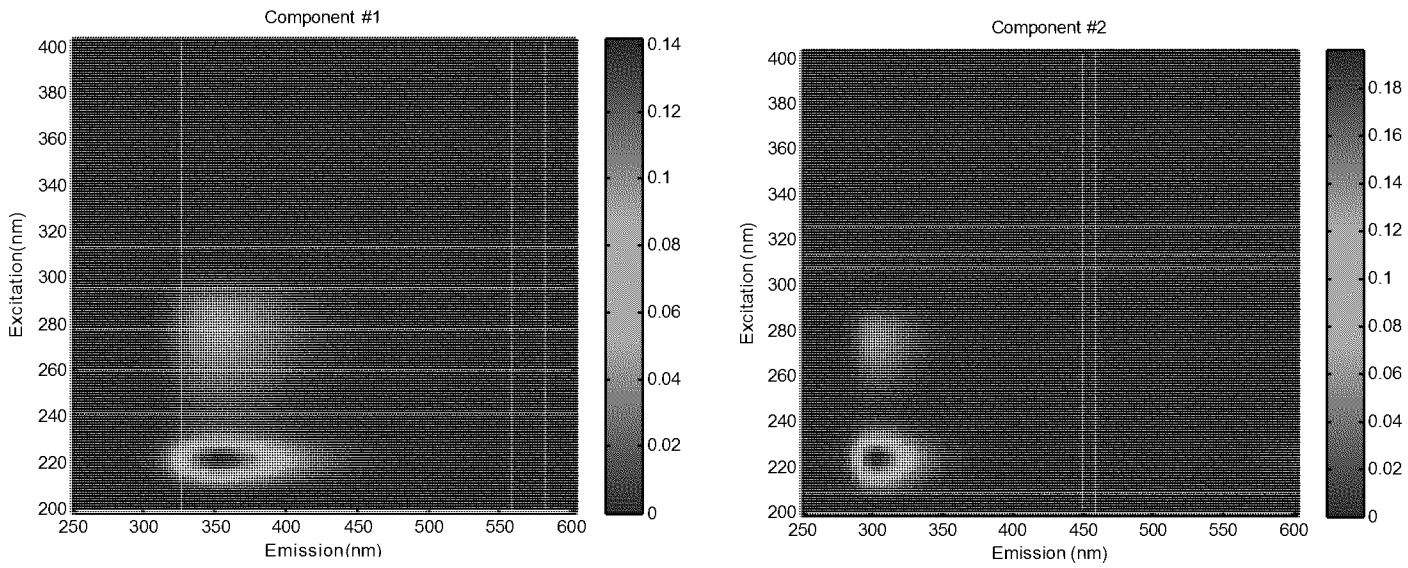


**Figure 90. EEM view of factor 1 with $F_{max}$ at Ex/Em = 221/353 nm (above) and factor 2 with $F_{max}$ at Ex/Em = 224/300 nm (below).**



ED_001324_00000953-00154

# REFERENCES

Alliance for Coastal Technologies Report (2008) Hydrocarbon sensors for oil spill prevention and response. Ref # [UMCES]CBL08-095, 28 pp.

Andersen, C. M., R. Bro (2003) Practical aspects of PARAFAC modeling of fluorescence excitation-emission data. J. Chemom., 17:200-217.

Bieroza, M., A. Baker, J. Bridgeman (2010) Classification and calibration of organic matter fluorescence data with multiway analysis methods and artificial neural networks: an operational tool for improved drinking water treatment. Envirometrics, 22: 256-270.

Boehme, J.R., PG. Coble, R.N. Conmy (2004) Examining CDOM fluorescence variability using principal component analysis: seasonal and regional modeling of three-dimensional fluorescence in the Gulf of Mexico. Marine Chemistry, 89:3-14.

Bahram, M., et al. (2006). "Handling of Rayleigh and Raman scatter for PARAFAC modeling of fluorescence data using interpolation." Journal of Chemometrics 20(3-4): 99-105.

Bugden, J.B.C., C.W. Yeung, P.E. Kepkay, K. Lee (2008) Application of ultraviolet fluorometry and (EEMS) to fingerprint oil and chemically dispersed oil in seawater. Marine Pollution Bulletin, 56(4): 677-85.

CRRC Report (2010) Coastal Response Research Center Deepwater Horizon Dispersants Meeting Report.

Christensen, A.B. Hansen, J. Mortensen, O. Andersen (2005) Characterization and matching of oil samples using fluorescence and PARAFAC. Anal. Chem., 77:2210-17.

Coble, P.G. (1996) Characterization of marine and terrestrial DOM in seawater using EEM spectroscopy. Mar. Chem., 51: 325-346.

Cole, M.G., T. King, K. Lee (2007) Analytical technique for extracting hydrocarbons from water using sample container as extraction vessel in combination with a roller apparatus. Anal. Chem., 77: 2210-17.

Conmy, R.N., P.G. Coble and C.E. Del Castillo (2004) Calibration and performance of the WetLabs' SAFIre in situ fluorometer using seawater. Contin. Shelf Res., 24: 431-42.

Conmy, R. N., et al. (2014a) Submersible Optical Sensors Exposed to Chemically Dispersed Crude Oil: Wave Tank Simulations for Improved Oil Spill Monitoring. Environ Sci Technol 48(3): 1803-1810.

Conmy, R.N., R.F. Chen, C.E. Del Castillo, B. Downing (2014b) Calibrations and Quality Control of In situ Sensors. In: Fluorescence Applications in Aquatic Science. Eds: A. Baker & P.G. Coble, Cambridge Univ. Press, 31 pp.



ED_001324_00000953-00155

Fuller, C.B., J.S. Bonner, C.A. Page, G. Arrambide, M.C. Sterling, Jr., T. Ojo (2003) Field instruments for real time in-situ crude oil concentration measurements. A Conrad Blucher Institute, Texas A&M Corpus Christi Report, 10 pp.

Johansen, O., et al. (2013) Droplet breakup in subsea oil releases - Part 2: Predictions of droplet size distributions with and without injection of chemical dispersants. Marine Pollution Bulletin 73(1): 327-335.

Joint Analysis Group Report (2010) Review of Data to Examine Subsurface Oil in the Vicinity of DWH MC-252, May 19-June 19, 2010; 29 pp.

Kepkay, P., W. Young, J.B.C. Bugden, Z. Li, K. Lee (2008) Ultraviolet fluorescence spectroscopy (UVFS): A new means of determining the effectiveness of chemical dispersants on oil spills. International Oil Spill Conference. API, Washington D.C., Savannah, GA, pp. 639-44.

King, T.L., B. Robinson, C. McIntyre, P. Toole, S. Ryan, F. Saleh, M.C. Boufadel, K. Lee (2015) Fate of surface spills of cold lake blend diluted bitumen treated with dispersant and mineral fines in a wave tank. In: Environmental Engineering Science, Vol. 32, No. 3, 01.03.2015, p. 250-261.

Lee, K., Li, Z., Boufadel, M.C., Venosa, A.D. and Scott Miles, M. (2009) Wave tank studies on dispersant effectiveness as a function of energy dissipation rate and particle size distribution. Final report submitted to NOAA/CRRC/UNH. Pp67+ appendix.

Li, Z., Lee, K., King, T., Boufadel, M.C. and Venosa, A.D., (2008) Oil droplet size distribution as a function of energy dissipation rate in an experimental wave tank 2008 International Oil Spill Conference. Americal Petroleum Institute, Washington D.C., Savannah, GA, pp. 621-626.

Li, Z., Lee, K., King, T., Boufadel, M.C. and Venosa, A.D., (2009a) Evaluating Chemical Dispersant Efficacy in an Experimental Wave Tank: 2, Significant Factors Determining In Situ Oil Droplet Size Distribution. Environmental Engineering Science, 26(9): 1407-1418.

Li, Z., Lee, K., King, T., Boufadel, M.C. and Venosa, A.D., (2009b) Evaluating crude oil chemical dispersion efficacy in a flow-through wave tank under regular non-breaking wave and breaking wave conditions. Marine Pollution Bulletin, 58: 735-744.

Li, Z., Lee, K., King, T., Boufadel, M.C. and Venosa, A.D., (2010) Effects of temperature and wave conditions on chemical dispersion efficacy of heavy fuel oil in an experimental flow-through wave tank. Marine Pollution Bulletin, In Press, Corrected Proof.

Li, Z., K. Lee, T. King, P.E. Kepkay, O. Mikkelsen, C. Pottsmith (2011) Monitoring dispersed oil droplet size distribution at the GOM Deepwater Horizon spill site. International Oil spill Conference Proceedings, March 2011.



ED_001324_00000953-00156

Masutani, S.M., E.E. Adams (2000) Experimental Study of Multiphase Plumes with Application to Deep Ocean Oil Spills," Final Report to U.S. Dept. of the Interior, Minerals Management Service, Contract No., 1435-01-98-CT-30946.

Murphy, K. R., et al. (2010). "Measurement of Dissolved Organic Matter Fluorescence in Aquatic Environments: An Interlaboratory Comparison." Environ Sci Technol 44(24): 9405-9412.

Murphy, K. R., C.A. Stedmon, D. Graeber, R. Bro (2013) Fluorescence Spectroscopy and mutli-way techniques, PARAFAC. Anal. Methods, 5: 6557-6566.

NOAA Technical Report NOS OR&R 25 (2010): Joint Analysis Group, Deepwater Horizon Oil Spill: Review of Preliminary Data to Examine Subsurface Oil in the Vicinity of MC252, May 19 – June 19, 2010, 168 pp.

Oil Budget Calculator (2010) NOAA Report Oil Budget Calculator: Deepwater Horizon, Federal Interagency Solutions Group, 217 pp.

NRC Report (2005) National Research Council Oil Spill Dispersants: Efficacy and Effects, Washington, DC, 400 pp.

Stedmon, C.A., S. Markager, R. Bro (2003) Tracing dissolved organic matter in aquatic environments using a new approach to fluorescence spectroscopy. Mar. Chem., 82: 239-54.

Stedmon, C.A., R. Bro (2003) Characterizing dissolved organic matter fluorescence with parallel factor analysis: a tutorial. Limnol. Oceanogr. Methods, 6: 572-579.

Venosa, A.D., D.W. King, G.A. Sorial (2002a) The Baffled Flask Test for Dispersant Effectiveness: A Round Robin Evaluation of Reproducibility and Repeatability. Spill Science &Technology Bulletin, 7(5-6): 299-308.

Venosa, A.D., K. Lee, M.T. Suidan, S. Garcia-Blanco, S. Cobanli, M. Moteleb, J.R. Haines, G. Tremblay, M. Hazelwood (2002b) Bioremediation and Biorestoration of a Crude Oil-Contaminated Freshwater Wetland on the St. Lawrence River. Bioremediation Journal,6(3):261-281.

Wickley-Olsen, E., Boufadel, M.C., King, T., Li, Z., Lee, K., Venosa, A.D. (2007) Regular and breaking waves in wave tank for dispersion effectiveness testing. In: Proceedings of the 30th Arctic and Marine Oil spill Program (AMOP) Technical Seminar, Edmonton, AB, Canada. Environment Canada, Ottawa, Ontario, Canada, pp. 161–187.

Zepp, R. G., et al. (2004). "Dissolved organic fluorophores in southeastern US coastal waters: correction method for eliminating Rayleigh and Raman scattering peaks in excitation-emission matrices." Marine Chemistry 89(1-4): 15-3.



ED_001324_00000953-00157

Zhao, L., et al. (2014). "Evolution of droplets in subsea oil and gas blowouts: Development and validation of the numerical model VDROP-J." Marine Pollution Bulletin 83(1): 58-69.



ED_001324_00000953-00158